REMOVAL OF TURBIDITY FROM PAINT AND BREWERY INDUSTRIAL WASTEWATERS USING SEQUENTIAL COAG-FLOCCULATION AND ADSORPTION PROCESSES

BY

OKOLO BERNARD IBEZIM

B.ENG (ASUTECH), M.ENG (ESUT)

NAU/2007217003F

A DISSERTATION PRESENTED TO THE DEPARTMENT OF CHEMICAL ENGINEERING IN PARTIAL FULLIMENT OF THE REQUIREMENT FOR THE AWARD OF THE DEGREE OF DOCTOR OF PHILOSOSPHY IN CHEMICAL ENGINEERING

OF

NNAMDI AZIKIWE UNIVERSITY, AWKA, ANAMBRA STATE

SEPTEMBER, 2018

CERTIFICATION

This is to certify that this research work titled, ''Removal of turbidityfrom paint and brewery industrial wastewaters using sequential coag-flocculation and adsorption processes'' was carried out by Okolo Bernard Ibezim under the supervision of Engr. (Prof) O.D. Onukwuli of the Department of Chemical Engineering, Faculty of Engineering, NnamdiAzikiwe University,Awka, Nigeria

_____ _____

Okolo Bernard Ibezim Date

APPROVAL PAGE

The Department of Chemical Engineering, NnamdiAzikiwe University, Awka hereby approves this Dissertation.

Engr. (Prof.) O. D. Onukwuli (Supervisor)	Date
Engr. (Dr.) R.O. Ajemba Head of Dept.	Date
External Examiner	Date
Engr. (Prof.) V.I.Idigo Dean, Fac. Of Engrg	Date
Prof. Harris Odimegwu Dean, SPGS	Date

ACKNOWLEDGEMENTS

I am very much grateful to the Almighty God, who gave me life and enables me to accomplish this project.

I would like to sincerely express my great gratitude and special appreciation to my supervisor Engr.(Prof.)O.D.Onukwuli for his valuable advice, guidance, wonderful encouragement and patience throughout the research without forgetting his human relationship.

Special thanks to Engr. (Dr) M.C Menkiti and Engr. P.C. Nnaji for their assistance in the laboratory works and data analysis.

I also express my gratitude to all staff in the department of chemical Engineering, Engr.(Dr) R.O. Ajemba head, Department of Chemical Engineering, Engr. Prof. (Mrs) P.K. Igbokwe, Engr. Prof. M.Kachi, Engr. (Dr.) J.T. Nwabanne, Engr.(Dr.) V.I. Ugonabo, and Engr. (Dr.) Stone Odera

I would like to express my appreciation to my friends and colleague especiallyto Engr.(Dr.) E.O. oke, Engr. Gabriel Ohabuike, and Dangote cement factory for instrumental characterization.

My profound appreciation goes to Engr. Maduabuchi Enemou (Serg) and my beloved brother Ifeanyi Okolo. I thank you for your support and understanding. I thank my –in-Laws for their support and best wishes.

I am most grateful to my wife Ifeoma, my beautiful daughters: Somtochukwu, Onyiyechukwu, Chinonso, Otitodirichukwu and my son Chukwudera. Thank you for your love, support and patience. I am truly blessed to have you as my family.

DEDICATION

I dedicate this work to God Almighty whom I found favour in, and my entire family for their unflinching support and belief in my success.

ABSTRACT

The continuous industrial development in Nigeria has resulted in the generation of industrial wastewaters. Th wastewaters are usually discharged without proper treatment which affects the environment. There are severa techniques applied in the treatment of wastewaters but coag-flocculation and adsorption processes was applied Thus, the present work focused on the utilization of natural coagulants/adsorbents in the removal of turbidity i wastewaters. The aim of this study was to investigate the removal of turbidity from paint and brewery industria wastewaters using sequential coag-flocculation and adsorption processes. Theobjectives were to: prepare an characterize biocoagulants from *Detaruim microcarpum* (DMC), *Xanthosoma* (CYC), *Hibiscus esculentus* (OSC and *Crassostrea virginica* (ODC) and biosorbents from *Mucuna pruriens* (MSA), *Canaruim schweirfurlhi* (AESA and *Crassostrea virginica* (OSA); study the various coag-flocculation/adsorption parameters such as pH, dosage and contact time; study the adsorption isotherms, kinetic and thermodynamic of the process; and optimize th process using response surface methodology (RSM).The biocoagulants and biosorbents were produced an characterized using Fourier transform infrared (FTIR) spectroscopy, scanning electron microscopy (SEM), X-ra diffraction (XRD) and X-ray fluorescence (XRF). Jar test and batch adsorption processes were carried out in order t determine the effects of process parameters on the turbidity removal. The experimental data were evaluated by fou isotherm models (Langmuir, Freundlich, Temkin, and Dubinin-Radushkevich) and four kinetic models (pseudo-first order, pseudo-second-order, Elovich and intraparticles diffusion). The process was optimized using RSM. Th resultsof characterization of biocoagulants and biosorbents showed that the materials are good for the removal o turbidity from the wastewaters. The removal efficiency of turbidity is dependent on the initial wastewater pH dosage and time. The optimum turbidity removal efficiency of 90.45% wasobtained at 100.53mg/L, pH 2 an settling time 24.45min for coagulationwhile the optimum removal efficiency of turbidity for of 99.8% was obtaine with 26.66mg, pH 6.66 and contact time 69.6min for adsorption. The experimental data fitted well to Langmui isotherm model and pseudo-second-order kinetic model.The thermodynamic study showed the adsorption proces was spontaneous and endothermic in nature.This work has shown that coag-flocculation and adsorption are ver effective in turbidity removal from paint and brewery wastewaters.This work has successfully transformed natura and abundant materials into coagulants/adsorbents that can be used for wastewater treatment. Hence, thes coagulants and adsorbents are recommended for wastewater treatment.

TABLE OF CONTENTS

CONTENT Pages

Title page i

Certification ii

Approval page iii

Dedication iv

Acknowledgement v

Abstract vi

Table of contents vii

List of table viii

List of figures ix

List of plates x

Abbreviations xi

Nomenclature xii

CHAPTER ONE

INTRODUCTION 1

1.1 Background of the Study 1

1.2 Statement of problem 3

1.3 Aim and objectives 3

1.4 Scope of the study 4

1.5 Significance of the study 4

CHAPTER TWO

2.0 Literature review 5

2.1 Sources of wastewater 5

2.2 Wastewater treatment methods 5

2.3 History of coag-flocculation process and its mechanism 5

2.3.1 Theory of coag-flocculation 6

2.4 Classification of Colloids 7

2.4.1 Stability of colloidal suspension 7

2.4.2 Destabilization of colloids

2.5 Flocculation Process 8

2.6 Factors that affect Coag-Flocculation Process 9

2.6.1 Composition of wastewater 9

2.6.2 The type of chemical used in treatment 11

2.6.2.1 Inorganic coagulants 11

2.6.2.2 Organic coagulants 11

2.7 Natural Materials used as Coagulants-Flocculants 12

2.7.1 *Hibiscusesculentus L*) 13

2.7.1.1 General description, growth and uses 13

2.7.2 Detarium *Microcarpum* 13

2.7.1.1Description and uses 13

2.7.3*Xanthosoma sagittifolium* 14

2.7.3.1Description and uses 14

2.7.4 *Crassostrea virginica* 14

2.7.4.1 Origin of chitosan and its extraction from chitin 15

2.7.4.2 Applications of chitosan 16

2.8 Adsorption Phenomenon and Process 16

2.8.1 Introduction 16

2.8.2 Adsorption mechanism 18

2.8.3 Types of adsorption 18

2.8.3.1 Physical adsorption 18

2.8.3.2 Chemical adsorption 19

2.9.1 Adsorption isotherms 19

2.9.1.1Langmuir isotherm model 20

2.9.1.2 Freundlich adsorption isotherm 20

2.9.1.3 Temkin isotherm 21

2.9.1.4 Dubinin- Radushkevich (D-R) isotherm 21

2.10 Adsorption Kinetics 21

2.10.1 Pseudo-first order model 22

2.10.2 Pseudo-second order model 23

2.10.3 Elovich equation 23

2.10.4 Intra particles diffusion model 23

2.10.5 Adsorption thermodynamic 24

2.11 Factors affecting adsorption 24

2.12 Properties of agricultural adsorbent 27

2.12.1*Mucuna pruriens* 27

2.12.1.1 Plant description 27

2.12.2*Canariumschweinfurthii* 28

2.12.2.1 Botanic description 28

2.12.2.3 Products and its applications 28

2.12.3*Crassostrea virginica* 29

2.13 Activated Carbon Production 29

2.13.1 Physical activation 29

2.13.2Chemical activation 30

2.13.3 Factors affecting activated carbon production 30

2.13.4 Properties of activated carbon 31

2.14 Characterization techniques 34

2.14.1 X-Ray diffraction measurement 34

2.14.2 Morphology analysis 35

2.14.3 Infrared spectroscopy analysis 35

2.14.4 X-ray fluorescence (XRF) spectroscopy 35

CHAPTER THREE

3.0 MATERIALSAND METHODS 36

3.1 Sample collections, preparations, characterization and equipment 36

3.1.1 Sample collection 36

3.1.2Sample preparations for biocoagulant and biosorbent 36

3.1.2.1Plant derived bio coagulants 36

3.1.2.2 Animal tissue derived bio coagulants 37

3.1.2.3 Carbonization and activation of adsorbent precursors 38

3.1.3 Sample characterization (Wastewaters, biocoagulants and biosorbent) 38

3.1.4Equipment used 39

3.2 Methods 39

3.2.1 Coag-flocculation test 39

3.2.2 Batch adsorption experiments 40

3.2.3 Mathematical methods 40

3.2.3.1 Kinetic of Coag-flocculation 40

3.2.3.2 Batch adsorption isotherm models 43

3.2.3.3 Adsorption kinetic model 45

3.3 Design of Experiments 47

3.3.1 Experimental design 47

CHAPTER FOUR

RESULTS AND DISCUSSION 50

4.1 Characterization Results for coag-flocculation and adsorption processes 54

4.1.1 Characterization for BRE and PW before and after coag-flocculation and adsorption processes

4.1.2 Characterization results for bio-coagulants and bio-sorbent 54

4.1.3Determination of point of zero charge 65

4.1.4FTIR spectra analysis 67

4.1.5X- ray fluorescence analysis (XRF) 74

4.1.6X-ray diffraction analysis (XRD) 76

4.1.7 SEM (Scanning Electron Microscope) 78

4.2 Effect of bio-coagulants parameters on BRE and PW treatment 82

4.2.1 Effects of dosage, pH and settling time on coag-flocculation of BRE and PW using DMC, CYC, ODC and OSC. 82

4.3 Coag-flocculation kinetic results for varying dosage and pH for DMC, CYC, OSC and ODC in BRE and PW 93

4.4 Time evolution of cluster size distribution 114

4.5 Development of regression model 123

4.6 Analysis of variance (ANOVA) 127

4.7 Adequacy of model 132

4.8 Optimization using the Desirability Functions 150

4.9 Model Validation and Confirmation Experiments 159

4.10 Adsorption studies 159

4.10.1 Effect of solution pH 159

4.10.2 Effect of adsorbent dosage 163

4.10.3 Effect of contact time 164

4.11Equilibrium isotherm studies for turbidity removal 166

4.12 Adsorption Thermodynamic Study 179

4.13Adsorption kinetic study for the removal of turbidity 180

4.14 Developmentof regression model 192

4.15 Analysis of variance (ANOVA) 199

4.16 Adequacy of a model 207

4.17 Optimization using the desirability functions 233

4.18 Model validation and Confirmation Experiments 247

CHAPTER FIVE

CONCLUSIONAND RECOMMENDATION 248

References 249

Appendix A: Raw materials used for coag-flocculation 268

Appendix B: Raw materials for adsorption 269

Appendix C:Adsorption isotherm plot 270

Appendix D:Adsorption kinetics 273

Appendix E:Thermodynamic plots 286

LIST OF TABLES **Pages**

Table 3.1 Equipment used, its model and functions 39

Table 3.2 Independence factors and their coded value level 47

Table 3.3 HDD Design matrix for three variables for coag-flocculation and adsorption processes 49

Table 4.1 Characterization results of BRE before and after coagulationusing DMC as biocoagulants 51

Table 4.2 Characterization results of BRE before and after coagulation using CYC as biocoagulants 52

Table 4.3 Characterization results of BRE before and after coagulationusing OSC as biocoagulants 53

Table 4.4 Characterization results of BRE before and after coagulation using ODC as biocoagulants 54

Table 4.5 Characterization results of PW before and after coagulationusing DMC as biocoagulants 55

Table 4.6 Characterization results of PWbefore and after coagulation using CYC as biocoagulants 56

Table 4.7 Characterization results of PWbefore and after coagulation using OSC as biocoagulants 57

Table 4.8 Characterization results of PWbefore and after coagulation using ODC as biocoagulants 58

Table 4.9 Characterization results of BRE before and after adsorption using MSA as biosorbent 59

Table 4.10 Characterization results of BRE before and after adsorption using AESA as biosorbent 60

Table 4.11 Characterization results of BRE before and after adsorption using OSA as biosorbent 61

Table 4.12 Characterization results of PW before and after adsorption using MSA as biosorbent 62

Table 4.13 Characterization results of PW before and after adsorption using AESA as biosorbent 63

Table 4.14 Characterization results of PW before and after adsorption using OSA as biosorbent 64

Table 4.15 Proximate analysis results of coagulants precursors 65

Table 4.16 Characterization results of activated carbon 66

Table 4.17 XRF results of acid and salt activated carbon for *Crassostrea virginica* 75

Table 4.18 XRF results of acid and salt activated carbon for *mucuna pruriens*l 75

Table 4.19 XRF results of acid and salt activated carbon for *Canarium schweinfurthii* 76

Table 4.20 X-ray diffraction results for the adsorbent 76

Table 4.21 Coag-flocculation kinetic parameter in BRE at pH2 and 50mg/L 94

Table 4.22 Coag-flocculation kinetic parameter in BRE at pH 2 and 100mg/L 94

Table 4.23 Coag-flocculation kinetic parameter in BRE at pH 2 and 200mg/L 95

Table 4.24 Coag-flocculation kinetic parameter in BRE at pH 2 and 300mg/L 95

Table 4.25 Coag-flocculation kinetic parameter in BRE at pH 2 and 400mg/L 95

Table 4.26 Coag-flocculation kinetic parameter in BRE at pH 2 and 500mg/L 96

Table 4.27 Coag-flocculation kinetic parameter in BRE at pH 4 and 50mg/L 96

Table 4.28 Coag-flocculation kinetic parameter in BRE at pH 4 and 100mg/L 96

Table 4.29 Coag-flocculation kinetic parameter in BRE at pH 4 and 200mg/L 97

Table 4.30 Coag-flocculation kinetic parameter in BRE at pH 4 and 300mg/L 97

Table 4.31 Coag-flocculation kinetic parameter in BRE at pH 4 and 400mg/L 97

Table 4.32 Coag-flocculation kinetic parameter in BRE at pH 4 and 500mg/L 98

Table 4.33 Coag-flocculation kinetic parameter in BRE at pH 6 and 50mg/L 98

Table 4.34 Coag-flocculation kinetic parameter in BRE at pH 6 and 100mg/L 98

Table 4.35 Coag-flocculation kinetic parameter in BRE at pH 6 and 200mg/L 99

Table 4.36 Coag-flocculation kinetic parameter in BRE at pH 6 and 300mg/L 99

Table 4.37 Coag-flocculation kinetic parameter in BRE at pH 6 and 400mg/L 99

Table 4.38 Coag-flocculation kinetic parameter in BRE at pH 6 and 500mg/L 100

Table 4.39 Coag-flocculation kinetic parameter in BRE at pH 8 and 50mg/L 100

Table 4.40 Coag-flocculation kinetic parameter in BRE at pH 8 and 100mg/L 100

Table 4.41 Coag-flocculation kinetic parameter in BRE at pH 8 and 200mg/L 101

Table 4.42 Coag-flocculation kinetic parameter in BRE at pH 8 and 300mg/L 101

Table 4.43 Coag-flocculation kinetic parameter in BRE at pH 8 and 400mg/L 101

Table 4.44 Coag-flocculation kinetic parameter in BRE at pH 8 and 500mg/L 102

Table 4.45 Coag-flocculation kinetic parameter in BRE at pH 10 and 50mg/L 102

Table 4.46 Coag-flocculation kinetic parameter in BRE at pH 10 and 100mg/L 102

Table 4.47 Coag-flocculation kinetic parameter in BRE at pH 10 and 200mg/L 103

Table 4.48 Coag-flocculation kinetic parameter in BRE at pH 10 and 300mg/L 103

Table 4.49 Coag-flocculation kinetic parameter in BRE at pH 10 and 400mg/L 103

Table 4.50 Coag-flocculation kinetic parameter in BRE at pH 10 and 500mg/L 104

Table 4.51 Coag-flocculation kinetic parameter in PW at pH 2 and 50mg/L 104

Table 4.52 Coag-flocculation kinetic parameter in PW at pH 2 and 100mg/L 104

Table 4.53 Coag-flocculation kinetic parameter in PW at pH 2 and 200mg/L 105

Table 4.54 Coag-flocculation kinetic parameter in PW at pH 2 and300mg/L 105

Table 4.55 Coag-flocculation kinetic parameter in PW at pH 2 and 400mg/L 105

Table 4.56 Coag-flocculation kinetic parameter in PW at pH 2 and 500mg/L 106

Table 4.57 Coag-flocculation kinetic parameter in PW at pH 4 and 50mg/L 106

Table 4.58 Coag-flocculation kinetic parameter in PW at pH 4 and 100mg/L 106

Table 4.59 Coag-flocculation kinetic parameter in PW at pH 4 and 200mg/L 107

Table 4.60Coag-flocculation kinetic parameter in PW at pH 4 and 300mg/L 107

Table 4.61 Coag-flocculation kinetic parameter in PW at pH 4 and400mg/L 107

Table 4.62 Coag-flocculation kinetic parameter in PW at pH 4 and 500mg/L 108

Table 4.63 Coag-flocculation kinetic parameter in PW at pH 6 and 50mg/L 108

Table 4.64 Coag-flocculation kinetic parameter in PW at pH 6 and 100mg/L 108

Table 4.65 Coag-flocculation kinetic parameter in PW at pH 6 and 200mg/L 109

Table 4.66 Coag-flocculation kinetic parameter in PW at pH 6 and 300mg/L 109

Table 4.67 Coag-flocculation kinetic parameter in PW at pH 6 and 400mg/L 109

Table 4.68 Coag-flocculation kinetic parameter in PWE at pH 6 and 500mg/L 110

Table 4.69 Coag-flocculation kinetic parameter in PW at pH 8 and 50mg/L 110

Table 4.70 Coag-flocculation kinetic parameter in PW at pH 8 and 100mg/L 110

Table 4.71 Coag-flocculation kinetic parameter in PW at pH 8 and 200mg/L 111

Table 4.72 Coag-flocculation kinetic parameter in PW at pH 8 and 300mg/L 111

Table 4.73 Coag-flocculation kinetic parameter in PW at pH 8 and 400mg/L 111

Table 4.74 Coag-flocculation kinetic parameter in PW at pH 8 and 500mg/L 112

Table 4.75 Coag-flocculation kinetic parameter in PW at pH 10 and 50mg/L 112

Table 4.76 Coag-flocculation kinetic parameter in PW at pH 10 and100mg/L 112

Table 4.77 Coag-flocculation kinetic parameter in PW at pH 10 and 200mg/L 113

Table 4.78 Coag-flocculation kinetic parameter in PW at pH 10 and 300mg/L 113

Table 4.79 Coag-flocculation kinetic parameter in PW at pH 10 and 400mg/L 113

Table 4.80 Coag-flocculation kinetic parameter in PW at pH 10 and 500mg/L 114

Table 4.81 Design matrixand HDD exptal and predicated results for turbidity removal from BRE 124

Table 4.82 Design matrix and HDD exptal and predicated results for turbidity removal from PW 125

Table 4.83 ANOVA for response surface quadratic model for turbidity removal in BRE using DMC 128

Table 4.84 Model coefficient for turbidity removal in BRE using DMC 128

Table 4.85ANOVA for response surface quadratic model for turbidity removal in BRE using CY128

Table 4.86Model coefficient for turbidity removal in BRE using CYC 128

Table 4.87 ANOVA response surface quadratic model for turbidity removal in BRE using OSC 129

Table 4.88Model coefficient for turbidity removal in BRE using OSC 129

Table 4.89 ANOVA for response surface quadratic model for turbidity removal in BRE using OD129

Table 4.90 Model coefficient for turbidity removal in BRE using ODC 129

Table 4.91 ANOVA for response surface quadratic model for turbidity removal in PW using D130

Table 4.92 Model coefficient for turbidity removal in BRE using DMC 130

Table 4.93 ANOVA for response surface quadratic model for turbidity removal in PW using CYC130

Table 4.94 Model coefficient for turbidity removal in BRE using CYC 130

Table 4.95 ANOVA for response surface quadratic model for turbidity removal in PW using OSC131

Table 4.96 Model coefficient for turbidity removal in BRE using OSC 131

Table 4.97 ANOVA for response surface quadratic model for turbidity removal in PW using ODC131

Table 4.98 Model coefficient for turbidity removal in BRE using ODC 131

Table 4.99 Result of optimization using desirability function of DMC in BRE 151

Table 4.100 Result of optimization using desirability function of CYC in BRE 151

Table 4.101 Result of optimization using desirability function of OSC in BRE 152

Table 4.102 Result of optimization using desirability function of ODC in BRE 152

Table 4.103 Result of optimization using desirability function of DMC in PW 153

Table 4.104 Result of optimization using desirability function of CYC in PW 153

Table 4.105 Result of optimization using desirability function of OSC in PW 154

Table 4.106 Result of optimization using desirability function of ODC in PW 154

Table 4.107 Validation of the models predicated using desirability function values for turbidity with DMC, CYC, OSC and ODC in BRE. 159

Table 4.108Validation of the models predicated using desirability function values for turbidity with DMC, CYC, OSC and ODC in PW 159

Table 4.109 Isotherm model constantsfor turbidity removal with MSA in BRE 167

Table 4.110 Isotherm model constants for turbidity removal with MSS in BRE 168

Table 4.111 Isotherm model constants for turbidity removal with AESA in BRE 169

Table 4.112 Isotherm model constants for turbidity removal with AESS in BRE 170

Table 4.113 Isotherm model constants for turbidity removal with OSA in BRE 171

Table 4.114 Isotherm model constants for turbidity removal with OSS in BRE 172

Table 4.115 Isotherm model constants for turbidity removal with MSA in PW 173

Table 4.116 Isotherm model constants for turbidity removal with MSS in PW 174

Table 4.117 Isotherm model constants for turbidity removal with AESA in PW 175

Table 4.118 Isotherm model constants for turbidity removal with AESS in PW 176

Table 4.119 Isotherm model constants for turbidity removal with OSA in PW 177

Table 4.120 Isotherm model constants for turbidity removal with OSS in PW 178

Table 4.121 Thermodynamic parameters for turbidity removal with acid treated adsorbent BRE 179

Table 4.122 Thermodynamic parameters for turbidity removal with salt treated adsorbent BRE 179

Table 4.123 Thermodynamic parameters for turbidity removal with acid treated adsorbent PW 180

Table 4.124Thermodynamic parameters for turbidity removal with salt treated adsorbent PW 180

Table 4.125 Kinetic model constants for turbidity removal with MSA in BRE 181

Table 4.126 Kinetic model constants for turbidity removal with MSS in BRE 182

Table 4.127 Kinetic model constants for turbidity removal with OSA in BRE 183

Table 4.128 Kinetic model constants for turbidity removal with OSS in BRE 184

Table 4.129 Kinetic model constants for turbidity removal with AESA in BRE 185

Table 4.130 Kinetic model constants for turbidity removal with AESS in BRE 186

Table 4.131 Kinetic model constants for turbidity removal with MSA in PW 187

Table 4.132 Kinetic model constants for turbidity removal with MSS in PW 188

Table 4.133Kinetic model constants for turbidity removal with AESA in PW 189

Table 4.134 Kinetic model constants for turbidity removal with AESS in PW 190

Table 4.135 Kinetic model constants for turbidity removal with OSA in PW 191

Table 4.136 Kinetic model constants for turbidity removal with OSS in PW 192

Table 4.137 Design matrix and HDD with experimental and predicated results for removal of turbidity with MSA, AESA and OSA from BRE 194

Table 4.138 Design matrix and HDD with experimental and predicated results for removal of turbidity with MSS, AESS and OSS from BRE 195

Table 4.139 Design matrix and HDD with experimental and predicated results for removal of turbidity with MSA, AESA and OSA from PW 196

Table 4.140 Design matrix and HDD with experimental and predicated results for removal of turbidity with MSS, AESS and OSS from PW 197

Table 4.141 ANOVA for response surface quadratic model for turbidity removal in BRE using MS 200

Table 4.142 Model coefficient for turbidity removal in BRE using MSA 200

Table 4.143 ANOVA for response surface quadratic model for turbidity removal in BRE using MSS 201

Table 4.144 Model coefficient for turbidity removal in BRE using MSS 201

Table 4.145 ANOVA for response surface quadratic model for turbidity removal in BRE using AES 201

Table 4.146 Model coefficient for turbidity removal in BRE using AESA 201

Table 4.147 ANOVA for response surface quadratic model for turbidity removal in BRE using AES 202

Table 4.148 Model coefficient for turbidity removal in BRE using AESS 202

Table 4.149 ANOVA for response surface quadratic model for turbidity removal in BRE using OSA 202

Table 4.150 Model coefficient for turbidity removal in BRE using OSA 202

Table 4.151 ANOVA for response surface quadratic model for turbidity removal in BRE using OSS 203

Table 4.152 Model coefficient for turbidity removal in BRE using OSS 203

Table 4.153 ANOVA for response surface quadratic model for turbidity removal in PW using MSA 203

Table 4.154 Model coefficient for turbidity removal in PWusing MSA 203

Table 4.155ANOVA for response surface quadratic model for turbidity removal in PW using MSS 204

Table 4.156 Model coefficient for turbidity removal in PWusing MSS 204

Table 4.157 ANOVA for response surface quadratic model for turbidity removal in PW using AES 204

Table 4.158 Model coefficient for turbidity removal in PWusing AESA 204

Table 4.159 ANOVA for response surface quadratic model for turbidity removal in PW using AES 205

Table 4.160 Model coefficient for turbidity removal in PWusing AESS 205

Table 4.161 ANOVA for response surface quadratic model for turbidity removal in PW using OSA 205

Table 4.162 Model coefficient for turbidity removal in PWusing OSA 205

Table 4.163 ANOVA for response surface quadratic model for turbidityremoval in PW using OS 206

Table 4.164 Model coefficient for turbidity removal in PW usingOSS 206

Table 4.165 Results of optimization using Desirability Functions with MSA in BRE 234

Table 4.166 Results of optimization using Desirability Functions with MSS in BRE 234

Table 4.167 Results of optimization using Desirability Functions with OSA in BRE 235

Table 4.168 Results of optimization using Desirability Functions with OSS in BRE 236

Table 4.169 Results of optimization using Desirability Functions with AESA in BRE 236

Table 4.170 Results of optimization using Desirability Functions with AESS in BRE 237

Table 4.171 Results of optimization using Desirability Functions with MSA in PW 237

Table 4.172 Results of optimization using Desirability Functions with MSS in PW 238

Table 4.173 Results of optimization using Desirability Functions with AESA in PW 238

Table 4.174 Results of optimization using Desirability Functions with AESS in PW 239

Table 4.175 Results of optimization using Desirability Functions with OSA in PW 239

Table 4.176 Results of optimization using Desirability Functions with OSS in PW 240

Table 4.177Validation of the models predicated using desirability function values for turbidity removal with acid and salt treated adsorbents in BRE. 247

Table 4.178 Validation of the models predicated using desirability function values for turbidity removal with acid and salt treated adsorbents in PW. 247

LIST OF FIGURES

Figure 2.1 Three steps of adsorption mechanism 18

Figure 2.2 Different types of porosity in a porous solid 33

Figure 4.1 Point of zero charge for acid treated adsorbents 66

Figure 4.2 Point of zero charge for salt treated adsorbents 67

Figure 4.3 FTIR spectra analysis of MSA adsorbent before adsorption in BRE 68

Figure 4.4 FTIR spectra analysis of MSA adsorbent after adsorption in BRE 69

Figure 4.5 FTIR spectra analysis of AESA adsorbent before adsorption in BRE 69

Figure 4.6 FTIR spectra analysis of AESA adsorbent after adsorption in BRE 70

Figure 4.7 FTIR spectra analysis of OSA adsorbent before adsorption in BRE 70

Figure 4.8 FTIR spectra analysis of OSA adsorbent after adsorption in BRE 71

Figure 4.9 FTIR spectra analysis of MSA adsorbent before adsorption in PW 71

Figure 4.10 FTIR spectra analysis of MSA adsorbent after adsorption in PW 72

Figure 4.11 FTIR spectra analysis of AESA adsorbent before adsorption in PW 72

Figure 4.12 FTIR spectra analysis of AESA adsorbent after adsorption in PW 73

Figure 4.13 FTIR spectra analysis of OSA adsorbent before adsorption in PW 73

Figure 4.14 FTIR spectra analysis of OSA adsorbent afteradsorption in PW 74

Figure 4.15 X-ray diffraction patterns of MSA and MSS 77

Figure 4.16 X-ray diffraction patterns of AESA and AESS 77

Figure 4.17 X-ray diffraction patterns of OSA and OSS 77

Figure 4.18 Turbidity removal efficiency in BRE at pH 2 and varying dosage with (initial concentration = 728.25mg/L, settling time = 30min) 83

Figure 4.19 Turbidity removal efficiency in BRE at pH 4 and varying dosage with (initial concentration = 728.25mg/L, settling time = 30min) 84

Figure 4.20 Turbidity removal efficiency in BRE at pH 6 and varying dosage with (initial concentration = 728.25mg/L, settling time = 30min) 85

Figure 4.21 Turbidity removal efficiency in BRE at pH 8 and varying dosage with (initial concentration = 728.25mg/L, settling time = 30min) 86

Figure 4.22 Turbidity removal efficiency in BRE at pH 10 and varying dosage with (initial concentration = 728.25mg/L, settling time = 30min) 87

Figure 4.23 Turbidity removal efficiency in PW at pH 2 and varying dosage with (initial concentration = 849.685mg/L, settling time = 30min) 88

Figure 4.24 Turbidity removal efficiency in PW at pH 4 and varying dosage with (initial concentration = 849.685mg/L, settling time = 30min) 89

Figure 4.25 Turbidity removal efficiency in PW at pH 6 and varying dosage with (initial concentration = 849.685mg/L, settling time = 30min) 90

Figure 4.26 Turbidity removal efficiency in PW at pH 8 and varying dosage with (initial concentration = 849.685mg/L, settling time = 30min) 91

Figure 4.27 Turbidity removal efficiency in PW at pH 10 and varying dosage with (initial concentration = 849.685mg/L, settling time = 30min) 92

Figure 4.28 Particle distributions for CYC in BRE at minimum half-lifeof 9.15min 115

Figure 4.29 Particle distributions for OSC in BRE at minimum half-life of 9.15min 115

Figure 4.30 Particle distributions for DMC in BRE at minimum half-life of 1.83min 116

Figure 4.31 Particle distributions for ODC in BRE at minimum half-lifeof 4.58min 116

Figure 4.32 Particle distributions for CYC in BRE at maximum half-lifeof 142.78min 117

Figure 4.33 Particle distributions for OSC in BRE at maximum half-life of 515.25min 117

Figure 4.34 Particle distributions for DMC in BRE at maximum half-life of 243.04min 118

Figure 4.35 Particle distributions for ODC in BRE at maximum half-life of 143.45min 118

Figure 4.36 Particle distributions for CYC in PW at minimum half-lifeof 3.92min 119

Figure 4.37 Particle distributions for OSC in PW at minimum half-lifeof 0.98min 119

Figure 4.38 Particle distributions for DMC in PW at minimum half-life of 0.87min 120

Figure 4.39 Particle distributions for ODC in PW at minimum half-life of 1.31min 120

Figure 4.40 Particle distributions for CYC in PW at maximum half-lifeof 81.17min 121

Figure 4.41 Particle distributions for OSC in PW at maximum half-life of 36.78min 121

Figure 4.42 Particle distributions for DMC in PW at maximum half-life of 43.04min 122

Figure 4.43 Particle distributions for ODC in PW at maximum half-life of 47.64min 122

Figure 4.44 Design-expert plots: (a) Normal probability plots (b) Residuals versus run number of data and (c) Predicted versus actual for turbidity removal in BRE using DMC 134

Figure 4.45 Design-expert plots: (a) Normal probability plots (b) Residuals versus run number of data and (c) Predicted versus actual for turbidity removal in BRE using CYC 135

Figure 4.46 Design-expert plots: (a) Normal probability plots (b) Residuals versus run number of data and (c) Predicted versus actual for turbidity removal in BRE using OSC 136

Figure 4.47 Design-expert plots: (a) Normal probability plots (b) Residuals versus run number of data and (c) Predicted versus actual for turbidity removal in BRE using ODC 137

Figure 4.48 Design-expert plots: (a) Normal probability plots (b) Residuals versus run number of data and (c) Predicted versus actual for turbidity removal in BRE using DMC 138

Figure 4.49 Design-expert plots: (a) Normal probability plots (b) Residuals versus run number of data and (c) Predicted versus actual for turbidity removal in PW using CYC 139

Figure 4.50 Design-expert plots: (a) Normal probability plots (b) Residuals versus run number of data and (c) Predicted versus actual for turbidity removal in PW using OSC 140

Figure 4.51 Design-expert plots: (a) Normal probability plots (b) Residuals versus run number of data and (c) Predicted versus actual for turbidity removal in PW using ODC 141

Figure 4.52 Response surface plots of the effects of (a) pH vs coagulant dosage (b) settling time vs pH (c) settling time vs coagulant dosage for turbidity removal in BRE using DMC 142

Figure 4.53 Response surface plots of the effects of (a) pH vs coagulant dosage (b) settling time vs pH (c) settling time vs coagulant dosage for turbidity removal in BRE using CYC 143

Figure 4.54 Response surface plots of the effects of (a) pH vs coagulant dosage (b) settling time vs pH (c) settling time vs coagulant dosage for turbidity removal in BRE using OSC 144

Figure 4.55 Response surface plots of the effects of (a) pH vs coagulant dosage (b) settling time vs pH (c) settling time vs coagulant dosage for turbidity removal in BRE using ODC 145

Figure 4.56 Response surface plots of the effects of (a) pH vs coagulant dosage (b) settling time vs pH (c) settling time vs coagulant dosage for turbidity removal in PW using DMC 146

Figure 4.57 Response surface plots of the effects of (a) pH vs coagulant dosage (b) settling time vs pH (c) settling time vs coagulant dosage for turbidity removal in PW using CYC 147

Figure 4.58 Response surface plots of the effects of (a) pH vs coagulant dosage (b) settling time vs pH (c) settling time vs coagulant dosage for turbidity removal in PW using OSC 148

Figure 4.59 Response surface plots of the effects of (a) pH vs coagulant dosage (b) settling time vs pH (c) settling time vs coagulant dosage for turbidity removal in PW using ODC 149

Figure 4.60 Desirability ramp of optimized DMC in BRE 155

Figure 4.61 Desirability ramp of optimized CYC in BRE 155

Figure 4.62 Desirability ramp of optimized OSC in BRE 156

Figure 4.63 Desirability ramp of optimized ODC in BRE 156

Figure 4.64 Desirability ramp of optimized DMC in PW 157

Figure 4.65 Desirability ramp of optimized CYC in PW 157

Figure 4.66 Desirability ramp of optimized OSC in PW 158

Figure 4.67 Desirability ramp of optimized ODC in PW 158

Figure 4.68Effects of pH on the efficiency removal of turbidity from BRE with acid and salt treated adsorbents (initial conc.=121 mg/L, adsorbent dosage= 60mg/L and contact time=40min) 160

Figure 4.69 Effects of pH on the efficiency removal ofturbidity from PW with acid and salt treated adsorbents (initial conc.=188 mg/L, adsorbent dosage= 60mg/L and contact time=40min) 161

Figure 4.70 Effects of dosage on the efficiency removal of turbidity from BRE with acid and salt treated adsorbents (initial conc.=121 mg/L, pH 8 and contact time=40min) 163

Figure 4.71 Effects of dosage on the efficiency removal of turbidity from PW with acid and salt treated adsorbents (initial concentration=188 mg/L, pH 8 and contact time=40min) 163

Figure 4.72 Effects of contact time on the efficiency removal of turbidity from BRE with acid and salt treated adsorbents (initial concentration=121 mg/L, adsorbent dosage= 60mg/L and pH=8) 165

Figure 4.73 Effects of contact time on the efficiency removal of turbidity from BRE with acid and salt treated adsorbents (initial concentration=188 mg/L, adsorbent dosage= 60mg/L and pH=8) 165

Figure 4.74 Design-expert plots: (a) Normal probability plots (b) Residuals versus run number of data and (c) Predicted versus actual for turbidity removal in BRE using MSA 209

Figure 4.75 Design-expert plots: (a) Normal probability plots (b) Residuals versus run number of data and (c) Predicted versus actual for turbidity removal in BRE using MSS 210

Figure 4.76 Design-expert plots: (a) Normal probability plots (b) Residuals versus run number of data and (c) Predicted versus actual for turbidity removal in BRE using OSA 211

Figure 4.77 Design-expert plots: (a) Normal probability plots (b) Residuals versus run number of data and (c) Predicted versus actual for turbidity removal in BRE using OSS 212

Figure 4.78 Design-expert plots: (a) Normal probability plots (b) Residuals versus run number of data and (c) Predicted versus actual for turbidity removal in BRE using AESA 213

Figure 4.79 Design-expert plots: (a) Normal probability plots (b) Residuals versus run number of data and (c) Predicted versus actual for turbidity removal in BRE using AESS 214

Figure 4.80 Design-expert plots: (a) Normal probability plots (b) Residuals versus run number of data and (c) Predicted versus actual for turbidity removal in PW using MSA 215

Figure 4.81 Design-expert plots: (a) Normal probability plots (b) Residuals versus run number of data and (c) Predicted versus actual for turbidity removal in PW using MSS 216

Figure 4.82 Design-expert plots: (a) Normal probability plots (b) Residuals versus run number of data and (c) Predicted versus actual for turbidity removal in PW using AESA 217

Figure 4.83 Design-expert plots: (a) Normal probability plots (b) Residuals versus run number of data and (c) Predicted versus actual for turbidity removal in PW using AESS 218

Figure 4.84 Design-expert plots: (a) Normal probability plots (b) Residuals versus run number of data and (c) Predicted versus actual for turbidity removal in PW using OSA 219

Figure 4.85 Design-expert plots: (a) Normal probability plots (b) Residuals versus run number of data and (c) Predicted versus actual for turbidity removal in PW using OSS 220

Figure 4.86 Response surface plots of the effects of (a) pH vs coagulant dosage (b) settling time vs pH (c) settling time vs coagulant dosage for turbidity removal in BRE using MSA 221

Figure 4.87 Response surface plots of the effects of (a) pH vs coagulant dosage (b) settling time vs pH (c) settling time vs coagulant dosage for turbidity removal in BRE using MSS 222

Figure 4.88 Response surface plots of the effects of (a) pH vs coagulant dosage (b) settling time vs pH (c) settling time vs coagulant dosage for turbidity removal in BRE using AESA 223

Figure 4.89 Response surface plots of the effects of (a) pH vs coagulant dosage (b) settling time vs pH (c) settling time vs coagulant dosage for turbidity removal in BRE using AESS 224

Figure 4.90 Response surface plots of the effects of (a) pH vs coagulant dosage (b) settling time vs pH (c) settling time vs coagulant dosage for turbidity removal in BRE using OSA 225

Figure 4.91 Response surface plots of the effects of (a) pH vs coagulant dosage (b) settling time vs pH (c) settling time vs coagulant dosage for turbidity removal in BRE using OSS 226

Figure 4.92 Response surface plots of the effects of (a) pH vs coagulant dosage (b) settling time vs pH (c) settling time vs coagulant dosage for turbidity removal in PW using MSA 227

Figure 4.93 Response surface plots of the effects of (a) pH vs coagulant dosage (b) settling time vs pH (c) settling time vs coagulant dosage for turbidity removal in PW using MSS 228

Figure 4.94 Response surface plots of the effects of (a) pH vs coagulant dosage (b) settling time vs pH (c) settling time vs coagulant dosage for turbidity removal in PW using AESA 229

Figure 4.95 Response surface plots of the effects of (a) pH vs coagulant dosage (b) settling time vs pH (c) settling time vs coagulant dosage for turbidity removal in PW using AESS 230

Figure 4.96 Response surface plots of the effects of (a) pH vs coagulant dosage (b) settling time vs pH (c) settling time vs coagulant dosage for turbidity removal in PW using OSA 231

Figure 4.97 Response surface plots of the effects of (a) pH vs coagulant dosage (b) settling time vs pH (c) settling time vs coagulant dosage for turbidity removal in PW using OSS 232

Figure 4.98 Desirability ramp of optimized MSA in BRE 240

Figure 4.99 Desirability ramp of optimized MSS in BRE 241

Figure 4.100 Desirability ramp of optimized OSA in BRE 241

Figure 4.101 Desirability ramp of optimized OSS in BRE 242

Figure 4.102 Desirability ramp of optimized AESA in BRE 242

Figure 4.103 Desirability ramp of optimized AESS in BRE 243

Figure 4.104 Desirability ramp of optimized MSA in PW 243

Figure 4.105 Desirability ramp of optimized MSS in PW 244

Figure 4.106 Desirability ramp of optimized AESA in PW 244

Figure 4.107 Desirability ramp of optimized AESS in PW 245

Figure 4.108 Desirability ramp of optimized OSA in PW 245

Figure 4.109 Desirability ramp of optimized OSS in PW 246

LIST OF PLATES

Plate	Tile	Page
4.1	SEM MSA	79
4.2	SEM MSS	79
4.3	SEM AESA	80
4.4	SEM AESS	80
4.5	SEM OSA	81
4.6	SEM OSS	81
A3	Bio coagulant raw materials for coag/flocculation process	341
A4	Bio sorbent raw materials for adsorption	342

LIST OF ABBREVIATIONS

AC	Activated carbon
AESA	Africa Elemi seed acid treated
AESS	Africa Elemi seed salt treated
ANOVA	Analysis of Variance
BBD	Box Behnken Design of Experiment
BET	Brunauer- Emmet and Teller
BoD_5	Biochemical oxygen demand
BRE	Brewery Effluent
CCD	Central composite Design
COD	Chemical oxygen demand
CV	Coefficient of variance
CYC	Cocoyam coagulant
DLVO	Deryagin and Landau, Verwery and Overbeck
DMC	*Detarium microcarpum* coagulant
DoE	Design of Experiment
D-R	Dubinin-Raduskevich
FTIR	Fourier Transform Infrared spectroscopy
2FI	Two factor interaction
IR	Impregnation Ratio
IUPAC	International Union of Pure and Applied Chemistry
MSA	Mucuna shell acid treated
MSS	Mucuna shell salt treated
NOM	Natural organic matter
NTU	NephelometricTurbibity Unit
ODC	Oyster derived coagulant

OSA	Oyster shell acid treated
OSC	Okra seed coagulant
OSS	Oyster shell salt treated
PW	Paint wastewater
RSM	Response surface methodology
SEM	Scanning electron microscopy
SD	Standard deviation
TDS	Total dissolved solid
TKN	Total Kjeldhal Nitrogen
TSS	Total suspended solid
WHO	World Health Organization
XRD	X-ray Diffraction
XRF	X-ray fluorescence
Zpc	zero point of charge

NOMENCLATURE

Symbol	Description	Units
A	Temkin constant	g^{-1}
β_i	Regression coefficient	dimensionless
C_e	Equilibrium liquid solute conc.	mg/L
C_o	initial liquid solute conc.	mg/L
C_t	Liquid solute conc. at time t	(min^{-1})
E	Mean free energy	kJ/mol
K_1	Pseudo-first-order rate constant	min^{-1}
K_2	Pseudo-second-order rat constant	$gmg^{-1}min^{-1}$
K_F	Freundlich adsorption capacity	mg/g
K_d	Intraparticle diffusion rate constant	($mg/gmin^{1/2}$)
K_L	Langmuir affinity constant	mg^{-1}
M	mass of dry adsorbent	(g)
n	Adsorbent intensity	(dimensionless)
q	Adsorption capacity	mg/g
q_e	Equilibrium adsorption capacity	mg/g
q_{max}	Maximum monolayer adsorption capacity	mg/g
q_t	Amount of solute adsorbed at time t	(mg/g)
q_D	Dubinin-Radushkevich constant	mg/g
R^2	Correlation Coefficient	(dimensionless)
R	Universal gas constant	J/K/mol

ΔG°	Gibbs free energy of Adsorption	J/mol
ΔH°	Enthalpy of Adsorption	KJ/mol
ΔS°	Change in the entropy of Adsorption	KJ/mol

CHAPTER ONE

INTRODUCTION

1.3 Background of the Study

The continuous industrial development in Nigeria has resulted in the generation of industrial wastewaters. This wastewater contains solid particles that causes turbidity, and are discharged into the environment without proper treatment.It occurs as a result of discharging poor quality treated wastewaters into the environmentwhich poses a serious threat to human life, aquatic organisms and ecosystem (Elhassadi, 2008; Simate, et al., 2011).

Paint and brewery industries due to varying degrees of chemicals used generate a lot of wastewaters with high concentration of biochemical oxygen demand(BOD), chemical oxygen demand (COD), suspended solids, toxic compounds and colour (Ajjabi and Chouba, 2009;Aboulhassen,*et al*., 2006). The wastewater from paint industries are generated primarily due to cleaning operation of mixers, reactors, blenders, packing machines and floors. Brewery industry is one of the industries that consume a large volume of water for its operations (Menkiti,*et al*., 2014; Simate,*et al.*, 2011). The wastewater contains a large amount of protein, fat, fiber, carbohydrates, yeast, hops residue, ethanol and total suspended solids (TSS) (Zheng,*et al*., 2011; Braeken, et al.,

2004). The main sources of brewery effluent are from bottle filling, cleaning and tank draining (Lemji and Eckstadt, 2013).Therefore, the need for treatment to meet the global demand and Nigerian Environmental regulatory standardsbefore discharging becomes imperative (Rajaram and Ashutosh, 2008; Ntuli,*et al*., 2011,NESREA, Act. 2007).

There are various techniques used in removingturbidity, suspended solids, dissolved solids and colour from industrial wastewaters such as biodegradation, adsorption, membrane filtration, coag-flocculation, advanced oxidation etc (Zhang, et al., 2007; Kabdasli, et al., 2007; Aboulhassan,*et al*., 2006; Keng,*et al*., 2014).Among these methods, coagulation-flocculation and adsorption processes wereapplied due to simplicity and efficient (Rodriguez,*et al*., 2007; Zouboulis and Tzoupanso, 2008). Coagulation process is usually completed in a very short period of time;(about ten seconds) whereas, flocculation occurs when destabilized particles are driven toward each other by the shear force in the rapid mix, usually over a long period of time (twenty to forty-five minutes).

Aluminium sulphate and ferric sulphate arethe conventionalcoagulants used for coagulation-flocculation process in primary treatment of water. However, previous research have shown that aluminium sulphate used for water treatment, causes serious health hazards, especially when an error occurs during the treatment process (Miller, *et al.*, 2008). High level of aluminium sulphate in the brain has been identified as a risk factor for Alzheimer's disease and as a causative agent in neurological disease. Other reports also suggest that alum may be carcinogenic in water application (Renuka and Yadhav,2012; Ayotunde,*et al*., 2011).Therefore, there is a need for the replacement of these inorganic coagulants with alternative natural coagulants that are environmentally friendly, cheap,more efficient and biodegradable (Cloete, 2010). Natural coagulants were the focus of many researchers through the last decade due to problems caused by the conventional coagulants. Theyhave been considerable interest in the development and usage of plant based natural coagulants such as *Moringa oleifera* (Menkiti,*et al*., 2012), *Strychnos potatorum*,*Pereskia aculeate* (Tripathi,*et al*., 1976),in treatment of water and wastewaters.

Adsorption is a mass transfer process by which an adsorbate is transferred from the liquid to the surface of the adsorbent, and becomes bound by physical or chemical interactions(Abdulhalim,*et al*., 2011; Amosa, 2015; Aber and Sheydaei, 2012). However, the main drawback of adsorption process is the high cost of commercial activated carbon; hence the need for cheap and locally available agricultural waste based adsorbents (DelRio,*et al*., 2011; Cobas,*et al*., 2014; EL-hadad, 2012). This has led to a growing research interest in the production of activated carbons from renewable and cheaper precursors(Padilla-Ortego, et al., 2013). Various kinds of activated carbon have been prepared from agro-byproducts, such as orange peels, melon seed (Ma, et al., 2014), coir pith (Banker, et al., 2009; Fomkin, 2009), coconut coir (Auta, 2012; Odoemelam,*et al*., 2011), bamboo dust, coconut shell,

groundnut shell, rice husk,corn cob, almond shell (Gupta,*et al*., 2006; Krishnani and Ayyapan, 2006; Akhtar,*et al.*, 2010) and palm shell (Alothman, et al., 2011; Park, et al., 2008) etc.The adsorptive properties of any activated carbon are highly dependent upon active surface sites including; functional groups, specific surface area, iodine number and modifications. The removal capabilities of these biosorbents can generally be improved through physical or chemical modification (Patel, 2012).

The aim of this work is to develop an efficient bio coagulants and biosorbents from *Hibiscus esculentus L*, *Detarium microcarpum, Xanthosoma* and *Crassostrea Virginica,* as biocoagulants while *Canarium schweinfurlhii*, *Mucuna Pruriens* and *Crassostrea Virginica* as biosorbents in removal of turbidity from brewery effluent (BRE) and paint wastewater (PW). The precursors used as adsorbents were modified with H_3PO_4 and NH_4Cl as activating agent.The adsorbents were characterized using Infrared spectra (FTIR), Scanning Electron Microscopy (SEM), X-ray diffraction (XRD) and X-ray fluorescence (XRF). Adsorption isotherms data were fitted to four different isotherm models: Langmuir, Frenudlich, Temkin and Dubinin-Radushkevich. Furthermore, four kinetic models including pseudo-first-order, pseudo-second-order, Elovich and intra particle diffusion models were also used to analyze the adsorption kinetics. Thermodynamic parameters such as standard free energy, enthalpy and entropy were also investigated to understand the spontaneity of the adsorption process.

1.2 Statement of Problem

Due to continuous industrial development in Nigeria, a lot of wastewater is generated and discharged into the environment without proper treatment. This affects human life, aquatic life and ecosystem; hence the need to meet Nigeria Environmental regulatory standards before discharge becomes imperative.

1.3 Aim and Objectives

The aim of this study is to investigate the removal of turbidity from paint and brewery industrial wastewaters using sequential coag-flocculation and adsorption processes.

The objectives of this study include:

(i) To prepareand characterize biocoagulant and biosorbent from *Hibiscus esculentus (L*), *Xanthosoma*, *Detarium microcarpum*, *Crassostrea virginica*, *Canarium schweinfurlhi* and *Mucuna Pruriens*.

(ii) To investigate the effects of some process parameters such as coagulants/adsorbents dose, pH, settling/contact time in removing turbidity.

(iii)To investigate the coag-flocculation kinetics, particle size distribution and adsorption isotherm, adsorption kinetic and thermodynamic parameters.

(iv) To investigate the removal efficiency of the processes using statistical design of experiment and response surface methodology.

1.4 Scope of the study

The scope of this study is to test the potential of some biomass in removing turbidity from paint wastewater (PW) and brewery effluent (BRE). The study is limited to the use of bio coagulants and biosorbents mentioned above. The experimental study was based on using combined methods coag-flocculation and adsorption.

1.5 Significance of the study

Since the treatment of these industrial wastewaters using traditional methods are expensive, hence the introduction of biocoag-flocculation and biosorption as an alternative technology with abundant biomass is expected to reduce the cost of treatment of industrial wastewaters. In this work, the focus was on the use of biomass to remove turbidity from paint and brewery wastewaters.

CHAPTER TWO

LITERATURE REVIEW

2.1 Sources of Wastewater

Wastewater can be defined as liquid effluent generated as a result of the use of water. The chief sources of wastewater in the environment are: domestic wastewater, runoff and industrial wastewater (MetCalf and Eddy, 2003). As explained by Metcalf and Eddy (2003) the major source of domestic wastewater are: residential areas, commercial areas, institutional and recreational areas. Runoff is generated by natural means for example after rainfall. The third major source is industrial wastewater and is basically produced from manufacturing and processing industries. The wastewater from brewery and paint manufacturing falls into this category.

2.2 Wastewater Treatment Methods

Industrial process wastewaters vary in terms of volume and pollutants present. But the type of treatment applied depends on the factors present. The contaminants may be classified as suspended solids, dissolved solids, organic and inorganic pollutants (Aboulhassan, *et al*., 2006). There are various techniques applied in removing pollutants from industrial wastewaters such as biodegradation, adsorption, membrane filtration, coagulation/flocculation and advanced oxidation processes (Aboulhassan,*et al*., 2006). However, there is no single technically viable method to solve this problem. But combination of two or three methods will achieve adequate removal of suspended and dissolved particles (Mondal, et al., 2009).

Coagulation-flocculation is one of the most practiced technologies extensively used on industrial scale for wastewater treatment (Jiang-Ping,*et al.,* 2007). The removal mechanism of this process is mainly due to the charge neutralization. Thus, after considering all the options above, and previous work done on water treatment, coagulation-flocculation was found to be most effective (Jiang-Ping,*et al.*, 2007; Trinh and Kang, 2011; Menkiti

and Onukwuli, 2012). Also adsorption techniques for wastewater treatment have been more popular in the removal of pollutants than other conventional methods (Hayashi, *et al.*, 2000).

2.3 Historyof Coagulation-Flocculation Processes and its Mechanism

The Romans were familiar with the use of alum in treating river water. Coagulation using organic and inorganic substances has been used in water purification since ancient times in Africa, Asia and other parts of the world. Ancient Egyptians discovered the principles of coagulation approximately in 2000 BC., using plant seeds and beans as natural coagulants for water purification. By 1757, alum was used for coagulation in water treatment in England for the treatment of public water supplies.

Modern use of coagulants for water treatment started about 100 years ago, wherein ferric chloride and aluminium sulphate were used as coagulants. The mechanism involved in removal of colloidal particles comes as: (i) the double layer compression, a process which allows the particles to overcome the repulsive forces and thus agglomerate and precipitate, and (ii) precipitate enmeshment, a process which physically enmeshed the smaller particles by metal precipitates when they are forming and settling.

Coagulation is the process of destabilization of the repulsive potential of colloids and dissolved particles in water which occurs in consecutive steps that neutralizes the forces stabilizing those particles, resulting in the formation of micro-particles (microflocs), followed by particle collision leading to the growth of a larger floc size (Jadhav and Mahajan, 2013). Coagulation of such colloids was achieved through controlling their surface electrical charges. This action was realized by adsorption of ions of opposite charge to the colloid surface. Particles in water are negatively charged and for this reason repels each other when they come in close contact. This will force them to remain in suspension rather than clump together and settle out of the water. The addition of positively charged coagulants destabilizes the dissolved particles in the water (Diaz,*et al*., 1999).

2.3.1 Theory of coag-flocculation

The coag-flocculation can be divided into two distinct procedures, which should be applied consecutively; coagulation, which occurs by injecting and scattering of chemical (coagulants) during relatively intense mixing to destabilize naturally occurring particles and macromolecules and/or to precipitate additional particles. Its function was to overcome the factors that promote the stability of a given system. It is achieved with the use of appropriate chemicals, usually aluminium or iron salts as coagulants (Duan,*et al*., 2003).

The second process which is flocculation refers to the successful collisions that occur when the destabilized particles are driven towards one another by the hydraulic shear forces in the rapid mix and flocculation basins.

An agglomerate of few colloids quickly bridge together to form micro flocs, which in turn gathered into visible quantity (Ravina, 1993; Duan, et al., 2003; Crittenden, *et al*., 2005; Simate,*et al.*, 2011).

2.4 Classification of Colloids

A colloid can be defined as a medium in which particulates of different size interact but with the highest particulate diameter less than 10µm. The particulates maximum settling velocity is less than 0.01cm/sec, for the particles that settle due to gravity while the rest remains in suspension (Faust and Aly, 1983).

The molecules and clay particles are the lower size particles, followed by that of microbes in water such as; viruses, bacteria and algae, while sand particles have the largest sized particles in water. When the size of particles is above 50µm agglomeration and sedimentation of particles occurs easily, but if particle size is below than 50µm, then the agglomeration of suspended particles in water becomes difficult (Faust& Aly, 1983)

2.4.1 Stability of colloidal suspension

Colloidal particles, invisible to the naked eye, undergo high-speed Brownian motion- the speed is between 0.004m/s and 100m/s for the larger and smaller particles, respectively (Crittenden *et al.*, 2005). These particles also have a very high specific surface area (inversely proportional to the diameter). They are therefore more sensitive to surface phenomena than to gravitational force. Thus, the larger colloid particle will have a natural settling time over a depth of 1m of water about two years.

The stability of a colloid suspension depends on the equilibrium between two types of opposing force involved. These are Van der Waal's force, the universal attractive force between atoms and molecules, and an electrostatic interaction force. These two forces act differently depending on the intrinsic nature of the colloids, which are either hydrophilic i.e, water molecules are adsorbed onto their surface, or conversely hydrophobic (Asadic,*et al.*, 2009, Han,*et al*., 2006).

Colloids of a hydrophobic nature (example clay) form stable suspensions because their surface charge is the same and they repel each other. The potential difference between the shear plane and the solution, which is zeta potential when reduced to zero or close to zero, the particles tend to agglomerate under the influence of the Van der Waal's forces and the colloidal suspension becomes destabilized.

2.4.2 Destabilization of colloids

Destabilization of colloidal particles is accomplished by coagulation through the addition of hydrolysing electrolytes such as metal salts and/ or synthetic organic polymers (Dental and Gosset, 1988; Licsko, 1997).

It undergoes dissolution, the formation of complex highly charged hydrolysed metal coagulants (hydroxides of metals), inter particle bridging, and the enmeshment of particles into flocs (Amirtharajah, 1982; O'Melia, 1972).

Amirtharajah et al, observed that coagulation mechanism depend on specific pH and coagulant dosage, and illustrated that operational coagulation mechanism are a function of pH and coagulation concentration. These methods may take place individually or collectively to destabilize colloidal particles, facilitating their removal from suspension (Letterman, et al., 1999; Dempsey and O'Melia, 1984; O' Melia, 1972; Amirtharajah, 1982).

2.5 Flocculation Process

The agglomeration of particles is a function of their rate of collisions. The function of flocculation is to optimize the rate of contact between the destabilized particles, hence increasing their rate of collisions and bringing about the attachment and aggregation of the particles into larger and denser floc (Faust and Aly, 1983).

There are three main mechanisms that particles can collide and form flocs while in the flocculation basin: Brownian motion (diffusion), fluid shear and differential sedimentation. Brownian motion is the random movement of particles in water due to the continual bombardment of water molecules against the particles. This mechanism causes particles to be continually moving in the water and can lead to collisions between two particles. Fluid shear occurs when there is a velocity gradient in the water due to mixing or the friction of the water against a surface. Collisions can occur between two particles that have different velocities caused by mixing the water. Differential sedimentation is similar to fluid shear, exceptit is caused by gravity instead of a velocity gradient in the water. In differential sedimentation, collisions occur when large particles or flocs settle at a higher velocity than the smaller particles underneath them. Differential sedimentation can occur in the flocculation basin as well as the sedimentation basin. The size of the particles or already formed flocs has a large role in which one of these collision mechanisms dominates in the flocculation basin; Brownian motion only occurs between two small particles, differential sedimentation only occurs between a large and small particle, but fluid shear collisions can occur between any size particles. For this reason, fluid shear is the primary mechanism of floc formation, making the mechanical mixing of the water important in flocculation (Menkiti and Onukwuli, 2012).

2.6 Factors that Affect Coagulation-Flocculation Process

There are two broad factors that influence the coag- flocculation process: compostion of wastewater and type of chemical used in treatment.

2.6.1 Composition of wastewater

Coag-flocculation process is related with alkalinity, pH, turbidity, colour, zeta potential, coagulants, mixing and temperature.

i) Alkalinity

For high colloidal concentration, low alkalinity requires small dosage of coagulant to coagulate the wastewater by adsorption and charge neutralization. But for low colloid concentration, low alkalinity, coagulation is difficult in such system (Peavy, *et al.*, 1985). The dosage of coagulants required for destabilization of a colloidal dispersion is stoichiometrically related to the amount of colloidal particles present in solution (Stumm and OMelia, 1968). However, for dilute colloidal systems, the rate of coagulation is very slow because of the small number of colloids in the suspension and therefore, not enough contact between particles is available.

ii). Zeta potential

The zeta potential reduces repulsive surface electrical charges, allowing the attractive forces between particles to dominate, and promoting the buildup of a continuous network of particles in flocs (Gustafsson, et al., 2003).

iii). Hydrophilic colloids

Hydrophilic (water loving) colloids are very stable. Because of their hydration shell, chemicals cannot readily replace absorbed water molecules and, consequently, they are difficult to coagulate and remove from suspension (Hammer, 1986).

The stability of hydrophilic dispersions depend more on their ‘’love’’ for water than on their electrostatic charge (Stumm and OMelia, 1968).

On the other hand, hydrophobic (water hating) particles are metal oxides that can be easily coagulated and destabilized. However, the bulk of colloidal particles in turbid water usually exhibit a mixture of hydrophobic-hydrophilic properties resulting in suspensions that are intermediate in the degree of their difficulty to coagulate (O’Melia, 1972).

iv). pH value

pH is a measure of H^+ and OH^- ion concentration. The presence of these ions in the solution may cause particle charge to be more positive or less negative at pH values below the isoelectric point. At high pH values above the

isoelectric point the reverse effect takes place, whereby particle charge becomes more negative or less positive (Amirtharajah and OMelia, 1999; Volk,*et al.*, 2000).

The solubility of colloidal dispersions affected radically by pH. The greatest adsorption occurs in the pH range where there is minimum solubility (Amirtharajah,*et al*., 1999). However, in the pH range from 5 to 7 the colloidal particles are re-stabilized due to charge reversal brought about by excess adsorption of the positively charged hydroxide species.

v). Turbidity

Turbidity can be classified as being anionic ally charged silica particles. In low turbidity water (< 10NTU) an organic polyelectrolyte should not be considered. The choice of inorganic coagulant should be used and will form a stable sludge. In moderate turbidity waters (<100NTU), the use of a general purpose inorganic salt is preferred (Black,*et al*., 1965).

vi). Temperature

Coagulation by metallic salts is adversely affected by low temperature. Low temperature affects the coagulation and flocculation process by altering the coagulant solubility, increasing the water viscosity and retarding the kinetic of hydrolysis reactions and particle flocculation (Gregory, 1993). However, the effect has been reported to be more pounced in using alum, hence the recommendation to switch to iron salts when operating under low water temperature.

vii). Mixing

In water and wastewater applications, shear forces in mixed fluids have been considered important owing to the necessity of preventing the rupture of delicate floc particles in the coagulation process. The purpose of rapid mixing is to achieve instantaneous, uniform dispersion of the chemicals through the water body (Hudson and Jenkins, 1998; Amuda and Amao, 2007). Proper mixing after addition of coagulants into raw water facilitates optimum removal of fine particles in the supernatant. This is because very fine particles become transformed into aggregate under good mixing condition.

2.6.2 Types of Chemicals used in treatment

The two main types of coag-flocculants used are inorganic and organic. The choice of coag-flocculants chemical depended upon the nature of the suspended solid to be removed, the raw water conditions and cost of the amount of chemical necessary to produce the desired result (Jadhav and Mahajan, 2013).

Coag-flocculants that are added to the water to achieve coagulation should have the following three properties:

(i) Trivalent metallic cations or polymers whose effectiveness as coag-flocculants has been known.

(ii) Non-toxic and has no adverse effects on human health.

(iii) Insoluble or low solubility in the pH ranges common in water treatment practice. This is necessary in order to have an efficient coagulation process and to be able to leave the lowest possible residual of the chemical in the treated water (Jiang et al.,, 2002; Duan and Gregory, 2003).

The most commonly used coag-flocculants in water and wastewater treatment include aluminium sulfate (alum), ferric chloride, ferric sulfate (copperas), sodium aluminate, polyalumin chloride, and organic polymers (O' Melia, 1978)

2.6.2.1 Inorganic coagulants

Aluminium sulfate (alum), ferric chloride, ferric sulfate and sodium aluminate will lower the alkalinity and pH of the solution while the sodium aluminate will add alkalinity and raise the pH of the solution (O' Melia, 1978). Aluminium and ferric compounds are the traditional coagulants for water and wastewater treatment, both are still widely used today (Bratby, 2006).

Aluminium and ferric coagulants are soluble salts. They are added in solution form and react with alkalinity in the water to form insoluble hydrous oxides that coagulate by sweep floc and charge neutralization (Geng, 2005).

2.6.2.2 Organic coagulants

Organic polymers are commonly used as primary coagulants or coagulant aids in drinking water treatment. These high molecular weight polymers, usually referred to as polyelectrolytes, are synthetic compounds that strongly tend to adsorb the particles on the surface in an aqueous suspension but produce poor quality floc (Edward and Amirtharajah, 1985)

Organic polymers are classified according to the electric charge of their dissociated macro ions in water: Cationic, anionic and nonionic. Cationic polymers are frequently used as primary coagulants. Anionic and nonionic polymers are referred to as either coagulants aids or flocculants (Stochi, 1990; WST, 2005). Polymers are different from inorganic coagulants in several ways. Polymers remove particles by a mechanism called bridging (Nozaic, *et al*., 2001).

2.7 Natural Materials as Coagulants/Flocculants

Natural materials have been used in water and wastewater treatment before the advent of the chemical coagulants (Ghebremichael, 2004). The unawareness on the mechanism by which they work has limited their wide spread

application. In recent years, there has been a revival of interest to use natural materials due to cost and associated health and environmental concerns of synthetic organic polymers and inorganic chemicals. These coagulants are derived from microorganisms, animals, plants, vegetables and derivatives of the mineral origins (Kwaambwa and Maikokera, 2007).

Apart from natural materials under investigation in this research, a number of effective coagulants have been identified from plant origin. Some of the common ones include: Nirmali tree (Menkiti, *et al.*, 2012), almonds, apricots and peaches (Jahn, 2001), *Plantago psyllium, Tamarindus,indica, trigonella foenum-graecum, Hibiscus esculentus* (okra) mucilages (Agarwal, *et al.*, 2001), *Malva sylvestris*(mallow) and *Moringa oleifera* (Abaliwano, 2008; Janh, 1988), has shown improvement in water treatment (Anastasakis, et al., 2009). Other natural flocculants include starch, they can be natural starch, anionic oxidized starches or amine treated cationic starches (Kawamura, 1991).

Studies had been conducted to evaluate the coagulation efficiency of many plant materials including extraction of Moringa seeds (Ndabigengesere, et al., 1995; Buba and Chaudhuri, 2005; Ghebremichael,*et al*., 2004; Bhuptawat,*et al.*, 2007); okra, nirmal, mango seeds, tamarind seeds and vegetable (Ozacar and Sengil, 2003).

Previous work showed that the crude extract of Nirmali seed reduced 50-52% of bacteria after 30min of settling time of turbid water coagulated by 0.5mg/L of seed extract (Tripathi,*et al.*, 1976).

The main merit of using natural coagulants as water treatment material is as a result of cost-effectiveness, and unlikely to produce treated water with extreme pH (Vijayaraghavan,*et al.*, 2011).

In general, the advantages of natural polyelectrolytes is that they are toxic free, and the raw products are often locally available. Presented below are details on the natural materials of interest applied as coag- flocculants in this dissertation.

2.7.1 *Hibiscus esculentus L*

2.7.1.1General description, Growth and uses

Okra is an economically important vegetable crop grown in tropical and sub-tropical part of the world. Okra is known by many local names in different parts of the world. It is called lady's finger in England, gumbo in United States of America, guino-gombo in Spanish, guiberiro Portuguese and Bhindi in India. Okra is mainly propagated by seeds and has duration of 90-100 days. It is generally an annual plant (FAOSTAT, 2008). Okra seed can be used as an alternative to conventional coagulants. The okra powder is natural organic matter, therefore, comprises hydrophilic colloids, low- molecular weight acids, proteins, polysaccharides, humic acids

and fulvic acids. When the coagulant obtained from the powdered seeds is added to raw water, the proteins produce positive charge acting like magnets and attracting the predominantly negatively charged particles

.2.7.2 *Detarium microcarpum*

2.7.2.1 Description and uses

Detarium microcarpum, commonly known as sweet detar, sweet dattock or tallow tree, is an underutilized tree legume that grows naturally in the drier regions of West and Central Africa. *Detarium microcarpum* is a member of the caesalpinioleal special family of the large leguminosae (Hopkins and Stanfield, 1966). It is known as taura in Hausa and ofor in Ibo. Among the Ibos in South eastern Nigeria, it is mythically conceived to be a chip of the primal tree that grows in God's own compound. It symbolizes truth and honesty (Ejizu, 1986).

Naturally, the seed which is used as a traditional soup thickener contains lipids, carbohydrates, protein, crude fibre and the essential elements: Na, K, Mg, Ca, S, P, and Fe (Abreu and Relva, 2002; Abreu *et al*., 1998). In Africa ethno-medicine, the plant and the closely related species *Detarium senegalese* are used in the treatment of syphilis, dysentery, bronchiolitis, leprosy, sore throat, pneumonia, diarrhea, malaria and meningitis (Burkil, 1995). Medicinal properties of *Detarium microcarpum* are in the roots, stems, bark, leaves and fruits to treat ailments (Abdalbasit,*et al*., 2009; Ebi and Afieroho, 2011).

The seed flour is a traditional emulsifying, flavoring and thickener agent used to prepare, cakes, bread, couscous, baby food and beer (Kouyate and van Damme, 2006).

2.7.3 *Xanthosoma sagittifolium*

2.7.3.1 Description and uses

Cocoyam belongs to the monocotyledonous family *Araceae* (the aroid) which contains several plants which are cultivated and used for food in various parts of the tropic (Onweme, 1978). They are mainly herbaceous plants, often with an enlarged root stock, which acts as a storage organ (Jirarat,*et al.*, 2006). It is widely grown as a staple food for millions of people living in the tropics. The corms and cornels are rich in minerals, vitamins and digestive starch grains. Despite these nutritional benefits, cocoyam is less valued in areas like Eastern Nigeria where it is produced in abundance (IITA, 1992). The two most important species of the edible aroids are *Colocasia esculenta* and *Xanthosoma sagittifolium* (Purseglove, 1972).

2.7.4 *Crassostrea virginica*

2.7.4.1 Origin of chitosan and its extraction from chitin

Chitosan is biodegradable modified natural carbohydrate polymer (polysaccharide) derived from chitin, which occurs predominantly in animals of arthropods and marine crustaceans (Singla and Chowla, 2001). Chitosan is

converted from chitin, which is a structural polysaccharide found in the skeleton of marine invertebrates, insects and some algae (Muzzarelli, 1977). Chitin is perhaps the second most important polysaccharide after cellulose and is abundantly availabl (Muzzarelli,*et al*., 1994; Dutta, *et al*., 1997; Ravikumar, *et al.*,2000). Isolation of chitin-chitosan from *Crassostrea Virginica* shell wastes involves four traditional steps:

1. Deproteinization (Fernandez-Kim, 2004)

Chitin occurs naturally in association with protein (chitinoprotein). Some of this protein can be extracted by mild methods, but other portion is not readily extracted, suggesting covalent bonding to chitin (Attwood and Zola, 1967).

Crustacean shell waste is usually ground and treated with dilute sodium hydroxide solution (1-10%) at elevated temperature (65-100^{o}C) to dissolve the protein present. Reaction time usually ranges from 0.5 to 12hr) depending on preparation methods. To obtain uniformity in reaction, it is recommended to use relatively high ratios of solid to alkali solution of 1: 10 or 1:15-20 with proper agitation.

The optimal conditions for deproteinization involves treatment of the crawfish shells with 3.5% (w/w) NaOH solution for 2hr at 65^{o}C with constant stirring and a solid ratio of 1:10 (w/v) (No, *et al*., 1989). Shahidi and Synowiecki (1991) suggested that optimal deproteinization can be achieved using dilute potassium hydroxide solution.

2. Demineralization (Fernandez-Kim, 2004)

Demineralization is usually accomplished by extraction with dilute hydrochloric acid (HCl) (up to 10%) at room temperature with agitation to dissolve calcium carbonate. Optimum demineralization is achieved by constant stirring of the dried ground crawfish shell with 1N HCl for 30min at ambient temperature and a solid to solvent ratio of 1: 15 (w/v) (No and Meyers, 1989). The ash content of the demineralized shell is an indicator of the effectiveness of the demineralization process.

During the demineralization process, excessive undesirable foams are produced due to the CO_2 generation ([$CaCO_3$ + 2HCL → $CaCl_2$ + CO_2 (↑) + H_2O]). To control or reduced the foam, (No and Meyer, 1998) recommended the use of commercial anti-foam comprising of 10% solution of active silicone polymer without an emulsifier. It is recommended that deproteinization followed by demineralization is a favorable sequence in terms of the amount of anti-foam required to control foaming.

3. Decoloration (Fernandez-Kim, 2004)

Acid and alkali treatments alone produced a colored chitin product. For commercial acceptability, the chitin produced from crustacean sources, needs to be decolorized or bleached to yield cream white powder (No and Meyers, 1989). During the process of decoloration, it should be noted that the chemical used should not affect the physicochemical or functional properties of chitin and chitosan. No and Meyers, (1989) was able to prepare a near white colored crawfish chitin by extraction with acetone and dried for 2h at ambient temperature, followed by bleaching with 0.315% (v/v) sodium hypochoride solution (containing 5.25% available chlorine)for 5min with a solid to solvent of 1:10 (w/v), based on dry shell. The color of chitin products varies from cream white to intermediate pink (No and Meyers, 1989).

4. Deacetylation (Fernandez-Kim, 2004).

Deacetylation is the process to convert chitin to chitosan by removal of acetyl group. It is generally achieved by treatment with concentrated sodium or potassium hydroxide solution (40-50%) usually at 100^{o}C or higher for 30min or longer to remove some or all of the acetyl groups from the polymer (No and Meyers, 1989). The N-acetyl groups cannot be removed by acidic reagents without hydrolysis of the polysaccharide, thus alkaline methods must be employed for N- deacetylation (Muzzarelli, 1977).

Depending upon the production sequence, deacetylation can be achieved by reaction of demineralized shells or crawfish chitin with 50% NaOH (w/w) solution at 100^{o}C for 30min in air using a solid to solvent ratio 1:10 (w/v).

2.7.4.2 Applications of chitosan

The poor solubility of chitosan is the major limiting factor in its utilization and investigation of its properties and structure. Despite these limitations, various applications of chitosan have been reported (Muzzarelli, 1977).Due to its physical and chemical properties, chitosan is being used in a vast array of widely different products and applications, ranging from pharmaceutical products and cosmetics products to water treatment and plant protection (Muzzarelli, 1977).

2.8 Adsorption Phenomenons and Process

2.8.1 Introduction

Since the discharge of treated industrial wastewater containing metal ions such as nickel, lead, copper, zinc, chromium, dye and aluminum, adsorption is widely used as an effective physical method of separation in order to eliminate or lower the concentration of wide range of dissolved pollutants (organic, inorganic) in an effluent (Demirbas, 2008).

Adsorption has significant advantages: low operating cost, high flexibility, simple design and operation, easy automation, lack of sensitivity to toxic pollutants and the capability to operate at very low concentrations, it could be highly selective, more efficient and can handle large volumes of wastewater containing low metal concentrations (Gadd, 1990; Minceva,*et al*., 2007).

Basically, adsorption is a mass transfer process by which a substance (adsorbate) is transferred from the liquid or gas phase to the surface of a solid (adsorbent), and becomes bound by physical and/or chemical interactions (Volesky, 2003). In an equilibrium system, adsorption and desorption occur simultaneously. Desorption is the process in which the solute is released back from or through the surface.

Adsorption or surface adsorption is a result of the attraction between negative and positive charges on the adsorbent system. The metal cations in the solution are attracted by an adsorbent because of the negative charges present in its framework structure. The adsorptive process may be even more promising when natural adsorbent produced from biomass are used, because they are renewable, low cost, highly available.

An adsorbent is a material that has the required properties for retaining compounds or ions or substance, which are collectively called adsorbates. Various materials ranging from agricultural wastes (Garg,*et al*., 2008) to commercial adsorbents (Genc-Fuhrmain,*et al*., 2007; Minceva,*et al*., 2007) have been investigated for the removal of metals from water.

Adsorption using low-cost adsorbent has attracted increasing attention of numerous researchers mainly due to its low cost, efficiency, effectiveness, technical flexibility and regeneration of used adsorbent (Keng,*et al*., 2014; Bailey,*et al*., 1999; Kurniawan, *et al*., 2006). Apparently, utilization of naturally occurring materials or industrial by-products or locally available agricultural waste materials as the adsorbents in removing heavy metals from wastewater is not only cost-effective in metal ion removal, but it also contributes to a zero waste situation in the environment (Coman, *et al*., 2013; Demirbas, 2008; Dhir, 2014; Keng,*et al*., 2014).

These biological material employed in adsorption processes is defined as ‘’biosorbent’’. Most of these biosorbent have shown their potential in metal removal without any modifications. But it is interesting to note that their removal capabilities can generally be improved through properly physical or chemical modification (Patel, 2012).

Adsorbent are used in various processes; activated carbons are among the most effective adsorbents used for removal of heavy metals from industrial wastewaters. Many studies have been undertaken to investigate the use of low-cost adsorbents such as peat, bentonite, steel-plant slag, fly ash, china clay,maize cob, silica,(Crini, 2006), bacterial biomass and biopolymers (Gupta, *et al.*, 2009), coir pith, (Mittal,*et al.*, 2008), sugar beet pulp (Aksu and Isoglu,2006), sugarcane bagasse pith (Amin, et al., 2008; Cronje,*et al*., 2011), jute fiber, hen feathers,

soybean (Gupta,*et al*., 2009) and wheat husk (Gupta, *et al.*, 2007), coconut shells, wood and cotton stalk (Deng, *et al*., 2010), rice husk and nut shells, etc. (Fierro,*et al*., 2010), for color removal.

The high adsorption capacity of activated carbon is related to the properties such as surface area, pore volume and pore size distribution. These unique characteristics depend on the type of raw materials employed for the preparation of activated carbon (AC) and the method of activation.

Due to increasing demand of AC, there is a strong need for sorting out new precursors for the preparation of AC which should be cost effective at par with the commercially available AC.

In water treatment, activated carbon is used to remove organic compounds that cause objectionable taste, odor, and color. Basically, there are two different processes for the preparation of AC: physical activation and chemical activation.

2.8.2 Adsorption mechanism

The classical mechanism of adsorption is divided into three steps as shown in Fig 2.5.The first step (fig.2.5a) shows the diffusion of adsorbate to adsorbent surface, (fig.2.5b) migration into pores of adsorbent and (fig.2.5c) monolayer build-up of adsorbate on the adsorbent. During the last step, when the adsorbate's particles are distributed on the surface and filled up the volumes of the pores, particles of the adsorbate are building monolayer of reacted molecules, ions and atoms to the active sites of adsorbent (Iakovalev and Sillanpaa, 2013).

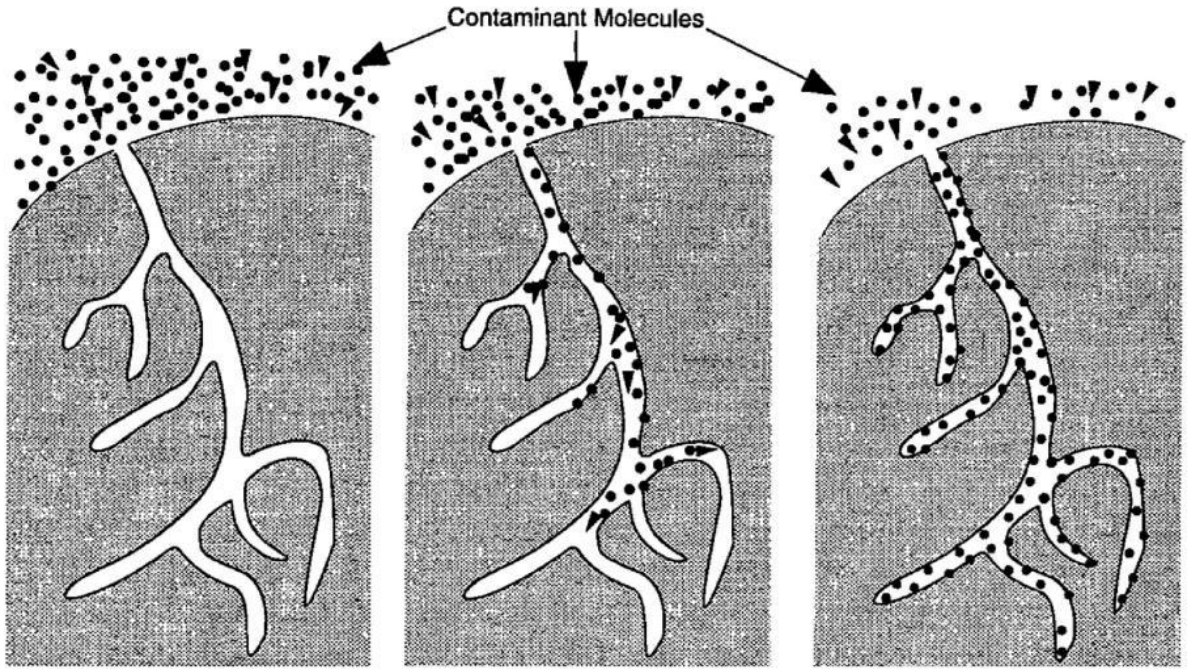

a b c

FIGURE 2.1 Three steps of adsorption mechanism: a) diffusion of adsorbate to adsorbent surface b) migration into pores of adsorbent c) monolayer build-up of adsorbate on adsorbent (Repo, 2011).

2.8.3 Types of adsorption

Adsorption may be classified as chemical adsorption or physical adsorption depending on the characteristics of the bonding between metal cations and the sorbent active sites (Jiaping, 2012). Adsorption can be classified into two types:

1. Physical adsorption (physisorption)
2. Chemical adsorption (chemisorption)

2.8.3.1 Physical adsorption

Physisorption is a physical adsorption involving intermolecular forces (Van der Waals forces), which do not involve a significant change in the electronic orbital patterns of the species (IUPAC, 1972). The adsorption processes can occur at an interface between any two phases, such as, liquid-liquid, gas-liquid, or liquid-solid interface. The energy of interaction between the adsorbate and adsorbent has the same order of magnitude as, but is usually greater than the energy of condensation of the adsorptive (Uluozlu,*et al.*, 2008). Therefore, no activation energy is needed. In this case, low temperature is favorable for the adsorption.

In physical adsorption, equilibrium is established between the adsorbate and the fluid phase. Physical adsorption is relatively nonspecific due to the operation of weak forces of attraction between molecules. The adsorbed molecule is not affixed to a particular site on the solid surface, but is free to move about over the surface.

Physical adsorption is generally reversible in nature; i.e., with a decrease in concentration the material is desorbed to the same extent that it was originally adsorbed (Inglezakis and Poupoulos, 2006). In this case, the adsorbed species are chemically identical with those in the fluid phase, so that the chemical nature of the fluid is not altered by adsorption and subsequent desorption; as a result, it is not specific in nature (Erdem,*et al*., 2004).

2.8.3.2 Chemical adsorption

Chemical adsorption is an inner sphere complexion phenomenon, in which adsorption caused by the formation of chemical bonds between the surfaces of solids (adsorbent) andheavy metals (adsorbate). Therefore, the energy of chemisorption is considered like chemical reactions. It may be exothermic or endothermic processes ranging from very small to very large energy magnitudes (Murzin and Salmi, 2005). The chemical bond involved is usually covalent bond and the adsorbent tends to find sites that will maximize its co-ordination number with

substrate. This means that the true equilibrium may be achieved slowly. In addition, high temperature is favoured for this type of adsorption; it increases with increase of temperatures (Lee and Johnson, 1980; Uberoi and Shadman, 1990).

2.9.1 Adsorption isotherms

Adsorption is usually described by isotherms which show how much solute can be adsorbed by an adsorbent at a given temperature. An adsorption isotherm relates the concentration of solute on the surface of the adsorbent to the concentration of the solute in the fluid with which the adsorbent is in contact. Adsorption isotherm models can also be used to calculate the maximum adsorption capacity of a sorbent and to establish the affinity series (Erdem,*et al*., 2004). It also helps to describe surface process of adsorbent, type of adsorbate monolayer or multilayer nature, which can be specifically useful to predict the type of adsorption mechanism involved (Kundu and Gupta, 2006;Dabrowski, 2001). The significance of adsorption isotherm is that they show how the adsorbate molecules (metal ion in aqueous solution) are distributed between the solution and the adsorbent solids at equilibrium concentration on the loading capacity at different temperatures.

The adsorption isotherm explain the interaction between adsorbate and adsorbent (John and Walther, 2003; Kundu and Gupta, 2006). To develop isotherms, a known quantity of adsorbate in a fixed volume of liquid exposed to various dosages of adsorbent. After sufficient time, the adsorption equilibrium is reached and the adsorption equilibrium capacity can be calculated from mass balance.

$$q_e = \frac{(C_o - C_e)V}{m} \quad (2.15)$$

where q_e =amount of solute adsorbed from the solution, V= the volume of liquid, m= mass of adsorbent, C_o= initial concentration in solution, C_e = adsorbate residual concentration in solute

In a multi-component system, the initial concentration of the target adsorbate influencesthe resultant isotherm. In order to describe the adsorption equilibrium mathematically, different models exist, differing in complexity and in the number of parameters necessary (Langmuir, 1918; Freundlich, 1906).

2.9.1.1 Langmuir isotherm model

Langmuir is the simplest type of theoretical isotherms. Langmuir adsorption isotherm describes quantitatively the formation of a monolayer of adsorbate on the outer surface of the adsorbent, and after that no further adsorption takes place. The Langmuir represents the equilibrium distribution of metal ions between the solid and liquid phases (Do Hee,*et al*., 2002).

Langmuir isotherm model is developed for an ideal homogeneous sorption type. Thus, every sorption site in the sorbent has equal affinity to sorb metal ions (Kundu and Gupta, 2006). Therefore, a rigid layer of only one molecule in thickness (a monolayer) is formed during ideal Langmuir sorption. Langmuir isotherm is more applicable to chemisorption, but is also often applied to physisorption isotherm of type I (Aksu,*et al*., 2003; Yu,*et al*., 2000; Ferda and Selen., 2012).

2.9.1.2 Freundlich isotherm

Freundlich isotherm is commonly used to describe the adsorption characteristics for the heterogeneous surface (Hutson and Yang, 1997; Azouam,*et al*., 2010). It represents an initial surface adsorption followed by a condensation effect resulting from strong adsorbate-adsorbent interaction. Freundlich isotherm curves are the opposite way of Langmuir isotherm and are exponential in form. The heat of adsorption, in many instances, decreases in magnitude with increasing extent of adsorption.

Thus, the isotherm sites have different degree of affinity for the adsorption of metal ions in such a way that stronger adsorption sites are occupied first by metal ions and adsorption continues until the weakest sites is occupied (Jiang,*et al*, 2002).

The Freundlich isotherm is represented by:

$$q_A = k_A C_A^{1/n} \quad (2.16)$$

Here k_A is an approximate indicator of adsorption capacity, while $1/n$ is a function of the strength of adsorption in the adsorption process, q_A is the amount of adsorbate adsorbed at equilibrium and C_A is the residual concentration of adsorbate in solution.

Freundlich isotherm provides a better fit to isotherm data than the Langmuir isotherm for activated carbon because many layers of adsorbate can absorb to the surface and there is distribution of site with different adsorption energies (Azouaon,*et al*., 2010).

2.9.1.3Temkin isotherm

This isotherm contains a factor that explicitly taking into account of adsorbent-adsorbate interactions. By ignoring the extremely low and large value of concentrations, the model assures that heat of adsorption of all molecules in the layer would decrease linearly rather than logarithmic with coverage (Temkin and Pyzhev, 1940).Temkin isotherm is a modification of the Langmuir isotherm.

2.10.1.4 Dubinin-Radushkevich (D-R) isotherm

Many micro porous adsorbents including activated carbons contain pores over a wide range of pore sizes, including micro and mesopores. The filling of micropores occurs at very low relative pressures and is entirely governed by the enhanced gas-solid interaction (Azouaou,*et al*., 2010; Elangovan,*et al*., 2008). In addition to the strong adsorption potential, a cooperative mechanism may play an important role in the micropore filling process. Dubinin and Radushkevich postulated an equation which allows the micropore volume to be calculated from the adsorption isotherm (Dubinin and Radushkevich, 1947).

The linear form of (D-R) isotherm model can be expressed as:

$$\ln q_e = \ln q_m - \beta\varepsilon^2 \qquad (2.17)$$

Where β is a constant corresponding to the biosorption energy, q_m the theoretical saturation capacity and ε is the Polanyi potential which is calculated from equation below,

$$\varepsilon = RT \ln\left(1 + \frac{1}{C_e}\right) \qquad (2.18)$$

Where R (8.314J mol^{-1} K^{-1}) is a gas constant and T (K) is the absolute temperature. The mean free energy of biosorption E can be defined as the free energy change when one mole of ion is transferred from infinity in solution to the biosorbent (Kundu and Gupta, 2006).

2.10 Adsorption Kinetics

The study of adsorption from a kinetic perspective can lead to a better understanding of the mechanism of the process. The kinetic studies describe the rate of adsorption, and this rate controls the equilibrium time. The results can establish the optimal time for adsorbate remover from the aquatic solution (Fogler, 2001; Ho, 2004).Various adsorption kinetic models have been used to describe the adsorption of metal ions.

2.10.1 Pseudo first order model

The pseudo-first order rate expression, popularly known as the lagergren equation, is generally described by the following equation (Yasemin and Zeki, 2007; Jaman, *et al*., 2009).

$$\frac{dq}{dt} = k_1(q_e - q_t) \qquad (2.19)$$

Where $q_e$the amount of adsorbate adsorbed at equilibrium per unit weight of adsorbent (mg/g), q_t is the amount of adsorbate adsorbed at any time (mg/g), and k_1 is the rate constant (min^{-1}). Integrating and applying the boundary conditions from t=0 and q=0 to t=t and $q = q_i$

Equation (2.19) takes the form

$$\ln(q_e - q_t) = \ln q_e - k_1 t \quad (2.20)$$

The plot of $\ln(q_e - q_t)$ versus t should give a straight line with slope of $k_1$and intercept$\ln q_e$, were used to determine pseudo first order rate constant (k_1) and theoretical amount of adsorbate adsorbed per unit mass of adsorbent $q_e(th)$, were compared with the q_e (exp) values. The $q_e\ (exp.)$ values differ from the corresponding $q_e\ (th)$ values showed that pseudo-first order model does not fit well with whole range of contact time, and hence not diffusion- controlled phenomen.

2.10.2 Pseudo second order model

The pseudo-second order kinetic model states that the interaction between solute and adsorbate molecules may be chemical forces of attraction on the solid surface of the adsorbent and adsorbate molecules. The mathematical form of the expression:

$$\frac{dq_t}{dt} = k_2(q_e - q_t)^2 \quad (2.21)$$

Where, k_2 is pseudo-second order rate constant (g/mg.min). After integrating, equation (2.21) for boundary conditions $q_t = 0\ at$ t=0 and $q_t = q_t$ at t=t, the following equation is obtained.

$$\frac{t}{q_t} = \frac{1}{K_2 q_e^2} + \frac{1}{q_e} t \quad (2.22)$$

A plot of t/q_t versus t is a straight line with slope $1/q_e$ and intercept$1/k_2 q_e^2$. Using the value of q_e calculated from the slope, the value of k_2 is determined from the intercept.

2.11.3 Elovich equation

Elovich equation is frequently used in describing chemisorption (Ozacar and Sengil,2003). The Elovich model equation is generally expressed as:

$$\frac{dq_t}{dt} = \alpha exp^{-\beta q_t} \quad (2.23)$$

Where α is the initial adsorption rate (mg/g min) and β is the adsorption constant (g/mg) during any experiment.

2.10.4 Intra particles diffusion model

The adsorption of adsorbate on adsorbent is the combination of four consecutive steps, diffusion in the bulk solution, and then diffusion across the thin film surrounding the adsorbent particles, followed by intra-particle diffusion and adsorption within the particles. Weber and Morris intra-particle model was used to elucidate the diffusion mechanism (Weber and Morris, 1963). The model is expressed as:

$$q_t = K_{ad} t^{1/2} + C \quad (2.24)$$

Where, q_t is the amount of adsorbate adsorbed, t is the contact time, C is the intercept and K_{ad} is the intra-particle diffusion rate constant. A plot of $q_t versus t^{1/2}$ gives a straight line with positive intercept for intra-particle diffusion controlled adsorption process, but does not pass through origin due to boundary layer effect. The high value of K_{ad} and intercept, illustrate an enhancement in the rate of adsorption. When the intercept is large, the greater the contribution of surface adsorption in rate determining step (Tan,*et al.*, 2008).

2.10.5 Adsorption thermodynamic

In adsorption, temperature has a great effect on it. Since the adsorption is a kinetic process, removal rate can be increased or decreased by increase or decrease in the system temperature.Thermodynamic parameters for adsorption process include change in free energy (ΔG), change in enthalpy (ΔH) and change in entropy (ΔS).

2.11 Factors Affecting Adsorption

In general, the adsorption reaction is known to proceed through the following three steps.

1 Transfer of adsorbate from bulk solution to adsorbent surface, which is usually mentioned as diffusion.
2 Migration of adsorbate (metal ions) into pores
3 Interaction of metal ions with available sites on the interior surface of pores.

The process is influenced by several factors, which have significant influence on the adsorption capacity of the adsorption rate. The most common one includes the nature and dose of adsorbents, nature and concentrations of adsorbate, temperature, modifying reagent (in case of natural adsorbent), contact time, speed of agitation, particle size and pH of the aqueous solution (Lee,*et al*., 2003).

(i) Surface area, pore structure, and pore size distribution of adsorbent

Larger surface area implies a greater adsorption capacity. Surface area is one of the principle characteristics affecting the adsorptive capacity of an adsorbent, since the adsorption process result in a concentration of solutes at the surface.

Pore structure and chemistry of activated carbon made from agricultural by-products are strongly dependent on pyrolysis temperature, composition and structure of the raw material.

Since surface properties of the granule activated carbon are a function of the precursor, pyrolysis and activation conditions, it is essential to characterize them with respect to the number and type of the chemical group on the surface, the polarity of the surface, pore size distribution and total surface area (Ahmedna,*et al*., 2000(b)).

(ii) Particle size of adsorbent

Activated carbon is a complex network of pores of varied shapes and sizes. The shape includes cylinders, rectangular cross section, as well as many irregular shapes and constriction. Size can range from less than 10Å to over 100,000 Å. Pore size distribution; will depend on the source materials used and on the method and extent of activation. Smaller particle sizes reduce internal diffusion and mass transfer limitation to the penetration of the adsorbate inside the adsorbent (Mohammad AL-Anber, 2010).Activated carbon (AC) are known as very effective adsorbent due to their highly developed porosity, large surface area, variable characteristics of surface chemistry and high degree of surface.

(iii) Contact time or residence time

The longer residence time means the more complete the adsorption will be. Therefore, the required contact time for adsorption to be completed is important to give insight into an adsorption process. This also provides information on the minimum time required for considerable adsorption to take place, and also the possible diffusion control mechanism between the adsorbate, as it moves from the bulk solution towards the adsorbent surface (Mohammad AL-Anber, 2010).

(iv)pH

The degree of ionization of a species is affected by the pH. This, in turn, affects adsorption, the precipitation of metal ions occurs at pH greater than 4.5. Therefore, the removal efficiency increases with increasing pH. At low pH, the concentration proton is high. As a result, the positively charged of the metal ions and the protons compete for binding on the adsorbent sites.The concentration of proton in the solution decrease as pH gradually increases in the ranges from 2 to 4.5, but above pH 4.5, the removal efficiency decreases as pH increases.

(v) Effect of dosage

The removal efficiency was found to increase with the increase of adsorbent dose in various studies and after reaching the optimum value, further increase in adsorbent dose does not show any significant change. The trend of increase in removal capacity is due to the fact that the availability of more adsorption sites for the metal ions. This can be explained by the fact that more mass available, more the contact surface offered to the adsorption (Mohammad Al-Anber., 2010). This is expected because the higher the dose of adsorbent in the solution, the greater availability of exchangeable sites for the ions, i.e., more active sites is available for binding of metal ions.

(vi) Effect of temperature

Since the process of adsorption is spontaneous, it is companied by a decrease in the system's free energy. There is always a decrease in entropy due to loss of degree of freedom of the solute in passing from the dissolved state to the adsorbed state. The decrease in entropy drives a decrease in enthalpy. An increase in temperature therefore results in a reduction of the equilibrium adsorptive capacity(Kobya, et al., 2006; Iakovaleva and Sillanpaa, 2013).

(vii) Solubility of solute (adsorbate) in liquid (wastewater)

Substance slightly soluble in water will be more easily removed from water than substance with high solubility. Also, non-polar substance will be more easily removed than polar substances, since the latter have a greater affinity for water. The rate of adsorption of solutes is inversely proportional to its solubility in the solvent. The greater the solubility, the stronger is solute-solvent bond, and the smaller the extent of the rate of adsorption (Lee, *et al*., 2003; Mohammad Al-Anber, *et al*., 2010).

(viii) Activated Carbon

Activated carbon (AC) is a solid, porous, black carbonaceous material and tasteless. Activated carbon is define as a porous carbon material, usually chars, which have been subjected to reaction with gases during or after carbonization in order to increases porosity. Activated carbon is distinguished from elemental carbon by the removal of all non-carbon impurities and the oxidation of the carbon surface. According to Norlia Baharun (1999), AC is an organic material that has an essentially graphitic structure. The main features common to all AC are; graphite like planes which show varying degrees of disorientation and the resulting spaces between these planes which constitute porosity, and the unit built of condensed aromatic rings. Activated carbon is a powerful adsorbent utilized by many industries and has been for many years. Water and wastewater treatment, industry effluents, brewery wastes, and textile discharges are some of the applications for activated carbon today (Nwabanne and Igbokwe, 2011). Early examples of rudimentary activated carbon use was found as early as the Egyptians and the Phoenicians (Dabrowski, 2001), but the activated carbon industry began when the Russian Ostrejko patented techniques for producing activated carbon using elevated temperatures and oxidant flows.

2.12 Propertties of Agricultural Adsorbent

Agricultural materials particularly those containing cellulose shows potential metal biosorption capacity. The materials are usually composed of lignin and cellulose as the main constituents. Other components are hemicellulose, extractives, lipids, protein, simple sugar, starch, water, hydrocarbons, ash and many more compounds that contain a variety of functional groups present in the binding process.

Materials with high lignin content develops AC with high macropores (> 50nm), whereas, material with high cellulose yield AC with microporous structure (Gani and Naruse, 2007)

Cellulose is a crystalline homo-polymer of glucose with β 1-4 glycosidic linkage and intra-molecular and inter-molecular hydrogen bonds. Lignin is three dimensional polymers of aromatic compounds covalently linked xylenes in hardwoods and galactoglucomannans in softwoods.

The functional groups present in biomass molecules acetamido groups, carbonyl, phenolic, structural polysaccharides, amido, amino, suphydryl carboxyl groups alcohols and esters. These groups have the affinity for metal complexation. Some biosorbents are non-selective and to a wide range of heavy metals with no specific priority, whereas others are specific for certain types of metals depending upon their composition (Sud,*et al*., 2008)

Agricultural waste usually has high moisture content, which is normal drying under the direct sunlight, room drying, and oven drying at certain temperature. Dried materials are normally ground to obtain the specific granular size of it before employed as adsorbent. Dried materials can directly be applied as adsorbent or transformed into carbonaeeous adsorbent by pyrolys.

2.12.1 *Mucuna pruriens*

2.12.1.1 Plant description

*Mucuna pruriens*is a vigorous annual climbing legume, vine and shrub that grow 3-18m in height. It was reported that originally the plant came from southern China and eastern India, where it was one time widely cultivated as green vegetable crop (Burkill, 1995). The genus mucuna (*Adans*), belong to the fubaceae family, covers perhaps 100 species of annual and perennial legumes including the annual velvet bean.

M. sloanei and *M. flagellipes* are generally utilized as a thickener in soup preparation. It is cracked by hitting it with a hard object before boiling. When cooked the seed is hulled, ground and mixed with red palm oil to form a yellow loose powder. The toxic principle can be removed by boiling and soaking the seeds in water for two hours, and change the water. In parts of Asia,the seeds are sometimes roasted before being eaten and in other parts; the immature pods and leaves are occasionally boiled and eaten as a vegetable.Mucuna bean seed is used in

treating numerous diseases, such as Parkinson disease, impotency, diarrhea, kidney stones, nerve pain, worm, tuberculosis, diabetes, intestinal gas etc. Also it is used as sources of nutrients in diets and as a thickener.

2.12.2 *Canarium schweinfurthii*

2.12.2.1 Botanic description

Canarium schweinfurthii is a large forest tree with its crown reaching to the upper canopy of the forest, with a long clean, straight and cylindrical bole exceeding 50m (Hutchinson,*et al*., 1993). Diameter above the heavy root swellings can be up to 4.5m. Bark thick, on young tree fairly smooth, becoming increasingly scaly and fissured with age. The slash is reddish or light brown with turpentine like odour, exuding a heavy, sticky oleoresin that colours to sulphur yellow and becomes solid (Burkill, 1995).

2.12.2.2 Producs and its applications

Canarium schweinfurthii is used in so many applications:

The slightly greenish outer pulp of the fruit is oily and edible. It can be eaten raw or soften in warm water to improve palatability. The pulp oil is about 71% palmitic acid 18% oleic acid. The seed-kernel is oily and edible. They are cooked, and in Nigeria, sometimes prepared into a vegetable-butter and eaten as a substitute for shea-butter. They contain several fatty acids including oleic (36%), linoleic (28%), palmiti acid (26%), stearic (7%).

The elemi makes a good fuel wood, igniting readily and burning with a lot of heat. The resin burns readily and is used as a bush candle. The sapwood, often very thick up to 15cm is white with pinkish reflections. Used as a substitute for true mahogany.

In the past, the resin was exported to Europe for pharmaceutical use. It was used as a substitute for gum mastic in making wound dressing in World War II.

2.12.3 *Crassostrea Virginica*

Two species of oyster, have been cultivated commercially in the UK, namely the native oyster (*Ostrea edulis*), and the Pacific oyster (*Crassostrea virginica*). This is a bivalve mollusc that occurs in sheltered coastal inlets and estuaries (Kwon,*et al*., 2010)

Pacific oyster is a bivalve molluse native to templet regions within the Pacific Ocean. It is naturally distributed around Japan and Korea but it has been introduced to many other countries worldwide for cultivation. Pacific oyster has a wider tolerance to salinity and tidal exposure. It will grow well in fully saline conditions but also in brackish water more typical of our estuaries.

2.13. Activated Carbon Production

Activated carbon can be produced from many different carbonaceous precursors. Ideal precursors have a high percentage of carbon content, are abundant and easy to recover. A high percentage of carbon content (i.e., low ash content) translates to more surface area available for adsorption. Common carbonaceous precursors utilized in the modern activated carbon industry include: peat, bituminous and lignite coal, wood and coconut shell (Wigmans, 1989; Derbyshire,*et al.*, 2011).

One area of activated carbon research involves the discovery of new, more efficient precursors for use in full-scale production. Precursors such as bituminous and lignite coal are non-renewable, and therefore should not be relied on for long- term usage (Dias,*et al*., 2007). Alternative sources of carbonaceous precursors allow these regions to produce activated carbon in an economic fashion, without the high cost of long distance shipping (Warhurt,*et al*., 1996).

Precursors used for activated carbon include: almond shell, olive stones, apricot stones, paper mill sludge, apple pulp, rice husks, cedar nutshells, and corncobs (Patel, 2012; Demirbas, et al., 2009; Abia, et al., 2003)

Many different techniques exist for producing or activating these precursors as well. These techniques are typically grouped into two main categories: physical or chemical activation (Sugumaran, 2009). The combination of the carbonaceous precursors and the activating technique employed, determines the physical and chemical characteristics of the finished activated.

2.13.1 Physical activation

Traditionally physical activation of a carbonaceous material is composed of two steps: first pyrolysis in an inert environment at elevated temperatures (650-850^{o}C), in the presence of suitable oxidized gases such as carbon dioxide, steam, air or their mixture. Carbonization temperature ranges between 400^{o}C to 800^{o}C, and activation temperature ranges between 800^{o}Cto 1100^{o}C (Aworn,*et al.*, 2009; Bonelli,*et al*., 2001; Cabel,*et al*., 2009; Petrov, *et al*., 2008). The purpose of activation is to create a porous structure that will readily adsorb pollutants whether in a gas or aqueous phase.

2.13.2 Chemical activation

Chemical activation is a single step process in which carbonization and activation is carried out simultaneously. Initially the precursor is mixed with chemical activating agent, which acts as dehydrating agent and oxidant. Chemical activation offers several advantages over physical activation which mainly include (1) lower activation temperature (<800^{o}C) compared to the physical activation temperature (800-1100^{o}C) (EL-Hendawy,*et al*., 2008). (II) Single activation step (III) higher yield, (IV) better porous characteristics, and (V) shorter activation times. The chemical activation agents used in practice includes zinc chloride, phosphoric acid or potassium hydroxide. The chemical is mixed with the precursor prior to a carbonization step.

After the impregnation step, the samples were carbonized in the horizontal furnace under inert atmosphere by using nitrogen gas by varying the operating parameter such as carbonization temperature and carbonization time. The carbonization process was carried out by loading the dried precursor into furnace and heating to a carbonization temperature of 650^{o}C for 30min (El- Hendawy,*et al*., 2008; Foo and Hameed, 2010). This carbonization is often milder in time and temperature than physical activation techniques.

2.13.3 Factors affecting activated carbon production

.(a) Raw material

Most organic material rich in carbon that do not fuse upon carbonization can be used as raw material for the production of activated carbon. Low content inorganic material is important to produce AC with low ash content. Raw material such as coconut shell and fruit stones are very popular for many type of AC, because their relatively high density, hardness and volatile content are ideal for the production of hard granular AC. Coconut shells, together with peach and olive stones are used commercially for the production of micro porous activated carbon, useful for a very wide range of application.

(b)Temperature

Temperature, particularly the final activated temperature, affects the characteristic of the activated carbon produced. Generally, for commercial activated carbon production, temperature above 800^{o}C in a mixture of steam and CO_2 is required. As reported by several authors, activated temperature significantly affects the production yield and also the surface area of the activated carbon (Haimour and Emeish, 2006).

The optimum temperature has been reported to be between 400^{o}C to 500^{o}C by most researchers irrespective of time of activation and impregnation ratio of different raw material. The increasing of activated temperature reduces the yield of the activated carbon continuously.

Haimour and Emeish (2006) suggested that the percentage of volatile matter decreased with an increased carbonization temperature and the variation of these parameters was at its maximum between 200^{o}C and 800^{o}C due to rapid carbonization occurring in this region.

(c)Activated time

Beside activated temperature, the activated time also affects the carbonization process and properties of activated carbon. From previous study, the activated time normally used was from 1 hour to 3 hour for palm shell and coconut shell. As the time increased, the percentage of yield decreased gradually and the surface area also increased. This result is possibly due to the volatilization of organic material from raw material, which resulted in formation of activated carbon (Kim,*et al*., 2001).

(d)Carbonization

During carbonization, most of the non-carbon elements, hydrogen and oxygen are first removed in gaseous form by pyrolytic decomposition of the starting materials. Then the free atoms of elementary carbon are grouped into organized crystallographic formations known as elementary graphite crystallites.

2.13.4 Properties of activated carbon

Physical properties of AC, such as ash content and moisture can affect the use of a granular AC and render them either suitable or unsuitable for specific applications. Furthermore, the porous structure of activated carbon also can be characterize by various techniques such as scanning electron microscopy (SEM), transmission electron microscopy (TEM), infrared spectroscopy analysis using Fourier transform infrared (FTIR), X-ray diffraction (XRD) and X-ray fluorescence (XRF).

(a) Moisture content

Activated carbon is generally priced on a moisture free basis, although occasionally some moisture content is stipulated, e.g.3, 8, 10%. Unless packaged in air-tight containers, some activated carbons when stored under humid condition will adsorb considerable moisture over a period of month. For many purposes, this moisture does not affect the adsorptive power, but obviously it dilutes the carbon. Therefore, an additional weight of moist carbon is needed to provide the required dry weight.

(b) Ash content

The ash content of a carbon is the residue that remains when the carbonaceous material is burned off. Ash content can lead to increase hydrophobicity and can have catalytic effects, causing restructuring process during regeneration of used activated carbon. The inorganic material contained in activated carbon is measured as ash content, generally in the range between 2 and 10% (Yang and Lua, 2003).

(c) Surface area

Generally, the larger the specific surface area of the adsorbent, the better its adsorption performance will be (Guo and Lua, 2003). The most widely used commercial active carbons have a specific surface area of the order of 600-1200m^2/g (Ng, et al., 2002). The pore volume limits the size of the molecules that can be adsorbed whilst the surface area limits the amount of material which can be adsorbed, assuming a suitable molecular size (Lartley and Acqual, 1999). The adsorptive capacity of adsorbent is related to its internal surface area and pore volume.The specific surface area (m^2/g) of porous carbon is most usually determined from gas adsorption measurement using the Brunaner-Emmett-Teller BET (Hu and Srinivasan, 1999).

(d) Iodine number

Many carbons preferentially adsorb small molecules. Iodine number is the most fundamental parameter used to characterize activated carbon performance. It is a measure of activity level of activated carbon. Iodine number is an important characteristic of activated carbon, it gives a measure of the micro pore volume of carbon, and it approximates the total internal surface of the carbon.

(e)Surface functional group of activated carbon

The selectivity of activated carbons for adsorption is a factor of their surface chemistry, as well as their pore size distribution (Radovic, et al., 2001). The chemical composition of the raw material influence the surface chemistry and offer a potentially lower cost method for adjusting the properties of activated carbons. Various functional groups containing oxygen, nitrogen and other hetero-atoms have been identified on activated carbon. Hence, activated carbons have a larger porosity, which makes heteroatom readily combined on the surface during production processes. These surface groups play a key role in the surface chemistry of activated carbon (Yang and Lua, 2003).

(f) Pore structure

The word comes from the Greek word, meaning a passage. A pore is a class of void which is connected to the external surface of a solid and will allow the passage of fluid into, out of, or through a material. Different types of pore are shown schematically in Figure 2.6

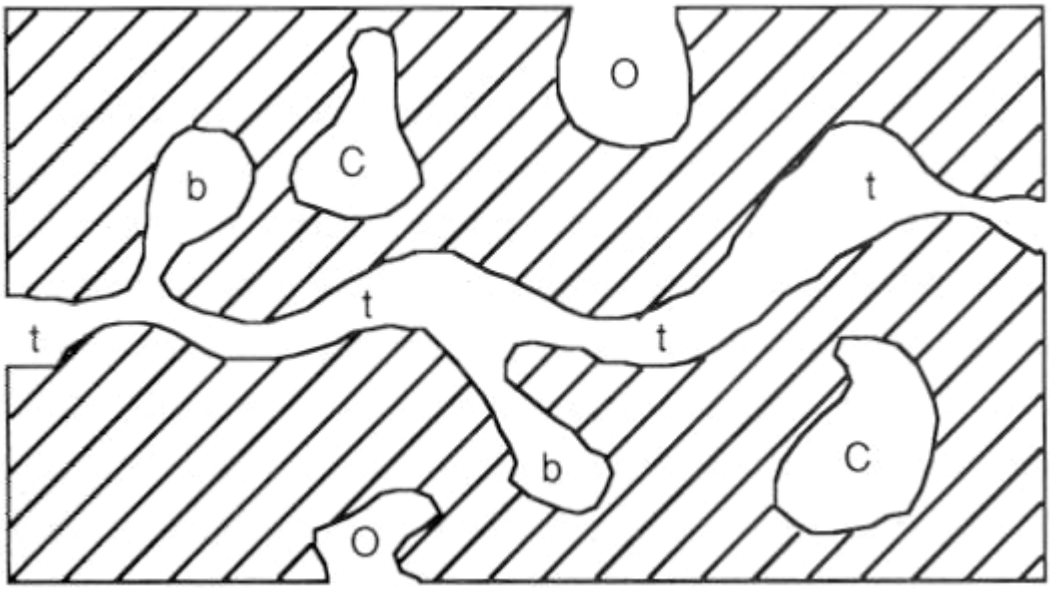

Figure 2.2: Different types of porosity in a porous solid.
O-open pores; C- closed pores; t-transport pores; b-blind pores

Transport pores are those pores in which a concentration gradient exist during steady state or time-independent fluid flow through the material. Blind pores are connected to transport pores by a single opening so that in them concentration gradient and hence fluid flow only occur during unsteady state or time independent flow.

Adsorption takes place in micro pores and mesopores with macropores acting as transport channels. The distribution of pores in activated carbons can vary significantly depending upon the raw material, the mesopores serves as the main transport arteries for the adsorbate (Hu and Srinivasan, 2001).

(g) Abrasion resistance

This accounts for the carbon's ability to withstand degradation during handling and is expressed in terms of abrasion number or handling number. It indicates carbon's ability to maintain its physical integrity and withstand frictional force imposed by backwashing and other factors. The harder the carbon, the lesser is the tendency to crumble.

(h) Bulk density

Bulk density is a measure of the weight of material that can be contained in a give volume under specified condition. Bulk density of carbon determines how much of it can be contained in a given container. Bulk density is affected by the raw material used and the degree of activation. The density does not affect the effectiveness of

the activated carbon measured in adsorptionper unit weight, but will have an effect on adsorption for unit volume. Higher density provides greater volume activity.

(i)pH at point zero of charge

The point zero of charge, pHpzc is defined as the pH of the aqueous solution in which the solid presents a neutral electric potential. It allows quantifying the acidic or basic character of the carbon. Depending on the precursor origin and the preparation mode (chemical or physical), activated carbons can have an acidic, basic or neutral nature depending on the pHpzc: the carbon surface is positively charged at pH<pH(pzc) and negatively charged at pH> pH(pzc). The pH(pzc)can be determined according to the method described by (Mondal, et al., 2009).

2.14 Characterization Techniques.

2.14.1 X-Ray diffraction measurement

X-ray scattering techniques are a family of non-destructive analytical techniques which reveal information about the crystallographic structure, chemical composition and physical properties of the materials and thin film. The adsorbents with broad peaks and absence of sharp peak revealed predominantly amorphous structure, which is an advantageous property for well-defined porous adsorbent (Tonypoothor,*et al*., 2011).

2.14.2 Morphology analysis

In order to know the structure sight at activated carbon, scanning electron microscopy (SEM), was generally employed to visualize sample morphology. Pore structure and structural charges happening after chemical activation could be also observed. The SEM images, shows the highly heterogeneous porous structure of the adsorbent particles (Arami,*et al*., 2005).

2.14.3 Infrared spectroscopy analysis

Fourier transform infrared spectral analysis was carried out to identify the different functional groups present in given samples. It is the most useful for identifying chemicals that are either organic or inorganic. It can be utilized to quantitate some component of an unknown mixture. It can be applied to the analysis of solids, liquids and gases. The pattern of adsorption of metals onto plant materials is attributable to the active groups and bonds present on the adsorbent surface.

2.14.4 X-ray fluorescence (XRF) spctroscopy

An XRF measurement probes the bulk composition of the amount of specific elements in a sample. The results of the elemental composition of the activated carbon is often presented as weight percent of the most common elemental oxide (Hossan,*et al*., 2012)

CHAPTER THREE

MATERIALS AND METHODS

3.1 Sample Collection, Preparations,Characterization and Equipment

3.1.1 Sample collections

The selected plants and animal materials used in this work were purchased in Enugu and Port Harcourt; *Detarium microcarpum, Xanthosoma, Hibiscus esculentus (L*), *Canarium schweinfurlhii* and *Mucuna pruriens were* purchased from Ogbette main market, in Enugu State, while *Crassostrea virginica* was bought from waterside market in Port Harcourt, River State. The plates were presented in Appendix A and B.The reagents used were also purchased from Conraw Nig. Ltd, Enugu. The effluent from brewery plant was collected at 9th

mile Corner Udi, Enugu State Nigeria, while paint wastewater was collected at Amechi Awkunanaw in Enugu State Nigeria.

3.1.2 Sample preparations for biocoagulants and biosorbents

The selected raw materials for coagulants were *Detarium microcarpum*, *Xanthosoma*, *Hibiscus esculentus (L*), and *Crassostrea virginica*. The *Xanthosoma* was peeled, washed and sliced into chips and sun dried with *Detarium microcarpum*, and *Hibiscus esculentus (L*) for one week, crushed and ground into powder using hand grinding machine. The *Crassostrea virginica* were washed with tap water to remove debris then dried in an oven at a temperature of 60^{o}C for 2 hours and ground into power. The *Canarium schweinfurlhii*, *Mucuna pruriens* and *Crassostrea virginica* used as adsorbents, were also washed, dried in an oven at a temperature of 105^{o}C for 24 hours to remove all moisture. All the samples were stored inair-tight containers to avoid moisture and for further treatment.

3.1.2.1*Plant derived biocoagulant*

2g of plant powders was mixed with 100ml of tap water and vigorously shaken for 30min. using magnetic stirrer to promote water extraction of coagulating agent. The suspension was filtered using Whatman No.1 filter paper. The filtrated solution was termed the coagulant (stock solution), and named as *Detarium microcarpum* coagulant (DMC), *Xanthosoma* coagulant as (CYC), *Hibiscus esculentus (L*) coagulant as (OSC) for plant the derived biocoagulants. Fresh solutions were prepared daily and kept refrigerated to prevent any aging effect.

3.1.2.2*Animal derived biocoagulant*

In preparing chitosan powder from *Crassostrea virginica* depends on lab scale requirement. In this method, 4 steps were involved in preparation of chitosan.

i) Preconditioning

The ground *Crassostrea virginica* was soaked in 0.05M acetic acid solution for 24 hours at room temperature. Then the sample was washed thoroughly with water and dried to remove excess water. Finally, the dried powder was weigh.

ii) Demineralization

The sample from preconditioning stage, were demineralized using 0.25L 1M HCL (hydrochloric acid) (1:10w/v) at room temperature (approximately 30^{o}C) and stirred for 6 hours. Then the residue was separated and washed with distilled water until pH of 6.5- 7.5 was obtained. Then the sample was dried and weighed.

iii) Deproteinization

The dried sample material obtain from demineralization step was deproteinized using 0.5L of 1M NaOH solution (1:10 w/v) at room temperature (approximately 30^{o}C) for about 16 hours. Then the sample was separated and washed with distilled water until pH is in the range of 6.5 – 7.5. The usefull product obtained in this process is known as chitin. The chitin was dried and ground, screen with sieve size 150μm. The amount obtained was weigh.

1v) Decolouration

The chitin from deprotienization were then treated with acetone at (1:10 w/v) ratio concentration, washed with distilled water and bleached with 0.315% NaOCL at 1:10 w/v) for 3 hours until the powder was crispy.

iv) De-acettylation

The chitin obtain from deproteinization step was de-acetylated in 25M NaOH (1:10 w/v) for about 20 hours at 65^{o}C. Then the product was separated and washed with distilled water until pH range of 6.5 – 7.5 was obtained. Then the useful product obtained in this process is known as chitosan named as *Crassostrea virginica* derived coagulant (ODC).

3.1.2.3 Carbonization and activation of adsorbent precursors

The dried samples of *Mucuna Pruriens*, *Canarium schweinfurlhii* and *Crassostrea virginica* were washed with tap water to remove dust on the materials and dried for two days. The samples were cut into small pieces and carbonized in a furnace for 2 hours at 500^{o}C. The samples were allowed cool down, washed several times with distilled water and dried in an oven at 110^{o}C overnight. The chemical activation procedure was carried out in 2L beakers. Two different parts of samples were immersed in 60% 1M of $H_3PO_4$and 60% 1M of NH_4CL solution, and stirred continuously for 24 hours so that the reagents were fully immersed into the samples. After this treatment, the modified samples were filtered, washed with distilled water for several times until the pH reached a constant value and was oven dried at 110^{o}C for 4 hours. The samples were stored in air-tight containers and lebelled as *Mucuna Prurien s*acid treated (MSA), *Mucuna Pruriens* salt treated (MSS), *Canarium schweinfurlhii*

acid treated (AESA), *Canarium schweinfurlhii* salt treated (AESS), *Crassostrea virginica* acid treated (OSA) and *Crassostrea virginica* salt treated (OSS) for characterization.

3.1.3 Sample characterization (wastewaters, biocoagulants and biosorbents)

3.1.3.1 *Characterization procedure for wastewaters, coag-flocculants and adsorbents*

The characterization of effluents was done according to the standard method of water and wastewater, APHA, AWWA (2005), while the bio coagulants and biosorbents were characterized using standard test, AOAC (2005) and ASTM (2002).

3.1.4 Equipment used

The equipment used during coag-flocculation and adsorption experiments; its model and functions are given in Table 3.1

Table 3.1: Equipmentused, its model and functions

Equipment	model	functions
Analytical balance		weight measurement
pH meter	Toledo 320	measurement of pH
Turbidimeter	No WZS-185	turbidity measurement
Magnetic stirrer	Gallenhamp APP No 688644	for stirring
Centrifuge	Techmel USA 800	for high speed stirring
Spectrophotometer	UV-1650, Shimadzu, Japan	for measuring TDS

Oven	Nemmert Din 40050-ip20	for drying
Blender	Model-242 superintermet	for mixing/blending
Centrifugal grinding mill	No DR 64857	for grinding
FTIR	SHIMADU IR PRESTIGE-21	functional group
SEM	JSM 5410, JECO	surface characteristic
XRD	XRD-6000 Shimadzu,	for crystalline structure
XRF	model PW 2400/0	for chemical composition
Beakers		for mixing
Furnace	Model KCQ 80750120 kgyn	carbonization/activation

3.2Methods

3.2.1 Coag-flocculation test

300ml of wastewater was transferred into a 1000ml beaker after adjustingthe initial pH using 0.1M HCL or 0.1M NaOH with pH meter (Toledo 320). Then varying doses of the biocoagulants were added into beaker containing the wastewater, and stirred rapidly for 1min at 250 rpm to obtain homogeneous dispersion of the biocoagulants using magnetic stirrer (Gallenhamp APP No 688644). Then followed by a slow stirring at 40 rpm for 10 minutes, for floc formation. Then the stirring was stopped and the suspension was allowed to settle for 30 minutes. At 5 minutes interval, the supernatant was analyzed using Turbidimeter (Model No WZS-185), by extracting from the beaker with a syringe 2cm below the water surface and filtered using Whatman No. 1 filter paper.The experiment was repeated for varying coagulant dosage (50, 100, 200, 300, 400 and 500mg/L), pH (2, 4, 6, 8 and 10) and settling times (3, 5, 10, 15, 20, 25 and 30 min) in order to study their effect in coagulation-flocculation and obtain the optimum condition for each parameter. The residual particle load of supernatant were measured and recorded. The experiment was perfomed in triplicate to obtain a more reliable result. The results from coagulation were measured in nephelometric turbidity unit (NTU) and converted to particle concentration by .using a conversion factor of 2.35.

3.2.2 Batch adsorption experiment

After coag-flocculation experiment, the pH of the supernatant was adjusted using 0.1M HCl or 0.1 M NaOH as required.Then 100ml of supernatant was transferred into 250 mL conical flasks and varying doses of biosorbents were added and agitated using a thermostatic mechanical shaker (HAAKE SWB20, Fission Ltd Germany) at 150 rpm. At pre-determined time interval, samples were withdrawn and put into centrifuge (Model: Sigma-301, Germany) at 3500rpm for 5min to separate the adsorbent from the effluent. Then the suspension was filtered, and the filtrate was analyzed using UV-Spectrophotometer(UV-1650A, Shimadzu, Japan) at 560nm to determine the final concentration of the turbidity removal.The effects of various operating parameters, pH of the supernatant

(2–10), adsorbent dosage (20-100mg), contact time (10-70 min) and temperature (30, 40 and 50 °C), on the adsorption of turbidity were investigated.

All the experiments were carried out in duplicates to avoid any discrepancy in experimental results and the average values were used for further data evaluation.

3.2.3Mathematical methods

3.2.3.1 Kinetic of Coag-flocculation

The kinetic of Brownian coagulation for colloidal particles is usually described by the Smolushowski equation (Von Smoluchowski, 1917; Menkiti,*et al*., 2010).

$$\frac{dn_k}{dt} = {}^{1}/_{2} \sum_{i+j=1} \beta_{BR}(i,j) n_i n_j - \sum_{i=1}^{\infty} \beta_{BR}(i,k) n_i n_k \qquad (3.1)$$

Where $\beta_{BR}(i,j)$ the Brownian aggregation factors for flocculation transport mechanism;n_i and $n_j$are concentration for aggretate particles size respectively.

$\beta_{BR}$is defined by (Jin, 2005).

$$\beta_{BR} = \frac{8}{3} \varepsilon_p \frac{K_B T}{\eta} \quad (3.2)$$

Where K_B is Boltzmann's constant (J/K), T is absolute temperature (K), ε_p is the collision efficiency, η is the viscosity of the medium.

Coagulation is controlled by Brownian diffusion and coagulation rate constant for dimmer formation of an initially monodisperse suspension is given by

$$K_{11} = \frac{8K_B T}{3\eta} \quad (3.3)$$

For rapid coagulation

$$K_R = \frac{4}{3} \frac{K_B T}{\eta} \quad (3.4)$$

Where K_R is the Von Smoluchowski rate constant for rapid coagulation (Menkiti, et al., 2012)

The kinetic of Brownian coagulation of mono-dispersed particles at the early stage is described generally by [Holthof, *et al.*, 1996; Jin, 2005]:

$$\frac{dN}{dt} = -KN^2 \quad (3.5)$$

whereN is the total number concentration of particles, t is the time and *K is* a second-order coagulation rate constant.

It has been reported that for a constant kernel i.e., $K_{ij} = K_{11}$. The Smoluchowski equation (1) can be solved exactly, resulting in the generic expression

$$\frac{N_t}{N_o} = \frac{(K_{11}N_o t/2)^{n-1}}{(1+K_{11}N_o t/2)^{n+1}} \quad (3.6)$$

Where N_o the initial particle concentration. For n = 1, i.e., a monomer, the following linear functions in time for the inverse square root of monomer concentration N_1 is obtained.

$$\frac{1}{\sqrt{N_t}} = \left(\frac{K_{11}N_o}{2\sqrt{N_o}}\right)t + \frac{1}{\sqrt{N_o}} \quad (3.7)$$

Therefore, a graphical representation of the inverse square root of monomer concentration N_t versus time should give a straight line and the coagulation rate constant can be measured from the slope of this function once the initial particle concentration N_o is known.

From the constant kernel solution of the Smoluchowski equation (Eq.6), is useful to introduce a coagulation-flocculation period, $\tau_{1/2}$ where the total number of concentration is reduced by a factor of 2.

$$\tau_{1/2} = \frac{1}{0.5KN_o} \quad (3.8)$$

Where $\tau' = 2\tau$

The concentration of singlets, doublet and triplets during coagulation can be evaluated by solving equation (3.6)

Hence, for singlets (n=1)

$$N_1 = N_o\left[\frac{1}{(1+t/\tau')^2}\right] \quad (3.9)$$

For doublets (n=2)

$$N_2 = N_o\left[\frac{t/\tau'}{(1+t/\tau')^3}\right] \quad (3.10)$$

For triplets (n=3)

$$N_3 = N_o \left[\frac{\left(t/\tau'\right)^2}{\left(1+t/\tau'\right)^4} \right] \quad (3.11)$$

Efficiency of coag-flocculation is expressed as:

$$E\ (\%) = \left[\frac{N_o - N_t}{N_o} \right] 100 \quad (3.12)$$

3.2.3.2 Batch adsorption isotherm models

(i) *Langmuir isotherm model*

Langmuir adsorption isotherm model exhibits the monolayer coverage of the adsorption surfaces and assumes structurally homogeneous adsorbent. It also assumes that all the adsorption sites as energetically identical. The Langmuir equation is given by (Langmuir, 1918).

$$q_e = \frac{q_m K_L C_e}{1+K_L C_e} \quad (3.13)$$

The linearization of equation (3.13) leads to the following form:

$$\frac{1}{q_e} = \frac{1}{q_m k_L C_e} + \frac{1}{q_m} \quad (3.14)$$

Where C_e, equilibrium adsorbate (turbidity) concentration, $q_m and k_L$ are the Langmuir constants related to maximum adsorption capacity (mg/L), and Langmuir isotherm constant (L/mg), respectively.The values of

q_{max} and $K_L$were computed from the slope and intercept of the Langmuir plot of$^1/_{q_e}$ $versus$ $^1/_{C_e}$ [Ahmad, et al., 2013]. The essential features of the Langmuir isotherm may be expressed in terms of equilibrium parameterR_L, which is a dimensionless constant referred to as separation factor or equilibrium parameter (Rangabhashiyam, *et al.*, 2013).

$$R_L = \frac{1}{1+K_L C_o} \quad (3.15)$$

Where: C_o= initial concentration, K_L = the constant related to the energy of adsorption (Langmuir Constant). $R_L$value indicates the adsorption nature to be either unfavourable if R_L>1), linear if R_L =1, favourable if 0< R_L<1 and irreversible if R_L=0.

(ii) *Frenudlich isotherm model*

This is commonly used to describe the adsorption characteristics for the heterogeneous surface. The Frenudlich equation is given by (Frenudlich, 1939):

$$q_e = k_f C_e^{1/n} \quad (3.16)$$

The logarithmic form of equation (3.16):

$$\ln q_e = \ln k_f + {}^1/_n \ln C_e \quad (3.17)$$

where,$q_e$the amount of adsorbate(turbidity) adsorbed per specific amount of adsorbent (mg/L), C_e is equilibrium concentration (mg/L). K_F is the freundlich characteristics and 1/n were obtained from intercept and slope of ln(qe) vs ln(Ce) linear plot respectively.The value 1/n indicates how
favourable the adsorption will be and how strong the bond is between the adsorbate and adsorbent.

(iii) *Temkin isotherm model*

Temkin isotherm is based on a factor that describes the adsorbent-adsorbate interaction which assures that the heat of adsorption of all the molecules in the layer would decrease linearly with coverage (Temkin and Pyzhev, 1940). The model is given by the following equation:

$$q_e = \frac{RT}{b} \ln(AC_e) \quad (3.18)$$

The linear form of Temkin is given as:

$$q_e = B \ln A + B \ln C_e$$

Where $B = \frac{RT}{b}$, R is the gas constant (8.314 J/molK), T is absolute temperature, C_e is equilibrium concentration (mg/L), and 'b' is related to heat of adsorption (J/mol) which is Temkin constant. A plot of $q_e \ versus \ \ln C_e$yields a linear line with B as the slope and B $\ln(A)$ as the intercept.A and B are the Temkin constants.

(iv) *Dubinin-Radushkevich isotherm (D-R).*

The adsorption data was applied to the D-R isotherm model to distinquish between physical and chemical adsorption.The following equation represents the D-R model:

$$q_e = q_o^{\exp(-\beta\varepsilon^2)} \qquad (3.19)$$

The linear form of this modelis expressed by:

$$\ln q_e = \ln q_o - \beta\varepsilon^2 \qquad (3.20)$$

Where β is a constant related to the adsorption energyand $\varepsilon = RT \ln\left(1 + {}^{1}/_{C_e}\right)$, where R is gas constant (KJ/molK) and T absolute temperature (K). The slope of plot of $\ln q_e \ versus \ \varepsilon^2$ gives β (mol^2/KJ^2) and the intercept yields the adsorption capacity, q_o (mg/g). The main adsorption energy (E) is defined when one mole of adsorbate is transferred from infinity in solution to the surface of the membrane. It is calculated from the β using the following equation

$$E = (2\beta)^{-1/2} \text{(KJ/mol)} \qquad (3.21)$$

(v) *Thermodynamic studies*

Thermodynamic study for the adsorption of turbidity onto adsorbents was conducted in the temperature range of 30-50^{o}C. Thermodynamic parameters such as change in free energy (ΔG), change in enthalpy (ΔH) and change in entropy (ΔS) was calculated using the following equations (Chowdhury and Papita, 2012; Gon calves,*et al.*, 2008).

$$\Delta G^\circ = -RT \ln K_c \qquad (3.22)$$

$$\Delta G^\circ = \Delta H^\circ - T\Delta S^\circ \qquad (3.23)$$

$$\ln K_c = \Delta S^\circ/R - \Delta H^\circ/RT \qquad (3.24)$$

The enthalpy change (ΔH°), and the entropy change (ΔS°) were calculated from the slope and the intercept in linear plots of $\ln K_c \; versus \; 1/T$.

3.2.3.3 Adsorption kinetic Models

Several adsorption kinetic models have been established to understand the adsorption kinetics and rate-limiting step. These are pseudo-first and second-order, Elovich and intra-particle diffusion models.

(i) *Pseudo-first-order*

The pseudo-first order rate expression of Lagergren model is generally expressed as (Tsenq,*et al.*, 2003, Ho, 2004).

$$\frac{dq_t}{dt} = k_1(q_e - q_t) \qquad (3.25)$$

Where $q_e and q_t$ refers to the amount adsorbed on the activated carbon at equilibrium and at time t (min), and k_1 as rate constant of the pseudo first order adsorption process(min^{-1}), respectively.

Integrating the above equation between the limits from t=0 to t= t and from $q_t = 0 \; to q_t = q_t$, becomes a linear equation as given by:

$$\log(q_e - q_t) = \log q_e - \frac{k_1}{2.303} t \qquad (3.26)$$

The plot of log (q_e−q_t) versus *t* gives a straight line for the pseudo first-order adsorption kinetics, from which the adsorption rate constant, k_1, is estimated.

(ii) *Pseudo-second-order*

The adsorption data were also studied by second order kinetic (Tseng, *et al*., 2003).

$$\frac{dq_t}{dt} = k_2(q_e - q_t)^2 \qquad (3.27)$$

where$k_2$is the equilibrium rate constant of pseudo second-order adsorption (g/mg.min). From the boundary conditions, $t = 0$ to t and $q_t = 0$ to q_t, the integrated form of the equation (3.27) is:

$$\frac{t}{q_t} = \frac{1}{k_2 q_e^2} + \frac{t}{q_e} \qquad (3.28)$$

where, $q_e and q_t$ (mg/g) are the amount of adsorbate that was adsorbed at the equilibrium and at time t (min), respectively and k_2 is the pseudo-second order rate constant of adsorption (g/mg.min).From the slopes and

intercepts of the linear plots obtained by plotting $^{t}/_{q_t} versus t$, the values of the pseudo-second order rate constants $q_e and k_2$ were calculated.

(iii) *Elovich kinetic equation*

The Elovich model equation is generally expressed as:

$$\frac{dq_t}{dt} = \alpha exp^{-\beta q_t} \quad (3.29)$$

Where α is the initial adsorption rate (mg/g min) and β is the adsorption constant (g/mg) during any experiment. To simplify the Elovich equation by applying the boundary conditions$q_t = 0 \; at \; t = 0 \; and q_t = q_t at \; t = t$, equation (3.29) becomes:

$$q_t = \frac{1}{\beta}\ln(\alpha\beta) + \frac{1}{\beta}\ln(t) \quad (3.30)$$

If turbidity adsorption fits the Elovich model, a plot of q_t versus $\ln(t)$ should yield a linear relationship with a slope of $\left(\frac{1}{\beta}\right)$ and an intercept $\left(\frac{1}{\beta}\right)\ln(\alpha\beta)$. The slope and intercept were used to determine the constant β and the initial adsorption rate α.

(iv) *Intra-particle diffusion*

According to intra-particle diffusion model, the initial rate of diffusion is given by the following equation (Cheung, et al., 2007)

$$q = k_{id}t^{1/2} + A \quad (3.31)$$

Where q is the adsorption capacity (mg/g) at time t (min), k_{id} is the diffusion rate constant (mg/gmin$^{1/2}$) and A (mg/g) is a constant that gives an indication of the thickness of the boundary layer. In this model, if the plot of $q_t versus t^{1/2}$ is linear and passes through the origin, then the intra-particle diffusion is the rate-controlling step (Cheung, et al., 2007).

3.3 Design of Experiments

In this study, response surface methodology (RSM) involving a historical data experimental design (HDD) was applied to identify the functional relationship between the variables (Aremu, *et al*., 2014). Also a second order polynomial equation was employed to identify the relationships between three independent variables: coagulant/adsorbent dose, pH and settling/contact time that influence the turbidty removal from PW and BRE. The percentage of turbidity removed was taken as the response (Y) and design expert software version 9.0.6., was

used for regression and graphical analyses.The statistical analysis of the model was performed in the form of analysis of variance (ANOVA) for the determination of significant variables.

3.3.1 Experimental design

The HDD was used to generate the experimental matrix and the model equations for optimization of the performance of the coagulants/adsorbents in removal of suspended solids, turbidity and total dissolved solid from BRE and PW. The manipulated variables were selected based on the results from historical data and varied at three levels: a high level, represented as (+1), a low level represented as (-1) a middle point (0). The response variables represented as Y are the percentage removal of turbidity.The following variables were selected for the study: coagulants/adsorbent (X_1), initial pH of solution (X_2) and settling/stirring time (X_3).The range and levels used in the experiment are listed in Table 3.2

Table 3.2: Independence factors and theircoded value levels

Variables	coded value level		
	Lower limit (-1)	middle (0)	up limit (+1)
Coagulant/adsorbent dose X_1	(-1)	(0)	(+1)
pH X_2	(-1)	(0)	(+1)
Settling/stirring time X_3	(-1)	(0)	(+1)

HDD matrix for experimental design coded values of the three factors ie coagulant/adsorbent, pH and settling/contact time, has been summarized in Table 3.3.

The A mathematical model, describing the relationships among the process dependent variables and independent variables in a second-order polynomial equation was developed. Design-based experimental were matched according to the following second-order polynomial equation:

$$Y = \beta_o + \sum_{i=1}^{k} \beta_i X_i + \sum_{i=1}^{k} \beta_{ii} X_i^2 + \Sigma \sum_{i<j} \beta_{ij} X_i X_j \qquad (3.32)$$

Where Y= the response variables to be modeled

$X_i and X_j are$ theindependent variables, $\beta_o, \beta_i, \beta_{ii} and \beta_{ij}$ are regression coefficients for intercept, linear, quadratic and interaction coefficient, respectively (Jadhave and Mahajan, 2013).

Table 3.3: HD Design matrix forthree variables for coag-flocculation and adsorption processes

Run no.	Coded values of independent variables		
	X_1	X_2	X_3
1	-1	-1	-1
2	-1	-1	0
3	-1	-1	1
4	-1	0	-1
5	-1	0	0
6	-1	0	1
7	-1	1	-1
8	-1	1	0
9	-1	1	1

10	0	-1	-1
11	0	-1	0
12	0	-1	1
13	0	0	-1
14	0	0	0
15	0	0	1
16	0	1	-1
17	0	1	0
18	0	1	1
19	1	-1	-1
20	1	-1	0
21	1	-1	1
22	1	0	-1
23	1	0	0
24	1	0	1
25	1	1	-1
26	1	1	0
27	1	1	1

CHAPTER FOUR

RESULTS AND DISCUSSION

4.1 Characterization Results for Coag-flocculation and Adsorption

4.1.1 Characterization results of BRE and PW before and after coag-flocculation and adsorption.

The characterization results of BRE and PW before and after coag-flocculation and adsorption were carried out according to the standard methods for the examination of water and wastewater (APHA, AWWA and WEF 2005) are presented in Tables4.1 to 4.14.The results indicated that turbidity, TDS, COD and BOD were present in significant quantities, which indicated that the wastewater can be classified as a pollutant because it exceeded the world health organization agency (WHO) standards for maximum effluent discharge and need to be

treated.From the results, it showed that turbidity,TDS, COD and BOD values were 334.74NTU,254.36mg/L, 2856.72mg/L and 1148 mg/L in BRE, and 440.21NTU,432.54mg/L, 986.87mg/L and 876.50mg/L in PW,respectively before coagulation. After coagulation and adsorption processes, the final removal of turbidity, TDS, COD and BOD were presented in Tables 4.1 to 4.14.

Table 4.1:Characterization results of BRE before and after coagulation using DMC as biocoagulant

Parameters	Before	After	WHO
pH	7.68	7.10	6.6-8.5
Turbidity (NTU)	334.74	8.92	< 11.75
Total hardness (mg/L)	156.24	76.64	500.00
Fe^{2+} (mg/L)	0.15	0.11	0.3
So_4^{2-}(mg/L)	38.17	48.63	250.00
Cl^- (mg/L)	20.864	165.32	200.00
TDS (mg/L)	254.36	5.36	50.00
TSS (mg/L)	30.52	2.52	30.00
COD (mg/L)	2856.72	69.32	NS
Total nitrogen (mg/L)	73.00	15.87	11.23

Total phosphorus (mg/L)	21.00	4.00	NS
Total coliform (MPN/100ml)	11.00	Nil	NS
Eschericha coli (cfu/100ml)	Nil	Nil	NS
Electrical conductivity (µmho/cm)	1590	1335	1250.00
BOD_5 (mg/L)	1148.63	8.18	< 1

Note: NTU-nephelometric turbidity unit, TDS-total dissolved solids, TSS-total suspended solids, MPN-most portable number, COD-chemical oxygen demand, BOD-biochemical oxygen demand, cfu-colony forming unit and NS-not stated.

Table 4.2: Characterization results of BRE before and after coagulation using CYC as biocoagulant

Parameters	Before	After	WHO
pH	7.68	7.25	6.6-8.5
Turbidity (NTU)	334.74	10.56	< 11.75
Total hardness (mg/L)	156.24	80.64	500.00
Fe^{2+} (mg/L)	0.15	0.10	0.3
So_4^{2-}(mg/L)	38.17	42.52	250.00
Cl^- (mg/L)	20.864	176.90	200.00
TDS (mg/L)	254.36	6.43	50.00
TSS (mg/L)	30.52	4.86	30.00
COD (mg/L)	2856.72	75.65	NS
Total nitrogen (mg/L)	73.00	23.68	11.23

Total phosphorus (mg/L)	21.00	5.43	NS
Total coliform (MPN/100ml)	11.00	Nil	NS
Eschericha coli (cfu/100ml)	Nil	Nil	NS
Electrical conductivity (µmho/cm)	1590	2346.87	1250.00
BOD_5 (mg/L)	1148.63	10.87	< 1

Note: NTU-nephelometric turbidity unit, TDS-total dissolved solids, TSS-total suspended solids, MPN-most portable number, COD-chemical oxygen demand, BOD-biochemical oxygen demand, cfu-colony forming unit and NS-not stated.

Table 4.3: Characterization results of BRE before and after coagulation using OSC as biocoagulant

Parameters	Before	After	WHO
pH	7.68	6.98	6.6-8.5
Turbidity (NTU)	334.74	8.76	< 11.75
Total hardness (mg/L)	156.24	72.65	500.00
Fe^{2+} (mg/L)	0.15	0.11	0.3
So_4^{2-}(mg/L)	38.17	47.86	250.00
Cl^- (mg/L)	20.864	154.43	200.00
TDS (mg/L)	254.36	5.01	50.00
TSS (mg/L)	30.52	3.24	30.00
COD (mg/L)	2856.72	82.65	NS
Total nitrogen (mg/L)	73.00	13.87	11.23

Total phosphorus (mg/L)	21.00	4.12	NS
Total coliform (MPN/100ml)	11.00	Nil	NS
Eschericha coli (cfu/100ml)	Nil	Nil	NS
Electrical conductivity (µmho/cm)	1590	1676.95	1250.00
BOD_5 (mg/L)	1148.63	9.87	< 1

Note: NTU-nephelometric turbidity unit, TDS-total dissolved solids, TSS-total suspended solids, MPN-most portable number, COD-chemical oxygen demand, BOD-biochemical oxygen demand, cfu-colony forming unit and NS-not stated.

Table 4.4: Characterization results of BRE before and after coagulation using ODC as biocoagulant

Parameters	Before	After	WHO
pH	7.68	6.56	6.6-8.5
Turbidity (NTU)	334.74	8.43	< 11.75
Total hardness (mg/L)	156.24	85.76	500.00
Fe^{2+} (mg/L)	0.15	0.10	0.3
So_4^{2-}(mg/L)	38.17	50.64	250.00
Cl^- (mg/L)	20.864	160.76	200.00
TDS (mg/L)	254.36	5.76	50.00
TSS (mg/L)	30.52	4.98	30.00
COD (mg/L)	2856.72	68.86	NS
Total nitrogen (mg/L)	73.00	14.76	11.23

Total phosphorus (mg/L)	21.00	4.34	NS
Total coliform (MPN/100ml)	11.00	Nil	NS
Eschericha coli (cfu/100ml)	Nil	Nil	NS
Electrical conductivity (µmho/cm)	1590	1432.65	1250.00
BOD_5 (mg/L)	1148.63	11.65	< 1

Note: NTU-nephelometric turbidity unit, TDS-total dissolved solids, TSS-total suspended solids, MPN-most portable number, COD-chemical oxygen demand, BOD-biochemical oxygen demand, cfu-colony forming unit and NS-not stated.

Table 4.5: Characterization results of PW before and after coagulation using DMC as biocoagulant

Parameters	Before	After	WHO
pH	6.70	5.64	6.6-8.5
Turbidity (NTU)	440.21	7.92	< 11.75
Total hardness (mg/L)	245.34	56.64	500.00
Fe^{2+} (mg/L)	10.68	12.65	0.3
So_4^{2-}(mg/L)	4568.00	4678.12	250.00
Cl^- (mg/L)	355.64	265.32	200.00
TDS (mg/L)	432.54	6.36	50.00
TSS (mg/L)	248.86	27.65	30.00
COD (mg/L)	986.87	53.42	NS
Total nitrogen (mg/L)	64.12	11.33	11.23

Total phosphorus (mg/L)	4.00	0.13	NS
Total coliform (MPN/100ml)	Nil	Nil	NS
Eschericha coli (cfu/100ml)	Nil	Nil	NS
Electrical conductivity (µmho/cm)	654.43	735.48	1250.00
BOD_5 (mg/L)	876.50	11.18	< 1

Note: NTU-nephelometric turbidity unit, TDS-total dissolved solids, TSS-total suspended solids, MPN-most portable number, COD-chemical oxygen demand, BOD-biochemical oxygen demand, cfu-colony forming unit and NS-not stated.

Table 4.6: Characterization results of PW before and after coagulation using CYC as biocoagulant

Parameters	Before	After	WHO
pH	6.70	4.89	6.6-8.5
Turbidity (NTU)	440.21	9.56	< 11.75
Total hardness (mg/L)	245.34	78.64	500.00
Fe^{2+} (mg/L)	10.68	14.65	0.3
So_4^{2-}(mg/L)	4568.00	4222.52	250.00
Cl^- (mg/L)	355.64	196.90	200.00
TDS (mg/L)	432.54	10.43	50.00
TSS (mg/L)	248.86	30.86	30.00
COD (mg/L)	986.87	75.86	NS
Total nitrogen (mg/L)	64.12	20.68	11.23

Total phosphorus (mg/L)	4.00	1.43	NS
Total coliform (MPN/100ml)	Nil	Nil	NS
Eschericha coli (cfu/100ml)	Nil	Nil	NS
Electrical conductivity (µmho/cm)	654.43	646.87	1250.00
BOD_5 (mg/L)	876.50	10.87	< 1

Note: NTU-nephelometric turbidity unit, TDS-total dissolved solids, TSS-total suspended solids, MPN-most portable number, COD-chemical oxygen demand, BOD-biochemical oxygen demand, cfu-colony forming unit and NS-not stated.

Table 4.7: Characterization results of PW before and after coagulation using OSC as biocoagulant

Parameters	Before	After	WHO
pH	6.70	3.65	6.6-8.5
Turbidity (NTU)	440.21	8.76	< 11.75
Total hardness (mg/L)	245.34	86.65	500.00
Fe^{2+} (mg/L)	10.68	11.65	0.3
So_4^{2-}(mg/L)	4568.00	4187.86	250.00
Cl^- (mg/L)	355.64	254.43	200.00
TDS (mg/L)	432.54	6.01	50.00
TSS (mg/L)	248.86	28.24	30.00
COD (mg/L)	986.87	48.95	NS
Total nitrogen (mg/L)	64.12	12.87	11.23

Total phosphorus (mg/L)	4.00	2.12	NS
Total coliform (MPN/100ml)	Nil	Nil	NS
Eschericha coli (cfu/100ml)	Nil	Nil	NS
Electrical conductivity (µmho/cm)	654.43	676.95	1250.00
BOD_5 (mg/L)	876.50	9.87	< 1

Note: NTU-nephelometric turbidity unit, TDS-total dissolved solids, TSS-total suspended solids, MPN-most portable number, COD-chemical oxygen demand, BOD-biochemical oxygen demand, cfu-colony forming unit and NS-not stated.

Table 4.8: Characterization results of PW before and after coagulation using ODC as biocoagulant

Parameters	Before	After	WHO
pH	6.70	4.87	6.6-8.5
Turbidity (NTU)	440.21	10.43	< 11.75
Total hardness (mg/L)	245.34	90.76	500.00
Fe^{2+} (mg/L)	10.68	15.60	0.3
So_4^{2-}(mg/L)	4568.00	5032.64	250.00
Cl^- (mg/L)	355.64	180.76	200.00
TDS (mg/L)	432.54	9.76	50.00
TSS (mg/L)	248.86	34.98	30.00
COD (mg/L)	986.87	60.42	NS
Total nitrogen (mg/L)	64.12	14.76	11.23

Total phosphorus (mg/L)	4.00	1.34	NS
Total coliform (MPN/100ml)	Nil	Nil	NS
Eschericha coli (cfu/100ml)	Nil	Nil	NS
Electrical conductivity (µmho/cm)	654.43	1132.65	1250.00
BOD_5 (mg/L)	876.50	11.65	< 1

Note: NTU-nephelometric turbidity unit, TDS-total dissolved solids, TSS-total suspended solids, MPN-most portable number, COD-chemical oxygen demand, BOD-biochemical oxygen demand, cfu-colony forming unit and NS-not stated.

Table 4.9: Characterization results of BRE before and after adsorption using MSA as biosorbent

Parameters	Before	After	WHO
pH	3.60	3.6	6.6-8.5
Turbidity (NTU)	6.21	1.25	< 11.75
Total hardness (mg/L)	76.64	66.64	500.00
Fe^{2+} (mg/L)	0.11	1.65	0.3
So_4^{2-}(mg/L)	48.63	40.55	250.00
Cl^- (mg/L)	165.32	165.32	200.00
TDS (mg/L)	5.36	1.36	50.00
COD (mg/L)	68.95	48.96	NS
Total nitrogen (mg/L)	Nil	Nil	11.23
Total phosphorus (mg/L)	Nil	Nil	NS

Total coliform (MPN/100ml)	Nil	Nil	NS
Eschericha coli (cfu/100ml)	Nil	Nil	NS
Electrical conductivity (µmho/cm)	2325.28	835.48	1250.00
BOD_5 (mg/L)	8.14	0.18	< 1

Note: NTU-nephelometric turbidity unit, TDS-total dissolved solids, MPN-most portable number, COD-chemical oxygen demand, BOD-biochemical oxygen demand, cfu-colony forming unit and NS-not stated.

Table 4.10: Characterization results of BRE before and after adsorption using AESA as biosorbent

Parameters	Before	After	WHO
pH	3.60	4.59	6.6-8.5
Turbidity (NTU)	6.21	1.56	< 11.75
Total hardness (mg/L)	76.64	78.64	500.00
Fe^{2+} (mg/L)	0.11	4.65	0.3
So_4^{2-}(mg/L)	48.63	42.52	250.00
Cl^- (mg/L)	165.32	176.90	200.00
TDS (mg/L)	5.36	1.43	50.00
COD (mg/L)	68.95	26.43	NS
Total nitrogen (mg/L)	Nil	Nil	11.23
Total phosphorus (mg/L)	Nil	Nil	NS

Total coliform (MPN/100ml)	Nil	Nil	NS
Eschericha coli (cfu/100ml)	Nil	Nil	NS
Electrical conductivity (µmho/cm)	2325.28	746.87	1250.00
BOD_5 (mg/L)	8.14	0.87	< 1

Note: NTU-nephelometric turbidity unit, TDS-total dissolved solids, MPN-most portable number, COD-chemical oxygen demand, BOD-biochemical oxygen demand, cfu-colony forming unit and NS-not stated.

Table 4.11: Characterization results of BRE before and after adsorption using OSA as biosorbent

Parameters	Before	After	WHO
pH	3.60	4.65	6.6-8.5
Turbidity (NTU)	6.21	1.38	< 11.75
Total hardness (mg/L)	76.64	66.65	500.00
Fe^{2+} (mg/L)	0.11	1.98	0.3
So_4^{2-}(mg/L)	48.63	41.86	250.00
Cl^- (mg/L)	165.32	194.43	200.00
TDS (mg/L)	5.36	1.01	50.00
COD (mg/L)	68.95	38.56	NS
Total nitrogen (mg/L)	Nil	Nil	11.23
Total phosphorus (mg/L)	Nil	Nil	NS

Total coliform (MPN/100ml)	Nil	Nil	NS
Eschericha coli (cfu/100ml)	Nil	Nil	NS
Electrical conductivity (µmho/cm)	2325.28	776.95	1250.00
BOD_5 (mg/L)	8.14	0.65	< 1

Note: NTU-nephelometric turbidity unit, TDS-total dissolved solids, MPN-most portable number, COD-chemical oxygen demand, BOD-biochemical oxygen demand, cfu-colony forming unit and NS-not stated.

Table 4.12: Characterization results of PW before and after adsorption using MSA as biosorbent

Parameters	Before	After	WHO
pH	5.6	3.6	6.6-8.5
Turbidity (NTU)	4.47	1.1	< 11.75
Total hardness (mg/L)	93.6	56.64	500.00
Fe^{2+} (mg/L)	1.45	1.05	0.3
So_4^{2-}(mg/L)	4765.97	40.55	250.00
Cl^- (mg/L)	438.83	145.32	200.00
TDS (mg/L)	3.86	0.36	50.00
COD (mg/L)	56.98	46.32	NS
Total nitrogen (mg/L)	Nil	Nil	11.23
Total phosphorus (mg/L)	Nil	Nil	NS

Total coliform (MPN/100ml)	Nil	Nil	NS
Eschericha coli (cfu/100ml)	Nil	Nil	NS
Electrical conductivity (µmho/cm)	785.34	835.48	1250.00
BOD_5 (mg/L)	11.98	0.18	< 1

Note: NTU-nephelometric turbidity unit, TDS-total dissolved solids, MPN-most portable number, COD-chemical oxygen demand, BOD-biochemical oxygen demand, cfu-colony forming unit and NS-not stated.

Table 4.13: Characterization results of PW before and after adsorption using AESA as biosorbent

Parameters	Before	After	WHO
pH	5.6	4.59	6.6-8.5
Turbidity (NTU)	4.47	1.24	< 11.75
Total hardness (mg/L)	93.6	68.64	500.00
Fe^{2+} (mg/L)	1.45	1.24	0.3
So_4^{2-}(mg/L)	4765.97	42.52	250.00
Cl^- (mg/L)	438.83	166.90	200.00
TDS (mg/L)	3.86	0.43	50.00
COD (mg/L)	56.98	38.65	NS
Total nitrogen (mg/L)	Nil	Nil	11.23
Total phosphorus (mg/L)	Nil	Nil	NS

Total coliform (MPN/100ml)	Nil	Nil	NS
Eschericha coli (cfu/100ml)	Nil	Nil	NS
Electrical conductivity (µmho/cm)	785.34	746.87	1250.00
BOD_5 (mg/L)	11.98	0.87	< 1

Note: NTU-nephelometric turbidity unit, TDS-total dissolved solids, MPN-most portable number, COD-chemical oxygen demand, BOD-biochemical oxygen demand, cfu-colony forming unit and NS-not stated.

Table 4.14: Characterization results of PW before and after adsorption using OSA as biosorbent

Parameters	Before	After	WHO
pH	5.6	4.65	6.6-8.5
Turbidity (NTU)	4.47	1.30	< 11.75
Total hardness (mg/L)	93.6	66.65	500.00
Fe^{2+} (mg/L)	1.45	1.65	0.3
So_4^{2-}(mg/L)	4765.97	41.86	250.00
Cl^- (mg/L)	438.83	174.43	200.00
TDS (mg/L)	3.86	0.23	50.00
COD (mg/L)	56.98	21.86	NS
Total nitrogen (mg/L)	Nil	Nil	11.23
Total phosphorus (mg/L)	Nil	Nil	NS

Total coliform (MPN/100ml)	Nil	Nil	NS
Eschericha coli (cfu/100ml)	Nil	Nil	NS
Electrical conductivity (µmho/cm)	785.34	776.95	1250.00
BOD_5 (mg/L)	11.98	0.65	< 1

Note: NTU-nephelometric turbidity unit, TDS-total dissolved solids, MPN-most portable number, COD-chemical oxygen demand, BOD-biochemical oxygen demand, cfu-colony forming unit and NS-not stated.

4.1.2Characterization results for biocoagulants and biosorbents

The results of proximate analysis of precursors used in preparation of biocoagulants were determine using the standard methods described in the (AOAC, 2005) are shown in Table 4.15. From the table, the crude protein for DMC and OSC are high, which agrees with the literature result that the active coagulating agent is dimeric cationic peptides, which are capable of destabilizing the anionic pollutants in the wastewaters (Obiora-Okafor and Onukwuli, 2015). Also the crude fibres contribute immensely to its ability of removing insoluble particles from wastewaters. While the characterization results of biosorbents using standard test (ASTM) were presented in Table 4.16 which shows that the acid treated biosorbents have high surface area and iodine number (Gupta, et al., 2003; Hossain, et al., 2012). Since adsorption is a surface phenomenon, the rate and extent of adsorption isa functions of the specific surface area of the adsorbent used. In this work, both the acid and salt treated adsorbents have a high surface area, of 864.02, 853.64 and 814.30m^2/g in MSA, AESA and OSA, and 783.63, 753.42 and 722.4m^2/gin MSS, AESS and OSS, respectively. This agrees with previous work (Ademiluyi, et al., 2009; Ahmenda, et al., 2000).

Since iodine number is the most fundamental parameters used to characterize activated carbon performance, it is a measure of activity level; higher number indicates higher degree of activation. Low ash content indictes a good activated carbon (Alam, et al., 2008). Also high ash content is undesirable for activated carbon since it reduces the mechanical strength of carbon and affects adsorption capacity (Valix, etal, 2004). The ash content in this study was between 3.24-4.86%.

Moisture content decreases as the temperature of activation increases. In this study, the moisture content was in the range of 2.63 to 3.64, compare to 19.5% obtained in the work done by (Ekpete, et al., 2010).

From the Table the iodine number obtained are high with values of 864.53, 754.07 and 675.25mg/g for MSA, AESA and OSA, and 800.4, 713.68 and 626.34mg/g for both acid and salt treated respectively.

Bulk density is important as it ensure sufficient mechanical strength, thereby reducing weight losses during treatment. The bulk density obtain in this study is comparable with the ones in literature (Eboibi and Eboibi, 2009; Zahangir, et al., 2008).

Table 4.15: Proximate analysis results of coagulant precursors (AOAC)

Parameter	OSC	DMC	CYC	ODC
Moisture contents (%	12.0	6.0	6.0	4.0
Ash contents (%)	7.2	2.0	3.0	6.0
Fat contents (%)	11.0	7.5	0.5	1.0
Crude protein (%)	23.0	28.0	14.9	16.8
Carbohydrate (%)	33.3	41.5	73.1	63.2
Crude fiber (%)	13.5	15.0	2.5	9.0

Table 4.16: Characterization results of Activated Carbon

Parameters/Adsorbent	**MSA**	**MSS**	**AESA**	**AESS**	**OSA**	**OSS**
Ash content (%)	4.86	3.24	4.75	3.46	4.25	3.08
Surface area (m^2/g)	864.02	783.63	853.64	753.42	814.3	722.4
Bulk density (g/cm^2)	0.39	0.42	0.42	0.55	0.54	0.63
Iodine number (mg/g)	864.53	800.4	754.07	713.68	675.25	626.34
Moisture content (%)	3.64	3.62	2.78	2.72	2.65	2.63
Yield (%)	21.43	27.52	22.85	26.05	24.60	26.30
Point of zero charge	8.0	7.56	6.1	7.0	5.4	5.0

4.1.3 Determination of point of zero charge

The point of zero charge is defined as the pH at which the surface has zero net charge (Cerovic, et al., 2007). A plot of $\Delta pH\ versus\ pH_i$, the point at which the curve cuts the horizontal line is defined as point of zero charge. Fig 4.1 and 4.2 shows the point of zero charge for acid and salt treated adsorbent. From the results it show that the adsorbent can remove cationic particles; since the adsorption of cationic particles is favoured at pH of the effluent is greater than the pH of point of zero charge (Mondal, 2009).

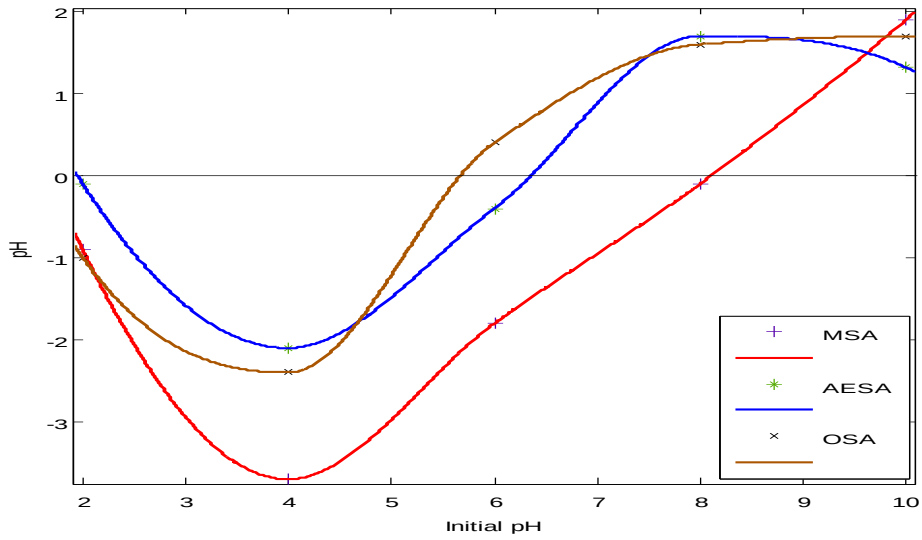

Fig.4.1: Point of zero charge for acid treated adsorbent.

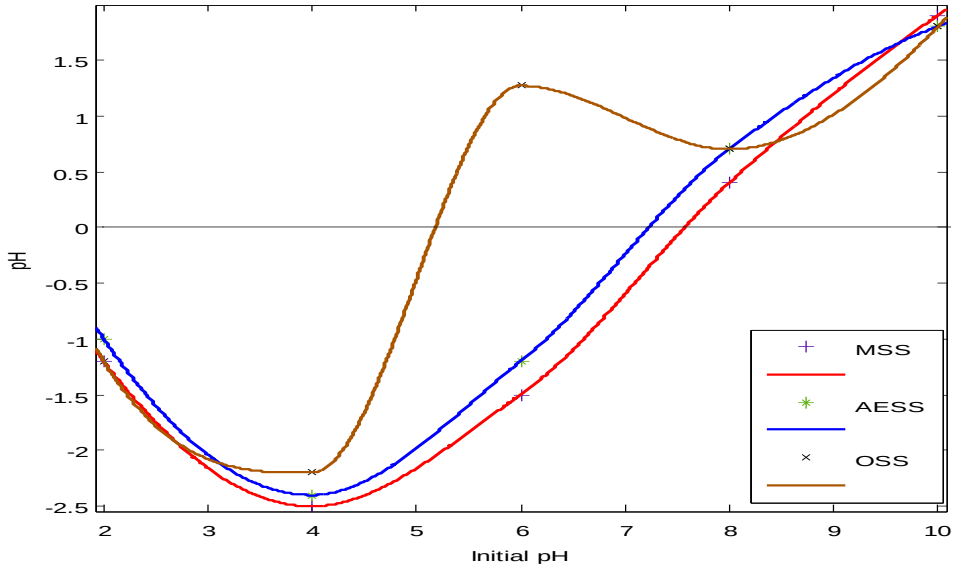

Fig 4.2: Point of zero charge for salt treated adsorbent.

4.1.4 FTIR spectra analysis

The FTIR technique is an important tool used to identify the characteristic functional groups on the surface of the biosorbent (Cherifi, et al., 2009; Danish, et al., 2011). The spectra of the biosorbent were measured within the range of 400-4000 cm^{-1} wave number. The FTIR spectra of MSA, AESA, OSA, MSS, AESS and OSS for acid and salt treated biosorbent before and after adsorption were shown in figures 4.7to 4.18. The FTIR spectra (Fig. 4.7 to 4.18) display a number of peaks pertaining to different functional groups, which reflects the complex nature of the biomassand is related with the standard in FTIR library (John Coates, 1996).The broad and intense

peak at 3429.43 $cm^{-1}$is due to the stretching of the N-H bond of amino groups and indicative of bonded hydroxyle group.The peak at 2372.44 is assigned C=C stretch of alkyn. The peaks at 1853.59, 1757.15 cm^{-1} is assigned to O-H, H bonded H stretch, carbonyl stretching of aldehyl (Bansal and Goyal, 2005 Wang, et al., 2009). The C=C stretch of aromatic alkene or N-H group of amino acid are represented by the bands at 1647.21, 1566.13 and 1517.98 cm^{-1} (Asgari, et al., 2013; Cherifi, et al., 2009). The peak at 1440.83 cm^{-1} is assigned to O-H bend in carboxylic acid.The peaks from 1300 to 1043.49 $cm^{-1}$are attributable to the presence of carboxyl and phosphate groups (Asgari, et al., 2013). The peaks at 879 cm^{-1} isassigned to C-C stretch, N-H rocking (Bansal and Goyal, 2005). The band at 428.2 cm^{-1} is assigned to C-I aromatic ring deformation. In fig.4.2, the peak at 3429.43 cm^{-1} is due to the stretching of the N-H bond of amino groups. Also the peak at 2372.44 is assigned C=C stretch of alkyn. The peaks at 1874.81, 1757.15 cm^{-1} is assigned to O-H, H bonded H stretch, carbonyl stretching of aldehyl. The C=C stretch of aromatic alhene or N-H group of amino acid are represented by the bands at 1654.92, 1568.13 cm^{-1}. The peak at 1440.83 and 1421.54 cm^{-1} is assigned to O-H bend in carboxylic acid. The peak 1111.00 and 1035.77 $cm^{-1}$is attributable to the presence of carboxyl and phosphate groups. The peak at 877.61 cm^{-1} shows the presence of aromatic –CH stretching. The peak at 713.66 and 603.77 are assigned to N-H rocking,C-H rocking, C-Cl stretching. The peaks 528.50, 493.78 428.27 cm^{-1} is assigned to C-Br stretching, C-I aromatic ring deformation. The results from fig.4.5 to 4.14, shows similar trend. From the study, the formation of new peaks and shift in wavenumber of fundamental groups indicates that functional groups were involved in adsorption process. From the result, it suggests that carbonyl, hydroxyl and amine are the main adsorption sites in the biosorbent.

Fig. 4.3: FTIR spectrum analysis of MSA adsorbent before adsorption in BRE

Fig. 4.4: FTIR spectrum analysis of MSA adsorbent after adsorptionof in BRE

Fig. 4.5 FTIR spectrum analysis ofAESA adsorbent before adsorption in BRE

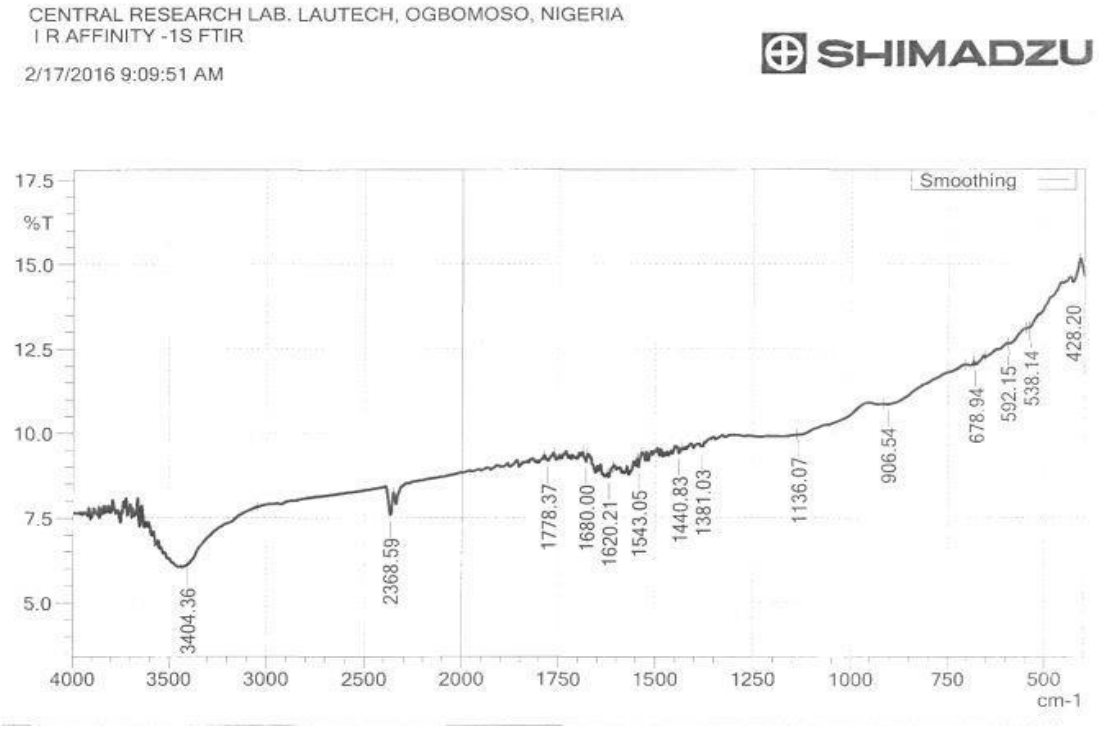

Fig.4.6: FTIR spectrum analysis of AESA adsorbent after adsorption in BRE

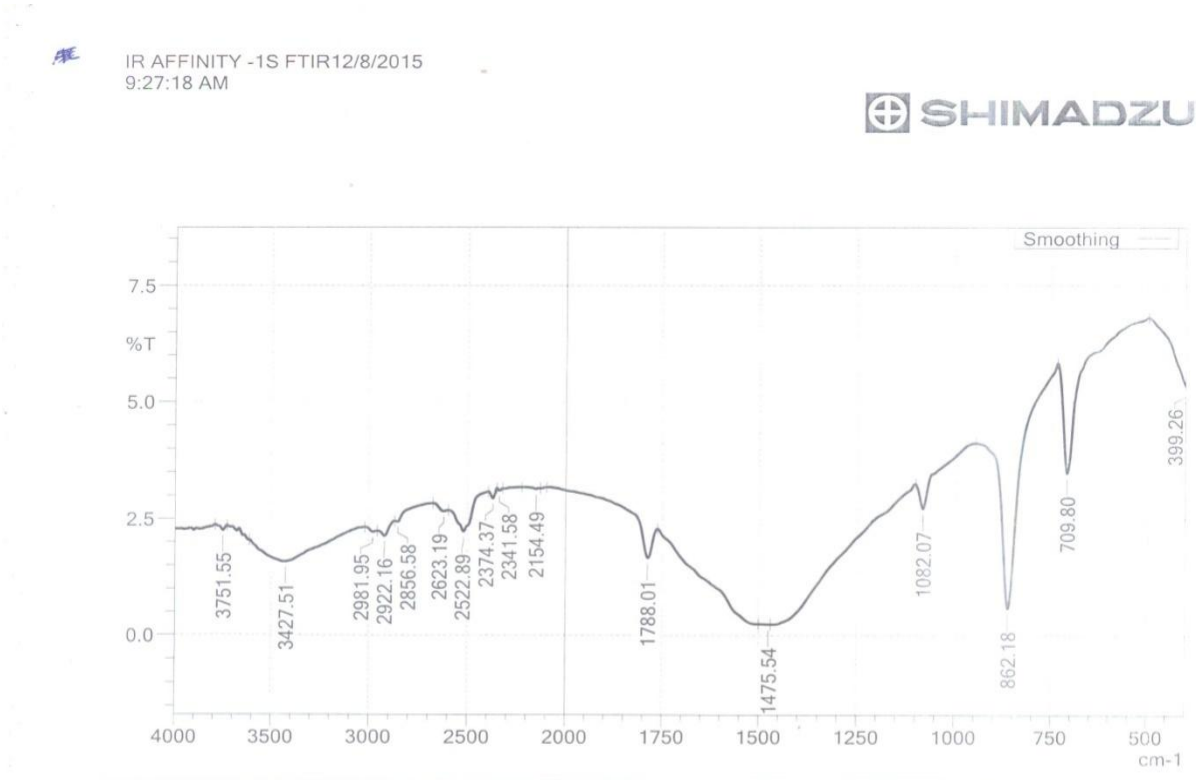

Fig.4.7: FTIR spectrum analysis of OSA adsorbent before adsorption in BRE

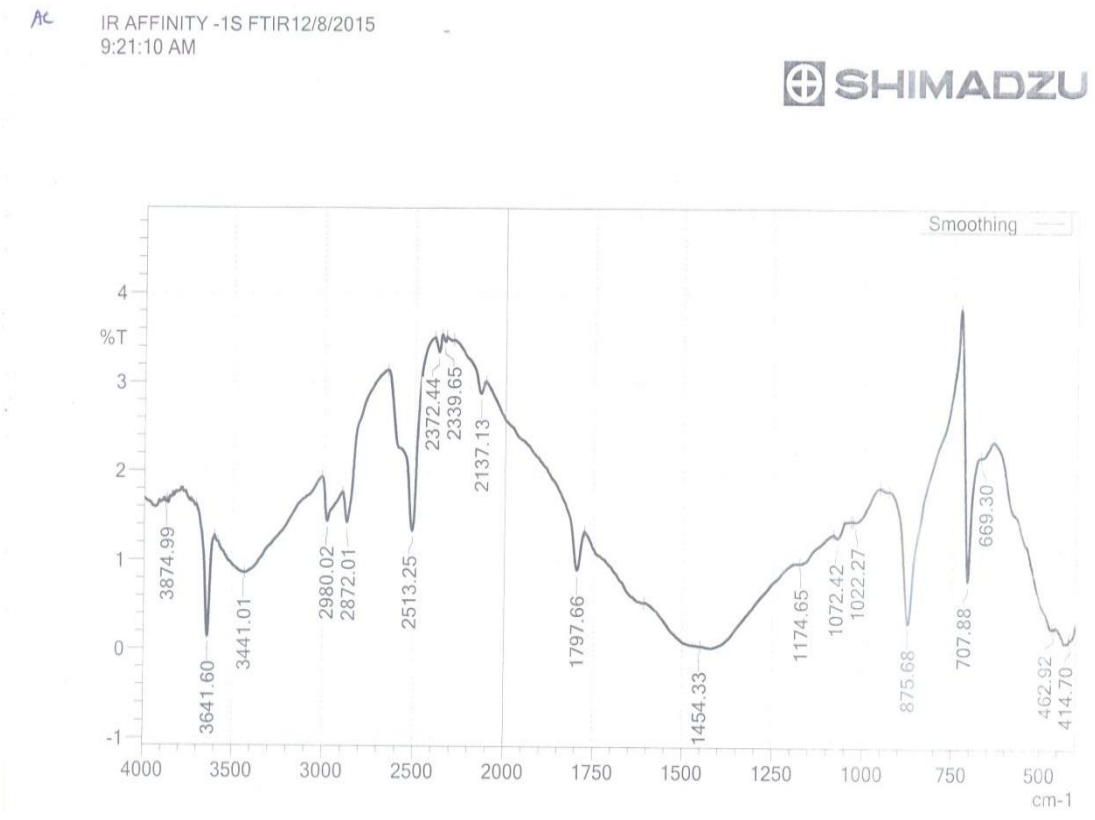

Fig. 4.8: FTIR spectrum analysis of OSA adsorbent after adsorption in BRE

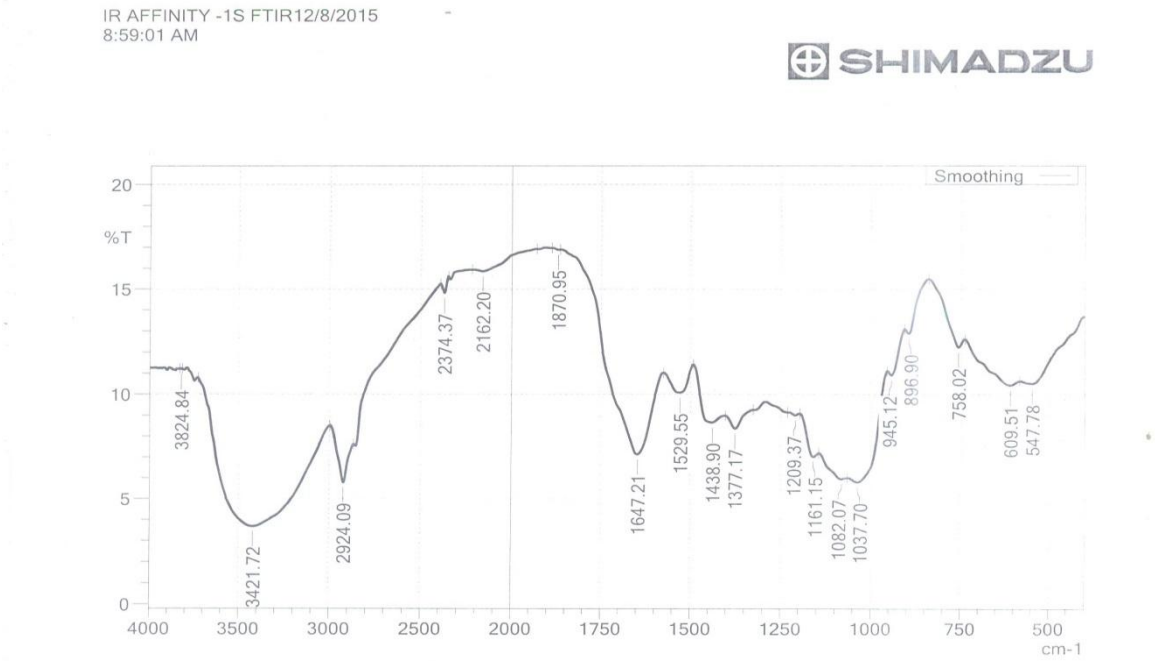

Fig 4.9: FTIR spectrum analysis of MSA adsorbent before adsorption in PW

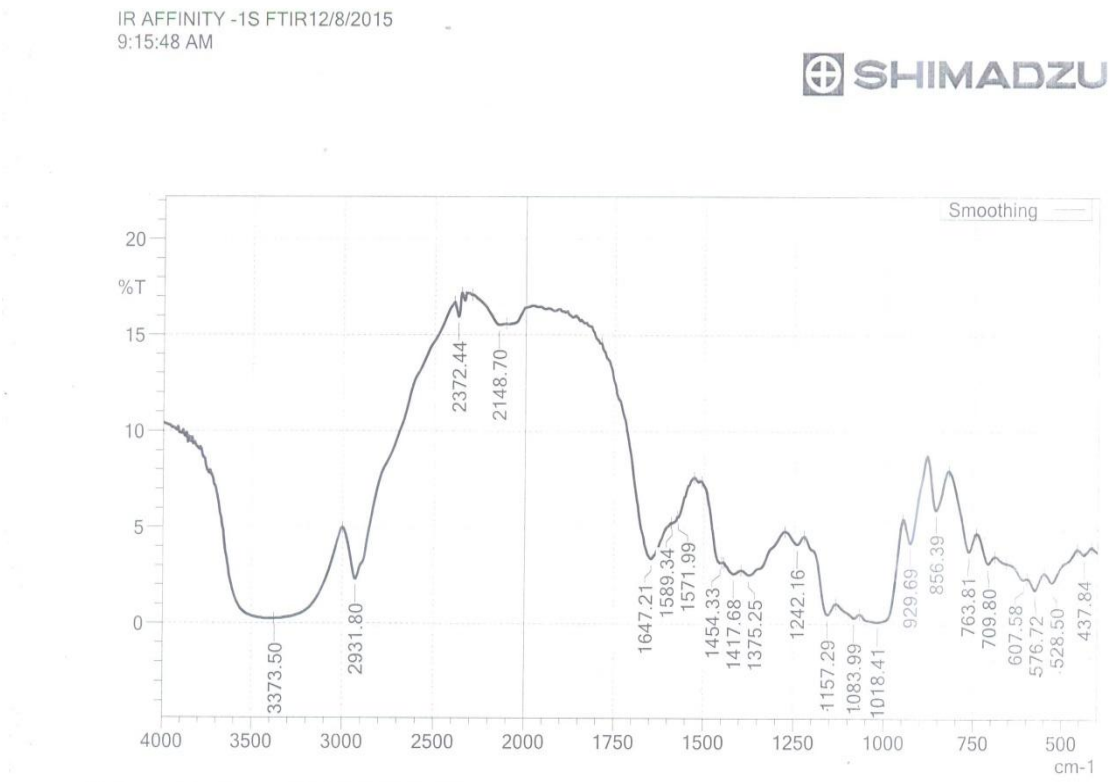

Fig 4.10: FTIR spectrum analysis of MSA adsorbent after adsorption in PW

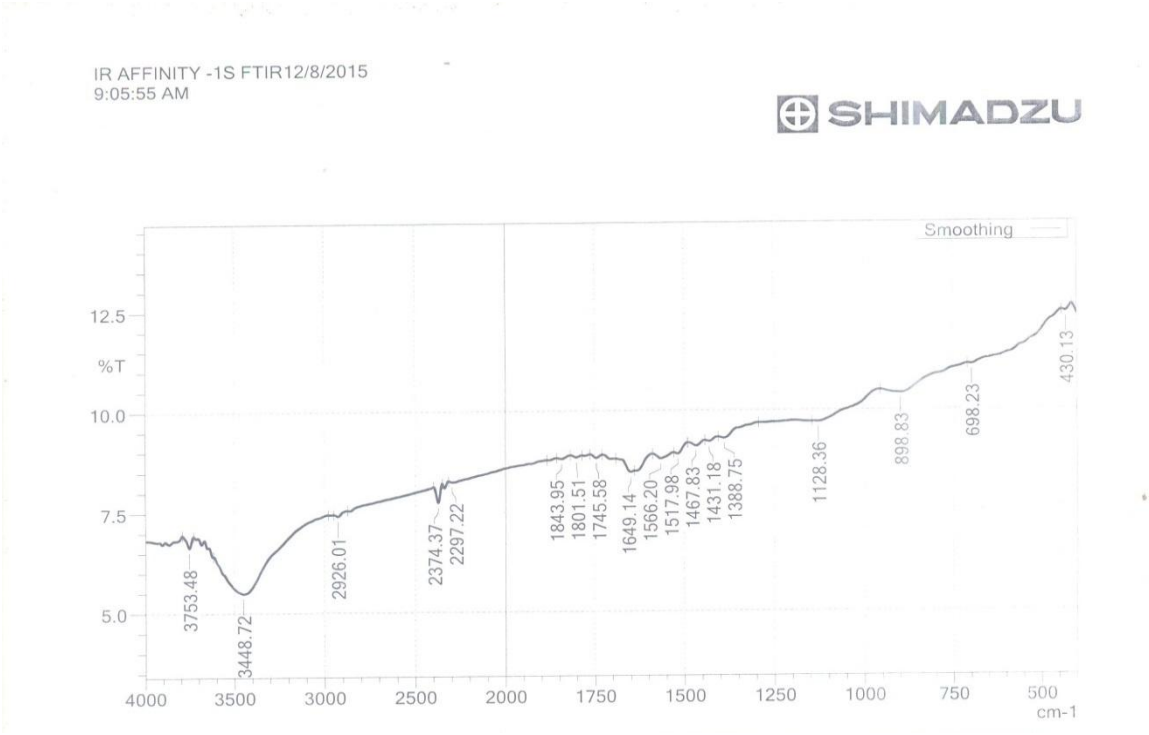

Fig 4.11: FTIR spectrum analysis of AESA adsorbent before adsorption in PW

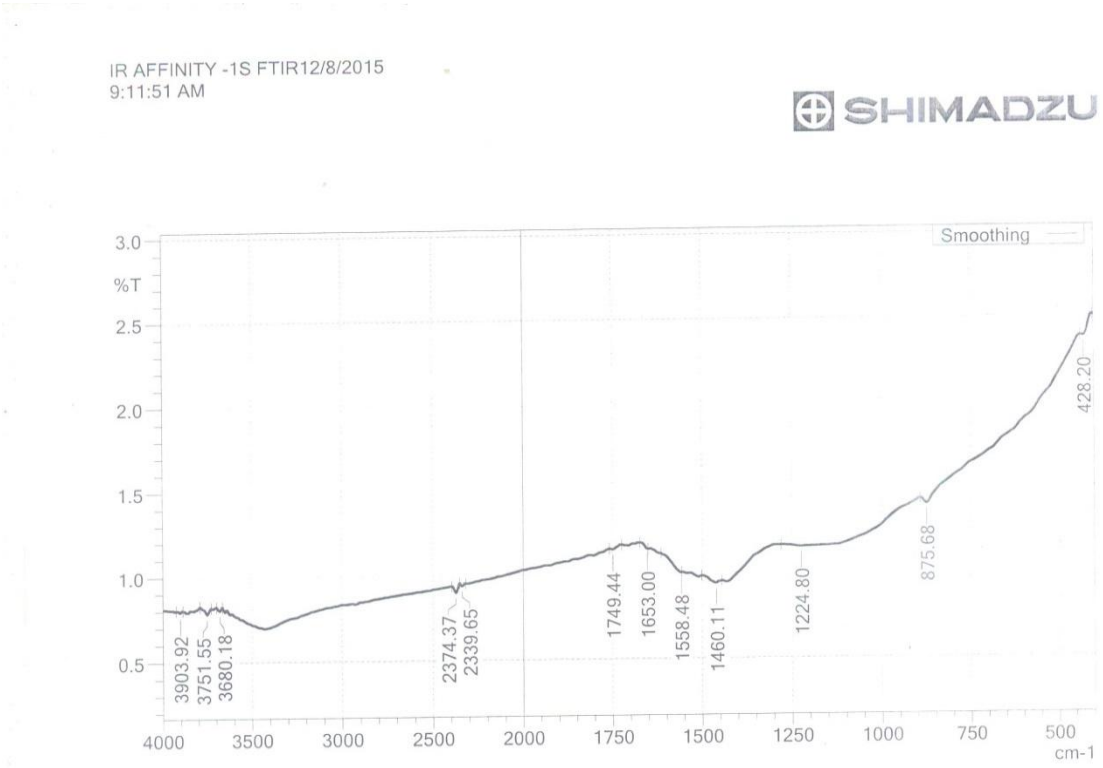

Fig. 4.12: FTIR spectrum analysis of AESA adsorbent after adsorption in PW

Fig. 4.13: FTIR spectrum analysis of OSA adsorbent before adsorption in PW

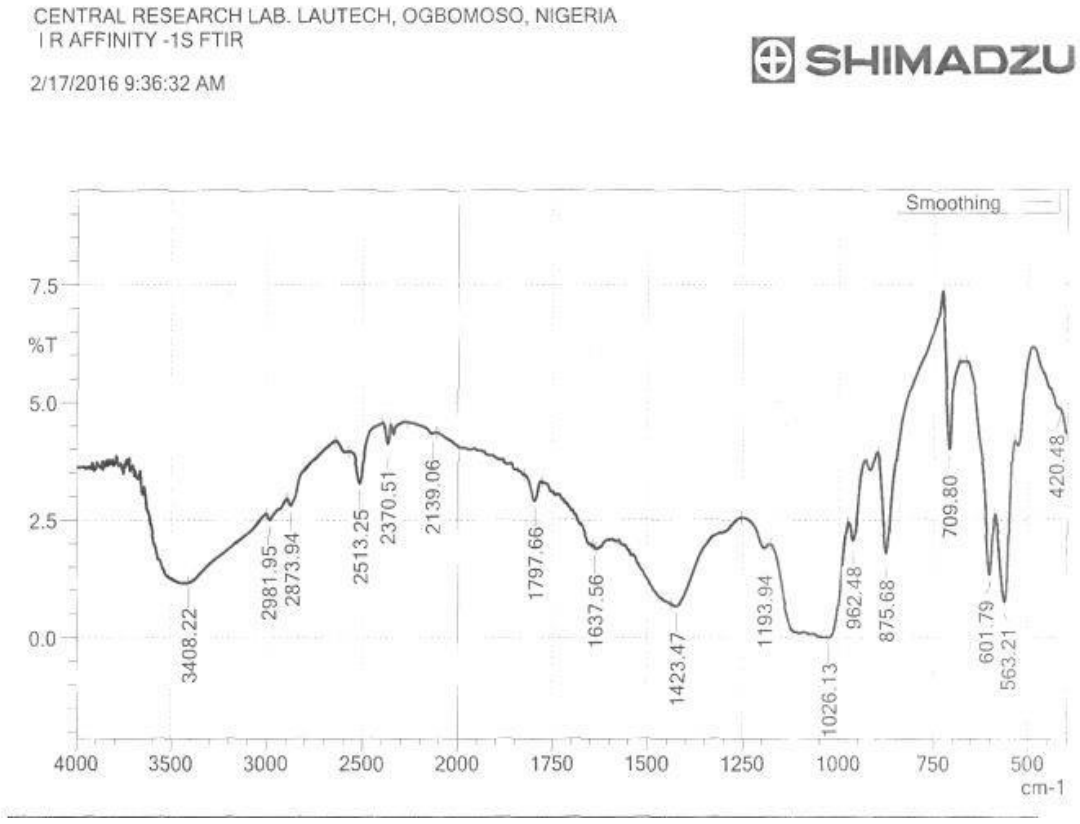

Fig. 4.14: FTIR spectrum analysis of OSA adsorbent after adsorption

4.1.5 X-ray fluorescence analysis (XRF)

The chemical composition of OSA, OSS, MSA, MSS, AESA and AESS were determined using X-ray fluorescence spectrometer. The results are shown in Tables 4.17 to 4.19 of the chemical analysis tested samples. Based on the result, calcium oxide and potassium oxide are present in relatively large amount, while other elements are low (Hossan,*et el*, 2012).

The acid treated activated carbon has higher percentage composition of those minerals than the salt activated carbon. According to Hossan,*et al* (2012), acid modification decreases the organic content of adsorbent and resulting to increased porosity.

Table 4.17: XRF results of acid and salt activated carbon from *Crassostrea virginica*

Chemical constitution	values (%)	
	OSA	OSS
SiO_2	5.91	4.84
Al_2O_3	1.63	1.24
Fe_2O_3	4.46	5.84
CaO	28.2	26.65
MgO	1.48	1.98
MnO	0.05	0.03
Na_2O	0.10	0.11
K_2O	12.6	10.52
TiO_2	1.65	2.47
P_2O_5	8.56	6.34
SO_2	0.24	0.26
LOI	33.12	36.72
Total	98.12	97.72

Note: LOI-loss-on-ignition

Table 4.18: XRF results of acid and salt activated carbon from *Mucuna pruriens*

Chemical constitution	values (%)	
	MSA	MSS
SiO_2	6.72	5.84
Al_2O_3	4.32	4.08
Fe_2O_3	1.4	1.32
CaO	26.73	24.65
MgO	0.14	0.11
SO_3	1.2	1.11

Na_2O	0.34	0.32
K_2O	11.53	10.83
TiO_2	2.45	1.89
P_2O_5	2.54	2.13
M_2O_3	0.40	0.32
Cr_2O_3	1.68	1.47
SrO	0.25	0.23
ZnO	1.1	0.92
LOI	37.2	40.78
Total	98.2	96.78

Note: LOI-loss-on-ignition

Table 4.19: XRF results of acid and salt activated carbon from *Canarium schweinfurlhii*,

Chemical constitution	values (%)	
	AESA	AESS
SiO_2	4.64	4.32
Al_2O_3	3.63	3.76
Fe_2O_3	2.86	2.53
CaO	23.21	22.87
MgO	0.18	0.16
SO_3	1.2	1.13
M_2O	0.04	0.01
Na_2O	0.64	0.60
K_2O	8.43	8.39
TiO_2	2.65	2.13
P_2O_5	7.63	6.60
SO_2	0.34	0.25
LOI	42.55	45.25
Total	98.55	98.35

Note: LOI-loss-on-ignition

4.1.6 X-ray diffraction analysis (XRD)

X-ray diffraction technique is a powerful tool used to analyze the crystalline nature of material. If the material under investigation is crystalline, well defined peaks are observed while non-crystalline or amorphous system show a hollow instead of a well-defined peaks (Nammasivan and Kavtha, 2006).

The X-ray defraction results for the activated carbon were presented in Table 4.20, whilethe X-ray diffraction pattern are presented in Figures 4.15 to 4.17. The XRD of MSA, MSS, AESA and AESS shows a broad peaks (fig. 4.15 and 4.16), which indicates the presence of high content of amorphous carbon, while in figs 4.17shows a clear crystalline of OSA and OSS. In addition, several other low intensity peaks corresponding to other crystalline phases of carbon have also been observed. The adsorbents with broad peaks and absence of sharp peaks, reveals predominantly amorphous structure which is an advantageous property for well-defined porous adsorbent (Tongpoothor et al., 2011). This result was also reported by other researchers (Jenkins and Snyder, 1996).

Table 4.20: X-ray diffraction results for the adsorbents

Phase	MSA	MSS	AESA	AESS	OSA	OSS
Smectite	0.00	0.00	1.22	0.89	0.15	0.00
Palygorskite	0.00	0.00	1.09	0.00	0.00	0.82
Kaolinite	16.80	25.45	94.56	93.15	0.00	2.87
quartz	0.00	0.00	0.35	0.00	16.90	15.74
Calcite	0.00	0.00	0.00	0.21	0.85	0.61
Dolomite	0.00	0.00	0.00	0.00	0.57	2.37
Mica/illite	83.20	74.55	2.72	5.75	81.54	77.59

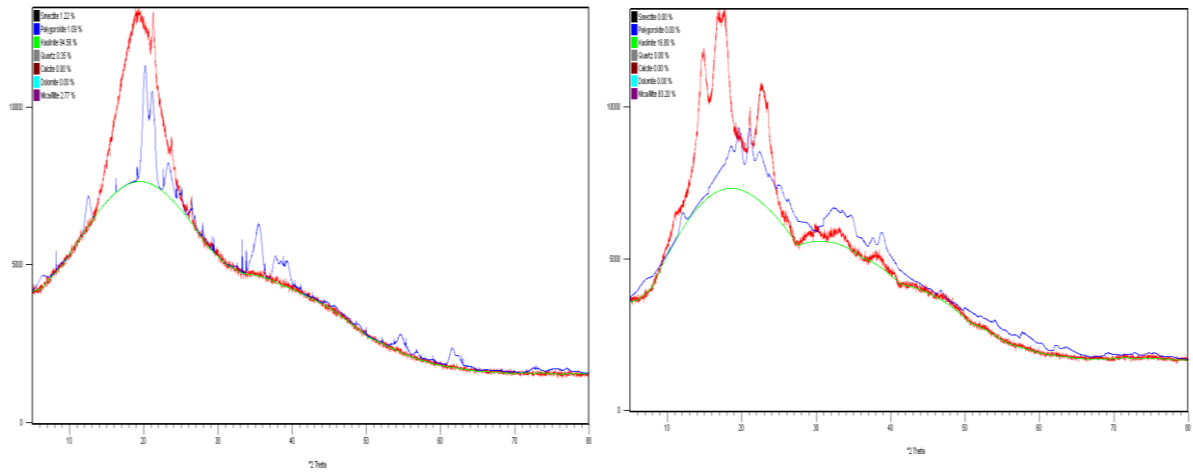

MSA MSS

Fig 4.15: X-ray diffraction pattern of *mucuna pruriens*acid (MSA) and salt treated (MSS) adsorbent

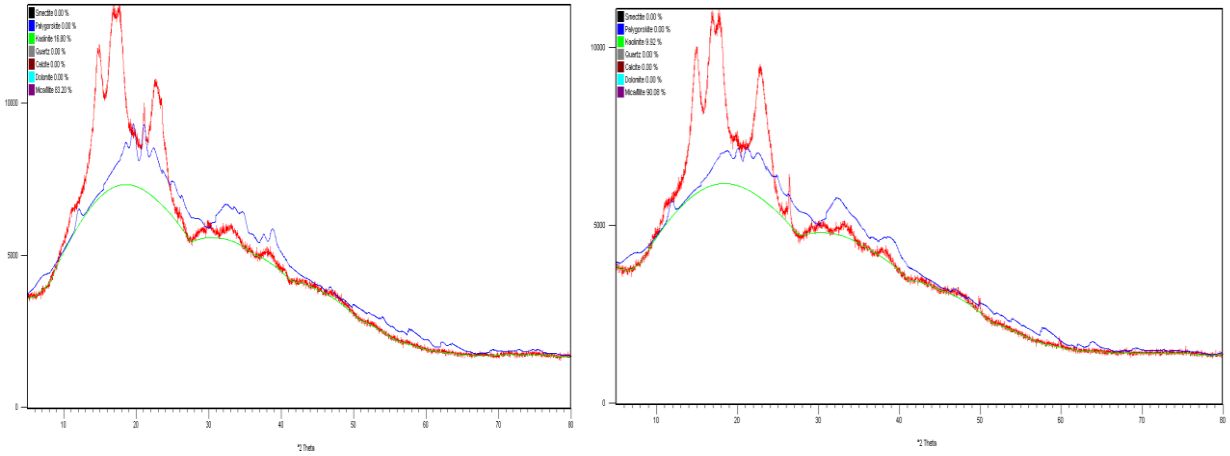

AESA AESS

Fig 4.16: X-ray diffraction pattern of *Canarium schweinfurthii* acid (AESA) and salt (AESS) treated adsorbent

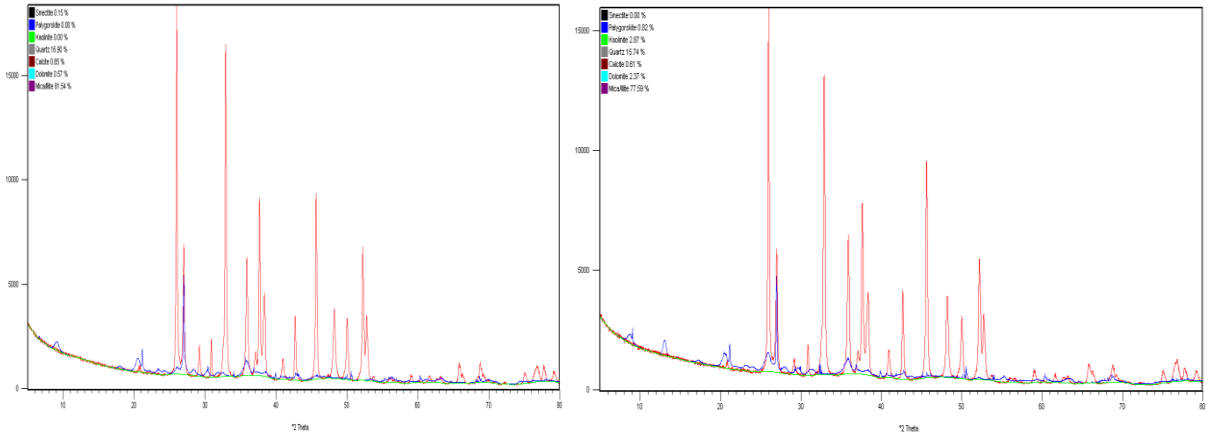

OSA OSS

Fig 4.17: X-ray diffraction pattern of *Crassostrea virginica* acid (OSA) and salt (OSS) treated adsorbent

4.1.7 SEM (Scanning electron microscopy)

The surface morphology of the biosorbent before and after adsorption was observed using SEM analysis. Plates 4.1 to 4.6 illustrate the SEM micrograph before and after adsorption. After modification with chemical agents, many various sizes of pores like honeycomb can be observed on some samples surface. From Plates 4.1A to 4.6A shows the pores and cavities which provide a large surface area for trapping of particles withinthe pores. This can be confirmed with Plates 4.1B to 4.6B, because the surface roughness changed significantly and the pores are packed with deposited particles after adsorption (Kumar, *et al*., 2011).Similar types of pore arrangement were observed in the activated carbon prepared from palm fiber jute and coconut fibers (Tan, 2008; Phan,*et al.*, 2006).

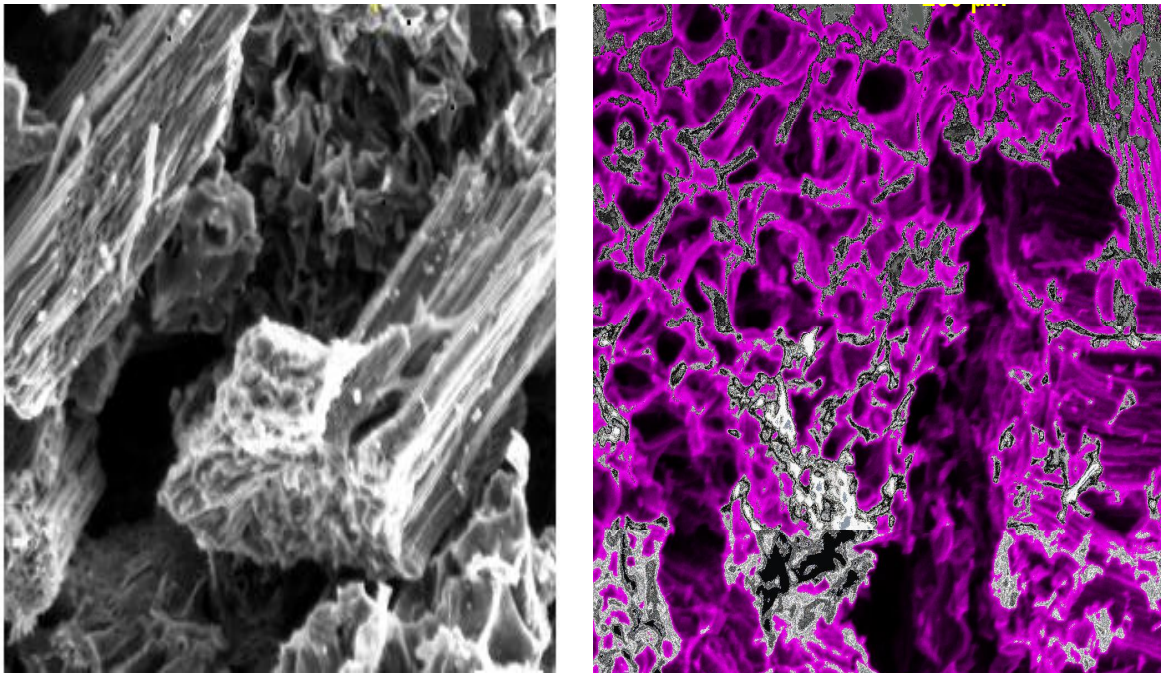

(A) Before **(B)** After

Plate 4.1: SEM micrographs of mucuma shell acid (MSA) treated adsorbent before and after adsorption at x 500 magnifications

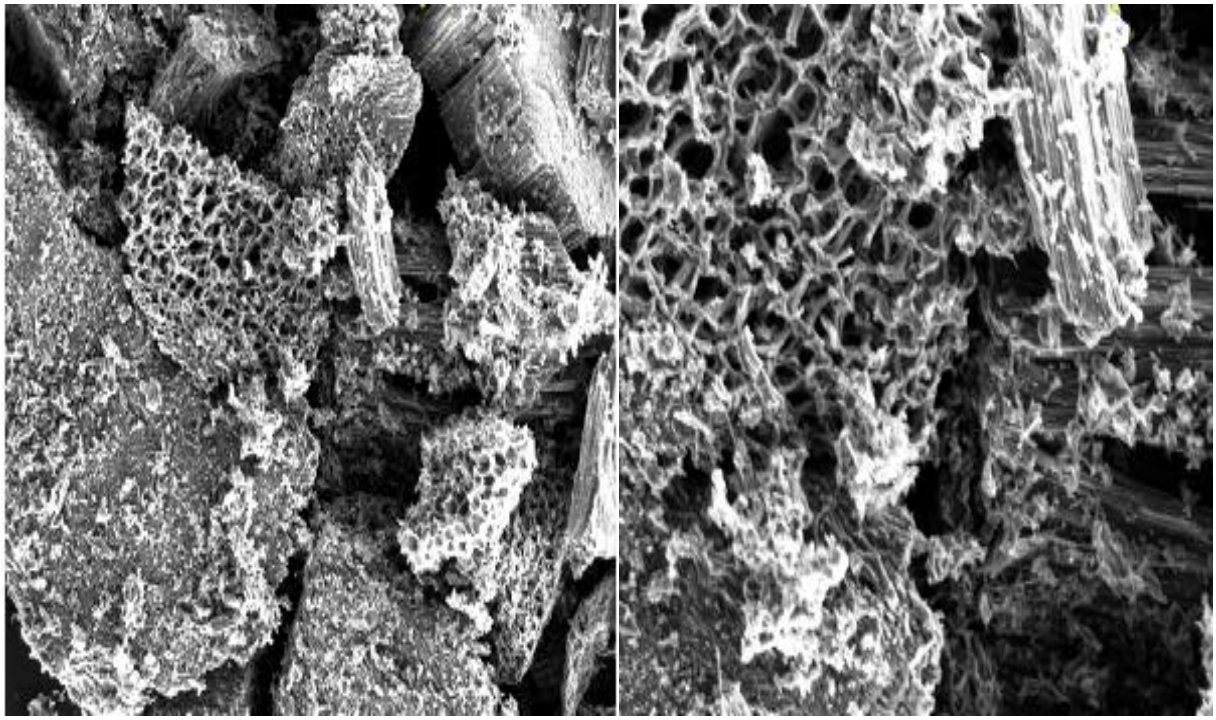

(A) Before **(B)** After

Plate 4.2: SEM micrographs of mucuma shell salt (MSS) treated adsorbent before and after adsorption at x 500 magifications

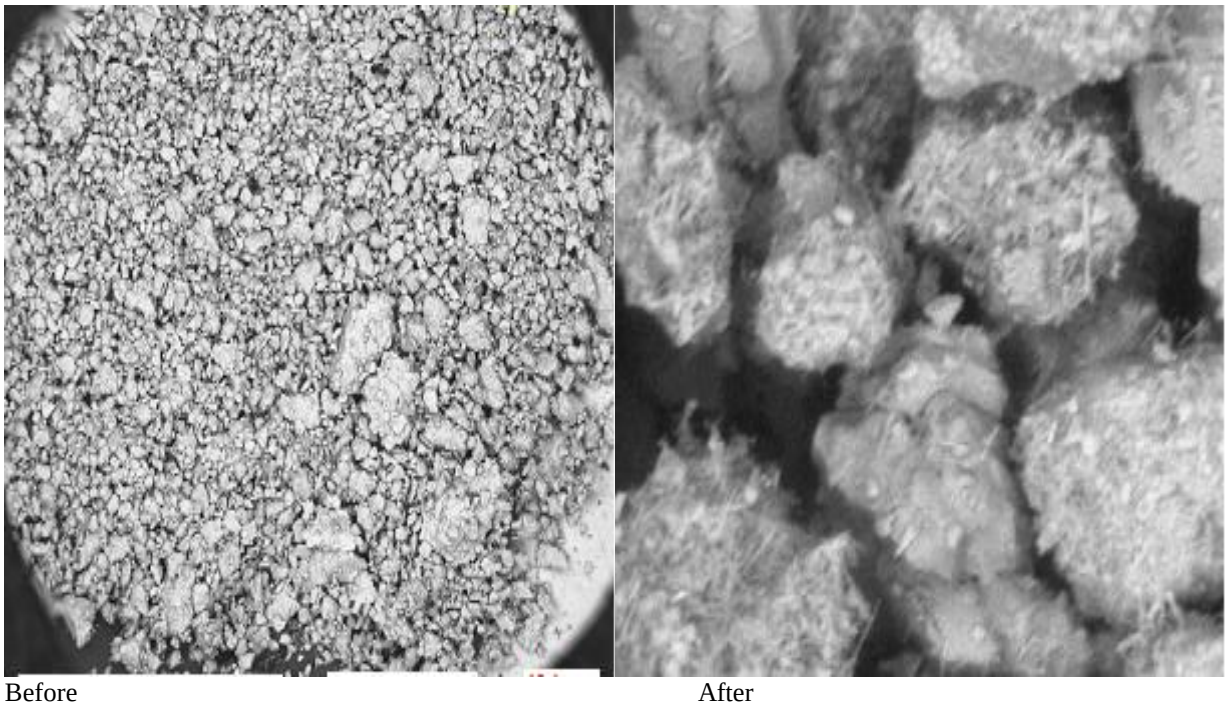

Before After

(A) **(B)**

Plate 4.3: SEM micrographs of Africa elemi seed acid (AESA) treated adsorbent before and after adsorption at x 500 maginification.

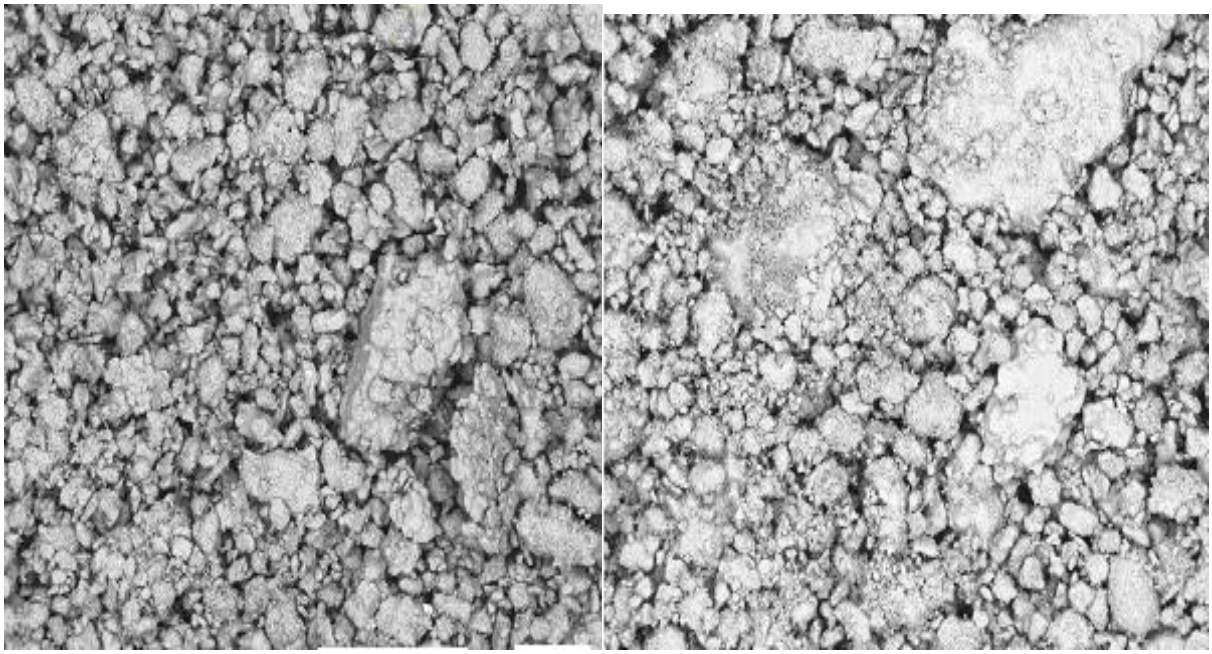

Before After

(A) **(B)**

Plate 4.4: SEM micrographs of Africa Elemi seed salt (AESS) treated adsorbent before and after adsorption at x 500 magnifications

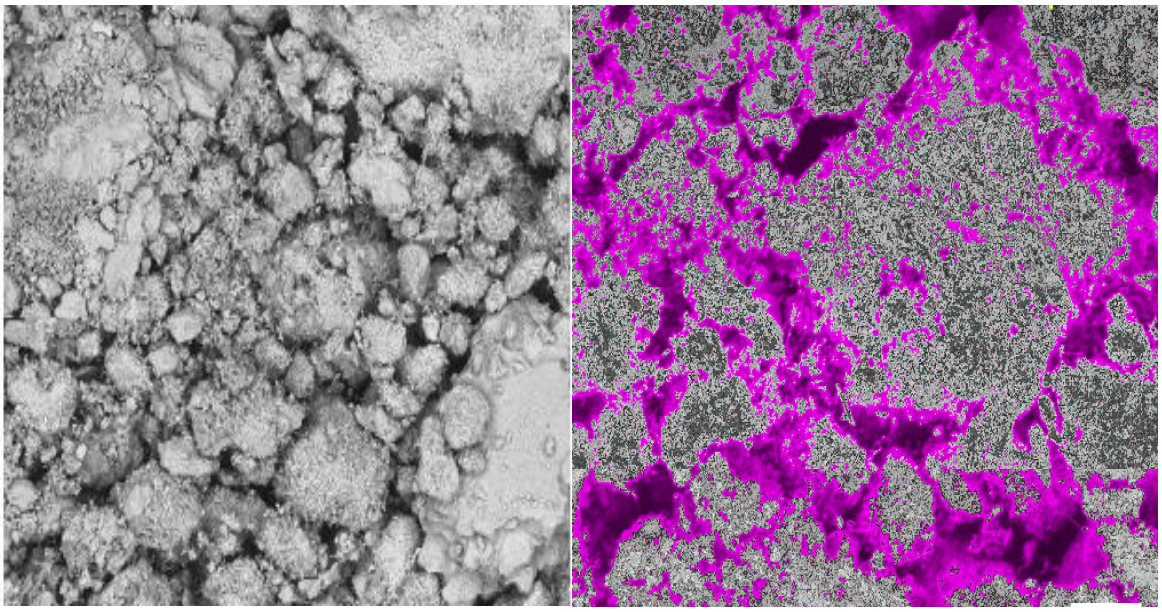

Before After

(A) **(B)**

Plate 4.5: SEM micrographs of oyster shell acid (OSA) treated adsorbent before and after adsorption at x 500 magnifications

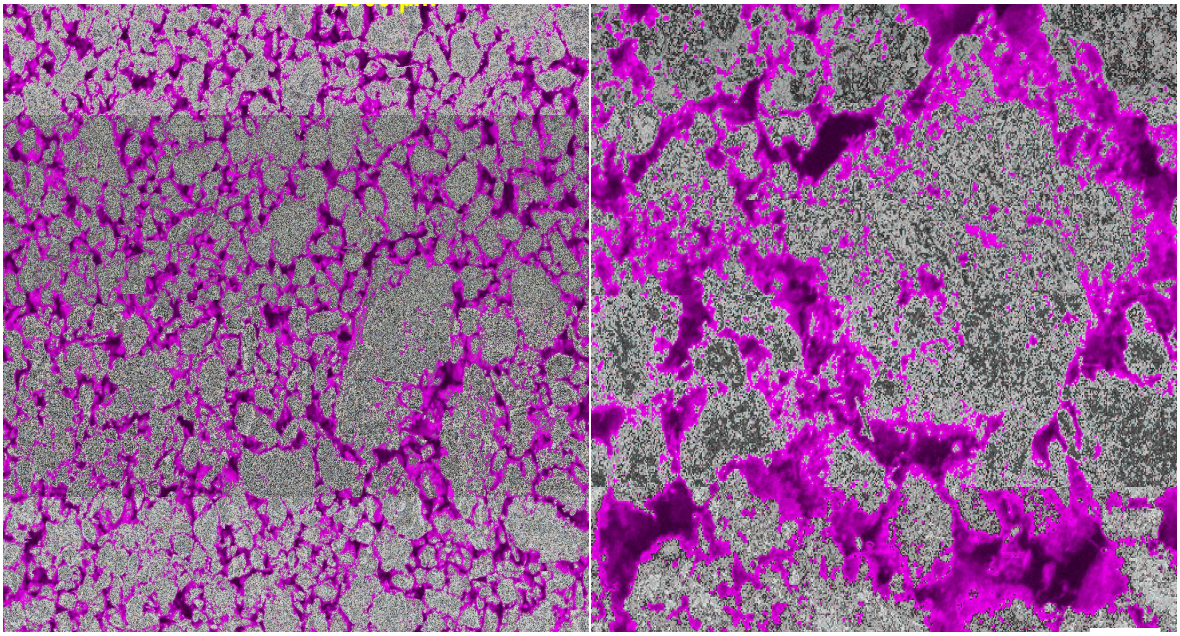

Before After

(A) **(B)**

Plate 4.6: SEM micrographs of oyster shell salt (OSS) treated adsorbent before and after adsorption at x 500 magnifications.

4.2 Effect of Biocoagulants Parameters, on BRE and PW Treatment

4.2.1 Effects of dosage, pH and settling time on coag-flocculation of BRE and PW using DMC, CYC, ODC and OSC

The effectiveness of coag-flocculation process is highly dependent on many factors such as coagulant dosage; pH and settling time of operation. In this study, DMC,CYC, ODC and OSC were used in removing turbidity from BRE and PW. Figures 4.18 to 4.27show the effect of pH, dosage and settling time with varying pH 2-10, dosage 50-500mg/L and settling time of 3- 30 minutes. In figure 4.18, the turbidity removal with 50mg/L dosage at pH 2in the first 3 minutes was in the range10-35%, as the settling increases to 30 minutes the removal was 50-80% with DMC showing as the best performing coagulant. Also with 100mg/L dosage, DMC shows 90.5% removal of turbidity, followed by OSC and ODC at 80% each respectively. The turbidity removal increases with the increase in coagulant dosage and pH, untill it reaches its highest value after which the removal will start to decrease based on previous work (Ugonabo, et al., 2012). At pH 2 and 4, dosage 100-200mg/L and settling time 30min, DMC and OSC shows high removal efficiency of turbidity in acidic medium. This could be attributed to higher degree of protonation of amino groups of the coagulants (Okolo, et al., 2014). According to Huang and Pan (2002), at low pH and lower dosage, the only mechanism for the destabilization of particles is charge

neutralization. From figures 4.20 -4.22, with increase in pH from 6 -10, ODC shows a high removal of turdity in PW. In PW, figures 4.23 - 4.27 removals followed the same pattern as in BRE.

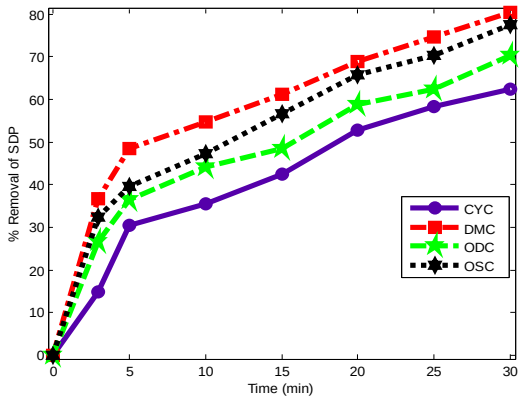

50mg/L

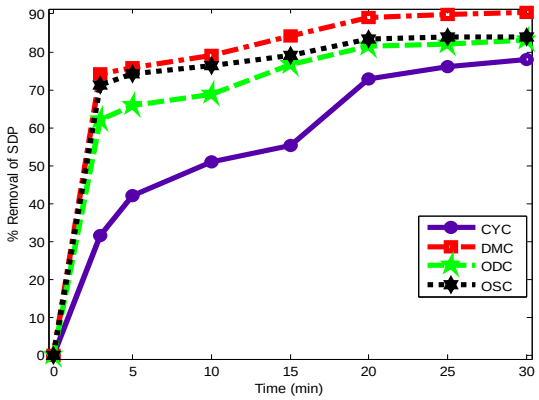

100mg/L

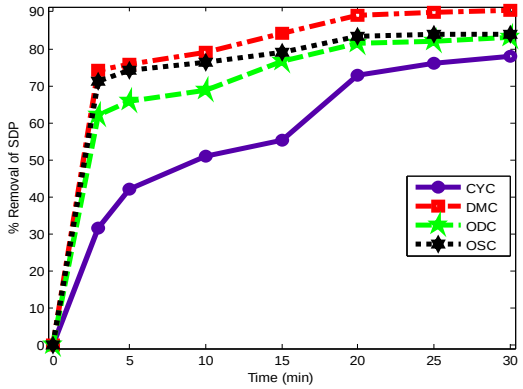

200mg/L

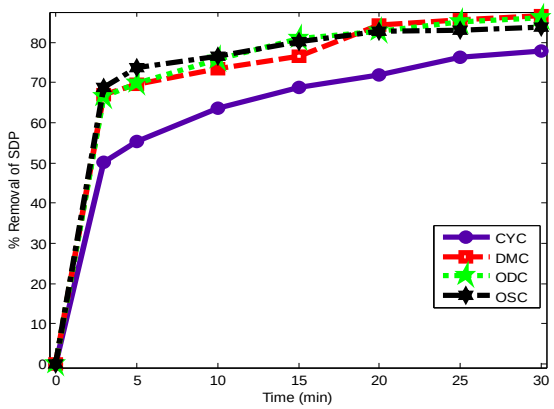

300mg/L

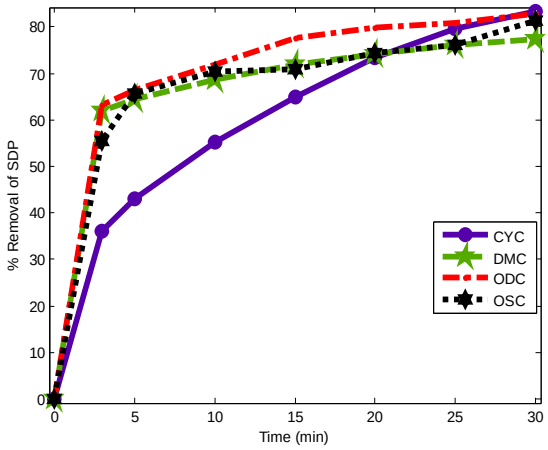

400mg/L

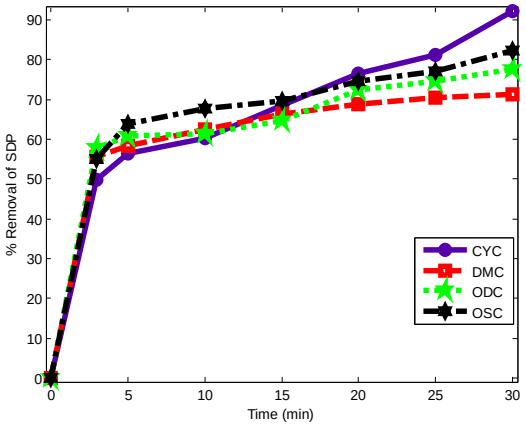

500,mg/L

Fig. 4.18 Turbidity removal efficiency in BRE at pH 2 and varying dosage with (initial concentration= 728.25mg/L, settling time = 30mins).

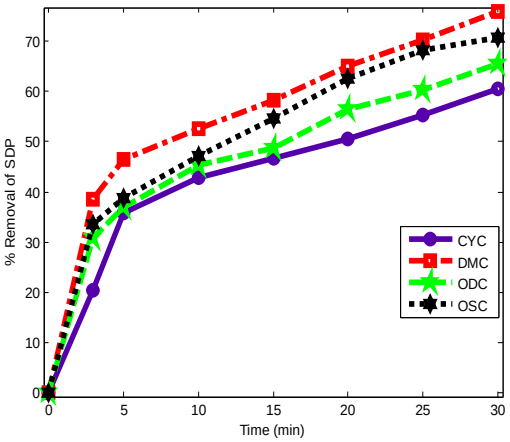

50mg/L

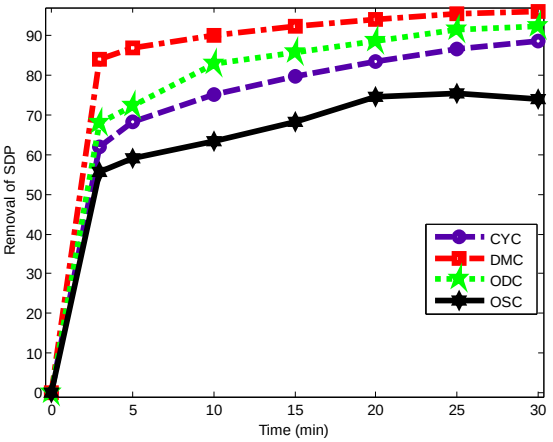

100mg/L

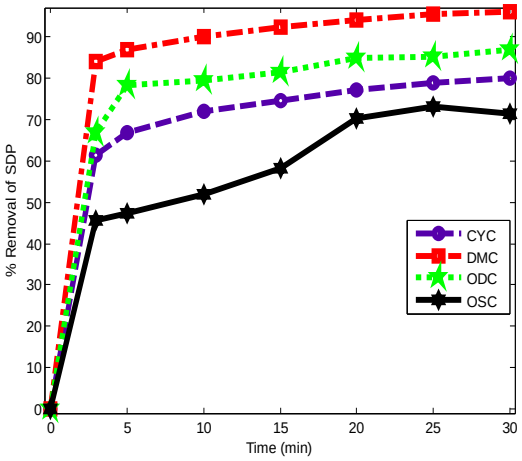

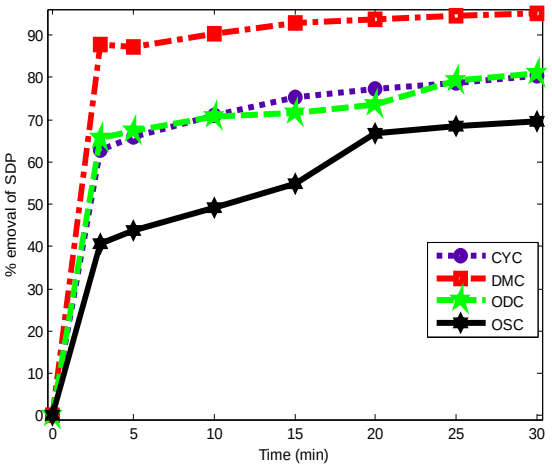

200mg/L

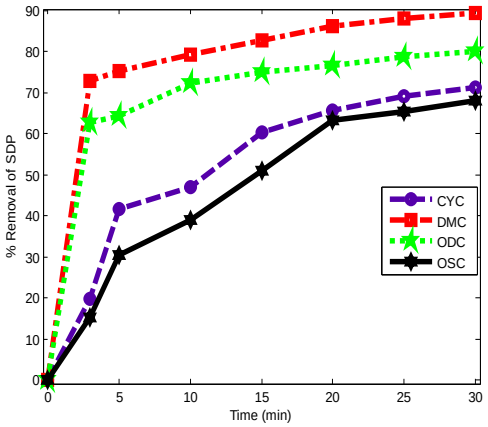

300mg/L

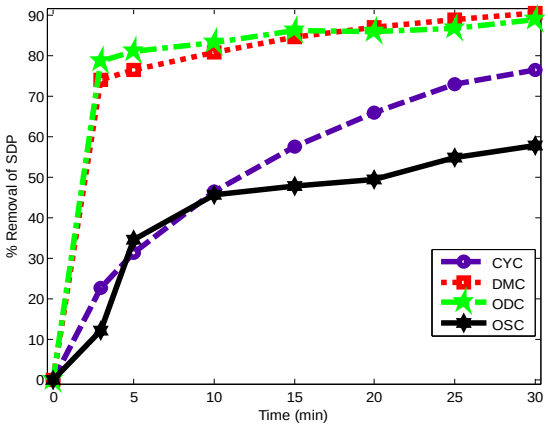

400mg/L

500mg/L

Fig. 4.19 Turbidity removal efficiency in BRE at pH 4 and varying dosage with (initial concentration= 728.25mg/L, settling time = 30mins).

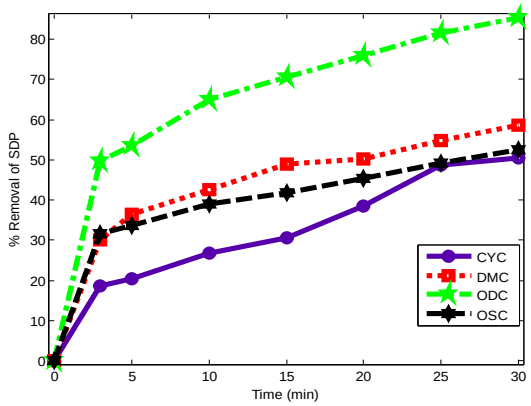

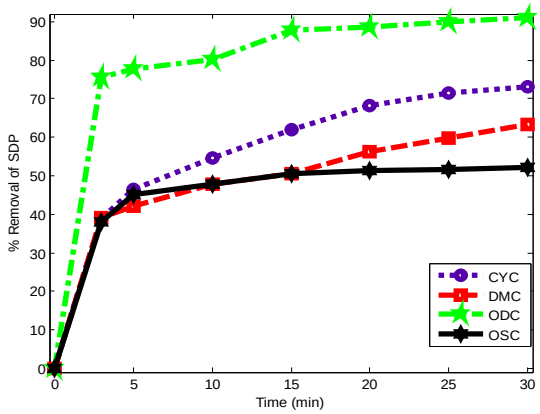

50mg/L

100mg/L

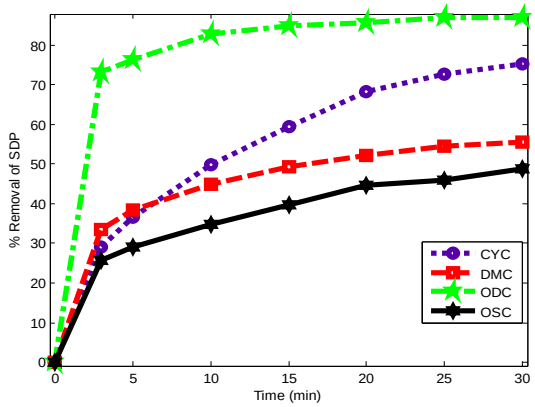

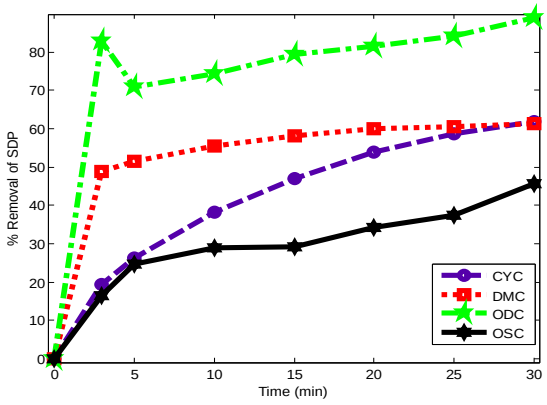

200mg/L

300mg/L

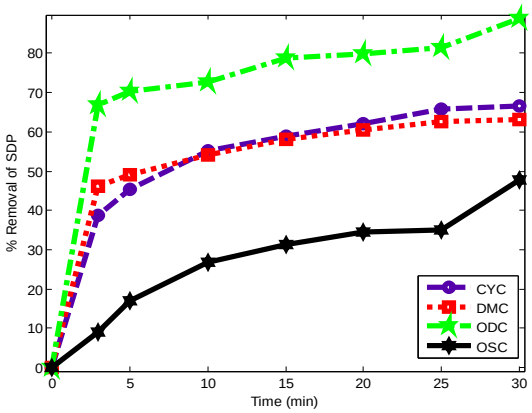

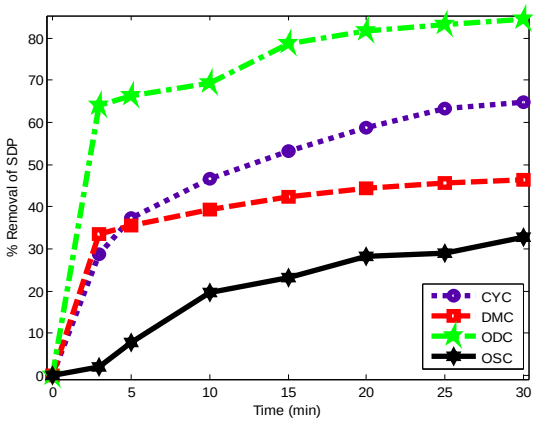

400mg/L

500mg/L

Fig. 4.20 Turbidity removal efficiency in BRE at pH 6 and varying dosage with (initial concentration= 728.25mg/L, settling time = 30mins)

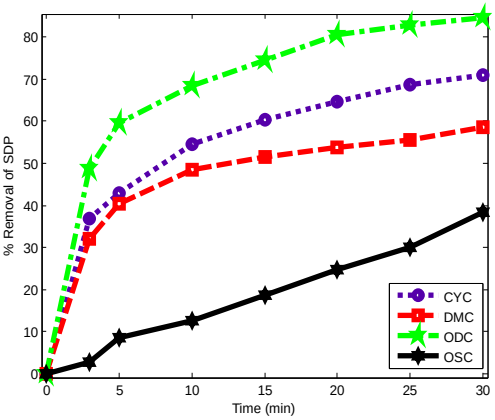

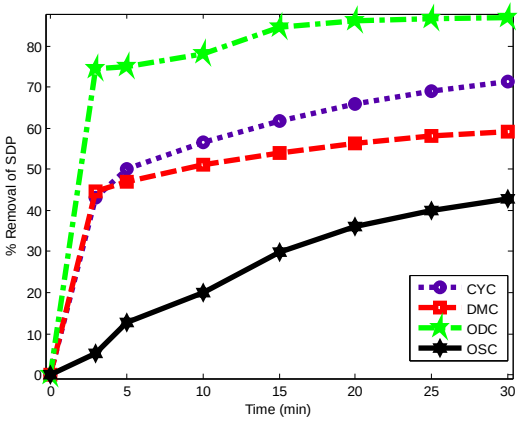

50mg/L

100mg/L

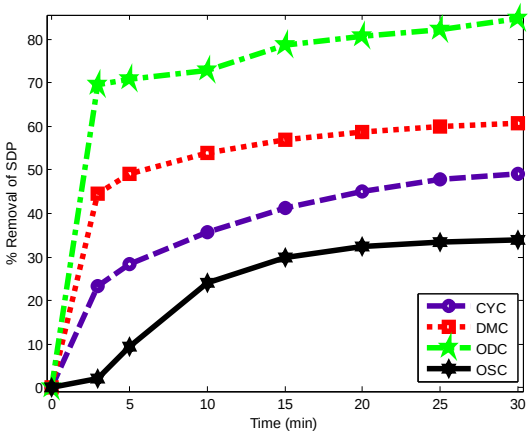

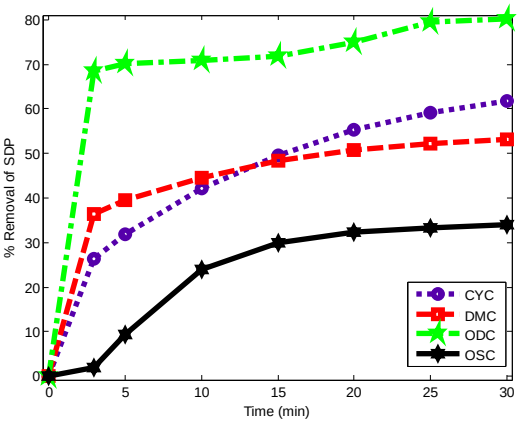

200mg/L

300mg/L

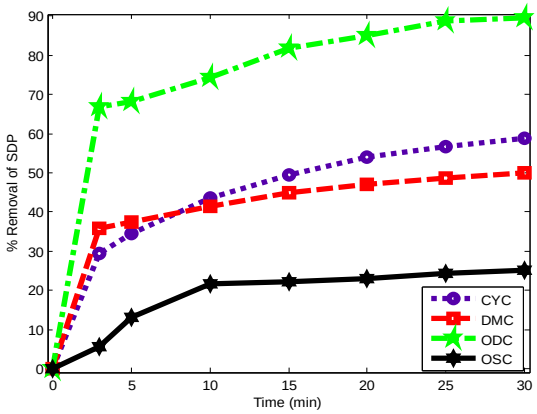

400mg/L

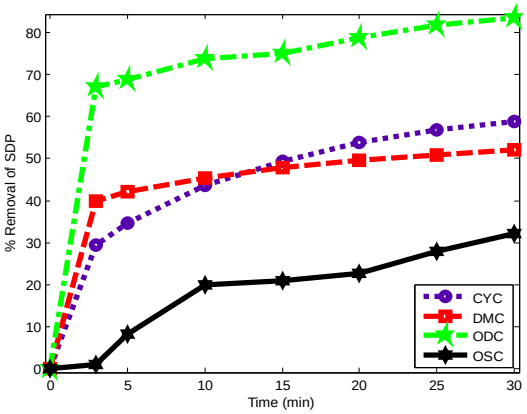

500mg/L

Fig. 4.21 Turbidity removal efficiency in BRE at pH 8 and varying dosage with (initial concentration= 728.25mg/L, settling time = 30mins).

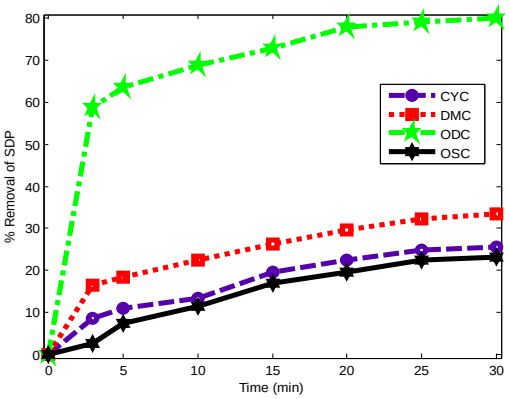

50mg/L

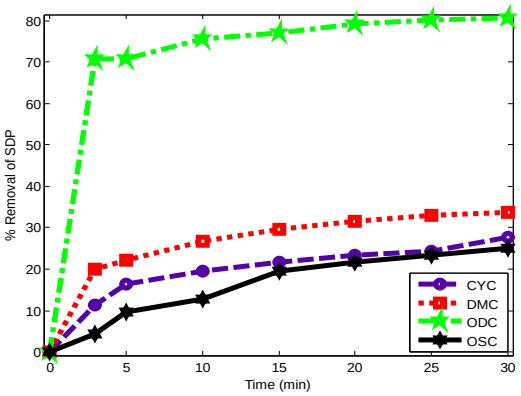

100mg/L

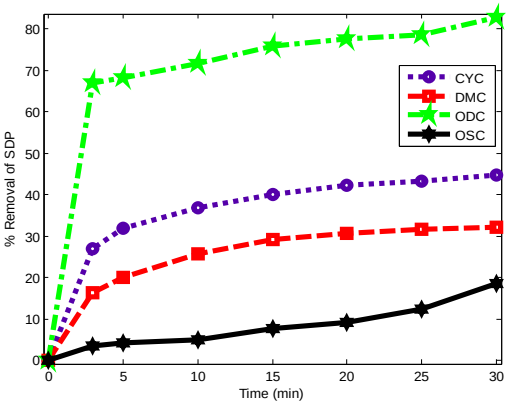

200mg/L

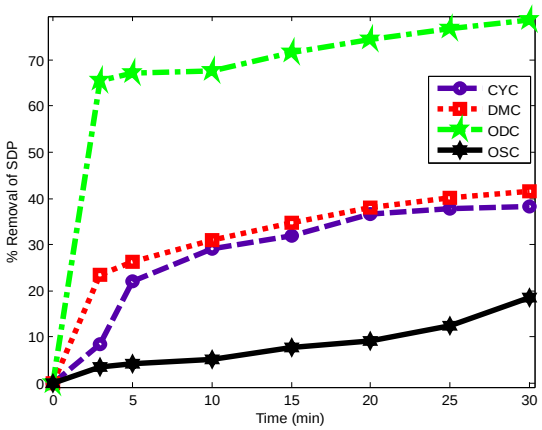

300mg/L

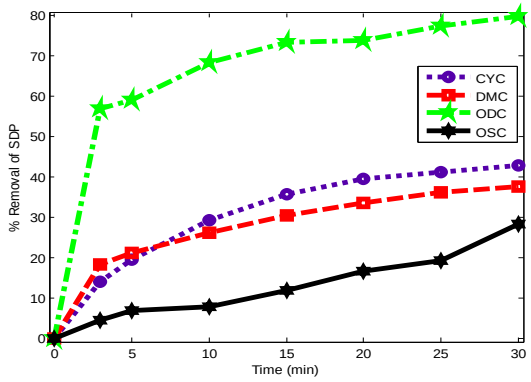

400mg/L

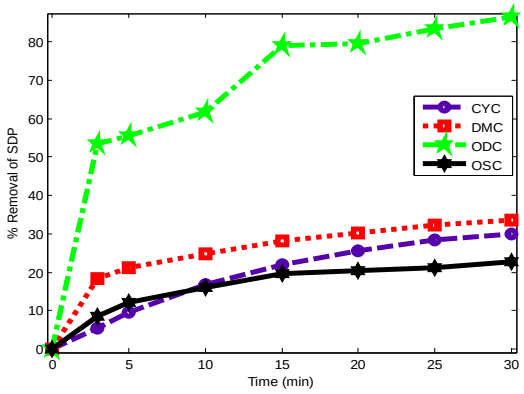

500mg/L

Fig. 4.22 Turbidity removal efficiency in BRE at pH 10 and varying dosage with (initial concentration= 728.25mg/L, settling time = 30mins).

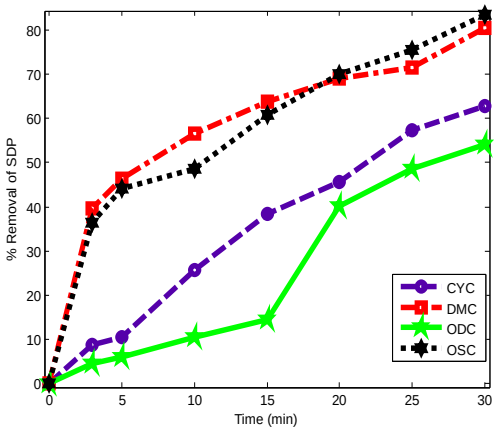

50mg/L

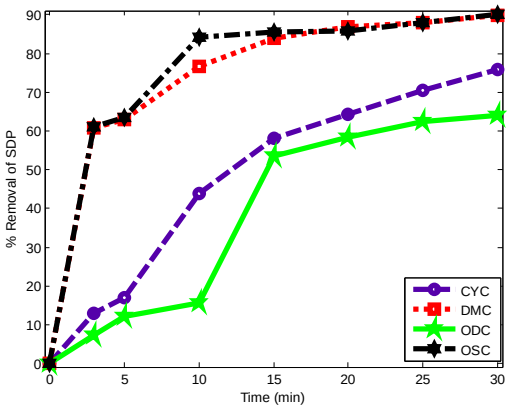

100mg/L

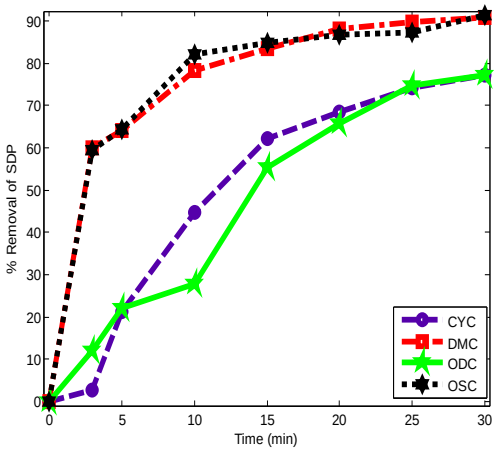

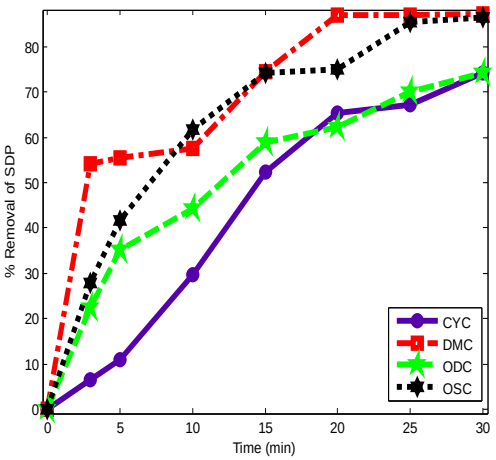

200mg/L

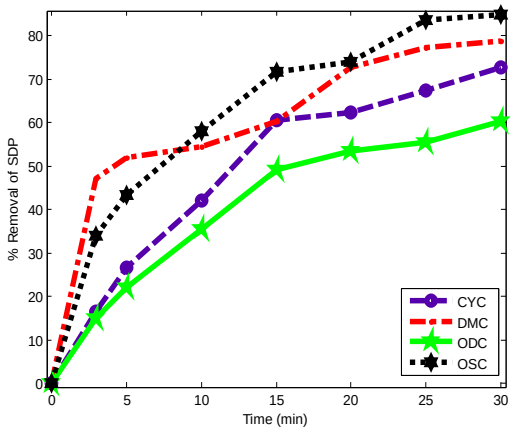

300mg/L

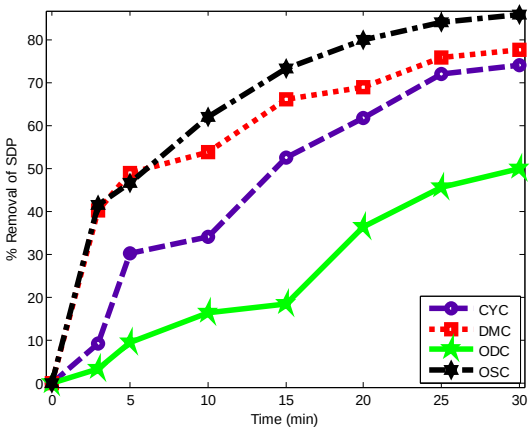

400mg/L

500mg/L

Fig. 4.23 Turbidity removal efficiency in PW at pH 2 and varying dosage with (initial concentration= 849.685mg/L, settling time = 30mins

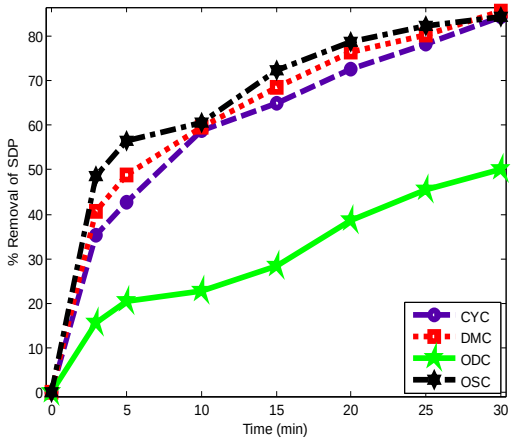

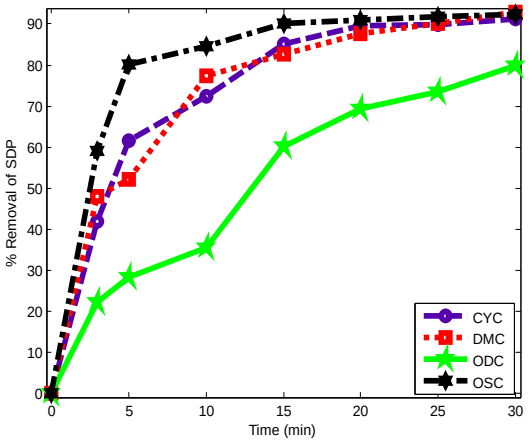

50mg/L

100mg/L

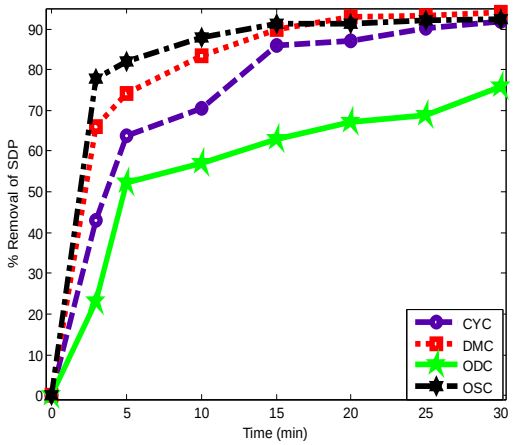

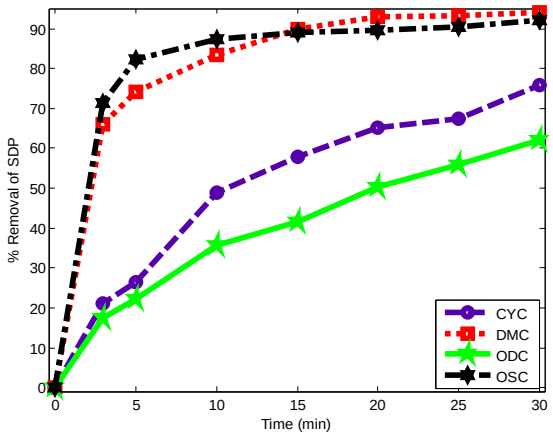

200mg/L

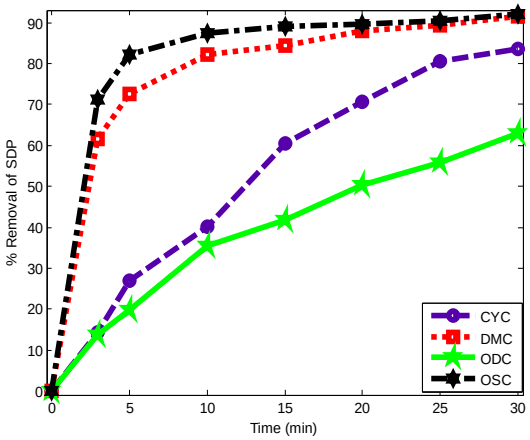

300mg/L

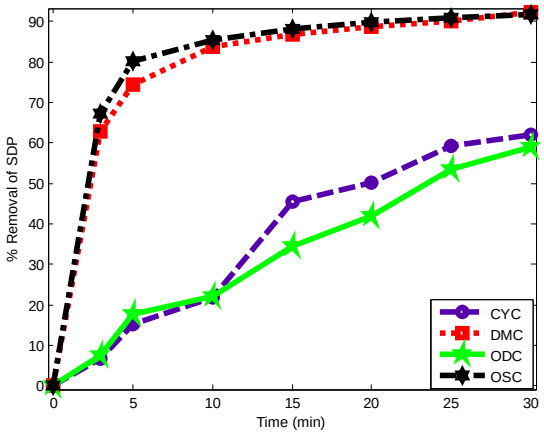

400mg/L

500mg/L

Fig. 4.24 Turbidity removal in PW at pH 4 and varying dosage with (initial concentration= 849.68mg/L, settling time = 30mins).

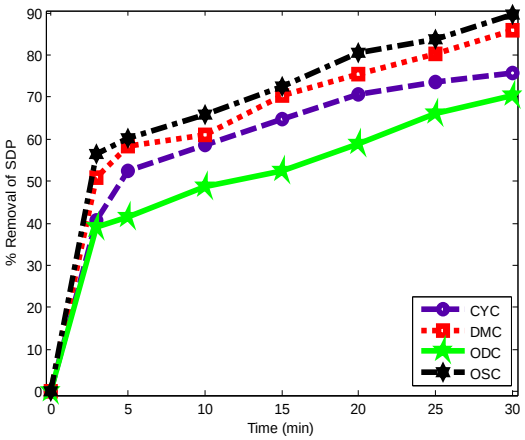

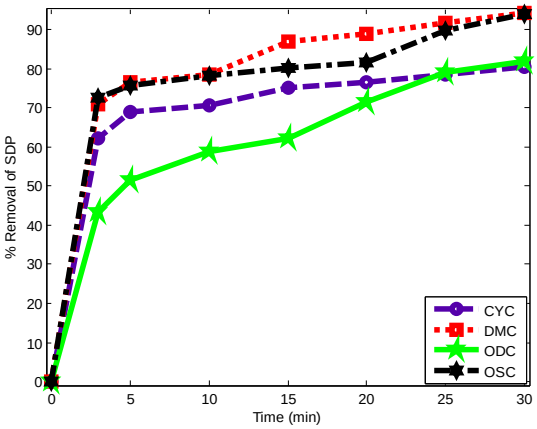

50mg/L

100mg/L

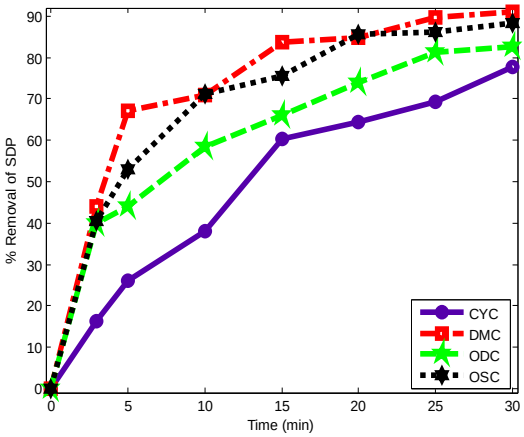

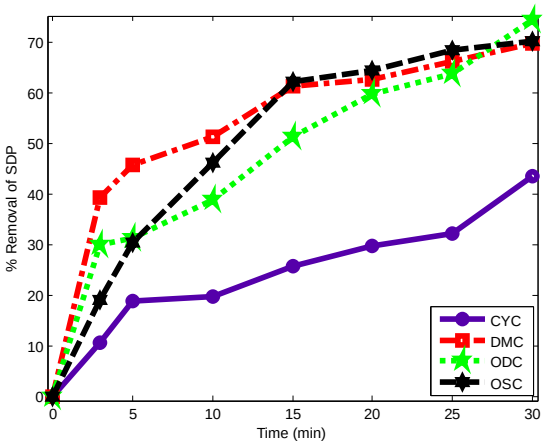

200mg/L

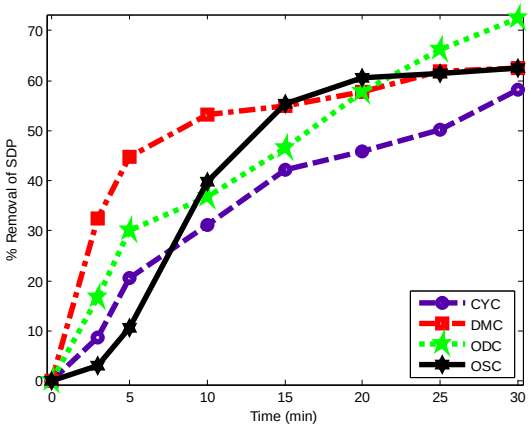

300mg/L

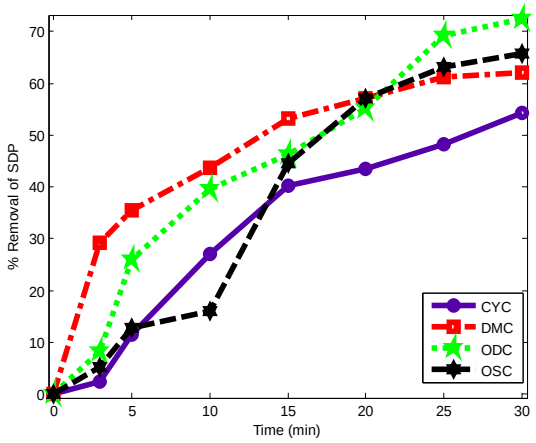

400mg/L

500mg/L

Fig. 4.25 Turbidity removal efficiency in PW at pH 6 and varying dosage with (initial concentration= 849.68mg/L, settling time = 30mins).

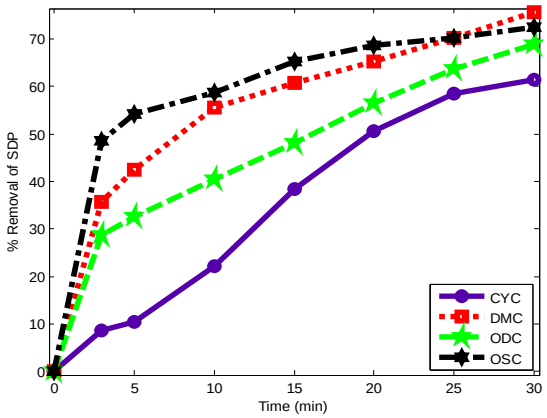

50mg/L

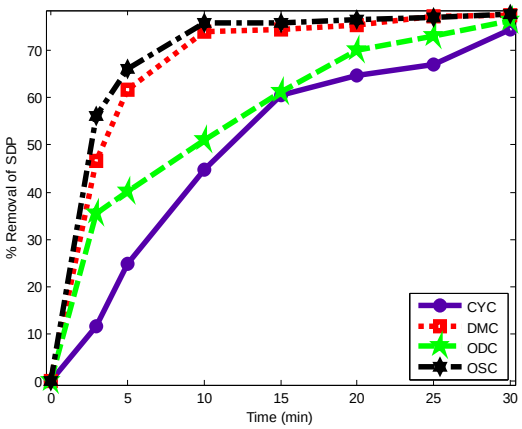

100mg/L

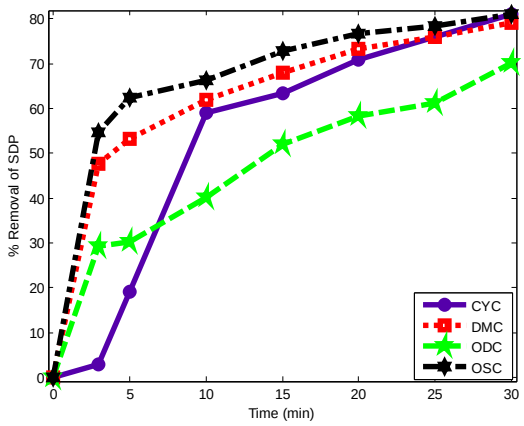

200mg/L

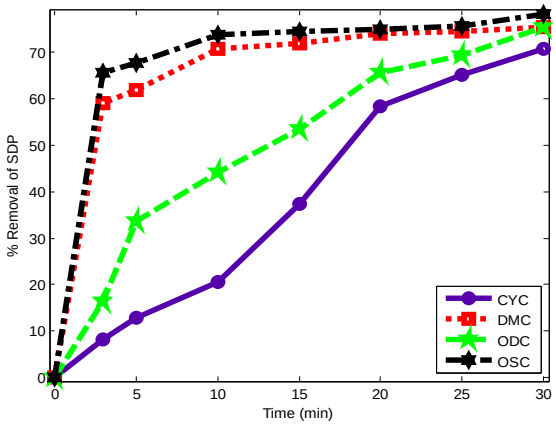

300mg/L

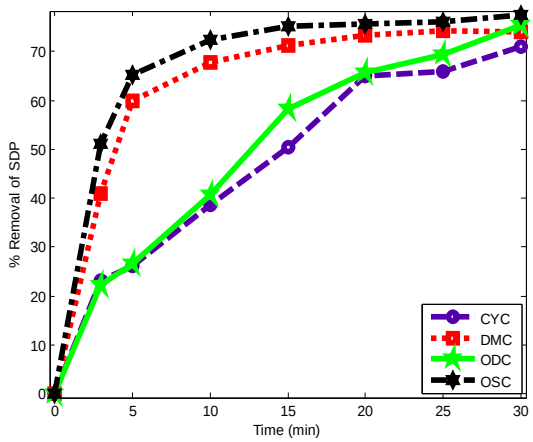

400mg/L

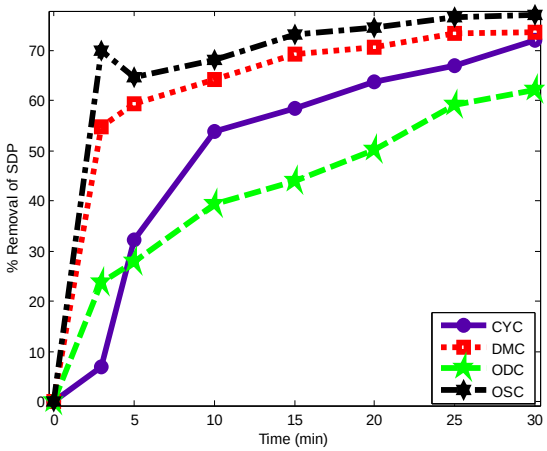

500mg/L

Fig. 4.26 Turbidity removal efficiency in PW at pH 8 and varying dosage with (initial concentration= 849.68mg/L, settling time = 30mins).

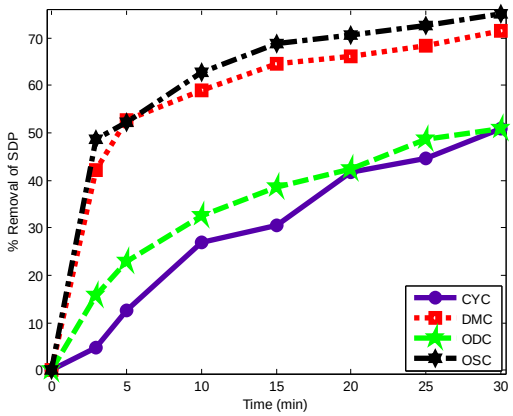

50mg/L

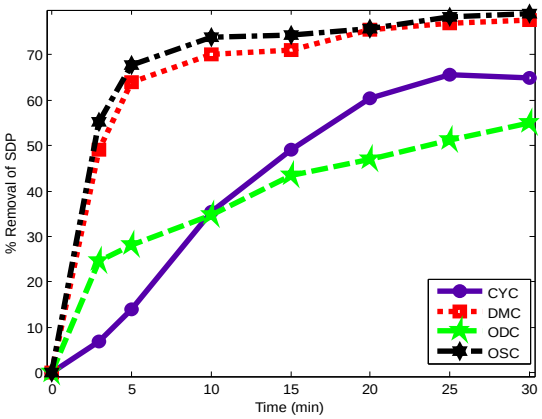

100mg/L

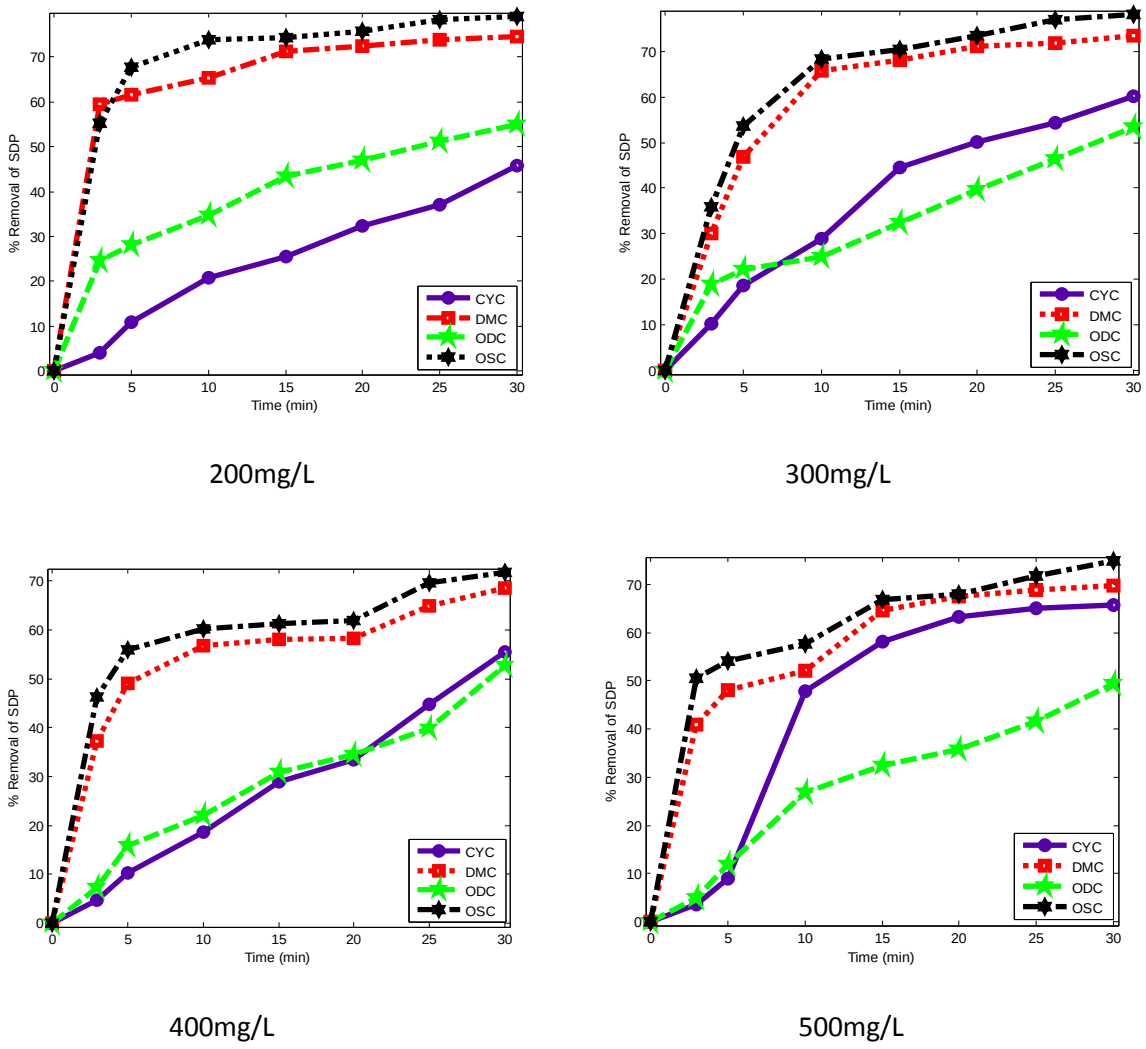

Fig. 4.27 Turbidity removal efficiency in PW at pH 10 and varying dosage with (initial concentration= 849.68mg/L, settling time = 30mins).

4.3 Coag-flocculation Kinetic Results for varying Dosage and pH for CYC, DMC, ODC and OSC in BRE and PW.

The kinetic parameters obtained for the coag-flocculation ofCYC, DMC, ODC and OSC in BRE and PW at pH 2, 4, 6, 8, 10 for 50, 100, 200, 300, 400, 500 mg/L dosages are presented in Tables 4.21 to 4.80. The plots were based on equation 3.18,with$K_{11} and \frac{1}{\sqrt{N_o}}$, as slope and intercept, respectively. The rate constantK_{11}, coefficient of determination,R^2, degree of freedom adjusted R-square, adj R^2, sum of square error, SSE and root mean square error (RMSE), obtained from the plots were depicted in Tables 4.21 to4.80. From the tables, the maximum and minimum coag-flocculation rate constant,K_{11}obtained at different pH and dosages were recorded.From table 4.34, the highest value of K_{11} was recorded at pH of 2 and 100mg/L as 0.0015 L/mg.min for DMC with $\tau_{1/2}$

(1.83min), while the in Table 4.39 the least K_{11} is 1.13×10^{-5}L/mg.min at pH 10 and 200mg/L with $\tau_{1/2}$(243.04min) for DMC. In Table 4.23, OSC at pH of 2 and 200mg/L recorded highest value of K_{11} as 0.0003L/mg.min with $\tau_{1/2}$ (9.15min), also with least K_{11}value of 5.33×10^{-6} at pH 10 and 300mg/L and $\tau_{1/2}$ (515.25 min) in Table 4.40. The ODC also recorded highest value of K_{11} in Tables 4.21, 4.29, 4.30, 4.35, 4.41, 4.45 and 4.47 of 0.0006L/mg.min at pH 2, 4, 6, 8 and 10 with $\tau_{1/2}$ (4.58 min), and the least value at pH 6 and 400mg/L as 0.0002 L/mg.min with $\tau_{1/2}$(127.79 min.). The CYC recorded the highest valueof K_{11} in Tables 4.23, 4.29, 4.30, 4.35, 4.41 and 4.47 of 0.0003 L/mg.min in BRE. The coagulation time $\tau_{1/2}$ which is time taken for the initial concentration of colloidal particles to reduce by half was calculated from equation (3.19). It was observed that the coagulation rate constants varied inversely with the coagulation time i.e. higher K_{11} goes with low$\tau_{1/2}$. This trend is consistence with previous studies (Menkiti, et al., 2010; Okolo, et al., 2014).

. For PW, the highest K_{11} for DMC was recorded in Table 4.37 at pH 2 and 400mg/L with K_{11} as 0.0027L/mg.min and$\tau_{1/2}$ (0.87mins), while the least was at pH 6 withK_{11} as 5.47E-5 and $\tau_{1/2}$ (43.03mins) .Also in Table 4.35, ODC recorded the highest valueat pH2 and 200mg/L with K_{11} as 0.0018L/mg.min and $\tau_{1/2}$(1.31mins) and the least $K_{11}$is 4.94E-5 at pH 10 with 200mg/L and $\tau_{1/2}$ (47.64) in Table 4.59. OSC recorded the highest and least values of K_{11} in Tables 4.58 and 4.61 as 0.0024 and 6.40E-5L/mg.minat pH 10 and with$\tau_{1/2}$ 0.98 and 36.78mins and dosage 100 and 400mg/L respectively.Also CYC recorded the highest and least of K_{11} as 0.0006 and 2.90E-5L/mg.min in Tables 4.41 and 4.48 at pH 4 and 6, with $\tau_{1/2}$ 3.92 and 81.17mins at 200 and 300mg/L dosage respectively. $K_{11}$is an important parameter that shows the speed of floc formation. The higher the value of K_{11}, the higher the efficiency in clarification (Menkiti, et al., 2012; Ugonabu, et al., 2012). Rapid coagulation constant, K_R was an indication that the variations in K_R values were minimal due to insignificant changes in temperature and viscosity of the effluent medium (Menkiti et al., 2010; Ugonabo et al., 2012).

The goodness of fit and the adequacy of experimental data to the primary model as expressed in equation (3.17) were evaluated using statistical parameters R^2 and adjusted R^2, SSE and RMSE to evaluate the quality of fit.Most values of R^2 and adjusted R^2 are relatively high with low values SSE and RMSE, indicates that the fit is in good agreement with experimental data. The results are consistent with previous work (AL. Ahmed et al., 2007; Menkiti et al., 2010).

Table 4.21: Coag-flocculation kinetic parameter in BRE at pH 2 and 50mg/L dosage

Parameter	CYC	DMC	ODC	OSC
α	2	2	2	2

R^2	0.9632	0.9405	0.9876	0.9325
adjR^2	0.9600	0.930	0.9752	0.9123
SSE	1.52E-6	357E-6	2.29E-6	2.26E-7
RMSE	0.0003	0.0055	0.0007	0.0002
K_{11}(L/m.min)	0.0003	0.0011	0.0006	0.0001
$\varepsilon_p(mg^{-1})$	5.37E5	2.68E5	6.21E4	1.05E4
$K_R(L/min)$	3.72E-10	3.52E-10	3.32E-10	3.72E-10
$\beta_{BR}(L/mg\ min)$	4E-4	2E-4	4.62E-5	7.84E-5
$\tau_{1/2}(min)$	9.15	2.49	4.58	27.46

Table 4.22: Coag-flocculation kinetic parameter in BRE at pH 2 and 100mg/L dosage

Parameter	CYC	DMC	ODC	OSC
α	2	2	2	2
R^2	0.9507	0.9559	0.9668	0.9397
adjR^2	0.9408	0.9489	0.9568	0.9212
SSE	8.87E-7	4.15E-6	1.604E-6	1.194E-6
RMSE	0.0004	0.0009	0.0006	0.0006
K_{11} (L/m.min)	0.0002	0.0004	0.0003	0.0002
$\varepsilon_p(mg^{-1})$	5.37E5	8.06E5	2.68E	2.32E5
$K_R(L/min)$	3.72E-10	3.32E-10	3.52E-10	3.72E-10
$\beta_{BR}(L/mg\ min)$	4E-4	6E-4	2E-4	1.73E-4
$\tau_{1/2}(min)$	13.73	6.86	9.15	13.73

Table 4.23: Coag-flocculation kinetic parameter in BRE at pH 2 and 200mg/L dosage

Parameter	CYC	DMC	ODC	OSC
α	2	2	2	2
R^2	0.9406	0.9787	0.9947	0.9691
adjR^2	0.932	0.9744	0.9937	0.9629
SSE	1.52E-6	3.57E-6	6.30E-8	2.25E-8
RMSE	0.0006	0.0008	0.0003	6.72E-5
K_{11} (L/m.min)	0.0002	0.0003	0.0002	0.0003
$\varepsilon_p(mg^{-1})$	5.37E5	2.68E5	2.78E5	9.11E4
$K_R(L/min)$	3.52E-10	3.73E-10	3.32E-10	3.52E-10
$\beta_{BR}(L/mg\ min)$	4E-4	2E-4	2E-4	6.78E-5

$\tau_{1/2}(min)$	13.73	9.15	13.73	9.15

Table 4.24: Coag-flocculation kinetic parameter in BRE at pH 2 and 300mg/L dosage

Parameter	CYC	DMC	ODC	OSC
α	2	2	2	2
R^2	0.9958	0.9484	0.9984	0.9455
adjR^2	0.9949	0.9478	0.9981	0.9434
SSE	6.69E-8	2.02E-6	4.38E-7	1.026E-6
RMSE	0.0001	0.0006	0.0003	0.00045
K_{11} (L/m.min)	0.0001	0.0002	0.0003	0.0002
$\varepsilon_p(mg^{-1})$	2.68E5	2.58E5	1.92E5	1.73E4
$K_R(L/min)$	3.72E-10	3.32E-10	2.72E-10	3.72E-10
$\beta_{BR}(L/mg\ min)$	2E-4	2E-4	1.43E-4	1.29E-4
$\tau_{1/2}(min)$	27.46	13.73	9.15	13.73

Table 4.25: Coag-flocculation kinetic parameter in BRE at pH 2 and 400mg/L dosage

Parameter	CYC	DMC	ODC	OSC
α	2	2	2	2
R^2	0.9722	0.9933	0.983	0.8721
adjR^2	0.9666	0.9918	0.980	0.8711
SSE	8.82E-7	3.578E-8	4.15E-7	1.81E-6
RMSE	0.0004	8.46E-5	0.0003	0.0006
K_{11} (L/m.min	0.0002	9.24E-5	0.0002	0.0001
$\varepsilon_p(mg^{-1})$	5.40E5	2.68E5	1.80E5	1.39E5
$K_R(L/min)$	3.42E-10	3.72E-10	3.22E-10	3.52E-10
$\beta_{BR}(L/mg\ min)$	4.0E-4	2.0E-4	1.34E-4	1.04E-4
$\tau_{1/2}(min)$	13.73	29.72	13.73	27.46

Table 4.26: Coag-flocculation kinetic parameter in BRE at pH 2 and 500mg/L dosage

Parameter	CYC	DMC	ODC	OSC
α	2	2	2	2
R^2	0.9551	0.974	0.9472	0.9394
adjR^2	0.9543	0.9723	0.9465	0.9376
SSE	1.51E-6	6.85E-8	5.87E-7	1.19E-6
RMSE	0.0005	0.0001	0.0003	0.0005

K_{11} (L/m.min)	0.0002	6.44E-5	0.0001	0.0002
$\varepsilon_p(mg^{-1})$	1.73E5	8.06E5	5.10E4	5.78E4
$K_R(L/min)$	3.22E-10	3.72E-10	3.56E-10	3.43E-10
$\beta_{BR}(L/mg\ min)$	1.28E-4	6E-4	3.8E-4	4.30E4
$\tau_{1/2}(min)$	13.73	42.65	27.46	13.73

Table 4.27: Coag-flocculation kinetic parameter in BRE at pH 4 and 50mg/L dosage

Parameter	CYC	DMC	ODC	OSC
α	2	2	2	2
R^2	0.9632	0.9405	0.9876	0.9325
adjR^2	0.9600	0.930	0.9752	0.9123
SSE	1.52E-6	357E-6	2.29E-6	2.26E-7
RMSE	0.0003	0.0055	0.0007	0.0002
K_{11} (L/m.min)	0.0003	0.0011	0.0006	0.0001
$\varepsilon_p(mg^{-1})$	5.37E5	2.68E5	6.21E4	1.05E4
$K_R(L/min)$	3.72E-10	3.52E-10	3.32E-10	3.72E-10
$\beta_{BR}(L/mg\ min)$	4E-4	2E-4	4.62E-5	7.84E-5
$\tau_{1/2}(min)$	9.15	2.49	4.58	27.46

Table 4.28: Coag-flocculation kinetic parameter in BRE at pH 4 and 100mg/L dosage

Parameter	CYC	DMC	ODC	OSC
α	2	2	2	2
R^2	0.9915	0.8303	0.9908	0.9792
adjR^2	0.9905	0.8143	0.9865	0.9754
SSE	4.99E-7	0.0002	2.29E-6	2.26E-7
RMSE	0.0003	0.0055	0.0007	0.0002
K_{11} (L/m.min)	0.0003	0.0011	0.0006	0.0001
$\varepsilon_p(mg^{-1})$	5.37E5	2.68E5	6.21E4	1.05E4
$K_R(L/min)$	3.72E-1	3.52E-10	3.32E-10	3.72E-10
$\beta_{BR}(L/mg\ min)$	4E-4	2E-4	4.62E-5	7.84E-5
$\tau_{1/2}(min)$	9.15	2.49	4.58	27.46

Table 4.29: Coag-flocculation kinetic parameter in BRE at pH 4 and 200mg/L dosage

Parameter	CYC	DMC	ODC	OSC

α	2	2	2	2
R^2	0.987	0.9357	0.9284	0.9006
adjR^2	0.9863	0.9285	0.9165	0.8896
SSE	1.08E-7	3.69E-6	3.06E-6	9.58E-7
RMSE	0.0001	0.0008	0.0008	0.0004
K_{11} (L/m.m)	0.0001	0.0003	0.0002	0.0001
$\varepsilon_p(mg^{-1})$	8.069E5	2.68E5	9.54E4	7.63E4
$K_R(L/min)$	3.42E-10	3.72E-10	3.62E-10	3.42E-10
$\beta_{BR}(L/mg\ min)$	6E-4	2E-4	7.1E-5	5.68E-5
$\tau_{1/2}(min)$	27.46	9.15	13.73	27.46

Table 4.30 Coag-flocculation kinetic parameter in BRE at pH 4 and 300mg/L dosage

Parameter	CYC	DMC	ODC	OSC
α	2	2	2	2
R^2	0.9857	0.9475	0.9226	0.9475
adjR^2	0.9796	0.9369	0.9071	0.9379
SSE	1.32E-7	0.0039	1.17E-6	3.68E-8
RMSE	0.0002	0.0279	0.0004	0.0003
K_{11} (L/m.min)	0.0001	0.0008	0.0001	0.0001
$\varepsilon_p(mg^{-1}$	5.37E5	2.68E5	8.06E4	5.86E4
$K_R(L/min)$	3.72E-10	3.48E-10	3.23E-10	3.72E-10
$\beta_{BR}(L/m)$	4E-4	2E-4	6E-4	4.36E-5
$\tau_{1/2}(min)$	27.46	3.43	27.46	27.46

Table 4.31 Coag-flocculation kinetic parameter in BRE at pH 4 and 400mg/L dosage

Parameter	CYC	DMC	ODC	OSC
α	2	2	2	2
R^2	0.9751	0.9929	0.9738	0.9744
adjR^2	0.9715	0.9912	0.9713	0.9699
SSE	1.97E-76	4.09E-7	3.72E-7	2.21E-7
RMSE	0.0002	0.0003	0.0002	0.0002
K_{11} (L/m.min)	0.0001	0.0003	0.0001	0.0001
$\varepsilon_p(mg^{-1})$	2.68E5	2.68 E5	1.03E5	3.68E4
$K_R(L/min)$	3.32E-10	3.62E-10	3.72E-10	3.42E-10
$\beta_{BR}(L/min)$	2E-4	2E-4	7.7E-5	2.74E-5
$\tau_{1/2}(min)$	27.46	9.15	27.46	27.46

Table 4.32: Coag-flocculation kinetic parameter in BRE at pH 4 and 500mg/L dosage

Parameter	CYC	DMC	ODC	OSC
α	2	2	2	2
R^2	0.9897	0.9947	0.9385	0.9078
adjR^2	0.9765	0.9876	0.9276	0.8976
SSE	1.47E-7	3.66E-7	2.15E-6	2.44E-7
RMSE	0.0002	0.0003	0.0007	0.0002
K_{11} (L/m.min)	0.0002	0.0003	0.0002	6.24E-5
$\varepsilon_p(mg^{-1})$	5.37E5	1.63 E5	6.74E5	6.45E4
$K_R(L/min)$	3.72E-10	3.54E-10	3.62E-10	3.54E-10
$\beta_{BR}(L/mg\ min)$	4E-4	1.2E-4	5.14E-5	4.8E-5
$\tau_{1/2}(min)$	13.73	9.15	13.73	44.01

Table 4.33: Coag-flocculation kinetic parameter in BRE at pH 6 and 50mg/L dosage

Parameter	CYC	DMC	ODC	OSC
α	2	2	2	2
R^2	0.9632	0.9405	0.9876	0.9325
adjR^2	0.9600	0.930	0.9752	0.9123
SSE	1.52E-6	357E-6	2.29E-6	2.26E-7
RMSE	0.0003	0.0055	0.0007	0.0002
K_{11} (L/m.min)	0.0003	0.0011	0.0006	0.0001
$\varepsilon_p(mg^{-1})$	5.37E5	2.68E5	6.21E4	1.05E4
$K_R(L/min)$	3.72E-10	3.52E-10	3.32E-10	3.72E-10
$\beta_{BR}(L/mg\ min)$	4E-4	2E-4	4.62E-5	7.84E-5
$\tau_{1/2}(min)$	9.15	2.49	4.58	27.46

Table 4.34: Coag-flocculation kinetic parameter in BRE at pH 6 and 100mg/L dosage

Parameter	CYC	DMC	ODC	OSC
α	2	2	2	2
R^2	0.991	0.8286	0.9621	0.776
adjR^2	0.9892	0.8117	0.9587	0.7654
SSE	6.70E-8	0.0003	5.07E-6	9.49E-
RMSE	0.0001	0.0077	0.0010	0.0001
K_{11} (L/m.min)	0.0001	0.0015	0.0006	2.31
$\varepsilon_p(mg^{-1})$	1.07E6	2.68 E6	1.45E5	8.81E4
$K_R(L/min)$	3.32E-10	3.72E-10	3.65E-10	3.42E-10

$\beta_{BR}(L/mg\ min)$	8E-5	2E-3	1.08E-4	6.56E-5
$\tau_{1/2}(min)$	27.46	1.83	42.59	118.88

Table 4.35: Coag-flocculation kinetic parameter in BRE at pH 6 and 200mg/L dosage

Parameter	CYC	DMC	ODC	OSC
α	2	2	2	2
R^2	0.9947	0.8079	0.9092	0.986
adjR^2	0.9915	0.7896	0.9001	0.9765
SSE	6.29E-8	0.0003	3.83E-6	1.05E-8
RMSE	0.0001	0.0071	0.0009	4.58E-5
K_{11} (L/m.min)	0.0001	0.0013	0.0002	3.55E-5
$\varepsilon_p(mg^{-1})$	8.06E5	8.06 E5	1.02E5	9.88E4
$K_R(L/min)$	3.72E-10	3.42E-10	3.56E-10	3.72E-10
$\beta_{BR}(L/mg\ min)$	6E-4	6E-4	7.6E-5	7.36E-5
$\tau_{1/2}(min)$	27.46	2.11	12.73	77.36

Table 4.36: Coag-flocculation kinetic parameter in BRE at pH 6 and 300mg/L dosage

Parameter	CYC	DMC	ODC	OSC
α	2	2	2	2
R^2	0.9984	0.7981	0.9067	0.9151
adjR^2	0.9922	0.7854	0.9012	0.9016
SSE	4.97E-8	0.0003	6.78E-6	5.05E-8
RMSE	3.16E-5	0.0083	0.0012	0.0001
K_{11} (L/m.min)	7.16E-5	0.0015	0.0003	2.97E-5
$\varepsilon_p(mg^{-1})$	5.36E5	1.88 E6	6.69E4	7.74E4
$K_R(L/min)$	3.42E-10	3.72E-10	3.62E-10	3.72E-10
$\beta_{BR}(L/mg\ min)$	4E-4	1.4E-4	4.98E-5	5.76E-5
$\tau_{1/2}(min)$	38.36	1.83	9.15	92.46

Table 4.37: Coag-flocculation kinetic parameter in BRE at pH 6 and 400mg/L dosage

Parameter	CYC	DMC	ODC	OSC
α	2	2	2	2
R^2	0.9652	0.9718	0.9656	0.9064
adjR^2	0.9543	0.9467	0.9578	0.8765
SSE	1.01E-8	3.64E-8	9.86E-7	9.45E-8

RMSE	0.0001	8.53E-5	0.0004	0.0001
K_{11} (L/m.min)	6.73E-5	4.51E-5	0.0002	3.85E-5
$\varepsilon_p(mg^{-1})$	2.51E5	8.06 E5	1.21E5	6.34E4
$K_R(L/min)$	3.53E-10	3.72E-10	3.72E-10	3.72E-10
$\beta_{BR}(L/mg\ min)$	1.87E-4	6E-4	9.02E-5	4.72E-5
$\tau_{1/2}(min)$	40.81	60.89	127.79	71.33

Table 4.38: Coag-flocculation kinetic parameter in BRE at pH 6 and 500mg/L dosage

Parameter	CYC	DMC	ODC	OSC
α	2	2	2	2
R^2	0.9898	0.9622	0.9716	0.94
adjR^2	0.9788	0.9486	0.9546	0.9245
SSE	3.46E-8	3.78E-9	1.09E-6	2.61E-8
RMSE	8.32E-5	4.19E-5	0.0005	7.23E-5
K_{11} (L/m.min)	7.39E-5	1.90E-5	0.0002	2.57E-5
$\varepsilon_p(mg^{-1})$	1.73E5	8.06 E5	5.11E5	5.75E4
$K_R(L/min)$	3.32E-10	3.72E-10	3.46E-10	3.62E-10
$\beta_{BR}(L/mg\ min)$	1.29E-4	6E-4	3.8E-5	4.28E-5
$\tau_{1/2}(min)$	37.16	144.54	13.73	106.86

Table 4.39: Coag-flocculation kinetic parameter in BRE at pH 8 and 50mg/L dosage

Parameter	CYC	DMC	ODC	OSC
α	2	2	2	2
R^2	0.9632	0.9405	0.9876	0.9325
adjR^2	0.9600	0.930	0.9752	0.9123
SSE	1.52E-6	357E-6	2.29E-6	2.26E-7
RMSE	0.0003	0.0055	0.0007	0.0002
K_{11}(L/m.min)	0.0003	0.0011	0.0006	0.0001
$\varepsilon_p(mg^{-1})$	5.37E5	2.68E5	6.21E4	1.05E4
$K_R(L/min)$	3.72E-10	3.52E-10	3.32E-10	3.72E-10
$\beta_{BR}(L/mg\ min)$	4E-4	2E-4	4.62E-5	7.84E-5
$\tau_{1/2}(min)$	9.15	2.49	4.58	27.46

Table 4.40: Coag-flocculation kinetic parameter in BRE at pH 8 and 100mg/L dosage

Parameter	CYC	DMC	ODC	OSC
α	2	2	2	2
R^2	0.9956	0.9783	0.928	0.9823
adjR^2	0.9760	0.9654	0.9054	0.9765
SSE	2.02E-8	1.48E-8	3.51E-6	1.69E-8
RMSE	6.36E-5	5.43E-5	0.0008	5.82E-5
K_{11}(L/m.min)	8.64E-8	3.28E-5	0.0003	3.91E-5
$\varepsilon_p(mg^{-1})$	8.06E5	1.61 E6	1.34E6	8.06E5
$K_R(L/min)$	3.72E-10	3.42E-10	3.56E-10	3.72E-10
$\beta_{BR}(L/mg\ min)$	6E-4	1.2E-3	1.0E-3	6E-4
$\tau_{1/2}(min)$	31.78	72.27	9.15	70.23

Table 4.41: Coag-flocculation kinetic parameter in BRE at pH 8 and 200mg/L dosage

Parameter	CYC	DMC	ODC	OSC
α	2	2	2	2
R^2	0.9656	0.9264	0.9808	0.8502
adjR^2	0.9468	0.9141	0.9723	0.8324
SSE	2.64E-8	6.61E-8	4.97E-7	8.76E-8
RMSE	7.63E-5	0.0001	0.0003	0.0001
K_{11}(L/m.min)	3.46E-5	3.68E-5	0.0002	2.84E-5
$\varepsilon_p(mg^{-1})$	3.17E5	8.06 E5	5.37E5	5.37 E5
$K_R(L/min)$	3.72E-10	3.72E-10	3.72E-10	3.72E-10
β_{BR} $9l/mg$ min)	4E-4	6E-3	4E-3	4E-4
$\tau_{1/2}(min)$	32.46	31.63	13.73	96.70

Table 4.42: Coag-flocculation kinetic parameter in BRE at pH 8 and 300mg/L dosage

Parameter	CYC	DMC	ODC	OSC
α	2	2	2	2
R^2	0.9945	0.9567	0.8999	0.9561
adjR^2	0.9884	0.9486	0.8882	0.9468
SSE	1.42E-8	2.36E-8	1.02E-6	1.34E-8
RMSE	5.33E-5	6.87E-5	0.0005	5.19E-5
K_{11}(L/m.min)	6.45E-5	2.23E-5	0.0001	2.18E-5
$\varepsilon_p(mg^{-1})$	8.06E5	2.68 E5	8.06E5	2.68 E5
$K_R(L/min)$	3.46E-10	3.33E-10	3.72E-10	3.72E-10
$\beta_{BR}(L/mg\ min)$	6E-4	2E-3	6E-3	2E-4
$\tau_{1/2}(min)$	42.58	6.12	27.46	125.98

Table 4.43: Coag-flocculation kinetic parameter in BRE at pH 8 and 400mg/L dosage

Parameter	CYC	DMC	ODC	OSC
α	2	2	2	2
R^2	0.9835	0.9778	0.9631	0.7441
adjR^2	0.9796	0.9685	0.9587	0.7228
SSE	2.81E-8	7.79E-9	4.92E-6	3.99E-6
RMSE	7.50E-5	3.95E-5	0.0010	8.93E-5
K_{11}(L/m.min)	5.20E-5	2.36E-5	0.0005	1.37E-5
$\varepsilon_p(mg^{-1})$	5.37E5	2.68 E5	5.37E5	1.07 E5
$K_R(L/min)$	3.72E-10	3.64E-10	3.42E-10	3.52E-10
$\beta_{BR}(L/mg\ min)$	4E-4	2E-4	4E-4	8E-4
$\tau_{1/2}(min)$	52.81	116.37	4.58	200.46

Table 4.44: Coag-flocculation kinetic parameter in BRE at pH 8 and 500mg/L dosage

Parameter	CYC	DMC	ODC	OSC
α	2	2	2	2
R^2	0.9914	0.9514	0.9841	0.9355
adjR^2	0.9737	0.9438	0.9765	0.9254
SSE	1.55E-8	1.38E-8	3.48E-7	2.41E-8
RMSE	5.57E-5	5.26E-5	0.0003	7.02E-5
K_{11}(L/m.min)	5.38E-5	2.09E-5	0.0002	2.41E-5
$\varepsilon_p(mg^{-1})$	2.68E5	5.37 E5	5.37E5	5.37 E5
$K_R(L/min)$	3.72E-10	3.43E-10	3.52E-10	3.72E-10
$\beta_{BR}(L/mg\ min)$	2E-4	4E-4	4E-4	4E-4
$\tau_{1/2}(min)$	51.05	131.40	13.73	113.95

Table 4.45: Coag-flocculation kinetic parameter in BRE at pH 10 and 50mg/L dosage

Parameter	CYC	DMC	ODC	OSC
α	2	2	2	2
R^2	0.9632	0.9405	0.9876	0.9325
adjR^2	0.9600	0.930	0.9752	0.9123
SSE	1.52E-6	357E-6	2.29E-6	2.26E-7
RMSE	0.0003	0.0055	0.0007	0.0002
K_{11} (L/m.min)	0.0003	0.0011	0.0006	0.0001
$\varepsilon_p(mg^{-1})$	5.37E5	2.68E5	6.21E4	1.05E4
$K_R(L/min)$	3.72E-10	3.52E-10	3.32E-10	3.72E-10

$\beta_{BR}(L/mg\ min)$	4E-4	2E-4	4.62E-5	7.84E-5
$\tau_{1/2}(min)$	9.15	2.49	4.58	27.46

Table 4.46: Coag-flocculation kinetic parameter in BRE at pH 10 and 100mg/L dosage

Parameter	CYC	DMC	ODC	OSC
α	2	2	2	2
R^2	0.9223	0.8889	0.9547	0.9083
adjR^2	0.9145	0.8650	0.9487	0.8976
SSE	2.28E-8	1.52E-8	7.63E-7	4.10E-9
RMSE	6.75E-5	5.52E-5	0.0004	2.56E-5
K_{11}(L/m.min)	2.09E-5	1.40E-5	0.0002	8.96E-5
$\varepsilon_p(mg^{-1})$	5.73E5	5.37 E5	2.68E5	5.37 E5
$K_R(L/min)$	3.61E-10	3.48E-10	3.72E-10	3.48E-10
$\beta_{BR}(L/mg\ min)$	4E-4	4E-4	2E-4	4E-4
$\tau_{1/2}(min)$	131.40	196.16	13.73	30.65

Table 4.47: Coag-flocculation kinetic parameter in BRE at pH 10 and 200mg/L dosage

Parameter	CYC	DMC	ODC	OSC
α	2	2	2	2
R^2	0.8499	0.9319	0.9561	0.9283
adjR^2	0.8276	0.9236	0.9432	0.9122
SSE	7.75E-8	5.72E-9	7.61E-7	3.75E-9
RMSE	0.0001	3.38E-5	0.0004	2.74E-5
K_{11}(L/m.min)	2.66E-5	1.13E-5	0.0002	8.87E-5
$\varepsilon_p(mg^{-1})$	8.06E5	2.68 E5	2.68E5	2.68 E5
$K_R(L/min)$	3.72E-10	3.65E-10	3.42E-10	3.72E-10
β_{BR} $(L/mg$min)	6E-4	4E-4	2E-4	2E-4
$\tau_{1/2}(min)$	103.24	243.04	13.73	30.96

Table 4.48: Coag-flocculation kinetic parameter in BRE at pH 10 and 300mg/L dosage

Parameter	CYC	DMC	ODC	OSC
α	2	2	2	2
R^2	0.8615	0.9805	0.9639	0.8747
adjR^2	0.8567	0.9786	0.9564	0.8652

SSE	5.74E-8	5.48E-9	2.85E-7	2.52E-9
RMSE	0.0001	3.31E-5	0.0002	2.24E-5
K_{11}(L/m.min	2.40E-5	2.11E-5	0.0001	5.33E-6
$\varepsilon_p(mg^{-1})$	2.68E5	2.68 E5	1.91E	1.80 E5
$K_R(L/min)$	3.54E-10	3.72E-10	3.48E-10	3.72E-10
$\beta_{BR}(L/mg\ min)$	2E-4	2E-4	1.42E-4	1.35E-4
$\tau_{1/2}(min)$	114.43	130.16	27.46	515.25

Table 4.49: Coag-flocculation kinetic parameter in BRE at pH 10 and 400mg/L dosage

Parameter	CYC	DMC	ODC	OSC
α	2	2	2	2
R^2	0.9429	0.9824	0.9806	0.9067
adjR^2	0.9312	0.9765	0.9765	0.8765
SSE	3.28E-8	4.35E-9	3.20E-7	1.95E-8
RMSE	8.09E-5	2.95E-5	0.0002	6.24E-5
K_{11}(L/m.min)	2.96E-5	1.98E-5	0.0002	1.74E-5
$\varepsilon_p(mg^{-1})$	2.32E5	9.29 E4	1.73E5	1.39 E5
$K_R(L/min)$	3.47E-10	3.52E-10	3.72E-10	3.72E-10
$\beta_{BR}(L/mg\ min)$	1.73E-4	6.9E-5	1.29E-4	1.04E-4
$\tau_{1/2}(min)$	92.78	138.70	13.73	156.93

Table 4.50: Coag-flocculation kinetic parameter in BRE at pH 10 and dosage 500mg/L dosage

Parameter	CYC	DMC	ODC	OSC
α	2	2	2	2
R^2	0.9682	0.9305	0.962	0.909
adjR^2	0.9543	0.9120	0.958	0.8765
SSE	7.41E-9	7.53E-8	2.72E-6	7.29E-9
RMSE	3.84E-5	5.53E-5	0.0007	3.82E-5
K_{11}(L/m.min)	1.91E-5	1.82E-5	0.0003	1.09E-5
$\varepsilon_p(mg^{-1})$	2.96E4	5.62 E4	6.45E4	7.95 E4
$K_R(L/min)$	3.52E-10	3.72E-10	3.43E-10	3.63E-10
$\beta_{BR}(L/mg\ min)$	2.2E-5	4.2E-5	4.8E-5	5.92E-5
$\tau_{1/2}(min)$	143.78	150.89	9.15	251.96

Table 4.51: Coag-flocculation kinetic parameter in PW at pH 2 and 50mg/L dosage

Parameter	CYC	DMC	ODC	OSC
α	2	2	2	2
R^2	0.9632	0.9405	0.9876	0.9325
adjR^2	0.9600	0.930	0.9752	0.9123
SSE	1.52E-6	357E-6	2.29E-6	2.26E-7
RMSE	0.0003	0.0055	0.0007	0.0002
K_{11} (L/m.min)	0.0003	0.0011	0.0006	0.0001
$\varepsilon_p(mg^{-1})$	5.37E5	2.68E5	6.21E4	1.05E4
$K_R(L/min)$	3.72E-10	3.52E-10	3.32E-10	3.72E-10
$\beta_{BR}(L/mg\ min)$	4E-4	2E-4	4.62E-5	7.84E-5
$\tau_{1/2}(min)$	9.15	2.49	4.58	27.46

Table 4.52: Coag-flocculation kinetic parameter in PW at pH 2 and 100mg/L dosage

Parameter	CYC	DMC	ODC	OSC
α	2	2	2	2
R^2	0.9935	0.9887	0.465	0.92
adjR^2	0.9905	0.9765	0.423	0.8824
SSE	1.04E-7	1.00E-6	0.0009	5.13E-6
RMSE	0.0001	0.00044	0.0134	0.0010
K_{11}(L/m.min)	0.0002	0.0003	0.0011	0.0003
$\varepsilon_p(mg^{-1})$	1.07E6	8.06 E5	5.37E5	2.48 E5
$K_R(L/min)$	3.72E-10	3.62E-10	3.34E-10	3.62E-10
$\beta_{BR}(L/mg\ min)$	8E-4	6E-4	4E-4	1.85E-4
$\tau_{1/2}(min)$	11.77	7.85	2.14	7.85

Table 4.53: Coag-flocculation kinetic parameter in PW at pH 2 and 200mg/L dosage

Parameter	CYC	DMC	ODC	OSC
α	2	2	2	2
R^2	0.9971	0.9927	0.4634	0.9378
adjR^2	0.9853	0.9892	0.4232	0.9018
SSE	6.09E-8	9.12E-7	0.022	5.09E-6
RMSE	0.0001	0.0004	0.0214	0.0010
K_{11}(L/m.min)	0.0002	0.0004	0.0018	0.0003
$\varepsilon_p(mg^{-1})$	2.42E6	8.06 E5	1.88E5	8.06 E5
$K_R(L/min)$	3.72E-10	3.32E-10	3.65E-10	3.42E-10
$\beta_{BR}(L/mg\ min)$	1.8E-4	6E-4	1.4E-3	6E-4

$\tau_{1/2}(min)$	11.77	5.88	1.31	7.85

Table 4.54: Coag-flocculation kinetic parameter in PW at pH 2 and 300mg/L dosage

Parameter	CYC	DMC	ODC	OSC
α	2	2	2	2
R^2	0.9763	0.8893	0.4509	0.4663
adjR^2	0.9643	0.8742	0.3653	0.4126
SSE	3.55E-7	9.30E-6	0.0018	0.0031
RMSE	0.0003	0.0013	0.0191	0.0250
K_{11}(L/m.min)	0.0001	0.0003	0.0016	0.0021
$\varepsilon_p(mg^{-1})$	1.45E5	1.02 E5	6.66E4	1.21 E5
$K_R(L/min)$	3.71E-10	3.48E-10	3.64E-10	3.72E-10
$\beta_{BR}(L/mg\ min)$	1.08E-4	7.58E-5	4.96E-5	9.02E-5
$\tau_{1/2}(min)$	23.54	7.85	1.47	1.12

Table 4.55: Coag-flocculation kinetic parameter in PW at pH 2 and 400mg/L dosage

Parameter	CYC	DMC	ODC	OSC
α	2	2	2	2
R^2	0.9811	0.84	0.9156	0.4632
adjR^2	0.9739	0.7986	0.8879	0.4123
SSE	2.05E-7	0.00086	3.02E-7	0.0022
RMSE	0.0002	0.0131	0.0002	0.0211
K_{11}(L/m.min)	0.0001	0.0027	7.29E-5	0.0018
$\varepsilon_p(mg^{-1})$	8.81E5	9.88 E4	7.74E4	6.31 E4
$K_R(L/min)$	3.31E-10	3.56E-10	3.72E-10	3.42E-10
$\beta_{BR}(L/mg\ min)$	6.65E-5	7.36E-5	5.76E-5	4.7E-5
$\tau_{1/2}(min)$	23.54	0.87	32.29	1.31

Table 4.56: Coag-flocculation kinetic parameter in PW at pH 2 and 500mg/L dosage

Parameter	CYC	DMC	ODC	OSC
α	2	2	2	2
R^2	0.9685	0.9817	0.9436	0.9908
adjR^2	0.9557	0.9765	0.9276	0.9878
SSE	4.85E-7	2.44E-7	1.43E-7	3.48E-7
RMSE	0.0003	0.0002	0.0002	0.0002
K_{11}(L/m.min)	0.0002	0.0001	6.22E-5	0.0002

$\varepsilon_p(mg^{-1})$	3.62E4	3.76E4	5.67E4	5.32 E4
$K_R(L/min)$	3.43E-10	3.72E-10	3.45E-10	3.72E-10
$\beta_{BR}(L/mg\ min)$	2.7E-5	2.8E-5	4.22E-5	3.96E-5
$\tau_{1/2}(min)$	11.77	23.54	37.84	11.77

Table 4.57: Coag-flocculation kinetic parameter in PW at pH 4 and 50mg/L dosage

Parameter	CYC	DMC	ODC	OSC
α	2	2	2	2
R^2	0.9632	0.9405	0.9876	0.9325
adjR^2	0.9600	0.930	0.9752	0.9123
SSE	1.52E-6	357E-6	2.29E-6	2.26E-7
RMSE	0.0003	0.0055	0.0007	0.0002
K_{11} (L/m.min)	0.0003	0.0011	0.0006	0.0001
$\varepsilon_p(mg^{-1})$	5.37E5	2.68E5	6.21E4	1.05E4
$K_R(L/min)$	3.72E-10	3.52E-10	3.32E-10	3.72E-10
$\beta_{BR}(L/mg\ min)$	4E-4	2E-4	4.62E-5	7.84E-5
$\tau_{1/2}(min)$	9.15	2.49	4.58	27.46

Table 4.58: Coag-flocculation kinetic parameter in PW at pH 4 and 100mg/L dosage

Parameter	CYC	DMC	ODC	OSC
α	2	2	2	2
R^2	0.9685	0.9625	0.9646	0.9245
adjR^2	0.9576	0.9587	0.9534	0.9110
SSE	6.05E-6	8.33E-6	1.21E-6	9.96E-6
RMSE	0.0011	0.0012	0.0005	0.0014
K_{11} (L/m.min)	0.0005	0.0006	0.0002	0.0004
$\varepsilon_p(mg^{-1})$	8.06E5	5.37E5	8.06E5	5.37 E5
$K_R(L/min)$	3.63E-10	3.72E-10	3.43E-10	3.72E-10
$\beta_{BR}(L/mg\ min)$	6E-4	4E-4	6E-4	4E-4
$\tau_{1/2}(min)$	4.71	3.92	11.77	5.88

Table 4.59: Coag-flocculation kinetic parameter in Pw at pH 4 and 200mg/L dosage

Parameter	CYC	DMC	ODC	OSC

α	2	2	2	2
R^2	0.9797	0.976	0.8945	0.9738
adjR^2	0.9685	0.968	0.8945	0.9685
SSE	4.11E-6	3.05E-6	1.17E-6	3.72E-7
RMSE	0.0009	0.0008	0.0005	0.0003
K_{11}(L/m.min)	0.0006	0.0003	0.0001	0.0001
$\varepsilon_p(mg^{-1})$	1.61E5	8.06E5	2.68E5	2.68 E5
$K_R(L/min)$	3.71E-10	3.72E-10	3.72E-10	3.72E-10
$\beta_{BR}(L/mg\ min)$	1.2E-5	6E-4	2E-4	2E-4
$\tau_{1/2}(min)$	3.92	7.85	23.54	23.54

Table 4.60: Coag-flocculation kinetic parameter in PW at pH 4 and 300mg/L dosage

Parameter	CYC	DMC	ODC	OSC
α	2	2	2	2
R^2	0.9725	0.9832	0.9896	0.925
adjR^2	0.9646	0.9786	0.9762	0.902
SSE	3.68E-7	2.82E-6	5.01E-6	5.80E-6
RMSE	0.0003	0.0008	0.0001	0.0011
K_{11}(L/m.min)	0.0001	0.0005	8.76E-5	0.0003
$\varepsilon_p(mg^{-1})$	1.34E6	5.37E5	8.06E5	5.37 E5
$K_R(L/min)$	3.56E-10	3.42E-10	3.72E-10	3.45E-10
$\beta_{BR}(L/mg\ min)$	1.0E-3	4E-4	6E-4	4E-4
$\tau_{1/2}(min)$	23.54	4.71	26.87	7.85

Table 4.61: Coag-flocculation kinetic parameter in PW at pH 4 and 400mg/L dosage

Parameter	CYC	DMC	ODC	OSC
α	2	2	2	2
R^2	0.9548	0.9869	0.9914	0.9518
adjR^2	0.9423	0.9773	0.9879	0.9412
SSE	2.15E-6	1.51E-6	5.26E-8	2.538E-6
RMSE	0.0006	0.0005	0.0001	0.0007
K_{11}(L/m.min)	0.0003	0.0004	9.91E-5	0.0003
$\varepsilon_p(mg^{-1})$	8.06E5	5.37E5	2.86 E5	1.07 E6
$K_R(L/min)$	3.71E-10	3.46E-10	3.72E-10	3.56E-10
$\beta_{BR}(L/mg\ min)$	6E-4	4E-4	2E-4	8E-4
$\tau_{1/2}(min)$	7.85	5.88	23.75	7.85

Table 4.62: Coag-flocculation kinetic parameter in PW at pH 4 and 500mg/L dosage

Parameter	CYC	DMC	ODC	OSC
α	2	2	2	2
R^2	0.9786	0.9826	0.9646	0.9355
adjR^2	0.9661	0.9765	0.9551	0.9108
SSE	1.07E-7	2.55E-6	1.59E-7	5.11E-6
RMSE	0.0001	0.0007	0.0002	0.0010
K_{11}(L/m.min)	8.91E-5	0.0004	8.37E-5	0.0003
$\varepsilon_p(mg^{-1})$	2.68E5	5.37E5	2.86 E5	5.37 E5
$K_R(L/min)$	3.43E-10	3.54E-10	3.72E-10	3.48E-10
$\beta_{BR}(L/mg\ min)$	2E-4	4E-4	2E-4	4E-4
$\tau_{1/2}(min)$	26.42	5.88	28.12	7.85

Table 4.63: Coag-flocculation kinetic parameter in PW at pH 6 and 50mg/L dosage

Parameter	CYC	DMC	ODC	OSC
α	2	2	2	2
R^2	0.9632	0.9405	0.9876	0.9325
adjR^2	0.9600	0.930	0.9752	0.9123
SSE	1.52E-6	357E-6	2.29E-6	2.26E-7
RMSE	0.0003	0.0055	0.0007	0.0002
K_{11} (L/m.min)	0.0003	0.0011	0.0006	0.0001
$\varepsilon_p(mg^{-1})$	5.37E5	2.68E5	6.21E4	1.05E4
$K_R(L/min)$	3.72E-10	3.52E-10	3.32E-10	3.72E-10
$\beta_{BR}(L/mg\ min)$	4E-4	2E-4	4.62E-5	7.84E-5
$\tau_{1/2}(min)$	9.15	2.49	4.58	27.46

Table 4.64: Coag-flocculation kinetic parameter in PW at pH 6 and 100mg/L dosage

Parameter	CYC	DMC	ODC	OSC
α	2	2	2	2
R^2	0.9739	0.9239	0.9451	0.7378
adjR^2	0.9657	0.9115	0.9346	0.6985
SSE	2.47E-7	2.14E-5	1.94E-6	4.74E-5
RMSE	0.0002	0.0021	0.0006	0.0031
K_{11}(L/m.min)	0.0001	0.0006	0.0002	0.0005
$\varepsilon_p(mg^{-1})$	5.37E5	8.06 E5	5.37 E5	2.68 E5
$K_R(L/min)$	3.71E-10	3.53E-10	3.32E-10	3.72E-10

$\beta_{BR}(L/mg\ min)$	4E-4	6E-4	4E-4	2E-4
$\tau_{1/2}(min)$	23.54	3.92	11.77	4.71

Table 4.65: Coag-flocculation kinetic parameter in PW at pH 6 and 200mg/L dosage

Parameter	CYC	DMC	ODC	OSC
α	2	2	2	2
R^2	0.9617	0.6983	0.9736	0.2509
adjR^2	0.9587	0.6457	0.9654	0.2389
SSE	6.81E-7	0.0084	1.28E-6	0.0041
RMSE	0.0003	0.0409	0.0005	0.0287
K_{11}(L/m.min)	0.0002	0.0010	0.0003	0.0015
$\varepsilon_p(mg^{-1})$	2.68E5	2.68 E5	2.68 E5	2.68 E5
$K_R(L/min)$	3.71E-10	3.57E-10	3.48E-10	3.72E-10
$\beta_{BR}(L/mg$min)	2E-4	2E-4	2E-4	2E-4
$\tau_{1/2}(min)$	11.77	2.35	7.85	1.57

Table 4.66: Coag-flocculation kinetic parameter in PW at pH 6 and 300mg/L dosage

Parameter	CYC	DMC	ODC	OSC
α	2	2	2	2
R^2	0.9035	0.9814	0.9181	0.9625
adjR^2	0.8711	0.9786	0.9098	0.9587
SSE	5.56E-8	7.68E-8	1.15E-6	2.26E-7
RMSE	0.0001	0.0001	0.0005	0.0002
K_{11}(L/m.min)	2.90E-5	8.11E-5	0.0001	9.69E-5
$\varepsilon_p(mg^{-1})$	2.68E5	2.68 E5	2.68 E5	2.68 E5
$K_R(L/min)$	3.65E-10	3.72E-10	3.43E-10	3.53E-10
$\beta_{BR}(L/mg\ min)$	2E-4	2E-4	2E-4	2E-4
$\tau_{1/2}(min)$	81.17	29.02	23.54	24.29

Table 4.67: Coag-flocculation kinetic parameter in PW at pH 6 and 400mg/L dosage

Parameter	CYC	DMC	ODC	OSC
α	2	2	2	2
R^2	0.9827	0.9149	0.9576	0.8127
adjR^2	0.9798	0.9087	0.9478	0.8112
SSE	4.49E-8	1.73E-7	5.81E-7	0.0003
RMSE	9.47E-5	0.0002	0.0003	0.0073
K_{11}(L/m.min)	6.43E-5	5.47E-5	0.0001	0.0014

$\varepsilon_p(mg^{-1})$	6.20E4	9.53 E4	7.98 E4	1.03 E5
$K_R(L/min)$	3.56E-10	3.72E-10	3.48E-10	3.54E-10
$\beta_{BR}(L/mg\ min)$	4.62E-5	7.1E-5	5.94E-5	7.7E-5
$\tau_{1/2}(min)$	36.61	43.03	23.54	1.68

Table 4.68: Coag-flocculation kinetic parameter in PW at pH 6 and 500mg/L dosage

Parameter	CYC	DMC	ODC	OSC
α	2	2	2	2
R^2	0.9841	0.9758	0.9759	0.8396
adjR^2	0.9788	0.9659	0.9685	0.8124
SSE	3.68E-8	6.57E-8	1.04E-7	0.0002
RMSE	8.58E-5	0.0001	0.0001	0.0070
K_{11}(L/m.min)	6.07E-5	6.55E-5	8.25E-5	0.0014
$\varepsilon_p(mg^{-1})$	1.05E5	7.63 E4	5.85 E4	3.68 E4
$K_R(L/min)$	3.52E-10	3.72E-10	3.43E-10	3.72E-10
$\beta_{BR}(L/mg\ min)$	7.8E-5	5.68E-5	4.34E-5	2.74E-5
$\tau_{1/2}(min)$	38.77	35.94	28.53	1.68

Table 4.69: Coag-flocculation kinetic parameter in PW at pH 8 and 50mg/L dosage

Parameter	CYC	DMC	ODC	OSC
α	2	2	2	2
R^2	0.9632	0.9405	0.9876	0.9325
adjR^2	0.9600	0.930	0.9752	0.9123
SSE	1.52E-6	357E-6	2.29E-6	2.26E-7
RMSE	0.0003	0.0055	0.0007	0.0002
K_{11} (L/m.min)	0.0003	0.0011	0.0006	0.0001
$\varepsilon_p(mg^{-1})$	5.37E5	2.68E5	6.21E4	1.05E4
$K_R(L/min)$	3.72E-10	3.52E-10	3.32E-10	3.72E-10
$\beta_{BR}(L/mg\ min)$	4E-4	2E-4	4.62E-5	7.84E-5
$\tau_{1/2}(min)$	9.15	2.49	4.58	27.46

Table 4.70: Coag-flocculation kinetic parameter in PW at pH 8 and 100mg/L dosage

Parameter	CYC	DMC	ODC	OSC
α	2	2	2	2
R^2	0.9778	0.8042	0.9913	0.7091
adjR^2	0.9743	0.7986	0.9843	0.6874
SSE	2.48E-7	1.99E-6	1.68E-7	1.77E-6
RMSE	0.0003	0.0006	0.0002	0.0006
K_{11}(L/m.min)	0.0001	0.0002	0.0002	8.35E-5
$\varepsilon_p(mg^{-1})$	4.46E4	1.26 E4	1.43 E4	4.70 E4
$K_R(L/min)$	3.71E-10	3.58E-10	3.33E-10	3.72E-10
$\beta_{BR}(L/mg\ min)$	3.32E-5	9.42E-6	1.07E-5	3.5E-5
$\tau_{1/2}(min)$	23.54	11.77	11.77	28.19

Table 4.71: Coag-flocculation kinetic parameter in PW at pH 8 and 200mg/L dosage

Parameter	CYC	DMC	ODC	OSC
α	2	2	2	2
R^2	0.9877	0.9893	0.9622	0.99
adjR^2	0.9743	0.97986	0.9543	0.9876
SSE	3.32E-7	1.29E-7	3.24E-7	8.45E-8
RMSE	0.0002	0.0002	0.0003	0.0001
K_{11}(L/m.min)	0.0002	0.0001	0.0001	0.0001
$\varepsilon_p(mg^{-1})$	4.46E4	1.26 E4	1.43 E4	4.70 E4
$K_R(L/min)$	3.46E-10	3.58E-10	3.33E-10	3.72E-10
$\beta_{BR}(L/mg\ min)$	3.32E-5	9.42E-6	1.07E-5	3.5E-5
$\tau_{1/2}(min)$	11.77	23.54	23.54	23.54

Table 4.72: Coag-flocculation kinetic parameter in PW at pH 8 and 300mg/L dosage

Parameter	CYC	DMC	ODC	OSC
α	2	2	2	2
R^2	0.9523	0.873	0.9799	0.8864
adjR^2	0.9474	0.8657	0.9654	0.8765
SSE	5.27E-7	5.78E-7	3.80E-7	3.26E-7
RMSE	0.0003	0.0003	0.0003	0.0003
K_{11}(L/m.min)	0.0001	8.02E-5	0.0002	6.42E-5
$\varepsilon_p(mg^{-1})$	4.46E4	1.26 E4	1.43 E4	4.70 E4
$K_R(L/min)$	3.46E-10	3.58E-10	3.33E-10	3.72E-10
$\beta_{BR}(L/mg\ min)$	3.32E-5	9.42E-6	1.07E-5	3.5E-5
$\tau_{1/2}(min)$	23.54	29.35	11.77	36.66

Table 4.73: Coag-flocculation kinetic parameter in PW at pH 8 and 400mg/L dosage

Parameter	CYC	DMC	ODC	OSC
α	2	2	2	2
R^2	0.9709	0.8332	0.9774	0.8029
adjR^2	0.9675	0.8126	0.9654	0.7876
SSE	2.74E-7	1.32E-6	5.70E-7	1.20E-6
RMSE	0.0002	0.0005	0.0003	0.0005
K_{11}(L/m.min)	0.0001	0.0001	0.0002	0.0002
$\varepsilon_p(mg^{-1})$	4.46E4	1.26 E4	1.43 E4	4.70 E4
$K_R(L/min)$	3.46E-10	3.58E-10	3.33E-10	3.72E-10
$\beta_{BR}(L/mg\ min)$	3.32E-5	9.42E-6	1.07E-5	3.5E-5
$\tau_{1/2}(min)$	23.54	23.54	11.77	11.77

Table 4.74: Coag-flocculation kinetic parameter in PW at pH 8 and 500mg/L dosage

Parameter	CYC	DMC	ODC	OSC
α	2	2	2	2
R^2	0.9668	0.9574	0.9759	0.9635
adjR^2	0.9568	0.9486	0.9654	0.9598
SSE	3.25E-7	1.86E-7	1.04E-7	1.51E-7
RMSE	0.0003	0.0002	0.0001	0.0001
K_{11}(L/m.min)	0.0001	8.26E-5	8.25E-5	8.03E-5
$\varepsilon_p(mg^{-1})$	4.46E4	1.26 E4	1.43 E4	4.70 E4
$K_R(L/min)$	3.46E-10	3.58E-10	3.33E-10	3.72E-10
$\beta_{BR}(L/mg\ min)$	3.32E-5	9.42E-6	1.07E-5	3.5E-5
$\tau_{1/2}(min)$	23.54	28.50	28.53	29.31

Table 4.75: Coag-flocculation kinetic parameter in PW at pH 10 and 50mg/L dosage

Parameter	CYC	DMC	ODC	OSC
α	2	2	2	2
R^2	0.9632	0.9405	0.9876	0.9325
adjR^2	0.9600	0.930	0.9752	0.9123
SSE	1.52E-6	357E-6	2.29E-6	2.26E-7
RMSE	0.0003	0.0055	0.0007	0.0002
K_{11} (L/m.min)	0.0003	0.0011	0.0006	0.0001
$\varepsilon_p(mg^{-1})$	5.37E5	2.68E5	6.21E4	1.05E4
$K_R(L/min)$	3.72E-10	3.52E-10	3.32E-10	3.72E-10

$\beta_{BR}(L/mg\ min)$	4E-4	2E-4	4.62E-5	7.84E-5
$\tau_{1/2}(min)$	9.15	2.49	4.58	27.46

Table 4.76: Coag-flocculation kinetic parameter in PW at pH 10 and 100mg/L dosage

Parameter	CYC	DMC	ODC	OSC
α	2	2	2	2
R^2	0.9821	0.9187	0.9828	0.8294
adjR^2	0.9798	0.8976	0.9788	0.8115
SSE	1.54E-7	8.02E-7	2.89E-8	0.0007
RMSE	0.0002	0.0004	7.61E-5	0.0119
K_{11}(L/m.min)	0.0001	0.0001	5.18E-5	0.0024
$\varepsilon_p(mg^{-1})$	4.46E4	1.26 E4	1.43 E4	4.70 E4
$K_R(L/min)$	3.46E-10	3.58E-10	3.33E-10	3.72E-10
$\beta_{BR}(L/mg\ min)$	3.5E-5	7.42E-6	9.42E-6	3.85E5
$\tau_{1/2}(min)$	23.54	23.54	45.44	0.98

Table 4.77: Coag-flocculation kinetic parameter in PW at pH 10 and 200mg/L dosage

Parameter	CYC	DMC	ODC	OSC
α	2	2	2	2
R^2	0.9795	0.9186	0.9653	0.8741
adjR^2	0.9689	0.8976	0.9601	0.8654
SSE	1.74E-7	8.01E-7	5.42E-8	8.24E-7
RMSE	0.0002	0.0004	0.0001	0.0004
K_{11}(L/m.min)	0.0001	0.0001	4.94E-5	9.62E-5
$\varepsilon_p(mg^{-1})$	4.46E4	1.26 E4	1.43 E4	4.70 E4
$K_R(L/min)$	3.58E-10	3.46E-10	3.25E-10	3.72E-10
$\beta_{BR}(L/mg\ min)$	8E-4	6E-4	4E-4	4.96E-5
$\tau_{1/2}(min)$	23.54	23.54	47.64	24.52

Table 4.78: Coag-flocculation kinetic parameter in PW at pH 10 and 300mg/L dosage

Parameter	CYC	DMC	ODC	OSC
α	2	2	2	2
R^2	0.9781	0.8617	0.9537	0.9396
adjR^2	0.9689	0.8564	0.9487	0.9287

SSE	2.16E-8	1.22E-6	9.29E-8	6.08E-7
RMSE	6.51E-5	0.0005	0.0001	0.0003
K_{11}(L/m.min)	3.95E-5	0.0001	5.57E-5	0.0001
$\varepsilon_p(mg^{-1})$	4.46E4	1.26 E4	1.43 E4	4.70 E4
$K_R(L/min)$	3.73E-10	3.65E-10	3.64E-10	3.72E-10
$\beta_{BR}(L/mg\ min)$	6E-4	4E-4	9.42E-6	3.5E-5
$\tau_{1/2}(min)$	59.59	23.54	42.26	23.54

Table 4.79: Coag-flocculation kinetic parameter in PW at pH 10 and 400mg/L dosage

Parameter	CYC	DMC	ODC	OSC
α	2	2	2	2
R^2	0.9385	0.923	0.9729	0.9131
adjR^2	0.9286	0.9115	0.9685	0.9086
SSE	1.47E-7	2.32E-7	5.09E-8	2.418E-7
RMSE	0.0002	0.0002	0.0001	0.0002
K_{11}(L/m.min)	6.03E-5	6.71E-5	5.44E-5	6.40E-5
$\varepsilon_p(mg^{-1})$	4.46E4	1.26 E4	1.43 E4	4.70 E4
$K_R(L/min)$	3.73E-10	3.64E-10	3.58E-10	3.72E-10
$\beta_{BR}(L/mg\ min)$	1.26E-5	3.32E-5	4E-4	9.42E-6
$\tau_{1/2}(min)$	39.04	35.08	43.26	36.78

Table 4.80: Coag-flocculation kinetic parameter in PW at pH 10 and 500mg/L dosage

Parameter	CYC	DMC	ODC	OSC
α	2	2	2	2
R^2	0.9043	0.9304	0.9746	0.9802
adjR^2	0.8987	0.9287	0.9685	0.9768
SSE	8.09E-7	3.58E-7	4.69E-8	8.89E-8
RMSE	0.0004	0.0004	9.68E-8	0.0001
K_{11}(L/m.min)	0.0001	8.81E-5	5.40E-5	8.42E-5
$\varepsilon_p(mg^{-1})$	4.46E4	1.26 E4	1.43 E4	4.70 E4
$K_R(L/min)$	3.46E-10	3.58E-10	3.33E-10	3.72E-10
$\beta_{BR}(L/mg\ min)$	3.32E-5	9.42E-6	1.07E-5	3.5E-5
$\tau_{1/2}(min)$	23.54	26.71	35.04	34.86

4.4 Time Evolution of Cluster Size Distribution

Particle size distribution was illustrated graphically by the interactions of singlets, doublet and triplets, based on the maximum and minimum coagulation period of the coagulant/flocculants under study. A plot of number of particles (N_i) versus time (t) is presented graphically by using Equation (3.18), to determine the concentration of singlets, doublets and triplets during coagulation.

In particle distribution, N_o is the initial particle concentration, while singlets are composed of single monomers, doublets are double monomers and triplets are three monomers. The graphs of the particles distribution curves are displayed in figures 4.28 to 4.43. From the figures, the decrease in the total number of particles and change of the number of singlets, doublets and triplets is shown as a function of time. In figures 4.28, 4.29, 4.30 and 4.31 for both BRE and PW, shows that the number of singlet particles decreases more rapidly than the sum. This indicates that early stage of coag-flocculation process is affected by colliadal destabilization and rapid sweep (Menkiti, et al., 2012; Ugonabo, et al., 2012). It also shows that there is a narrow margin difference in concentration of suspended particles (SP) between singlets, doublets, triplets and sum of particles. The minimum values of $\tau_{1/2}$ correspond to the period of rapid coagulation, which indicates that there are greater force of attraction than repulsion.

While in figures 4.13, 4.14, 4.17 and 4.18 the sum of particles and singlets decreases linearly with time under the influence of moderate shear force between them. There is a wide gap between the pairs of (sum of particles and singlets) and (doublets and triplets) which narrow down as the coag-flocculation process progresses. The values of $\tau_{1/2}$ was maximum corresponding to low collision, suggesting inability of particles to acquire energy needed for effective coagulation. This is an indication that there is no particle sweep, only a fraction of the particles flocculated. Similar results have been reported by Menkiti, et al., (2011).

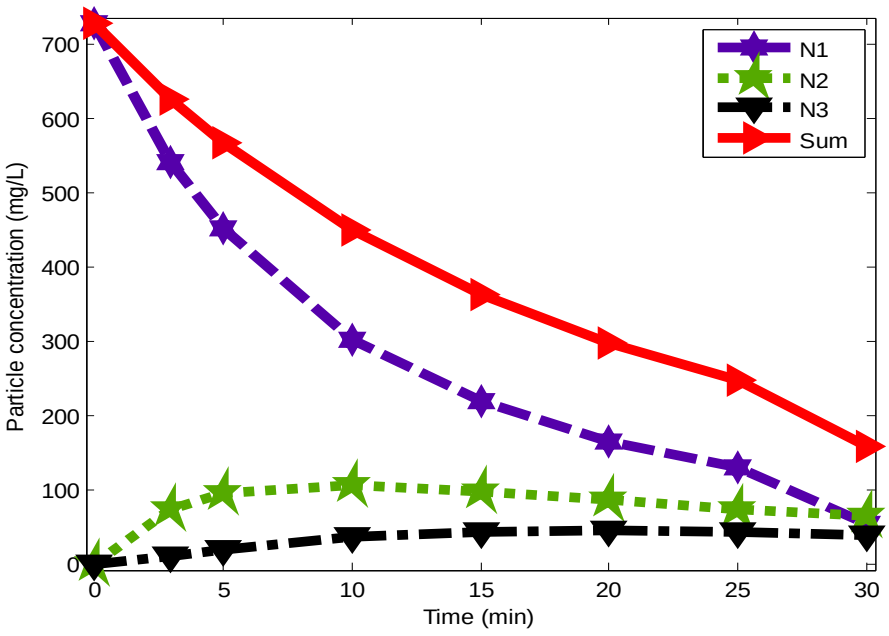

Fig. 4.28: Particle distribution for CYC in BRE at minimum half- life **(9.15mins)**
Note: N1-singlet particles, N2-doublet particles, N3- triplet particles

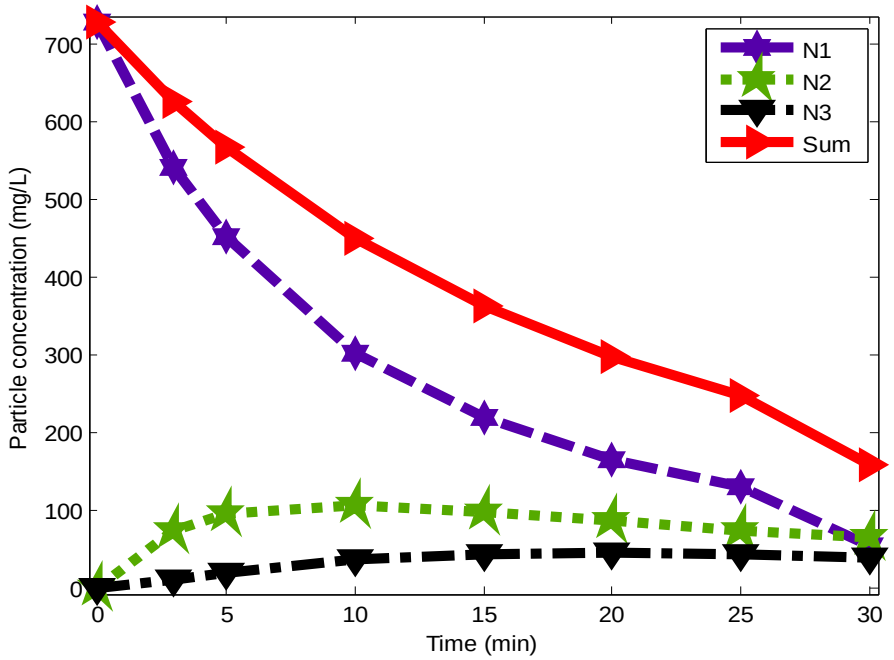

Fig. 4.29: Particle distribution for OSC in BRE at minimum half- life (9.15min).
Note: N1-singlet particles, N2-doublet particles, N3- triplet particles

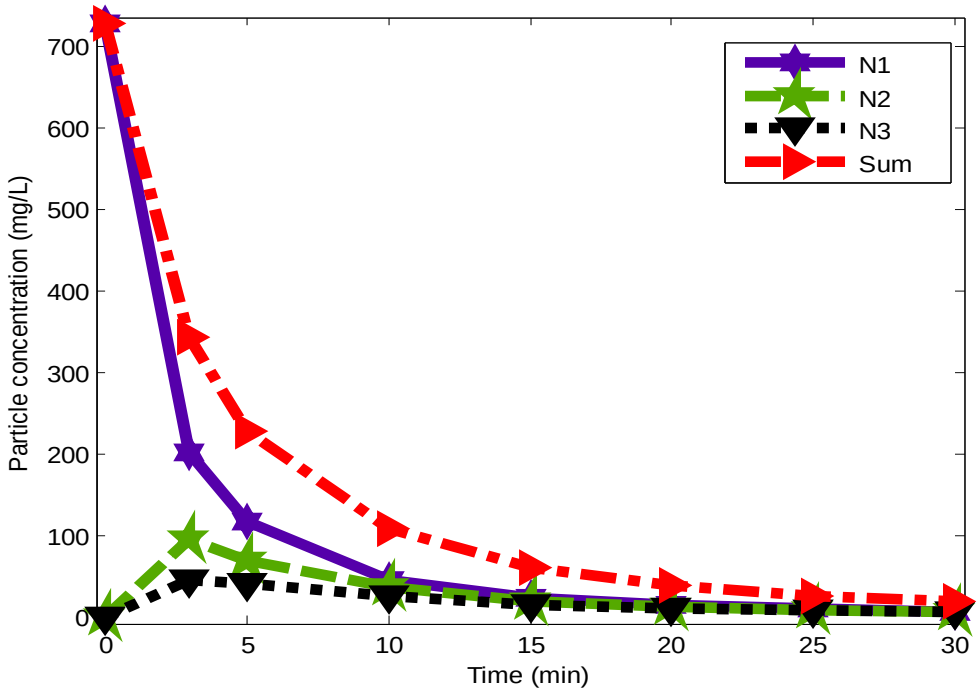

Fig. 4.30: Particle distribution for DMC in BRE at minimum half- life **(1.83mins)**

Note: N1-singlet particles, N2-doublet particles, N3- triplet particles

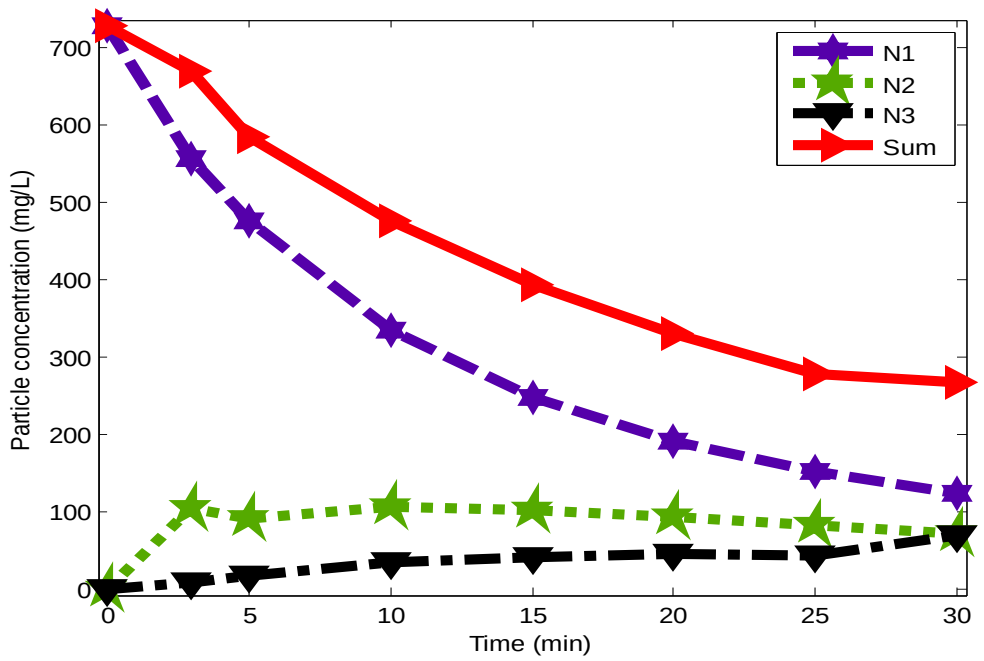

Fig. 4.31: Particle distribution for ODC in BRE at minimum half- life **(4.58mins)**
Note: N1-singlet particles, N2-doublet particles, N3- triplet particles

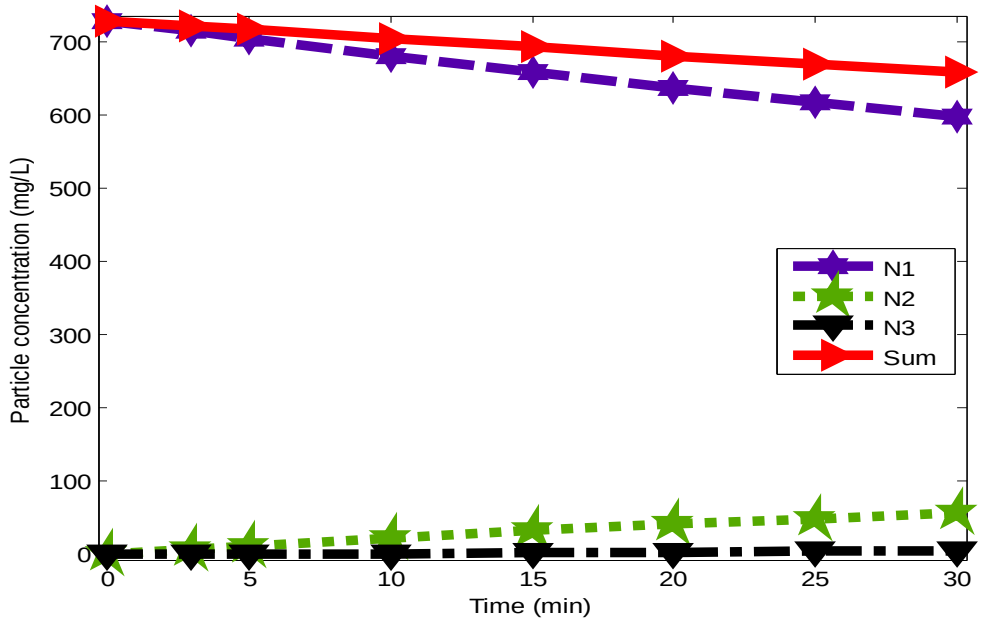

Fig. 4.32: Particle distribution for CYC in BRE at maximum half- life (143.78min)
Note: N1-singlet particles, N2-doublet particles, N3- triplet particles

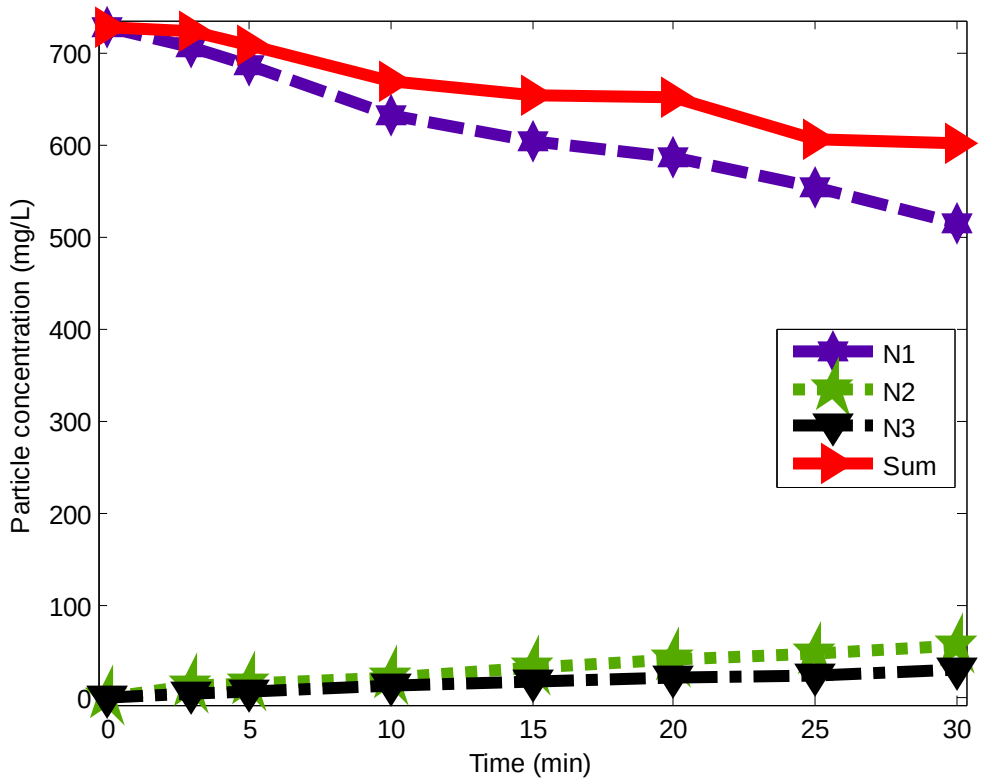

Fig. 4.33: Particle distribution for OSC in BRE at maximum half- life **(515.25mins)**
Note: N1-singlet particles, N2-doublet particles, N3- triplet particles

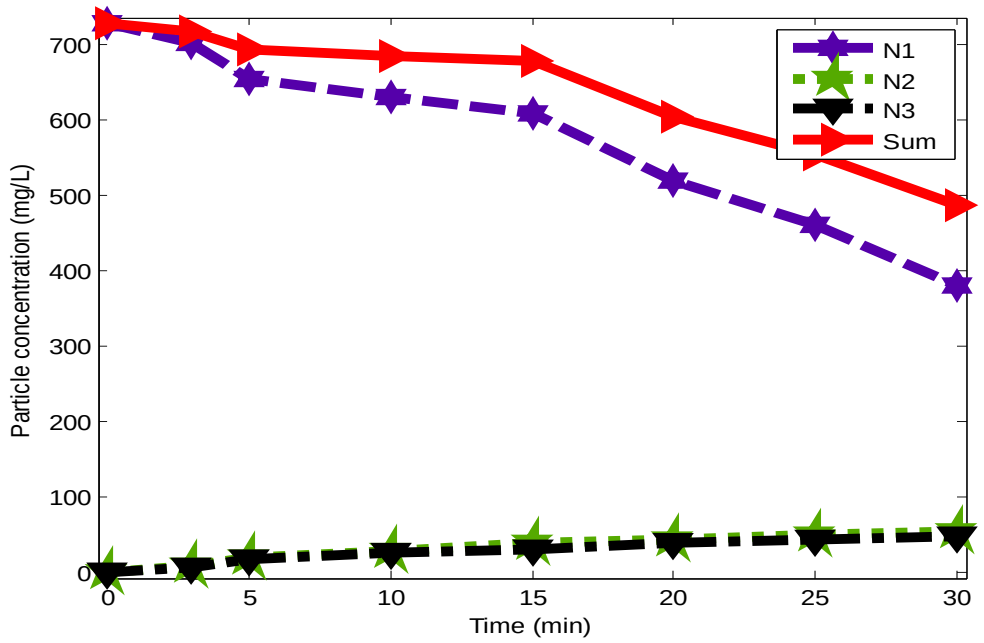

Fig. 4.34: Particle distributions for DMC in BRE at maximum half- life (243.04min)
Note: N1-singlet particles, N2-doublet particles, N3- triplet particles

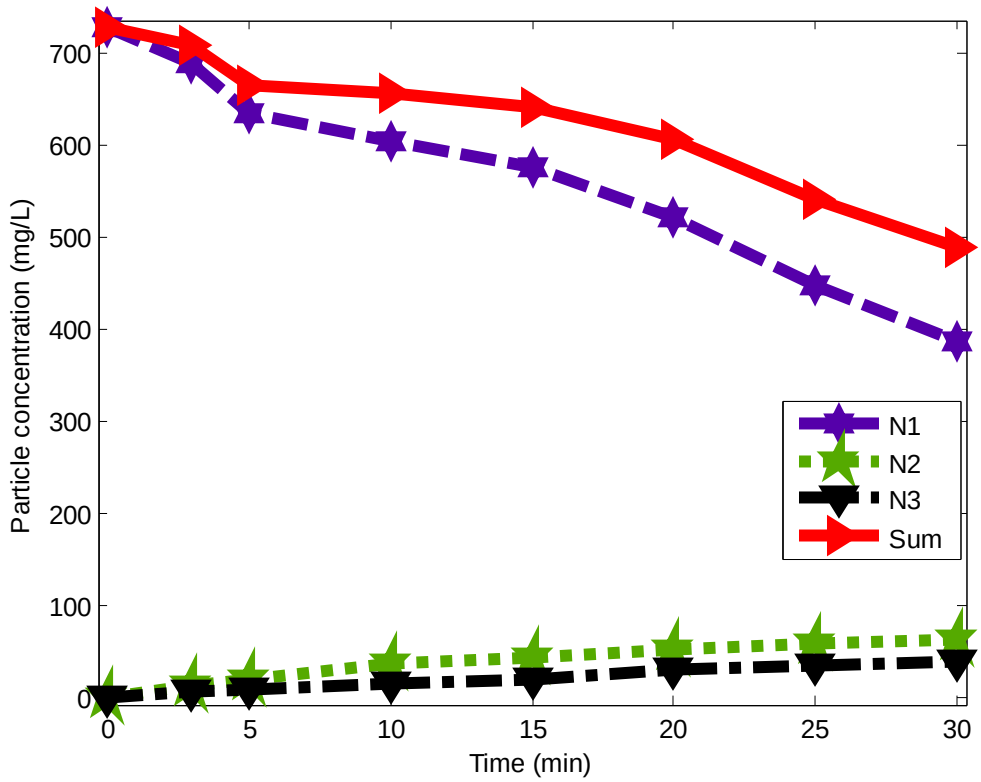

Fig. 4.35: Particle distributions for ODC in BRE at maximum half- life. (143.45min)
Note: N1-singlet particles, N2-doublet particles, N3- triplet particles

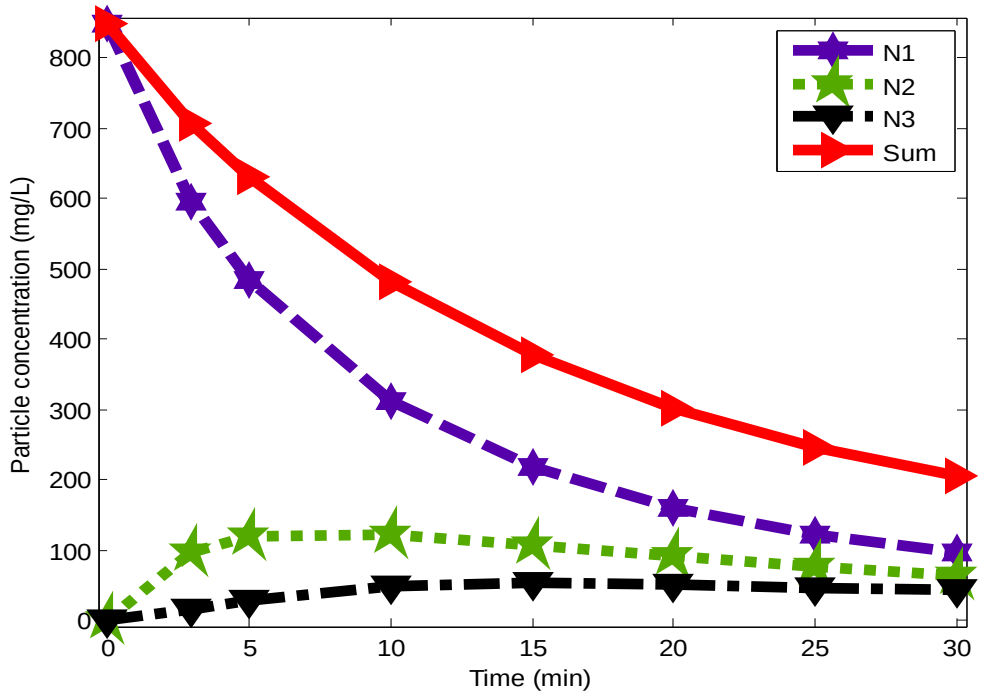

Fig.4.36: Particle distribution for CYC in PW at minimum half- life (3.92min)
Note: N1-singlet particles, N2-doublet particles, N3- triplet particles

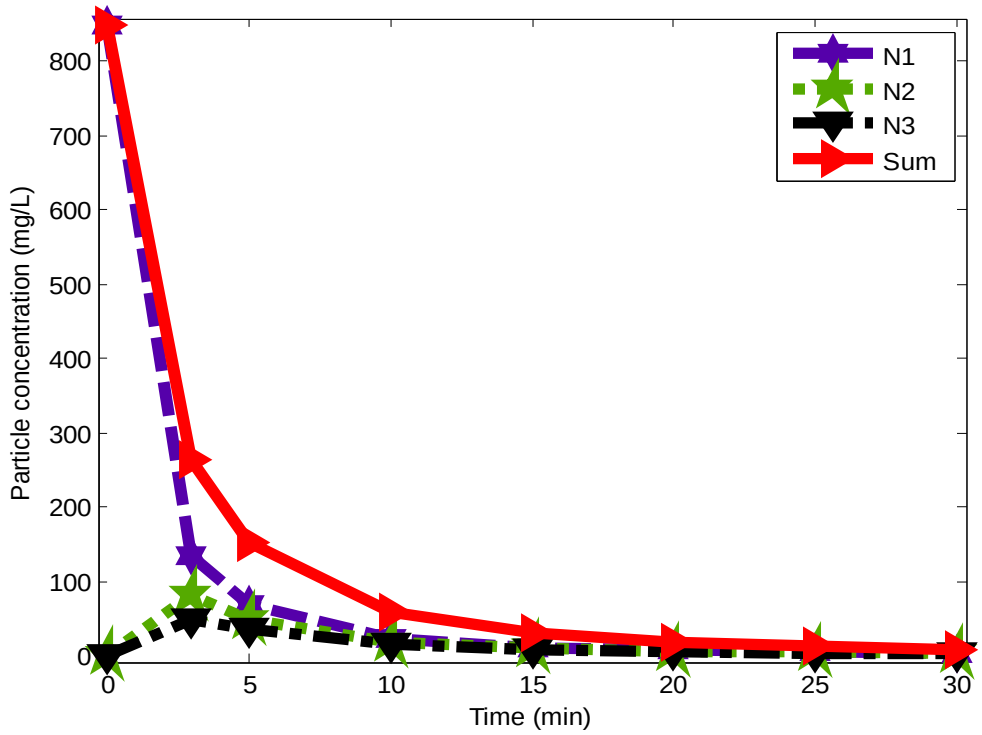

Fig.4.37: Particle distribution for OSC in PW at minimum half- life (0.98min)
Note: N1-singlet particles, N2-doublet particles, N3- triplet particles

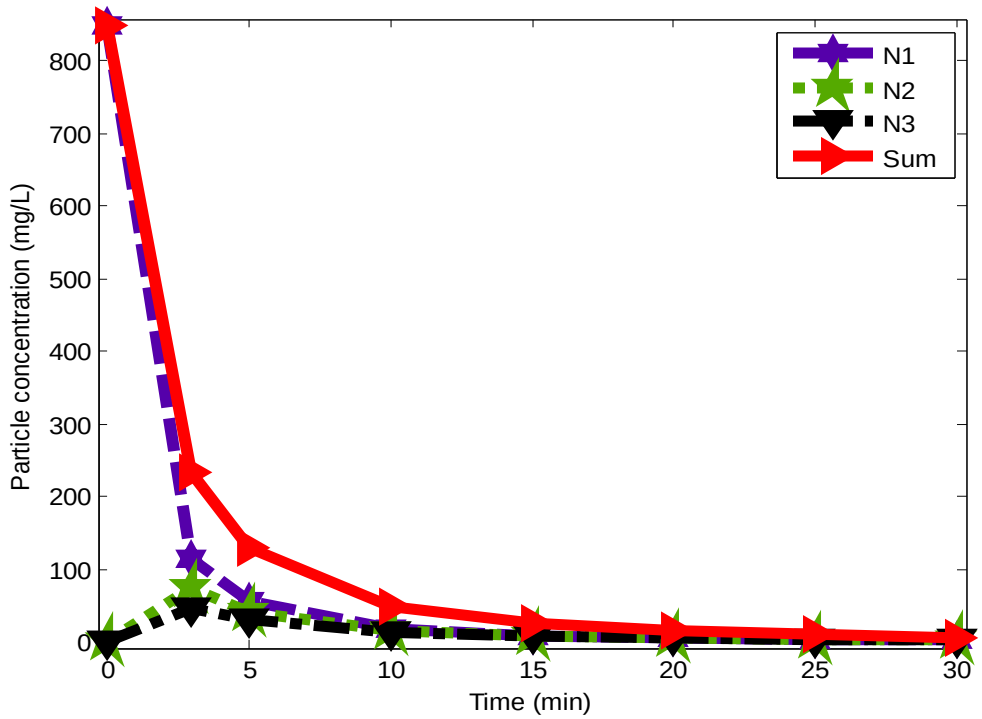

Fig.4.38: Particle distribution for DMC PW solution at minimum half- life (0.87min)
Note: N1-singlet particles, N2-doublet particles, N3- triplet particles

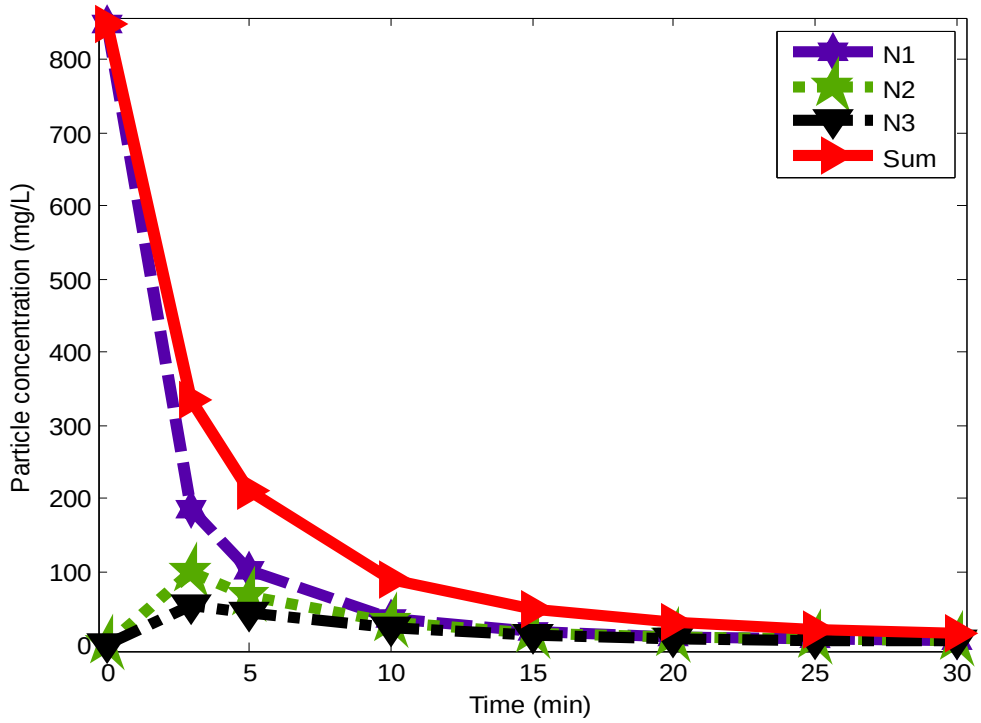

Fig.4.39: Particle distribution for ODC in PW solution at minimum half- life (1.31min).
Note: N1-singlet particles, N2-doublet particles, N3- triplet particles

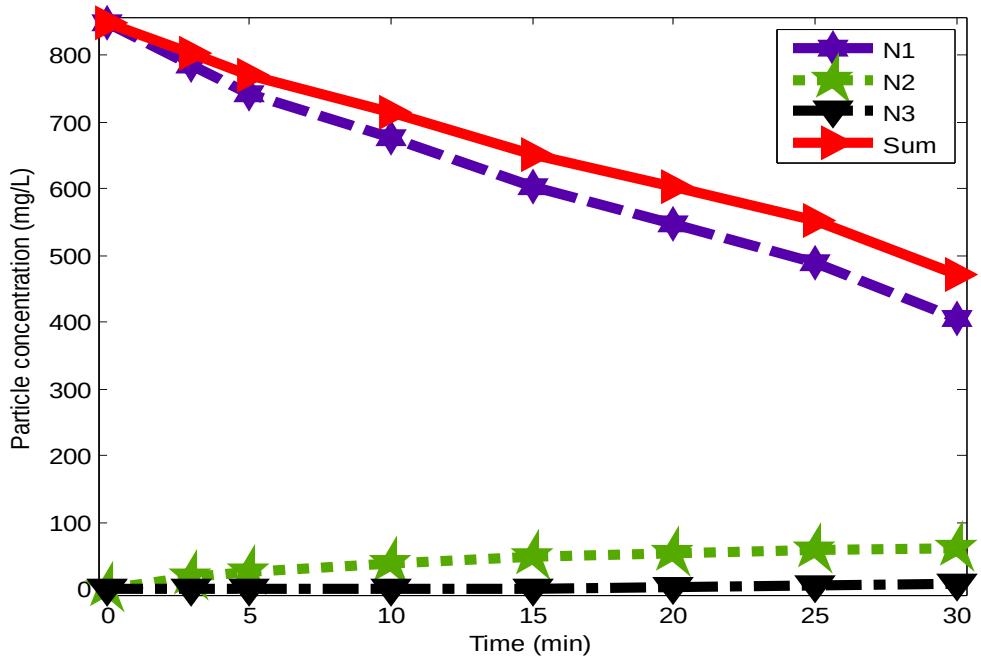

Fig.4.40: Particle distribution for CYC in PW solution at maximum half- life (81.17min)
Note: N1-singlet particles, N2-doublet particles, N3- triplet particles

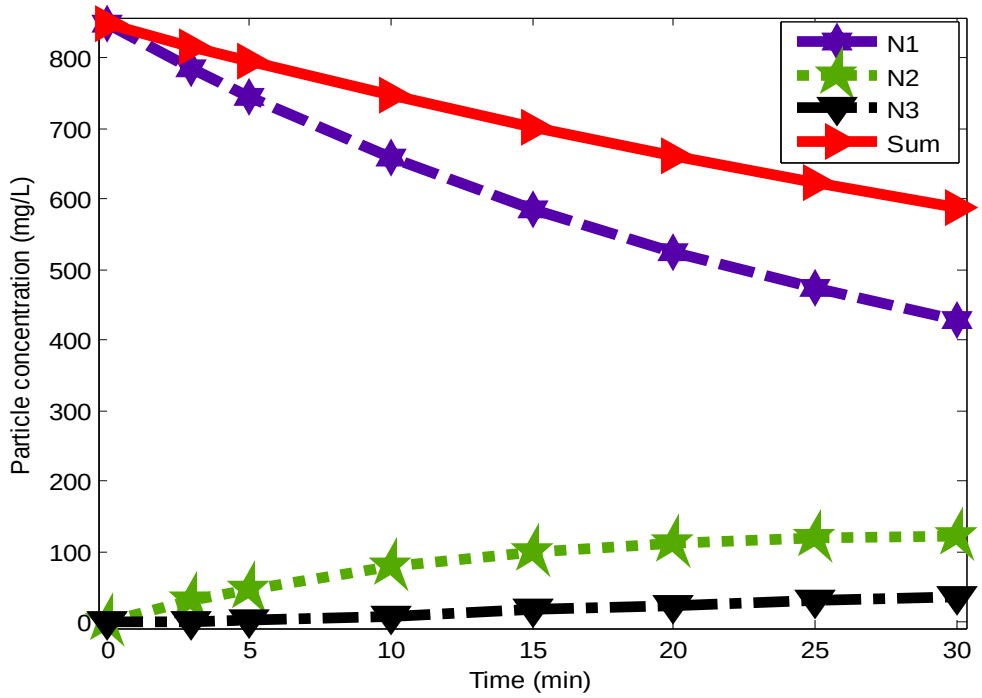

Fig.4.41: Particle distribution for OSC in PW solution at maximum half- life (36.78min)
Note: N1-singlet particles, N2-doublet particles, N3- triplet particles

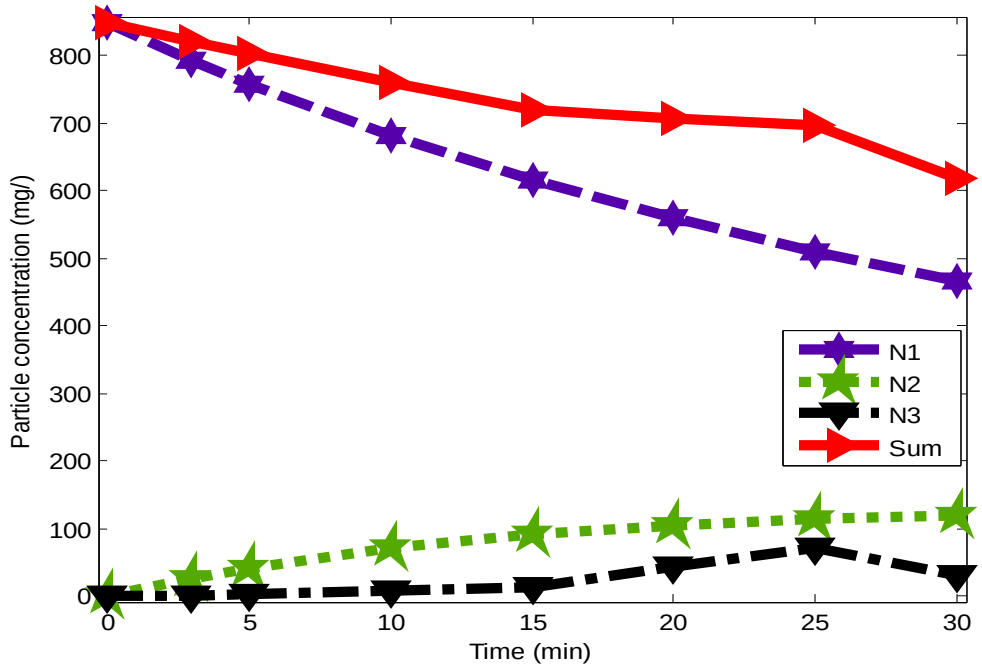

Fig.4.42: Particle distribution for DMC in PW solution at maximum half- life (43.03min)
Note: N1-singlet particles, N2-doublet particles, N3- triplet particles

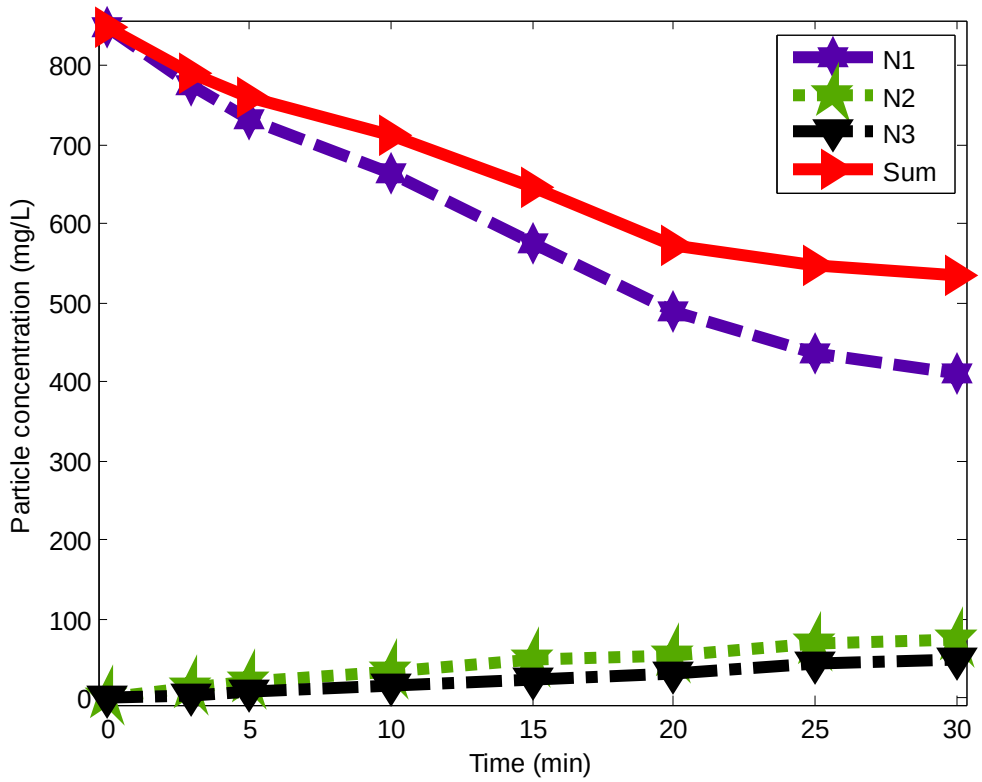

Fig.4.43: Particle distribution for ODC in PW solution at maximum half- life (47.64min)
Note: N1-singlet particles, N2-doublet particles, N3- triplet particles

4.5 Development of Regression Model

A total of 27 experiments were run using historical data design (HDD) in implementing RSM. HDD matrixfor experimental design (real and coded values of the three factors ie coagulant dosage, pH and settling time) for observed and predicted responses for the removal of turbidity have been summarized in Tables 4.81and 4.82, using Design expert software version 9.0.6. Second order polynomial equations were used to draw relationship between independent variables and responses. The effects of the parameters and response behavior of the system was explained by equations 4.2 to 4.9 shown below. Within the chosen range of experiments shown on theTables, the optimum pH, dosage and settling time for DMC was at 100mg/L, pH 2 and settling time of 30minutes with 92.42% removal of turbidity. With CYCthe removal was 89.76% with 100mg/L, pH 2 and settling time of 15minutes. The OSC and ODC removed 86.67 and 92.73% with 300mg/L, pH 2, settling times 30minutes and 100mg/L, pH 6 and 30minutes settling time, respectively.

Table 4.81: Design matrix and HDD experimental and predicted results for removal of turbidity from BRE.

Run no.	Real (coded) values			Turbidity removal (%)							
				DMC		CYC		OSC		ODC	
	X_1	X_2	X_3	Exp.	Pred.	Exp.	Pred.	Exp.	Pred.	Exp.	Pred.
1	100(-1)	10(+1)	15(0)	29.66	29.83	21.77	21.64	28.75	27.45	81.42	80.86
2	500(+1)	2(-1)	3(-1)	55.68	56.56	49.96	49.62	57.54	58.65	65.79	73.65
3	500(+1)	2(-1)	30(+1)	71.25	72.80	84.86	85.78	84.26	82.84	81.79	80.32
4	500(+1)	10(+1)	15(0)	28.12	28.78	21.92	21.76	28.94	29.23	82.91	83.65
5	500(+1)	2(-1)	15(0)	66.33	65.23	68.51	70.48	73.04	72.65	71.51	73.75
6	500(+1)	10(+1)	30(+1)	34.02	34.12	29.94	29.65	19.03	18.39	89.10	90.12
7	300(0)	6(0)	3(-1)	48.73	49.85	19.49	19.45	26.01	25.84	86.08	88.49
8	100(-1)	6(0)	15(0)	50.50	50.32	61.83	61.33	56.19	55,62	90.09	89.13
9	300(0)	10(+1)	15(0)	34.71	35.76	31.86	31.46	18.00	17.89	76.87	77.89
10	500(+1)	10(+1)	3(-1)	13.45	13.64	5.41	5.85	31.64	31.56	62.23	86.57

11	100(-1)	6(0)	3(-1)	39.16	39.06	38.77	38.12	45.09	44.67	81.04	79.15
12	**100(-1)**	**6(0)**	**30(+1)**	63.26	63.52	73.04	73.65	57.55	58.10	**92.73**	**90.45**
13	**100(-1)**	**2(-1)**	**15(0)**	84.09	83.64	**89.76**	**88.64**	81.47	80.65	83.74	82.65
14	300(0)	2(-1)	3(-1)	67.00	67.12	49.40	49.52	72.30	71.45	72.75	70.89
15	500(+1)	6(0)	30(+1)	46.52	46.65	64.80	64.12	40.58	39.64	87.46	71.32
16	300(0)	2(-1)	15(0)	90.72	89.86	68.82	68.10	82.52	81.86	84.56	83.65
17	500(+1)	6(0)	3(-1)	33.56	32.87	28.67	27.76	13.21	12.54	70.79	72.59
18	100(-1)	10(+)	3(-1)	19.90	19.82	11.30	11.54	15.24	15.86	76.34	75.86
19	100(-1)	10(+)	30(+)	33.80	33.10	27.71	27.21	33.61	33.86	84.32	82.41
20	100(-1)	2(-1)	3(-1)	74.33	74.63	33.23	33.76	74.59	76.87	69.23	70.52
21	**100(-1)**	**2(-1)**	**30(+)**	**92.42**	**92.15**	75.98	74.43	85.80	84.86	88.08	87.65
22	300(0)	6(0)	30(+1)	61.24	61.64	61.97	61.64	51.58	82.96	86.08	89.21
23	500(+1)	6(0)	15(0)	42.40	42.54	53.31	54.85	32.05	32.97	82.66	80.84
24	**300(0)**	**2(-1)**	**30(+1)**	86.63	86.80	77.93	78.65	**86.67**	**87.54**	88.76	87.65
25	300(0)	10(+)	30(+)	41.44	41.76	38.22	39.65	23.35	23.43	82.66	80.53
26	300(0)	10(+)	3(-1)	23.41	23.54	8.57	8.95	14.75	15.65	71.95	72.56
27	300(0)	6(0)	15(0)	58.18	58.65	47.08	46.86	37.23	36.54	83.22	80.68

Table 4.82: Design matrix and HDD experimental and predicted results for removal of turbidity from PW.

Run no.	Real (coded) values			Turbidity removal %							
				DMC		CYC		OSC		ODC	
	X_1	X_2	X_3	Exp.	Pred.	Exp.	Pred.	Exp.	Pred.	Exp.	Pred.
1	100(-1)	10(+1)	15(0)	75.07	75.83	59.07	59.64	74.26	74.45	60.96	60.86
2	500(+1)	2(-1)	3(-1)	48.72	48.56	34.60	35.62	41.41	41.10	33.30	33.65
3	500(+1)	2(-1)	30(+1)	36.78	36.80	79.16	79.78	85.85	85.84	65.52	65.32
4	500(+1)	10(+1)	15(0)	72.29	72.78	66.30	66.76	66.81	66.23	53.31	53.65
5	500(+1)	2(-1)	15(0)	70.91	70.23	61.84	62.59	73.35	72.85	43.75	42.75
6	500(+1)	10(+1)	30(+1)	74.18	74.98	72.37	72.65	50.54	50.39	65.36	65.12
7	300(0)	6(0)	3(-1)	48.00	47.85	27.99	27.45	19.20	19.84	58.95	58.49
8	100(-1)	6(0)	15(0)	88.83	88.32	79.95	79.33	80.24	80.64	73.82	73.13
9	300(0)	10(+1)	15(0)	72.61	72.76	40.05	40.46	70.33	69.89	53.28	53.89

10	500(+1)	10(+1)	3(-1)	49.38	49.64	72.37	73.85	74.96	74.56	65.36	65.57
11	100(-1)	6(0)	3(-1)	81.16	81.86	69.55	70.12	72.66	73.67	60.83	60.15
12	**100(-1)**	**6(0)**	**30(+1)**	**95.08**	**95.52**	**84.25**	**84.65**	**93.98**	**93.10**	78.49	78.45
13	100(-1)	2(-1)	15(0)	85.93	85.64	66.33	66.64	85.41	85.65	67.90	67.65
14	300(0)	2(-1)	3(-1)	60.78	60.12	24.75	24.52	28.00	28.45	46.41	47.89
15	500(+1)	6(0)	30(+1)	67.47	67.65	63.14	64.12	43.38	43.64	81.00	81.32
16	300(0)	2(-1)	15(0)	78.08	78.86	61.56	61.10	74.20	74.86	71.56	72.65
17	500(+1)	6(0)	3(-1)	39.34	39.87	21.47	22.76	40.62	39.54	36.61	37.59
18	100(-1)	10(+)	3(-1)	56.37	56.82	25.76	24.98	55.38	55.86	47.92	47.86
19	100(-1)	10(+)	30(+)	80.78	80.10	71.69	71.21	79.10	79.86	68.98	68.41
20	100(-1)	2(-1)	3(-1)	75.05	75.63	29.84	29.76	60.97	61.87	35.98	35.52
21	100(-1)	2(-1)	30(+)	66.39	66.15	80.52	79.43	90.12	90.86	75.12	75.65
22	**300(0)**	**6(0)**	**30(+1)**	80.79	80.64	54.53	54.64	70.21	70.96	**82.33**	**83.21**
23	500(+1)	6(0)	15(0)	59.94	59.54	51.93	51.45	65.68	65.97	63.00	64.84
24	300(0)	2(-1)	30(+1)	73.96	74.12	79.14	78.65	86.62	87.54	82.14	83.65
25	300(0)	10(+)	30(+)	78.44	78.76	56.34	56.65	83.35	82.43	67.82	67.53
26	300(0)	10(+)	3(-1)	40.99	40.54	22.77	22.95	78.12	78.65	44.08	44.56
27	300(0)	6(0)	15(0)	72.61	72.65	40.18	39.86	62.10	62.54	66.35	67.68

The regression equation for the optimization of the turbidity (Y) removal is a function of coagulant dosage (X_1), pH (X_2) and settling time (X_3), which resulted in the following equations. 4.1 to 4.8 for both BRE and PW.

For BRE

$$Y_{DMC} = 84.11777 + 0.046668X_1 - 11.72382X_2 + 1.52777X_3 + 9.54875E-003X_1X_2 - 5.76427E-004X_1X_3 - 0.040756X_2X_3 - 1.84230E-004X_1^2 + 0.39710X_2^2 - 0.0175X_3^2 \quad (4.1)$$

$$Y_{CYC} = 18.994455 + 0.06768X_1 + 4.81193X_2 + 2.28686X_3 - 4.98742E-003X_1X_2 + 4.59595E-005X_1X_3 - 0.056277X_2X_3 - 5.77000E-005X_1^2 - 0.62001X_2^2 - 0.025584X_3^2 \quad (4.2)$$

$$Y_{OSC} = 105.16701 - 0.063956X_1 - 14.15601X_2 + 1.27380X_3 + 5.36233E-004X_1X_2 + 1.05424E-003X_1X_3 - 3.21568E-003X_2X_3 + 1.66837E-005X_1^2 + 0.58279X_2^2 - 0.026795X_3^2$$

(4.3)

$$Y_{ODC} = 90.46476 - 0.089770X_1 - 0.27014X_2 + 1.04953X_3 + 5.89071E-003X_1X_2 + 4.81084E-004X_1X_3 - 0.015904X_2X_3 + 4.42714E-005X_1^2 - 0.13124X_2^2 - 0.017863X_3^2 \quad (4.4)$$

For PW,

$$Y_{DMC} = 83.86423 - 0.058215X_1 - 8.88403X_2 + 2.29769X_3 + 3.90680E-003X_1X_2 + 3.94348E-004X_1X_3 + 6.56204E-003X_2X_3 - 1.87399E-006X_1^2 + 0.57129X_2^2 - 0.047585X_3^2$$

(4.5)

$$Y_{CYC} = 43.21938 - 0.097950X_1 - 10.44038X_2 + 4.51909X_3 + 9.36382E-004X_1X_2 - 4.00038E-005X_1X_3 - 0.020335X_2X_3 + 1.72576E-004X_1^2 + 0.78394X_2^2 - 0.0767125X_3^2 \quad (4.6)$$

$$Y_{OSC} = 74.04609 - 0.15520X_1 - 6.02469X_2 + 3.40117X_3 + 1.22391E-003X_1X_2 - 1.05750E-003X_1X_3 - 0.023722X_2X_3 + 2.20795E-004X_1^2 + 0.42280X_2^2 - 0.047388X_3^2 \quad (4.7)$$

$$Y_{ODC} = 47.39851 - 0.066797X_1 + 6.74900X_2 + 1.04157X_3 + 3.24567E-003X_1X_2 + 1.24119E-003X_1X_3 - 3.68468E-003X_2X_3 - 1.08171E-005X_1^2 - 0.66342X_2^2 - 0.010291X_3^2$$

(4.8)

where, X_1, X_2, X_3 and E are the coagulant dosage, pH of effluents, settling time and expontial sign, respectively. The coefficients in front of X_1, X_2 *and* X_3 represent the linear coefficient, while the coefficients in front of X_1X_2, X_1X_3 *and* X_2X_3 represent the interaction between factors and, that of X_3^2, X_3^2 *and* X_3^2 represent the quadratic effect, respectively.

4.6 Analysis of Variance (ANOVA)

The results obtained from regression model equation were then analysed by ANOVA to determine the goodness of fit.The statistical significance of the second order model equations were checked by an F-test and also the probability (P) values were used as a tool to check the significance of each of the coefficient shown in Tables 4.83 to 4.90 for BRE and in Table 4.91 to 4.98 for PW. The quadratic regression for turbidity removal efficiency shows that all the models were significant because the F-value of 45.8056, 34.7208, 45.1971 and 55.3049 for DMC, CYC, OSC and ODC in BRE, and 69.5835, 44.233, 30.1264 and 53.6249 for DMC, CYC, OSC and ODC in PW are high. The greater the F-value, the more certain it is that the model explains adequately the variation in the data and the estimated significant terms of the coagulants variables are closer to the actual value (Montogoney, 2005; Trinh and Kaug, 2011). Also the P-values for the quadratic models for four coagulants were

less than 0.05, indicating that the model is significant. Also the coefficient of determination R^2 is close to 1, which means a better correlation between the experimental and predicted (Sharma et al., 2009; Abu Amr, et al., 2014). In Tables 4.83 to 4.90, the R^2 values of 0.9440, 0.9513, 0.9598 and 0.9803 for DMC, CYC, OSC and ODC in BRE, indicates that the models could not explain 5.60%, 4.87%, 4.02% and 1.97% of the total variations, respectively. Similar results were obtained with paint wastewater. The predicted R^2 of 0.9012, 0.8786, 0.8947 and 0.9231, were in reasonable agreement with adjusted R^2 of 0.9527, 0.9238, 0.9598 and 0.9626, which indicates that the models were significant. The coefficient of variation (CV) indicates the degree of precision with which the experiments are compared. A relatively lower value indicates a better precision and reliability of the experiments carried out (Kousha, et al., 2012). The CV values of 7.86, 6.78, 3.26 and 1.70, for DMC, CYC, OSC and ODC in BRE, from Tables 4.84, 4.86, 4.88 and 4.90, illustrated that the models can be considered reasonably reproducible. Also the standard deviation (SD) indicates the degree of precision. The low CV and SD show the adequacy with which the experiments were conducted. Adequate precision (AP) is a measure of the experimental signal to noise ratio; an AP that exceeds 4 usually indicates that the model will give a reasonable performance in prediction, which is shown in Tables above. Similar results were also obtained with PW.

Table 4.83: ANOVA for response surface quadratic model for turbidityremoval in BRE using DMC

Source	Sum of Squares	Df	Mean Square	F Value	p-value Prob > F	
Model	7892.032	9	876.8924	45.80562	1.92E-07	Significant
X_1	111.8219	1	111.8219	5.841163	0.034197	
X_2	4300.531	1	4300.531	224.6438	1.15E-08	
X_3	560.9983	1	560.9983	29.30448	0.000212	
X_1X_2	429.4784	1	429.4784	22.43437	0.000613	
X_1X_3	21.96403	1	21.96403	1.14732	0.30705	
X_2X_3	42.0101	1	42.0101	2.194452	0.166576	
X_1^2	211.4834	1	211.4834	11.04711	0.006786	
X_3^2	153.3068	1	153.3068	8.008182	0.016376	
X_3^2	38.7482	1	38.7482	2.024063	0.182559	
Residual	210.5815	11	19.14377			
Cor Total	8102.613	20				

Table 4.84: Model coefficient for turbidity removal BRE using DMC

Std. Dev.	4.37536	R-Squared	0.974011
C.V. %	7.856699	Adj RSquared	0.952747
AdeqPrecision	23.45953	PredRSquared	0.901167

Table 4.85: ANOVA for response surface quadratic model for turbidity removal in BRE using CYC

Source	Sum of Squares	Df	Mean Square	F Value	p-value Prob > F	
Model	12299.01	9	1366.557	34.7208	7.92E-09	Significant
X_1	10.9216	1	10.9216	0.277491	0.00578	
X_2	7338.232	1	7338.232	186.4462	3.1E-10	
X_3	3819.085	1	3819.085	97.03341	3.39E-08	
X_1X_2	191.035	1	191.035	4.853723	0.042588	
X_1X_3	0.185542	1	0.185542	0.004714	0.946111	
X_2X_3	111.2783	1	111.2783	2.827304	0.112086	
X_1^2	29.05567	1	29.05567	0.738232	0.402918	
X_2^2	536.7726	1	536.7726	13.63805	0.001971	
X_3^2	122.9459	1	122.9459	3.123747	0.096223	
Residual	629.7352	16	39.35845			
Cor Total	12928.75	25				

Table 4.86: Model coefficient forturbidity removal in BRE using CYC

Std. Dev.	6.273632	R-Squared	0.951292
C.V. %	6.76682	Adj RSquared	0.923894
AdeqPrecision	20.26773	PredRSquared	0.87855

Table 4.87: ANOVA for response surface quadratic model for turbidity removal in BRE using OSC

Source	Sum of Squares	Df	Mean Square	F Value	p-value Prob > F	
Model	15841.33	9	1760.147	45.19713	4.08E-10	Significant
X_1	761.6966	1	761.6966	19.55888	0.000373	
X_2	13647.11	1	13647.11	350.4311	8.8E-13	
X_3	1427.852	1	1427.852	36.66444	1.29E-05	
X_1X_2	2.015136	1	2.015136	0.051745	0.822768	
X_1X_3	88.12857	1	88.12857	2.262969	0.150852	
X_2X_3	0.327976	1	0.327976	0.008422	0.927953	
X_1^2	2.616365	1	2.616365	0.067183	0.798596	
X_2^2	510.8098	1	510.8098	13.11659	0.002107	
X_3^2	134.6513	1	134.6513	3.45758	0.080358	
Residual	662.0443	17	38.94378			
Cor Total	16503.37	26				

Table 4.88: Model coefficient for turbidity in BRE using OSC

Std. Dev.	6.240496	R-Squared	0.959884
C.V. %	3.26606	Adj RSquared	0.938647

AdeqPrecision	21.03581	PredRSquared	0.894745

Table 4.89: ANOVA for response surface quadratic model for turbidity removal in BRE using ODC

Source	Sum of Squares	Df	Mean Square	F Value	p-value Prob > F	
Model	991.3997	9	110.1555	55.30487	2.39E-07	Significant
X_1	141.0007	1	141.0007	70.79104	7.55E-06	
X_2	15.42758	1	15.42758	7.745599	0.019348	
X_3	622.5833	1	622.5833	312.5752	7.14E-09	
X_1X_2	83.68059	1	83.68059	42.01282	7.06E-05	
X_1X_3	12.24215	1	12.24215	6.146316	0.032589	
X_2X_3	5.32615	1	5.32615	2.674056	0.133041	
X_1^2	10.4583	1	10.4583	5.250709	0.044903	
X_2^2	16.36407	1	16.36407	8.215773	0.016774	
X_3^2	39.56855	1	39.56855	19.86585	0.001222	
Residual	19.91787	10	1.991787			
Cor Total	1011.318	19				

Table 4.90: Model coefficient for turbidity removal in BRE using ODC

Std. Dev.	1.411307	R-Squared	0.980305
C.V. %	1.719435	Adj RSquared	0.96258
AdeqPrecision	28.07969	PredRSquared	0.923119

Table 4.91: ANOVA for response surface quadratic model for turbidity removal in PW using DMC

Source	Sum of Squares	Df	Mean Square	F Value	p-value Prob > F	
Model	3526.875	9	391.875	69.58352	2.07E-08	Significant
X_1	389.2722	1	389.2722	69.12134	4.52E-06	
X_2	110.9618	1	110.9618	19.703	0.000997	
X_3	1532.031	1	1532.031	272.036	4.18E-09	
X_1X_2	101.7674	1	101.7674	18.07039	0.001364	
X_1X_3	9.493692	1	9.493692	1.685753	0.220723	
X_2X_3	0.842089	1	0.842089	0.149526	0.706364	
X_1^2	0.021375	1	0.021375	0.003795	0.951981	
X_2^2	244.5986	1	244.5986	43.4323	3.91E-05	
X_3^2	309.9712	1	309.9712	55.04022	1.33E-05	
Residual	61.94894	11	5.631722			
Cor Total	3588.824	20				

Table 4.92: Model coefficient for turbidity removal in PW using DMC

Std. Dev.	2.373125	R-Squared	0.982738
C.V. %	3.518225	Adj RSquared	0.968615

AdeqPrecision	30.8734	PredRSquared	0.944086

Table 4.93: ANOVA for response surface quadratic model for turbidity removal in PW using CYC

Source	Sum of Squares	Df	Mean Square	F Value	p-value Prob > F	
Model	9134.598	9	1014.955	44.23383	7.77E-08	significant
X_1	10.93524	1	10.93524	0.47658	0.50311	
X_2	315.9751	1	315.9751	13.77084	0.002976	
X_3	7931.411	1	7931.411	345.6671	3.26E-10	
X_1X_2	6.733909	1	6.733909	0.293478	0.597916	
X_1X_3	11.39683	1	11.39683	0.496697	0.494407	
X_2X_3	14.52008	1	14.52008	0.632815	0.441776	
X_1^2	216.8296	1	216.8296	9.449879	0.009644	
X_2^2	526.2685	1	526.2685	22.93586	0.000442	
X_3^2	881.0493	1	881.0493	38.39793	4.61E-05	
Residual	275.3427	12	22.94523			
Cor Total	9409.94	21				

Table 4.94: Model coefficient for turbidity removal in PW using CYC

Std. Dev.	4.790118	R-Squared	0.970739
C.V. %	4.266752	Adj RSquared	0.948794
AdeqPrecision	19.82557	PredRSquared	0.902519

Table 4.95: ANOVA for response surface quadratic model for turbidity removal in PW using OSC

Source	Sum of Squares	Df	Mean Square	F Value	p-value Prob > F	
Model	4208.1	9	467.5666	30.12639	4.38E-06	significant
X_1	506.7428	1	506.7428	32.6506	0.000195	
X_2	194.438	1	194.438	12.52809	0.005361	
X_3	2953.291	1	2953.291	190.2873	7.8E-08	
X_1X_2	6.30869	1	6.30869	0.406483	0.538083	
X_1X_3	37.9166	1	37.9166	2.443054	0.149111	
X_2X_3	8.714163	1	8.714163	0.561474	0.470926	
X_3^2	321.7155	1	321.7155	20.72887	0.001054	
X_2^2	139.317	1	139.317	8.976515	0.013433	
X_3^2	320.9464	1	320.9464	20.67931	0.001062	
Residual	155.2017	10	15.52017			
Cor Total	4363.301	19				

Table 4.96: Model coefficient for turbidity removal in PW using OSC

Std. Dev.	3.939564	R-Squared	0.96443
C.V. %	5.687857	Adj RSquared	0.932417
AdeqPrecision	18.41825	PredRSquared	0.871357

Table 4.97: ANOVA for response surface quadratic model for turbidity removal in PW using ODC

Source	Sum of Squares	Df	Mean Square	F Value	p-value Prob > F	
Model	5207.382	9	578.598	53.62487	2.63E-09	Significant
X_1	726.0375	1	726.0375	67.28967	1.02E-06	
X_2	19.65366	1	19.65366	1.821515	0.198554	
X_3	2991.239	1	2991.239	277.2302	1.27E-10	
X_1X_2	69.32121	1	69.32121	6.424739	0.023813	
X_1X_3	117.2317	1	117.2317	10.86511	0.005302	
X_2X_3	0.362533	1	0.362533	0.0336	0.857189	
X_1^2	0.858974	1	0.858974	0.07961	0.781954	
X_2^2	612.7708	1	612.7708	56.79203	2.73E-06	
X_3^2	17.96131	1	17.96131	1.664667	0.217878	
Residual	151.0562	14	10.78973			
Cor Total	5358.438	23				

Table 4.98: Model coefficient for turbidity removal in PW using ODC

Std. Dev.	3.284773	R-Squared	0.97181
C.V. %	5.511084	Adj RSquared	0.953687
AdeqPrecision	25.44753	PredRSquared	0.915101

Neglecting the coefficients of non significant terms at 95% confidence level, the final regression equations becomes 4.10 to 4.17 for BRE and PW.

Final equation for BRE:

$$Y_{DMC} = 84.11777 + 0.046668X_1 - 11.72382X_2 + 1.52777X_3 + 9.54875E-003X_1X_2 - 1.84230E-004X_1^2 + 0.39710X_2^2$$

(4.9)

$$Y_{CYC} = 18.994455 + 4.81193X_2 + 2.28686X_3 - 4.98742E-003X_1X_2 - 0.62001X_2^2 - 0.025584X_3^2$$

(4.10)

$$Y_{OSC} = 105.16701 - 0.063956X_1 - 14.15601X_2 + 1.27380X_3 + 0.58279X_2^2 \quad (4.11)$$

$$Y_{ODC} = 90.46476 - 0.089770X_1 - 0.27014X_2 + 1.04953X_3 + 5.89071E - 003X_1X_2 + 4.42714E - 005X_1^2 - 0.13124X_2^2 - 0.017863X_3^2$$
(4.12)

Final equation for PW
$$Y_{DMC} = 83.86423 - 0.058215X_1 - 8.88403X_2 + 2.29769X_3 + 3.90680E - 003X_1X_2 + 0.57129X_2^2 - 0.047585X_3^2$$
(4.13)

$$Y_{CYC} = 43.21938 - 10.44038X_2 + 4.51909X_3 + 1.72576E - 004X_1^2 + 0.78394X_2^2 - 0.0767125X_3^2$$
(4.14)

$$Y_{OSC} = 74.04609 - 0.15520X_1 - 6.02469X_2 + 3.40117X_3 + 2.20795E - 004X_1^2 + 0.42280X_2^2 - 0.047388X_3^2$$
(4.15)

$$Y_{ODC} = 47.39851 - 0.066797X_1 + 1.04157X_3 + 3.24567E - 003X_1X_2 + 1.24119E - 003X_1X_3 - 0.66342X_2^2$$
(4.16)

4.7 Adequacy of a Model

It is usually necessary to check the fitted model to ensure it provides an adequate approximation to the real system. Normalization plots in figures 4.44 to 4.51, helps in judging if the models are satisfactory. The data were plotted against a theoretical normal distribution in such a way that the points should form an approximate straight line and a departure from this line would indicate a departure from a normal distribution. From the result, figures 4.44a to 4.51a shows that the data points are slightly deviating from the normal distribution given, but not very critical. Figures 4.44b to 4.51b for residual plots shows that the data points are scattered randomly and does not form a trend, but all the data points in the plot are within the boundaries marked by the red lines. Therefore, there were no outlier data. The predicted versus actual, in figures 4.44c to 4.51c shows that all the data points are distributed along the 45 degree line, indicating that the model can provides an acceptable fit for the experimental data (Chen, et al., 2011).

The 3D response surface plots are the graphical representation of the regression equations used to visualize the relationship between the responses and experimental levels of each factor. These plots can be observed in figures 4.52 to 4.59 for DMC, CYC, OSC and ODC for BRE and PW. The removal of turbidity was display on z- axis showing the three dimensional relationship with factor variables on y and x axis respectively. The interactions of two factors are reflected in the contour of the plots, so that rounded contour line indicates a weak interaction of

two factors and a distorted contour indicates a significant interaction of two factors (Holetz, et al., 2003). In figures 4.52a and 4.52b, the contour are distorted which indicates a significant interaction of pH vs coagulant dosage and pH vs settling time with DMC. The turbidity removal of 60% was within the pH range (2-4) and dosage (340-500mg/L). While in fig. 4.52b, turbidity removal of 80% was achieved within pH range (2-4) and settling time (27-30mins). In fig. 4.52c, the contour plot was almost circular indicating that the settling time and coagulant dosage did not effect the turbidity removal significantly, while the interaction between other factors had significant effect.In fig. 4.53a, the rounded contour line indicates a weak interaction of two factors ie pH and dosage, while in fig. 4.53b and 4.53c the interactions indicates that settling time vesus dosage and pH was significant in turbidity removal. The other figures for three interaction factors follow similar trends.

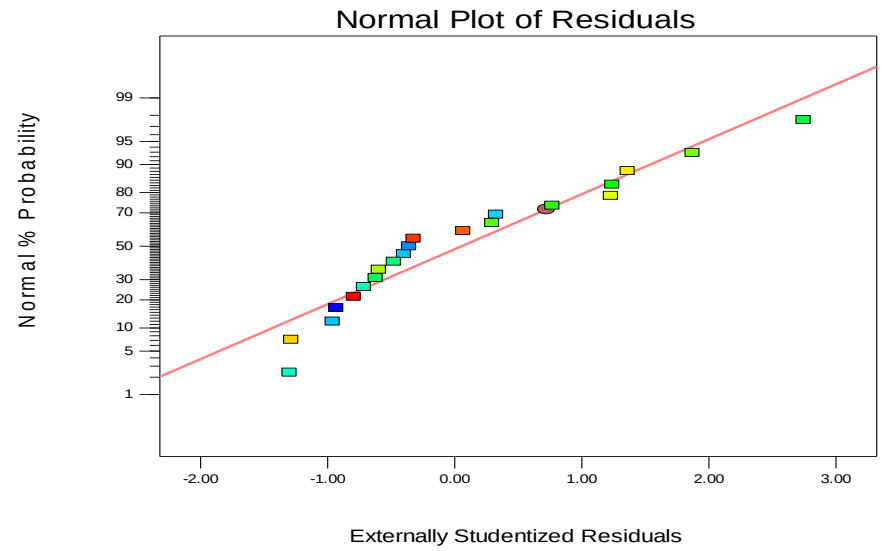

(a)

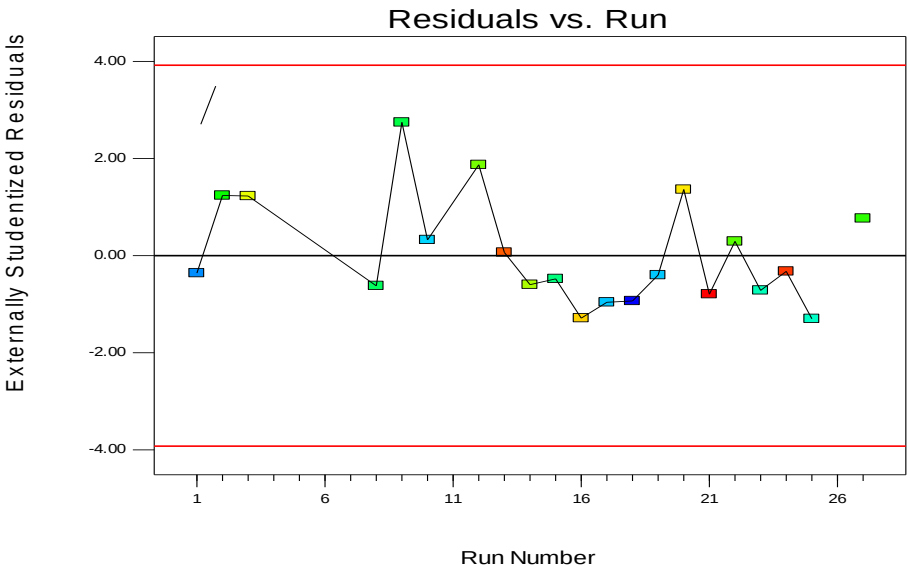

(b)

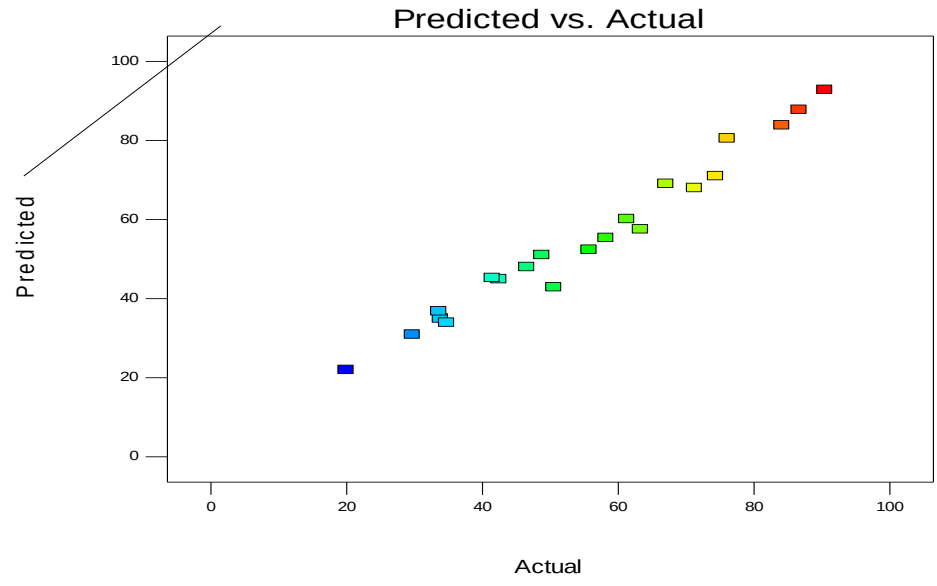

(c)

Fig. 4.44: Design-expert plots: (a) Normal probability plots, (b) Residuals versus run number of data and (c) Predicted versus actual for turbidity removal in BRE using DMC.

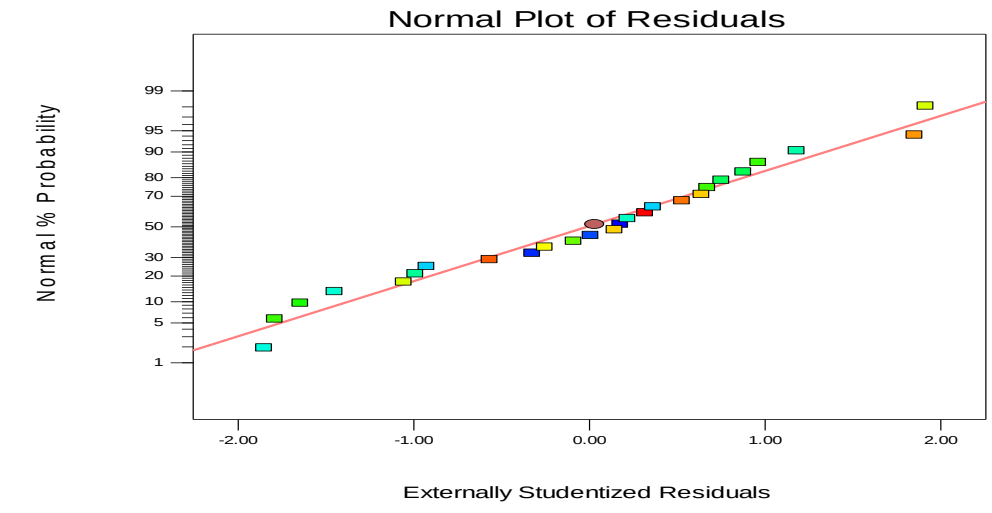

(a)

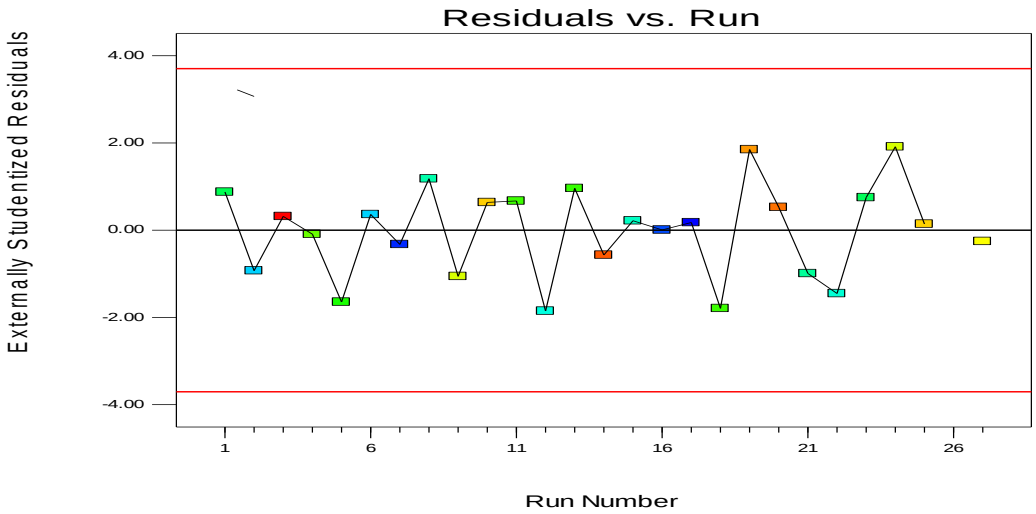

(b)

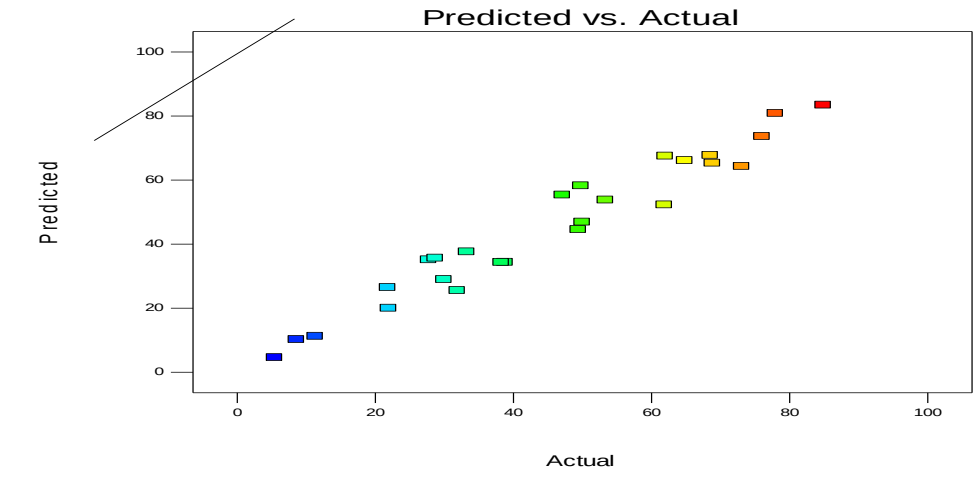

(c)

Fig. 4.45: Design-expert plots: (a) Normal probability plots, (b) Residuals versus run number of data and (c) Predicted versus actual for turbidity removal in BRE using CYC

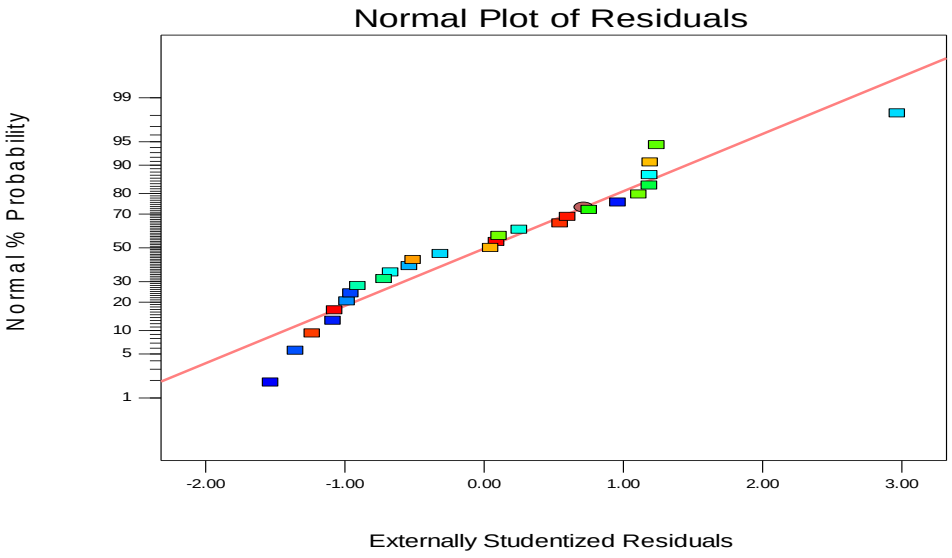

(a)

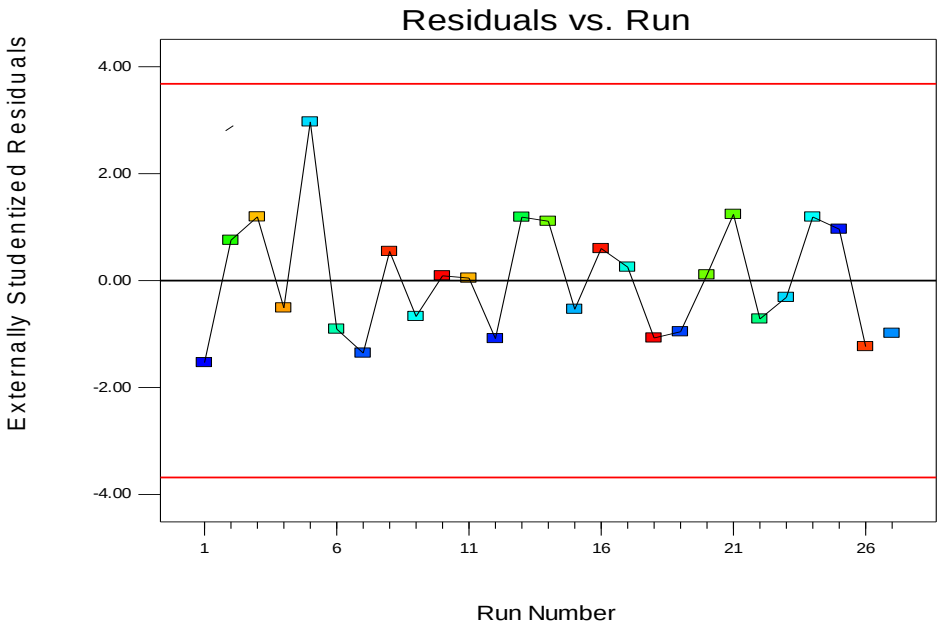

(b)

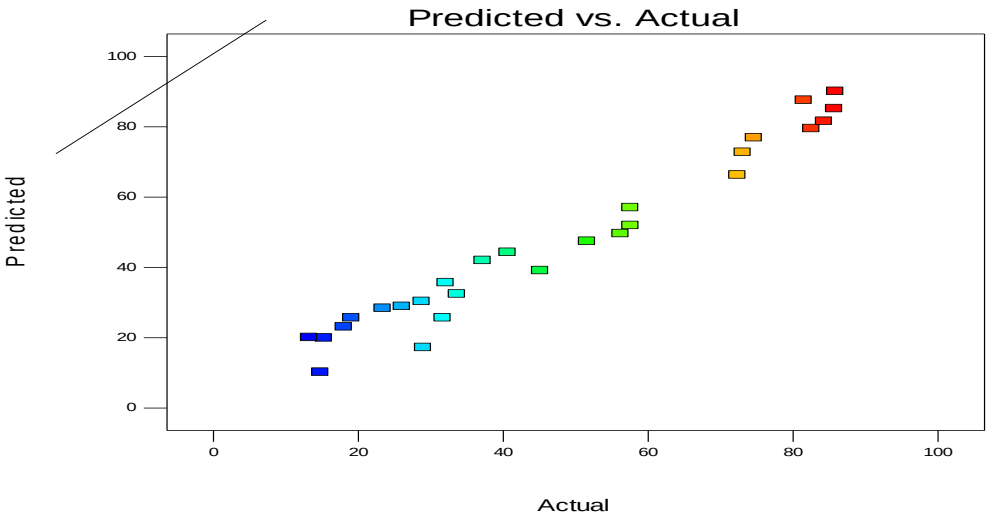

(c)

Fig 4.46: Design-expert plots: (a) Normal probability plots, (b) Residuals versus run number of data and (c) Predicted versus actual for turbidity removal in BRE using OSC.

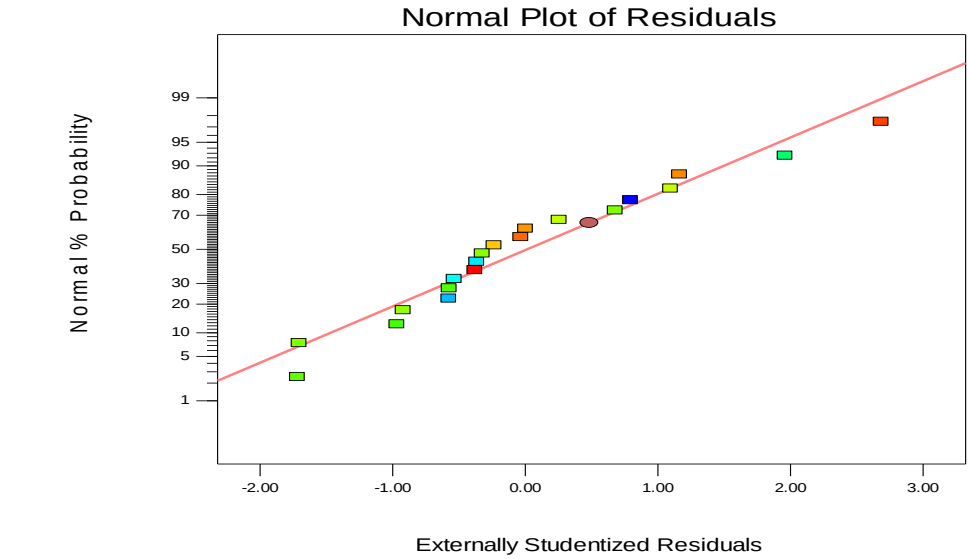

(a)

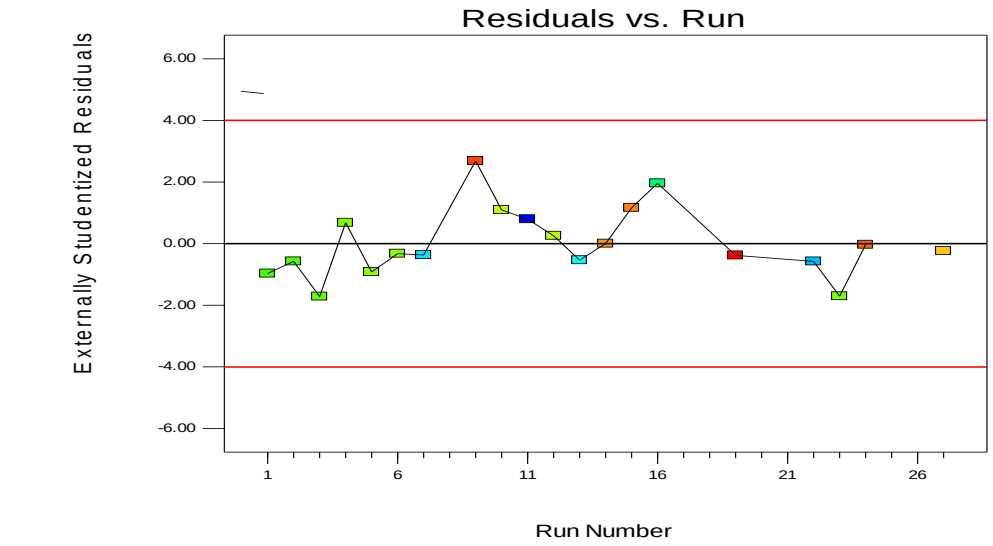

(b)

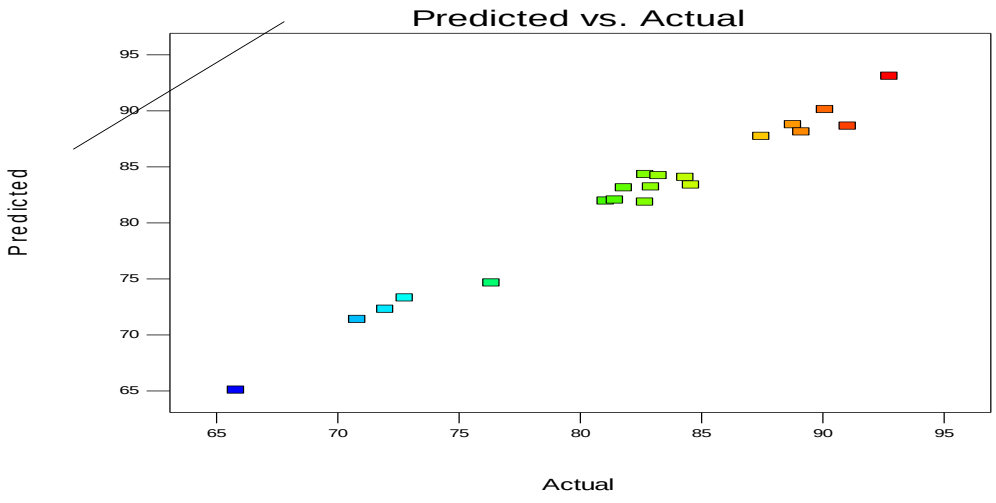

(c)

Fig. 4.47: Design-expert plots: (a) Normal probability plots, (b) Residuals versus run number of data and (c) Predicted versus actual for turbidity removal in BRE using ODC.

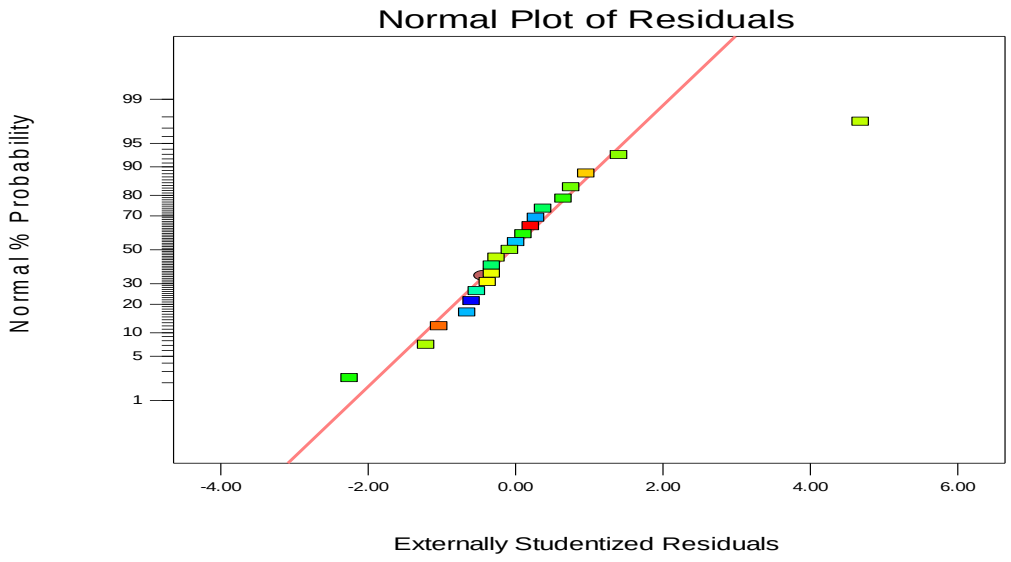

(a)

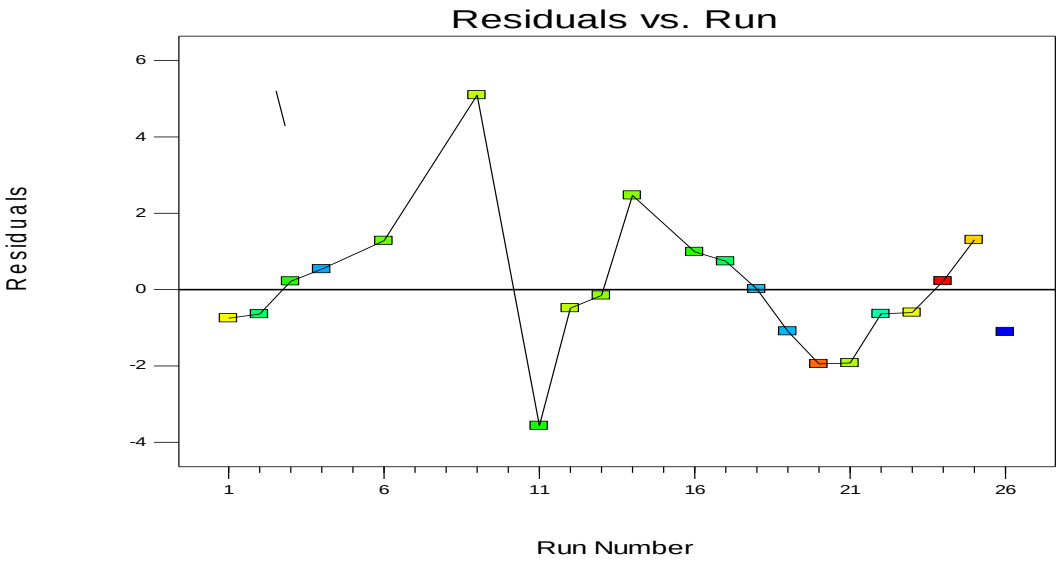

(b)

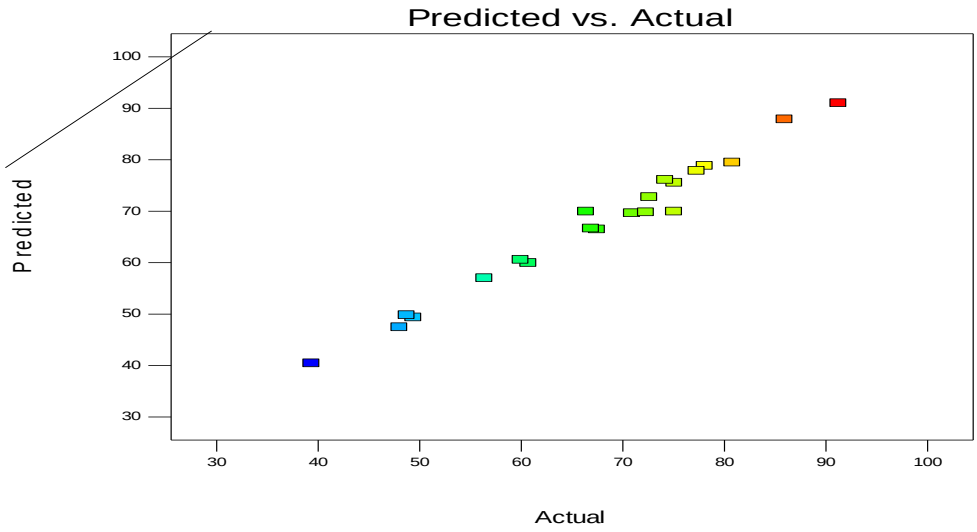

(c)

Fig. 4.48: Design-expert plots: (a) Normal probability plots, (b) Residuals versus run number of data and (c) Predicted versus actual for turbidity removal in PW using DMC.

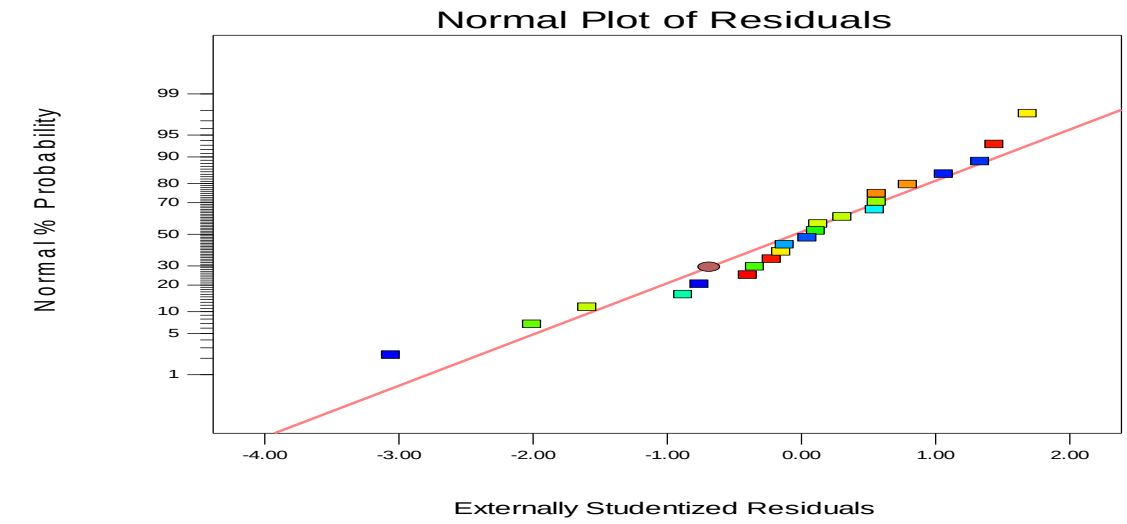

(a)

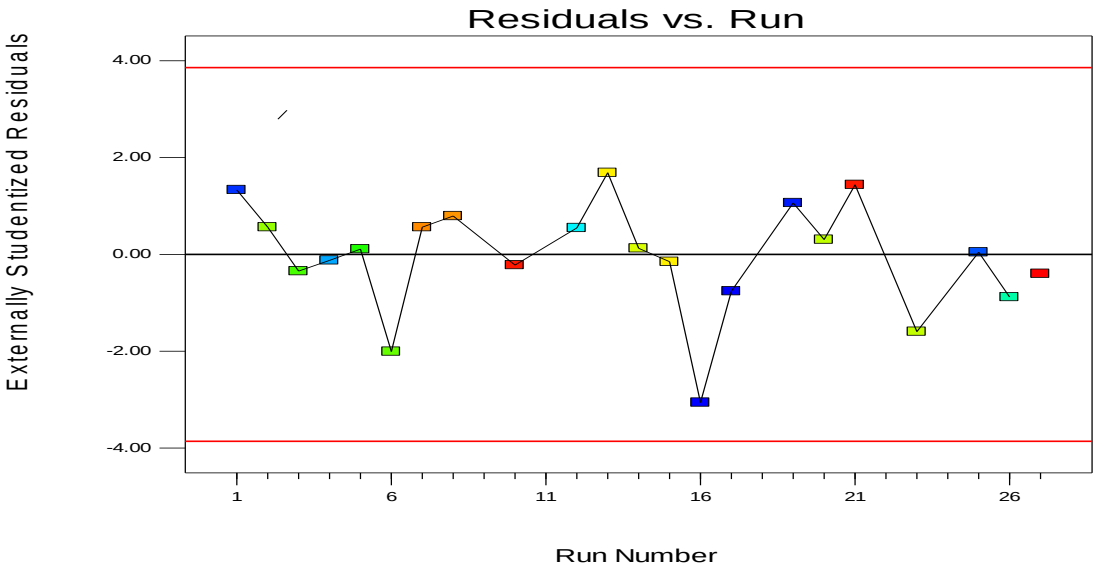

(b)

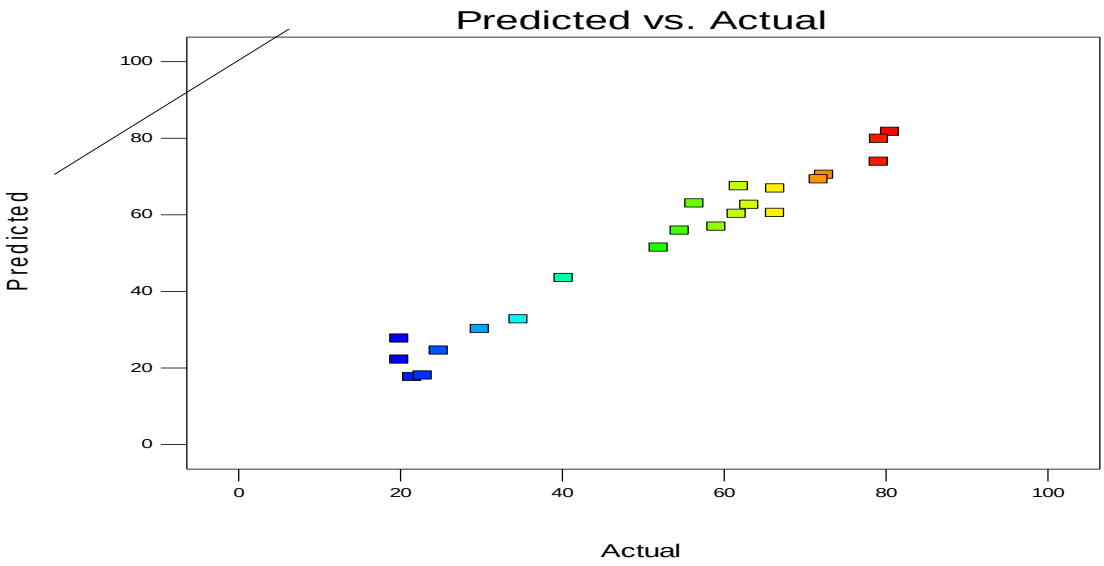

(c)

Fig. 4.49: Design-expert plots: (a) Normal probability plots, (b) Residuals versus run number of data and (c) Predicted versus Actual for turbidity removal in PW using CYC

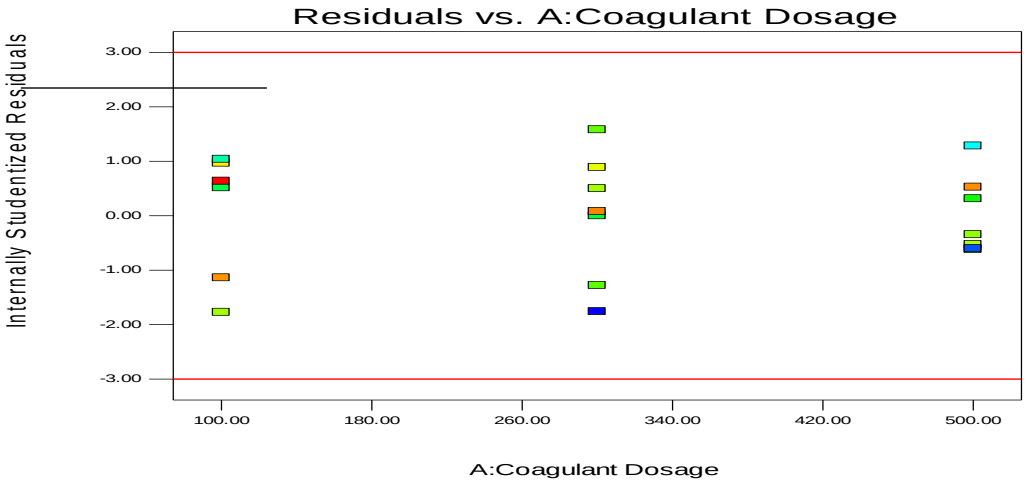

(a)

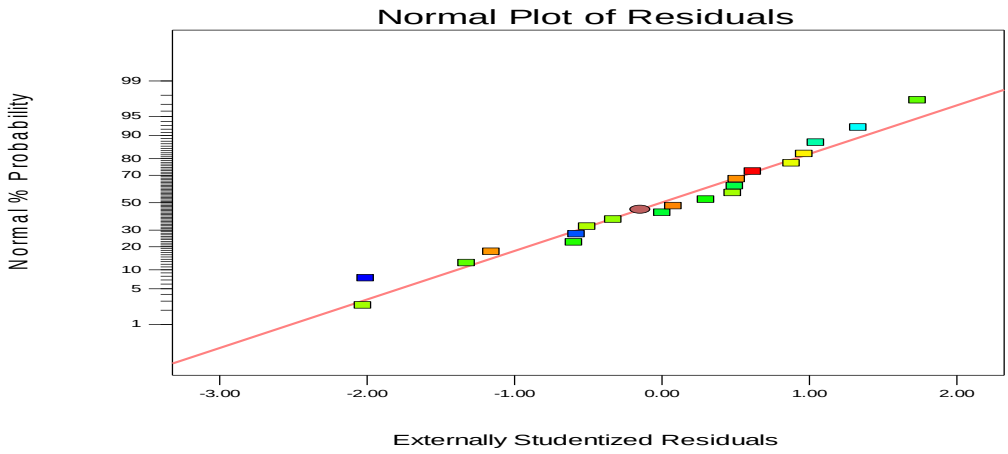

(b)

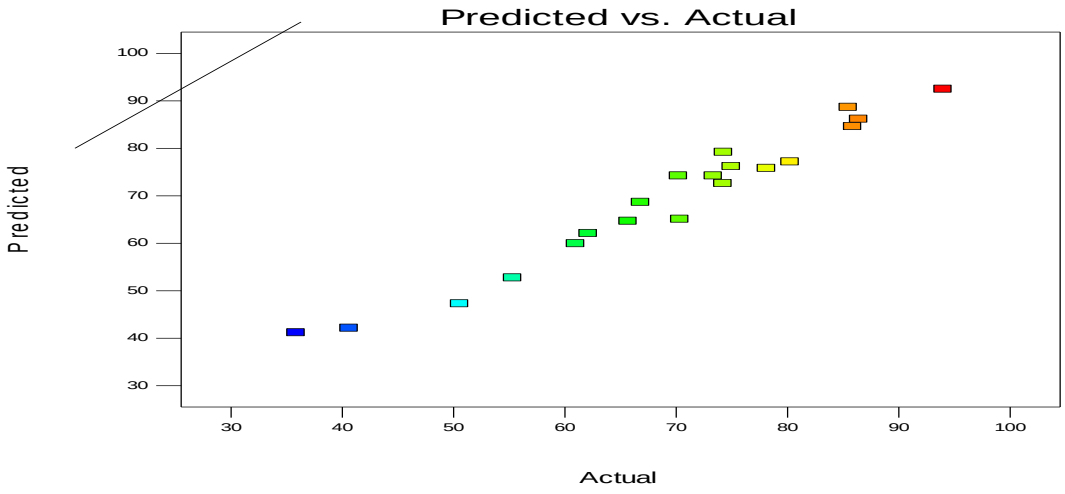

(c)

Fig. 4.50: Design-expert plots: (a) Normal probability plots, (b) Residuals versus run number of data and (c) Predicted versus Actual for turbidity removal in PW using OSC

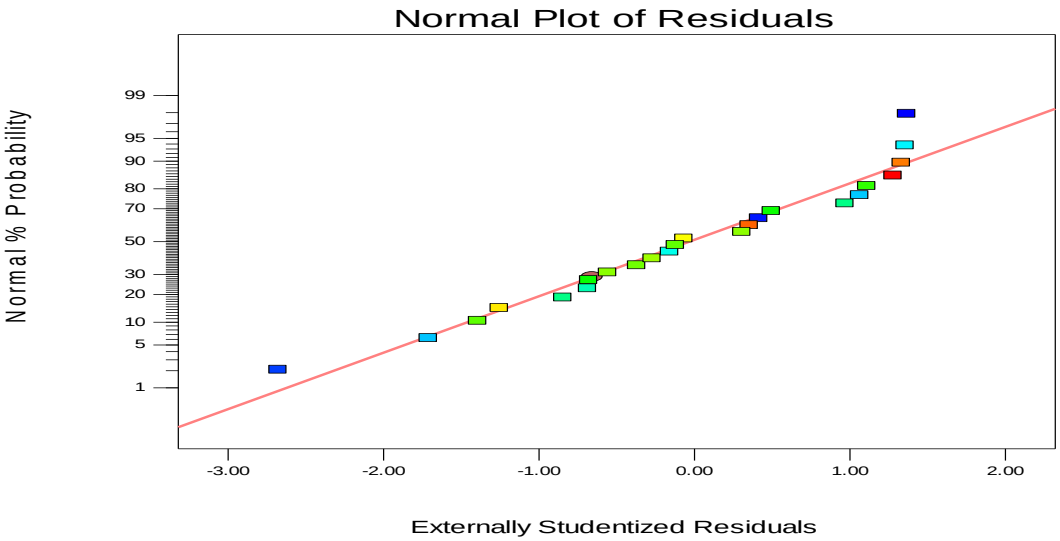

(a)

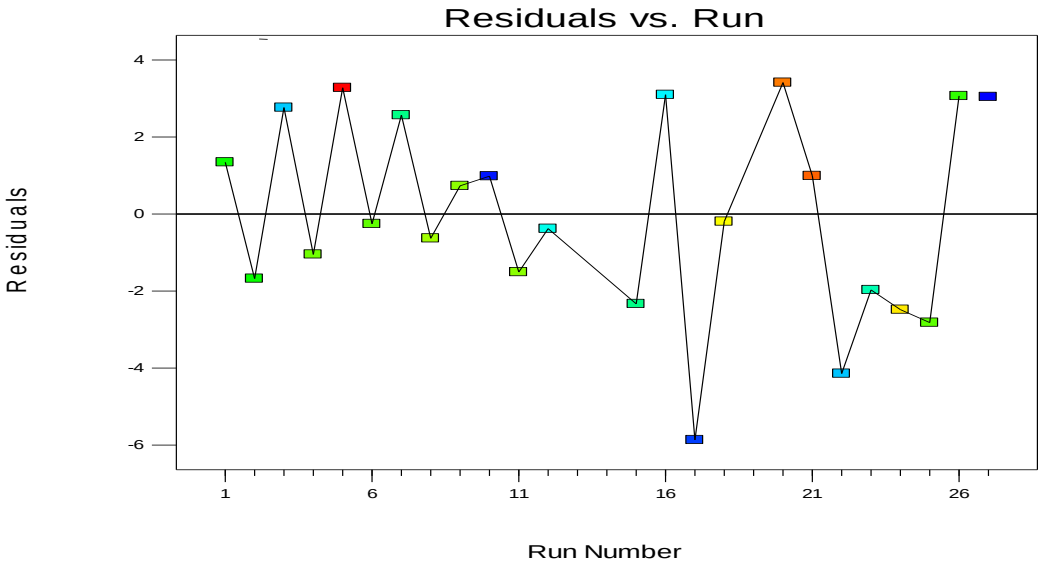

(b)

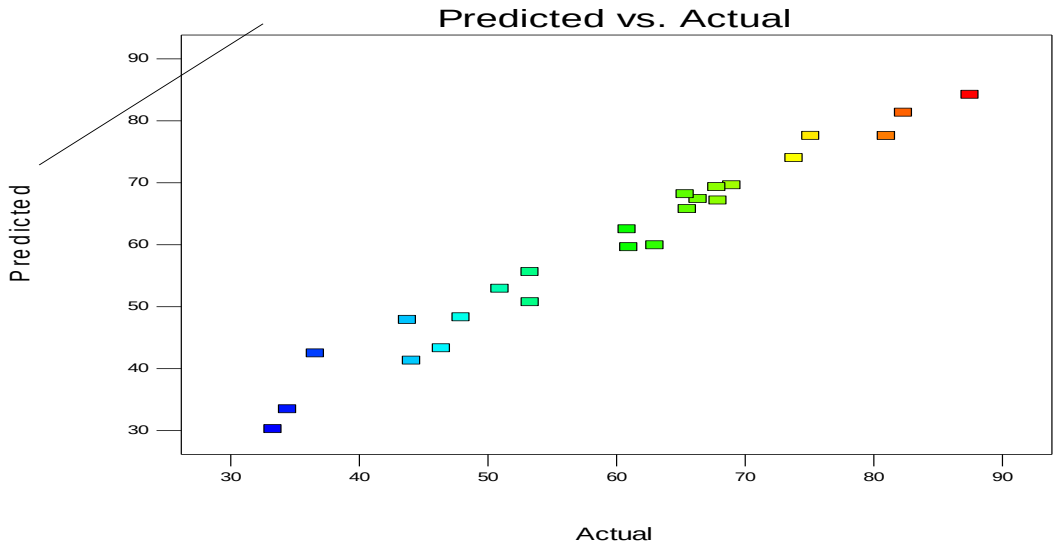

(c)

Fig 4.51: Design-expert plots: (a) Normal probability plots, (b) Residuals versus run number of data and (c) Predicted versus actual for turbidity removal in PW using ODC.

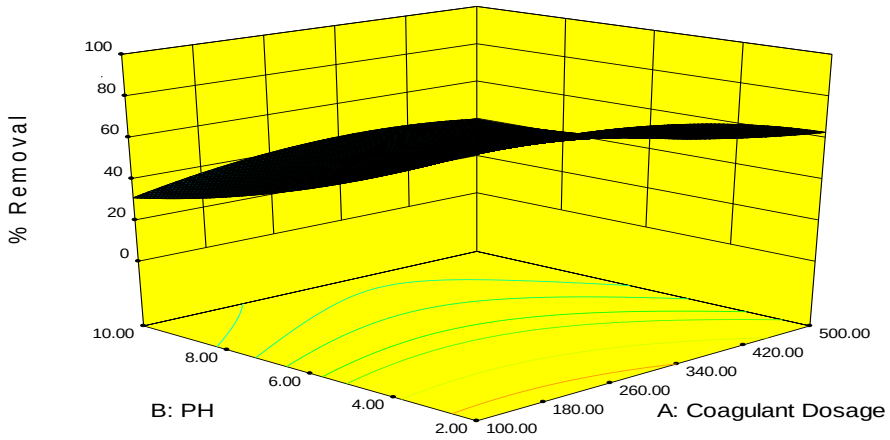

(a)

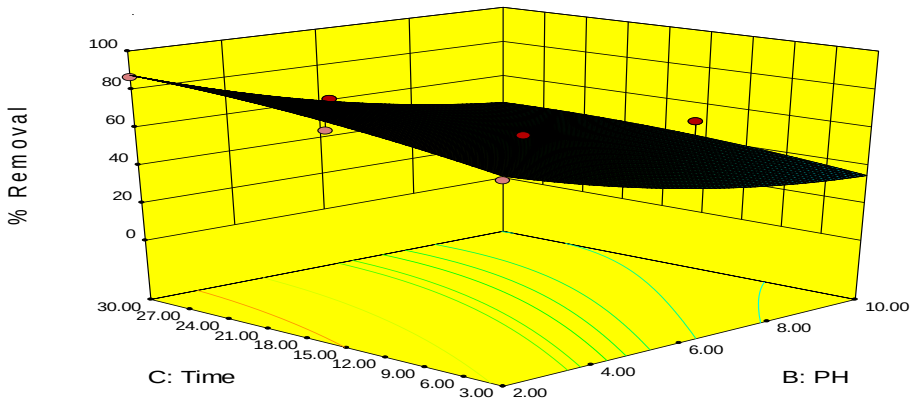

(b)

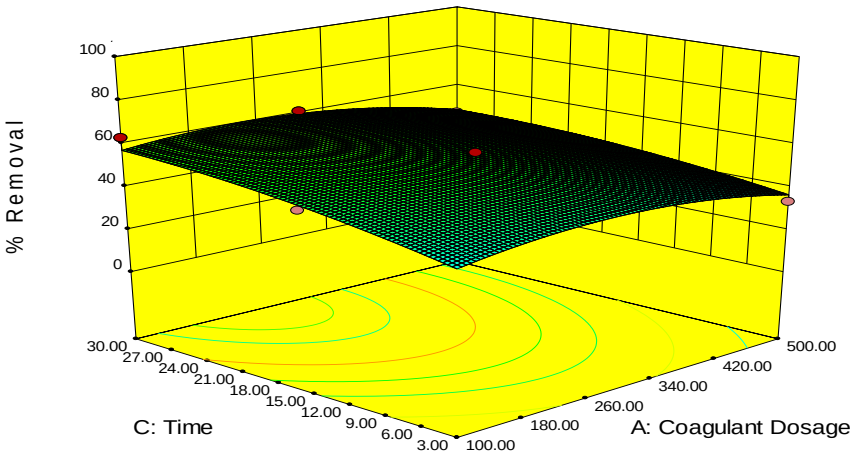

(c)

Fig 4.52: Response surface plots of the effects of (a) pH vs coagulant dosage (b) Settlig time vs pH (c) settling time vs coagulant dosage for turbidity removal in BRE using DMC.

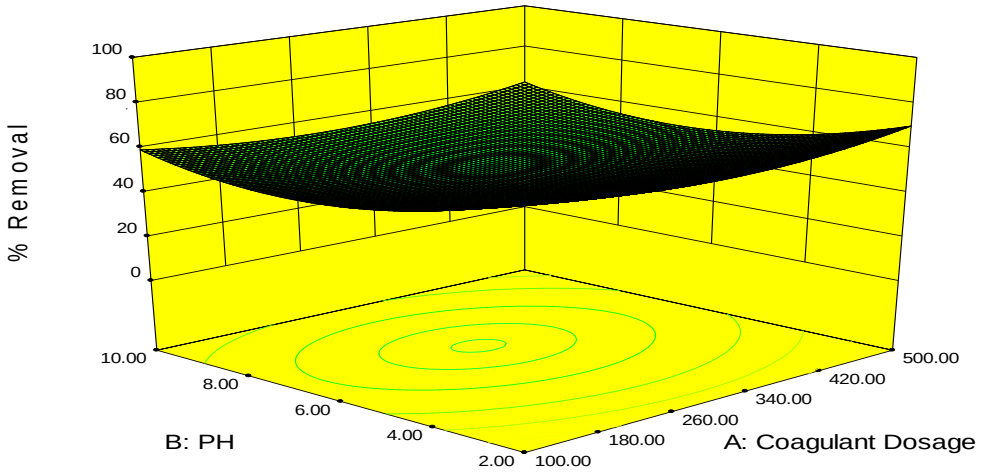

(a)

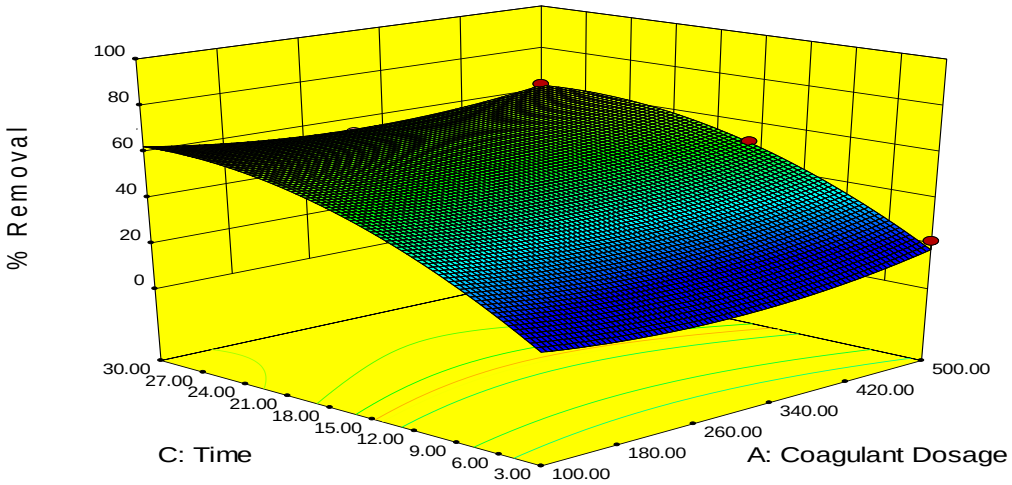

(b)

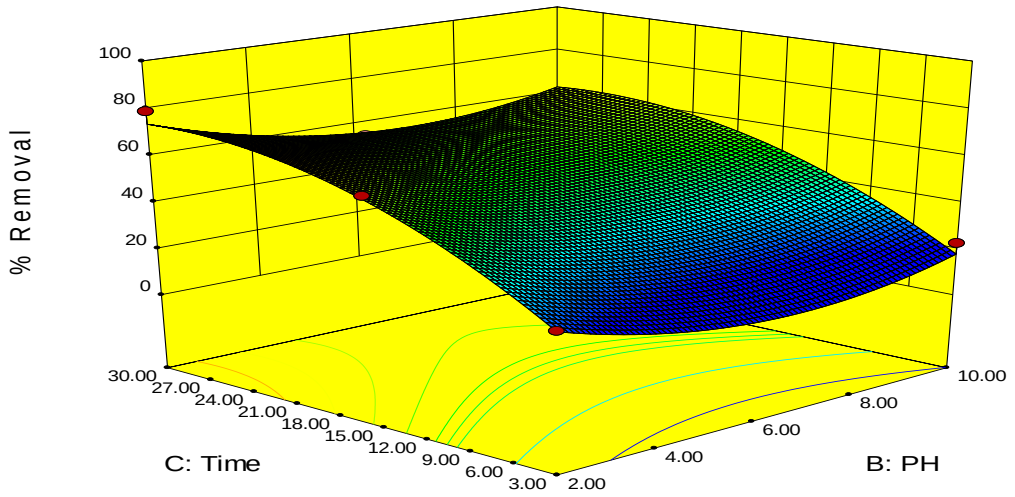

(c)

Fig 4.53: Response surface plots of the effects of (a) pH vs coagulant dosage (b) settling time vs coagulant dosage(c) settlig time vs pH for turbidity removal in BRE using CYC.

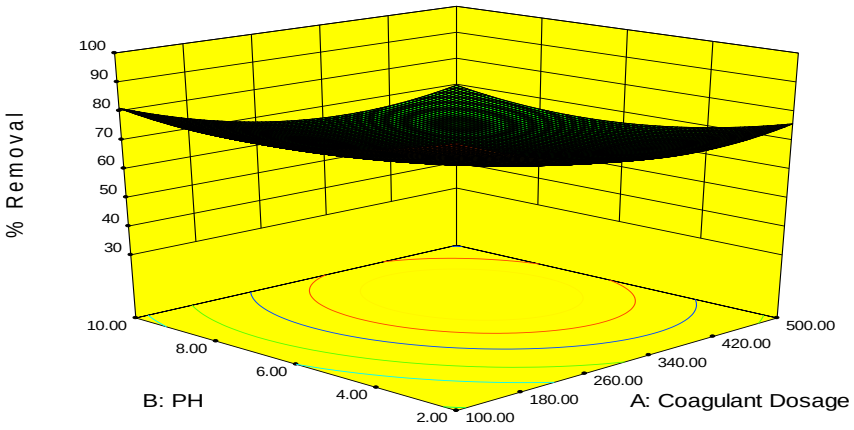

(a)

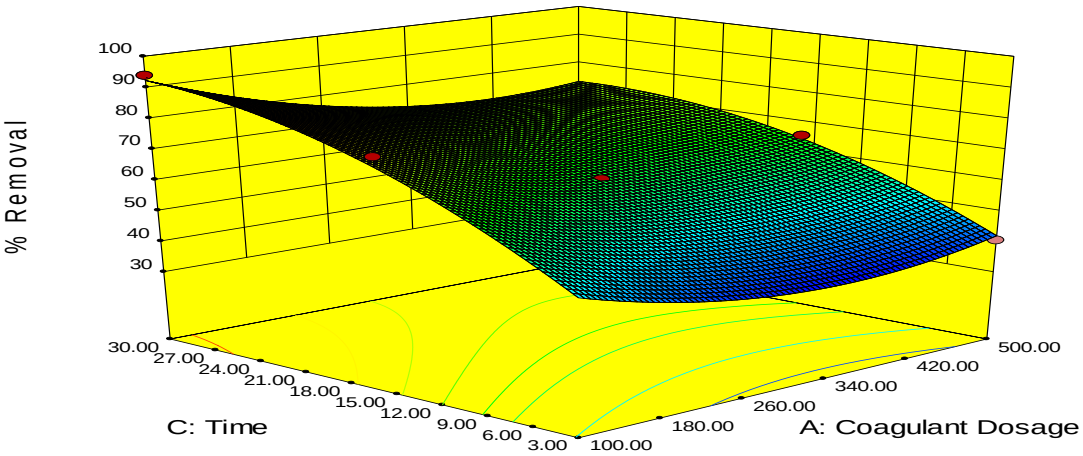

(b)

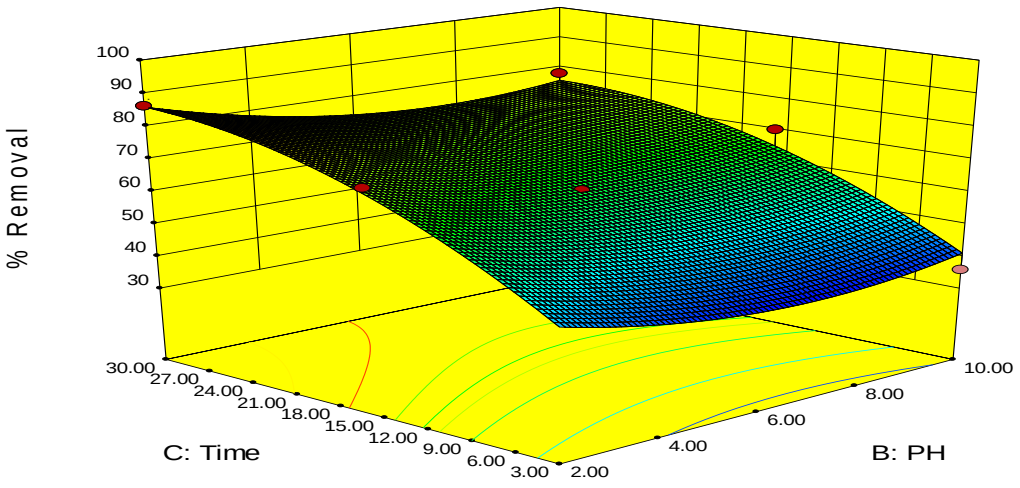

(c)

Fig 4.54: Response surface plots of the effects of (a) pH vs coagulant dosage (b) settling time vs coagulant dosage(c) settlig time vs pHfor turbidity removal in BRE using OSC.

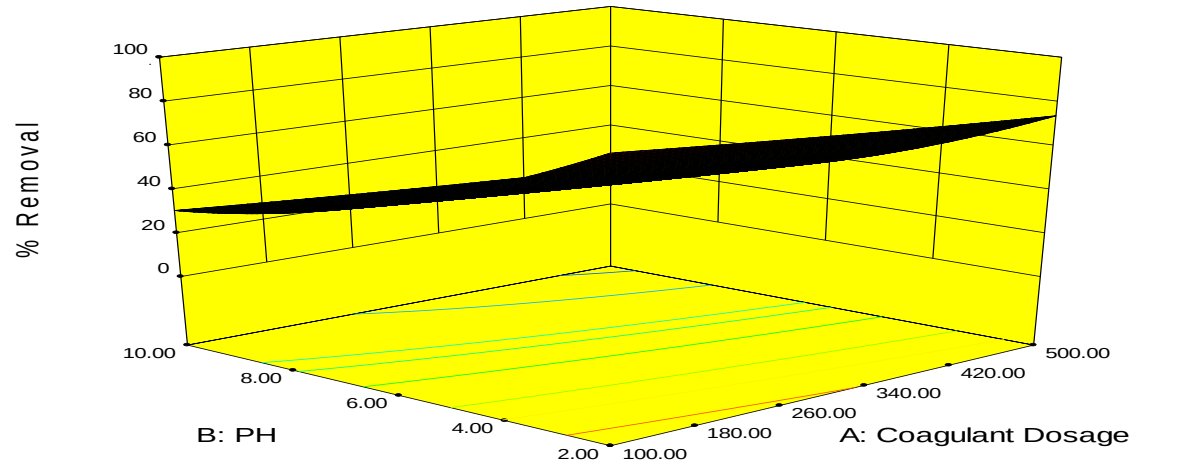

(a)

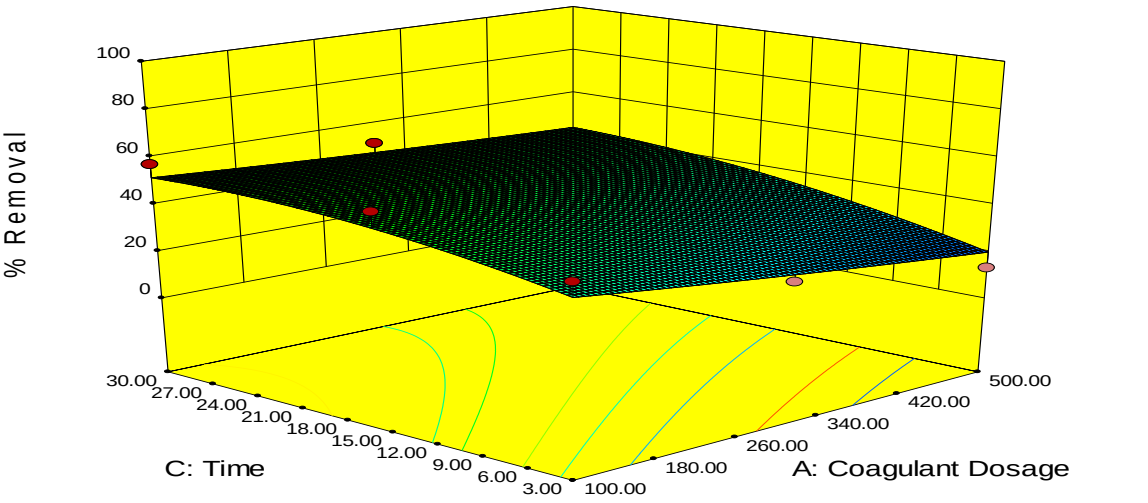

(b)

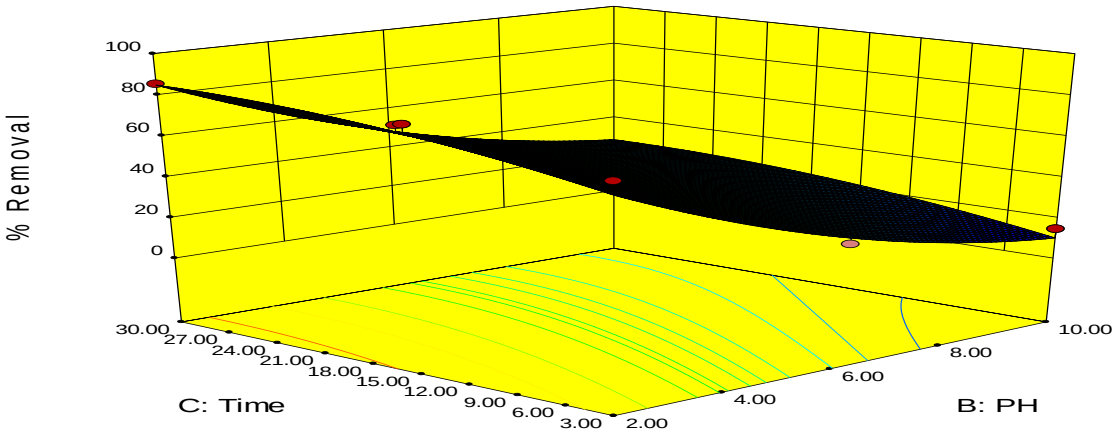

(c)

Fig 4.55: Response surface plots of the effects of (a) pH vs coagulant dosage (b) settling time vs coagulant dosage (c) Settlig time vs pH for turbidity removal in BRE using ODC.

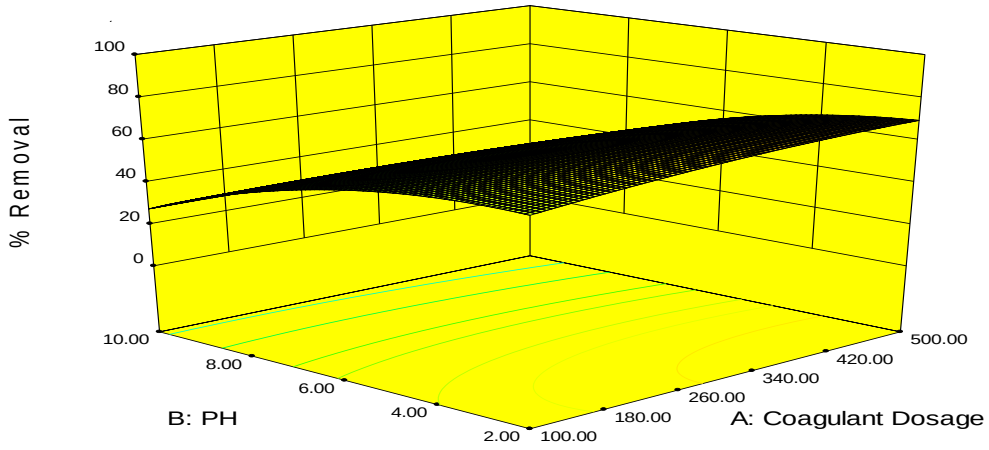

(a)

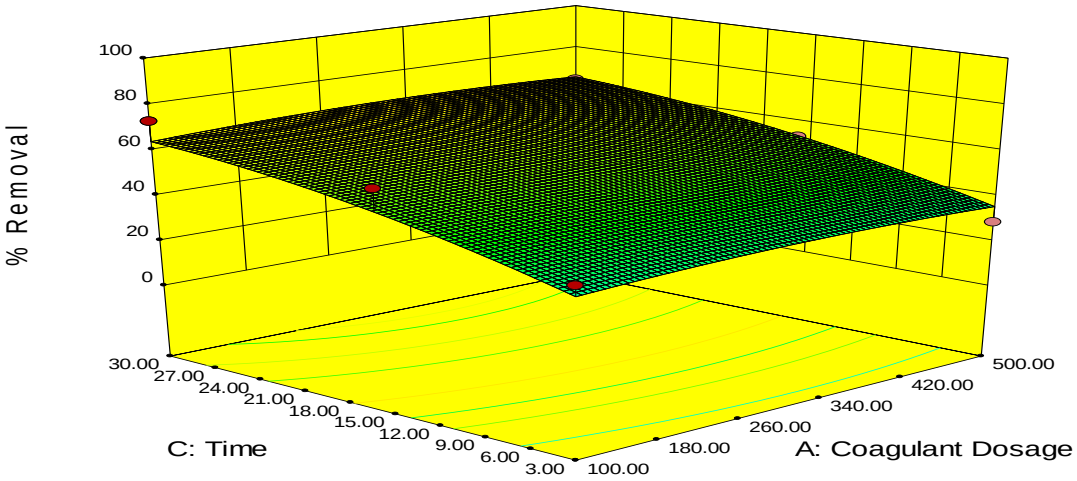

(b)

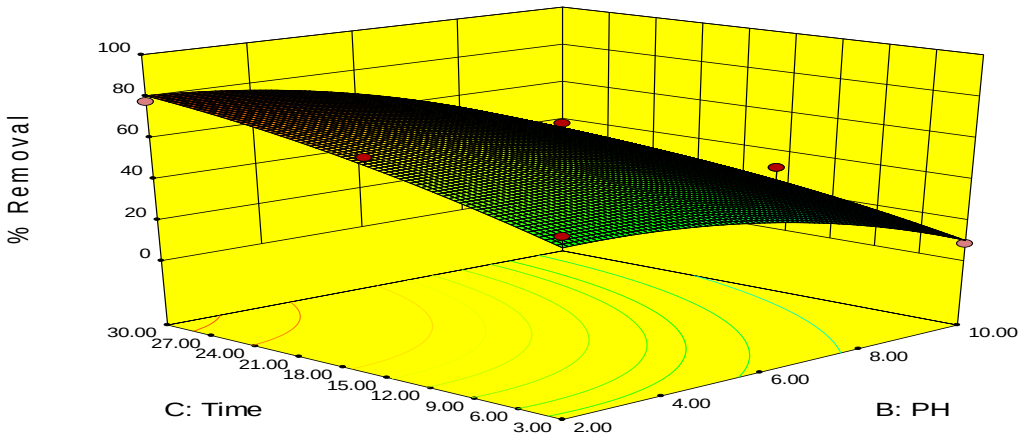

(c)

Fig 4.56: Response surface plots of the effects of (a) pH vs coagulant dosage (b) settling time vs coagulant dosage (c) Settlig time vs pH for turbidity removal in PW using DMC.

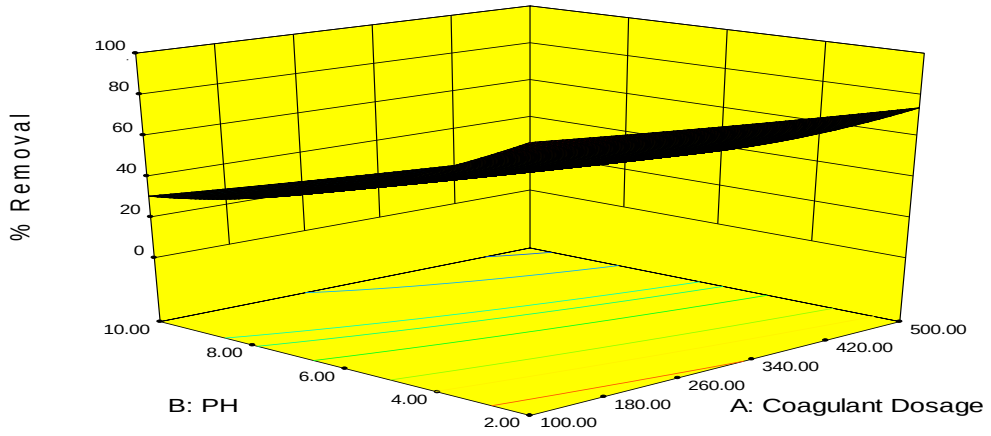

(a)

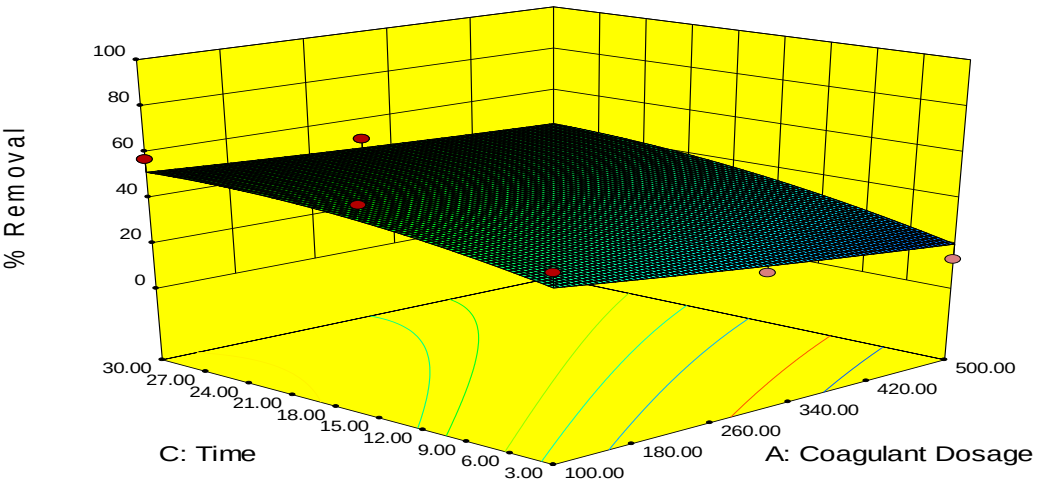

(b)

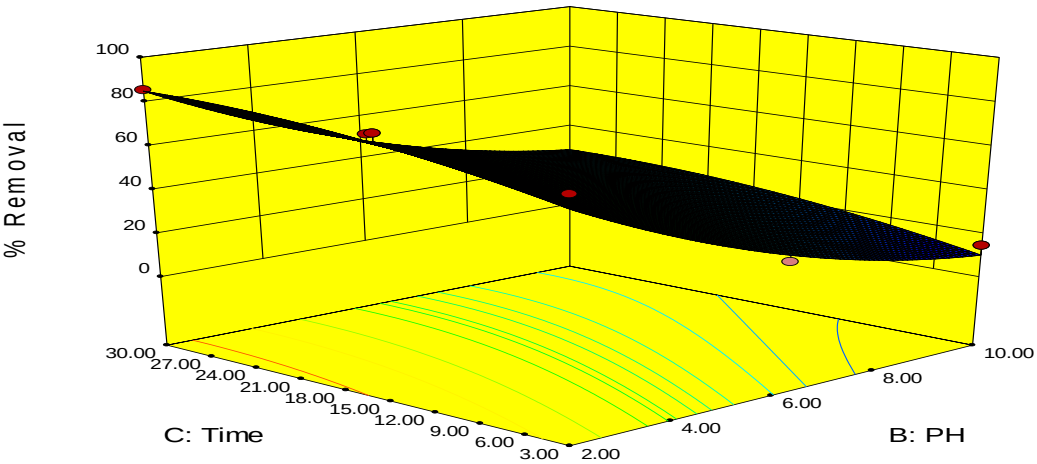

(c)

Fig 4.57: Response surface plots of the effects of (a) pH vs coagulant dosage (b) settling time vs coagulant dosage (c) settlig time vs pH for turbidity removal in PW using CYC.

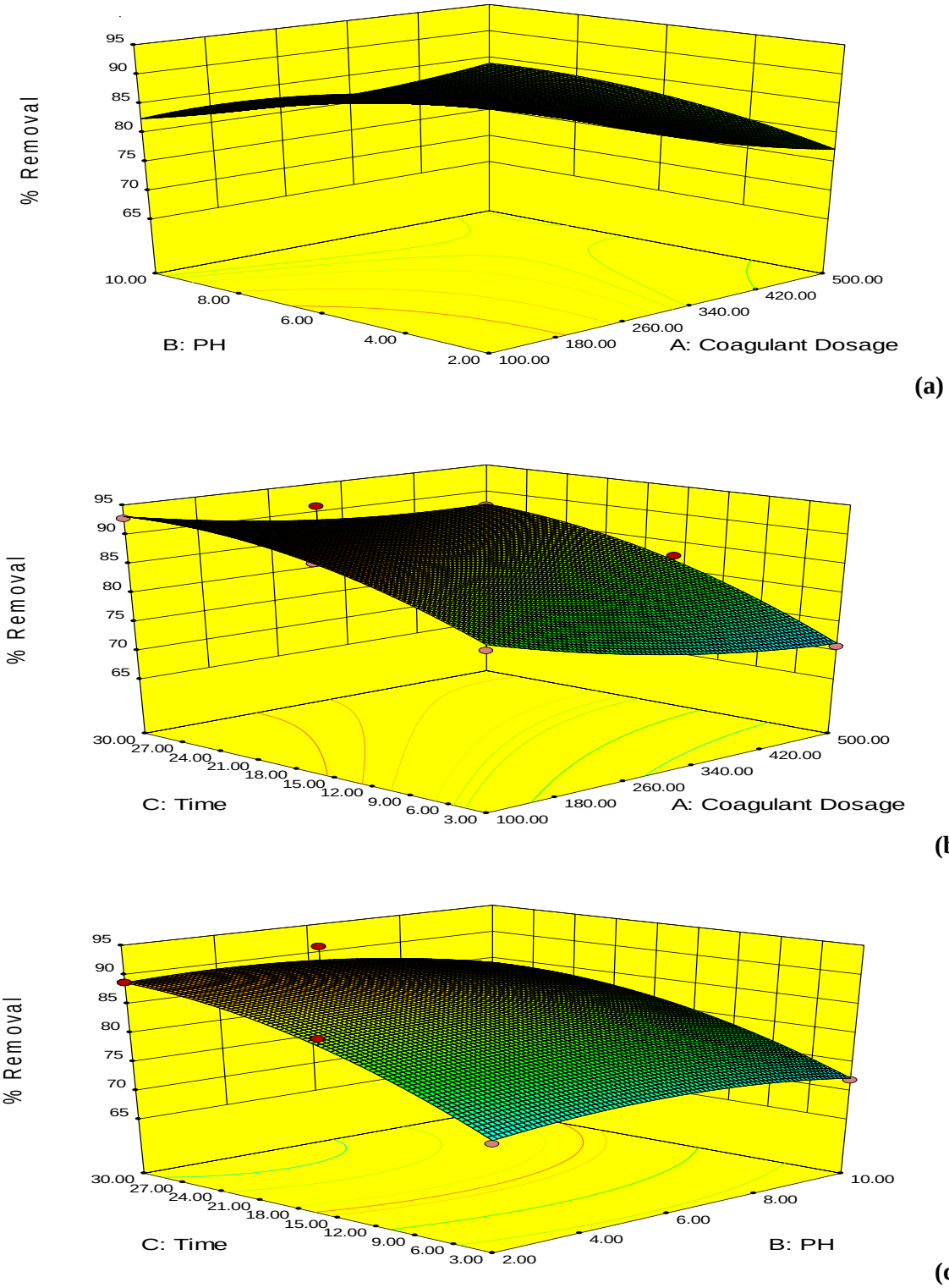

Fig 4.58: Response surface plots of the effects of (a) pH vs coagulant dosage (b) settling time vs coagulant dosage (c) Settlig time vs pH for turbidity removal in PW using OSC.

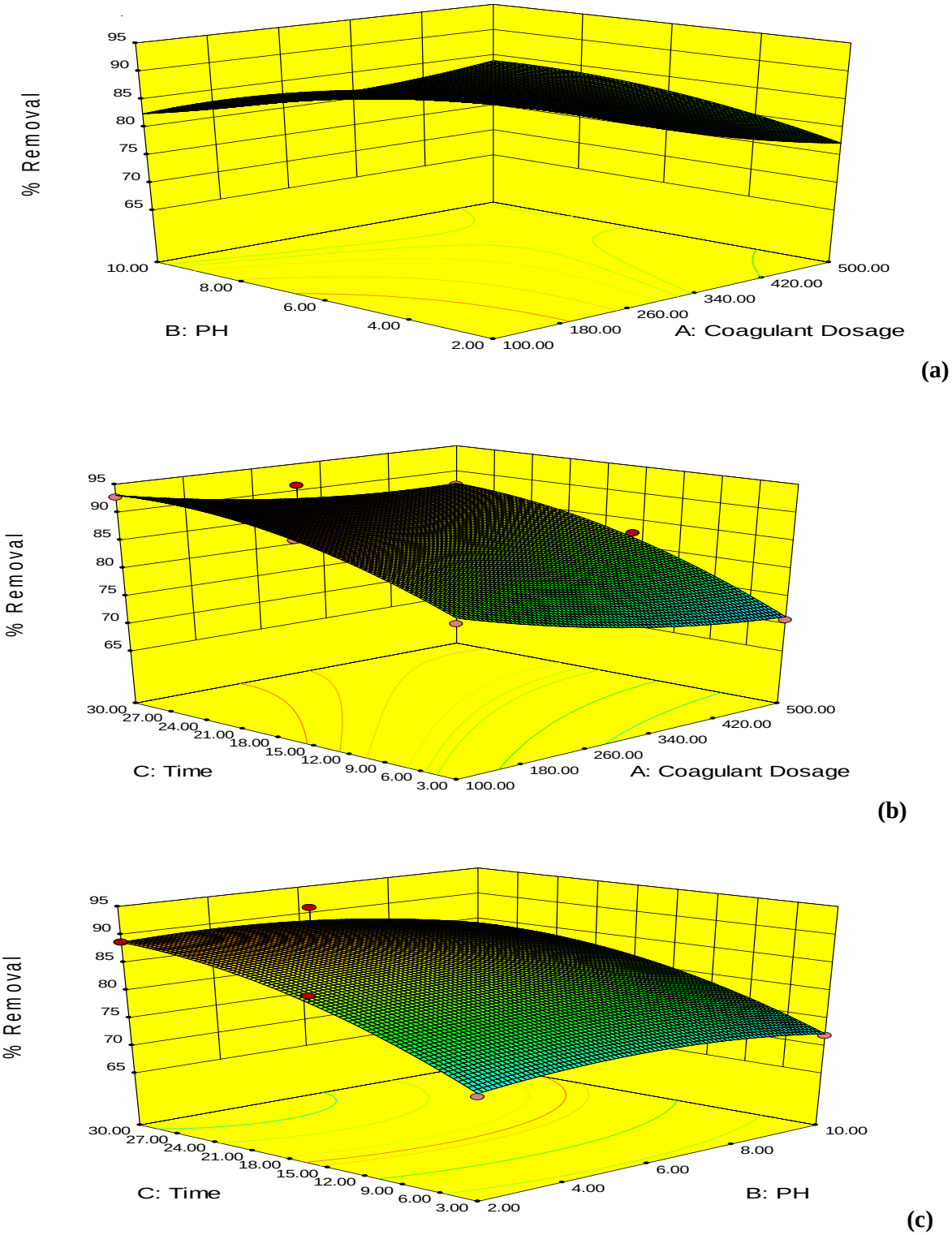

Fig 4.59: Response surface plots of the effects of (a) pH vs coagulant dosage (b) settling time vs coagulant dosage (c) Settlig time vs pH for turbidity removal in PW using ODC.

4.8 Optimization using the Desirability Functions

Optimization of turbidity removal was carried out by a multiple response methoed called desirability functions to optimize different combinations of process variables such as coagulant dosage, pH, and settling time. It is a value between 0 and 1, and increases as the corresponding response value becomes more desirable. By using numerical optimization, a desirable value for each input factor and response can be selected. In this study, the input variables were given specific ranged values, whereas the response was design to achieve a maximum. Tables 4.99 to 4.106, shows the optimum values for the responses and the factors for both BRE and PW. The values were calculated by means of the desirability function using design expert software. Figures 4.60 to 4.67 shows the most desirable points for DMC, CYC, OSC and ODC are (100.53, 2, 24.48), (476.97, 2, 30.00), (101.34, 2.08, 14.94) and (104.19, 3.3, 27.54) where the turbidity removal was 90.45, 83.40, 86.61 and 96.55 with 1.000, 0.982, 1.000 and 1.000 as overall desirability in BRE. While in PW, the desirable points are (100.15, 2, 20.10), (104.54, 2, 26.72), (101.98, 2.5, 28.98) and (100.00, 5.25, 30.00) also the turbidity removal was 91.29, 80.92, 95.49 and 84.59% with 1.000, 1.000, 1.000 and 0.946 as overall desirability.

Table 4.99: Results of optimization using Desirability function of DMC in BRE

Number	Coagulant	PH	Time	% Removal	Desirability

	Dosage					
1	159.460	2.137	28.361	90.991	1.000	
2	119.499	2.054	25.358	90.569	1.000	
3	218.547	2.042	27.982	90.618	1.000	
4	221.055	2.002	27.797	90.851	1.000	
5	203.825	2.006	28.387	91.504	1.000	
6	164.341	2.160	28.295	90.705	1.000	
7	195.826	2.030	26.522	90.787	1.000	
8	181.586	2.061	28.310	91.426	1.000	
9	119.715	2.092	27.029	90.948	1.000	
10	127.742	2.036	26.149	91.165	1.000	
11	172.504	2.042	27.057	91.289	1.000	
12	124.696	2.098	28.381	91.446	1.000	
13	166.936	2.153	29.695	91.206	1.000	
14	100.533	2.001	24.476	90.446	1.000	Selected
15	179.865	2.017	26.303	91.110	1.000	
16	175.903	2.076	28.485	91.435	1.000	
17	138.965	2.110	27.187	90.894	1.000	
18	141.437	2.227	29.727	90.649	1.000	

Table 4.100: Results of optimization using Desirability function of CYC in BRE

Number	Coagulant Dosage	PH	Time	% Removal	Desirability	
1	499.982	2.000	30.000	83.461	0.982	
2	497.991	2.000	30.000	83.458	0.982	
3	494.425	2.000	29.999	83.451	0.982	
4	491.395	2.000	30.000	83.444	0.982	
5	487.056	2.002	30.000	83.429	0.982	
6	485.578	2.000	30.000	83.429	0.982	
7	482.987	2.000	30.000	83.421	0.982	
8	481.123	2.000	30.000	83.414	0.982	
9	479.513	2.000	30.000	83.408	0.982	
10	476.973	2.000	30.000	83.398	0.982	Selected
11	499.946	2.000	29.886	83.385	0.981	
12	499.408	2.047	30.000	83.372	0.981	
13	469.173	2.000	30.000	83.363	0.981	
14	464.158	2.000	30.000	83.337	0.981	
15	486.780	2.046	29.976	83.333	0.981	

Table 4.101: Results of optimization using Desirability function of OSC in BRE

Number	Coagulant Dosage	PH	Time	% Removal	Desirability	
1	154.232	2.111	18.626	85.922	1.000	
2	224.387	2.035	24.485	86.259	1.000	
3	266.578	2.000	27.312	85.909	1.000	
4	165.741	2.176	25.762	86.529	1.000	
5	135.000	2.300	27.863	85.977	1.000	
6	112.270	2.198	20.266	87.092	1.000	
7	121.852	2.348	25.875	85.896	1.000	
8	169.844	2.190	23.571	85.969	1.000	
9	123.634	2.054	15.000	85.964	1.000	
10	133.128	2.136	23.603	87.813	1.000	
11	232.003	2.079	28.479	85.890	1.000	
12	131.797	2.030	15.667	86.293	1.000	
13	198.244	2.040	21.761	86.349	1.000	
14	167.959	2.160	25.231	86.605	1.000	
15	263.434	2.018	28.870	85.841	1.000	
16	101.343	2.079	14.944	86.609	1.000	Selected
17	255.661	2.008	26.958	86.066	1.000	

Table 4.102: Results of optimization using Desirability function of ODC in BRE

Number	Coagulant Dosage	PH	Time	% Removal	Desirability	
1	128.519	3.479	21.292	94.151	1.000	
2	118.173	2.498	16.830	93.612	1.000	
3	129.959	5.095	23.267	92.982	1.000	
4	119.163	4.009	28.628	95.240	1.000	
5	133.292	2.058	17.034	93.019	1.000	
6	133.333	5.244	28.050	93.219	1.000	
7	180.505	2.189	27.056	93.538	1.000	
8	113.333	3.689	19.500	94.132	1.000	
9	126.977	5.280	24.888	93.131	1.000	
10	129.924	4.218	23.530	94.000	1.000	
11	137.590	5.011	24.966	93.095	1.000	
12	153.508	2.479	20.462	93.194	1.000	
13	102.129	2.269	14.823	93.661	1.000	
14	122.445	4.916	29.160	94.036	1.000	
15	104.189	3.337	27.537	96.551	1.000	Selected
16	126.667	2.533	24.600	95.684	1.000	
17	148.680	4.639	28.079	93.404	1.000	
18	144.774	3.202	27.181	94.755	1.000	

Table 4.103: Results of optimization using Desirability function of DMC in PW

Number	Coagulant Dosage	PH	Time	% Removal	Desirability	
1	100.218	2.001	29.419	91.267	1.000	
2	104.892	2.008	26.497	91.945	1.000	
3	100.536	2.049	21.071	91.398	1.000	
4	103.011	2.024	25.361	92.052	1.000	
5	109.605	2.038	27.347	91.395	1.000	
6	109.360	2.105	24.356	91.326	1.000	
7	116.045	2.040	25.091	91.439	1.000	
8	106.536	2.033	28.347	91.255	1.000	
9	102.667	2.104	27.475	91.251	1.000	
10	107.216	2.042	22.962	91.647	1.000	
11	101.743	2.053	21.658	91.513	1.000	
12	114.657	2.048	26.023	91.381	1.000	
13	104.506	2.070	27.588	91.345	1.000	
14	112.688	2.050	26.494	91.380	1.000	
15	111.127	2.006	28.296	91.249	1.000	
16	109.393	2.002	22.455	91.698	1.000	
17	112.126	2.043	23.778	91.542	1.000	
18	102.309	2.008	27.699	91.773	1.000	
19	109.706	2.053	27.157	91.352	1.000	
20	100.150	2.007	20.101	91.292	1.000	Selected

Table 4.104: Results of optimization using Desirability function of CYC in PW

Number	Coagulant Dosage	PH	Time	% Removal	Desirability	
1	106.047	2.003	25.645	80.513	1.000	
2	104.543	2.022	26.717	80.921	1.000	Selected
3	100.271	2.053	28.261	81.328	1.000	
4	106.667	2.044	29.250	80.959	1.000	
5	108.756	2.052	28.546	80.751	1.000	
6	106.889	2.066	27.317	80.592	1.000	
7	109.943	2.001	27.361	80.895	1.000	
8	101.324	2.004	29.120	81.664	1.000	
9	102.844	2.122	29.204	80.643	1.000	
10	105.100	2.005	27.321	81.190	1.000	
11	109.624	2.063	29.300	80.607	1.000	
12	100.055	2.156	29.415	80.574	1.000	
13	112.085	2.050	29.387	80.530	1.000	
14	111.555	2.022	26.961	80.514	1.000	

Table 4.105: Results of optimization using Desirability function of OSC in PW

Number	Coagulate Dosage	PH	Time	% Removal	Desirability	
1	100.667	2.790	23.060	96.735	1.000	
2	101.975	2.464	28.983	95.494	1.000	Selected
3	100.004	4.852	29.997	94.809	1.000	
4	115.336	2.355	27.718	100.511	1.000	
5	111.871	4.104	28.470	94.688	1.000	
6	103.333	2.067	29.325	104.328	1.000	
7	101.134	4.459	27.271	94.413	1.000	
8	109.353	2.149	21.317	96.424	1.000	
9	130.000	2.600	27.525	97.442	1.000	
10	118.593	2.537	23.835	96.274	1.000	
11	108.512	4.039	26.412	94.118	1.000	
12	126.667	2.533	24.600	95.992	1.000	
13	187.564	2.095	29.723	94.273	1.000	
14	114.769	2.739	26.455	98.082	1.000	
15	100.753	2.206	20.864	96.707	1.000	

Table 4.106: Results of optimization using Desirability function of ODC in PW

Number	Coagulant Dosage	PH	Time	% Removal	Desirability	
1	100.000	5.247	30.000	84.590	0.946	Selected
2	100.001	5.276	30.000	84.589	0.946	
3	100.007	5.214	30.000	84.589	0.946	
4	100.000	5.307	30.000	84.587	0.946	
5	100.002	5.180	30.000	84.586	0.946	
6	100.005	5.377	30.000	84.578	0.946	
7	100.007	5.111	30.000	84.577	0.946	
8	100.046	5.040	30.000	84.560	0.946	
9	102.498	5.229	30.000	84.552	0.946	
10	102.348	5.343	30.000	84.550	0.946	
11	100.001	4.990	30.000	84.545	0.946	
12	100.002	5.257	29.882	84.527	0.945	
13	100.012	5.567	30.000	84.522	0.945	
14	100.003	5.128	29.841	84.496	0.945	
15	106.771	5.293	30.000	84.489	0.945	

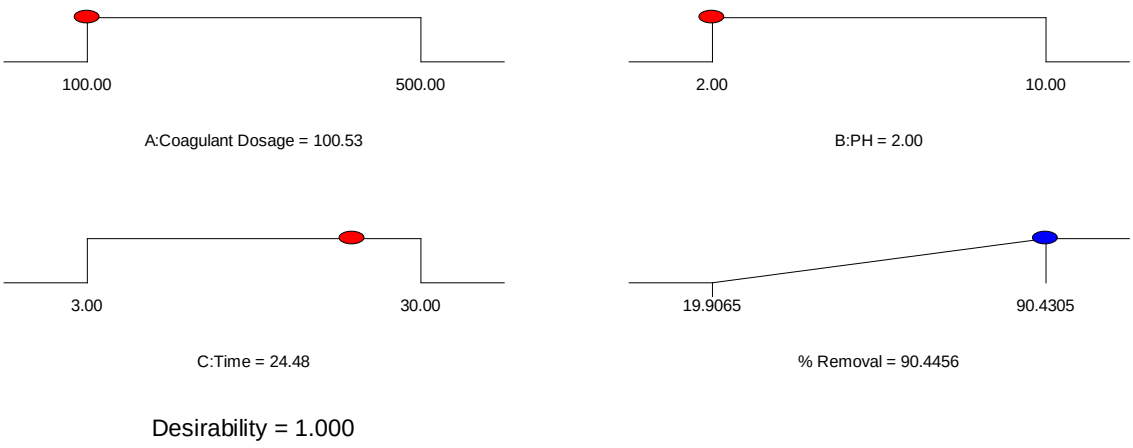

Fig. 4.60: Desirability ramp of optimized DMC in BRE.

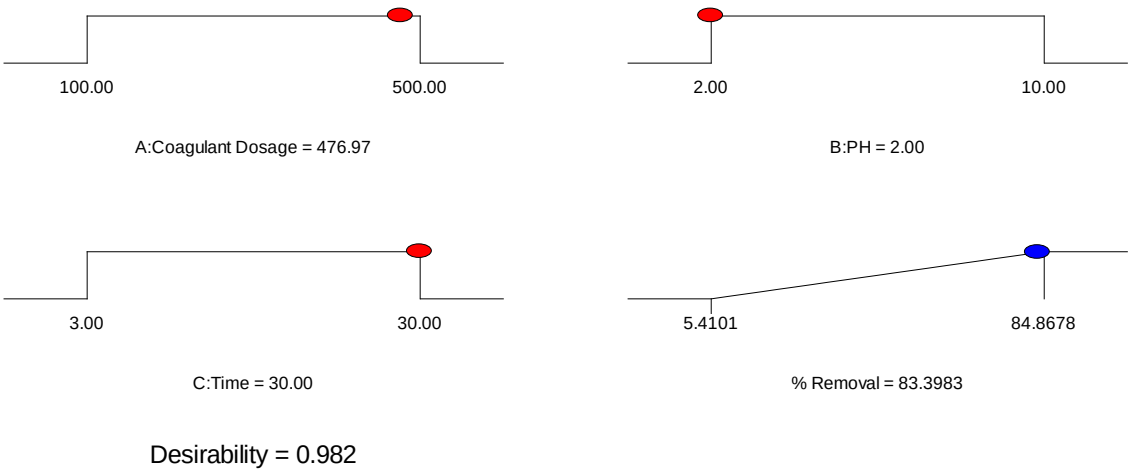

Fig 4.61: Desirability ramp of optimized CYC in BRE.

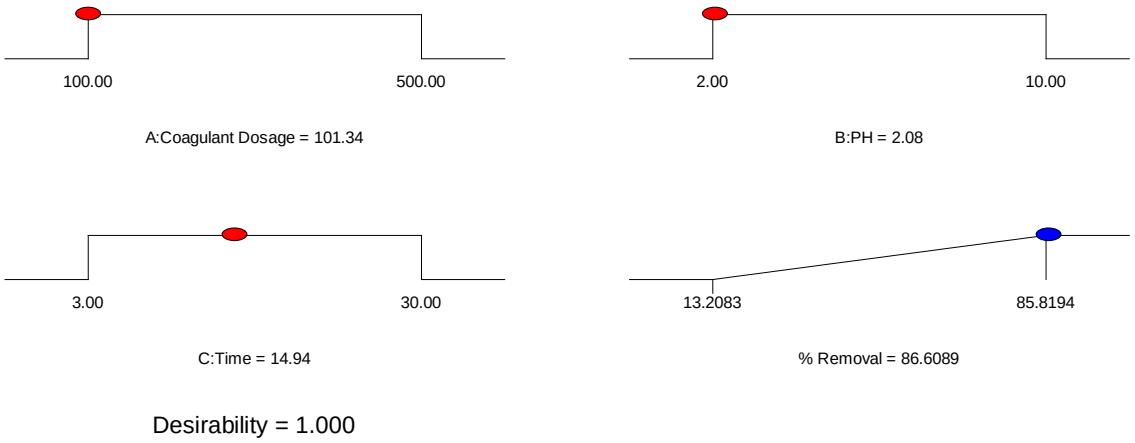

Fig 4.62: Desirability ramp of optimized OSC in BRE.

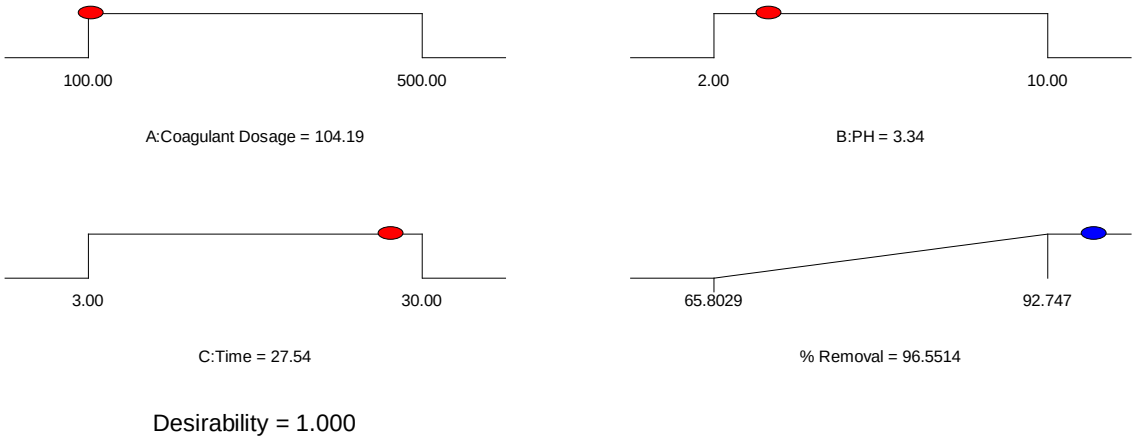

Fig 4.63: Desirability ramp of optimized ODC in BRE.

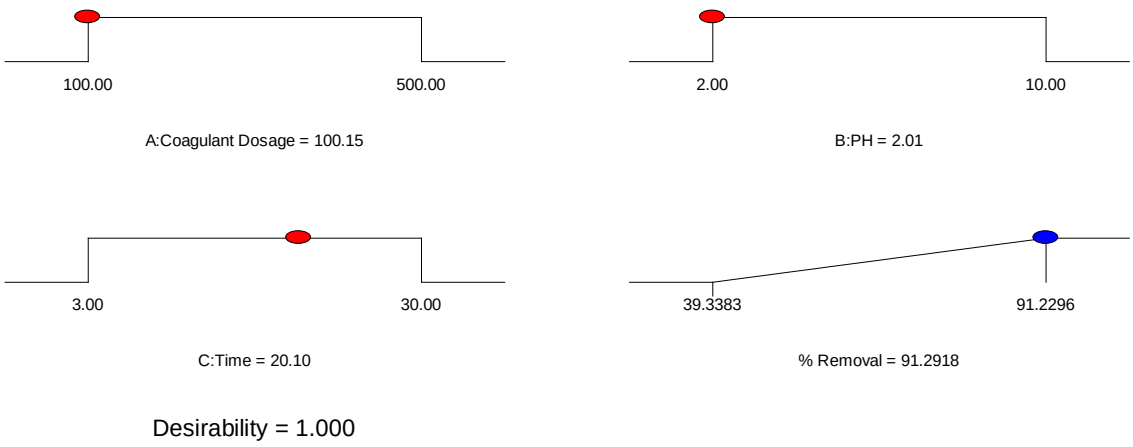

Fig 4.64: Desirability ramp of optimized DMC in PW.

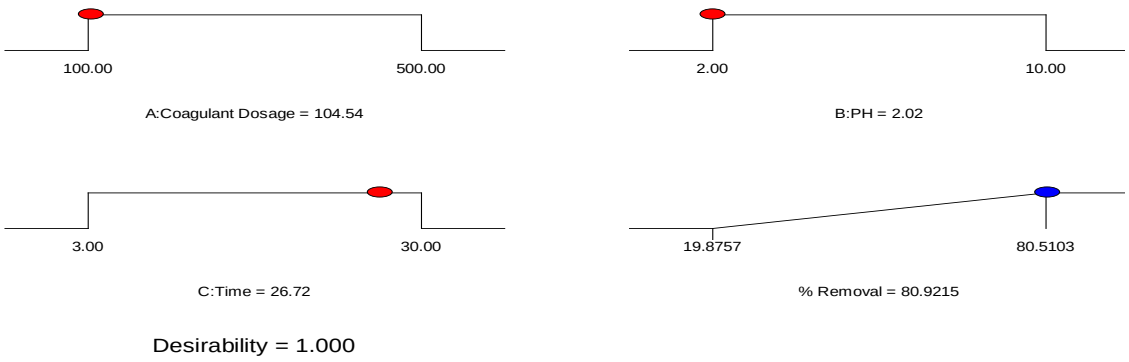

Fig 4.65: Desirability ramp of optimized CYC in PW.

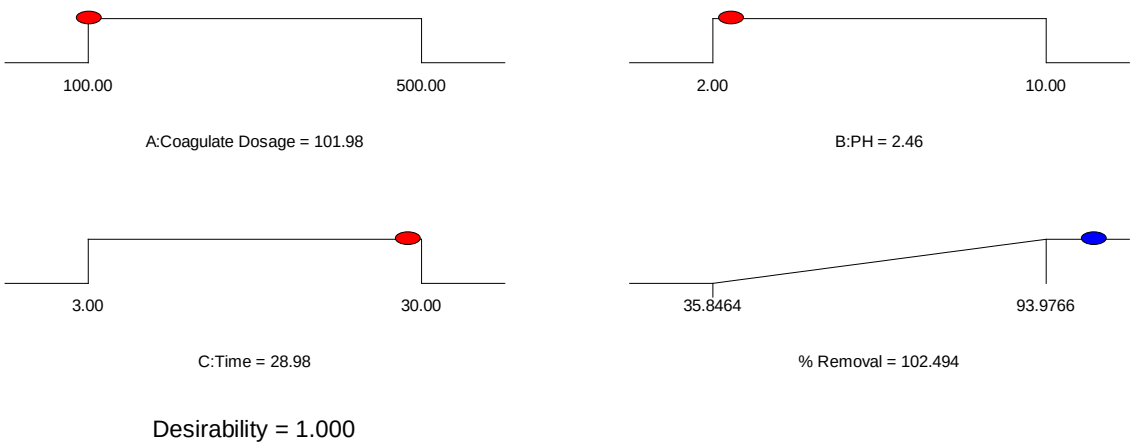

Fig 4.66: Desirability ramp of optimized OSC in PW.

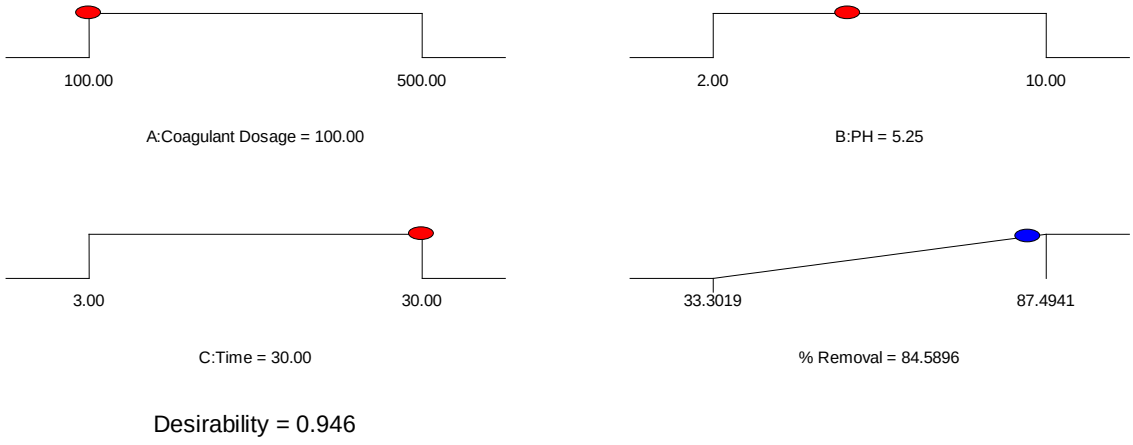

Fig 4.67: Desirability ramp of optimized ODC in PW.

4.9 Model Validation and Confirmation Experiments

The optimized conditions generated during response surface methodology were validated by conducting coag-flocculation experiment with the optimum parameters. Details of the experiments conducted, predicted and measured values of the output variables are given in Tables 4.107 and 4.108 for BRE and PW. Also the maximum error (%) between the predicted values and experimental values were less than 3% indicating that the quadratic models adopted could predict experimental results well (Shama et al., 2009).

Table 4.107:Validation of the models for turbidity removal in BRE.

Coagulants	pH	Dosage (mg/L)	Settling time (min)	Predicted values (%)	Experimental values (%)	Error (%)
DMC	2.0	100.53	24.48	90.45	89.35	1.22
CYC	2.0	476.97	30.00	83.40	81.63	2.12
OSC	2.0	101.34	14.94	86.61	85.24	1.58
ODC	3.3	104.19	27.53	96.55	94.85	1.76

Table 4.108: Validation of the models for turbidity removal in PW.

Coagulants	pH	Dosage (mg/L)	Settling time (min)	Predicted values (%)	Experimental values (%)	Error (%)
DMC	2.0	100.15	20.00	91.29	89.63	1.82
CYC	2.0	104.54	26.72	80.92	79.63	1.59
OSC	2.5	101.98	28.98	93.97	92.88	1.16
ODC	5.3	100.00	30.00	84.59	82.78	2.14

4.10 Adsorption studies

The adsorption study was carried out to evaluate the effects of various parameters via: Contact time, pH and adsorbent dosage in removal of turbidity from BRE and PW.

4.10.1 Effect of pH

The effluent pH is considered as a very important parameter in adsorption process. The pH optimization was done by varying the pH in the range 2-10, shown in fig.4.68 and 4.69. It was observed that maximum removal of turbidity was established at pH 8, and further increase in pH beyond pH 8 results in the formation of precipitation. The highest removal was in the range 99.0 to 99.9% for the three biosorbent in BRE and PW. Similar reults was presented by Bharathi, et al., 2012.

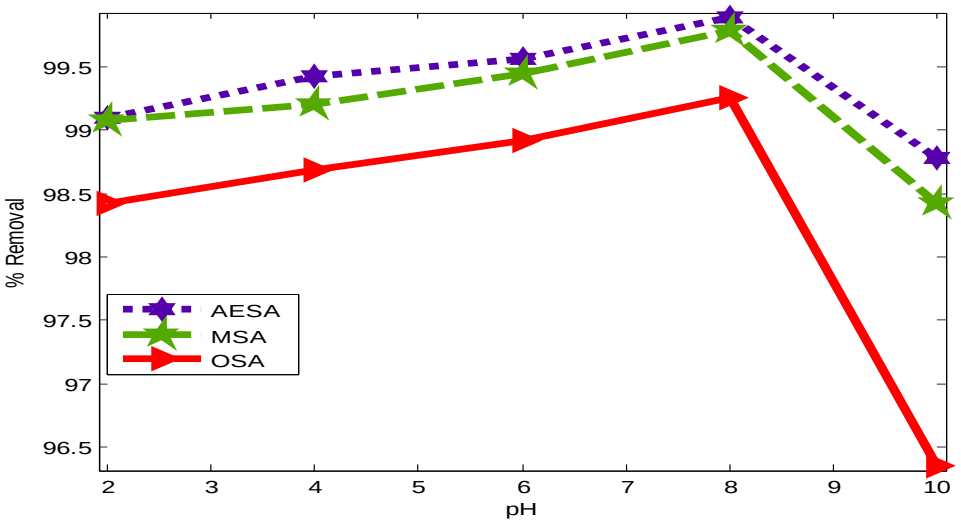

MSA, AESA and OSA (acid treated)

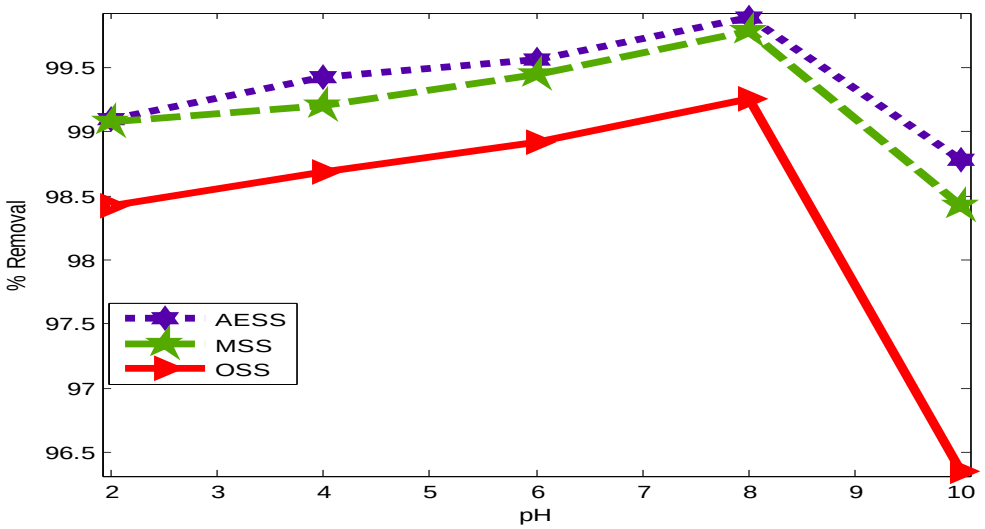

MSS, AESS and OSS (salt treated)

Fig 4.68: Effect of pH on the efficiency removal of turbidity from BRE with acid and salt treated biosorbent (initial concentration =121mg/L, adsorbent dosage = 60mg/L and contact time = 40mins).

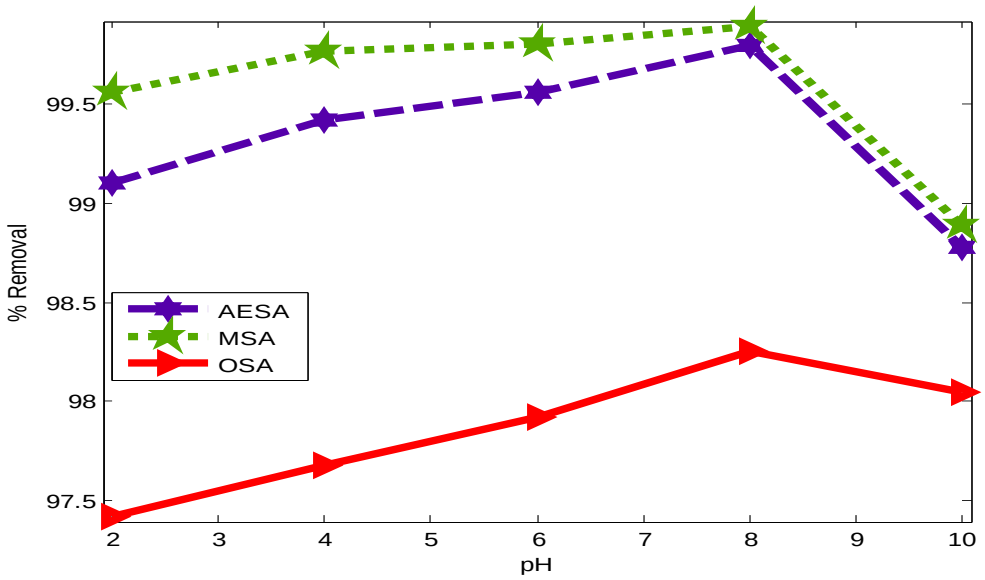

MSA, AESA and OSA (acid treated)

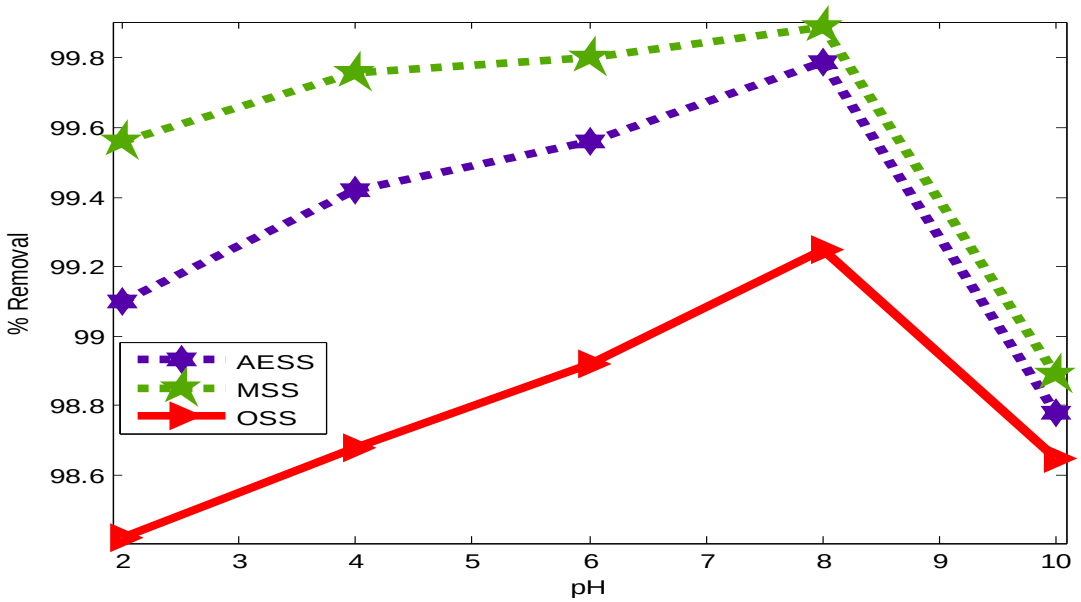

MSS, AESS and OSS (salt treated)

Fig 4.69: Effect of pH on the efficiency removal of turbidity from PW with acid and salt treated biosorbent (initial concentration =188mg/L, adsorbent dosage = 60mg/L and contact time = 40mins).

4.10.2 Effect of adsorbent dosage

Adsorbent dosage is one of the important parameters studied while conducting adsorption experiment. The effects of adsorbent dosage on the removal of turbidity was studied by varying dosage from 20 -100mg/L. From the results shown in Fig 4.70 and 4.71, the maximum removal of 99.8% of turbidity was observed at 60mg/L. This is as a result of more active binding sites on the surface of the adsorbent. Further increase in the adsorbent dosage did not significantly change the adsorption yield. This is due to the non-avaliability of active sites on the adsorbent and establishment of equilibrium between the turbidity on the adsorbent surface and the effluent. Similar report was observed by (Hammaini, et al., 2006; Kumar, et al., 2009; Mittal, et al., 2008; Chiou, et al., 2003; Al-Qodah, 2006).

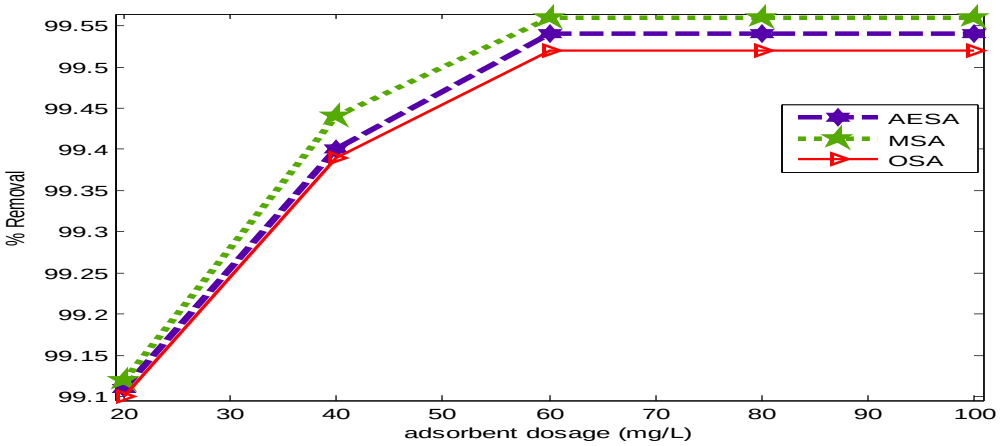

MSA, AESA and OSA (acid treated adsorbent)

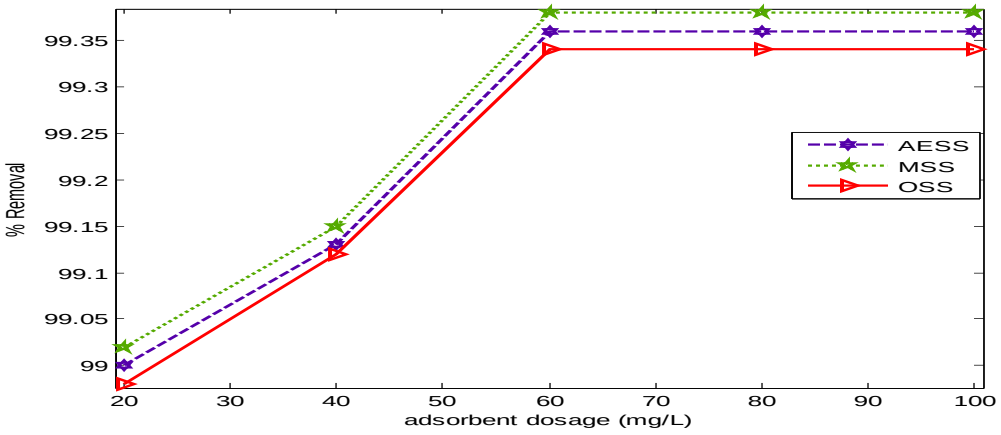

MSS, AESS and OSS (salt treated adsorbent)

Fig 4.70: Effect of dosage on the efficiency removal of turbidity from BRE with acid and salt treated biosorbent (initial concentration =121mg/L, pH 8 and contact time = 40mins).

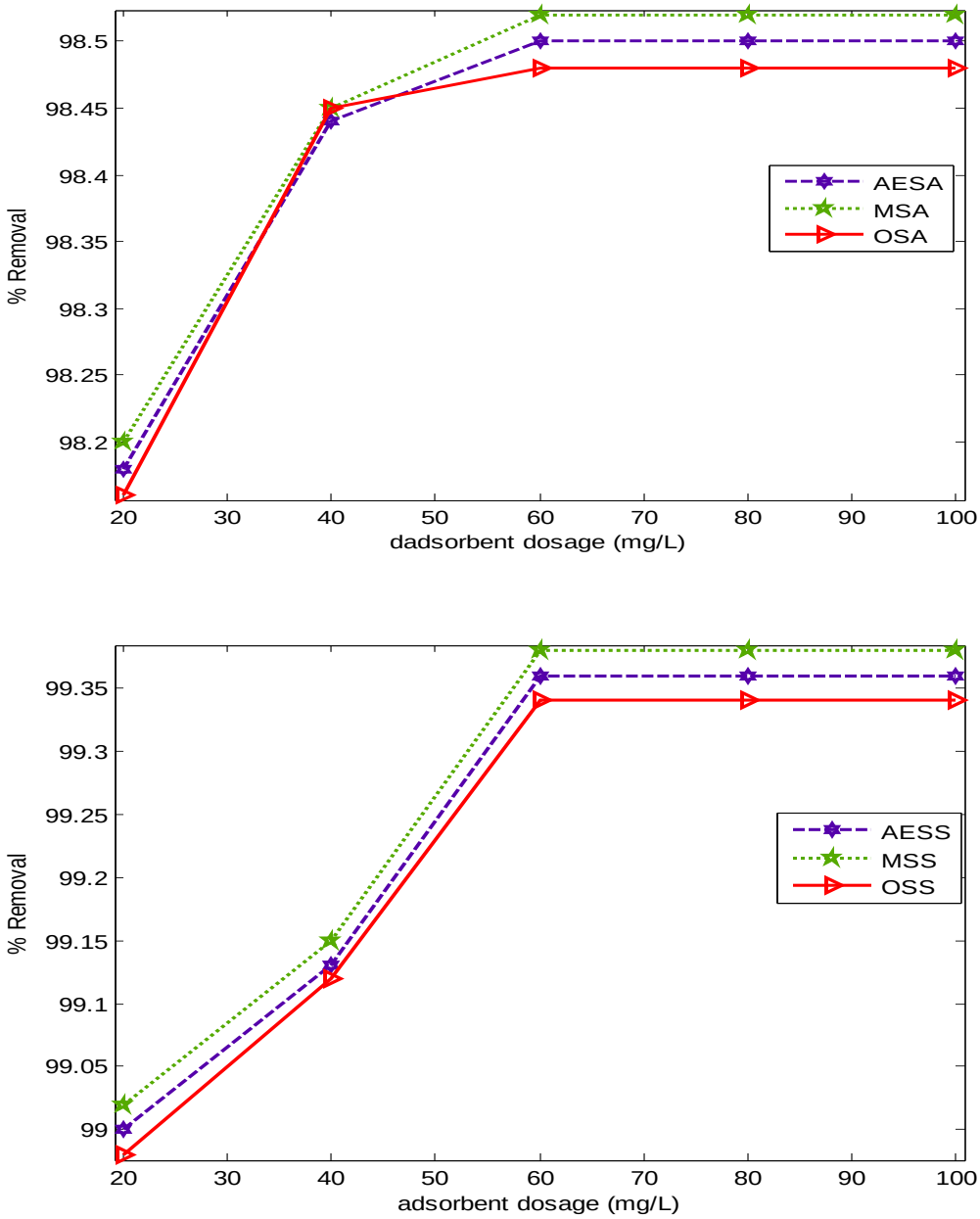

Fig 4.71: Effect of dosage on efficiency removalof turbidity from PW with acid and salt treated biosorbent (initial concentration =188mg/L, pH 8 and contact time = 40mins).

4.10.3 Effect of contact time

The effects of contact time was shown in Fig. 4.72, from the figure the rate of uptake turbidity was quite rapid in the first 10min, this was due to fast transfer of pollutants onto the empty adsorption sites on the surface of adsorbent. The equilibrium was observed at 40min and after that no significant increase in removal. This show that the remaining empty sites on the adsorbent have been occupied leading to repulsive force between pollutants on the surface of adsorbent and pollutants in the effluent. .The removal efficiency was in the range. Similar findings on other adsorbent have been reported by some researcers (Azouaou, et al., 2010; Nandi, et al., 2009; Kavitha, et al., 2007).

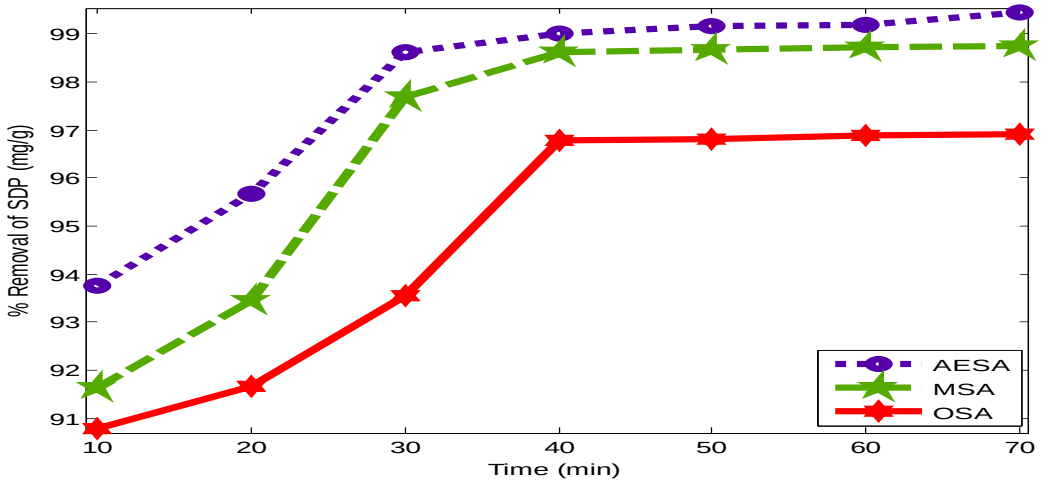

MSA, AESA and OSA

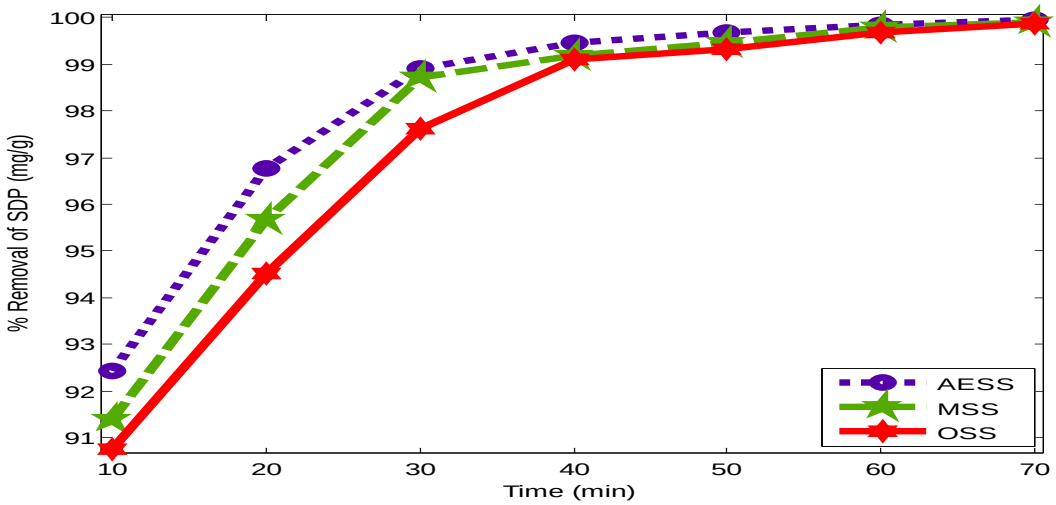

MSS,AESS and OSS

Fig.4.72: Effect of contact time on efficiency removal of turbidity from BRE with acid and salt treated biosorbent (initial concentration =121mg/L, pH 8 and dosage 60mg/L).

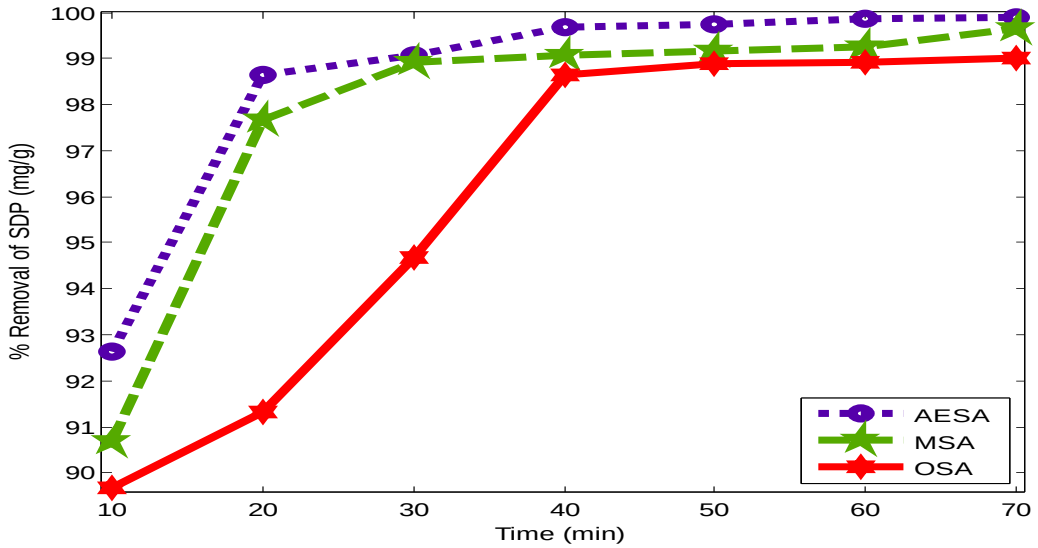

MAS, AESA and OSA

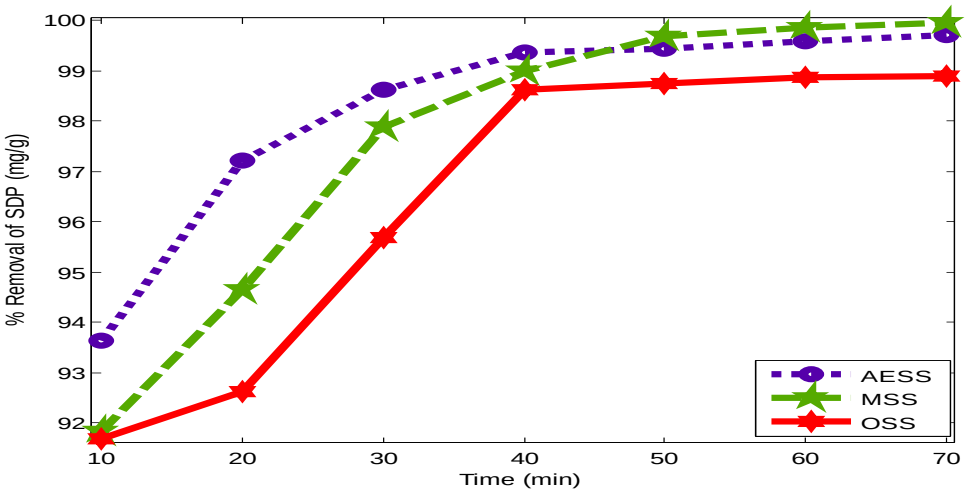

MSS, AESS and OSS

Fig.4.73: Effect of contact time on efficiency removal of turbidity from PW with acid and salt treated biosorbent (initial concentration =188mg/L, pH 8 and dosage 60mg/L).

4.11 Equilibrium Isotherm Studies for Turbidity Removal

An adsorption isotherm describes the relationship between the amounts of turbidity taken up by the adsorbents and the turbidity concentration remaining in the effluent. In this study, four commonly used isotherms Langmuir (Langmuir, 1918), Freundlich (Freundlich, 1939), Temkin (Temkin, 1940) and Dubinin Radushkevich (Dubinin, et al., 1947) were applied in this work.The equilibrium adsorption studies for the removal of turbidity from BRE and PW onto the acid and salt treated adsorbent was conducted at 303K, 313K and 323K. The graphical representation of all the isotherm models using equations 3.35, 3.28, 3.29 and 3.31 (see Appendix C) and determined parameters are presented in Table 4.109 to 4.120. The equilibrium study gave a good fit for the Langmuir isotherm model with high regression coefficient (> 0.99) in comparison to the other tested isotherm models. This confirms the surface homogeneity of the adsorbent. Freundlich isotherm model is usually applied for non-ideal reversible adsorption procrss and it gives the imformation regarding multilayer adsorption with non-uniform distribution of heat which takes place on the heterogeneous surface (Freundlich, 1906). In this study, a low regression coefficient (R^2) less than 0.99, suggest that the mode of adsorption is not heterogeneous in nature. The Temkin isotherm model gives the information regarding the adsorbent/adsorbate interaction. It is based on the assumption that the free energy of adsorption is a function of surface coverage (Temkin & Pyzhev, 1940). Low R^2 value, obtained from the model, implied that the heat of the adsorption of all turbidity in a layer did not decrease with the surface coverage of the adsorbent interaction. When the D-R model was applied to check whether the turbidity adsorption by the biosorbent follows the physisorption or chemisorption process (Dubinin, 1960), the obtained value of mean free energy (E) was found to be greater than 8KJ/mol. The (E) value corresponds with the mechanism of turbidity adsorption onto the biosorbent. The fitness of the models with the experimental data was determined on the bases of regression coefficient, R^2, sum of the square error SSE% and root meam square error RMSE. The higher the value of R^2 and lower SEE and RMSE, the better is the goodness of fit. From the Tables, the Langmuir has the best fit on the data among the four isotherms, also the value of R^2> 0.99 and SSE and RMSE < 0.1 as shown in the tables. Further analysis of the Langmuir model using (equation 3.26) can be predicted with Langmuir parameter K_L from the dimensionless constant separation factor R_L. The value of R_L indicates information as to whether the adsorption is favourable or not. The adsorption process is unfavourable whenR_L>1, linear when R_L = 1, favourable when 0 < R_L< 1 and irreversible when R_L = 0. From the tables, the value of R_L shows that the adsorption is favourable. For Freundlich isotherm, the favourability of the process would be achieved if n lies in range 1-10. From the tables n lies between 1 and 10 that means that the system could be considered favourable.

Table 4.109: Isotherm model constants for turbidity removal with MSA in BRE

pH	Model	2	4	6	8	10

	Parameters					
Langmuir	q_m	214.35	317.86	212.95	487.32	328.45
	K_L	0.0236	0.0167	0.044	0.1454	0.255
	R^2	0.9967	0.9800	0.9932	0.9987	0.9876
	SSE	0.0043	0.0012	0.0085	0.0456	0.0865
	RMSE	0.0235	0.0086	0.0458	0.0643	0.0756
	R_L	0.2594	0.3310	0.0940	0.0538	0.0314
Freundlich	k_f	4.42	9.56	13.54	18.11	19.68
	n	1.18	1.093	4.65	1.061	2.654
	R^2	0.9883	0.986	0.9115	0.8567	0.9767
	SSE	0.0033	0.0041	0.0268	0.0426	0.0070
	RMSE	0.0334	0.0367	0.0945	0.1192	0.0482
Temkin	A	0.559	1.049	4.53	1.801	1.688
	B	33.30	29.51	33.04	33.39	43.09
	R^2	0.9115	0.9548	0.7638	0.9536	0.9529
	SSE	0.0065	0.0087	0.0655	0.0054	0.0867
	RMSE	0.023	0.076	0.0439	0.0085	0.0912
D-R	K_D	0.1797	0.0713	0.12	0.4675	0.4105
	q_S	46.99	47.66	61.68	75.19	74.0
	E	9.563	10.65	8.965	12.86	10.43
	R^2	0.8396	0.8489	0.7743	0.8456	0.8865
	SEE	0.0567	0.0654	0.0034	0.0075	0.0086
	RMSE	0.2385	0.0564	0.0236	0.0876	0.0542

Table 4.110: Isotherm model constants for turbidity removal with MSS in BRE

pH	Model Parameters	2	4	6	8	10
Langmuir	q_m	414.35	155.28	317.16	138.58	160.18
	K_L	0.0167	0.3183	0.1368	0.5256	0.025
	R^2	0.9934	0.7905	0.9264	0.8043	0.9614
	SSE	0.0006	0.0076	0.0054	0.0087	0.0865
	RMSE	0.0235	0.0658	0.0458	0.0684	0.0756
	R_L	0.2594	0.3310	0.0940	0.0538	0.0314
Freundlich	k_f	6.616	15.86	9.87	14.86	12.98
	n	2.56	1.093	3.68	1.061	2.654
	R^2	0.9883	0.986	0.9115	0.8567	0.9767
	SSE	0.0033	0.0041	0.0268	0.0426	0.0070
	RMSE	0.0334	0.0367	0.0945	0.1192	0.0482
Temkin	A	0.559	1.049	4.53	1.801	1.688
	B	30.47	26.65	30.68	78.25	34.52
	R^2	0.9242	0.8816	0.7017	0.9483	0.8744
	SSE	0.0034	0.0087	0.0655	0.0054	0.0867
	RMSE	0.023	0.076	0.0439	0.0085	0.0912
D-R	K_D	0.1154	0.1031	0.12	0.4675	0.4105
	q_S	46.99	47.66	61.68	75.19	74.0
	E	10.67	14.87	8.965	12.86	10.43
	R^2	0.8396	0.8489	0.7743	0.8456	0.8865
	SEE	0.0567	0.0654	0.0034	0.0075	0.0086
	RMSE	0.2385	0.0564	0.0236	0.0876	0.0542

Table 4.111: Isotherm model constants for turbidity removal with AESA in BRE

pH	Model Parameters	2	4	6	8	10
Langmuir	q_m	82.645	383.44	62.31	61.96	338.29
	K_L	0.360	0.078	0.221	0.030	0.0126
	R^2	0.9208	0.9174	0.8104	0.9923	0.9677
	SSE	0.0023	0.0045	0.0085	0.0456	0.0865
	RMSE	0.0235	0.0086	0.0458	0.0643	0.0756
	R_L	0.0244	0.026	0.0359	0.2168	0.3961
Freundlich	k_f	21.48	2.335	18.75	0.749	3.729
	n	1.205	2.678	1.876	3.654	2.654
	R^2	0.9883	0.986	0.9115	0.8567	0.9767
	SSE	0.0033	0.0041	0.0268	0.0426	0.0070
	RMSE	0.0334	0.0367	0.0945	0.1192	0.0482
Temkin	A	2.93	0.33	1.702	0.221	2.182
	B	23.54	28.63	38.93	41.96	19.75
	R^2	0.8112	0.6972	0.9706	0.9536	0.9529
	SSE	0.0065	0.0087	0.0655	0.0054	0.0867
	RMSE	0.023	0.076	0.0439	0.0085	0.0912
D-R	K_D	0.1797	0.0713	0.12	0.4675	0.4105
	q_S	46.99	47.66	61.68	75.19	74.0
	E	9.563	10.65	8.965	12.86	10.43
	R^2	0.8396	0.8489	0.7743	0.8456	0.8865
	SEE	0.0567	0.0654	0.0034	0.0075	0.0086
	RMSE	0.2385	0.0564	0.0236	0.0876	0.0542

Table 4.112: Isotherm model constants for turbidity removal with AESS in BRE

pH	Model Parameters	2	4	6	8	10
Langmuir	q_m	26.95	378.3	160.53	70.27	100.64
	K_L	0.050	0.0334	0.0985	0.0151	0.1824
	R^2	0.9322	0.9964	0.9678	0.9449	0.9677
	SSE	0.0023	0.0045	0.0085	0.0456	0.0865
	RMSE	0.0235	0.0086	0.0458	0.0643	0.0756
	R_L	0.0244	0.026	0.0359	0.2168	0.3961
Freundlich	k_f	21.48	2.335	18.75	0.749	3.729
	n	1.205	2.678	1.876	3.654	2.654
	R^2	0.9883	0.986	0.9115	0.8567	0.9767
	SSE	0.0033	0.0041	0.0268	0.0426	0.0070
	RMSE	0.0334	0.0367	0.0945	0.1192	0.0482
Temkin	A	2.93	0.33	1.702	0.221	2.182
	B	23.54	28.63	38.93	41.96	19.75
	R^2	0.8112	0.6972	0.9706	0.9536	0.9529
	SSE	0.0065	0.0087	0.0655	0.0054	0.0867
	RMSE	0.023	0.076	0.0439	0.0085	0.0912
D-R	K_D	0.1797	0.0713	0.12	0.4675	0.4105
	q_S	46.99	47.66	61.68	75.19	74.0
	E	9.563	10.65	8.965	12.86	10.43
	R^2	0.8396	0.8489	0.7743	0.8456	0.8865
	SEE	0.0567	0.0654	0.0034	0.0075	0.0086
	RMSE	0.2385	0.0564	0.0236	0.0876	0.0542

Table 4.113: Isotherm model constants for turbidity removal with OSA in BRE

pH	Model Parameters	2	4	6	8	10
Langmuir	q_m	7.45	964.32	192.42	9.09	11.94
	K_L	0.0503	0.012	0.0275	0.058	0.058
	R^2	0.8947	0.9305	0.8765	0.9223	0.9677
	SSE	0.0023	0.0045	0.0085	0.0456	0.0865
	RMSE	0.0235	0.0086	0.0458	0.0643	0.0756
	R_L	0.1411	0.4078	0.1243	0.2168	0.3961
Freundlich	k_f	8.654	5.643	8.234	0.749	3.729
	n	1.205	2.678	1.876	3.654	2.654
	R^2	0.9883	0.986	0.9115	0.8567	0.9767
	SSE	0.0033	0.0041	0.0268	0.0426	0.0070
	RMSE	0.0334	0.0367	0.0945	0.1192	0.0482
Temkin	A	2.93	0.33	1.702	0.221	2.182
	B	23.54	28.63	38.93	41.96	19.75
	R^2	0.8112	0.6972	0.9706	0.9536	0.9529
	SSE	0.0065	0.0087	0.0655	0.0054	0.0867
	RMSE	0.023	0.076	0.0439	0.0085	0.0912
D-R	K_D	7.809	0.654	0.4698	39.27	29.16
	q_S	204.59	46.76	22.74	114.66	98.59
	E	9.563	10.65	8.965	12.86	10.43
	R^2	0.8396	0.8489	0.7743	0.8456	0.8865
	SEE	0.0567	0.0654	0.0034	0.0075	0.0086
	RMSE	0.2385	0.0564	0.0236	0.0876	0.0542

Table 4.114: Isotherm model constants for turbidity removal with OSS in BRE

pH	Model Parameters	2	4	6	8	10
Langmuir	q_m	515.46	11.776	9.099	5.548	6.26
	K_L	0.042	0.047	0.0546	0.058	0.047
	R^2	0.8601	0.9305	0.8765	0.9223	0.9677
	SSE	0.0023	0.0045	0.0085	0.0456	0.0865
	RMSE	0.0235	0.0086	0.0458	0.0643	0.0756
	R_L	0.1411	0.4078	0.1243	0.2168	0.3961
Freundlich	k_f	2.687	10.589	8.234	0.749	3.729
	n	1.205	2.678	1.876	3.654	2.654
	R^2	0.9883	0.986	0.9115	0.8567	0.9767
	SSE	0.0033	0.0041	0.0268	0.0426	0.0070
	RMSE	0.0334	0.0367	0.0945	0.1192	0.0482
Temkin	A	2.93	0.33	1.702	0.221	2.182
	B	23.54	28.63	38.93	41.96	19.75
	R^2	0.8112	0.6972	0.9706	0.9536	0.9529
	SSE	0.0065	0.0087	0.0655	0.0054	0.0867
	RMSE	0.023	0.076	0.0439	0.0085	0.0912
D-R	K_D	7.809	0.654	0.4698	39.27	29.16
	q_S	204.59	46.76	22.74	114.66	98.59
	E	9.563	10.65	8.965	12.86	10.43
	R^2	0.8396	0.8489	0.7743	0.8456	0.8865
	SEE	0.0567	0.0654	0.0034	0.0075	0.0086
	RMSE	0.2385	0.0564	0.0236	0.0876	0.0542

Table 4.115: Isotherm model constants for turbidity removal with MSA in PW

pH	Model Parameters	2	4	6	8	10
Langmuir	q_m	12.837	74.869	61.126	56.275	29.96
	K_L	0.167	0.5743	0.394	0.5796	0.626
	R^2	0.9651	0.8562	0.9882	0.9912	0.9662
	SSE	0.9561	0.0016	0.0013	0.0093	0.0865
	RMSE	0.0036	0.0086	0.0133	0.0643	0.0756
	R_L	0.1453	0.4078	0.1243	0.2168	0.3961
Freundlich	k_f	33.88	37.41	42.07	66.07	54.70
	n	2.436	4.987	1.876	3.654	2.654
	R^2	0.8912	0.7635	0.9115	0.8567	0.9767
	SSE	0.0033	0.0719	0.0046	0.0426	0.0070
	RMSE	0.105	0.155	0.0945	0.1192	0.0482
Temkin	A	1.257	1.468	1.93	2.66	2.182
	B	175.9	115.6	76.09	78.87	100.3
	R^2	0.7407	0.5948	0.9625	0.9536	0.9529
	SSE	0.0065	0.0087	0.0655	0.0054	0.0867
	RMSE	0.023	0.076	0.0439	0.0085	0.0912
D-R	K_D	0.9141	0.654	0.4698	39.27	29.16
	q_S	204.59	46.76	22.74	114.66	98.59
	E	9.563	10.65	8.965	12.86	10.43
	R^2	0.8396	0.8489	0.7743	0.8456	0.8865
	SEE	0.0567	0.0654	0.0034	0.0075	0.0086
	RMSE	0.2385	0.0564	0.0236	0.0876	0.0542

Table 4.116: Isotherm model constants for turbidity removal with MSS in PW

pH	Model Parameters	2	4	6	8	10
Langmuir	q_m	28.977	81.10	156.48	146.48	54.35
	K_L	0.116	0.2966	0.394	0.5796	0.626
	R^2	0.9315	0.9349	0.9648	0.9912	0.9662
	SSE	0.0039	0.0087	0.0016	0.0093	0.0865
	RMSE	0.0051	0.0074	0.0133	0.0643	0.0756
	R_L	0.1453	0.4078	0.1243	0.2168	0.3961
Freundlich	k_f	30.97	36.56	36.81	8.16	4.65
	n	2.436	4.987	1.876	3.654	2.654
	R^2	0.8912	0.7635	0.9115	0.8567	0.9767
	SSE	0.0033	0.0719	0.0046	0.0426	0.0070
	RMSE	0.105	0.155	0.0945	0.1192	0.0482
Temkin	A	1.386	1.796	1.93	2.66	2.182
	B	109.5	74.31	57.46	61.15	100.3
	R^2	0.9686	0.8337	0.9656	0.9536	0.9529
	SSE	0.0065	0.0087	0.0655	0.0054	0.0867
	RMSE	0.023	0.076	0.0439	0.0085	0.0912
D-R	K_D	0.6449	0.3409	0.305	39.27	29.16
	q_S	222.07	110.60	105.05	114.66	98.59
	E	10.98	15.786	8.965	12.86	10.43
	R^2	0.8396	0.8489	0.7743	0.8456	0.8865

	SEE	0.0567	0.0654	0.0034	0.0075	0.0086
	RMSE	0.2385	0.0564	0.0236	0.0876	0.0542

Table 4.117: Isotherm model constants for turbidity removal with AESA in PW

pH	Model Parameters	2	4	6	8	10
Langmuir	q_m	77.459	110.62	23.96	22.65	59.45
	K_L	0.181	0.136	0.130	0.5473	0.258
	R^2	0.9777	0.9865	0.9921	0.9866	0.8032
	SSE	0.0025	0.0027	0.0016	0.0093	0.0865
	RMSE	0.0029	0.0025	0.0133	0.0643	0.0756
	R_L	0.0285	0.037	0.1243	0.2168	0.3961
Freundlich	k_f	15.74	16.52	0.673	29.04	21.96
	n	2.436	4.987	1.876	3.654	2.654
	R^2	0.8912	0.7635	0.9115	0.8567	0.9767
	SSE	0.0033	0.0719	0.0046	0.0426	0.0070
	RMSE	0.105	0.155	0.0945	0.1192	0.0482
Temkin	A	1.091	1.122	1.93	2.66	2.182
	B	70.26	63.41	61.96	61.15	100.3
	R^2	0.8276	0.9121	0.9656	0.9536	0.9529
	SSE	0.0065	0.0087	0.0655	0.0054	0.0867
	RMSE	0.023	0.076	0.0439	0.0085	0.0912
D-R	K_D	0.6913	0.6691	5.362	0.677	0.7145
	q_S	102.72	97.13	153.78	114.66	98.59
	E	8.965	13.856	8.965	12.86	10.43

	R^2	0.8396	0.8489	0.7743	0.8456	0.8865
	SEE	0.0567	0.0654	0.0034	0.0075	0.0086
	RMSE	0.2385	0.0564	0.0236	0.0876	0.0542

Table 4.118: Isotherm model constants for turbidity removal with AESS in PW

pH	Model Parameters	2	4	6	8	10
Langmuir	q_m	44.863	127.29	27.43	53.447	47.89
	K_L	0.2897	0.056	0.1966	0.258	0.030
	R^2	0.9805	0.9643	0.9457	0.9866	0.8032
	SSE	0.0027	0.0046	0.0056	0.0093	0.0865
	RMSE	0.0029	0.0025	0.0133	0.0643	0.0756
	R_L	0.0567	0.037	0.1243	0.2168	0.3961
Freundlich	k_f	3.359	5.50	0.673	29.04	21.96
	n	2.436	4.987	1.876	3.654	2.654
	R^2	0.8912	0.7635	0.9115	0.8567	0.9767
	SSE	0.0033	0.0719	0.0046	0.0426	0.0070
	RMSE	0.105	0.155	0.0945	0.1192	0.0482
Temkin	A	0.493	0.531	1.122	2.66	2.182
	B	87.27	61.59	63.42	61.15	100.3
	R^2	0.8276	0.9121	0.9656	0.9536	0.9529
	SSE	0.0065	0.0087	0.0655	0.0054	0.0867
	RMSE	0.023	0.076	0.0439	0.0085	0.0912
D-R	K_D	2.266	1.86	2.437	0.677	0.7145

	q_S	105.95	78.03	158.54	114.66	98.59
	E	8.965	13.856	8.965	12.86	10.43
	R^2	0.8396	0.8489	0.7743	0.8456	0.8865
	SEE	0.0567	0.0654	0.0034	0.0075	0.0086
	RMSE	0.2385	0.0564	0.0236	0.0876	0.0542

Table 4.119: Isotherm model constants for turbidity removal with OSA in PW

pH	Model Parameters	2	4	6	8	10
Langmuir	q_m	104.537	12.85	89.456	60.445	113.87
	K_L	0.0789	0.055	0.1966	0.258	0.030
	R^2	0.9805	0.9643	0.9457	0.9866	0.8032
	SSE	0.0027	0.0046	0.0056	0.0093	0.0865
	RMSE	0.0029	0.0025	0.0133	0.0643	0.0756
	R_L	0.0567	0.037	0.1243	0.2168	0.3961
Freundlich	k_f	7.94	5.50	16..33	3.56	6.78
	n	1.235	4.987	1.876	3.654	2.654
	R^2	0.8912	0.7635	0.9115	0.8567	0.9767
	SSE	0.0033	0.0719	0.0046	0.0426	0.0070
	RMSE	0.105	0.155	0.0945	0.1192	0.0482
Temkin	A	0.493	0.531	1.122	2.66	2.182
	B	32.93	163.7	73.93	119.0	100.3
	R^2	0.8276	0.9121	0.9656	0.9536	0.9529
	SSE	0.0065	0.0087	0.0655	0.0054	0.0867
	RMSE	0.023	0.076	0.0439	0.0085	0.0912

D-R	K_D	2.266	1.86	2.437	0.677	0.7145
	q_S	105.95	78.03	158.54	114.66	98.59
	E	8.965	13.856	8.965	12.86	10.43
	R^2	0.8396	0.8489	0.7743	0.8456	0.8865
	SEE	0.0567	0.0654	0.0034	0.0075	0.0086
	RMSE	0.2385	0.0564	0.0236	0.0876	0.0542

Table 4.120: Isotherm model constants for turbidity removal with OSS in PW

pH	Model Parameters	2	4	6	8	10
Langmuir	q_m	25.06	72.05	73.69	19.45	394.79
	K_L	0.0789	0.055	0.1966	0.258	0.030
	R^2	0.9805	0.9643	0.9457	0.9866	0.8032
	SSE	0.0027	0.0046	0.0056	0.0093	0.0865
	RMSE	0.0029	0.0025	0.0133	0.0643	0.0756
	R_L	0.0567	0.037	0.1243	0.2168	0.3961
Freundlich	k_f	5.90	6.43	16..33	3.56	6.78
	n	1.235	4.987	1.876	3.654	2.654
	R^2	0.8912	0.7635	0.9115	0.8567	0.9767
	SSE	0.0033	0.0719	0.0046	0.0426	0.0070
	RMSE	0.105	0.155	0.0945	0.1192	0.0482
Temkin	A	0.493	0.531	1.122	2.66	2.182
	B	32.93	163.7	73.93	119.0	100.3
	R^2	0.8276	0.9121	0.9656	0.9536	0.9529

	SSE	0.0065	0.0087	0.0655	0.0054	0.0867
	RMSE	0.023	0.076	0.0439	0.0085	0.0912
D-R	K_D	2.266	1.86	2.437	0.677	0.7145
	q_S	105.95	78.03	158.54	114.66	98.59
	E	8.965	13.856	8.965	12.86	10.43
	R^2	0.8396	0.8489	0.7743	0.8456	0.8865
	SEE	0.0567	0.0654	0.0034	0.0075	0.0086
	RMSE	0.2385	0.0564	0.0236	0.0876	0.0542

4.12 Adsorption Thermodynamic Study

The thermodynamic study was to determine whether the process is spontaneous and to observe the effect of temperature on adsorption of turbidity onto biosorbent. The thermodynamic parameters such as free energy (ΔG°), enthalpy (ΔH°) and entropy (ΔS°) were estimated using equations 3.22, 3.23 and 3.24.The values of $(\Delta H^\circ)$and (ΔS°) were estimated from the slope and intercept of the linear plot of equation 3.24 (see Appendix E) and the parameters presented in Tables 4.121-4.124(Horsfall and Spiff, 2005; Dwivedi,*et al*., 2008). The calculated negative (ΔG°) values at all temperature for acid and salt treated biosorbent, confirmed that the adsorption process was feasible and spontaneous in nature and the magnitudeof the Gibbs free change, increased with the rising temperature (Hameed, et al., 2007). The calculated (ΔG°) for turbidity adsorption onto MSA was -581.96, -619.17 -652.83, AESA -933.84, -1018.21, -1102.74, OSA -319.14, -353.93, -388.72 at a given temperature (303 to 323K). The sign of the positive standard entropy change (ΔS°) value describes the increased randomness at the biosorbent/effluent interface during the adsorption of turbidity (Hameed,*et al.*,2007). The positive values of (ΔH°) for the three biosorbent which indicates that the interaction between turbidity removed and biosorbent surface is endothermic.

Table4.121: Thermodynamic Parameters for the removal of turbidity on acid treated adsorbents in brewery wastewater

Adsorbents	ΔH^O(KJ/mol)	ΔS^O(J/mol)	R^2	SSE	RMSE	ΔG^O(KJ/mol)		
						303K	313K	323K
MSA	545.5	3.721	0.9993	4.35E-6	2.082E-3	-581.96	-619.17	-652.83
AESA	1625.0	8.445	0.9777	1.20E-3	3.47E-2	-933.84	-1018.29	-1102.74
OSA	735.0	3.479	0.9162	9.88E-4	3.144E-2	-319.14	-353.93	-388.72

Table 4.122: Thermodynamic Parameters for the removal of turbidity on salt treated adsorbents in brewery effluent

Adsorbents	ΔH^O(KJ/mol)	ΔS^O(J/mol)	R^2	SSE	RMSE	ΔG^O(KJ/mol)		
						303K	313K	323K
MSS	140.0	2.538	0.9932	2.67E-6	1.633E-3	-629.01	-654.39	-679.77
AESS	525.0	3.224	0.8480	9.88E-4	3.144E-2	-451.87	-484.11	-516.35
OSS	455.0	2.863	1.0	1.67E-7	4.08E-4	-412.49	-441.12	-469.75

Table4.123: Thermodynamic Parameters for the removal of turbidity on acid treated adsorbents in Paint effluent

Adsorbents	ΔH^O(KJ/mol)	ΔS^O(J/mol)	R^2	SSE	RMSE	ΔG^O(KJ/mol)		
						303K	313K	323K
MSA	85.0	4.630	0.7500	4.82E-5	6.94E-3	-1317.89	-1364.19	-1410.49
AESA	1135.0	7.264	0.9995	1.35E-5	3.674E-3	-1065.99	-1138.63	-1211.27
OSA	355.0	3.263	0.9968	8.17E-6	2.858E-3	-633.69	-666.32	-698.95

Table4.124: Thermodynamic Parameters for the removal of turbidity on salt treated adsorbents in Paint effluent

Adsorbents	ΔH^O(KJ/ml)	ΔS^O(J/ml)	R^2	SSE	RMSE	ΔG^O(KJ/mol)		
						303K	313K	323K
MSS	1015.0	7.377	0.9890	2.28E-4	1.511E-2	-1220.231	-1294.00	-1367.77
AESS	1125.0	7.044	0.9997	8.17E-6	2.858E-3	-1009.332	-1079.77	-1150.21
OSS	135.0	2.431	0.9781	8.17E-6	2.850E-3	-601.592	-625.90	-650.21

4.13 Adsorption Kinetic Study for the Removal of Turbidity.

Several kinetic models are available to understand the behavior of the adsorbent and also to examine the controlling mechanism of the adsorption process. To study the adsorption kinetics for turbidity removal onto MSA, MSS, AESA, AESS, OSA and OSS, pseudo-first order, pseudo-second order, Elovich equation and intra particle diffusion models were applied to the batch experimental data. The kinetics of adsorption describes the

solute uptake rate, which in turn governs the residence time of adsorption reaction. A linear plot of equations 3.26, 3.28, 3.30 and 3.31 (see Appendix D) and evaluated kinetics parameters shown in Tables 4.125 to 4.136. From the Tables, the adsorption capacity q_e (calculated) determined from the plot of pseudo first-order, differs from that obtain experimentally, q_e (experimentally).This implies that the model is not very good in explaining the kinetic of the removal of turbidity. On the other hand, the pseudo second-order model as shown in the Tables, fits the kinetic models, better as their correlation coefficient is close to 1 (0.99). The estimated values of q_e are also close to the q_e, experimental. It points to the fact second order best explain the observed rate, suggesting that adsorption is the rate- limiting step (Boudrahem, et al., 2009; Karthikeyam, et al., 2007; Sag and Aktay, 2001). The linear plot of intrparticle diffusion for wide range contact time between adsorbent and turbidity removal does not pass through the origin. This deviation from the origin may be due to the variation of mass transfer in the initial and and final stages of adsorption. Such a deviation from the origin indicates the pore diffusion is the only controlling step and film diffusion (Oguz, 2005; Gomez, et al., 2007).

Table 4.125: Kinetic model constants for turbidity removal using MSA in BRE

pH	Model Parameters	2	4	6	8	10
Pseudo first order	$q_e exp\ (mg/g$	56.375	57.475	60.033	58.85	59.40
	$K_1(min^{-1})$	0.0313	0.0312	0.0099	0.022	0.0212
	$q_e cal.\ (mg/g)$	6.4173	5.6406	2.057	2.397	2.4860
	R^2	0.5639	0.7507	0.0185	0.354	0.3865
	SSE	0.0029	0.0025	0.0133	0.0643	0.0756
	RMSE	0.0567	0.037	0.1243	0.2168	0.3961
Pseudo second order	$q_e cal.$(mg/g)	57.736	59.032	60.35	57.636	59.52
	$k_2(min^{-1})$	0.0096	0.0106	0.0522	0.020	0.0724
	R^2	0.9998	0.9990	0.9990	0.9980	0.9982
	SSE	0.0002	0.0001	0.0001	0.00015	0.0002
	RMSE	0.0064	0.0046	0.0011	0.002	0.0174
Elovich	$\alpha\ (mg/g)$	3.3292	2.9902	1.002	1.637	1.637
	$\beta\ (g.mg^{-1})$	0.3226	0.3555	1.015	0.653	0.626
	R^2	0.8814	0.9944	0.8343	0.980	0.9828
	SSE	0.5122	0.1567	0.0655	0.0054	0.0867

	RMSE	0.023	0.076	0.0439	0.0085	0.0912
Intrapartices diffusion	K_{id} (min)	1.127	1.029	0.3381	0.586	0.5801
	A (mg/g)	47.47	49.68	53.58	54.32	54.85
	R^2	0.7495	0.9712	0.718	0.944	0.95
	SEE	0.0567	0.0654	0.0034	0.0075	0.0086
	RMSE	0.2385	0.0564	0.0236	0.0876	0.0542

Table 4.126: Kinetic model constants for turbidity removal onto MSS in BRE

pH	Model Parameters	2	4	6	8	10
Pseudo first order	$q_e exp\ (mg/g$	56.925	60.00	60.05	59.60	56.375
	$K_1(min^{-1})$	0.0289	0.031	0.0163	0.026	0.0276
	$q_e cal.\ (mg/g)$	6.322	3.618	1.0503	3.346	4.349
	R^2	0.909	0.304	0.0689	0.468	0.6977
	SSE	0.1923	0.340	0.0133	0.0643	0.0756
	RMSE	0.0567	0.037	0.1243	0.2168	0.3961
Pseudo second order	$q_e cal.$(mg/g)	58.139	61.05	60.459	60.57	57.438
	$k_2(min^{-1})$	0.0095	0.014	0.0364	0.016	0.0128
	R^2	0.9998	1	1	0.9980	0.9982
	SSE	0.0002	0.0001	0.0001	0.00015	0.0002
	RMSE	0.0064	0.0046	0.0011	0.002	0.0174
Elovich	$\alpha\ (mg/g)$	3.3292	2.9902	1.002	1.637	1.637
	$\beta\ (g.mg^{-1})$	0.3226	0.3555	1.015	0.653	0.626
	R^2	0.9814	0.9944	0.8343	0.980	0.9828
	SSE	0.5122	0.1567	0.0655	0.0054	0.0867
	RMSE	0.023	0.076	0.0439	0.0085	0.0912
Intrapartices diffusion	K_{id} (min)	1.127	1.029	0.3381	0.586	0.5801

	A (mg/g)	47.47	49.68	53.58	54.32	54.85
	R^2	0.9495	0.9712	0.718	0.944	0.95
	SEE	0.0567	0.0654	0.0034	0.0075	0.0086
	RMSE	0.2385	0.0564	0.0236	0.0876	0.0542

Table 4.127: Kinetic model constants for turbidity removal onto OSA in BRE

pH	Model Parameters	2	4	6	8	10
Pseudo first order	$q_e exp\ (mg/g$	51.425	58.58	56.10	53.63	53.625
	$K_1(min^{-1})$	0.0252	0.014	0.025	0.045	0.0214
	$q_e cal.\ (mg/g)$	2.7508	1.5742	3.1143	10.655	2.9624
	R^2	0.3529	0.2303	0.4450	0.6436	0.6046
	SSE	3.256	1.899	2.136	3.226	0.8393
	RMSE	0.808	0.6163	0.6537	0.8032	0.4097
Pseudo second order	$q_e cal.$(mg/g)	52.356	59.066	56.974	56.338	54.585
	$k_2(min^{-1})$	0.0166	0.027	0.0163	0.0057	-.0086
	R^2	1	1	0.9999	0.9999	0.9965
	SSE	0.0002	0.0003	0.0008	0.0001	0.0002
	RMSE	0.0239	0.0025	0.0042	0.0005	0.0255
Elovich	$\alpha\ (mg/g)$	2.6946	1.0873	1.8183	7.1168	1.7243
	$\beta\ (g.mg^{-1})$	0.3946	0.9380	0.5701	0.1707	0.6010
	R^2	0.8722	0.9718	0.9575	0.9395	0.9767
	SSE	2.647	0.0926	0.3837	6.215	0.1861

	RMSE	0.7276	0.1361	0.277	1.115	0.1929
Intrapartices diffusion	K_{id} (min)	0.8808	0.3964	0.6533	2.069	0.6158
	A (mg/g)	44.54	55.42	50.94	38.12	48.68
	R^2	0.7685	0.9809	0.9689	0.8597	0.9836
	SEE	0.0567	0.0654	0.0034	0.0075	0.0086
	RMSE	0.2385	0.0564	0.0236	0.0876	0.0542

Table 4.128: Kinetic model constants for turbidity removal onto OSS in BRE

pH	Model Parameters	2	4	6	8	10
Pseudo first order	$q_e exp\ (mg/g$	53.652	52.80	52.525	51.70	50.875
	$K_1(min^{-1})$	0.0253	0.019	0.118	0.038	0.0214
	$q_e cal.\ (mg/g)$	3.3939	2.2139	1.6730	8.3563	7.4857
	R^2	0.4659	0.3507	0.4255	0.7662	0.7701
	SSE	2.51	1.847	0.5262	1.249	1.092
	RMSE	0.6405	0.6078	0.3244	0.499	0.4674
Pseudo second order	$q_e cal.$(mg/g)	56.592	50.05	53.163	53.676	52.604
	$k_2(min^{-1})$	0.0051	0.998	0.0176	0.0073	0.0082
	R^2	0.9996	0.9904	0.9993	0.9999	0.9999
	SSE	0.0003	0.0108	0.006	0.0001	0.0002
	RMSE	0.0239	0.0025	0.0042	0.0005	0.0255
Elovich	$\alpha\ (mg/g)$	1.8163	1.3172	1.0346	8.2418	4.009
	$\beta\ (g.mg^{-1})$	57.18	0.7800	0.5701	0.1707	0.6010

	R^2	0.9345	0.9504	0.9575	0.9395	0.9767
	SSE	0.6033	0.0926	0.3837	6.215	0.1861
	RMSE	0.3473	0.1361	0.277	1.115	0.1929
Intrapartices diffusion	K_{id} (min)	0.6583	0.3964	0.6533	2.069	0.6158
	A (mg/g)	48.36	55.42	50.94	38.12	48.68
	R^2	0.9654	0.9809	0.9689	0.8597	0.9836
	SEE	0.0567	0.0654	0.0034	0.0075	0.0086
	RMSE	0.2385	0.0564	0.0236	0.0876	0.0542

Table 4.129: Kinetic model constants for turbidity removal onto AESA in BRE

pH	Model Parameters	2	4	6	8	10
Pseudo first order	$q_e exp\ (mg/g$	59.125	54.175	52.525	51.70	50.875
	$K_1(min^{-1})$	0.0258	0.01844	0.118	0.038	0.0214
	$q_e cal.\ (mg/g)$	3.3635	1.9311	1.6730	8.3563	7.4857
	R^2	0.468	0.3962	0.4255	0.7662	0.7701
	SSE	2.122	1.847	0.5262	1.249	1.092
	RMSE	0.6405	0.6078	0.3244	0.499	0.4674
Pseudo second order	$q_e cal.$(mg/g)	54.05	50.05	53.163	53.676	52.604
	$k_2(min^{-1})$	0.0132	0.998	0.0176	0.0073	0.0082
	R^2	0.9973	0.9904	0.9993	0.9999	0.9999
	SSE	0.0003	0.0108	0.006	0.0001	0.0002
	RMSE	0.0239	0.0025	0.0042	0.0005	0.0255

Elovich	$\alpha\ (mg/g)$	2.1152	1.3172	1.0346	8.2418	4.009
	$\beta\ (g.mg^{-1})$	0.4924	0.7800	0.5701	0.1707	0.6010
	R^2	0.9345	0.9504	0.9575	0.9395	0.9767
	SSE	0.6033	0.0926	0.3837	6.215	0.1861
	RMSE	0.3473	0.1361	0.277	1.115	0.1929
Intrapartices diffusion	K_{id} (min)	0.734	0.3964	0.6533	2.069	0.6158
	A (mg/g)	53.37	55.42	50.94	38.12	48.68
	R^2	0.9654	0.9809	0.9689	0.8597	0.9836
	SEE	0.0567	0.0654	0.0034	0.0075	0.0086
	RMSE	0.2385	0.0564	0.0236	0.0876	0.0542

Table 4.130: Kinetic model constants for turbidity removal onto AESS in BRE

pH	Model Parameters	2	4	6	8	10
Pseudo first order	$q_e exp\ (mg/g$	29.838	27.563	29.975	27.775	28.188
	$K_1(min^{-1})$	0.0053	0.0066	0.0208	0.038	0.0214
	$q_e cal.\ (mg/g)$	1.0974	1.6422	2.9329	1.4436	1.6128
	R^2	0.468	0.3962	0.4255	0.7662	0.7701
	SSE	2.122	1.847	0.5262	1.249	1.092
	RMSE	0.6405	0.6078	0.3244	0.499	0.4674
Pseudo second order	$q_e cal.$(mg/g)	30.138	27.979	30.339	26.925	28.645
	$k_2(min^{-1})$	0.0368	0.998	0.0176	0.0073	0.0082
	R^2	0.9999	0.9904	0.9993	0.9999	0.9999

	SSE	0.0003	0.0108	0.006	0.0001	0.0002
	RMSE	0.0239	0.0025	0.0042	0.0005	0.0255
Elovich	$\alpha\ (mg/g)$	0.7262	0.7786	1.0346	8.2418	4.009
	$\beta\ (g.mg^{-1})$	1.4132	1.3245	0.5701	0.1707	0.6010
	R^2	0.9345	0.9504	0.9575	0.9395	0.9767
	SSE	0.6033	0.0926	0.3837	6.215	0.1861
	RMSE	0.3473	0.1361	0.277	1.115	0.1929
Intrapartices diffusion	$K_{id}\ (\text{min})$	0.2654	0.3964	0.6533	2.069	0.6158
	A (mg/g)	27.67	25.33	24.85	25.27	28.97
	R^2	0.9654	0.9809	0.9689	0.8597	0.9836
	SEE	0.0567	0.0654	0.0034	0.0075	0.0086
	RMSE	0.2385	0.0564	0.0236	0.0876	0.0542

Table 4.131: Kinetic model constants for turbidity removal onto MSA in PW

pH	Model Parameters	2	4	6	8	10
Pseudo first order	$q_e exp\ (mg/g$	93.445	93.432	93.225	93.528	93.500
	$K_1(min^{-1})$	0.0115	0.0115	0.0065	0.0083	0.0189
	$q_e cal.\ (mg/g)$	1.2231	1.2231	0.8594	0.4785	1.4483
	R^2	0.1330	0.1330	0.0418	0.1256	0.0985
	SSE	2.122	1.847	0.5262	1.249	1.092
	RMSE	0.6405	0.6078	0.3244	0.499	0.4674
Pseudo second order	$q_e cal.$(mg/g)	100.23	139.178	127.23	102.40	161.78

	$k_2(min^{-1})$	0.0023	0.1291	0.0010	0.0073	0.0082
	R^2	0.9808	0.9999	0.9993	0.9999	0.9999
	SSE	0.0003	0.0108	0.006	0.0001	0.0002
	RMSE	0.0239	0.0025	0.0042	0.0005	0.0255
Elovich	$\alpha\ (mg/g)$	0.9878	0.7786	1.0346	8.2418	4.009
	$\beta\ (g.mg^{-1})$	1.4132	1.3245	0.5701	0.1707	0.6010
	R^2	0.9906	0.9504	0.9575	0.9395	0.9767
	SSE	0.6033	0.0926	0.3837	6.215	0.1861
	RMSE	0.3473	0.1361	0.277	1.115	0.1929
Intrapartices diffusion	K_{id} (min)	0.356	0.3964	0.6533	2.069	0.6158
	A (mg/g)	90.65	90.64	90.56	90.43	90.12
	R^2	0.9654	0.9809	0.9689	0.8597	0.9836
	SEE	0.0567	0.0654	0.0034	0.0075	0.0086
	RMSE	0.2385	0.0564	0.0236	0.0876	0.0542

Table 4.132: Kinetic model constants for turbidity removal onto MSS in PW

pH	Model Parameters	2	4	6	8	10
Pseudo first order	$q_e exp\ (mg/g$	93.225	93.225	92.950	91.575	91.30
	$K_1(min^{-1})$	0.010	0.0085	0.0117	0.0157	0.0029
	$q_e cal.(mg/g)$	1.2051	1.2631	1.3240	1.6971	0.8016
	R^2	0.1330	0.1330	0.0418	0.1256	0.0985
	SSE	2.122	1.847	0.5262	1.249	1.092

	RMSE	0.6405	0.6078	0.3244	0.499	0.4674
Pseudo second order	$q_e cal.$(mg/g)	98.425	93.721	93.270	92.081	91.827
	$k_2(min^{-1})$	0.0151	0.1291	0.0010	0.0073	0.0082
	R^2	0.9808	0.9999	1	1	1
	SSE	0.0003	0.0108	0.006	0.0001	0.0002
	RMSE	0.0239	0.0025	0.0042	0.0005	0.0255
Elovich	$\alpha\ (mg/g)$	0.8923	1.1631	1.0346	8.2418	4.009
	$\beta\ (g.mg^{-1})$	1.1318	1.3245	0.5701	0.1707	0.6010
	R^2	0.9906	0.9504	0.9575	0.9395	0.9767
	SSE	0.6033	0.0926	0.3837	6.215	0.1861
	RMSE	0.3473	0.1361	0.277	1.115	0.1929
Intrapartices diffusion	K_{id} (min)	0.3273	0.3964	0.6533	2.069	0.6158
	A (mg/g)	90.6	90.05	88.14	90.05	87.56
	R^2	0.9654	0.9809	0.9689	0.8597	0.9836
	SEE	0.0567	0.0654	0.0034	0.0075	0.0086
	RMSE	0.2385	0.0564	0.0236	0.0876	0.0542

Table 4.133: Kinetic model constants for turbidity removal onto AESA in PW

pH	Model Parameters	2	4	6	8	10
Pseudo first order	$q_e exp\ (mg/g$	92.675	92.40	91.025	93.363	92.675
	$K_1(min^{-1})$	0.0142	0.0116	0.0142	0.0157	0.0029
	$q_e cal.\ (mg/g)$	1.7131	1.3260	1.3240	1.6971	0.8016

	R^2	0.2302	0.1713	0.0418	0.1256	0.0985
	SSE	2.122	1.847	0.5262	1.249	1.092
	RMSE	0.6405	0.6078	0.3244	0.499	0.4674
Pseudo second order	$q_e cal.$(mg/g)	93.109	139.118	231.80	92.081	91.827
	$k_2(min^{-1})$	0.0292	0.0139	0.0010	0.0073	0.0082
	R^2	1	0.9999	1	1	1
	SSE	0.0001	0.0108	0.006	0.0001	0.0002
	RMSE	0.0239	0.0025	0.0042	0.0005	0.0255
Elovich	$\alpha\ (mg/g)$	1.079	1.1631	1.0346	8.2418	4.009
	$\beta\ (g.mg^{-1})$	0.9380	1.3245	0.5701	0.1707	0.6010
	R^2	0.9906	0.9504	0.9575	0.9395	0.9767
	SSE	0.6033	0.0926	0.3837	6.215	0.1861
	RMSE	0.3473	0.1361	0.277	1.115	0.1929
Intrapartices diffusion	K_{id} (min)	0.3964	0.3964	0.6533	2.069	0.6158
	A (mg/g)	89.52	89.61	87.87	90.72	90.33
	R^2	0.9809	9680	0.9689	0.8597	0.9836
	SEE	0.0567	0.0654	0.0034	0.0075	0.0086
	RMSE	0.2385	0.0564	0.0236	0.0876	0.0542

Table 4.134: Kinetic model constants for turbidity removal onto AESS in PW

pH	Model Parameters	2	4	6	8	10
Pseudo first order	$q_e exp\ (mg/g$	91.575	91.025	92.125	92.675	91.575

	$K_1(min^{-1})$	0.0153	0.0099	0.0205	0.0157	0.0029
	$q_e cal.(mg/g)$	2.1593	1.205	1.3240	1.6971	0.8016
	R^2	0.562	0.1388	0.3368	0.1014	0.0985
	SSE	1.899	1.847	0.5262	1.249	1.092
	RMSE	0.6163	0.6078	0.3244	0.499	0.4674
Pseudo second order	$q_e cal.$(mg/g)	92.081	87.873	88.809	90.851	91.966
	$k_2(min^{-1})$	0.0218	0.0139	0.0010	0.0073	0.0082
	R^2	0.9999	0.9996	0.9942	0.9976	1
	SSE	0.0001	0.0108	0.006	0.0001	0.0002
	RMSE	0.0239	0.0025	0.0042	0.0005	0.0255
Elovich	$\alpha\ (mg/g)$	1.1922	0.8925	1.5524	0.7709	1.1366
	$\beta\ (g.mg^{-1})$	0.8503	1.1319	0.5701	0.1707	0.6010
	R^2	0.9234	0.9783	0.9575	0.9395	0.9767
	SSE	0.6033	0.0926	0.3837	6.215	0.1861
	RMSE	0.3473	0.1361	0.277	1.115	0.1929
Intrapartices diffusion	K_{id} (min)	0.446	0.3273	0.5575	0.288	0.6158
	A (mg/g)	89.52	89.61	87.87	90.72	90.33
	R^2	0.9809	0.9680	0.9689	0.8597	0.9836
	SEE	0.0567	0.0654	0.0034	0.0075	0.0086
	RMSE	0.2385	0.0564	0.0236	0.0876	0.0542

Table 4.135: Kinetic model constants for turbidity removal onto OSA in PW

pH	Model Parameters	2	4	6	8	10
Pseudo first order	$q_e exp\ (mg/g$	88.00	86.075	90.475	85.80	91.85
	$K_1(min^{-1})$	0.0149	0.0310	0.0232	0.0294	0.0217
	$q_e cal.\ (mg/g)$	2.2794	4.645	3.2740	3.463	2.519
	R^2	0.7526	0.5228	0.6213	0.3718	0.3893
	SSE	0.2041	0.567	2.403	1.249	1.092
	RMSE	0.6163	0.6078	0.3244	0.499	0.4674
Pseudo second order	$q_e cal.$(mg/g)	89.047	87.642	77.042	86.880	73.909
	$k_2(min^{-1})$	0.02086	0.0139	0.0010	0.0073	0.0082
	R^2	0.9999	0.9959	0.9959	0.9976	1
	SSE	0.0004	0.0108	0.006	0.0001	0.0002
	RMSE	0.0239	0.0025	0.0042	0.0005	0.0255
Elovich	$\alpha\ (mg/g)$	1.2668	2.7731	1.8763	2.549	1.6687
	$\beta\ (g.mg^{-1})$	0.8013	0.3737	0.5701	0.1707	0.6010
	R^2	0.932	0.9551	0.9575	0.9395	0.9767
	SSE	0.6033	0.0926	0.3837	6.215	0.1861
	RMSE	0.3473	0.1361	0.277	1.115	0.1929
Intrapartices diffusion	K_{id} (min)	0.4681	0.3273	0.5575	0.288	0.6158
	A (mg/g)	84.65	78.62	85.08	78.97	87.18
	R^2	0.9566	0.9053	0.9689	0.8597	0.9836
	SEE	0.0567	0.0654	0.0034	0.0075	0.0086
	RMSE	0.2385	0.0564	0.0236	0.0876	0.0542

Table 4.136: Kinetic model constants for turbidity removal onto OSS in PW

pH	Model Parameters	2	4	6	8	10
Pseudo first order	$q_e exp\ (mg/g$	88.00	89.925	86.900	86.625	84.975
	$K_1(min^{-1})$	0.0183	0.0112	0.01705	0.03324	0.0163
	$q_e cal.\ (mg/g)$	2.6834	1.4563	1.8056	6.443	1.6631
	R^2	0.6235	0.2603	0.2666	0.7607	0.3893
	SSE	0.2041	0.567	2.403	1.249	1.092
	RMSE	0.6163	0.6078	0.3244	0.499	0.4674
Pseudo second order	$q_e cal.$(mg/g)	86.207	88.731	82.305	80.775	86.616
	$k_2(min^{-1})$	0.02086	0.0139	0.0010	0.0073	0.0082
	R^2	0.999	0.9817	0.9962	0.9962	1
	SSE	0.0004	0.0108	0.006	0.0001	0.0002
	RMSE	0.0239	0.0025	0.0042	0.0005	0.0255
Elovich	$\alpha\ (mg/g)$	1.3639	2.7731	1.8763	2.549	1.6687
	$\beta\ (g.mg^{-1})$	0.7453	0.3737	0.5701	0.1707	0.6010
	R^2	0.932	0.9551	0.9575	0.9395	0.9767
	SSE	0.6033	0.0926	0.3837	6.215	0.1861
	RMSE	0.3473	0.1361	0.277	1.115	0.1929
Intrapartices diffusion	K_{id} (min)	0.512	0.3273	0.5575	0.288	0.6158
	A (mg/g)	83.74	78.62	85.08	78.97	87.18
	R^2	0.9566	0.9053	0.9689	0.8597	0.9836
	SEE	0.0567	0.0654	0.0034	0.0075	0.0086
	RMSE	0.2385	0.0564	0.0236	0.0876	0.0542

4.14 Development of Regression Model

The process parameters affecting the removal of turbidity from BRE and PW using biosorbent were studied using historical data design (HDD) in implementing RSM. Also a total of 27 experiments were conducted. HDD matrix for experimental design (real and coded values of the three factors ie adsorbent dose, pH and contact time) for observed and predicted responses for the removal of turbidity have been summarized in Tables 4.137 and

4.140, using Design expert software version 9.0.6. Second order polynomial equations were used to draw relationship between independent variables and responses. The effects of the parameters and response behavior of the system was explained by equations 4.18 to 4.29 as shown below. Within the chosen range of experiments shown on the Tables, for acid treated adsorbent, the optimum adsorbent dose, pH and contact time for MSA was at 100mg/L, pH 6 and contact time of 40minutes at 99.59% removal of turbidity. With AESA the removal was 99.59% with 100mg/L, pH 2 and contact time of 70minutes. The OSA removed 98.18% with 100mg/L, pH 6, contact times 40minutes.For salt treated adsorbent, MSS was 100mg/L, pH 6 and contact time 40minutes at 99.59%, AESS was 60mg/L, pH 6 and contact time 70minutes at 99.18% and OSS with 100mg/L, pH2 and contact time 70minutes at 95.10% in BRE. PW with acid treated adsorbent, the optimum removal of turbidity was obtained with MSA 100mg/L, pH 10 and contact time 70minutes at 99.68%, AESA 100mg/L, pH 10 and contact time 70minutes at 99.44% and OSA 20mg/L, pH 2 and contact time 10minutes at 99.44%. With MESS, 100mg/L, pH 2 and contact time 70minutes at 99.65%, AESS 20mg/L, pH 10 and contact time 10minutes at 99.50% and OSS 100mg/L, pH 2 and contact time 70minutes at 96.49%.

Table 4.137: Design matrix and HDD with experimental and predicted results for removal of turbidity with MSA, AESA and OSA from BRE.

Run no.	Real (coded) values			Turbidity removal %					
				MSA		AESA		OSA	
	X_1	X_2	X_3	Exp.	Pred.	Exp.	Pred.	Exp.	Pred.
1	100(+1)	6(0)	10(+1)	99.10	99.68	96.83	95.64	86.36	87.12
2	**100(+1)**	**2(-1)**	**70+1)**	98.18	98.64	**99.59**	**98.62**	83.81	82.65
3	20(-1)	10(+1)	70(+1)	98.18	97.65	90.90	89.78	88.64	87,84
4	60(0)	2(-1)	40(0)	93.18	92.62	98.18	98.76	85.91	84.23
5	100(+1)	2(-1)	10(-1)	91.81	90.76	96.82	96.59	83.18	82.85
6	60(-1)	2(-1)	10(-1)	88.64	88.21	95.00	94.76	85.91	85.39
7	20(-1)	2(-1)	40(0)	90.00	90.12	95.91	94.65	84.09	83.84
8	60(0)	10(-1)	70(+1)	99.09	98.65	95.91	95.33	91.36	92.64
9	60(0)	6(0)	70(+1)	99.18	99.76	99.18	98.46	96.36	95.89
10	60(0)	6(0)	40(0)	98.18	97.85	98.18	97.85	88.64	87.56
11	20(-1)	6(0)	10(-1)	92.73	91.69	92.73	91.12	92.73	93.67
12	100(+1)	10(-1)	40(+1)	99.00	99.52	95.00	94.65	89.55	88.10
13	100(+1)	2(-1)	40(0)	95.91	94.76	95.91	96.64	83.18	84.65
14	60(0)	6(-1)	10(-1)	98.18	98.12	95.00	94.52	89.09	88.45
15	20(-1)	2(0)	10(-1)	83.18	83.65	91.36	90.12	76.36	74.64
16	100(+1)	10(-1)	70(+)	99.41	98.86	97.73	96.10	93.18	92.86
17	**100(+1)**	**6(0)**	**40(0)**	**99.59**	**99.87**	98.64	98.12	**98.18**	**99.54**
18	60(-1)	10(-)	10(-1)	95.91	96.82	89.09	90.23	85.00	85.86
19	100(+1)	10(-1)	10(-1)	96.82	96.10	95.00	94.21	86.36	86.86
20	20(-1)	10(-1)	40(0)	96.82	95.63	88.64	89.76	87.27	86.87
21	100(+1)	6(0)	40(0)	99.59	99.15	98.64	97.54	95.00	94.86
22	60(0)	10(-1)	40(0)	98.64	97.64	91.82	91.64	93.18	92.96
23	20(-1)	10(-1)	10(-1)	93.18	92.54	85.91	86.45	83.64	82.97
24	20(-1)	6(0)	70(+1)	99.23	98.12	97.73	98.65	92.73	93.54
25	20(-1)	6(0)	40(0)	99.09	98.76	95.91	96.65	91.36	90.43
26	20(-1)	6(0)	70(+1)	93.18	92.54	97.73	97.95	92.73	93.65
27	60(0)	2(-1)	70(+1)	96.82	96.65	99.00	89.86	88.64	87.54

Table 4.138: Design matrix and HDD with experimental and predicted results for removal of turbidity with MSS, AESS and OSS from BRE.

Run no.	Real (coded) values			Turbidity removal %					
				MSS		AESS		OSS	
	X_1	X_2	X_3	Exp.	Pred.	Exp.	Pred.	Exp.	Pred.
1	100(+1)	6(0)	10(+1)	99.09	99.68	96.82	95.64	86.36	87.12
2	**100(+1)**	**2(-1)**	**70+1)**	98.64	98.64	95.00	96.62	**95.91**	**94.65**
3	20(-1)	10(+1)	70(+1)	93.18	97.65	95.91	96.78	88.64	87,84
4	60(0)	2(-1)	40(0)	94.09	92.62	90.00	89.76	89.55	88.23
5	100(+1)	2(-1)	10(-1)	92.27	90.76	88.18	88.59	83.18	82.85
6	60(-1)	2(-1)	10(-1)	89.09	88.21	86.82	87.76	87.73	86.39
7	20(-1)	2(-1)	40(0)	90.00	90.12	88.64	87.65	86.82	85.84
8	60(0)	10(-1)	70(+1)	95.91	98.65	99.09	98.33	87.27	86.64
9	**60(0)**	**6(0)**	**70(+1)**	99.50	99.76	**99.18**	**98.46**	89.09	88.89
10	60(0)	6(0)	40(0)	99.09	97.85	97.73	97.85	88.18	87.56
11	20(-1)	6(0)	10(-1)	95.45	91.69	92.27	91.12	83.64	82.67
12	100(+1)	10(-1)	40(+1)	96.36	99.52	98.63	97.65	86.36	87.10
13	100(+1)	2(-1)	40(0)	95.91	94.76	92.27	91.64	91.36	90.65
14	60(0)	6(-1)	10(-1)	90.00	98.12	95.00	94.52	85.45	84.45
15	20(-1)	2(0)	10(-1)	85.91	83.65	83.18	82.12	83.64	84.64
16	100(+1)	10(-1)	70(+)	97.41	98.86	99.32	98.10	88.64	87.86
17	100(+1)	6(0)	40(0)	99.32	99.87	99.00	98.12	89.09	88.54
18	60(-1)	10(-)	10(-1)	90.00	96.82	94.09	93.23	78.64	77.86
19	100(+1)	10(-1)	10(-1)	92.20	96.10	97.27	96.21	83.18	82.86
20	20(-1)	10(-1)	40(0)	91.36	95.63	94.09	93.76	87.27	86.87
21	**100(+1)**	**6(0)**	**40(0)**	**99.59**	**99.15**	99.00	98.54	89.09	88.86
22	60(0)	10(-1)	40(0)	95.00	97.64	96.82	95.64	85.45	84.96
23	20(-1)	10(-1)	10(-1)	85.45	92.54	90.91	89.45	72.73	72.97
24	20(-1)	6(0)	70(+1)	99.18	98.12	97.73	98.65	86.82	85.54
25	20(-1)	6(0)	40(0)	99.00	98.76	95.91	96.65	85.45	84.43
26	20(-1)	6(0)	70(+1)	99.18	92.54	97.73	97.95	86.82	85.65
27	60(0)	2(-1)	70(+1)	97.82	96.65	92.27	91.86	91.36	92.54

Table 4.139: Design matrix and HDD with experimental and predicted results for removal of turbidity with MSA, AESA and OSA from PW.

Run no.	Real (coded) values			Turbidity removal %					
				MSA		AESA		OSA	
	X_1	X_2	X_3	Exp.	Pred.	Exp.	Pred.	Exp.	Pred.
1	100(+1)	6(0)	10(+1)	98.83	99.68	95.91	95.64	95.32	96.12
2	100(+1)	2(-1)	70+1)	99.68	98.64	99.42	98.62	98.53	97.65
3	20(-1)	10(+1)	70(+1)	99.42	98.65	98.83	97.78	97.66	97,84
4	60(0)	2(-1)	40(0)	99.27	98.62	98.18	98.76	94.74	94.23
5	100(+1)	2(-1)	10(-1)	98.83	97.76	97.66	96.59	94.44	93.85
6	60(-1)	2(-1)	10(-1)	98.25	98.68	97.07	96.76	92.98	91.39
7	20(-1)	2(-1)	40(0)	98.82	97.12	97.95	96.65	92.98	92.84
8	60(0)	10(-1)	70(+1)	99.56	98.65	99.36	98.33	98.54	97.64
9	60(0)	6(0)	70(+1)	99.44	99.76	97.66	98.46	94.74	95.89
10	60(0)	6(0)	40(0)	99.42	98.85	97.66	97.85	96.98	97.56
11	20(-1)	6(0)	10(-1)	98.82	97.69	94.74	93.12	92.69	93.67
12	100(+1)	10(-1)	40(+1)	99.44	99.52	99.12	97.65	99.12	98.10
13	100(+1)	2(-1)	40(0)	99.44	98.76	99.12	98.64	97.08	96.65
14	60(0)	6(-1)	10(-1)	98.25	98.12	95.32	94.52	93.56	94.45
15	20(-1)	2(0)	10(-1)	97.36	95.65	96.49	95.12	91.52	92.64
16	**100(+1)**	**10(-1)**	**70(+)**	**99.68**	**98.86**	**99.44**	**98.10**	99.44	97.86
17	100(+1)	6(0)	40(0)	99.62	99.87	98.28	98.12	97.95	99.54
18	60(-1)	10(-)	10(-1)	98.25	96.82	97.66	95.23	96.49	95.86
19	100(+1)	10(-1)	10(-1)	98.83	97.10	98.25	97.21	97.36	96.86
20	20(-1)	10(-1)	40(0)	98.83	97.63	97.95	99.76	96.78	97.87
21	100(+1)	6(0)	40(0)	99.62	99.15	98.28	97.54	97.95	95.86
22	60(0)	10(-1)	40(0)	99.36	98.64	99.12	96.64	97.66	96.96
23	**20(-1)**	**10(-1)**	**10(-1)**	97.36	95.54	97.07	96.45	**99.44**	**98.97**
24	20(-1)	6(0)	70(+1)	99.12	98.12	96.78	98.65	92.39	93.54
25	20(-1)	6(0)	40(0)	98.83	98.76	96.78	96.65	95.32	94.43
26	20(-1)	6(0)	70(+1)	99.12	97.54	96.78	97.95	93.57	93.65
27	60(0)	2(-1)	70(+1)	99.44	98.65	99.12	99.86	99.12	98.54

Table 4.140: Design matrix and HDD with experimental and predicted results for removal of turbidity with MSS, AESS and OSS from PW.

Run no.	Real (coded) values			Turbidity removal %					
				MSS		AESS		OSS	
	X_1	X_2	X_3	Exp.	Pred.	Exp.	Pred.	Exp.	Pred.
1	100(+1)	6(0)	10(+1)	99.36	99.68	97.07	95.64	91.81	92.12
2	**100(+1)**	**2(-1)**	**70+1)**	**99.65**	**98.64**	98.83	96.62	**96.49**	**94.65**
3	20(-1)	10(+1)	70(+1)	97.07	97.65	97.36	96.78	90.35	87,84
4	60(0)	2(-1)	40(0)	99.36	97.62	97.36	99.76	93.57	92.23
5	100(+1)	2(-1)	10(-1)	99.12	98.76	96.78	98.59	93.27	92.85
6	60(-1)	2(-1)	10(-1)	98.53	98.21	96.20	97.76	92.11	89.39
7	20(-1)	2(-1)	40(0)	98.85	97.12	96.20	97.65	92.11	90.84
8	60(0)	10(-1)	70(+1)	98.25	98.65	98.83	98.33	92.11	93.64
9	60(0)	6(0)	70(+1)	99.50	99.76	98.83	98.46	94.74	92.89
10	60(0)	6(0)	40(0)	98.53	97.85	97.66	97.85	93.27	91.56
11	20(-1)	6(0)	10(-1)	96.78	95.69	99.50	97.12	90.06	88.67
12	100(+1)	10(-1)	40(+1)	97.07	99.52	98.25	97.65	92.40	97.10
13	100(+1)	2(-1)	40(0)	99.44	97.76	97.95	96.64	95.03	94.65
14	60(0)	6(-1)	10(-1)	98.53	98.12	96.49	94.52	91.23	90.45
15	20(-1)	2(0)	10(-1)	85.91	83.65	99.50	98.12	90.93	87.64
16	100(+1)	10(-1)	70(+)	97.36	98.86	99.36	98.10	95.32	93.86
17	100(+1)	6(0)	40(0)	99.50	99.87	98.25	98.12	94.44	92.54
18	60(-1)	10(-)	10(-1)	96.20	96.82	96.20	95.23	90.06	89.86
19	100(+1)	10(-1)	10(-1)	97.07	96.10	99.34	97.21	90.94	90.46
20	20(-1)	10(-1)	40(0)	94.44	95.63	97.78	96.76	89.77	86.87
21	100(+1)	6(0)	40(0)	99.50	99.15	98.25	98.54	94.44	92.86
22	60(0)	10(-1)	40(0)	97.66	97.64	97.66	95.64	90.93	86.96
23	**20(-1)**	**10(-1)**	**10(-1)**	97.07	94.54	**99.50**	**97.45**	87.13	85.97
24	20(-1)	6(0)	70(+1)	98.83	98.12	97.95	98.65	92.40	91.07
25	20(-1)	6(0)	40(0)	98.25	98.76	97.36	96.65	91.81	89.43
26	20(-1)	6(0)	70(+1)	98.83	96.54	97.95	97.95	92.42	91.65
27	60(0)	2(-1)	70(+1)	99.44	96.65	98.25	95.86	95.03	92.54

For BRE

$$Y_{(MSA)} = 72.42350 + 0.15309X_1 + 4.03523X_2 + 0.25639X_3 - 6.25946E-003X_1X_2 - 7.33172E-004X_1X_3 - 9.89710E-003X_2X_3 - 3.22048E-004X_1^2 - 0.21911X_2^2 - 8.53832E-004X_3^2$$

(4.18)

$$Y_{(MSS)} = 74.37794 + 0.16158X_1 + 3.22864X_2 + 0.26977X_3 - 2.70833E-004X_1X_2 - 8.91940E-004X_1X_3 - 2.7916E-003X_2X_3 - 4.86292E-004X_1^2 - 0.25902X_2^2 - 1.15341E-003X_3^2$$

(4.19)

$$Y_{(AESA)} = 88.96827 + 0.089505X_1 + 0.82886X_2 + 0.11205X_3 + 5.2220E-003X_1X_2 - 3.77887E-004X_1X_3 + 4.24976E-003X_2X_3 - 4.34725E-004X_1^2 - 0.15962X_2^2 - 4.34148E-004X_3^2$$

(4.20)

$$Y_{(AESS)} = 73.10150 + 0.10448X_1 + 4.09936X_2 + 0.19603X_3 + 2.95029E-003X_1X_2 - 6.37459E-003X_1X_3 - 2.55597E-003X_2X_3 - 4.32102E-004X_1^2 - 0.27290X_2^2 - 8.54267E-004X_3^2$$

(4.21)

$$Y_{(OSA)} = 63.04734 + 0.13823X_1 + 5.55190X_2 + 0.20385X_3 - 6.34818E-003X_1X_2 + 1.48210E-004X_1X_3 - 4.50520E-003X_2X_3 - 3.6307E-004X_1^2 - 0.38030X_2^2 - 8.42182E-004X_3^2$$

(4.22)

$$Y_{(OSS)} = 81.32437 + 0.092164X_1 + 0.057438X_2 + 0.11756X_3 - 4.99248E-004X_1X_2 + 2.24900E-004X_1X_3 - 1.13230E-003X_2X_3 - 4.07131E-004X_1^2 - 0.043088X_2^2 - 5.99351E-004X_3^2$$

(4.23)

For PW

$$Y_{(MSA)} = 72.42350 + 0.15309X_1 + 4.03523X_2 + 0.25639X_3 - 6.25946E-003X_1X_2 - 7.33172E-004X_1X_3 - 9.89710E-003X_2X_3 - 3.22048E-004X_1^2 - 0.21911X_2^2 - 8.53832E-004X_3^2$$

(4.24)

$$Y_{(MSS)} = 96.03023 + 0.045980X_1 + 0.16951X_2 + 0.046317X_3 + 1.51590E-003X_1X_2 - 2.04084E-004X_1X_3 + 2.26969E-003X_2X_3 - 2.24945E-004X_1^2 - 0.048292X_2^2 - 3.06727E-004X_3^2$$

(4.25)

$$Y_{(AESA)} = 96.66498 + 0.026740X_1 - 1.07427X_2 + 0.096699X_3 + 1.56250E-005X_1X_2 - 1.73611E-005X_1X_3 - 1.04167E-003X_2X_3 - 9.47917E-003X_1^2 + 0.095937X_2^2 - 7.25926E-004X_3^2$$

(4.26)

$$Y_{(AESS)} = 73.10150 + 0.10448X_1 + 4.09936X_2 + 0.19603X_3 + 2.95029E-003X_1X_2 - 6.37459E-003X_1X_3 - 2.55597E-003X_2X_3 - 4.32102E-004X_1^2 - 0.27290X_2^2 - 8.54267E-004X_3^2$$

(4.27)

$$Y_{(OSA)} = 88.13434 + 0.047958X_1 + 0.43966X_2 + 0.11529X_3 - 2.57292E-003X_1X_2 + 1.11586E-004X_1X_3 - 1.26052E-003X_2X_3 + 1.14911E-005X_1^2 + 0.010110X_2^2 - 8.20771E-004X_3^2$$

(4.28)

$$Y_{(OSS)} = 90.05157 + 0.023410X_1 + 0.052986X_2 + 0.043787X_3 + 1.67708E-003X_1X_2 + 3.04167708E-003X_1X_3 + 6.11111E-004X_2X_3 - 5.20833E-005X_1^2 - 0.041563X_2^2 - 1.44444E-004X_3^2$$

(4.29)

where, X_1, X_2, X_3 and E are the adsorbent dose, pH of effluents, contact time and expontial sign, respectively. The coefficients in front of X_1, X_2 and X_3 represent the linear coefficient, while the coefficients in front of X_1X_2, X_1X_3 and X_2X_3 represent the interaction between factors and, that of X_3^2, X_3^2 and X_3^2 represent the quadratic effect, respectively.

4.15Analysis of Variance (ANOVA)

The results obtained from regression model equation were then analysed by ANOVA to determine the goodness of fit. The quadratic regression for turbidity removal efficiency shows in Tables 4.141 to 4.164, indicates that all the models were significant because the F-value for acid treated adsorbent in BRE are 31.76222, 42.83089 and 229.9161 for MSA, AESA and OSA, while that of salt treated are 37.36444, 238.7495 and 67.88743 for MSS,

AESS and OSS are high. For PW, the F-values are 31.76222, 54.08241 and 59.82023 for MSA, AESA and OSAand for salt treated, 59.71978, 238.7496 and 72.17147.The greater the F-value, the more certain it is that the model explains adequately the variation in the data and the estimated significant terms of the adsorbents variables are closer to the actual value (Montogoney, 2005; Trinh and Kaug, 2011). Also the P-values for the quadratic models for the adsorbents both acid and salt treated were less than 0.05, indicating that the model is significant. Also the coefficient of determination R^2 is close to 1, which means a better correlation between the experimental and predicted (Sharma, et al., 2009; Abu Amr, et al., 2014). In Tables 4.140, 4.142. 4.144. 4.146, 4.148, and 4.150 shows the R^2 values of 0.9470, 0.9354 and 0.9923 for MSA, AESA and OSA for acid treated and 0.9343, 0.9931 and 0.9776 for salt in BRE, indicates that the models could not explain 5.3%, 6.46%, 0.77% and 6.577%, 0.76% and 2.24% for acid/salt treated adsorbent. Similar results were obtained with paint wastewater. The predicted R^2 of 0.8720, 0.8871, 0.0.9807 for MSA, AESA and OSA for acid treated and 0.0.8777, 0.8871 and 0.9807 MESS, AESS and OSS for salt treated were in reasonable agreement with adjusted R^2 of 0.9172, 0.9354, 0.9889 for acid treted and 0.9343, 0.9889 and 0.9632 for salt treated, which indicates that the models were significant. The ‘’Adequate Precision’’ ratio should be higher than 4 so that the predicated models can be used to navigate the space (Kousla, et al., 2012). Small values of CV and SD reflect reproducibility of the models; the values of CV, SD and AP are also presented in Tables mentioned above. The CV values of 1.23, 0.98 and 0.67 for acid treated, while 1.17, 0.507 and 0.577 for salt treated, Adequate precision (AP) results showns, that any value that exceeds 4 usually indicates that the model will give a reasonable performance in prediction (Kousha, et al., 2012). Similar results were also obtained with PW.

Table4.141: ANOVA for response surface quadratic model for turbidity removal in BRE using MSA

Source	Sum of Squares	Df	Mean Square	F Value	p-value Prob > F	
Model	399.4754	9	44.38615	31.76222	1.54E-08	significant
X_1	57.61855	1	57.61855	41.23117	8.46E-06	
X_2	104.177	1	104.177	74.54783	2.03E-07	
X_3	98.29206	1	98.29206	70.33666	2.99E-07	
X_1X_2	10.29602	1	10.29602	7.367712	0.015315	
X_1X_3	7.080508	1	7.080508	5.06673	0.038802	
X_2X_3	14.47884	1	14.47884	10.36089	0.005361	
X_1^2	1.52453	1	1.52453	1.090936	0.311789	
X_2^2	69.38956	1	69.38956	49.65437	2.76E-06	
X_3^2	3.515262	1	3.515262	2.515481	0.132297	
Residual	22.35922	16	1.397451			
Cor Total	421.8346	25				

Table 4.142: Model coefficient for (turbidity) removal in BRE using MSA

Std. Dev.	1.18	R-Squared	0.9470

C.V. % 1.23 Adj R-Squared 0.9172
Adeq Precision 22.660 Pred R-Squared 0.8720

Table 4.143: ANOVA for response surface quadratic model for turbidity removal in BRE using MSS

Source	Sum of Squares	Df	Mean Square	F Value	p-value Prob > F	
Model	415.7435	9	46.19372	37.36444	2.92E-08	Significant
X_1	103.2589	1	103.2589	83.52239	2.82E-07	
X_2	0.0162	1	0.0162	0.013104	0.91049	
X_3	153.681	1	153.681	124.3071	2.39E-08	
X_1X_2	0.022533	1	0.022533	0.018226	0.89453	
X_1X_3	12.05844	1	12.05844	9.753638	0.007481	
X_2X_3	1.3467	1	1.3467	1.089297	0.314315	
X_1^2	3.187099	1	3.187099	2.57793	0.130677	
X_2^2	70.49029	1	70.49029	57.01706	2.67E-06	
X_3^2	5.672994	1	5.672994	4.58868	0.050249	
Residual	17.30823	14	1.236302			
Cor Total	433.0517	23				

Table 4.144: Moel coefficient for (turbidity) removal in BRE using MSS

Std. Dev.	1.111891	R-Squared	0.960032
C.V. %	1.175117	Adj RSquared	0.934338
AdeqPrecision	22.57123	PredRSquared	0.877739

Table 4.145: ANOVA for response surface quadratic model for removal of turbidity in BRE using AESA

Source	Sum of Squares	Df	Mean Square	F Value	p-value Prob > F	
Model	334.3875	9	37.15417	42.83089	6.28E-10	Significant
X_1	77.54059	1	77.54059	89.38789	3.5E-08	
X_2	94.37521	1	94.37521	108.7946	8.32E-09	
X_3	99.36823	1	99.36823	114.5505	5.67E-09	
X_1X_2	7.186621	1	7.186621	8.284653	0.010431	
X_1X_3	2.304461	1	2.304461	2.656555	0.121511	
X_2X_3	2.876377	1	2.876377	3.315854	0.086263	
X_1^2	2.840983	1	2.840983	3.275052	0.088056	
X_2^2	38.30057	1	38.30057	44.15246	4.14E-06	
X_3^2	0.804157	1	0.804157	0.927023	0.349134	
Residual	14.74685	17	0.867462			
Cor Total	349.1343	26				

Table 4.146: Model coefficient for (turbidity) removal in BRE using AESA

Std. Dev.	0.93	R-Squared	0.9578
C.V. %	0.98	Adj R-Squared	0.9354
Adeq Precision	27.179	Pred R-Squared	0.8871

Table 4.147: ANOVA for response surface quadratic model for removal of turbidity in BRE using AESS

Source	Sum of Squares	Df	Mean Square	F Value	p-value Prob > F	
Model	492.0737	9	54.67486	238.7495	1.53E-14	Significant
X_1	43.42512	1	43.42512	189.6251	6.45E-10	
X_2	174.7982	1	174.7982	763.2938	2.8E-14	
X_3	78.30558	1	78.30558	341.9381	9.8E-12	
X_1X_2	1.783755	1	1.783755	7.78915	0.013709	
X_1X_3	5.833833	1	5.833833	25.47468	0.000145	
X_2X_3	0.937908	1	0.937908	4.095576	0.061188	
X_1^2	2.581608	1	2.581608	11.27314	0.004318	
X_2^2	102.9714	1	102.9714	449.6467	1.35E-12	
X_3^2	3.176231	1	3.176231	13.86969	0.002036	
Residual	3.435077	15	0.229005			
Cor Total	495.5088	24				

Table 4.148: Model coefficient for (turbidity) removal in BRE using AESS

Std. Dev.	0.478545	R-Squared	0.993068
C.V. %	0.507305	Adj RSquared	0.988908
AdeqPrecision	52.30417	PredRSquared	0.978207

Table 4.149: ANOVA for response surface quadratic model for turbidity removal in BRE using OSA

Source	Sum of Squares	Df	Mean Square	F Value	p-value Prob > F	
Model	715.5977	9	79.51085	229.9161	1.23E-13	Significant
X_1	87.07683	1	87.07683	251.7941	2.41E-10	
X_2	40.72689	1	40.72689	117.7672	3.36E-08	
X_3	182.0345	1	182.0345	526.3768	1.66E-12	
X_1X_2	9.42281	1	9.42281	27.2473	0.00013	
X_1X_3	0.288906	1	0.288906	0.835411	0.376186	
X_2X_3	3.148507	1	3.148507	9.104323	0.009229	
X_1^2	1.802815	1	1.802815	5.213078	0.038557	
X_2^2	157.3492	1	157.3492	454.996	4.48E-12	
X_3^2	2.608757	1	2.608757	7.543563	0.015751	
Residual	4.841557	14	0.345826			
Cor Total	720.4393	23				

Table 4.150: Model coefficient for (turbidity) removal in OSA

Std. Dev.	0.588069	R-Squared	0.99328
C.V. %	0.668698	Adj RSquared	0.98896
AdeqPrecision	56.50938	PredRSquared	0.980764

Table 4.151: ANOVA for response surface quadratic model for turbidity removal in BRE using OSS

Source	Sum of Squares	Df	Mean Square	F Value	p-value Prob > F	
Model	154.0081	9	17.11201	67.88743	5.36E-10	Significant
X_1	59.42583	1	59.42583	235.7565	3.74E-10	
X_2	60.86923	1	60.86923	241.4828	3.19E-10	
X_3	69.70356	1	69.70356	276.5306	1.29E-10	
X_1X_2	0.047217	1	0.047217	0.187321	0.671749	
X_1X_3	0.53897	1	0.53897	2.138223	0.165752	
X_2X_3	0.109644	1	0.109644	0.434983	0.520256	
X_1^2	2.173963	1	2.173963	8.624628	0.010826	
X_2^2	2.324548	1	2.324548	9.222036	0.00888	
X_3^2	1.42306	1	1.42306	5.64562	0.032316	
Residual	3.528903	14	0.252065			
Cor Total	157.537	23				

Table 4.152: Model coefficient for turbidity removal in BRE using OSS

Std. Dev.	0.50206	R-Squared	0.9776
C.V. %	0.577413	Adj RSquared	0.963199
AdeqPrecision	26.88766	PredRSquared	0.920203

Table 4.153: ANOVA for response surface quadratic model for turbidity removal in PW using MSA

Source	Sum of Squares	Df	Mean Square	F Value	p-value Prob > F	
Model	399.4754	9	44.38615	31.76222	1.54E-08	Significant
X_1	57.61855	1	57.61855	41.23117	8.46E-06	
X_2	104.177	1	104.177	74.54783	2.03E-07	
X_3	98.29206	1	98.29206	70.33666	2.99E-07	
X_1X_2	10.29602	1	10.29602	7.367712	0.015315	
X_1X_3	7.080508	1	7.080508	5.06673	0.038802	
X_2X_3	14.47884	1	14.47884	10.36089	0.005361	
X_1^2	1.52453	1	1.52453	1.090936	0.311789	
X_2^2	69.38956	1	69.38956	49.65437	2.76E-06	
X_3^2	3.515262	1	3.515262	2.515481	0.132297	
Residual	22.35922	16	1.397451			
Cor Total	421.8346	25				

Table 4.154: Model coefficient for (turbidity) removal in PW using MSA

Std. Dev.	1.18	R-Squared	0.9470

C.V. %	1.23	Adj R-Squared	0.9172
Adeq Precision	22.660	Pred R-Squared	0.8720

Table 4.155: ANOVA for response surface quadratic model for turbidity removal in PW using MSS

Source	Sum of Squares	Df	Mean Square	F Value	p-value Prob > F	
Model	28.83362	9	3.203735	59.71978	1.3E-10	Significant
X_1	10.24881	1	10.24881	191.0447	2.59E-10	
X_2	13.51712	1	13.51712	251.9682	3.26E-11	
X_3	7.975469	1	7.975469	148.6681	1.63E-09	
X_1X_2	0.56933	1	0.56933	10.61269	0.00494	
X_1X_3	0.603258	1	0.603258	11.24513	0.004038	
X_2X_3	0.805312	1	0.805312	15.01156	0.001344	
X_1^2	0.674028	1	0.674028	12.56433	0.002697	
X_2^2	3.381397	1	3.381397	63.03151	6.12E-07	
X_3^2	0.391179	1	0.391179	7.29184	0.015761	
Residual	0.858338	16	0.053646			
Cor Total	29.69195	25				

Table 4.156: Model coefficient for (turbidity) removal in PW using MSS

Std. Dev.	0.231616	R-Squared	0.971092
C.V. %	0.235486	Adj RSquared	0.954831
AdeqPrecision	24.51716	PredRSquared	0.927276

Table 4.157: ANOVA for response surface quadratic model for removal of turbidity in PW using AESA

Source	Sum of Squares	df	Mean Square	F Value	p-value Prob > F	
Model	39.59007	9	4.398897	54.08241	9.58E-11	Significant
X_1	6.277606	1	6.277606	77.18026	9.97E-08	
X_2	0.37845	1	0.37845	4.652868	0.045608	
X_3	15.9048	1	15.9048	195.5422	9.38E-11	
X_1X_2	7.5E-05	1	7.5E-05	0.000922	0.976129	
X_1X_3	0.005208	1	0.005208	0.064034	0.803265	
X_2X_3	0.1875	1	0.1875	2.305226	0.147317	
X_1^2	0.138017	1	0.138017	1.696851	0.210071	
X_2^2	14.13735	1	14.13735	173.8122	2.36E-10	
X_3^2	2.561067	1	2.561067	31.48713	3.11E-05	
Residual	1.382728	17	0.081337			
Cor Total	40.9728	26				

Table 4.158: Model coefficient for (turbidity) removal in PW using AESA

Std. Dev.	0.285196	R-Squared	0.966253
C.V. %	0.291483	Adj RSquared	0.948386
AdeqPrecision	26.61028	PredRSquared	0.917215

Table 4.159: ANOVA for response surface quadratic model for removal of turbidity in PW using AESS

Source	Sum of Squares	Df	Mean Square	F Value	p-value Prob > F	
Model	492.0737	9	54.67486	238.7495	1.53E-14	Significant
X_1	43.42512	1	43.42512	189.6251	6.45E-10	
X_1	174.7982	1	174.7982	763.2938	2.8E-14	
X_3	78.30558	1	78.30558	341.9381	9.8E-12	
X_1X_2	1.783755	1	1.783755	7.78915	0.013709	
X_1X_3	5.833833	1	5.833833	25.47468	0.000145	
X_2X_3	0.937908	1	0.937908	4.095576	0.061188	
X_1^2	2.581608	1	2.581608	11.27314	0.004318	
X_2^2	102.9714	1	102.9714	449.6467	1.35E-12	
X_3^2	3.176231	1	3.176231	13.86969	0.002036	
Residual	3.435077	15	0.229005			
Cor Total	495.5088	24				

Table 4.160: Model coefficient for (turbidity) removal in PW using AESS

Std. Dev.	0.478545	R-Squared	0.993068
C.V. %	0.507305	Adj RSquared	0.988908
AdeqPrecision	52.30417	PredRSquared	0.978207

Table 4.161: ANOVA for response surface quadratic model for removal of turbidity in PW using OSA

Source	Sum of Squares	Df	Mean Square	F Value	p-value Prob > F	
Model	117.7708	9	13.08564	59.82023	1.26E-09	Significant
X_1	38.624	1	38.624	176.5673	2.5E-09	
X_2	33.49791	1	33.49791	153.1337	6.3E-09	
X_3	24.49214	1	24.49214	111.9644	4.62E-08	
X_1X_2	2.033633	1	2.033633	9.296635	0.008666	
X_1X_3	0.175033	1	0.175033	0.800153	0.386168	
X_2X_3	0.241679	1	0.241679	1.104822	0.311016	
X_1^2	0.001616	1	0.001616	0.007386	0.932729	
X_2^2	0.114358	1	0.114358	0.522781	0.481564	
X_3^2	2.830008	1	2.830008	12.93722	0.002917	
Residual	3.062492	14	0.218749			
Cor Total	120.8333	23				

Table 4.162: Model coefficient for (turbidity) removal in PW using OSA

Std. Dev.	0.47707	R-Squared	0.974655
C.V. %	0.487385	Adj RSquared	0.958362
AdeqPrecision	29.29512	PredRSquared	0.895718

Table 4.163: ANOVA for response surface quadratic model for removal of turbidity in PW using OSS

Source	Sum of Squares	Df	Mean Square	F Value	p-value Prob > F	
Model	127.1245	9	14.12495	72.17147	9.1E-12	Significant
X_1	44.68276	1	44.68276	228.3067	2.76E-11	
X_2	29.61934	1	29.61934	151.3401	6.87E-10	
X_3	47.49876	1	47.49876	242.6951	1.7E-11	
X_1X_2	0.864033	1	0.864033	4.414781	0.050848	
X_1X_3	1.5987	1	1.5987	8.168564	0.010887	
X_2X_3	0.064533	1	0.064533	0.329733	0.573337	
X_1^2	0.041667	1	0.041667	0.212896	0.650356	
X_2^2	2.65335	1	2.65335	13.5573	0.001849	
X_3^2	0.1014	1	0.1014	0.518104	0.481431	
Residual	3.327133	17	0.195714			
Cor Total	130.4517	26				

Table 4.164: Model coefficient for (turbidity) removal in PW using OSS

Std. Dev.	0.442395	R-Squared	0.974495
C.V. %	0.478237	Adj RSquared	0.960993
AdeqPrecision	33.30032	PredRSquared	0.929157

Neglecting the coefficients of non significant terms at 95% confidence level, the final regression equations becomes 4.30 to 4.41 for BRE and PW.

Final equation for BRE

$$Y_{(MSA)} = 72.42350 + 0.15309X_1 + 4.03523X_2 + 0.25639X_3 - 6.25946E - 003X_1X_2 - 7.33172E - 004X_1X_3 - 9.89710E - 003X_2X_3 - 0.21911X_2^2$$

(4.30)

$$Y_{(MSS)} = 74.37794 + 0.16158X_1 + 0.26977X_3 - 8.91940E-004X_1X_3 - 0.25902X_2^2 - 1.15341E-003X_3^2$$

(4.31)

$$Y_{(OSA)} = 63.04734 + 0.13823X_1 + 5.55190X_2 + 0.20385X_3 - 6.34818E-003X_1X_2 - 4.50520E-003X_2X_3 - 3.6307E-004X_1^2 - 0.38030X_2^2 - 8.42182E-004X_3^2$$

(4.32)

$$Y_{(OSS)} = 81.32437 + 0.092164X_1 + 0.057438X_2 + 0.11756X_3 - 4.07131E-004X_1^2 - 0.043088X_2^2 - 5.99351E-004X_3^2$$

(4.33)

$$Y_{(AESA)} = 88.96827 + 0.089505X_1 + 0.82886X_2 + 0.11205X_3 + 5.2220E-003X_1X_2 - 0.15962X_2^2$$

(4.34)

$$Y_{(AESS)} = 73.10150 + 0.10448X_1 + 4.09936X_2 + 0.19603X_3 + 2.95029E-003X_1X_2 - 6.37459E-003X_1X_3 - 4.32102E-004X_1^2 - 0.27290X_2^2 - 8.54267E-004X_3^2$$

(4.35)

Final equation for PW

$$Y_{(MSA)} = 72.42350 + 0.15309X_1 + 4.03523X_2 + 0.25639X_3 - 6.25946E-003X_1X_2 - 7.33172E-004X_1X_3 - 9.89710E-003X_2X_3 - 0.21911X_2^2$$

(4.36)

$$Y_{(MSS)} = 96.03023 + 0.045980X_1 + 0.16951X_2 + 0.046317X_3 + 1.51590E-003X_1X_2 - 2.04084E-004X_1X_3 + 2.26969E-003X_2X_3 - 2.24945E-004X_1^2 - 0.048292X_2^2 - 3.06727E-004X_3^2$$

(4.37)

$$Y_{(AESA)} = 96.66498 + 0.026740X_1 - 1.07427X_2 + 0.096699X_3 - 9.47917E-003X_1^2 + 0.095937X_2^2 - 7.25926E-004X_3^2$$

(4.38)

$$Y_{(AESS)} = 73.10150 + 0.10448X_1 + 0.19603X_3 + 2.95029E-003X_1X_2 - 6.37459E-003X_1X_3 - 2.55597E-003X_2X_3 - 4.32102E-004X_1^2 - 0.27290X_2^2 - 8.54267E004X_3^2$$

(4.39)

$$Y_{(OSA)} = 88.13434 + 0.047958X_1 + 0.43966X_2 + 0.11529X_3 - 2.57292E - 003X_1X_2 - 8.20771E - 004X_3^2$$

(4.40)

$$Y_{(OSS)} = 90.05157 + 0.023410X_1 + 0.052986X_2 + 0.043787X_3 + 1.67708E - 003X_1X_2 + 3.04167708E - 003X_1X_3 - 0.041563X_2^2$$

(4.41)

Positive sign in front of the terms represents synergistic effect, whereas negative sign in front of the term represent antagonistic effect.

4.16 Adequacy of a Model

It is usually necessary to check the fitted model to ensure it provides an adequate approximation to the real system. Normalization plots in figures 4.74 to 4.85, helps in judging if the models are satisfactory. The data were plotted against a theoretical normal distribution in such a way that the points should form an approximate straight line and a departure from this line would indicate a departure from a normal distribution. From the result, figures 4.74a to 4.85a shows that the data points are slightly deviating from the normal distribution given, but not very critical. Figures 4.74b to 4.85b for residual plots shows that the data points are scattered randomly and does not form a trend, but all the data points in the plot are within the boundaries marked by the red lines. Therefore, there were no outlier data. The predicted versus actual, in figures 4.74c 4.85c shows that all the data points are distributed along the 45 degree line, indicating that the model can provides an acceptable fit for the experimental data (Chen, et al., 2011).

The 3D response surface plots are the graphical representation of the regression equations used to visualize the relationship between the responses and experimental levels of each factor. These plots can be observed in figures 4.86 to 4.97 for MSA, MSS, AESA, AESS, OSA and OSS for BRE and PW. The removal of turbidity was display on z- axis showing the three dimensional relationship with factor variables on y and x axis respectively. The interactions of two factors are reflected in the contour of the plots, so that rounded contour line indicates a weak interaction of two factors and a distorted contour indicates a significant interaction of two factors (Holetz, et al., 2003). From figures 4.88 and 4.90, the contour are distorted which indicates a significant interaction of pH vs adsorbent dose and pH vs contact time with the three adsorbent both in BRE and PW. The turbidity removal of 80 -90% was within the pH range (6-8), dosage (60-80mg/L) and contact time (40-70min) for the adsorbents both acid and salt treated.

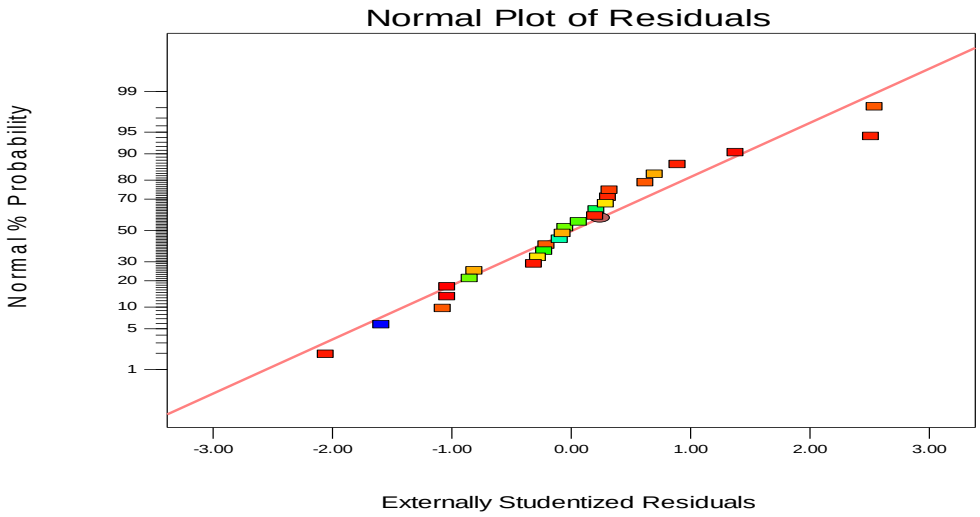

(a)

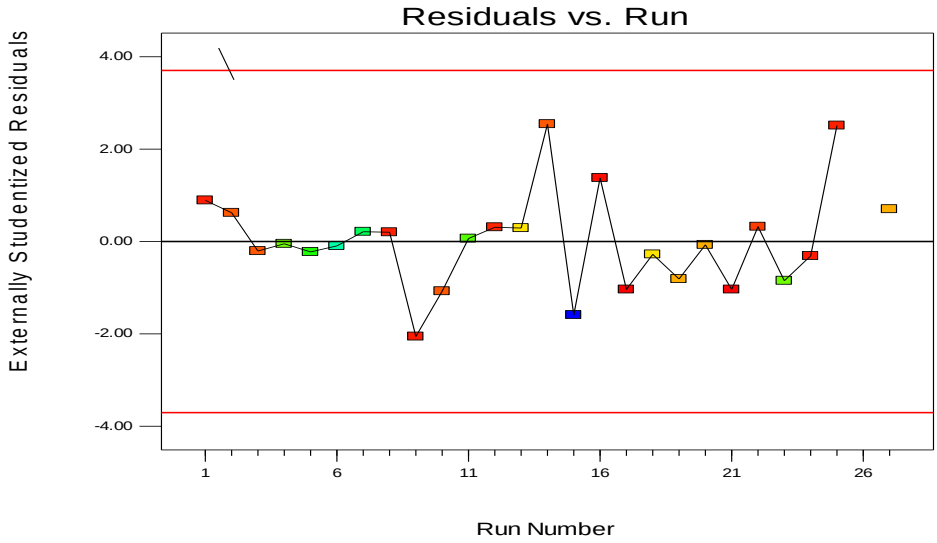

(b)

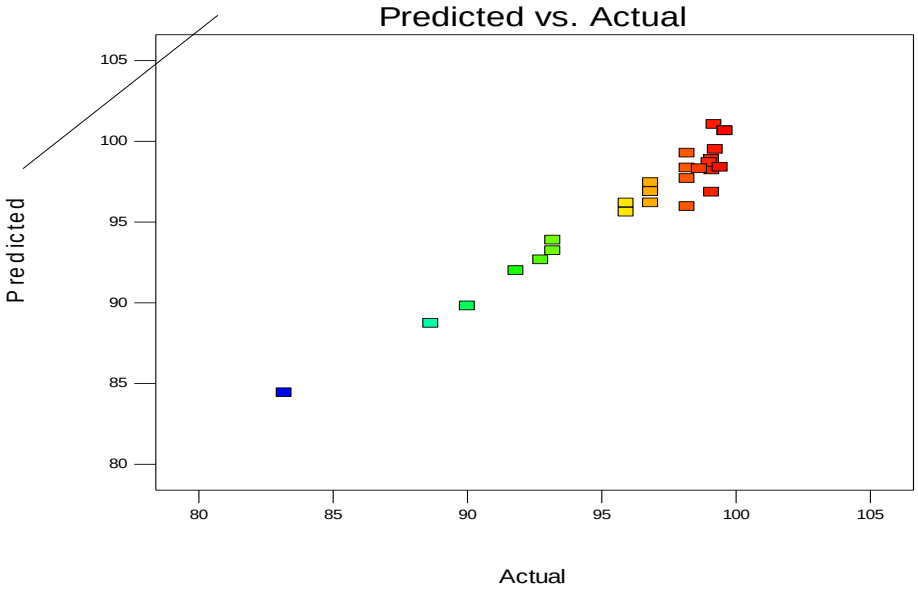

(c)

Figure 4.74: Design-expert plots: (a) Normal probability plots, (b) Residuals versus run number of data and (c) Predicted versus actual for turbidity removal using MSA in BRE.

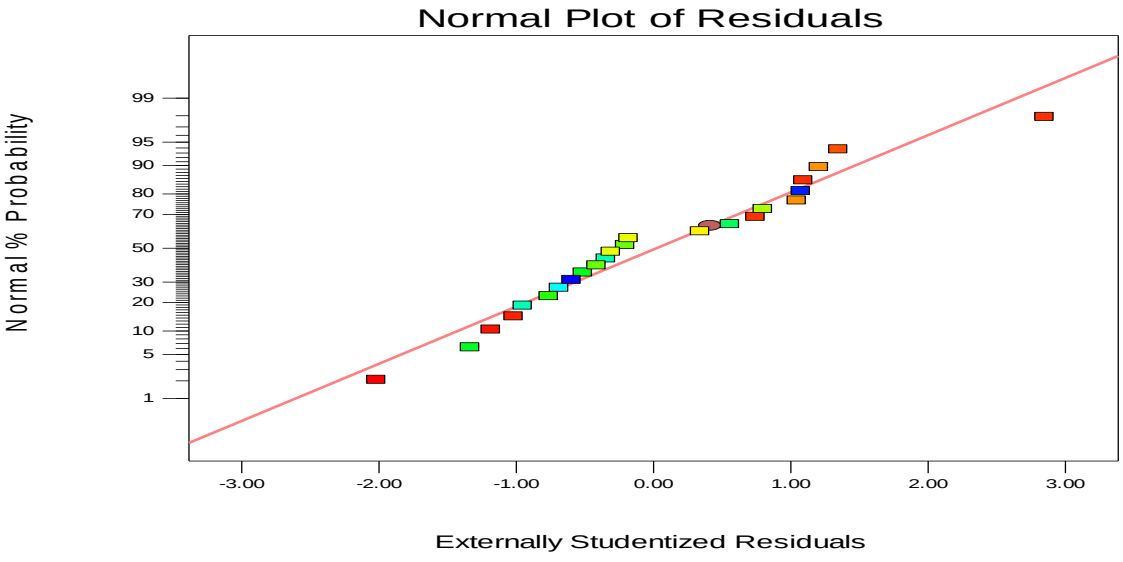

(a)

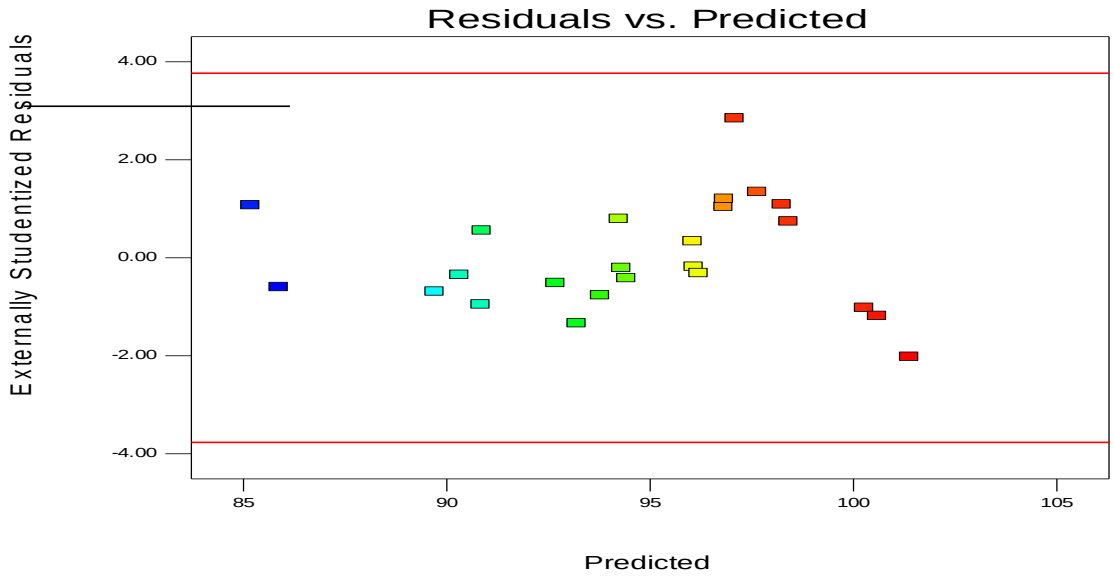

(b)

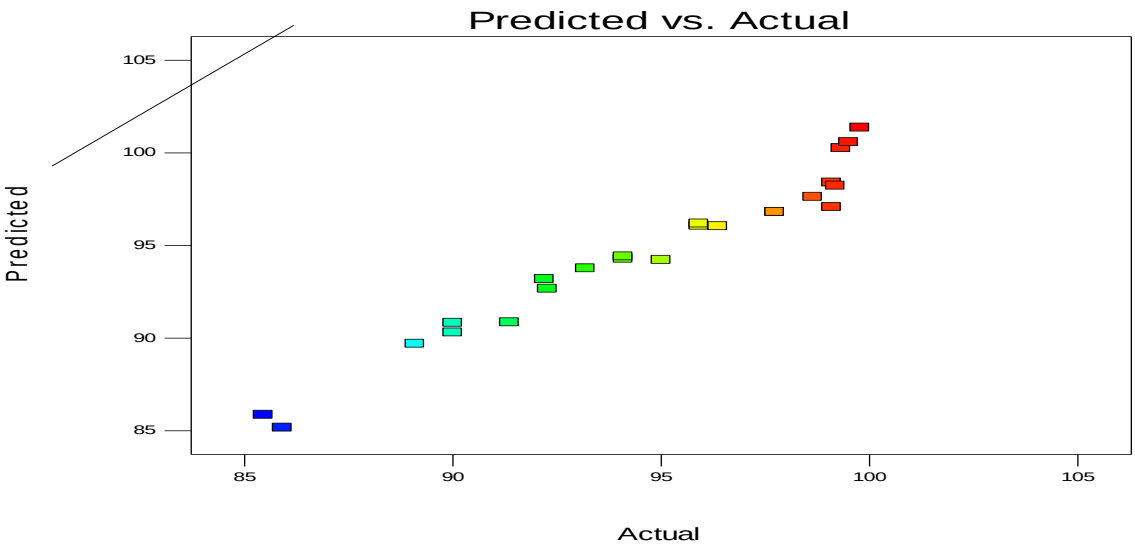

(c)

Figure 4.75: Design-expert plots: (a) Normal probability plots, (b) Residuals versus run number of data and (c) Predicted versus actual for turbidity removal in BRE usingMSS.

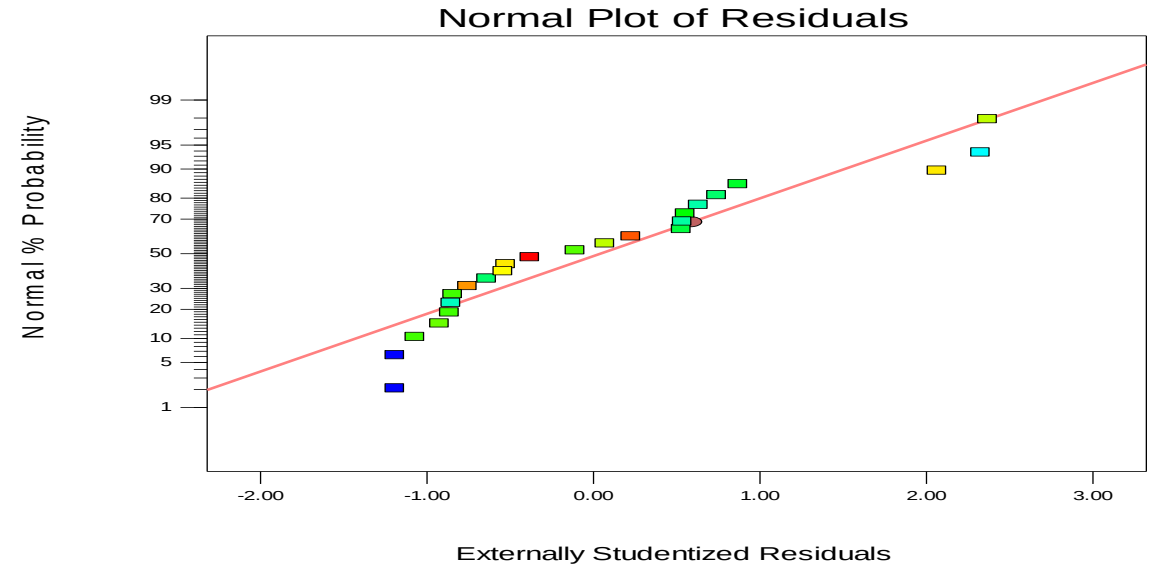

(a)

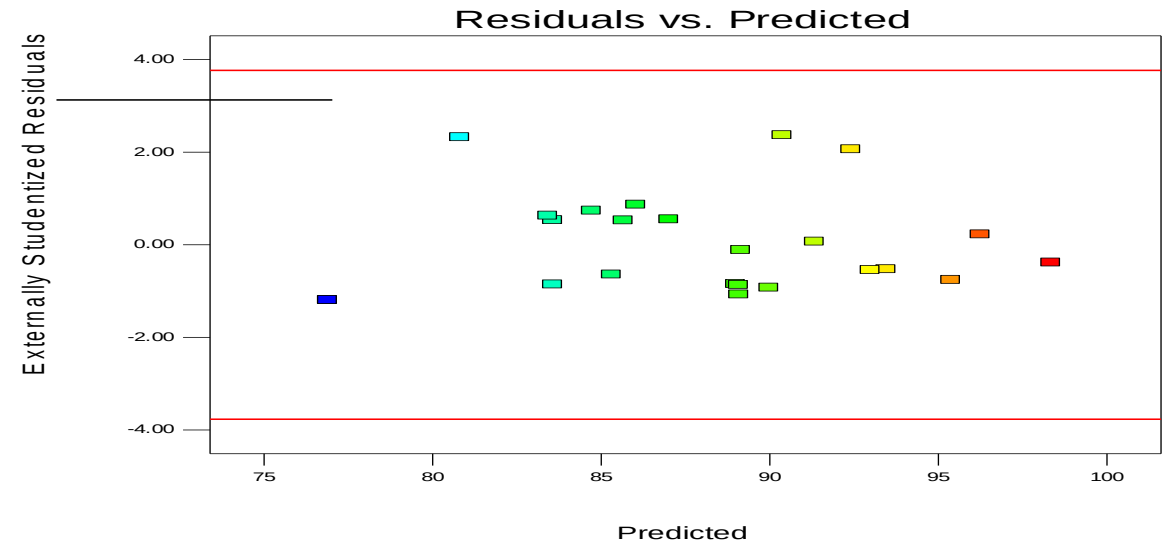

(b)

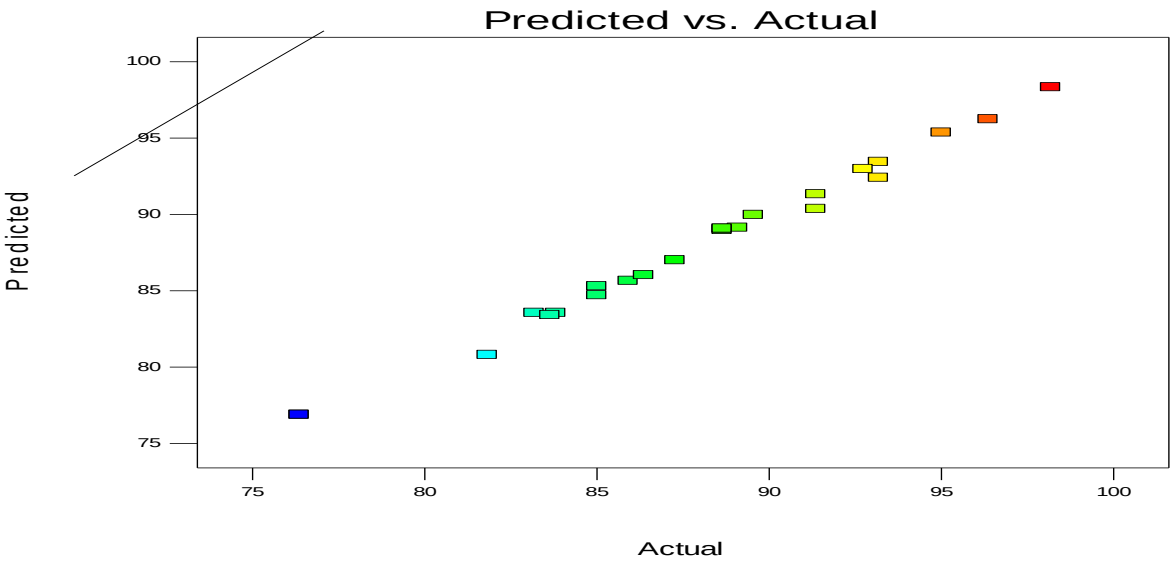

(c)

Fig. 4.76: Design-expert plots: (a) Normal probability plots, (b) Residuals versus run number of data and (c) Predicted versus actual for turbidity removal in BRE using OSA.

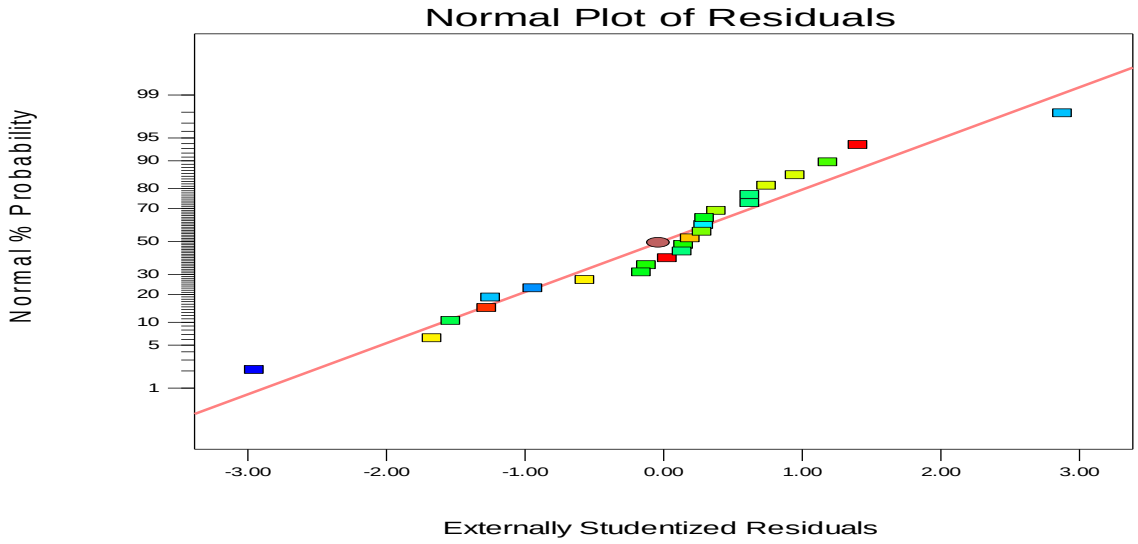

(a)

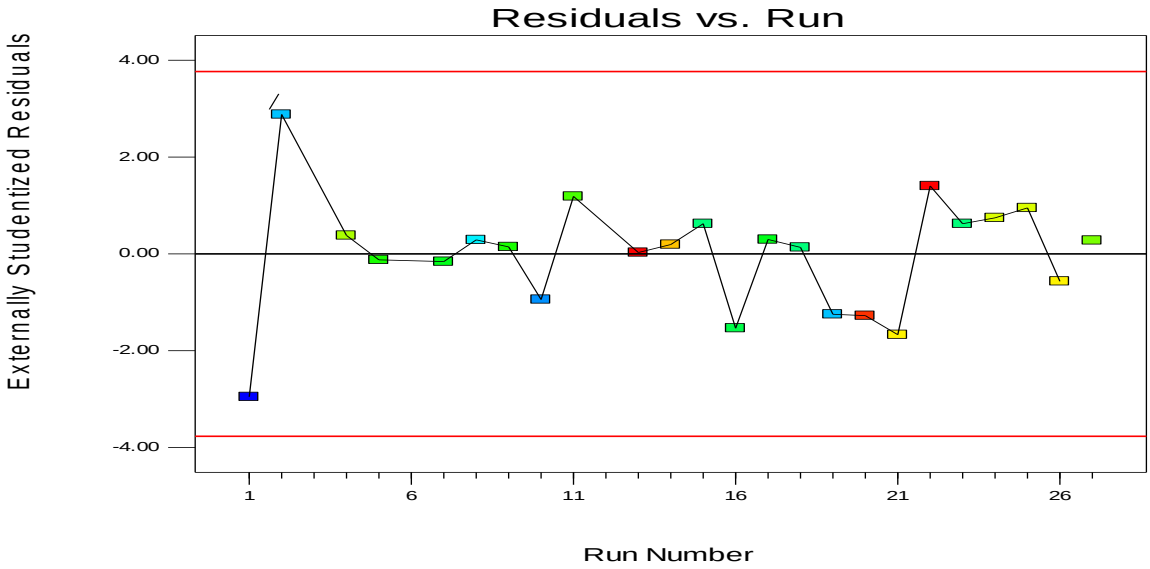

(b)

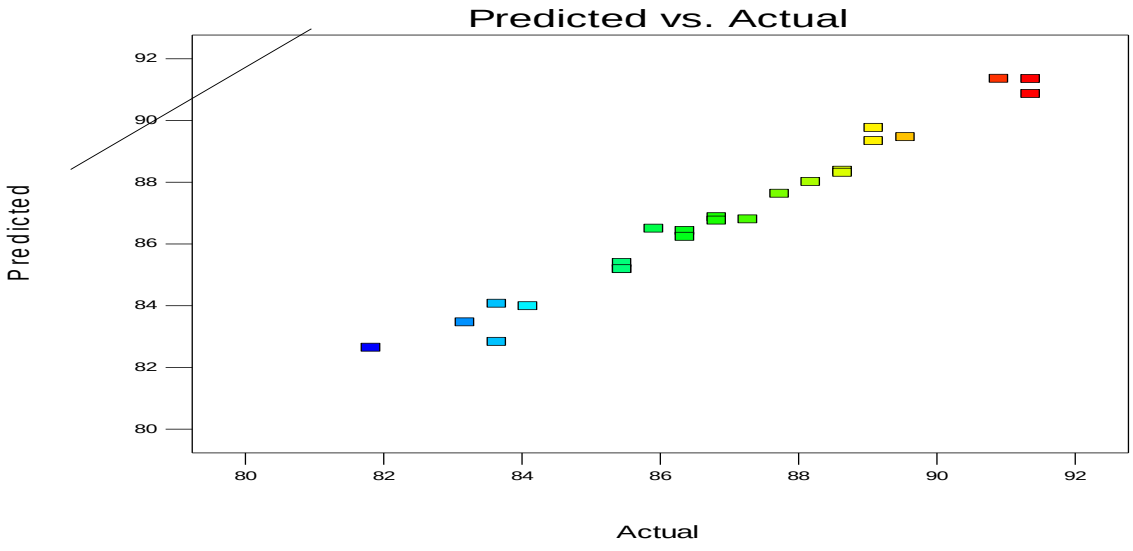

(c)

Fig.4.77: Design-expert plots: (a) Normal probability plots, (b) Residuals versus run number of data and (c) Predicted versus actual for turbidity removal in BRE using OSS.

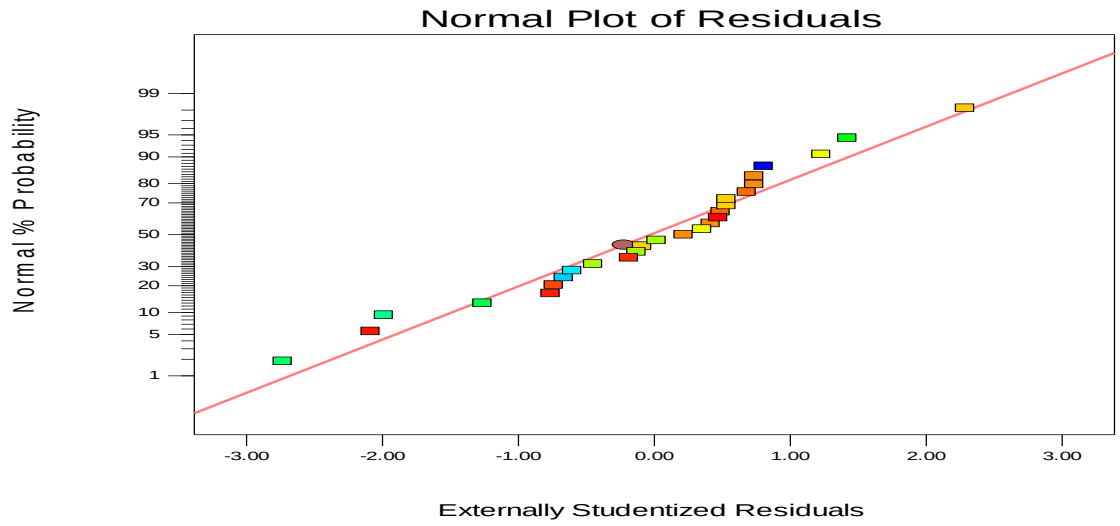

(a)

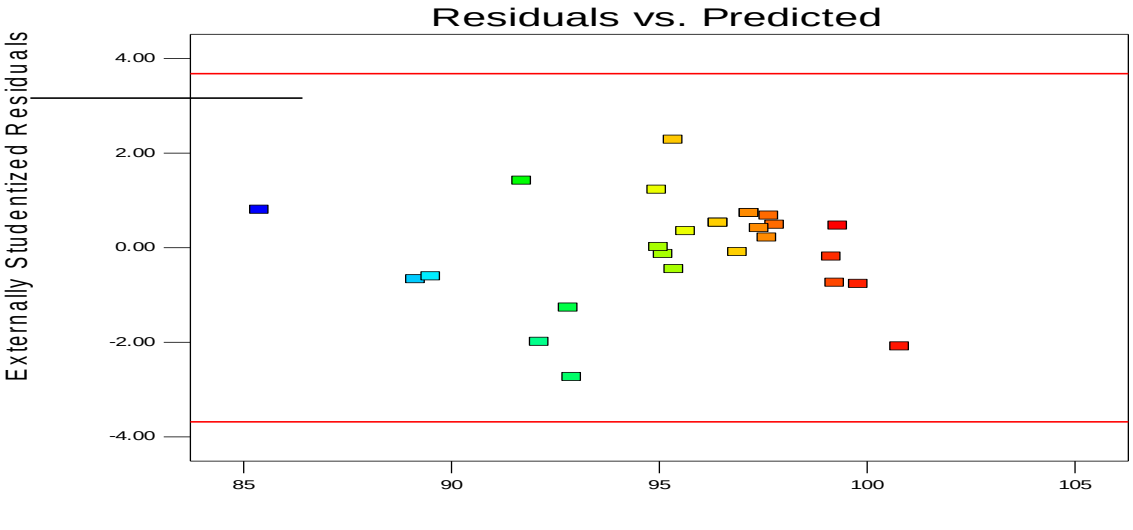

(b)

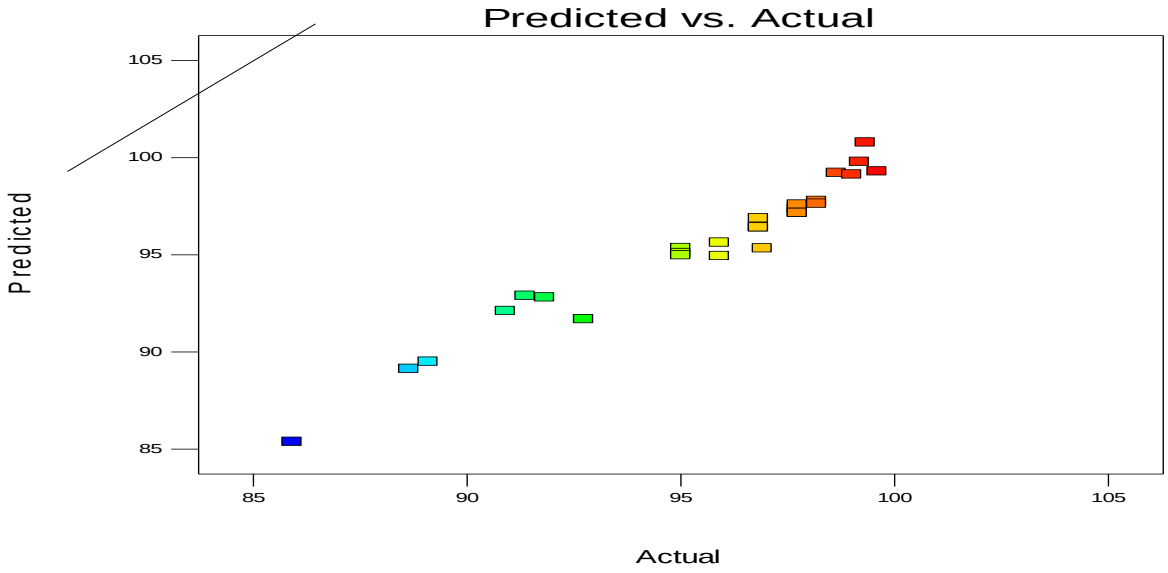

(c)

Fig.4.78: Design-expert plots: (a) Normal probability plots, (b) Residuals versus run number of data and (c) Predicted versus actual for turbidity removal in BRE using AESA.

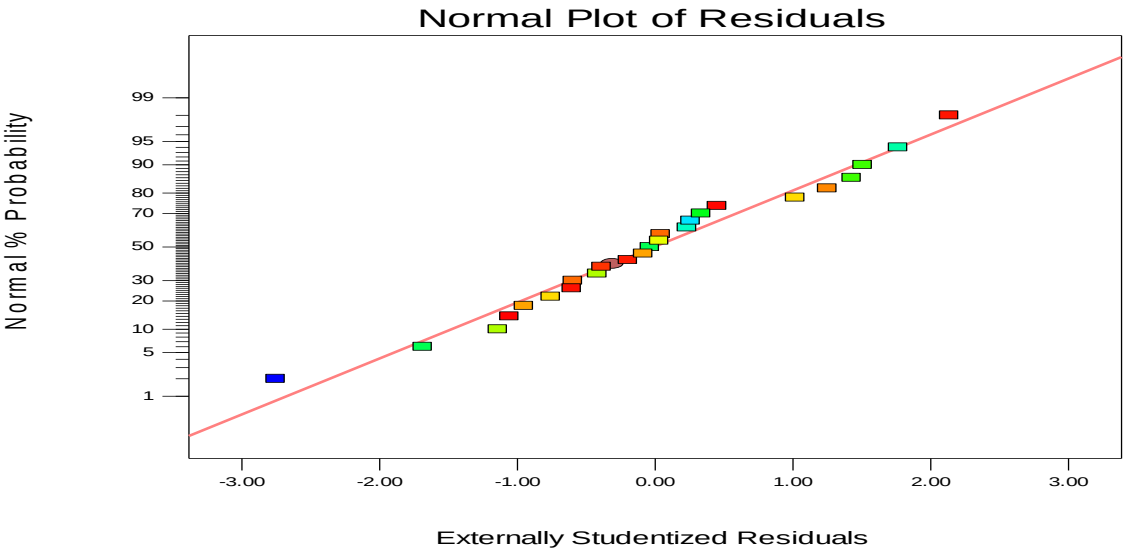

(a)

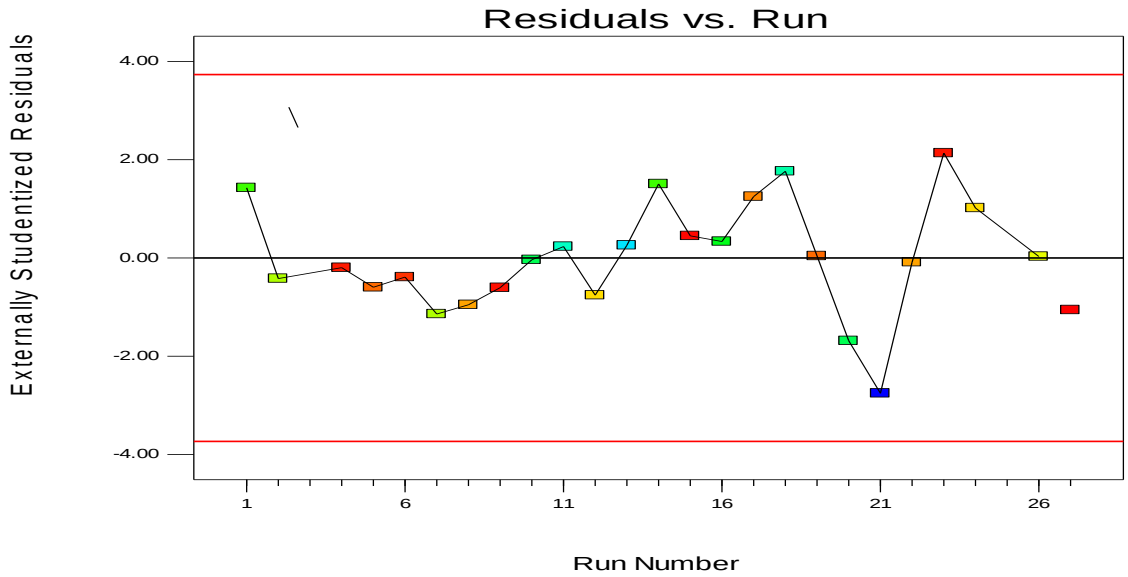

(b)

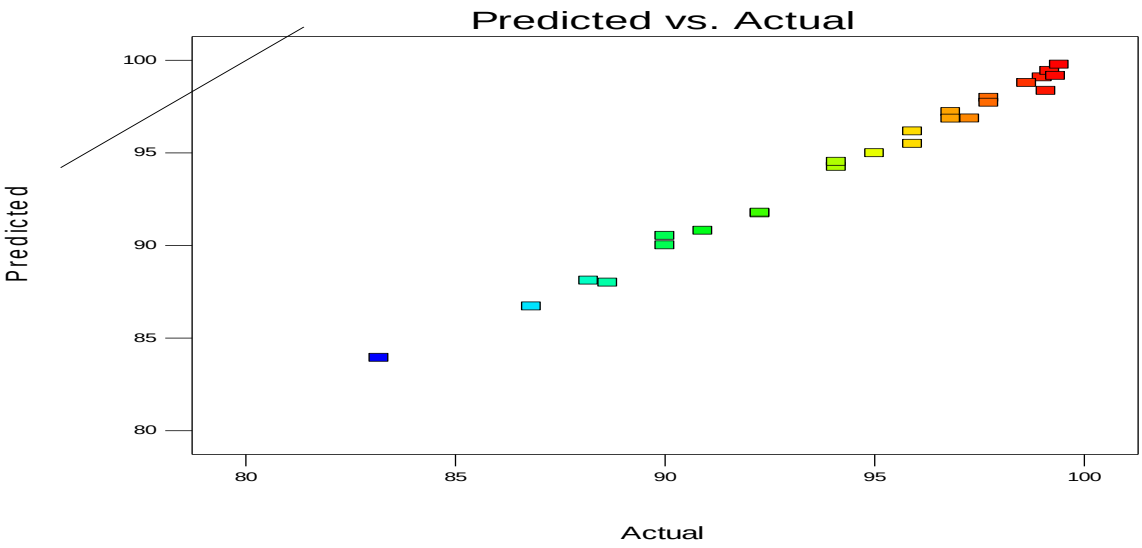

(c)

Fig. 4.79: Design-expert plots: (a) Normal probability plots, (b) Residuals versus run number of data and (c) Predicted versus actual for turbidity removal in BRE using AESS.

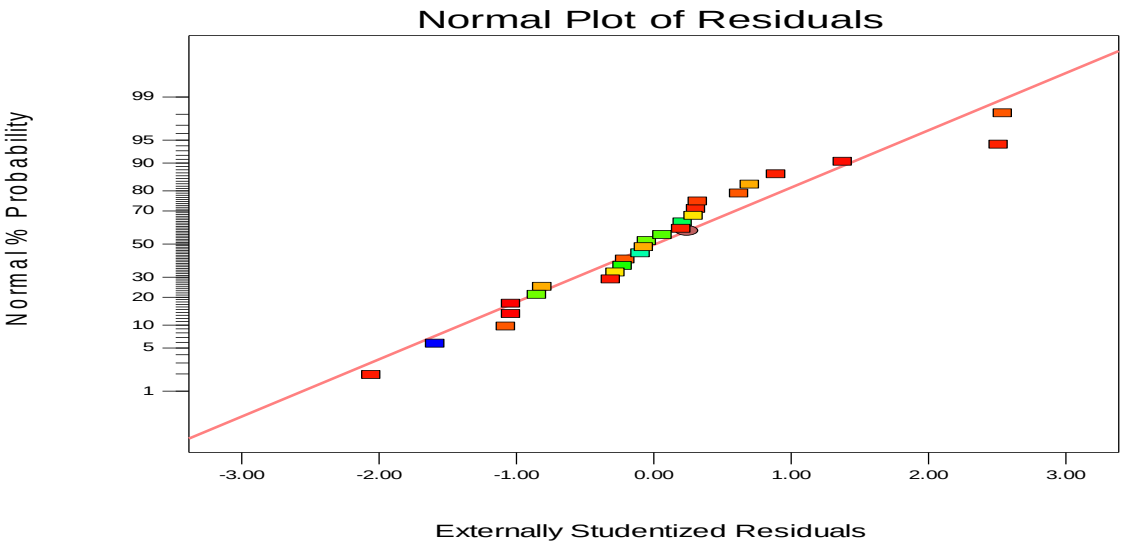

(a)

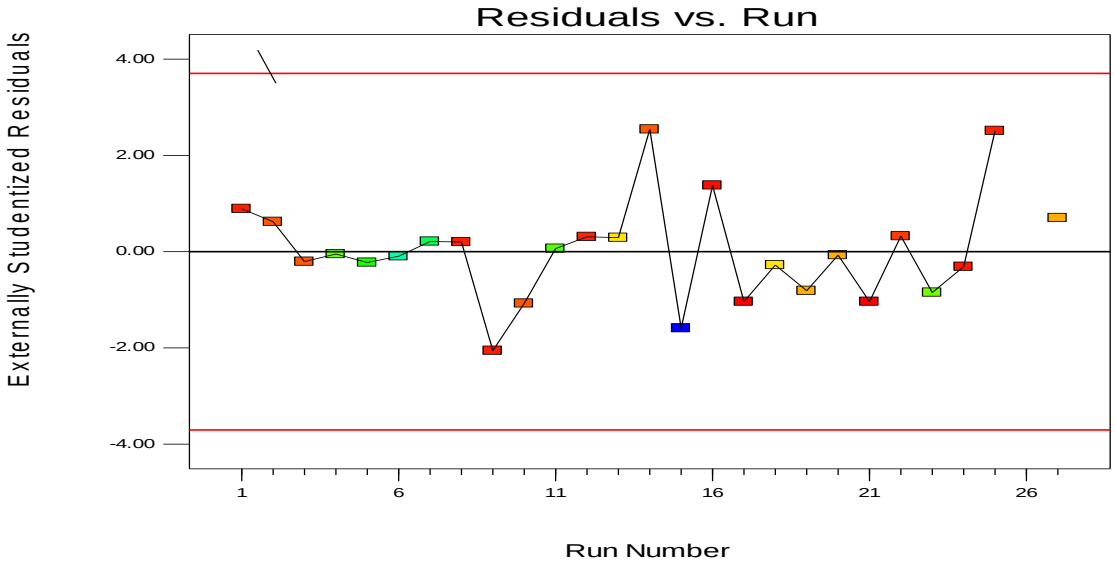

(b)

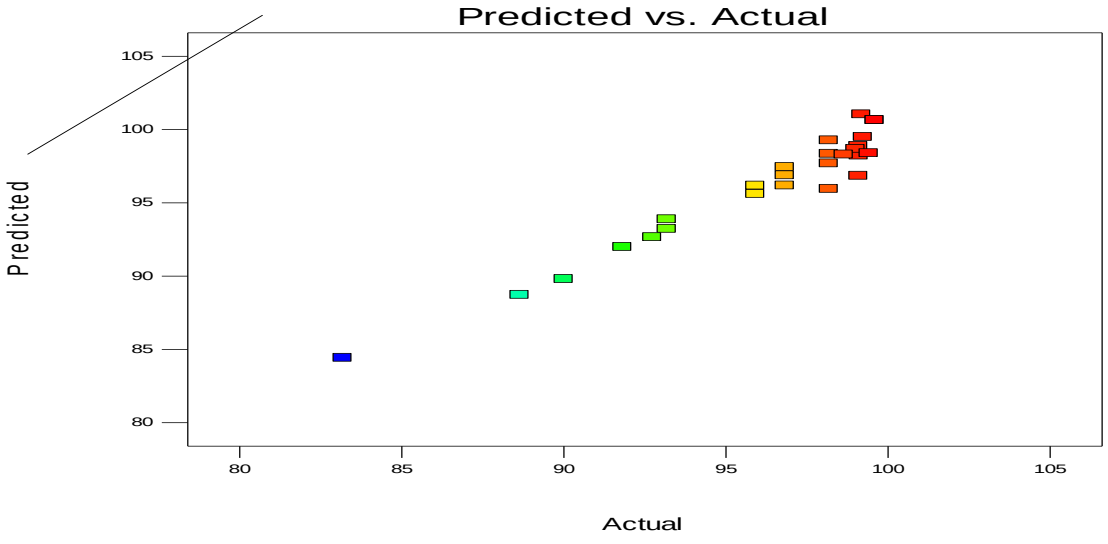

(c)

Fig.4.80: Design-expert plots: (a) Normal probability plots, (b) Residuals versus run number of data and (c) Predicted versus actual for turbidity removal in PW using MSA.

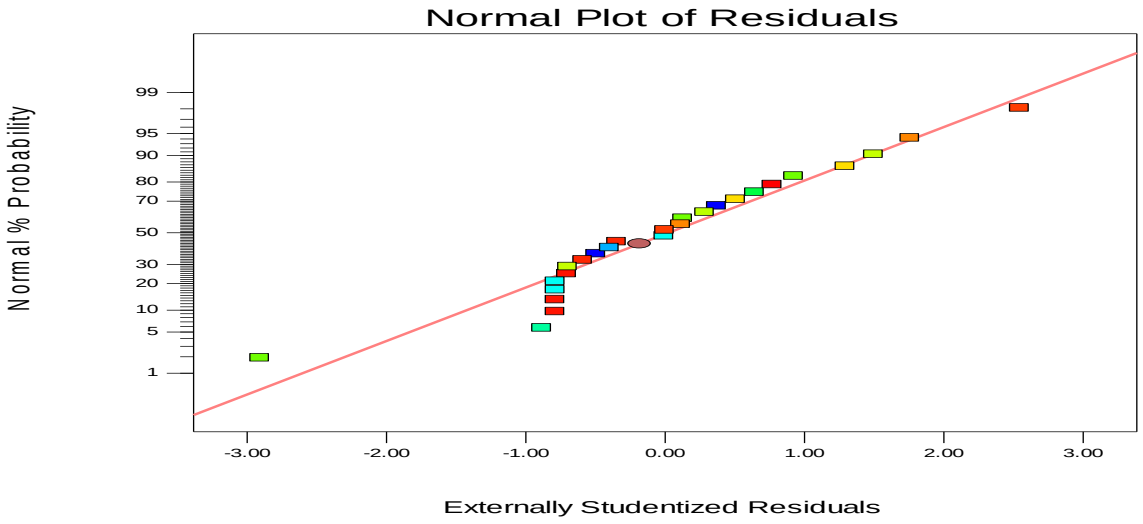

(a)

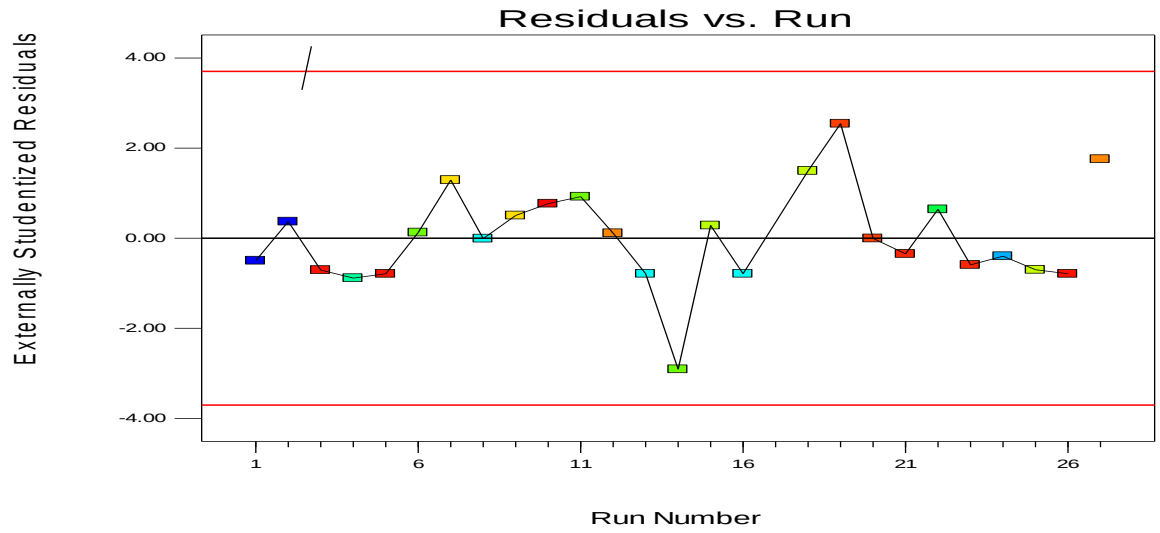

(b)

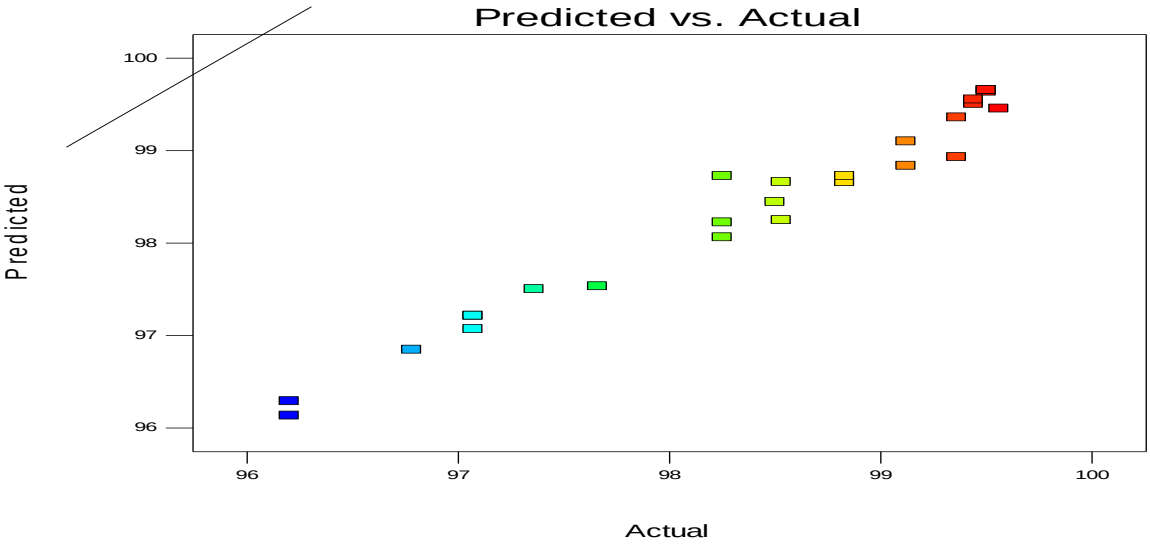

(c)

Figure 4.81: Design-expert plots: (a) Normal probability plots, (b) Residuals versus run number of data and (c) Predicted versus actual for turbidity removal in PW using MSS.

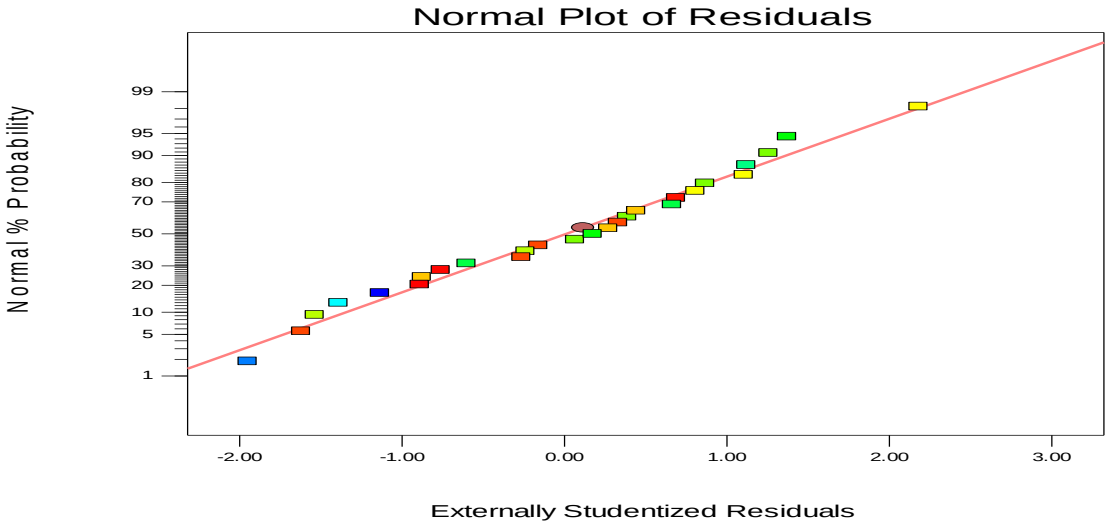

(a)

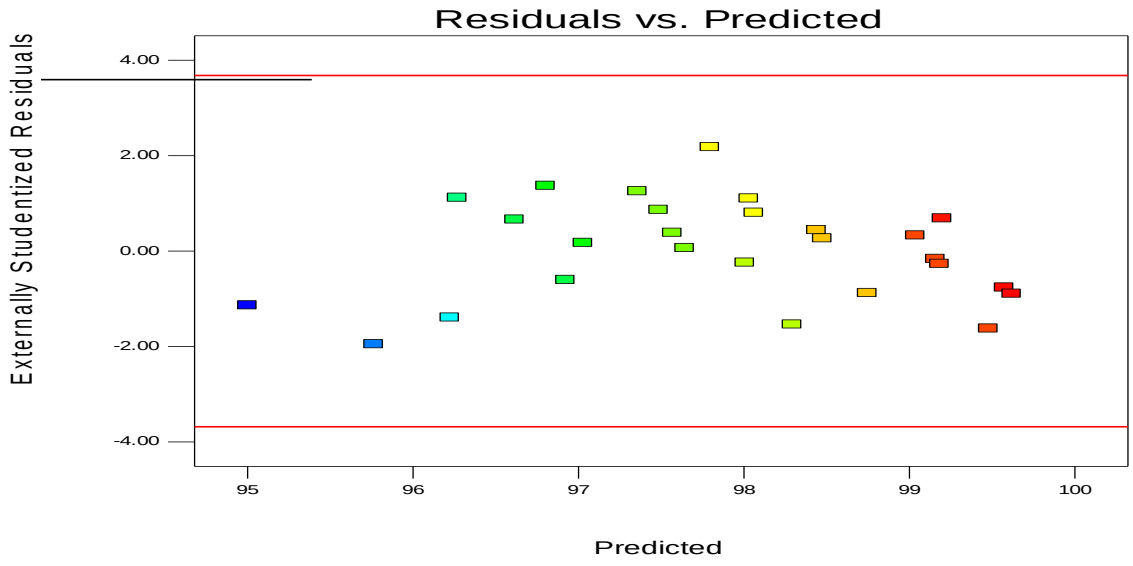

(b)

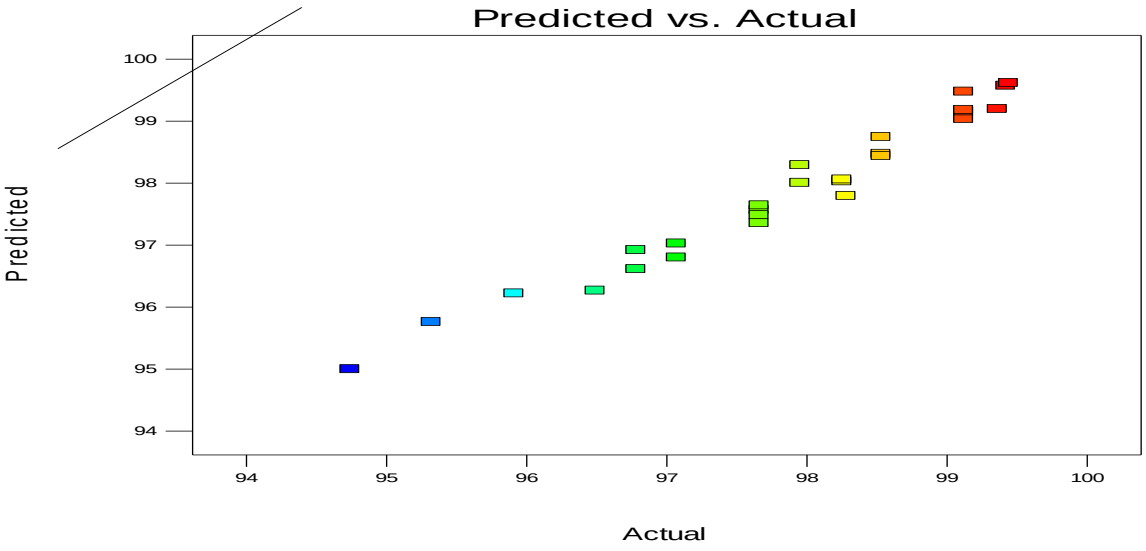

(c)

Figure 4.82: Design-expert plots: (a) Normal probability plots, (b) Residuals versus run number of data and (c) Predicted versus actual for turbidity removal in PW using AESA.

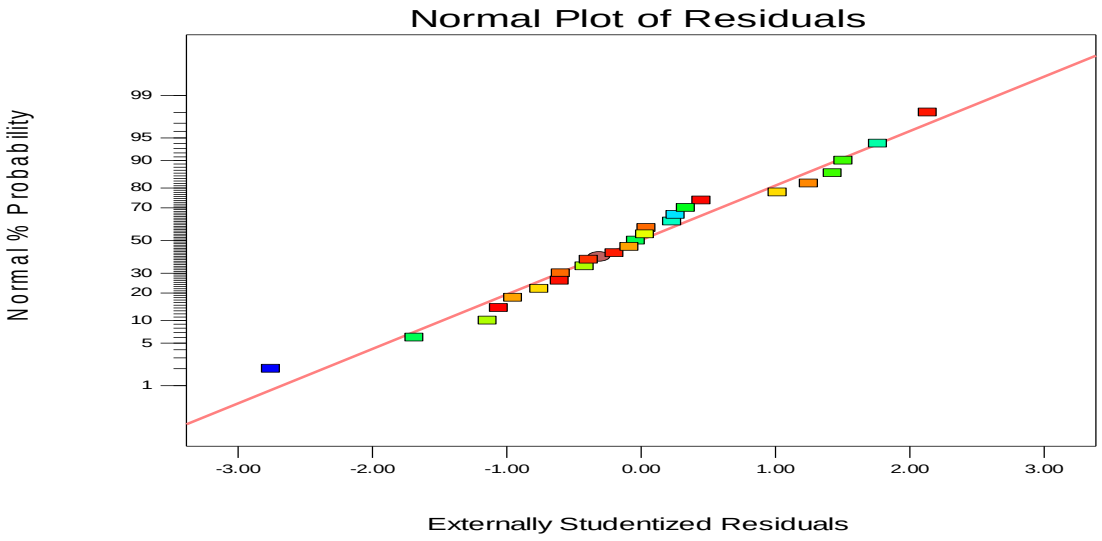

(a)

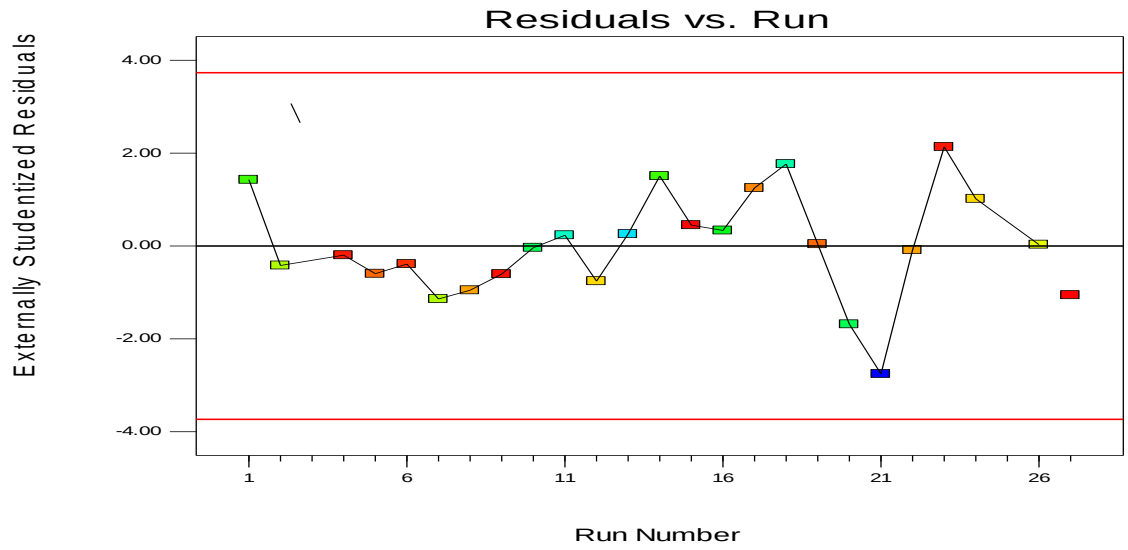

(b)

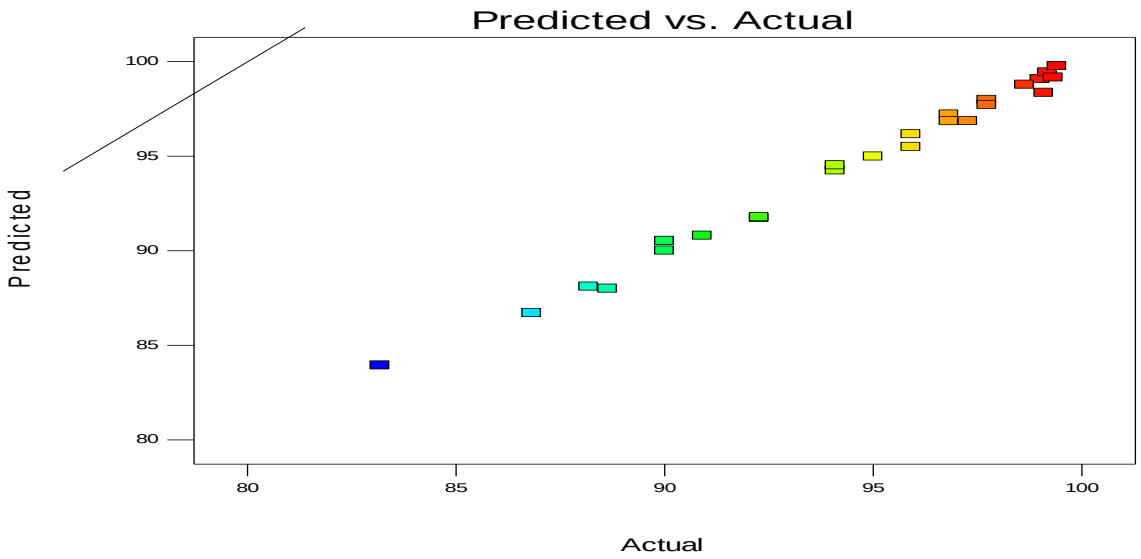

(c)

Figure 4.83: Design-expert plots: (a) Normal probability plots, (b) Residuals versus run number of data and (c) Predicted versus actual for turbidity removal in PW using AESS.

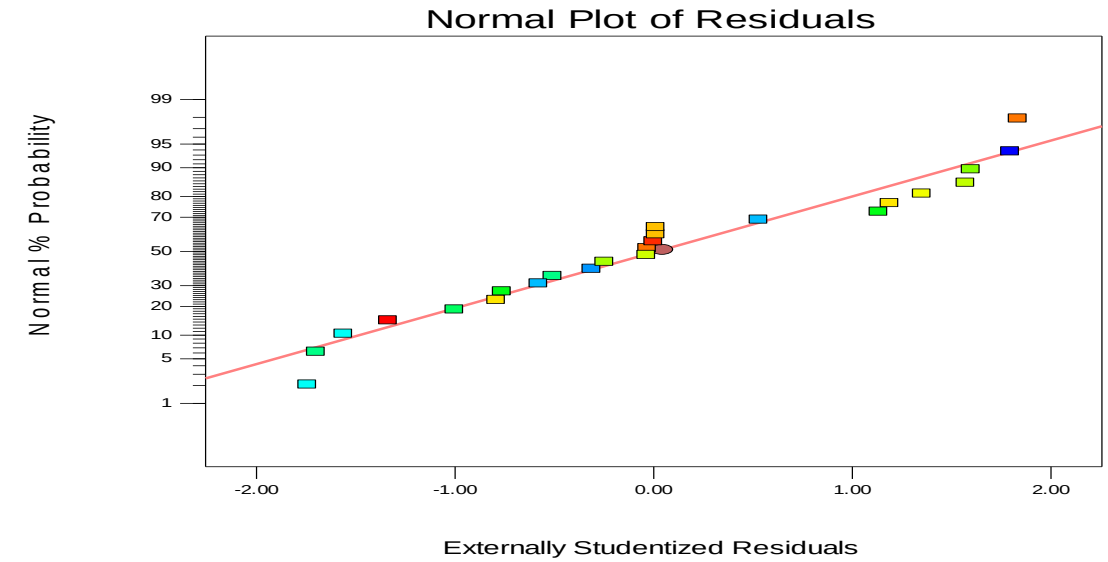

(a)

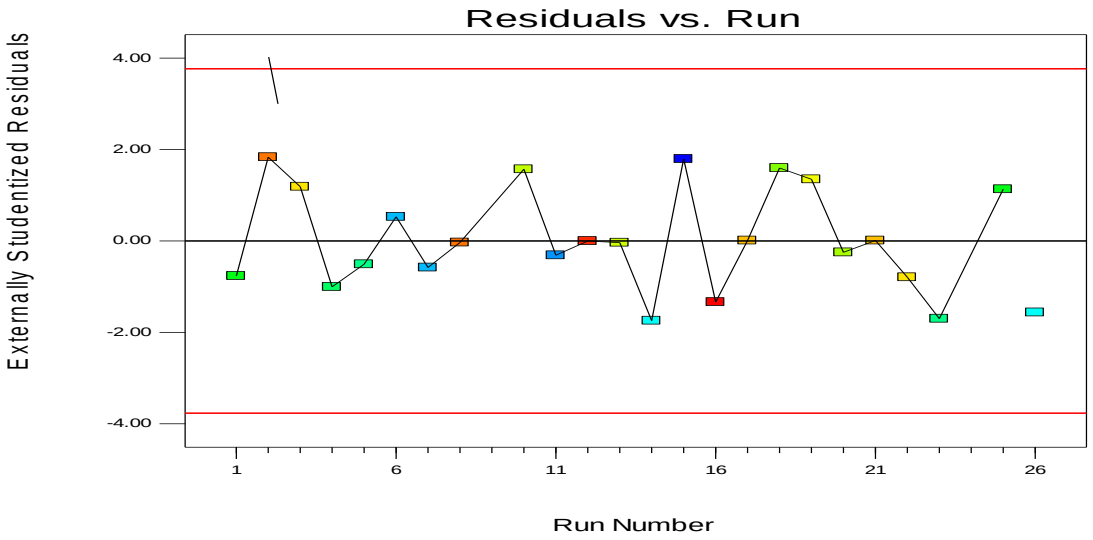

(b)

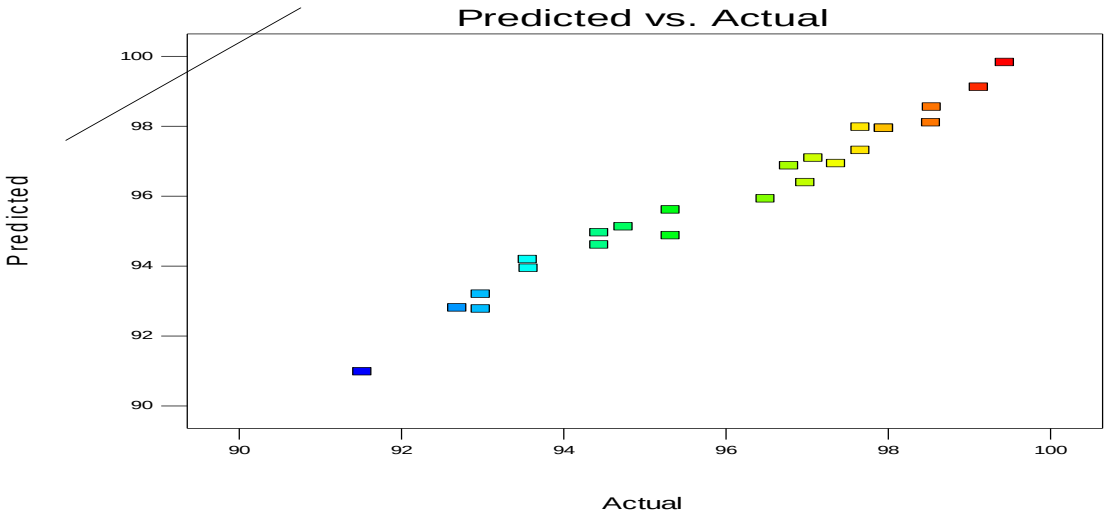

(c)

Figure 4.84: Design-expert plots: (a) Normal probability plots, (b) Residuals versus run number of data and (c) Predicted versus actual for turbidity removal in PW using OSA.

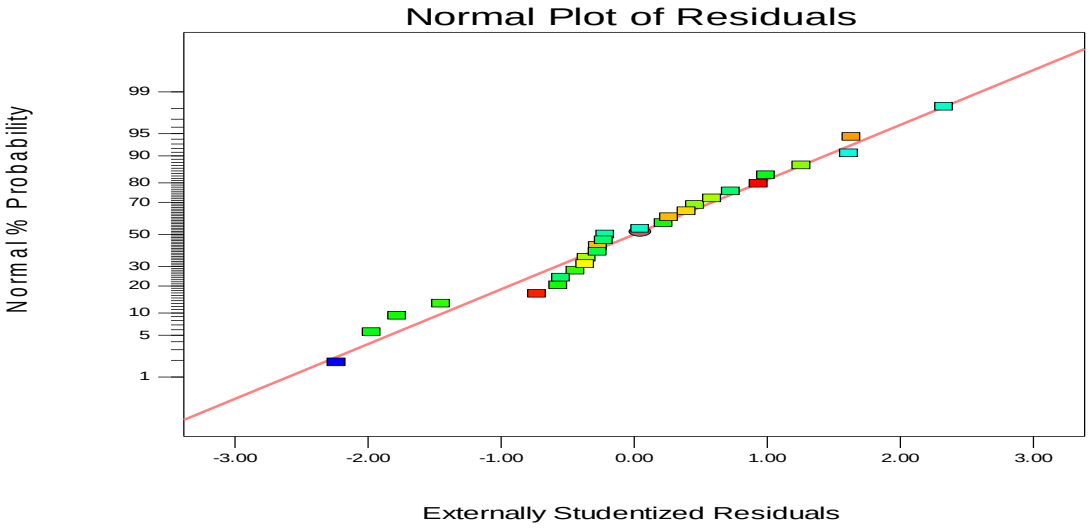

(a)

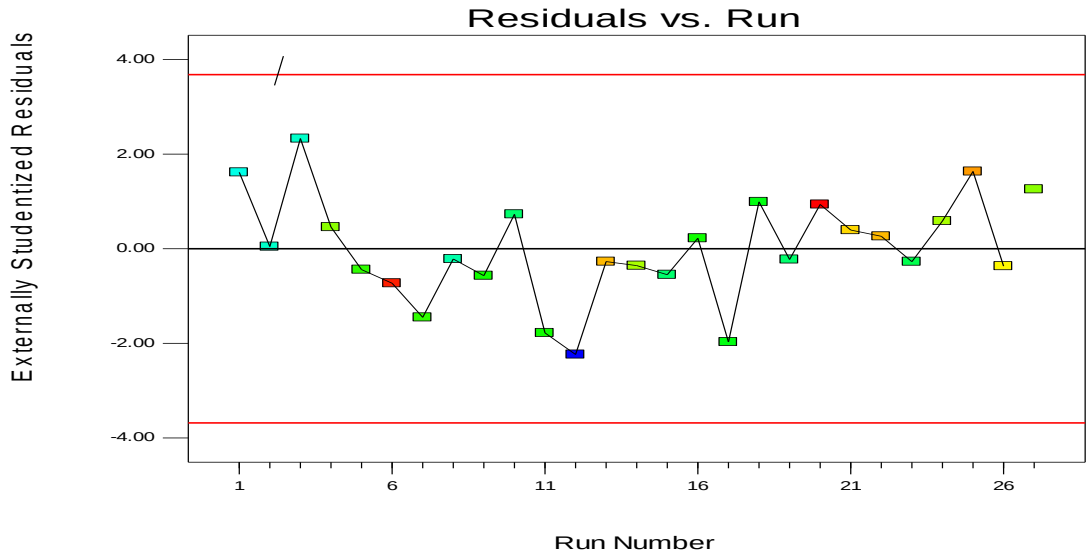

(b)

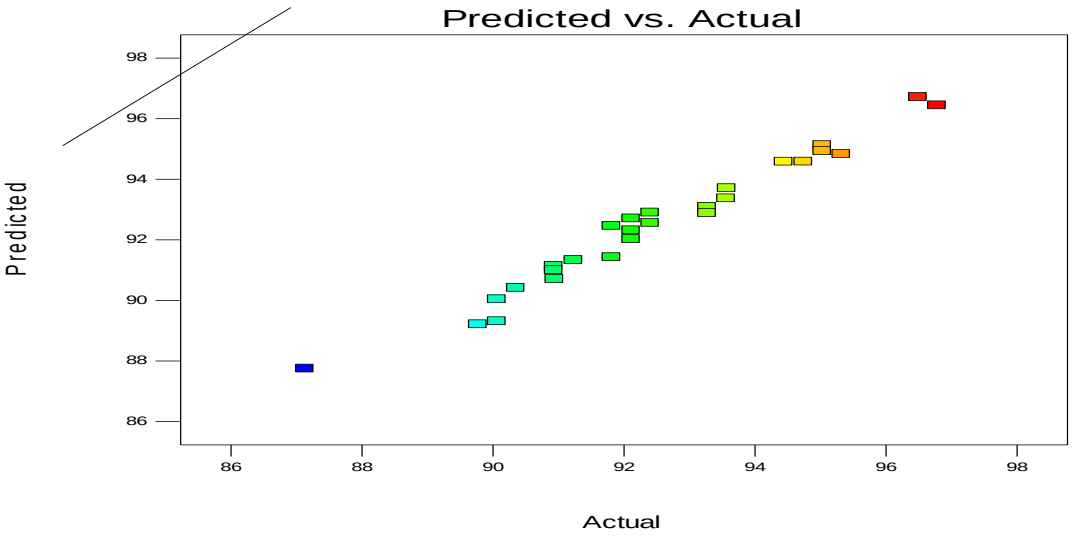

(c)

Figure 4.85. Design-expert plots: (a) Normal probability plots, (b) Residuals versus run number of data and (c) Predicted versus actual for turbidity removal in PW using OSS.

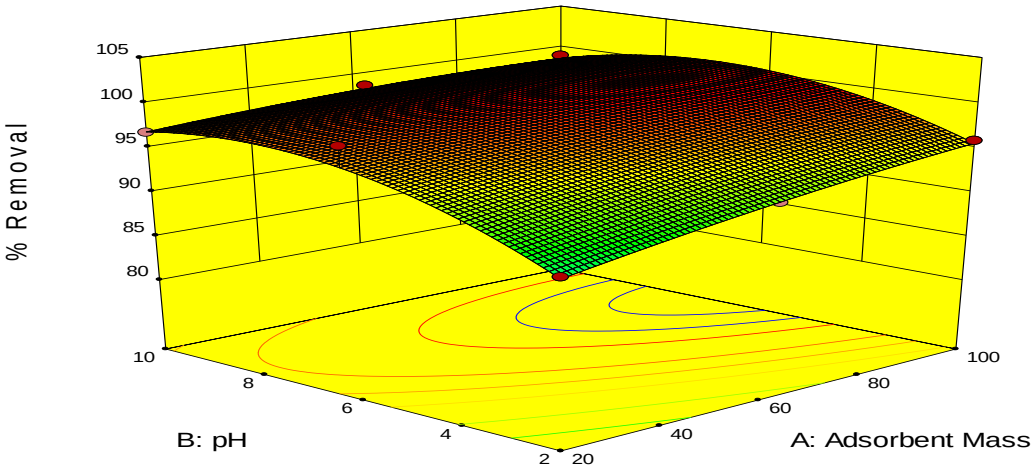

(a)

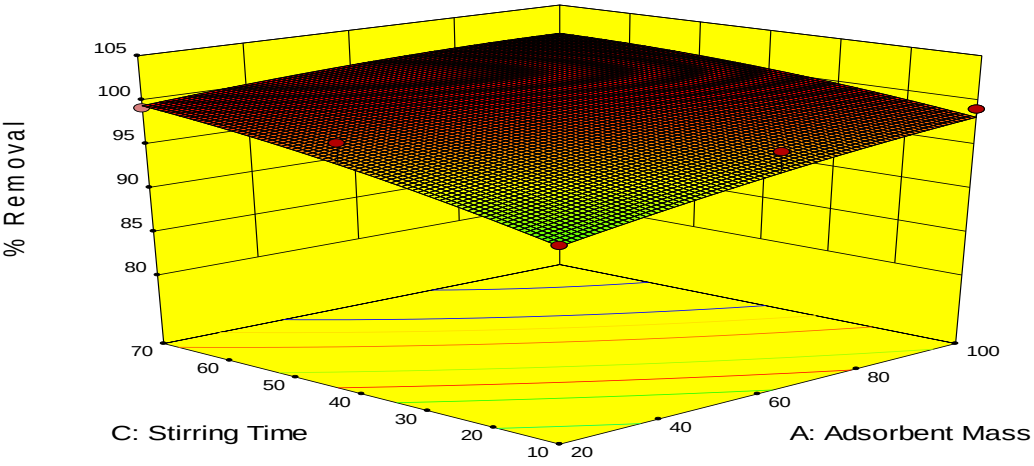

(b)

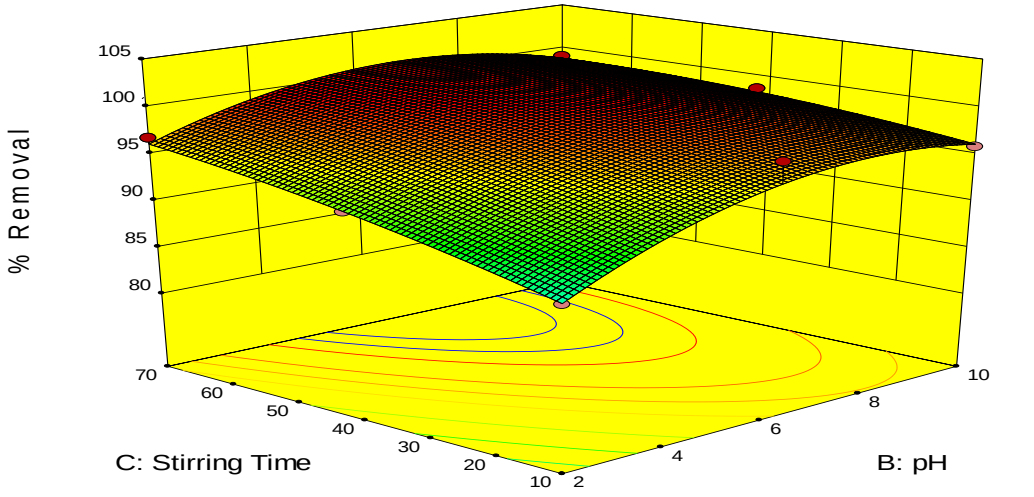

(c)

Fig 4.86: Response surface plots of the effects of (a) pH vs adsorbent dosage (b) contact time vs adsorbent dose (c) contact time vs pH for turbidity removal in BRE using MSA

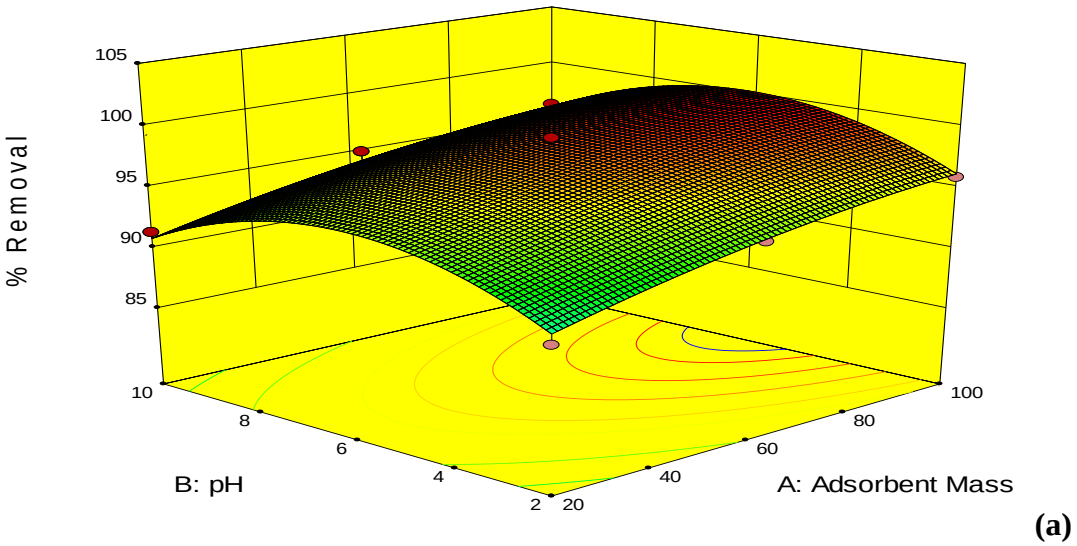

(a)

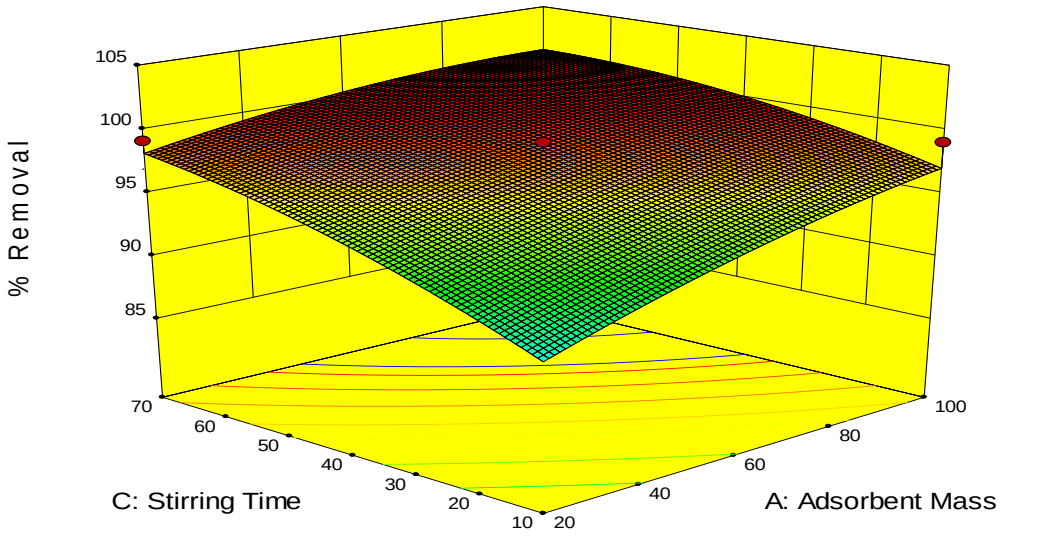

(b)

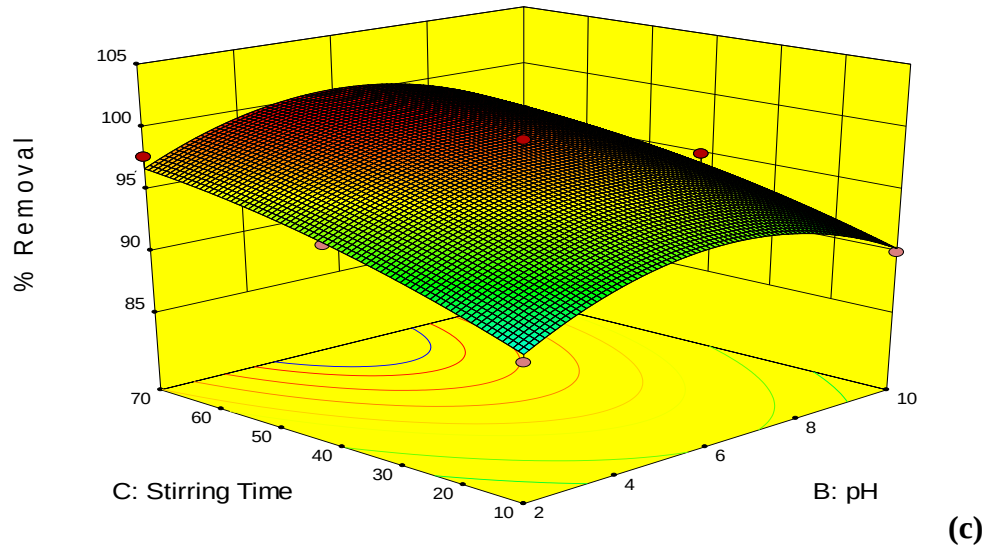

(c)

Fig 4.87: Response surface plots of the effects of (a) pH vs adsobent dosage (b) contact time vs adsorbent dosage (c) contact time vs pH for turbidity removal in BRE using MSS

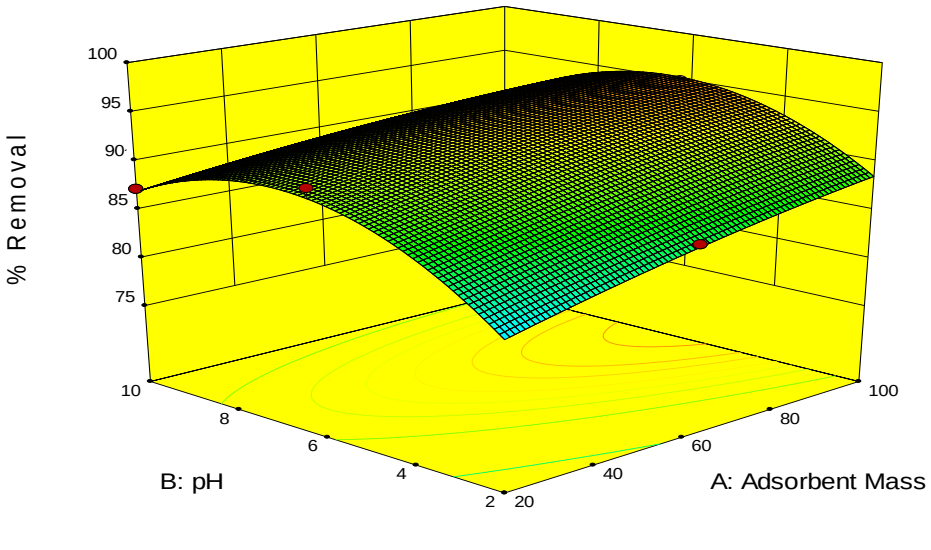

(a)

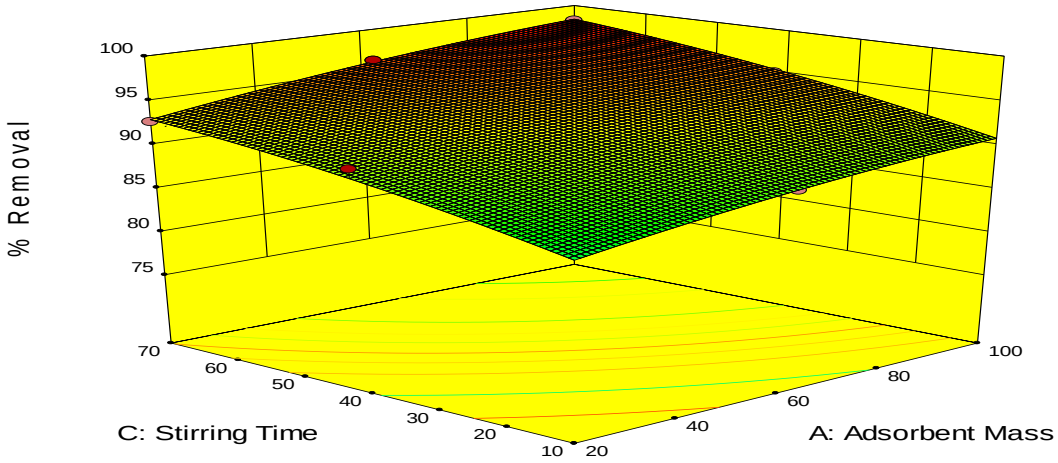

(b)

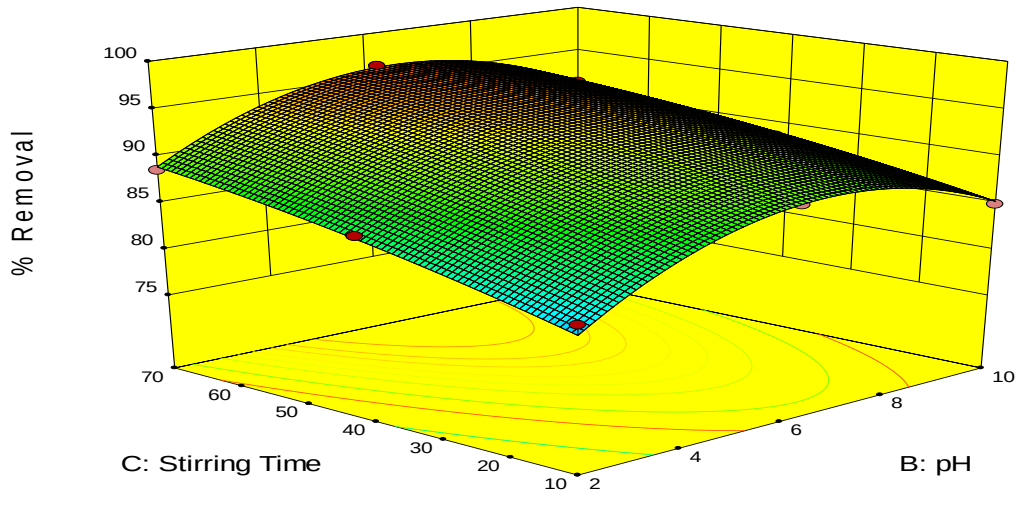

(c)

Fig 4.88: Response surface plots of the effects of (a) pH vs adsobent dosage (b) contact time vs adsorbent dosage (c) contact time vs pH for turbidity removal in BRE using AESA

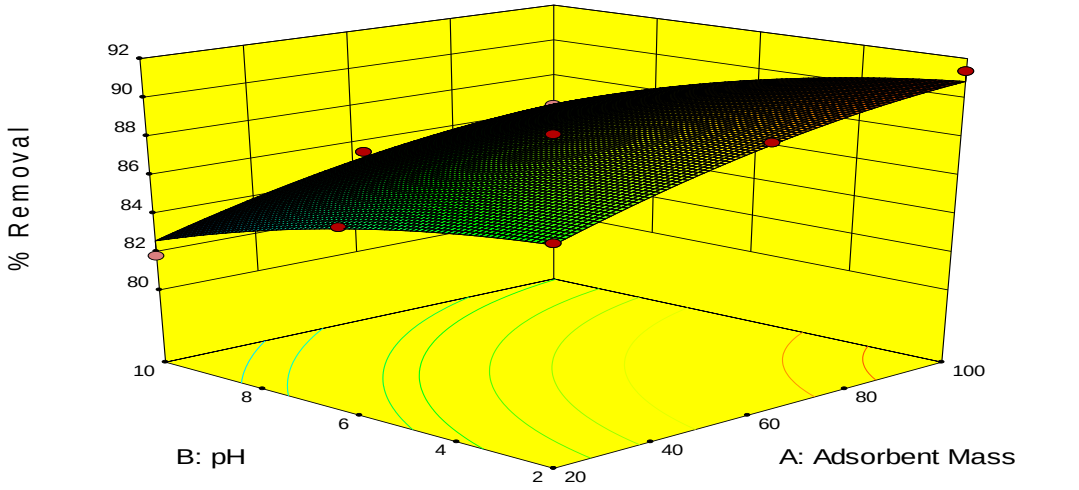

(a)

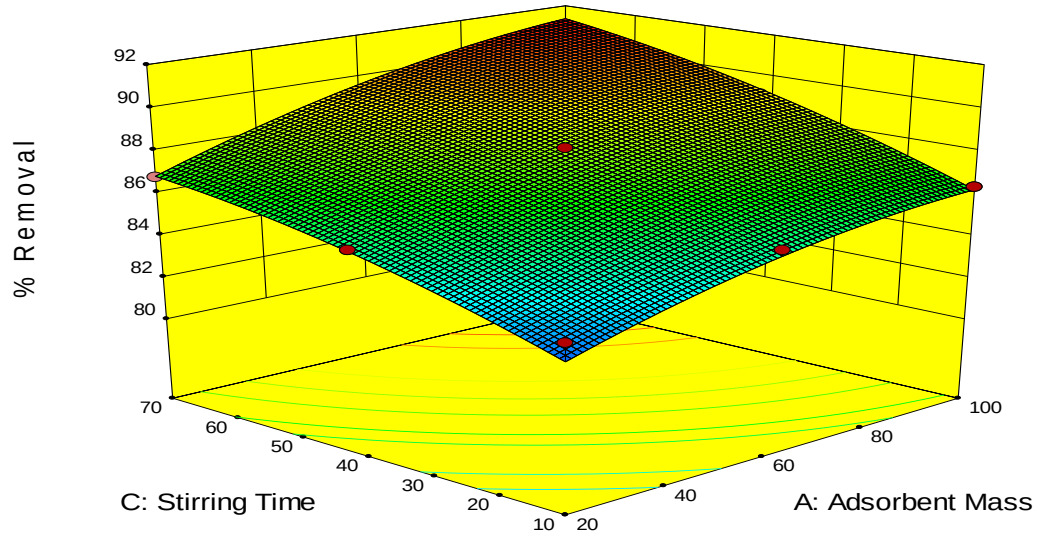

(b)

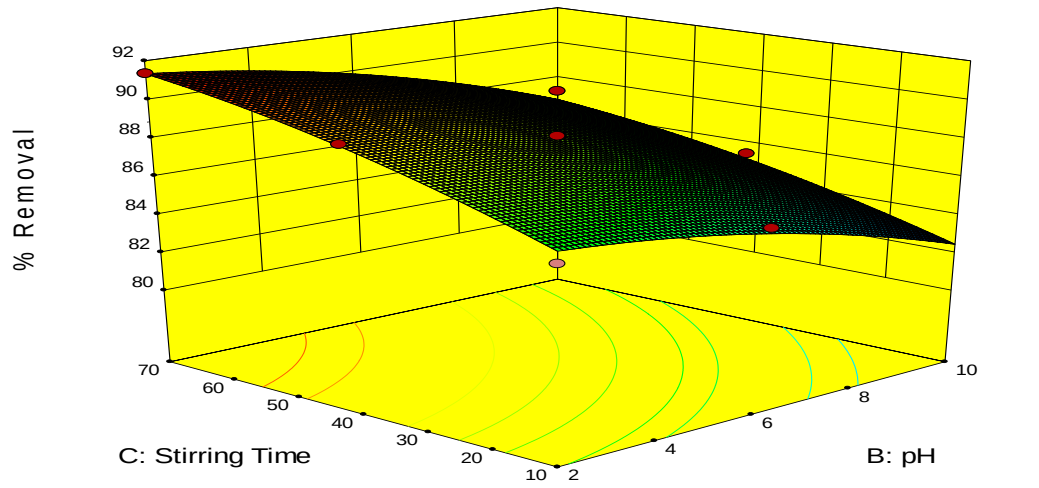

(c)

Fig 4.89: Response surface plots of the effects of (a) pH vs adsobent dosage (b) contact time vs adsorbent dosage (c) contact time vs pH for turbidity removal in BRE using AESS

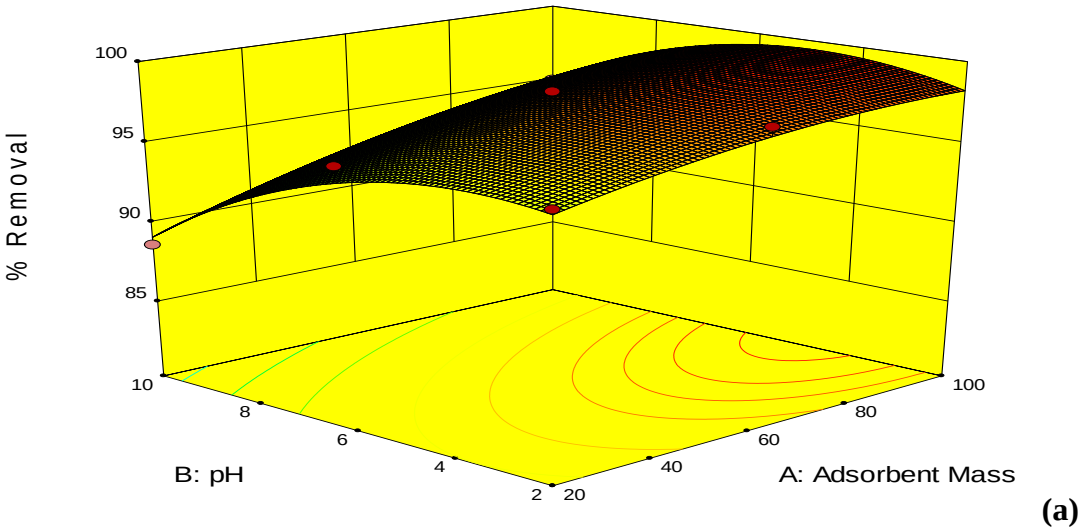

(a)

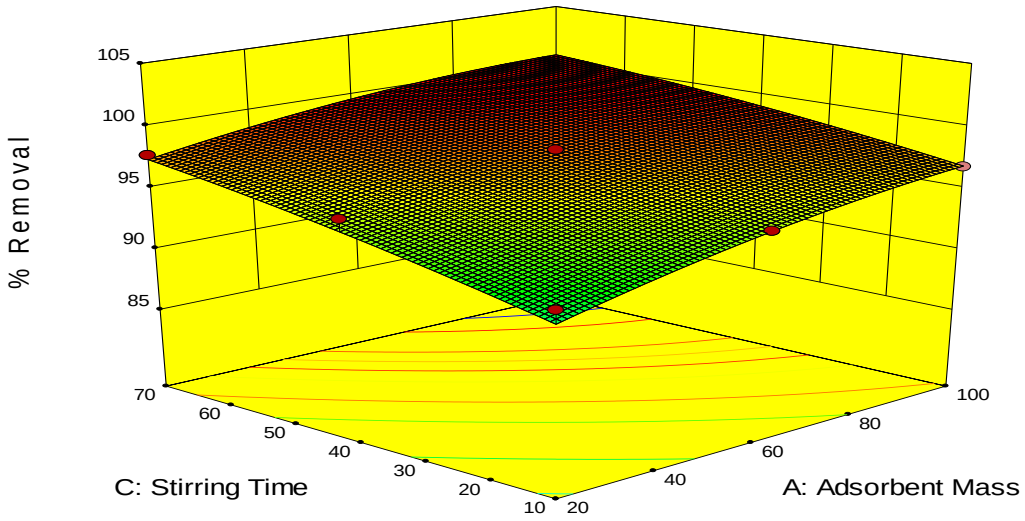

(b)

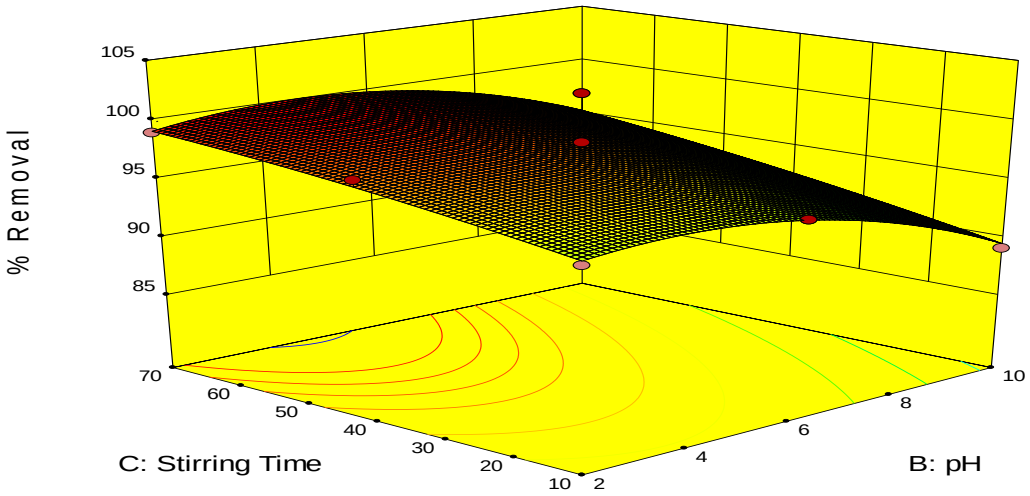

(c)

Fig 4.90 Response surface plots of the effects of (a) pH vs adsobent dosage (b) contact time vs adsorbent dosage (c) contact time vs pH for turbidity removal in BRE using OSA

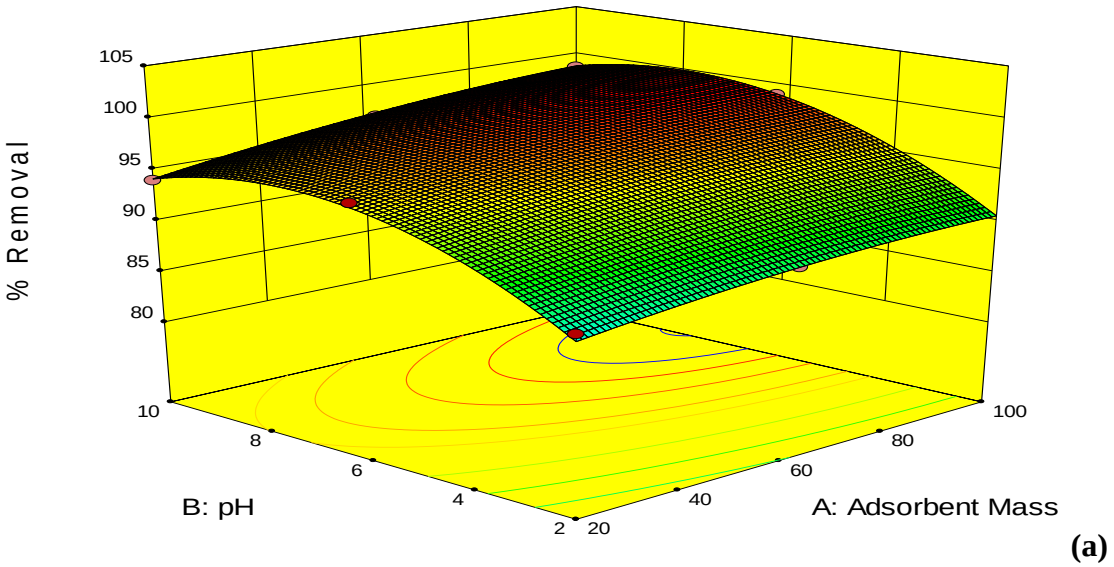

(a)

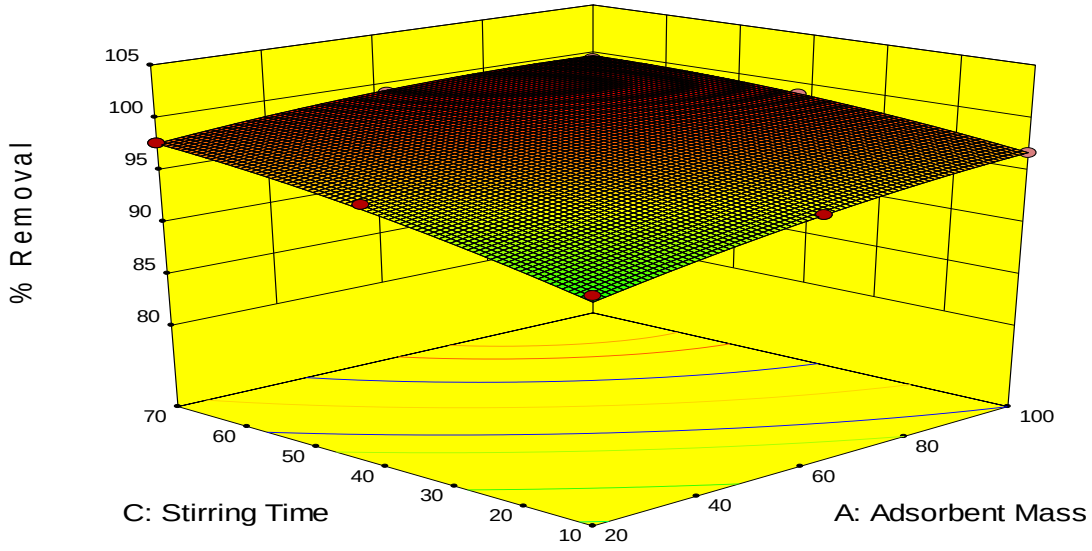

(b)

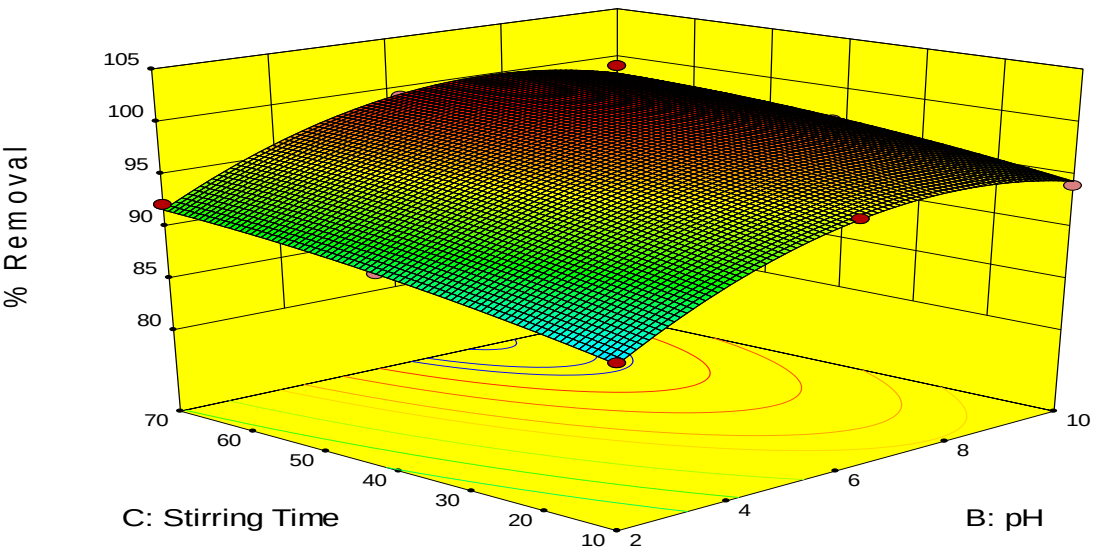

(c)

Fig 4.91: Response surface plots of the effects of (a) pH vs adsobent dosage (b) contact time vs adsorbent dosage (c) contact time vs pH for turbidity removal in BRE using OSS

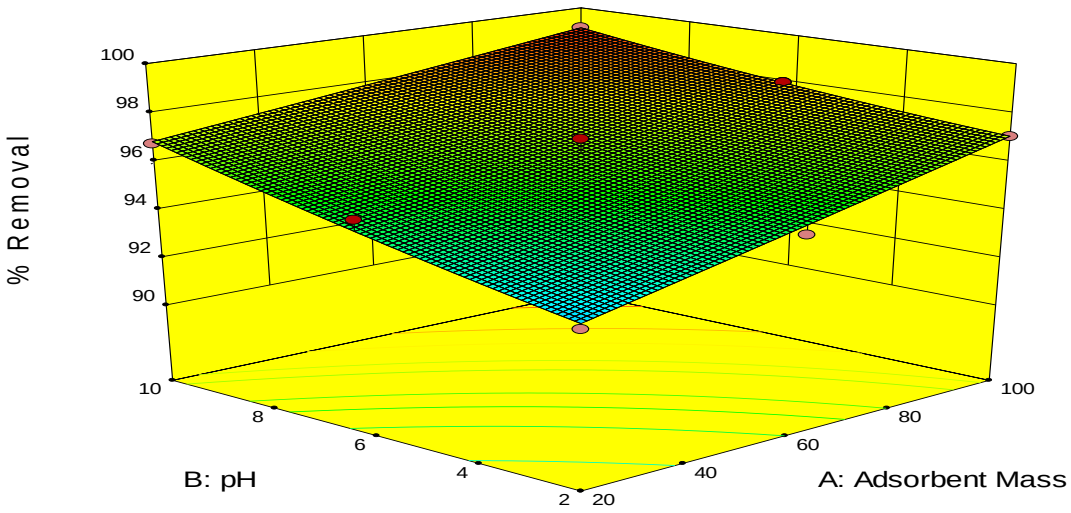

(a)

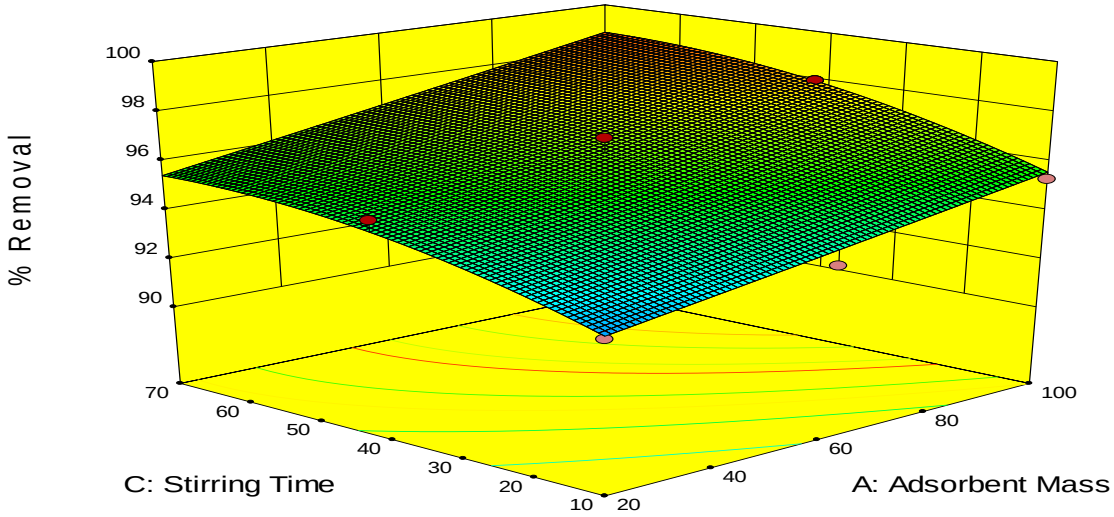

(b)

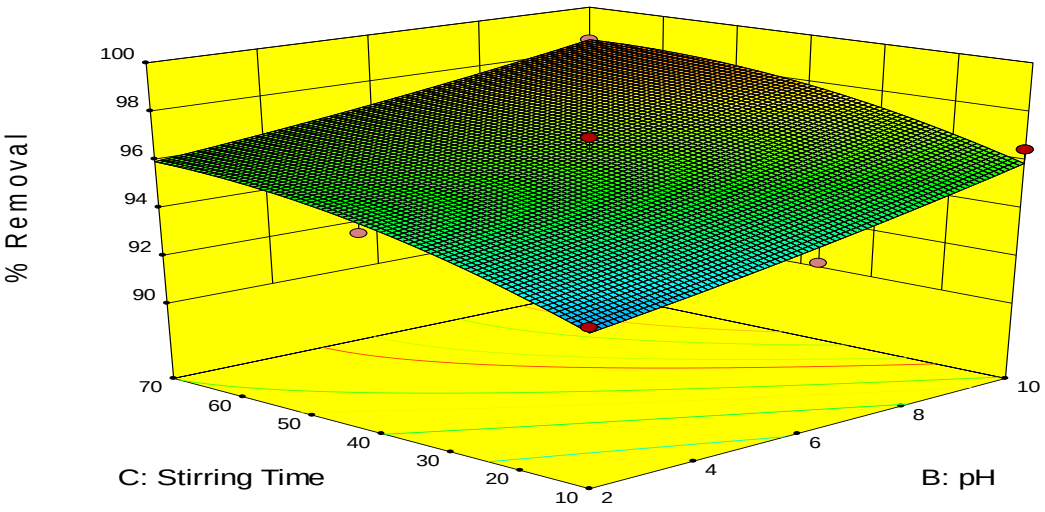

(c)

Fig 4.92: Response surface plots of the effects of (a) pH vs adsobent dosage (b) contact time vs adsorbent dosage (c) contact time vs pH for turbidity removal in PW using MSA

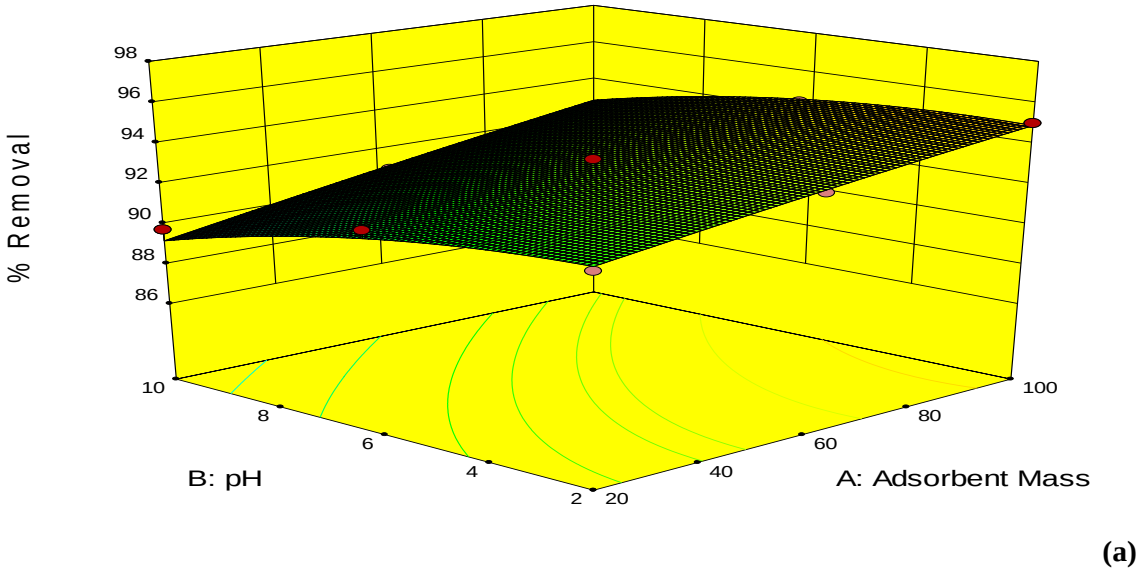

(a)

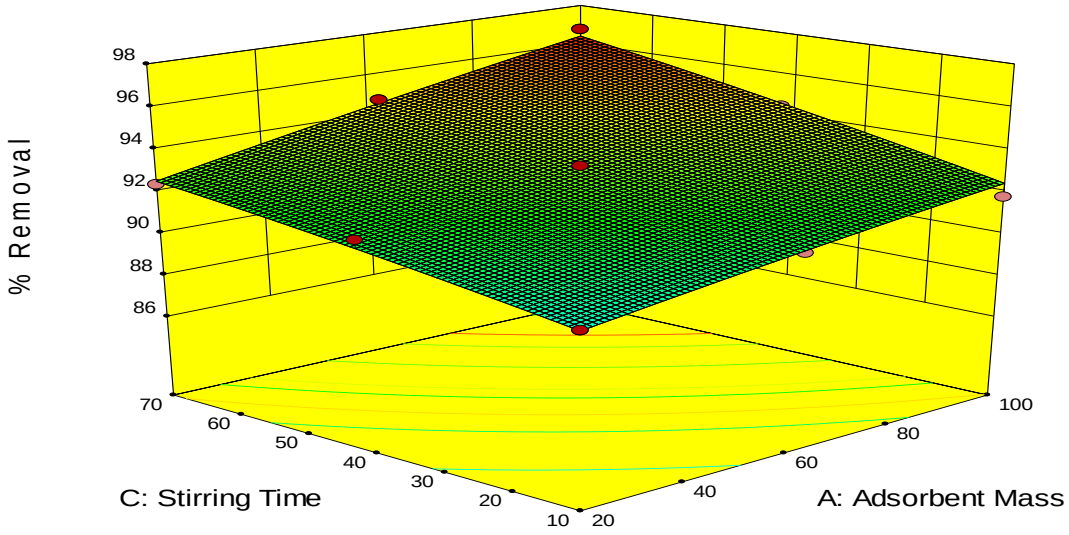

(b)

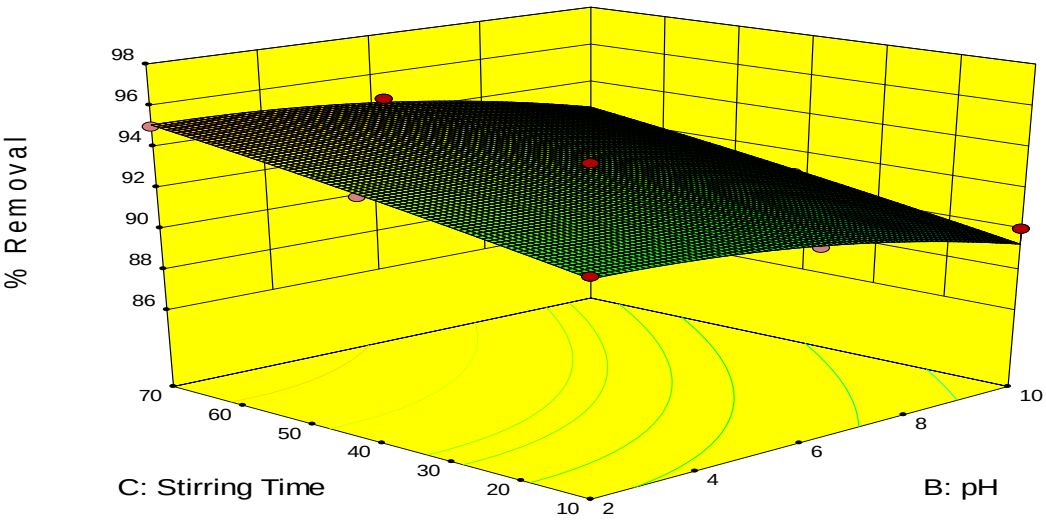

(c)

Fig 4.93: Response surface plots of the effects of (a) pH vs adsobent dosage (b) contact time vs adsorbent dosage (c) contact time vs pH for turbidity removal in PW using MSS

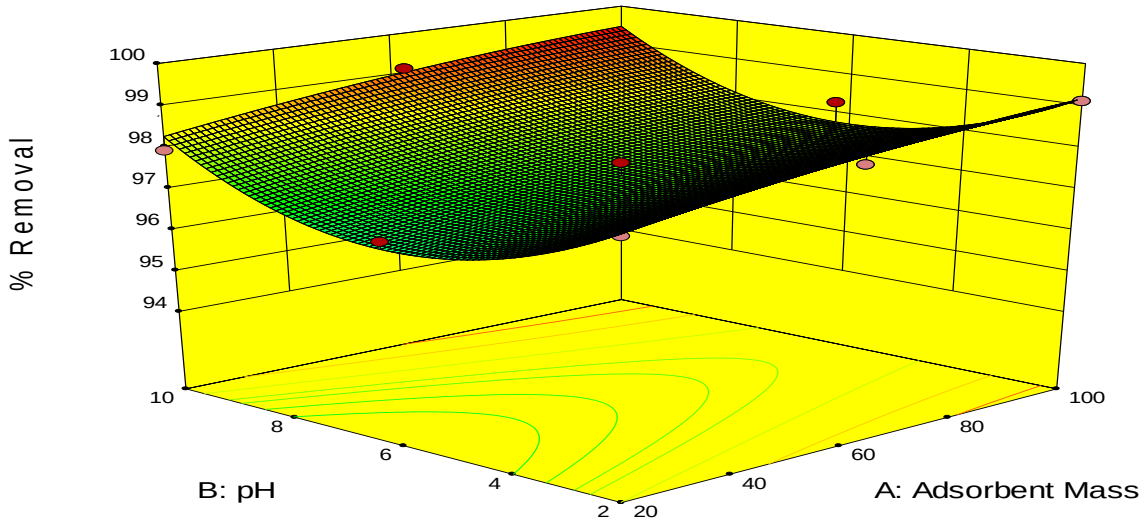

(a)

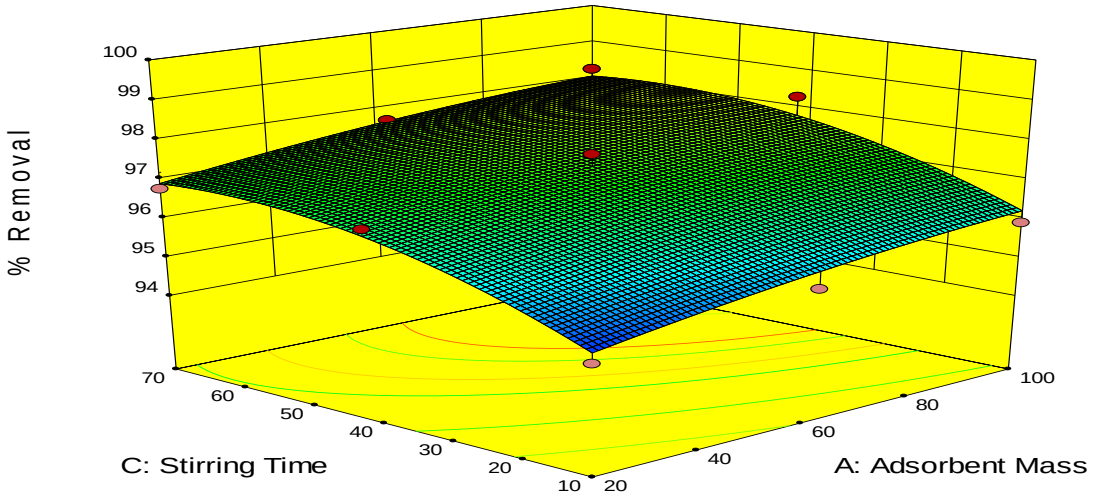

(b)

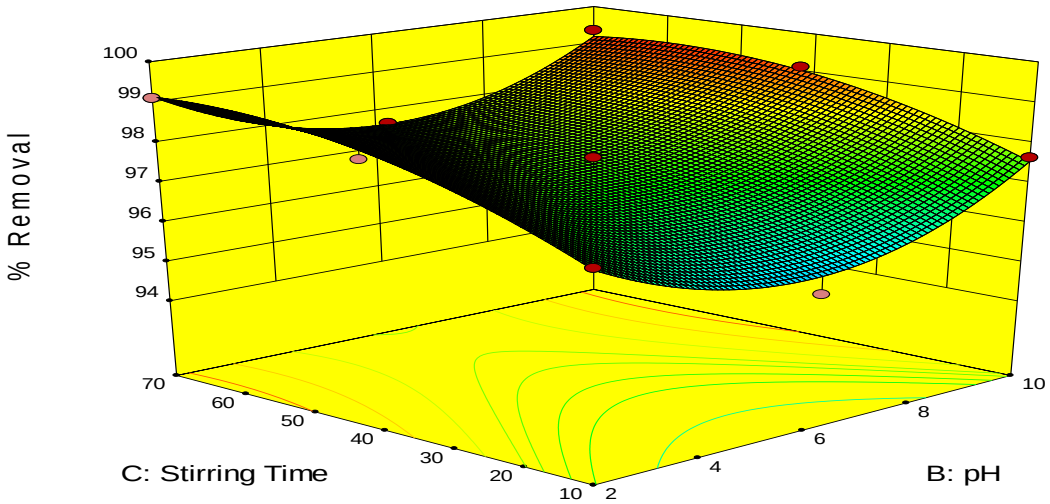

(c)

Fig 4.94: Response surface plots of the effects of (a) pH vs adsobent dosage (b) contact time vs adsorbent dosage (c) contact time vs pH for turbidity removal in PW using AESA

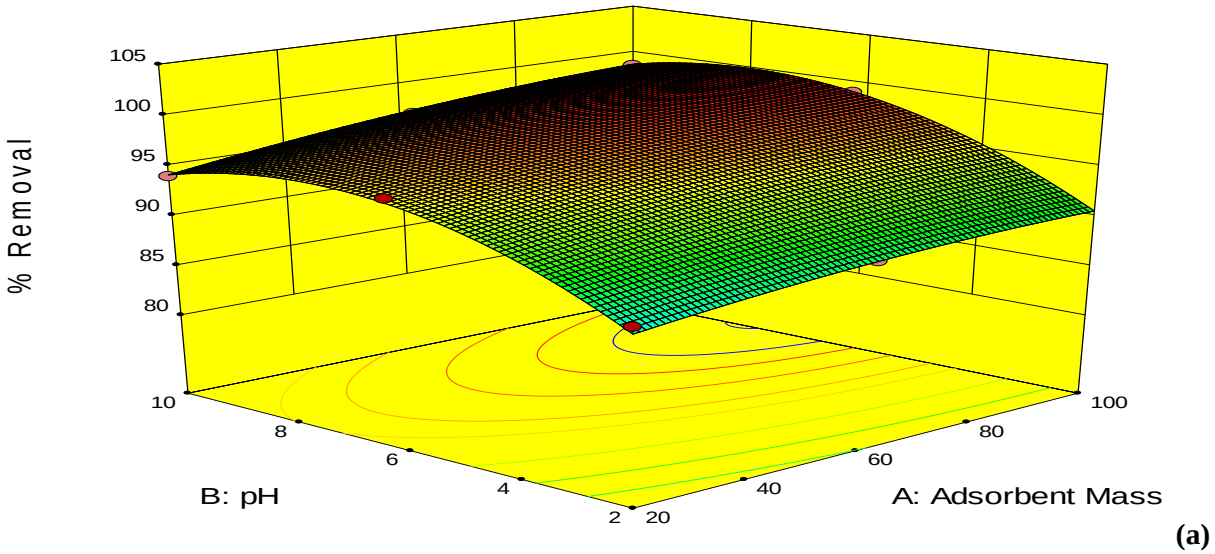

(a)

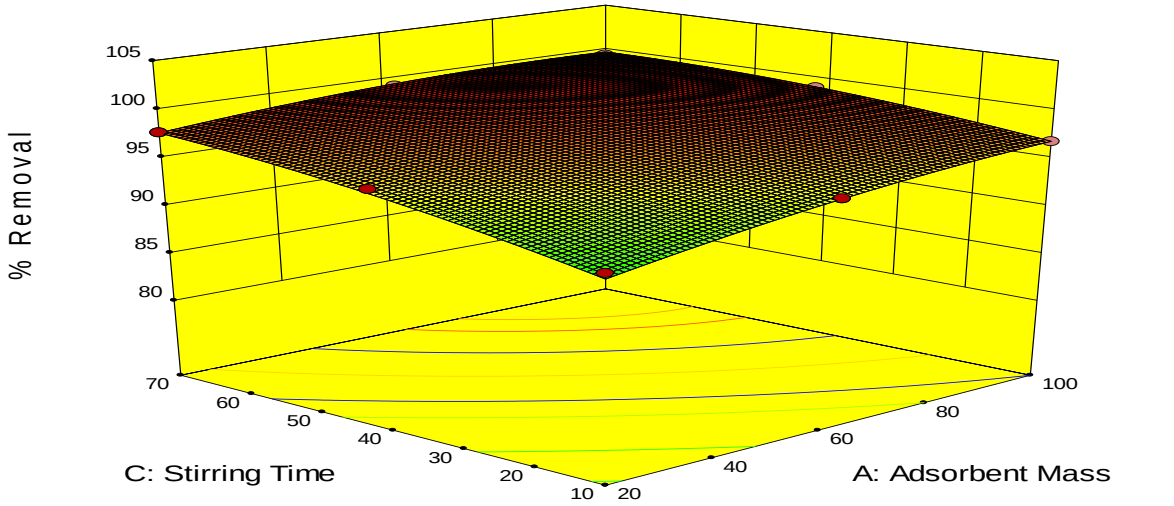

(b)

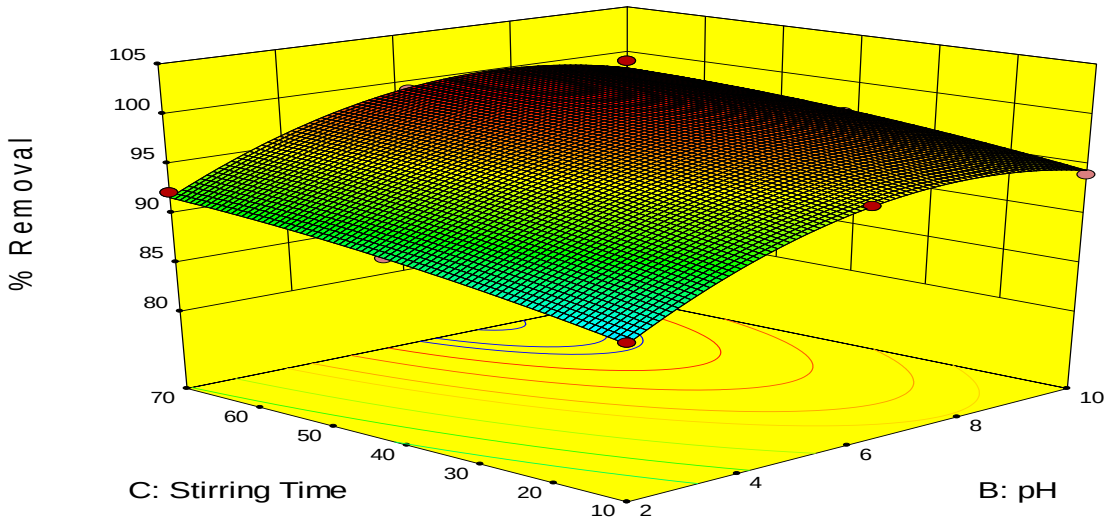

(c)

Fig 4.95: Response surface plots of the effects of (a) pH vs adsobent dosage (b) contact time vs adsorbent dosage (c) contact time vs pH for turbidity removal in PW using AESS

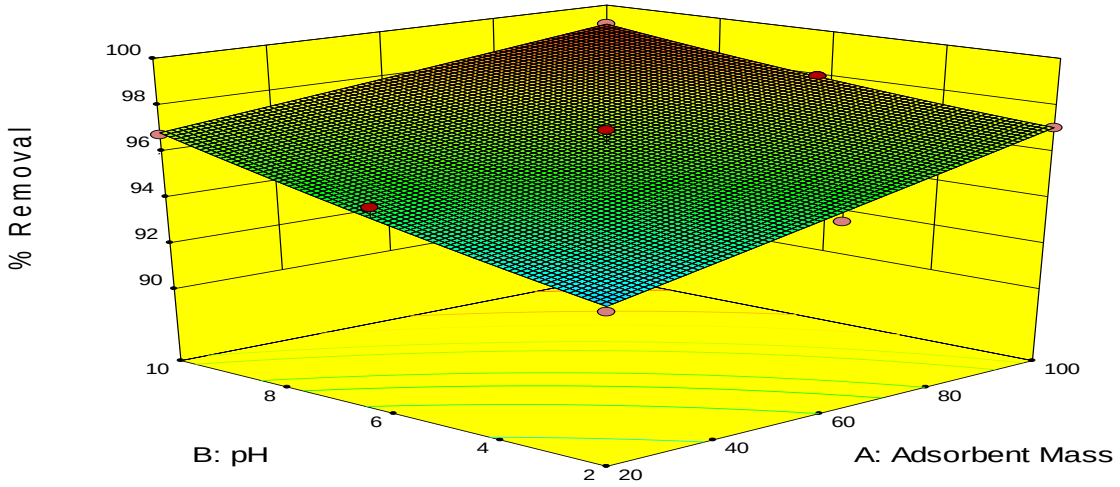

(a)

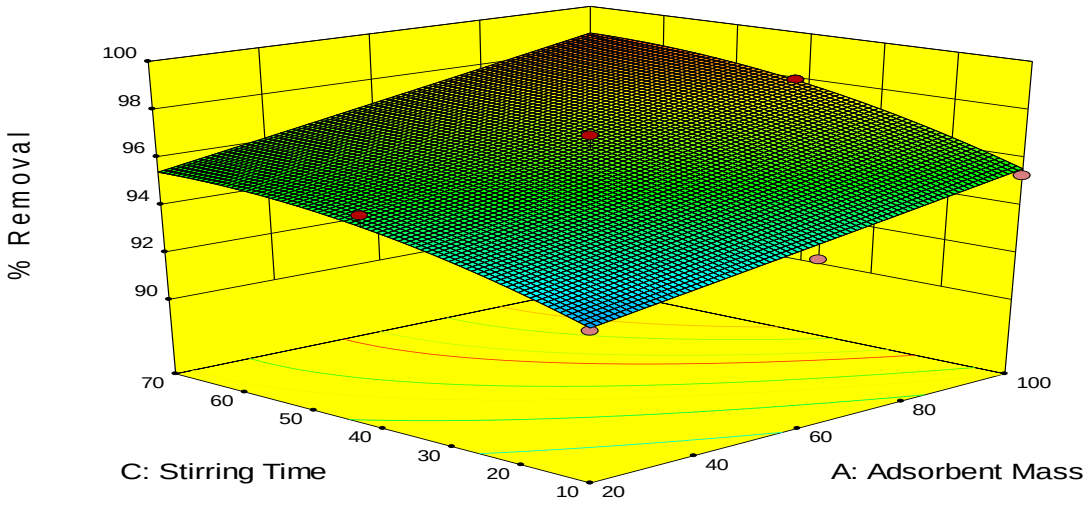

(b)

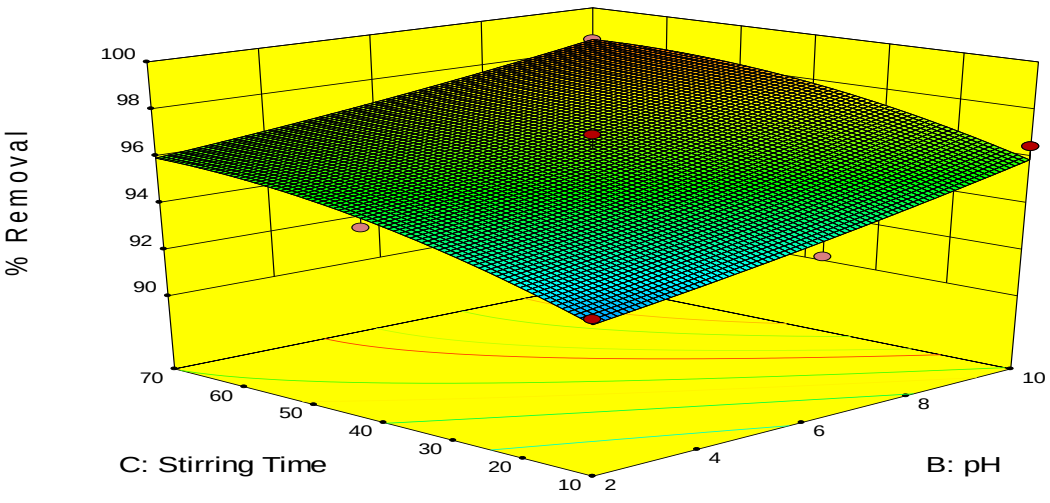

(c)

Fig 4.96: Response surface plots of the effects of (a) pH vs adsobent dosage (b) contact time vs adsorbent dosage (c) contact time vs pH for turbidity removal in PW using OSA

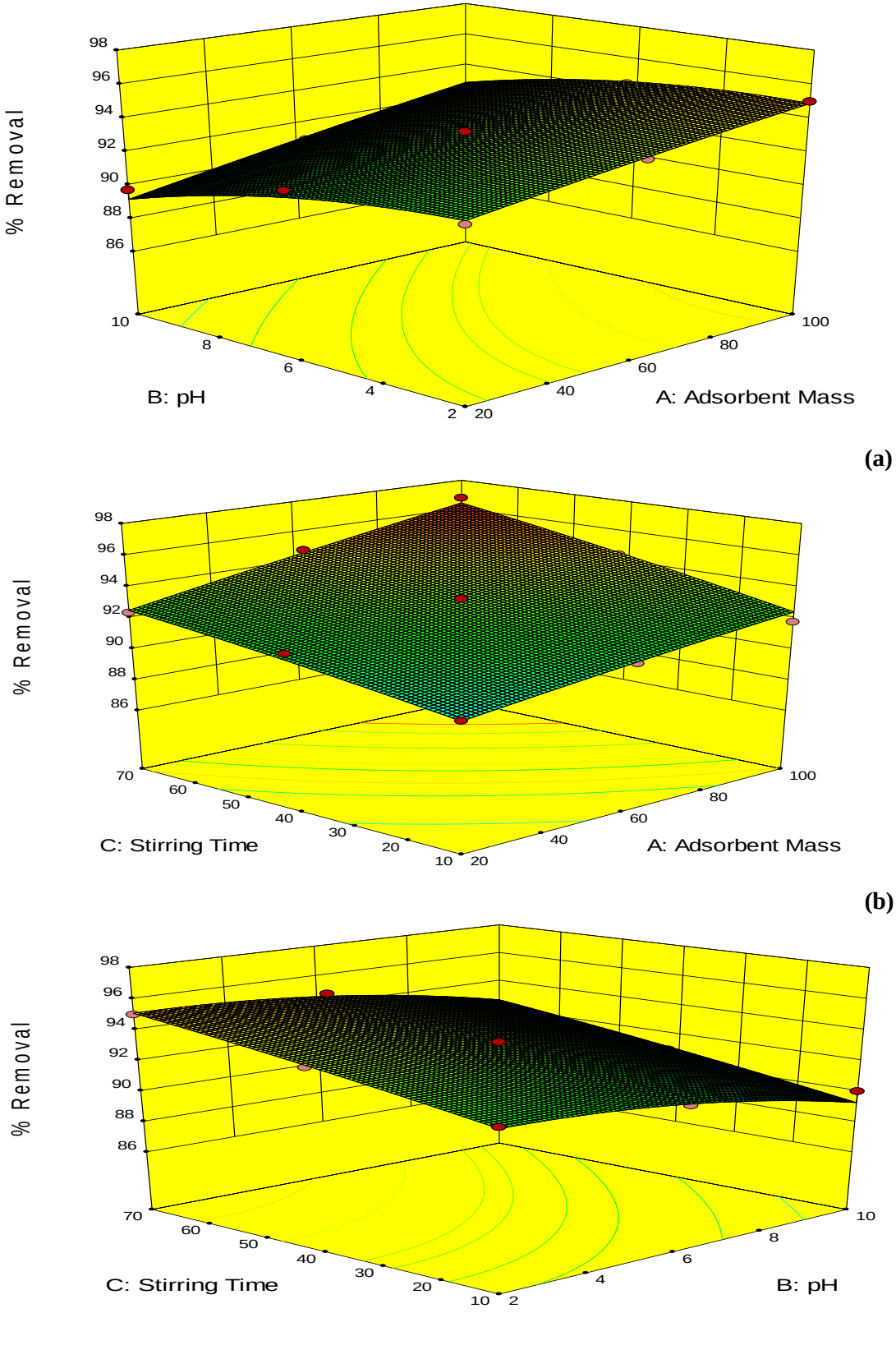

Fig 4.97: Response surface plots of the effects of (a) pH vs adsobent dosage (b) contact time vs adsorbent dosage (c) contact time vs pH for turbidity removal in PW using OSS

4.17 Optimization using the Desirability Functions

Optimization of turbidity removal was carried out by a multiple response methoed called desirability functions to optimize different combinations of process variables such as coagulant dosage, pH, and settling time. It is a value between 0 and 1, and increases as the corresponding response value becomes more desirable. By using numerical optimization, a desirable value for each input factor and response can be selected. In this study, the input variables were given specific ranged values, whereas the response was design to achieve a maximum. Tables 4.165 to 4.176, shows the optimum values for the responses, factors and its desirability for both BRE and PW. The values were calculated by means of the desirability function using design expert software. Figures 4.98 to 4.109 shows the most desirable points for both acid and salt treated adsorbent.

Table 4.165: Results of optimization using Desirability Function of MSA in BRE.

Number	Adsorbent Mass	pH	Stirring Time	% Removal	Desirability	
1	44.889	4.756	68.000	99.593	1.000	
2	70.667	8.489	42.444	99.923	1.000	
3	21.027	7.882	67.979	99.788	1.000	
4	26.667	6.667	69.000	99.999	1.000	Selected
5	100.000	6.000	40.000	100.661	1.000	
6	88.889	5.037	45.444	100.112	1.000	
7	66.420	8.805	45.630	99.776	1.000	
8	93.778	6.454	28.370	99.899	1.000	
9	83.369	5.220	42.841	99.902	1.000	
10	54.667	9.111	63.333	99.853	1.000	

Table 4.166: Results of optimization using Desirability Function of MSS in BRE.

Number	Adsorbent Mass	pH	Stirring Time	% Removal	Desirability	
1	60.000	6.000	70.000	100.585	1.000	
2	88.543	5.170	50.963	100.509	1.000	
3	91.671	7.172	68.691	100.854	1.000	
4	98.815	4.005	60.519	100.356	1.000	
5	73.333	5.200	50.000	99.902	1.000	
6	48.860	5.908	66.527	99.913	1.000	
7	96.570	5.237	44.879	100.376	1.000	
8	52.853	5.411	69.790	100.233	1.000	
9	75.111	7.067	51.333	99.865	1.000	
10	96.667	4.111	51.833	100.061	1.000	
11	88.543	6.830	50.963	100.433	1.000	
12	99.914	7.372	65.193	100.726	1.000	
13	70.683	6.914	58.716	100.206	1.000	
14	48.686	5.756	66.321	99.891	1.000	
15	63.926	4.111	67.500	99.875	1.000	
16	80.593	6.588	49.741	100.200	1.000	
17	57.581	6.358	62.921	99.999	1.000	Selected
18	96.570	6.763	44.879	100.329	1.000	
19	98.353	3.846	69.777	100.386	1.000	
20	91.671	4.828	68.691	101.080	1.000	

Table 4.167: Results of optimization using Desirability Function of OSA in BRE.

Number	Adsorbent Mass	pH	Stirring Time	% Removal	Desirability	
1	98.700	5.873	69.363	98.231	1.000	
2	99.394	5.777	69.390	98.243	1.000	
3	99.756	5.604	69.714	98.234	1.000	
4	99.279	6.156	68.731	98.216	1.000	
5	97.432	5.752	69.848	98.192	1.000	
6	99.104	5.575	69.861	98.208	1.000	
7	98.992	5.685	69.521	98.214	1.000	
8	97.306	6.214	69.544	98.196	1.000	
9	99.301	6.540	69.406	98.183	1.000	
10	99.676	6.290	69.503	98.271	1.000	
11	98.493	6.099	69.399	98.239	1.000	
12	97.964	6.078	68.939	98.185	1.000	
13	97.883	5.876	69.941	98.242	1.000	
14	99.350	5.586	69.393	98.187	1.000	
15	98.997	5.850	68.670	98.186	1.000	
16	98.602	6.205	69.086	98.213	1.000	
17	96.872	5.923	69.865	98.201	1.000	Selected
18	99.429	6.030	69.321	98.269	1.000	
19	99.263	6.258	69.799	98.283	1.000	
20	97.063	6.118	69.729	98.207	1.000	

Table 4.168: Results of optimization using Desirability Function of OSS in BRE.

Number	Adsorbent Mass	pH	Stirring Time	% Removal	Desirability	
1	67.150	2.707	68.419	91.488	1.000	
2	89.481	4.178	62.111	91.559	1.000	
3	100.000	2.000	70.000	93.021	1.000	
4	95.559	2.264	67.855	92.717	1.000	
5	97.336	3.963	55.757	91.459	1.000	
6	82.255	3.537	58.840	91.365	1.000	
7	96.467	5.703	69.351	91.405	1.000	
8	80.222	2.991	58.969	91.477	1.000	
9	97.923	5.035	62.907	91.447	1.000	
10	96.638	2.121	55.238	91.988	1.000	
11	93.926	3.644	55.444	91.474	1.000	
12	83.556	2.607	55.444	91.485	1.000	
13	95.754	4.675	63.811	91.618	1.000	
14	79.523	2.471	66.016	92.005	1.000	
15	94.235	2.223	53.616	91.786	1.000	
16	97.820	2.123	46.751	91.371	1.000	
17	92.790	3.225	67.185	92.309	1.000	
18	62.969	2.353	69.351	91.404	1.000	Selected
19	92.167	2.330	50.802	91.498	1.000	
20	72.955	2.110	64.891	91.749	1.000	

Table 4.169: Results of optimization using Desirability Function of AESA in BRE.

Number	Adsorbent Mass	pH	Stirring Time	% Removal	Desirability	
1	93.185	5.378	47.778	99.764	1.000	
2	66.222	2.622	68.000	99.640	1.000	
3	64.060	5.038	64.379	99.962	1.000	
4	84.000	5.486	51.704	99.766	1.000	
5	65.580	5.256	66.428	100.081	1.000	
6	73.720	5.133	67.910	100.426	1.000	
7	92.704	7.122	68.644	100.103	1.000	
8	64.920	4.391	61.404	99.880	1.000	
9	68.613	6.656	69.968	99.773	1.000	
10	51.890	3.594	69.013	99.699	1.000	
11	63.543	4.868	68.808	99.998	1.000	Selected
12	65.690	5.508	67.170	100.057	1.000	
13	98.118	4.163	45.228	99.686	1.000	
14	96.050	5.218	45.670	99.718	1.000	

Table 4.170: Results of optimization using Desirability Function of AESS in BRE.

Number	Adsorbent Mass	pH	Stirring Time	% Removal	Desirability	
1	65.816	7.288	48.971	99.486	1.000	
2	100.000	6.000	70.000	99.770	1.000	
3	76.274	7.207	53.177	99.991	1.000	
4	63.841	8.015	55.597	99.701	1.000	
5	97.333	9.378	44.667	99.522	1.000	
6	70.960	5.930	67.471	99.556	1.000	
7	88.609	7.753	53.412	100.329	1.000	
8	65.474	7.337	61.730	100.004	1.000	
9	66.046	7.241	68.832	99.996	1.000	Selected
10	53.128	7.976	63.778	99.585	1.000	
11	87.127	7.817	42.163	99.865	1.000	
12	90.700	8.143	47.974	100.153	1.000	
13	77.307	8.619	64.997	100.118	1.000	
14	69.048	7.304	53.437	99.812	1.000	
15	92.804	6.089	58.063	99.749	1.000	
16	92.921	7.909	32.859	99.506	1.000	

Table4.171: Results of optimization using Desirability Function of MSA in PW.

Number	Adsorbent Mass	pH	Stirring Time	% Removal	Desirability	
1	44.889	4.756	68.000	99.593	1.000	
2	70.667	8.489	42.444	99.923	1.000	
3	21.027	7.882	67.979	99.788	1.000	
4	26.667	6.667	69.000	99.999	1.000	Selected
5	100.000	6.000	40.000	100.661	1.000	
6	88.889	5.037	45.444	100.112	1.000	
7	66.420	8.805	45.630	99.776	1.000	
8	93.778	6.454	28.370	99.899	1.000	
9	83.369	5.220	42.841	99.902	1.000	
10	54.667	9.111	63.333	99.853	1.000	

Table 4.172: Results of optimization using Desirability Function of MSS in PW.

Number	Adsorbent Mass	pH	Stirring Time	% Removal	Desirability	
1	65.333	2.533	66.000	99.665	1.000	
2	98.118	6.840	68.168	99.719	1.000	
3	62.074	2.474	59.778	99.625	1.000	
4	68.000	2.800	46.000	99.637	1.000	
5	67.259	3.170	61.667	99.767	1.000	
6	51.556	4.444	59.000	99.589	1.000	
7	63.292	4.591	56.667	99.738	1.000	
8	86.568	3.580	29.852	99.607	1.000	
9	82.222	4.591	42.469	99.766	1.000	
10	99.133	4.342	25.670	99.576	1.000	
11	50.748	3.033	64.072	99.573	1.000	Selected
12	73.436	6.084	47.901	99.573	1.000	
13	82.368	4.628	43.456	99.779	1.000	
14	87.796	6.956	68.711	99.689	1.000	
15	90.713	6.867	59.707	99.678	1.000	
16	98.099	4.581	36.114	99.746	1.000	

Table 4.173: Results of optimization using Desirability Function of AESA in PW.

Number	Adsorbent Mass	pH	Stirring Time	% Removal	Desirability	
1	98.511	2.004	51.719	99.478	1.000	
2	94.542	9.822	66.604	99.494	1.000	
3	93.619	9.898	53.659	99.576	1.000	
4	86.253	9.906	60.492	99.530	1.000	
5	100.000	2.000	70.000	99.574	1.000	
6	76.193	9.985	65.383	99.455	1.000	
7	91.585	2.095	59.802	99.454	1.000	
8	78.728	9.988	67.536	99.460	1.000	
9	98.131	2.102	62.123	99.509	1.000	
10	96.710	2.084	58.019	99.489	1.000	
11	73.717	9.986	61.817	99.453	1.000	Selected
12	80.865	10.000	62.156	99.542	1.000	
13	90.917	2.043	62.144	99.497	1.000	
14	94.865	2.065	54.295	99.446	1.000	
15	82.486	9.961	48.041	99.460	1.000	
16	86.979	9.822	61.143	99.472	1.000	

Table 4.174: Results of optimization using Desirability Function of AESS in PW.

Number	Adsorbent Mass	pH	Stirring Time	% Removal	Desirability	
1	65.816	7.288	48.971	99.486	1.000	
2	100.000	6.000	70.000	99.770	1.000	
3	76.274	7.207	53.177	99.991	1.000	
4	63.841	8.015	55.597	99.701	1.000	
5	97.333	9.378	44.667	99.522	1.000	
6	70.960	5.930	67.471	99.556	1.000	
7	88.609	7.753	53.412	100.329	1.000	
8	65.474	7.337	61.730	100.004	1.000	
9	66.046	7.241	68.832	99.999	1.000	Selected
10	53.128	7.976	63.778	99.585	1.000	
11	87.127	7.817	42.163	99.865	1.000	
12	90.700	8.143	47.974	100.153	1.000	
13	77.307	8.619	64.997	100.118	1.000	
14	69.048	7.304	53.437	99.812	1.000	
15	92.804	6.089	58.063	99.749	1.000	
16	92.921	7.909	32.859	99.506	1.000	

Table 4.175: Results of optimization using Desirability Function of OSA in PW.

Number	Adsorbent Mass	pH	Stirring Time	% Removal	Desirability	
1	96.831	9.747	69.994	99.648	1.000	
2	96.689	9.960	58.987	99.624	1.000	
3	98.596	9.756	62.070	99.665	1.000	
4	90.217	9.968	62.222	99.469	1.000	Selected
5	93.142	9.643	62.800	99.463	1.000	
6	99.701	8.686	68.483	99.442	1.000	
7	98.451	9.558	67.955	99.644	1.000	
8	99.528	9.497	61.838	99.614	1.000	
9	92.513	9.982	67.072	99.578	1.000	
10	99.955	9.898	49.230	99.461	1.000	
11	96.808	9.408	60.321	99.477	1.000	
12	91.743	9.668	67.951	99.456	1.000	
13	92.999	9.729	64.542	99.501	1.000	
14	98.979	9.729	52.096	99.466	1.000	
15	100.000	10.000	70.000	99.827	1.000	

Table 4.176: Results of optimization using Desirability Function of OSS in PW.

Number	Adsorbent Mass	pH	Stirring Time	% Removal	Desirability	
1	100.000	3.176	70.000	96.776	1.000	
2	100.000	3.117	70.000	96.776	1.000	Selected
3	100.000	3.245	70.000	96.775	1.000	
4	100.000	3.041	70.000	96.775	0.999	
5	99.972	3.306	70.000	96.774	0.999	
6	100.000	3.387	70.000	96.774	0.999	
7	100.000	2.950	70.000	96.774	0.999	
8	99.926	2.985	70.000	96.771	0.999	
9	100.000	2.823	70.000	96.771	0.999	
10	99.972	3.480	70.000	96.771	0.999	
11	100.000	3.582	70.000	96.769	0.999	
12	99.896	3.521	70.000	96.766	0.999	
13	100.000	2.695	70.000	96.766	0.999	
14	100.000	3.667	70.000	96.765	0.998	
15	100.000	2.651	70.000	96.765	0.998	

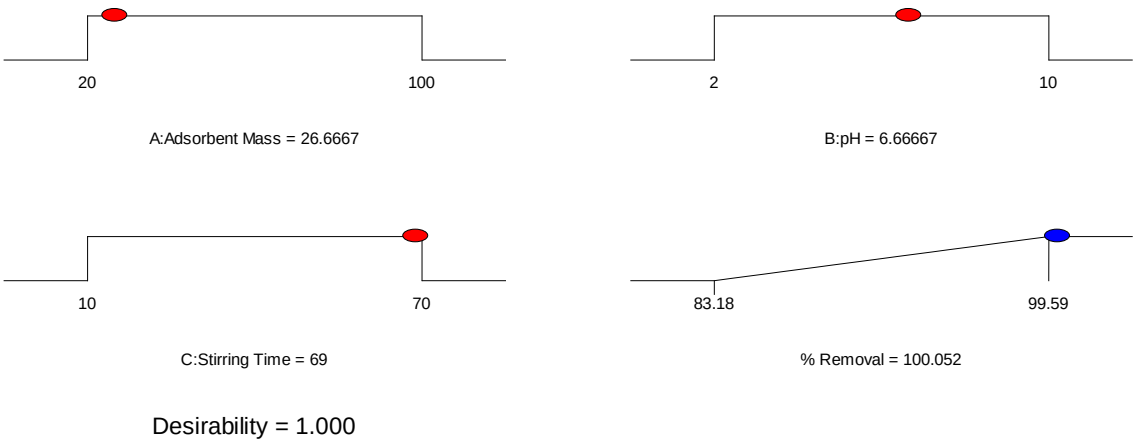

Fig 4.98: Desirability ramp of optimization using MSA in BRE.

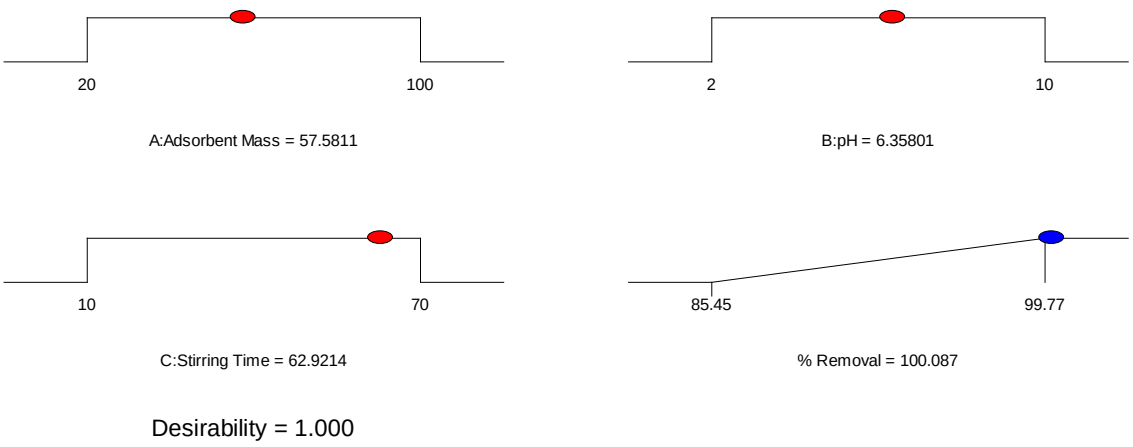

Fig 4.99: Desirability ramp of optimization using MSS in BRE.

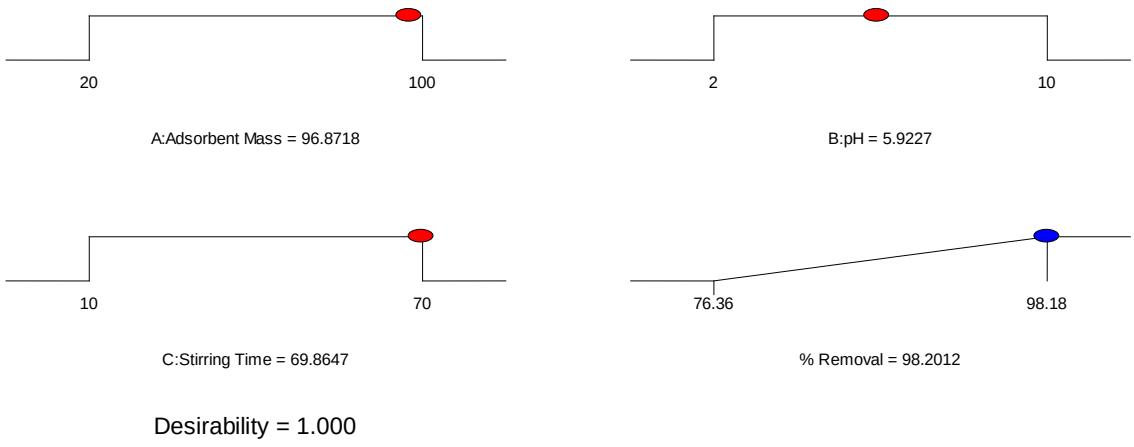

Fig 4.100: Desirability ramp of optimization using OSA in BRE.

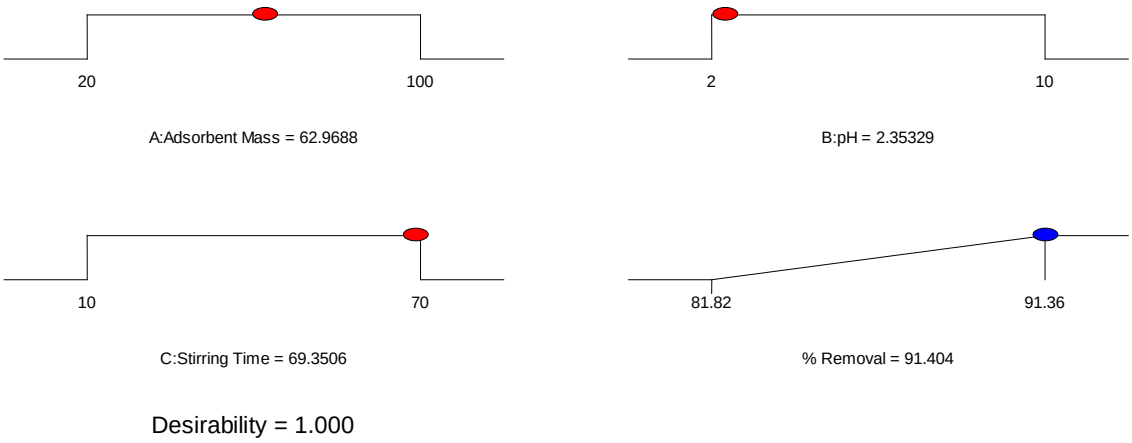

Fig 4.101: Desirability ramp of optimization using OSS in BRE.

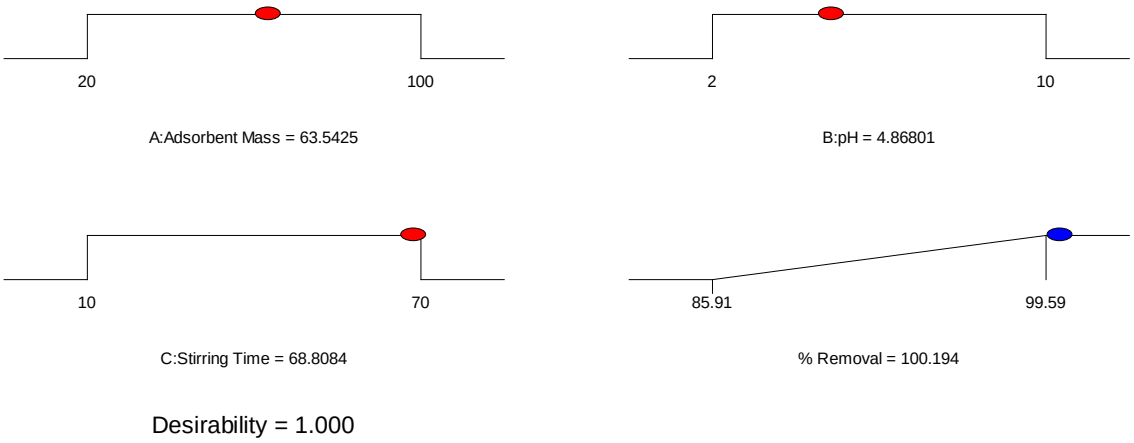

Fig 4.102: Desirability ramp of optimization using AESA in BRE.

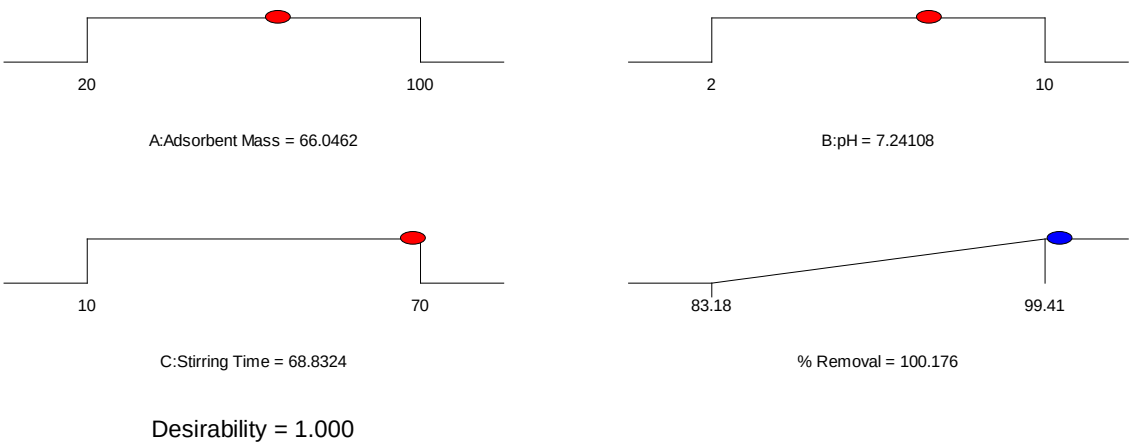

Fig 4.103: Desirability ramp of optimization using AESS in BRE.

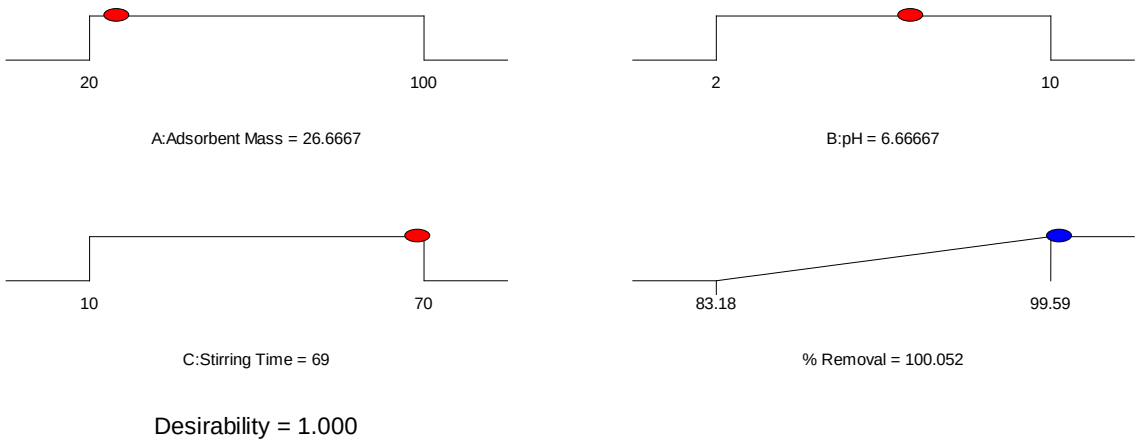

Fig 4.104: Desirability ramp of optimization using MSA in PW.

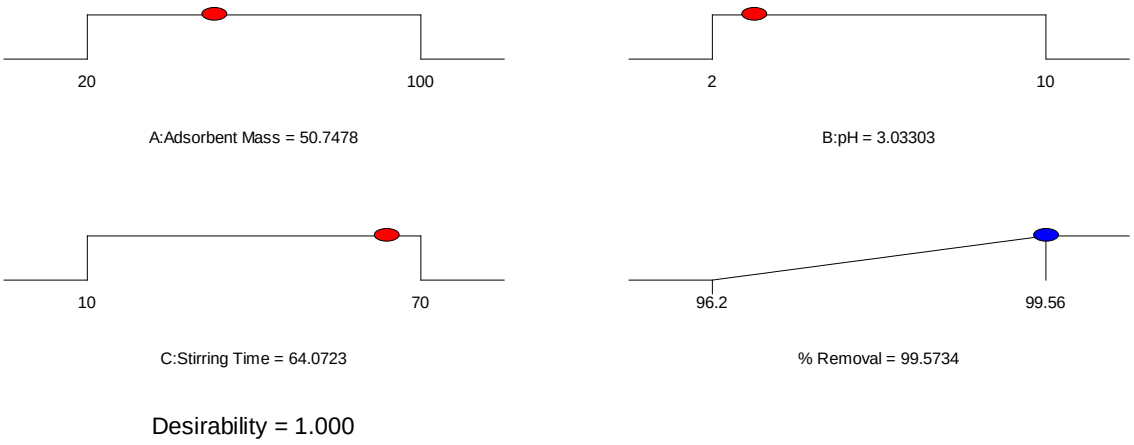

Fig 4.105: Desirability ramp of optimization using MSS in PW.

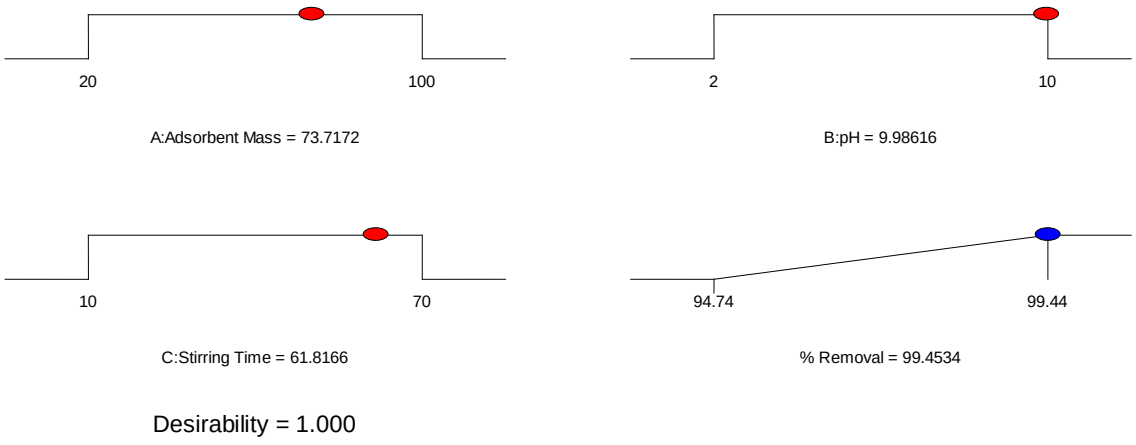

Fig 4.106: Desirability ramp of optimization using AESA in PW.

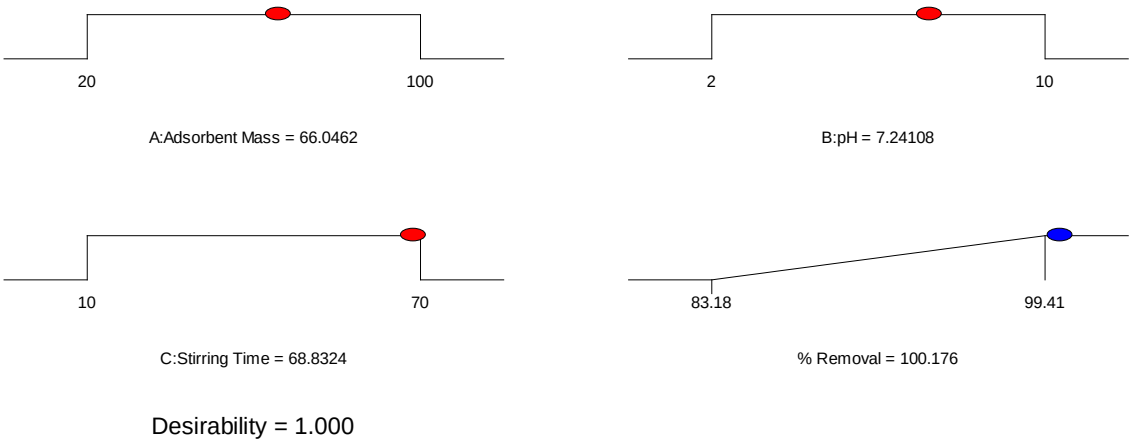

Fig 4.107: Desirability ramp of optimization using AESS in PW.

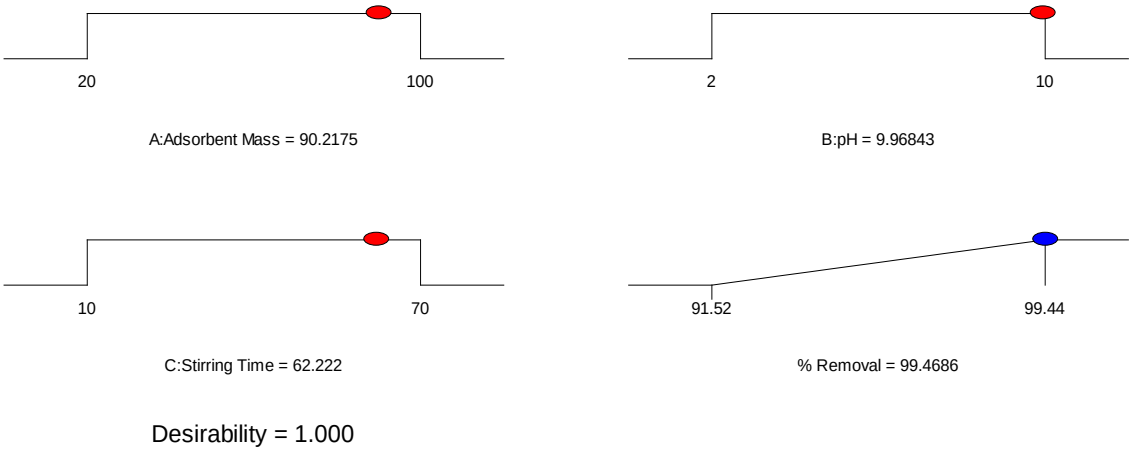

Fig 4.108: Desirability ramp of optimization using OSA in PW.

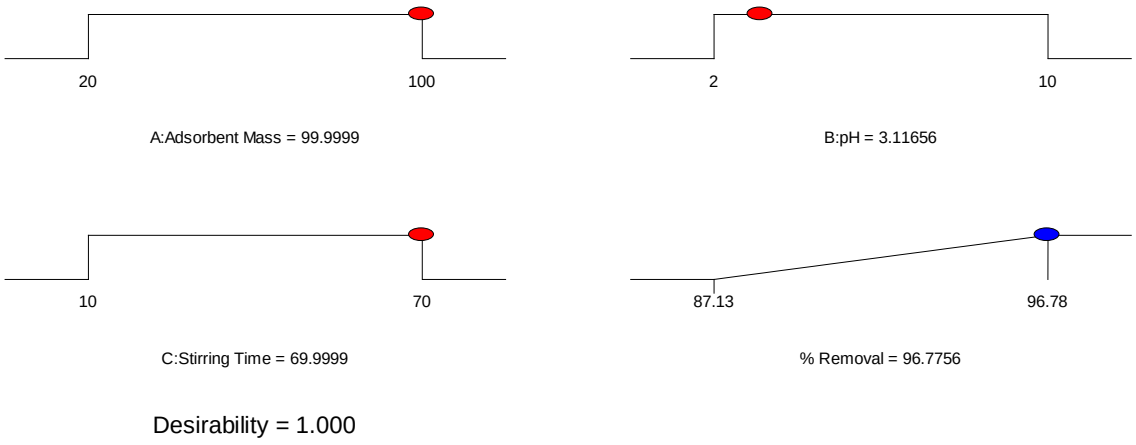

Fig 4.109: Desirability ramp of optimization using OSS in PW.

4.18 Model Validation and Confirmation Experiments

The optimized conditions generated during response surface methodology were validated by conducting adsorption experiments with the optimum parameters. Experimental validation is the final step in the modeling process to investigate the accuracy and robustness of the established models. The results of predicted and measured values of the output variables are given in Tables 4.95 and 4.96 for BRE and PW. Also the maximum error (%) between the predicted values and experimental values were less than 3% indicating that the quadratic models adopted could predict experimental results well (Shama, et al., 2009). Therefore, it can be concluded that the models acculately represent turbidity removals over the experimental range studied.

Table 4.177: Validation of the models predicated using desirability function values for turbidity with acid and salt treated adsorbents in BRE.

Adsorbents	pH	Adsorbent mass (mg)	Stirring time (min)	Predicted values (%)	Experimantal values (%)	Error (%)
MSA	6.67	26.68	69.0	99.99	97.64	2.35
MSS	6.35	57.58	62.90	99.99	98.85	1.14
AESA	4.87	63.54	68.81	99.98	97.32	2.66
AESS	7.2	66.05	68.8	99.99	98.58	1.41
OSA	5.9	96.87	69.86	98.20	96.52	1.71
OSS	2.35	63.00	69.35	91.4	89.67	1.89

Table 4.178: Validation of the models predicated using desirability function values for turbidity with acid and salt treated adsorbents inPW.

Adsorbents	pH	Adsorbent mass (mg)	Stirring time (min)	Predicted values (%)	Experimantal values (%)	Error (%)
MSA	6.66	26.67	69.00	99.99	97.64	2.35
MSS	3.03	50.75	64.07	99.57	97.85	1.73
AESA	9.98	73.72	61.8	99.45	98.32	1.14
AESS	7.24	66.05	68.8	98.41	96.58	1.86
OSA	9.97	90.22	62.22	99.47	96.52	2.96
OSS	3.18	100.00	70.00	96.78	94.67	2.18

5.0 Conclusion and Recommendation

Based on the results obtained from this study, it shows that coag-flocculation and adsorption are very effective in turbidity removal from paint and brewery wastewaters. This work has successfully transformed natural and abundant materials into coagulants/adsorbents that can be used for wastewater treatment. Hence, these coagulants and adsorbent are recommended for wastewater treatment. Also since most industries in Nigeria discharge their effluents without proper treatment, the environmental agency must monitor the industrial factories and classify the contaminants of each factory according to its toxicity and issue limitations with law to the control on the water pollution.

References

Abaliwano, J.K. (2008).Application of the purified coagulant from Moringa oleifera for surface water treatment.*Watermill*, 5, 701-710.

Abdalbasit, A., Mohammed, E.S.M. and Ahamed, B.U. (2009).*Detarium microcarpum* guill and perr fruit proximate chemical analysis and sensory characteristic of concentrated juice and jam. *Afri. J. Biotechnol*, 8(17), 4217-4221

Abdulhalim, A., ZainalAbidin, N. N., Awang, N., Ithnin, A., Othman, M. and Wahab, M. (2011). Ammonia andCOD removal from synthetic leachate using rice husk composite adsorbent. *J Urban Environ Eng, 5*, 24–31.

Aber, S., and Sheydaei, M. (2012). Removal of COD from industrial effluent containing indigo dye using adsorption method by activated carbon cloth: Optimization, kinetic, andisotherm studies. *Clean—Soil, Air, Water, 40*, 87–94

Abia, A.A., Horsfall, M. Jnr and Didi, O. (2003). The use of chemically modified and unmodified cassava waste for the removal of Cd^{2+},Cu^{2+} and Zn^{2+} ions from aqueous solution. *J. Bioresources Technol*, 90, 345-345

Aboulhassan,M. A., Souabi, S., Yaacpubi, A. and Baudu, M. (2006). Improvement of part effluent coagulation using natural and synthetic coagulant aids. *J. Hazard Mater*138, 40-45

Abreu P. and Relva, A. (2002). Carbohydrates from *Detarium microcarpum* bark extract. *Carbohy. Res.* 337, 1663-1666.

Abreu P. M., Rosa V.S., Araujo E.M., Canda, A.B., Kayer, O., Bindseli K. V., Siems K. and Seeman A. (1998). Phytochemical analysis and anti-microbial evaluation of *Detarium microcarpum* bark. *Pharm. Pharmacol. Let*. 8, 107-111.

Abu Amr, S.S., Aziz, H.A. and Bashir, M.J.K. (2014). Application of surface response methodology (RSM) for optimization of semi-aerobic landfill leachate treatment using ozone .*Appl. Water Sci*. doi:10.1007/s13201-014.0156-z

Ademiluyi, F.T., Gumus, R.H., Adeniji, S.M and Jasem, O.I. (2009). Effects of process conditions on the characterization of activated carbon from waste Nigeria Bamboo, *Journal of Nigeria Society of Chemical Engineers*, 24(1),83-93

Agarwal M., Srinivasan R.and Mishira A. (2001).Study on flocculation efficiency of okra gum in sewage wastewater. *Macromol. Water and Eng*., 286,560-563.

Ahmad, R.; Kumar, R. and Laskar, M.A. (2013).Adsorptive removal of Pb2+ form aqueous solution by macrocyclic calyx[4]naphthalene: Kinetic, thermodynamic, and isotherm analysis. *Environ. Sci.Pollut. Res., 20*, 219–226.

Ahmedna, A., Marchall, W.E. and Rad, R.M. (2000b). Production of granular activated carbon from selected agricultural products and evaluation of their physical, chemical and adsorption properties, *Bioresource Technol.*71, 2920-2925

Ajjabi, L.C. and Chouba, L. (2009). Biosorption of $Cu^{2+}$and Zn^{2+} from aqueous solution by dried marine green macroalga, *Chaetomorpha Linum, J. Environ. Manage*, 90, 3485-3489

Akhtar, M., Igbal, S., Kausar, A., Bhanger, M.I. and Shahee, M.A. (2010).An economically viable method for the removal of selected divalent metal ions from aqueous solution using activated rice husk.*Colloids Surf B*: *Biointerf*, 75(1), 149-155

Aksu, Z. and I.A. Isoglu.(2006). Use of agricultural waste sugar beet pulp for the removal of Gemazol turquoise blue-G reactive dye from aqueous solution. *J. Hazard. Mater.*, 137, 418-430

Aksu, Z. and F. Gonen. (2003). Biosorption of phenol by immobilized activated sludge in a continuous packed bed: prediction of breakthrough curves. *Proc. Biochem.*, 39, 599–613.

Alam, Z., Muyibi, S.A., and Tormae, Y. (2008). Statistical optimization of adsorption processes for removal of 2,4-dichlorophenol by activated carbon derived from oil palm empty fruit bunches, *J. Environ. Sci*. 19(6), 674-677.

Al-Qodah, Z. (2006).Biosorption of heavy metal ions from aqueous solutions by activated sludge.*Desalination J.*, 196, 164-176.

Althoman, Z. A., Habila, M.A. and Ali, R. (2011).Preparation of activated carbon using the copyrolysis of agricultural municipal solid wastes at a low carbonization temperature.*International conference on Biology, Environment and Chemistry,IPCBEE,* 24 IACSIT Press, Singapore.

Amini, M., Younesi, H., Bahramifar, N., Loretstani, A. A. Z., Ghorbani, F., Daneshi, A., and Sharfzadeh, M. (2008). Application of response surface methodology for optimization of lead biosorption in an aqueous solution by *aspergillus niger*. *J.Haz. mater*. 154, 694-702

Amirtharajah, A. and O'Melia C.R. (1999); *Water Quality and Treatment* AWWA, 5th ed. American Water Works Association, Denver, Co.

Amirtharajah, A. (1982).Coagulation-Rejuvenation for a classical process.*Water Eng Manag*. 137, 25-28

Amosa, M. K. (2015).Process optimization of Mn and H_2S removals from POME using an enhanced empty fruit bunch (EFB)-based adsorbent produced by pyrolysis.*Environmental Nanotechnology, Monitoring& Management*, *4*, 93–105. doi:10.1016/j.enmm.2015.09.002

Amuda, O. and Amoo, J. (2007).Coagulation/flocculation process and sludge conditioning in beverage industrial wastewater treatment. *J.H.Mater*. 141(3), 778

Anastasakis,K., Kalderis, D. and Diamadopoulos (2009). Flocculation behavior of mallow and okra mucilage in treating waste water, *Desalination* 249, 786-791

AOAC, (2005). Official Method of Analysis 14th Edition, Association of Official Analytical Chemist, Gaitherburg,

APHA, (2005."Standard Methods for the Examination of Water and Wastewater",American Public Health Association, New York, NY, USA, 21st edition,

Arami, M., Limaee, N.Y., Mahmoodi, N.M., and Tabrizi, N.S. (2005). Equilibrium andkinetics studies for the adsorption of direct and acid dyes from aqueous solutionby soy meal hull.*Journal of Hazardous Materials* 135, 171-179.

Aremu,M.O., Oke, E.O., Arinkoola, A.O. and Salam, K.K. (2014).Development of optimum operating parameters for Bioelectricity generation from sugar wastewater using response surface methodology.*Journal of Scientific Research and Reports*, 3(15), 2098-2109.

Asadi, A., Huat, B.B.K., Hanafi, M.M., Mohamed, T.A. and Shariatmadari, N. (2009).Role of organic matter on electrosomotic properties and ionic modification of organic soils.*GeoSciences J*. 13, 175-181.

Asgari, G., Ramavandi, B., Sahebi, S., (2013).Removal of a cationic dye from wastewater during purification by Phoenix dactylifera*Desalin. Water Treat*. http://dx.org/10.1080/19443994.2013.823358,

ASTM D-3172-89(2002).*Standard Practice for proximate analysis of coal and coke*,(ASTM, USA).

Attwood, N.A. and Zola, H. (1967).The association between chitin and protein in some chitinous tissues.*Comp. Biochem. Physiol*.. 20, 993

Auta M.(2012).Fixed Bed Adsorption Studies Of Rhodamine B Dye Using Oil Palm Empty Fruits Bunch Activated Carbon, *Journal of Engineering Research and Studies (JERS)*, 3(3),3-6

AWWA, APHA andWEF (2002);*Standard Method for the Examination of Water and Wastewater*, 22nd Edition, New York

Aworn, A., Thiravetyan, P. and Nakbanpote, W. (2009). Preparation of CO2 activated carbon from corncob for methylene glycol adsorption. *Colloids and Surfaces A: Physicochemical EngineeringAspects*, 333,19-25.

Ayotunde, E.O., Fagbenro, O.A. and Adebanyo, O.T. (2011).Toxicity of Aqueous Extract of Moringa oleifera Seed Powder to Nile Tilapia (*Oreochromis niloticus*) Fingerling.*International Research Journal of Agriculture Science* 1(4),142-150

Azouaou.N,Sadaoui.Z,Djaafri.A and Mokaddem.H (2010).Adsorption of cadmium from aqueous solution onto untreated coffee grounds: Equilibrium, kinetics and thermodynamics,*Journal of Hazardous Materials*, 184, 126-134.

Bailey, S.E., Olin, T.J., Mark Bricka, R., and Dean Adrian, D. (1999).A review of potentially low-cost sorbent for heavy metals.*Water Res*., 33, 2469 -2479.

Babu R. and Chavudhari M. (2005).Home water treatment by direct filtration with natural coagulant.*J. water Health* 3, 27-30

Banker, A. V., Kumar, A. R. and Zingarde, S. S. (2009). Removal of Cr(IV) ions from aqueous solution by adsorption onto two marine isolates of yawowia lipolytical. *J. Hazardous Materials*, 170, 487-494

Bansal R.C. and Goyal M (2005).*Activated carbon Adsorption.* CRC Press 1st edition, USA, 1-5

Bhuptawat, H., Folkard, G. K., and Chaudhari, S. (2007).Innovative physic-chemical treatment treatment of wastewater in operating moringa olerifera seed coagulant.*Journal of Hazardous Material* 142, 477-482.

Black, A. P., Birkner F. B. and Morgan J. J.(1965). America Water Works Assoc., 57, 1547.

Bonelli, P.R., Della Rocca, P.A., Cerrella, E.G. and Cukierman, A.L. (2001). Effect of pyrolysis temperature on composition, surface properties and thermal degradation rates of Brazil Nut shells. *Bioresource Technology*, 76 (1),15-22,

Braeken, L., Van der Bruggen, B. and Vandecasteele, C. (2004).Regeneration of brewery wastewater using nanofiltration.*Water Research* 38(13), 3075-3082.

Brathy, J.(2006). *Coagulants in coagulation and flocculation in water and wastewater Treatment*, second ed., IWA Publishing, London, 50-68.

Bouchrahem, F., Aissani-Benissad, H. and Ait-Amar, E. (2009). Batch sorption dynamic and equilibrium for removal of lead ions from aqueous phase using activated carbon develop from coffee residue activated with zinc chloride. *Journal of Environmental Managemant*, 90, 3031-3039.

Burkil, H. M (1995);*The useful plants of West Tropical Africa, Royal Botanic Gardens. London* ,3:101.

Cabal, B., Budinova, T., Ania, C.O., Tsyntsarski, B., Parra, J.B. and Petrova, B. (2009).Adsorption of naphthalene from aqueous solution on activated carbons obtained from bean pods. *Journal of Hazardous Materials*, 161 (2-3), 1150-1156.

Cerovic, L. S., Milonjic, S. K., Todorovic, M. B., Trtanj, M. I. and Pogozhev, Y. S. (2007). Blagoveschenskii, Y. and Levashov, E. A., Point of zero charge of different carbides. *Colloids Surf. A***297**,

Chen, Y., Nie, J., Chen, M. and Zhang, D. (2011).Biosorptional removal of lead and cadmium from water by waste materials.Jiangxi University of Science and Technology, School of Resource and Environmental Engineering. Ganzhou Jiangxi: IEEE.

Cherifi, H., Haninia, S. and Bentaher, F. (2009).Adsorption of phenol from waste water using vegetal cords as a new adsorbent.*Desalination*, 244, 177-187

Cheung, W.H., Szeto, Y.S. and McKay, G. (2007).Intraparticle diffusion processes during acid dye adsorption onto chitosan. *Bioresour.Technol.* 98, 2897–2904.

Chiou, M.S. and Hsing,Y. L. (2003).Adsorption behavior of reactive dye in aqueos solution on chemical cross-linked chitosan beads.*Chemosphere* 50(8),1095-1105

Chowdhury, S. and Papita, D.S. (2012).Scale-up of a dye adsorption process using chemically modified rice husk: optimization using response surface methodology.*Desalination and Water Treatment* 37(1-3), 331-336.

Cloete, T.E. (2010).*Nanotechnology in water treatment application*.(Caister Academic Press, Norfolk, UK).

Cobas, M., Sanromán, M.A. and Pazos, M. (2014). Box–Behnken methodology for Cr(VI) and leather dyes removal by an eco-friendly biosorbent: *F. vesiculosus. Bioresour. Technol.* 160, 166–174.

Coman, V., Robotin, B. and Ilea, P. (2013). Nickel recovery/removal from industrial wastes: A review Resour. Conserv.Recy., 73, 229-238

Coates, J.P. (1996).Into the Unknown: the First in the Series, *Spectroscopy*, **11**(5), 32–39

Crini, G. (2006). Non-Conventional Low-cost adsorbents for dye removal: A review. *Bioresearch Technology* 97, 1061-1085.

Critternden, J. C., Trussell, R. R., Hand, D.W., Howe, K. J. and Tchobanoglous, G. (2005). Coagulation, mixing and flocculation, in: Water Treatment: Principles and Design, second ed., John Wiley & Sons, USA, pp. 643-779.

Cronje, K.J., Chetty, K., Carsky, M., Sahu, J.N. and Meikap, B.C. (2011).Optimization of chromium(VI) sorption potential using developed activated carbon from sugarcane bagasse with chemical activation by zinc chloride. *Desalination*, 275, 276-284.

Dabrowski, A. (2001).*Adsorption – from theory to practice,* Advances in Colloid and Interface Science. Faculty of Chemistry, M.Curie-Sklodowska University, Lublin, Poland.93(1-3), 135-224.

Danish, M., Hashim, R., Ibrahim, M.N.M., Rafatullah, M., Ahmad, T. and Sulaiman, O. (2011).Characterization of Acacia mangium wood, based activated carbons in presence of basic activating agents. *BioResources* 6(3), 3019-3033.

Demirbas, A. (2008). Heavy metal adsorption onto agro-based waste material: A review *J. Hazard. Mater.*, 157, 220-229

Demirbas.E,Dizge.N,Sulak.M.T and Kobya.M (2009). Adsorption kinetics and equilibrium of copper from aqueous solutions using hazelnut shell activated carbon.*Chemical Engineering Journal*, 148, 480-487.

Dempsey, B.A. and O'Melia, C.R.(1984).*News in environmental control*, 14, 311

Deng, H., Zhang, G., Xu, X., Tao, G. and Dai, J. (2010). Optimization of preparation of activated carbon from cotton stalk by microwave assisted phosphoric acid – chemical activation. *Journal of Hazardous Materials*, 182, 217-224.

Dentel, S.K and Gosset, M.J. (1988).Mechanism of coagulation with aluminium salts, *Journal of American Water Works Association; Research & Technology*, 80(4),187-198.

Derbyshire, F., Andrews, R., Jaques, D., Jagtoyen, M., Kimber, G. and Rantell, T. (2011).Synthesis of isotropic carbon fibers and activated carbon fibers from pitch precursors.*Fuel*, 80(3), 345-356.

DelRı´o, A.I., Ferna´ndez, J., Molina, J., Bonastre, J. and Cases, F. (2011).Electrochemical treatment of a synthetic wastewater containing a sulphonated azo dye. Determination of naphthalenesulphonic compounds produced as main by-products. *Desalination* 273,428–435.

Dhir, B. (2014).Potential of biological material for removing heavy metals from wastewater.*Environ. Sci. Pollut. Res.*, 21, 1614-1627

Dias, J.M., Alvias-Feeraz, C.M., Almeida, M.F., Rivella-Utrilla, J. and Sanchez Polo, M. (2007).Waste materials for activated carbon preparation and its use in aqueous-phase treatment: A review, *J. Environ. Manag*. 85(4), 833-846

Diaz, A., Rincon, N., Escorihulela, A., Fernandez, N., Chacin, E., and Forster, C.F. (1999).A preliminary evaluation of turbidity removal by material coagulants indigenous to Venezuela.*Process Biochemistry*, 35(3-5), 391-395

Dubinin, M.M. and Radushkevich, L.V. (1947).Equationof the characteristic curve of activated charcoal.*Chem.Zentralbl.* 1, 875–890.

Do Hee, K., Seung-Hyeon M. and Jaeweon, Ch.(2003). Investigation of the Adsorption and Transport of Natural Organic Matter (NOM) in Ion Exchange Membranes, *Desalination*, 151, 11–20

Duan, J. and Gregory, J. (2003). Coagulation by hydrolyzing metal salts, *Advances in colloids and interface science*, 100-102 (28), 475-502..

.

Dutta P. K., Vishwanathan P., Mimrot L.and Ravikumar MNV (1997). Use of chitosan-amine-oxide gel as drug carrier, *J. Polym Mater,* 14, 531

Dwivedi, C.P., Sahu, J.N., Mohanty, C.R., Ray Mohan, B. and Maikap, B.C. (2008).Colum performance of granular activated carbon packed bed for Pb(II) removal. *Journal of Hazardous Materials*, 156(1-3), 596-603

Ebi, G. C., and Afieroho, O.E. (2011).Phytochemical and antimicrobial studies on Detarium Microcarpum Guill and sperr (*Caesalpinioceae*) seed coat.*African journal of Biotechnology* . 10(3), 457-462.

Eboibi, B.E., and Eboibi, O. (2009). Activated carbon production from ground nut shells, *Journal of Nigeria Society of Chemical Engineers*, 24(1and2), 95-99

Edwards, A.G. and Amirtharajah, A. (1985). Removing colour caused by humic acids, *Journal of American water works Association; research & Technology*, 77(3),50-57.

Ejizu C.I. (1986).*Ofo Igbo ritual Symbol*. Fourth Dimension Publication, 190

Ekpete, O.A., Horsfall, M. Jnr., and Tarawou, T. (2010).Potentials of fluted and commercial activated carbon for phenol removalin aqueous solution, ARPN.*Journal of Engineering and Applied Science*, 5, 39-47

Elangovan, R., Philip, L. and Chandraraj, K. (2008). Biosorption of chromium species by aquatic weeds: kinetics and mechanism studies. *J Hazard Mater* 152, 100–112. PMID: 17689012

El-hadad, E. (2012).Sorption and Desorption Processes of Organic Contaminants on Carbonaceous Materials (Ph.D. thesis).Fac. of Sci. Technissche University. 80.

Elhassadi, A. (2008). Pollution of water resources from industrial effluents: Case study-Benghazi, Libya, *Desalination* 222

EL- Hendawy, A.N.A. (2008). An insight into the KOH activated mechanism through the production of microporous activated carbon for the removal of Pb^{2+} cations, *Appl. Surf, Sci* 255(6), 3723- 3730.

Erdem, E., Karapinar, N., and Donat, R. (2004).The removal of heavy metal cations by natural zeolites.*Journal of colloid and Interface Science* 280(2), 309-314.

FAOSTAT (2008). Food and Agricultural Organization of the United Nations.http://faostat.fao.org/faoastat

Faust, S.D. and Aly, O.M. (1983).Chemistry of Water Treatment, Butterworth Publishers, Stoneham, 277-363.

Ferda.G and Selen.S.D (2012). Adsorption study on orange peel: Removal of Ni(II) ions from aqueous solution, *African Journal of Biotechnology*,11, 1250-1258

Fernadez-Kim, S (2004). Physiochemical and functional properties of crawfish chitosan as affected by Different Processing Protocols, M.Sc. Thesis, Department food science, Louisiana State University and Agricultural and Mechanical College, USA, 1-99

Fierro, V., Muniz, G., Basta, A.H., El-Saied, H. and Celzard, A. (2010).Rice straw as precursor of activated carbons: Activation with ortho-phosphoric acid. *Journal of Hazardous Materials*, 181, 27-34.

Fomkin A. (2009).Nanoporous Material and Their Adsorption Properties. Institute of Physical Chemistry and Electrochemistry, *Russian Academy of Sciences,* Vol. 45(2), 133–149

Foo, K.Y., and Hameed, B. H. (2010). Insights into the modeling of adsorption isotherm systems, *Chemical Engineering Journal*, 156 (1), 2-10

Fogler, S. (2001).*Elements of Chemical Reaction Engineering* 3rd Edition. Spain: Prentice Hall Inc.

Freundlich, H. (1906).Over the Adsorption in solution.*Journal of Physical Chemistry* 57, 385-470

Gadd.G.M. (1990).*Fungi and yeasts for metal accumulation' In Microbial Mineral Recovery,* Ehrlich, H.L. and Brierly, C. (Eds.). New York, McGraw- Hill, 249-276

Gani, A. and Naruse, I. (2007).Effect of cellulose and lignin content on pyrolysis and combustion characteristics for several types of biomass.*Renewable Energy,* 32, 649-661.

Garg, U., Kaur, M.P, Jawa, G.K, Sud, D. and Garg, V.K. (2008).Removal of cadmium (II) from aqueous solutions by adsorption on agricultural waste biomass, *Journal of Hazardous Materials* 154, 1149-1157.

Genç-Fuhrman, H., Mikkelsen, P.S. and Ledin, A. (2007). Simultaneous removal of As, Cd, Cr, Cu, Ni and Zn from stormwater: Experimental comparison of 11 different sorbents,*Water Research,* 41(3), 591-602.

Geng, Y. (2005). Application of flocs analysis for Coagulation Optimization at the split lake water treatment plant. A Thesis submitted to Department of civil and Geological Engineering, University of Manitoba, Winnipeg, Manitob

Ghebremichael, K. (2004). In Land and Water Resources Engineering, PhD thesis (Royal Institue of Technology; KTH, Stockholm, Sweden. ISSN 1650-8602;

Gómez, V., Larrechi, M. S. and Callao, M. P.(2007). Kinetic and adsorption study of acid dye removal using activated carbon. *Chemosphere*, 69,1151.

Gon calves,M., Oliveira,L. C. A. and Guerreiro, M. C. (2008). Magnetic niobia as adsorbent of organic contaminants in aqueous medium: effect of temperature and pH, *Qu´ımica Nova*, 31(3), 518–522

Gregory, J.(1993). Stability and flocculation of suspensions, in Proc. Solid-Liuid Dispersions, P. Ayazi Shamlou ed., Butterworth-Heinemam Ltd

Guo, J., and Lua, A.C. (2003). Textural and chemical properties of adsorbent prepared from palm shell by phosphoric acid activation, *Mater. Chem. Phys.* 80(1), 114-119.

Gupta, V.K., Carrott, P.J.M., Ribeiro Carrott, M.M.L. and Suhas, (2009). Low-costadsorbents: growing approach to wastewater treatment a review. Crit. *Rev.Environ. Sci. Technol*. 39, 783–842..

Gupta.V.K and Rastogi.A (2007). 'Biosorption of lead from aqueous solutions by green algae *Spirogyra species*: Kinetic and equilibrium studies' *Journal ofHazardous Materials*,152, 407-414.

Gupta, V.K., Jain, C.k., Ali, I., Sharma, M. and Saini, V.K. (2003). Removalof cadmium and Nickel from wastewater using Bagasse Fly Ash. *Journal of water Resource*, 37, 4038-4044

Gustafsson, J., Nordenswan, E. and Rosenholm, J.B. (2003).Effectof pH on the sedimentation, -potential, and rheology of anatase suspensions.*Colloids and Surfaces A: Physicochemical and Engineering Aspects*, 212(2-3), 235-247.

Haimour, N.M. and Emeish, S. (2006). Utilization of date stones for production of activated carbon using phosphoric acid. *Waste Management*, 26 (6), 651-660.

Hameed, B. H., Tan, I. A. W. and Ahmad,A. L. (2007). Optimization of basic dye removal by oil palm fibre-based activated carbon using response surface methodology."*Journal of hazardous materials* 158(2), 324-332.

Hammaini, A., Ballester, F. A.,Blazquez, M.L.and Munoz, J.A. (2006).Biosorption ofheavy metals by activated sludge and theirdesorption characteristics, *J. Environ. Manage*, 84(4), 419-426.

Hammer, M. J.(1986). *Water and Wastewater Technology*, John Wiley and Sons, New York, NY

Han, H., Li, Y., Li, J., Zhang, H.X. and Shi, J. (2006). Biosorption of copper and lead ions by waste beer yeast, *Journal of Hazardous Materials* (137), 1569–1576.

Hayashi, J., Kazehaya, A., Muroyama, K.and Watkinson, A.P.(2000).Preparation of activated carbon from lignin by chemical activation, *Carbon* 38, 1873-1878.

Ho, Y.S. (2004). Citation review of Lagergren kinetic rate equation on adsorption reactions. Scientometrics, 59, 171-177.

Holhof, H., Egelhaaf, S.U., Borkovee, M., Schurtenberger, P. and Sticher.(1996). Coagulation Rate Measurement of colloidal particles by Simultaneous static and Dynamic Light Scattering. Langmuir, 12, 5541

Holetz F.B, Ueda-Nakamura T, Filho B.P.D, CortezD.A.G, Morgado-Diaz J.A. and Nakamura C.V. (2003).Effect ofessential oil of Ocimum gratissimum on the trypanosomatid Herpetomonas samuelpessoai.Acta Protozoologica. 42(4), 269–276. doi: 10.13140/RG.2.1.1605.5208

Hopkins B. and Stanfied DP (1966).*Savannah Tree of Nigeria* University Press Ibadan. 6-7, 12
.
Horsfall, M., Jnr, and Spiff, A.I., (2005).Equilibrium sorption study of Al^{3+}, Co^{2+} and Ag^{+} in aqueous solutions by fluted pumkin (Telfairia occidentials Hook F) waste biomass, *ActaChim. Slov*, 52, 174-181

Hossain, M.A., Ngo, H.H., and Guo, W.S. (2012).Removal of copper from water by Adsorption onto Banana Peel as Bioadsorbent.*International Journal of Geomate* 2,227-234

Hu, Z. and Srinivasan, M.P.(1999). Preparation of high-surface-area activated carbons from coconut shell. *Microporous and Mesoporous Materials*, 27 (1), 11-18.

Hu Z, and Srinivasan, M.P. (2001).Mesoporous high surface area activated carbons. *Microporous Mesoporous Mater*., 34: 267–275.

Hudson, S.M. and Jenkins D. W. (1998).Chitin and chitosan.Encyclopedia of polymer Science and Technology. Third ed. (Wiley Interscience, New York)(Online version, www.interscience.com)

Huang, C. and Pan, J.R. (2002).Coagulation Approach to water Treatment Encyclopedia of surface and colloid science, 2nd edition, Marcl Dekker Inc. New York, 5667

Hutchinson, L.E., Berry, D.F., Mullins, D.E., Helzel, G.H. and Yong, R.W. (1993).Evaluation of economical sorbents for removal of metolachlor from rinsate wastewater.*Waste Manage.* 13, 83-87.
Hutson, N. D. and Yang, R. T.(1997). Adsorption.3, 189.

Iakovleva E. andSillanpää M. (2013).The Use of Low Cost Adsorbents for Wastewater Purification in Mining Industries.*Environmental Science and Pollution Research.* Vol. 20(11),7878-7899
.
IITA.(1992). International Institute of Tropical Agriculture, Substantial food production in sub-Saharan African, IITA Ibadan, 85

Inglezakis, V. and Poulopoulos, S. (2006). Adsorption ion exchange and catalysis design of operations and environmental applications. Elsevier Science Ltd.

IUPAC (1972).IUPAC Manual of Symbols and Terminology.*Pure and Applied Chemistry*, 31, 587.

Jadhav, M.V. and Mahajan, Y.S. (2013). Investigation of the performance of chitosan as a coagulant for flocculation of local clay suspension of different turbidities, *KSCE J.Civil Eng*. 17(2), 329-334

Jahn, S. A. (2001). Drinking water from Chinese River; Challenges of clarification, *Journal water supply Res. Technol.* 50, 15-27

Jaman H, Chakraborty D, and Saha P. (2009). A Study of the Thermodynamics and Kinetics of Copper Adsorption Using Chemically Modified Rice Husk. *Clean* 37, 704-711.

Janh, S.A.A. (1988).Using Moringa seed as coagulants in developing countries, *Journal of the American Water Works Association*, 80(6), 43-50

Jenkins, R. and Snyder, R.L. (1996).Introduction to X-ray powder diffractometry.J.D Winefordner series editor. John Willey& Sons, New York, pp. 47-94

Jiang, J. Q., Cooper, C., and Ouki, S. (2002).Comparison of modified monhmorillonite adsorbents: Part 1: Preparation Characterization and phenol adsorption. *Chemosphere* 47(7), 711-716

Jiaping.P.C (2012). 'Decontamination of Heavy Metals: Processes, Mechanisms, and Applications' CRC Press , Print ISBN: 978-1-4398- 1667-7

Jin, Y. (2005). Use of High Resolution Photographic Technique for Studying Coagulation/Flocculation in Water Treatment. M.Sc Thesis, University of Saskatchewan, Saskatoon, 22-29.

Jiang-Ping, W., Yong-Zhen, C., Xue-Wu, G.E. and Han-Qing, Y. (2007).Optimization of coagulation/flocculation process for paper-recucling wastewater Treatment using response surface methodology.*Colloids Surf.* 302, 204-210.

Jirarat, T., Sukruedee, A. and Pasawadee, P. (2006). Chemical and physical properties of flour extracted from Taro Colocasis esculenta (L) Schott grown in different regions of Thailand. Sci. Asia, 32, 279-284

John, S. B. and Walther, S. (2003). Surface Water Pesticide Contamination in the Upper Terrebonne Basin of Louisiana.Louisiana State University.1-54.

Kabdasli, I., Arslan-Alaton, I., Vardar, B. and Tunay, D. (2007). Comparison of electrocoagulation, coagulation and the fenton process for the treatment of reactive dye bath effluent, *Water Sci. Technol*, 55, 125-134

Karthiheyam, S., Sivakumar, P. and Palanisamy, P.N. (2008). Novel activated carbons from agricultural waste and their characterization, *E-Journal of chemistry,* 5, 409-426.

Kavitha, D., and Namasivayam, C. (2007). Experimental and kinetic studies on methylene blue, adsorption by coir pith carbon. *Bioresources Technology* 98(1), 14-21

Kawamura, S. (1991).Effectiveness of natural polyelectrolytes in water treatment.*Journal of the American Water Works Association*, 83(10), 88-91.

Keng, P.S., Lee, S.L.,Ha, S.T., Hung, Y.T. and Ono, S.T. (2014). Removal of hazardous heavy metals from aqeous environment by low-cost adsorption material.*Environ. Chem. Lett*., 12, 15-25

Kim, J., Nason, J.A. and Lawler D.F.(2001). Influence of surface charge distributions and particle size distributions on particle attachment in granular media filtration. *Environmental Science & Technology* 42, 2557-2562.

Kobya, M., Hiz, H., Senturk, E., Aydiner, C. and Demirbas, E. (2006).Treatment of potato chips manufacturing wastewater by electrocoagulation. *Desalination*, 190, 201-211

Kouyate, A.M. and Van Damme, P. (2006).Detarium Microcarpum Guill and Perr.In. Schmelzer, G.H & Gurib-Fakim, A. (Editor). Prota 11(1): Medicinal plants/ plantes medicinales. PROTA, Wageningen NetherLands.

Kousha, M., Daneshvar, E., Dopeikar, H., Taghavi, D. and Bhatnagar, A. (2012). Box-Behnken design optimizationof Acid Black I dye biosorption by different brown macroalgae, *Chem. Eng. J*.179,158-168

Kumar, S.D. Subbaiah, V. M. Reddy, A. S.and Krishnaiah, A. (2009). Biosorption of phenolic compounds from aqueous solutions onto chitosan-*abrusprecatorius* blended beads. *J ChemTechnolBiotechnol*. 84, 972-981..

Kundu, S. and Gupta, A. K. (2006). Arsenicadsorption onto iron oxide-coated cement (IOCC): regression analysis of equilibrium datawith several isotherm models and their optimization. *Chem. Eng. J.*, 122 (1-2), 93-106

Kurniawan, T.A., Chan, G.Y.S., Lo, W. and Babel, S. (2006). Comparisons of Low-cost adsorbent for treating wastewaters laden with heavy metals, *Science of the Total Environment* 366, 409-426

Kwaambwa, H.M. and Maikokera, R. (2007). A fluorescence spectroscopic study of a coagulating protein extracted from Moringa oleifera seeds. *Colloid Surf B* 60, 213-220.

Krishnani, K., and Ayyapan, S. (2006). Heavy Metals Remediation of Water Using Plants and Lignocellulosic Agrowastes.*Rev. Environ. Contam.Toxicol., 188*, 59-84.

Kwon, J.S., Yun, S.T., Lee, J.H., Kim, S.O. and Jo, H.Y. (2010). Removal of divalent heavy metals (Cd, Cu, Pb and Zn) and arsenic (III) from aqueous solutions using scoria: kinetic and equilibrium of sorption. *Journal of Hazardous materials* 174(1-3), 307-313

Langmuir, I. (1918).The adsorption of gases on plane surface of glass, mica and platinum.*Journal of American Chemical Society* (40),1361-1403

Lartey, R.B. and Acqual, F. (1999). Developing national capability for manufacture of activated carbon from agricultural wastes, *GhanaEngineer*

Lee, J.K., Park, G., Ryu, S.K. and Kim, J.H. (2003).Effect of Two-step surface Modification of Activated carbon on the Adsorption Characteristics of Metal ions in wastewater II. Dynamic Adsorption, *Carbon Science* 4, 14-20

Lee, S.H.D., and Johnson, I.J. (1980). Removal of gaseous alkali metal compounds from hot flue gas by particulate sorbents. *J. Engrg. Power*, 102, 397-402

Lemji, H.H. and Eckstadt, H. (2013). A pilot scale trickling filter with pebble graveedia and its performance to remove chemical oxygen demand from synthetic brewery wastewater, Journal of Zhejiang University-Science B (Biomedicine and Biotechnology), 14(10), 924-933.

Letterman, R.D., Amirtharajah, A., and O'Melia, C.R.(1999). Coagulation and flocculation.Water quality and treatment. A handbook of community water supplies, *American Water Works Association*, Mc.Grad=Hill. New York.

Licskó, I. (1997). Realistic coagulation mechanisms in the use of aluminium and iron (III) salts. *Water Science and Technology.* 36, 103–110.

Lyklema, J.(2009). Quest for ion-ion correlations in electric double layers and over charging phenol, *Advance Colloid Interface Sci.* 147-148, 205-213

Ma, W., Zong, P., Cheng, Z., Wang, B. and Sun, Q., 2014.Adsorption and bio-sorption of nickel ions and reuse for 2-chlorophenol catalytic ozonation oxidation degradation from water. *J. Hazard. Mater*. 266, 19–25.

Menkiti, M.C., Nnaji, P.C., Nwoye, C.I., and Onukwuli, O.D. (2010). Coag-flocculation kinetic and Functional Parameters Response of Mucuna coagulant to pH variation in organic Rich Coal Effluent medium, *Journal of Mineral and material characterization and Engineering,* 9(2), 89-103

Menkiti, M.C. and Onukwuli, O.D. (2012).Coag-flocculation of mucuna seed, coag-flocculation (MSC) in coal washery effluent (CME) using light scattering effect.*AICHE J.* 156(4), 303-313

Menkiti, M.C., Aneke, M.C., Ejikeme, P.M., Onukwuli, O.D. and Menkiti, N.U. (2014). Springer Plus 3, 213

MetCalf and Eddy (2003).*Wastewater Engineering Treatment and Reuse,* Tata McGrawHill, New Dellhi, 4th Ed, 42-55

Miller, S.M., Fugate, E.J., Craver, V.O., Smith, J.A. and Zimmerman,J.B. (2008). Towards understanding the efficacy and mechanism of Opuntia spp. as a natural coagulant for potential application in water treatment. *Environ. Sci. Technol*. 42, 4274–4279.

Minceva, M. Markovska, L.and Meshko,V.(2007). Removal of Zn2+, Cd2+ and Pb2+from binary aqueous solution by natural zeolite and granulated activated carbon,*Macedonian Journal of Chemistry and Chemical Engineering*, 26(20), 125–134,

Mittal, A., Gajbe, V. and Mittal, J. (2008). Removal and recovery of hazardous triphenylmethane dye, Methyl. Violet through adsorption over granulated waste materials.*Journal of Hazardous Material*, 150, 364-375.

Mohammad Al-Anber, (2010). Removal of High-level Fe3 + from Aqueous Solution using Jordanian Inorganic Materials: Bentonite and Quartz, *Desalination* 250, 885- 891.

Mondal, P., Mohanty, B. and Majamder, C.B. (2009). Treatment of simulated arsenic contaminated ground water using GAC-Cu in batch reactor: Optimization of process parameters, *Canadian Society for Chemical Engineering*, 87(5), 766-778

Montgomery, D.C. (2005).*Design and analysis of experiments*. 6th ed. Hoboken NJ: JohnWiley& Sons. Inc.

Murzin,D. and Salm T. (2005). *Catalytic Kinetic*, Elsevier Science Ltd. Amsterdam

Namasivayam, C. and Kavitha, D. (2006). IR, XRD and SEM studies on the mechanism of adsorption of dyes and phenols by coir pith carbon from aqueous phase, *Microchemical Journal* (82), 43-48

Nandi, B.K., Goswani, A. and Purkait, M.k. (2009). Adsorption characteristic of brilliant green dye on kaoline.*Journal of Hazardous Material*, 1611, 387-395

(**N**ESREA) Act. 2007. National Environmental (Standard for Discharge of Effluent into water or Land) Regulations.

Ndabigengesere, A., Narasiah, K.S. and Talbot, B.G. (1995).Active agents and Mechanism of coagulation of turbid waters using moringa oleifera.*Water Research* 29(2),703-710

Ng C, Marshal R, Rao M, Rishipal R.B, Jack N.L, and Ralph J.A (2002). Granulated activated carbons from agricultural by- products: Process description and estimated cost of production. LSU Ag center.Bulletin Number 881.

No, H.K. and Meyers, S.P. (1989). Crawfish chitosan as a coagulant in recovery of organic compounds from seafood processing stream *J.Agric. food Chem.,* 37, 580-583

Norlia, B., Kheng, L.L.,and Kamarudin, H.(1999). "Cyanide Removal using Commercially Available Resins".National Seminar on "Recent Techniques in Mineral Processing, *Wastes and Environmental Management"* (RETMEM), Bhubaneswar, India.207-214.

Nozaic, D. J., Freese, S. D. and Thompson, P., (2001). Longterm experience in the use of polymeric coagulants at Umgeni water.*Water Science and Technology* 1(1), 45-50.

Ntuli, F., Kupia, K.P. and Muzenda, E. (2011). Designing of sampling programmed for industrial effluent monitory, *Environmental Science and Pollution Research* 18, 479-484

Nwabanne, J.T. and Igbokwe, P.K. (2011).Copper (II) uptake by adsorption using palmyra palmnut, *Advances in Applied Science Research* 2(6), 166-175.

Obiora-Okafor, I.A. and Onukwuli, O.D. (2015). Optimization of coag-flocculation process for colour removal from synthetic dye wastewater using natural organic polymer: Response Surface Methodology applied. Internation journal of Scientific & Engineering Research, vol.6(12), 2229-5518.

Odoemelam, S.A., Iroh, C.U. and Igwe, J.C. (2011). Copper (II), Cadmium (II) and Lead (II) adsorption kinetics from, aqueous metal solutions using chemically modified and unmodified cocoa pod hush (Theobrma cacao) waste biomass. *Res. J. Applied Sci*., 6(1), 44-52

Oguz, E. (2005). Thermodynamic and kinetic investigation of Po_4^{3-} adsorption on bast furnace slag, *Journal of clloid and interface science*, 28(1), 62-67

Okolo, B.I., Nnaji, P.C., Menkiti, M.C., Ugonabo, V.I. and Onukwuli, O.D. (2014). Parametric Response Evaluation for Xanthosoma spp. Induce Coag-flocculation of brewery Effluent. *Journal of Green and Sustainable Chemistry*. 4,7-14

O'Meila C.R., (1978). Coagulation in waste water treatment : The scientific basis of flocculation (NATO Advanced study Inst. Series E, Appl.Sc.No 27), In : *Sijtholf andNoordhoff,Alpenan den Rijn*, pp 219-268, (Ives ,K.J., Ed.),Netherlands.

O'Melia, C.R.(1972).*In Physicochemical Processes for water Quality Control*, W.J. Webber, Jr., ed., Wiley-Inter science, New york NY, 61-109.

Onweme, I.C. (1987). Strategies for increasing Cocoyam (*Colocasia* and *Xanthosoma* sp.) in Nigerian Food Basket. In: O.B. Arene, L.S.O. Ene, S.O. Odurukwe and N.O.A. Ezeh (Eds.). Proc. 1st National Workshop on Cocoyam NRCRI Umudike Nigeria, 35-42

Ozacar, M. and Sengil, A. (2003).Evaluation of tannin biopolymer as a coagulant aid for coagulation of colloidal particles.*Colloids and Surfaces A:Physicochemical and Engineering Aspects* 229,85–96.

Padilla-Ortega, E., Leyva-Ramos, R. and Flores-Cano, J.V., (2013).Binary adsorption of heavy metals from aqueous solution onto natural clays.*Chem. Eng. J.* 225, 536–546.

Park, D., Lim, S.-R., Yun, Y.-S.and Park, J.M., (2008). Development of a new Cr(VI)-biosorbent from agricultural biowaste. *Bioresour.Technol.* 99, 8810–8818.

Patel, S. (2012). Potential of fruit and vegetable wastes as novel biosorbent: summarizing the recent studies. *Rev. Environ-Sci Biotechnol*., 11, 365-380.

Peavy, H. S., Rowe, D. R. and Tchobanglous, G. (1985). Environmental Engineering, New York: McGraw-Hill, Singapore, pp. 11-51, 131-140.

Petrov, N., Budinova, T., Razvigorova,M., Parra,J. and Galiatsatou, P. (2008). Conversion of olive wastes to volatiles and carbon adsorbents. *Biomass & Bioenergy*, 32(12), 1303-1310.

Phan, N.H., Rio, S., Faur, C., Le Coq, L., Le Cloirec, P. and Nguyen, T.H., (2006).Production of fibrous activated carbons fromnatural cellulose (jute, coconut) fibers for water treatment Applications.*Carbon* 44, 269-277

Purseglove, J. W. (1972) Araceae. *In Tropical Crops:Monocotyledons*, Longman, Essex, UK, 58-74.

Radovic, L. R., Moreno-Castilla, C. and Rivera-Utrilla, J. (2001).Carbon materials as adsorbents in aqueous solutions. In: Radovic, L.R. (Ed.). Chemistry and Physics of Carbon, A Series of Advances, ,27, 227-405.

Rajaram, T. and Ashutosh, D. (2008). Water pollution by industrial effluents in India: Discharge scenarios and case for participatory eco-system specific local regulation, Futms, 40, 51-69.

Rangabhashiyam, S., Anu, N. and Selvaraju N. (2013) Sequestration of Dye from Textile Industry Wastewater Using Agricultural Waste Products as Adsorbents.*Journal of Environmental Chemical Engineering*, **1**, 629-641. http://dx.doi.org/10.1016/j.jece.2013.07.014

Ravikumar, M.N.U.., Dutta, P.K. and Nakamura, S. (2000). Chitosan-amine oxide, a new gelling system, characterization and an vitro evaluation, *Indian J. Pharma-Sci*, 62, 55

Ravina L. (April 1993). Everythingyou wantto know about Coagulation and Flocculation", Zeta-Meter Inc. VirginiaUSA,

Renuka, A.B. and Yadhav, M.V. (2012).Assessment of Purification of water by using Natural Herbs.Lokavishkar, *International E-Journal*. 1(5): 1-21

Repo, E. (2011). EDTA- and DTPA- Functionalized Silica Gel and Chitosan Adsor-bents for the Removal of Heavy Metals From Aqueous Solutions. Lappeenranta Uni-versity of Technology.Thesis.

Rodriguez, J.P.M., Lugo, I.P.U., Rojas, A.V.C., and Malaver C.C. (2007).Evaluation of the coagulation process for designing of a water treatment plant.Threshold Scientific. Manuela Beltran University Foundation, Bogota, 8-16

Rosales, E., Pazos, M., Sanaroman, M. A. and Tavares, T. (2012). Application of zeolite-Arthrobacter viscosus system for removal of heavy metal and dyer: chromium and azure B. Desalination, 284, 150-156.

Sag, Y and Aktay, Y. (2001). Application of equilibrium and mass transfer models to dynamic removal of Cr (VI) ions by chitin in packed colum reactor. *Journal of Process Biochemistry,* 36, 1187-1197.

Shahidi, F. and Synowiecki, J. (1991). Isolation and characterization of nutrients and value-added products from snow crab (*Chionoecetes opil*io) and shrimp (*Pandalus borealis*) processing discards. *J Agri Food Chem*, 39, 1527-1532

Sharma, P., Singh, L. and Dilbaghi, N. (2009). Optimization of process variables for decolorization of Disperse Yellow 211 by *Bacillus* subtiles using Box-Behnken design. *J. Hazard. Mater.* 164, 1024-1029.

Simate, G.S, Cluett, J., Iyuke, S.E., Mustapatika, E.T., Ndloru, S., Walubita, L.F. and Alvarez, A.E.(2011).The Treatment of brewery wastewater for reuse: State of the art. *Desalination* 273, 235-247

Singla, A.K. and Chowla, M. (2001). Chitosan: Some pharmaceutical and biological aspects an update. *J.Pharm. Pharmacol*. 53, 1047-1067

Stochi, E. (1990). Industrial Chemistry Vol.1 Ellis, Horwood, New York.

Stumm,W. and O`Melia,C.R (1968). Stoichiometry of coagulation, *Journal of American Water Works Association*,.60(5), 514-539.

Sud D., Mahajan G. and Kaur M.P. (2008).Agricultural waste material as potential adsorbent for sequestering heavy metal ions from aqueous solution. A review *Bioresource Technology*, 99, 6017-6027.

Sugumaran, P. (2009). Production of activated carbon from agro-waste for application in textile effluent treatment. Ph.D Thesis, submitted to University of Madras.

Tan, I.A.W., Ahmad, A.I., and Hameed, B.H (2008). Adsorption of basic dye using activated carbon prepared from oil palm shell, batch and fixed bed studies. *Desalination* 225(1), 13-28. Doi 101016/j desal 2007.07.005.

Temkin, M.J. and Pyzhey, V. (1940).Recent modifications to Langmuir isotherms.*Acta Pgysiochim.* 12, 217-222

Tongpoothorn, W., Srittha, M., Homchan, P., Chanthai, S., and Ruangviriyachai, C. (2011).Preparation of activated carbon from Jatropha curcas fruit shell by simple thermo- chemical activations and characterization of their physio-chemical properties.*Chem. Eng. Res. Des* 89(3), 335-340

Trinh, T.K. and Kang, L.S. (2011).Response surface methodological approach to optimize the coagulation/flocculation process in drinking water treatment.*Chem. Eng. Res. Design;* 89, 1126-1130

Tripathi P .N., Chaudhari M. and Bokil S.D. (1976). *Nirmali* seed a naturally occurring coagulant, *Indian J. Environ Health*, 18,272–81

Tseng R. L, Wu F. C and Juang R.S. (2003).Liquid-phase adsorption of dyes and phenols using pinewood-based activated carbons.*Carbon* 41(3),487-495. http://dx.doi.org/10.1016/ S0008-6223(02)00367-6

Uberoi, M. and Shadman, F. (1990). Sobents for removal of lead compounds from hot flue gases *ALCHE J*., 36(2), 307-309

Ugonabo, V.I., Menkiti, M.C., Onukwuli, O.D. (2012).Effect of Coag-flocculation kinetic of Telfairia Occidentalis seed coagulant (TOC) in Pharmaceutical wastewater, *Int. J. Multidispinary Sci. Eng* (9)

Uluozlu, O. D., Sari, A., Tuzen, M. and Soylak, M. (2008). Biosorption of Pb(II) and Cr(II) from aqueous solution by lichen (*Parmelina tiliaceae*) biomass. *Bio resources Technology.* 99(8), 2972-2980

Valix, M., Cheang, W.H., and Mckay, G. (2004). Preparation of activated carbon using low temperature carbonization and physical activation of high ash raw bagasse for acid dye adsorption, *Chemosphere,* 56, 493-51

Vijayaraghavan,G., Sivakumar, T. and Vimal Kumar, A.(2011). Application of plant based coagulants for Wastewater Treatment, *International journal of Advanced Engineering Research and Studies*.1, 88-92

Volesky, B. (2003). Biosorption Process Simulation Tools. Hydro metalling, 71(1-2), 179-190

Volk, C., Bell, K., Ibrahim, E., Verges, D., Amy, G. and Lechevaller, M. (2000).Impact of enhanced and optimized coagulation on removal of organic matter and its biodegradable fraction in chemistry water.*Water Res*. 34, 3247-3257. Doi:10.1016/s0043-1354.00.000336

Von Smoluchowski, M. (1917).Versucheiner Mathematischen Theorie der Koagulation Kinetic kolloide Lousumgen Z.*The Journal of Physical Chemistry,* 92, 129-168.

Wang, J. and Chem, C. (2009).Biosorbents for heavy metals removal and their future.*Biotechnology Advances*, 27(2):195-226

Warhurst A. M., McConnachie G. L. and Pollard S. J. T., (1996). The Production of Activated Carbon for Water Treat-ment in Malawi from the Waste Seed Husks of Moringa Oleifera, *Water Science and Technology*, 34(11),177-184.

(**W**ST)(2005). Water Specialist Technology, About Coagulation and Flocculation; Information Bulletin, USA

Weber,W.J. and Morris, J.C. (1963). Kinetic of adsorption on carbon from solution: *J.Sanit.Eng. Div. Am. Soc. Civ. Eng.* 89, 31-60

Wigmans, T., 1989.Industrial aspects of production and use of activated carbons.*Carbon* 27, 13-22.

Yang, T., and Lua, A. (2003). Characterization of activated carbons prepared from pistachio-nut shells by physical activation. *Journal of colloid and interface, science*, 367, 408-417

Yasemin, B. and Zeki, T. (2007). 'Adsorption studies on ground shells of hazelnut and almond '*Journal of Hazardous Materials,* 149, 35-41.

Yu, B., Zhang, Y., Shukla, S.S. and Dorris, K.L. (2000).'The removal of heavy metal from aqueous solutions by sawdust adsorption - removal of copper' *Journal of Hazardous Materials*, .80, 33-42.

Zahangir, M.A., Suleyman, A.M. and Norami, K. (2008). Production of activated carbon from Oil palm empty fruit bunches for removal of zinc, Twelfth International Water Technology Conference (IWTC12), Alexandria, Egypt. . 373-383.

Zhang, W., Ricketts, T., Kreman, C., Carney, K. and Swinton, S.M. (2007). Ecosystem services and dis-services to agriculture, *Ecological Economics* 64(2), 253-260.

Zheng, H.L., Zhu, G.C., Jiang, S., Tshukudu, T., Xiang, X. and Zhang, P.(2011). Investigations of coagulation–flocculation process by performance optimization, model prediction and fractal structure of flocs. *Desalination*; 269(1–3),148–156.

Zouboulis, A. I. and Tzoupanos, N. D. (2008). Coagulation-flocculation processes in water/wastewater treatment: The application of new generation of chemical reagents. Paper presented at the *6th IASME/WSEAS International conference on heat transfer, thermal engineering and environment (hte'08)*. Rhodes, Greece, August 20-22, 2008.

APPENDIX A1

(A) ***Xanthosoma sagittifolium*****(B)** ***Xanthosoma sagittifolium*** **Powder**

(C)*Hibiscus esculentus L*(D) *Hibiscus esculentus L*powder

(E) *Detarium Microcarpum* (F) *Detarium Microcarpum*powder

(G) *Crassostrea virginica* **(H) *Crassostrea virginica* powder**

Plate A1: Bio coagulant raw materials for coagulation/flocculation process

APPENDIX B

(A) *Mucuna pruriens*(B)*Mucuna pruriens (AC)*

(C) *Crassostrea virginica* (D) *Crassostrea virginica (AC)*

(E) *Canarium schweinfurthii* (F)*Canarium schweinfurthii (AC)*

Plate B1: Bio sorbent raw materials for adsorption process

APPENDIX C

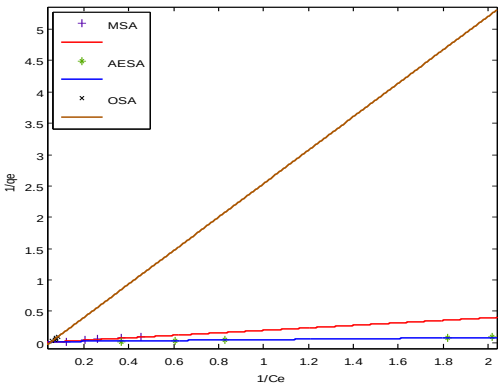

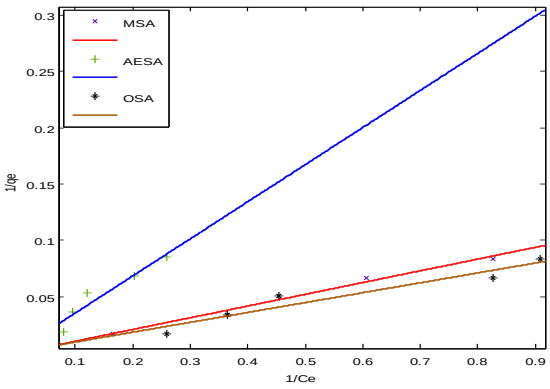

(pH2.0)

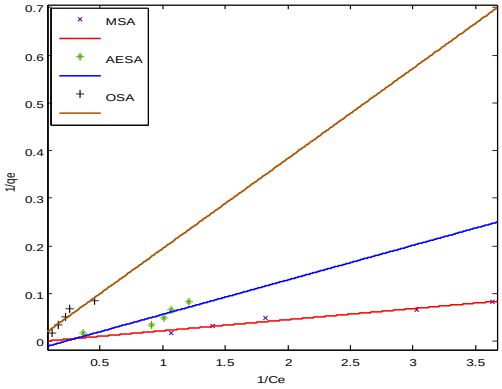

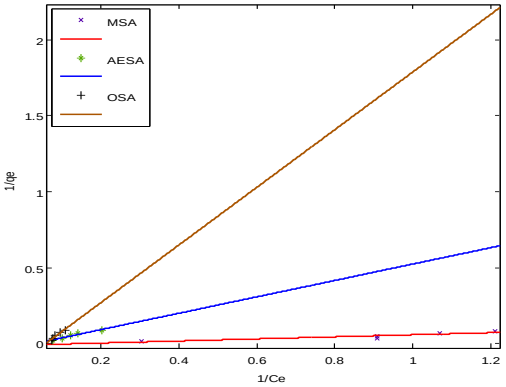

(pH4.0)

(pH6.0) (pH8.0)

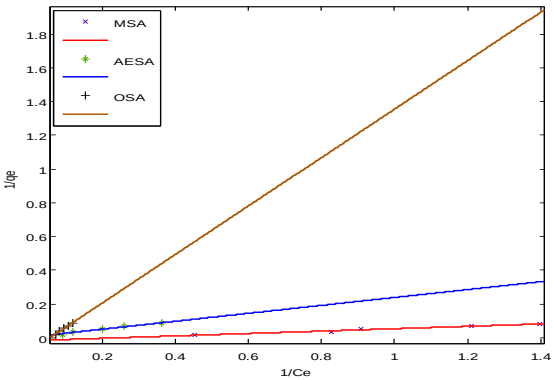

(pH10.0)

Figure C1 A plot of $1/q_e$ vs $1/C_e$at various pHs for acid treated adsorbent in brewery effluent (BRE)

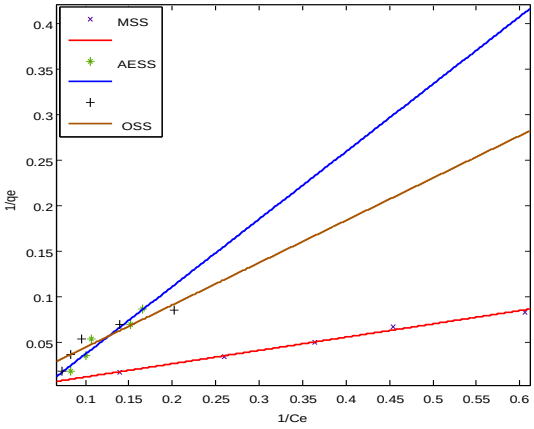

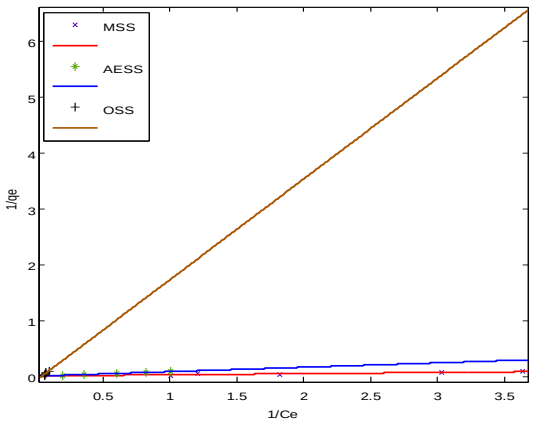

(pH2.0)

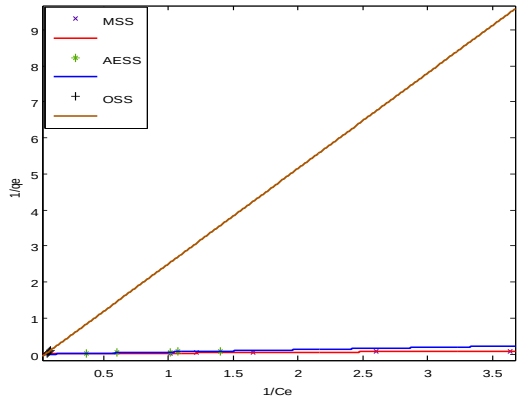

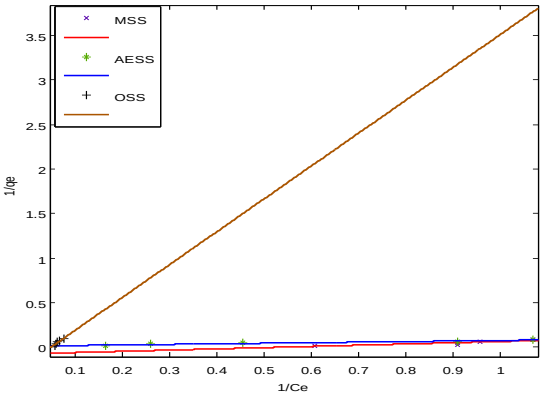

(pH4.0)

(pH6.0)

(pH8.0)

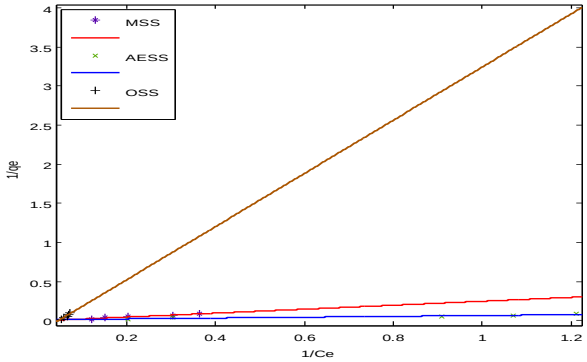

(pH10.0)

Figure C2 A plot of $1/q_e$ vs $1/C_e$at various pH for salt treated adsorbent in brewery (BRE)

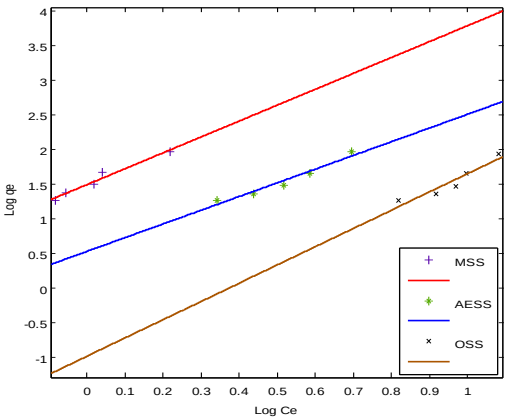

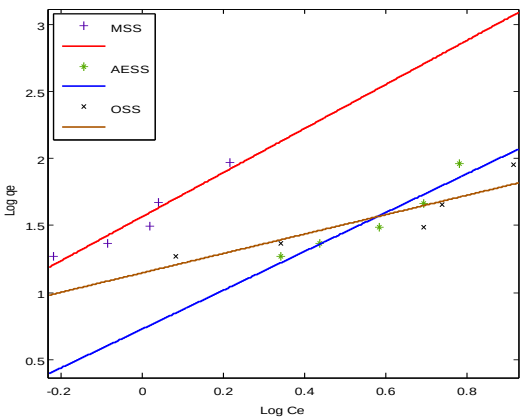

(pH2) (pH4)

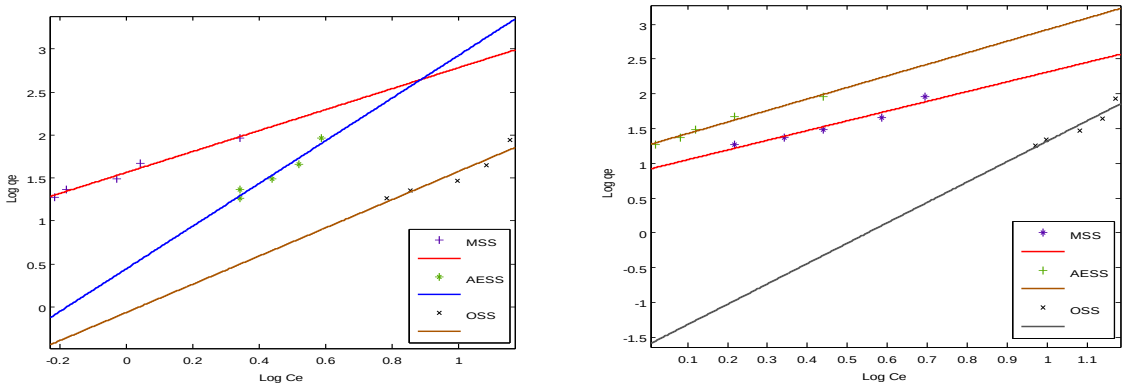

(pH6) (pH8)

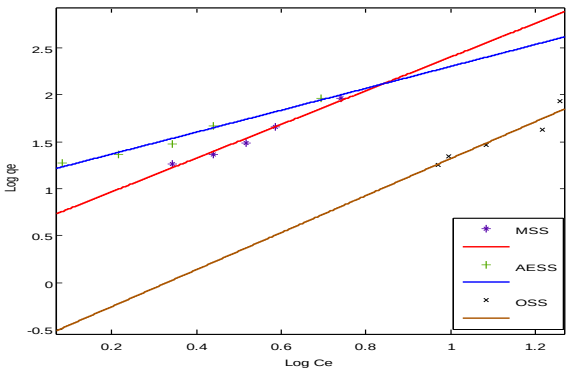

(pH10)

Figure C3 A plot of Logq_e vs LogCe at various pH for salt treated adsorbent in Paint effluent (PW)

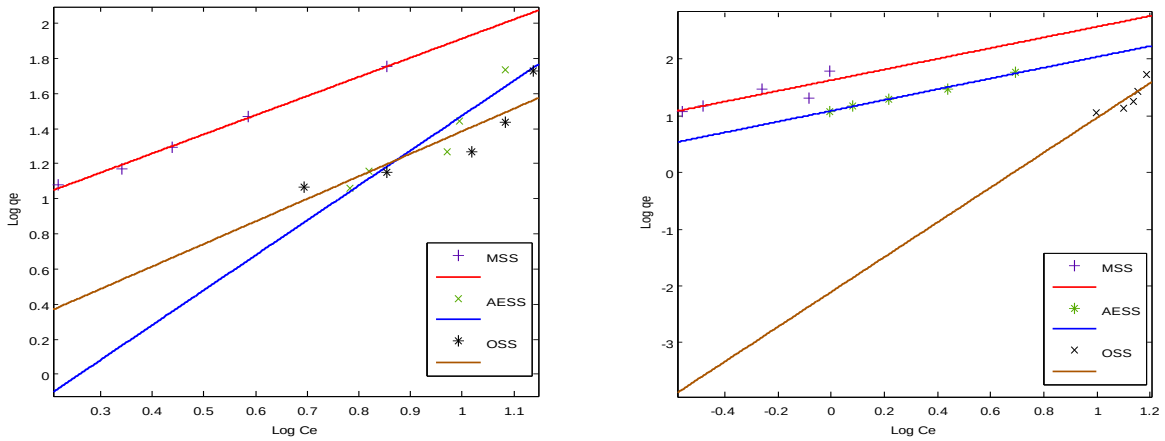

(pH2)

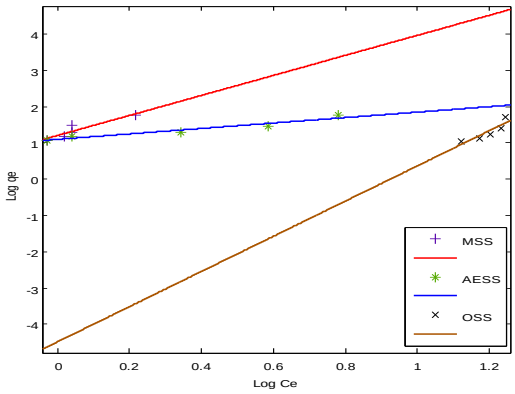

(pH4)

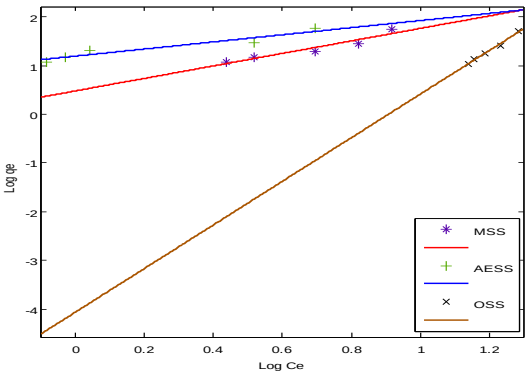

(pH6)

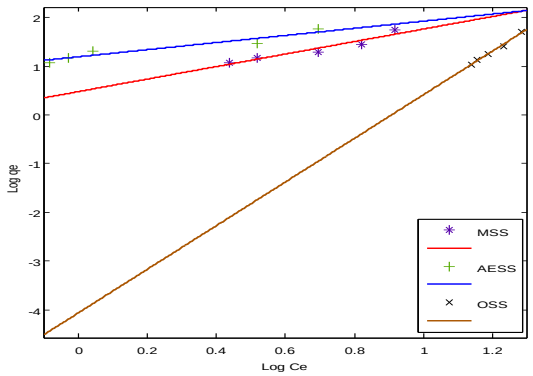

(pH8)

(pH10.0)

Figure C4 A plot of Log q_e vs Log $C_e$at various pH for salt treated adsorbent in brewery effluent (BRE)

APPENDIX C

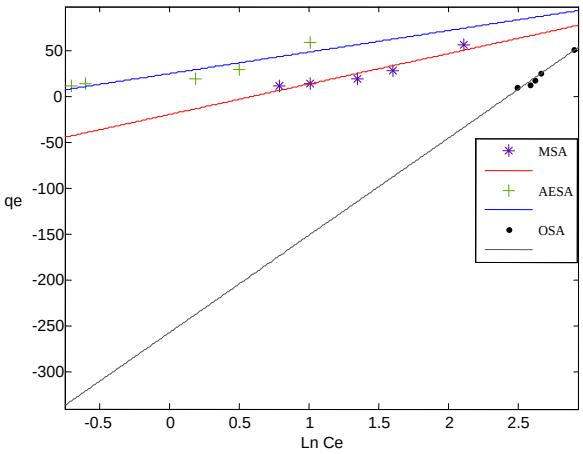

(pH 2)

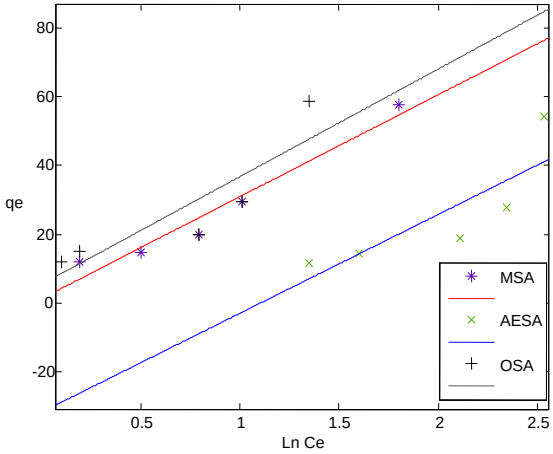

(pH 4)

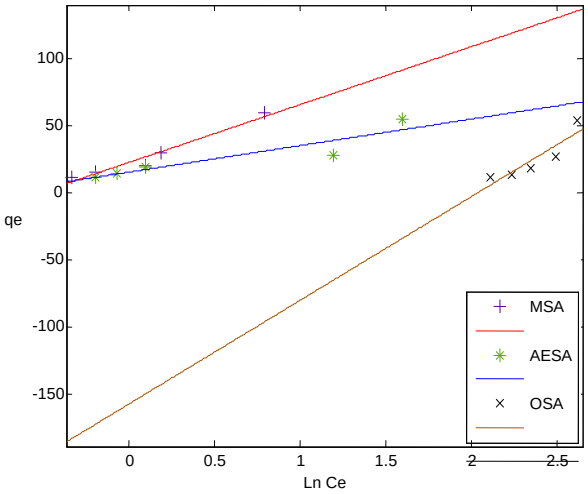

(pH6)

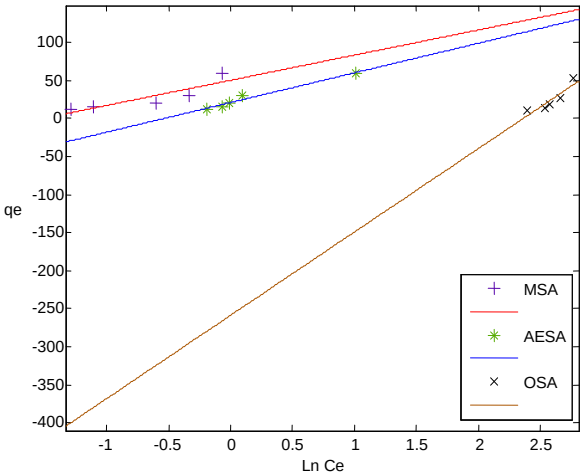

(pH8)

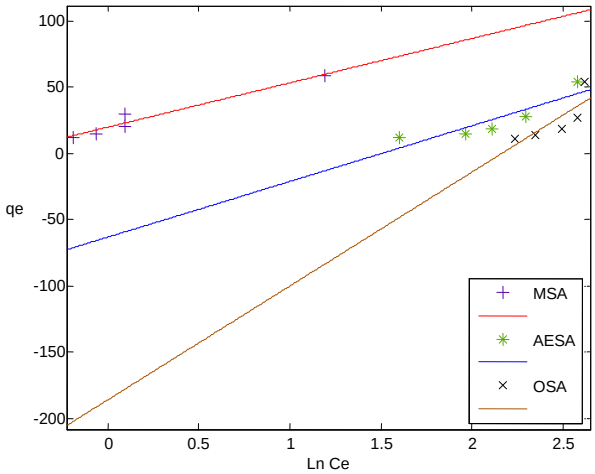

(pH10)

Figure C5 A plot of q_e vs Ln C_e at various pH using acid treated adsorbent on brewery effluent

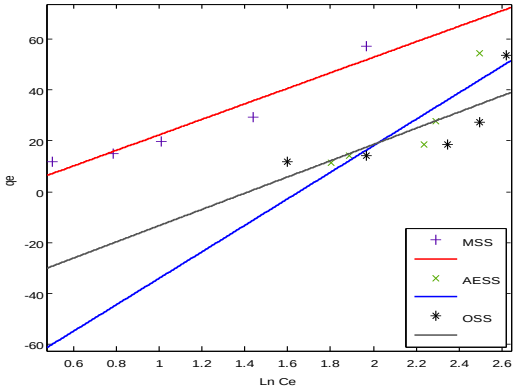

(pH2.0)

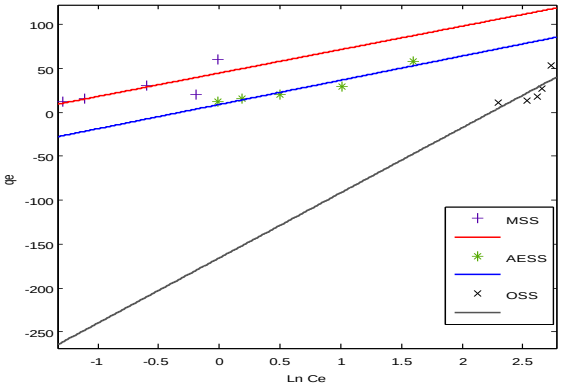

(pH4.0)

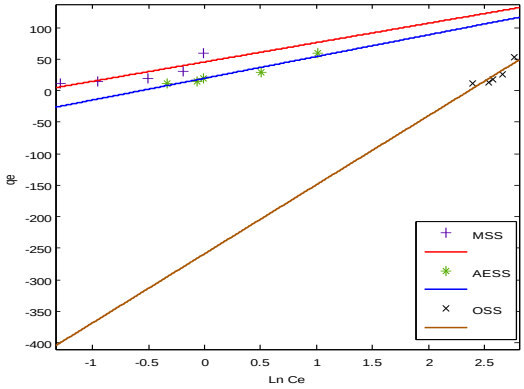

(pH6.0)

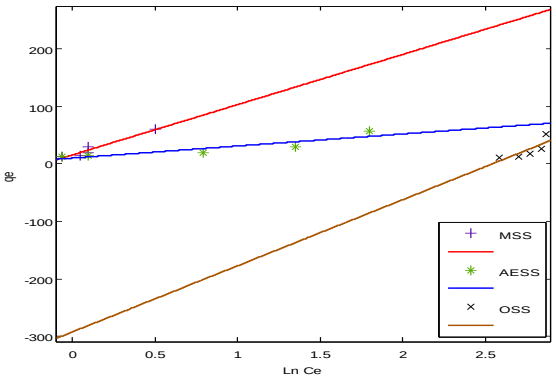

(pH8.0)

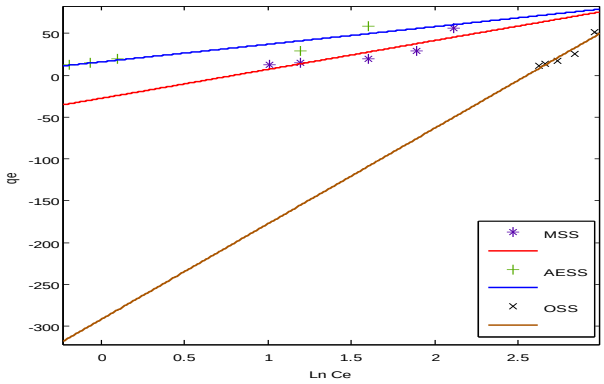

(pH10.0)

Figure C6A plot of q_e vs Ln C_e for various pH using salt treated adsorbent on brewery effluent (BRE)

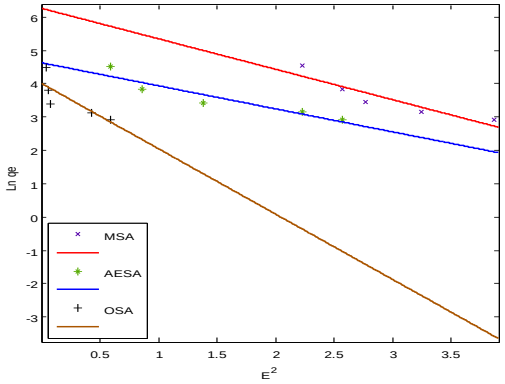

(pH2)

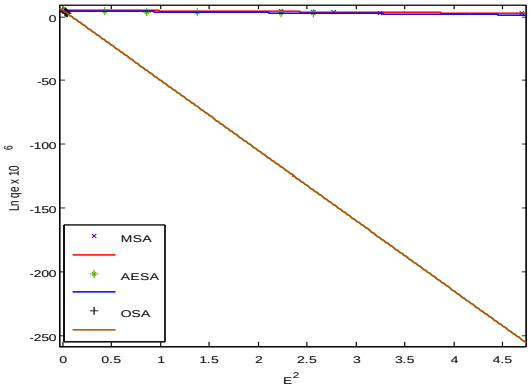

(pH4)

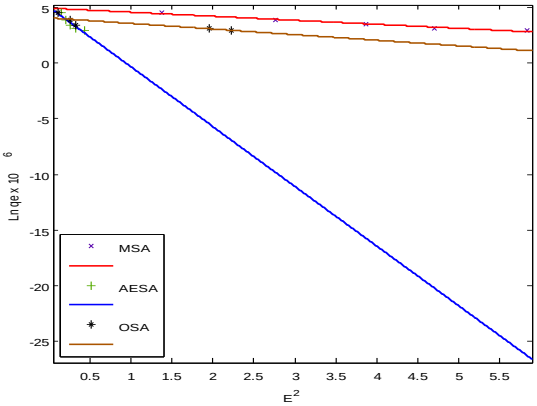

(pH6)

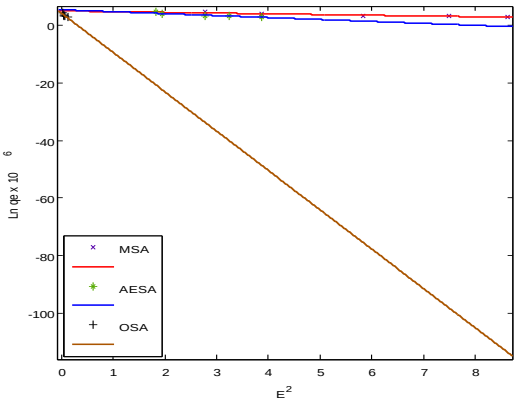

(pH8)

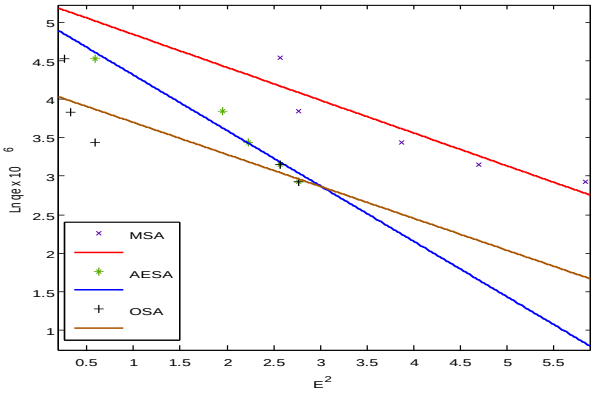

(pH10)

Figure C7A plot of Ln($1/q_e$) vs E^2 at various pH for acid treated adsorbent in paint effluent(PW)

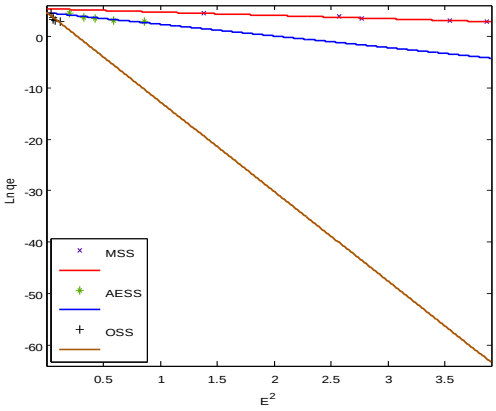

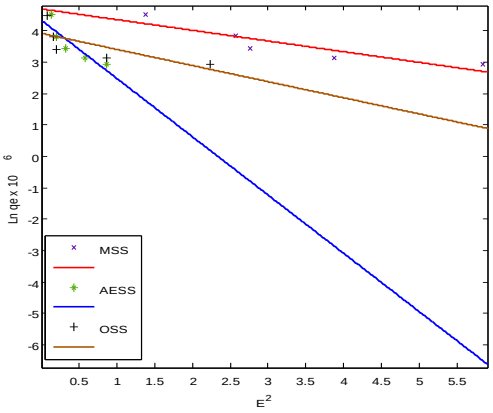

(pH2)

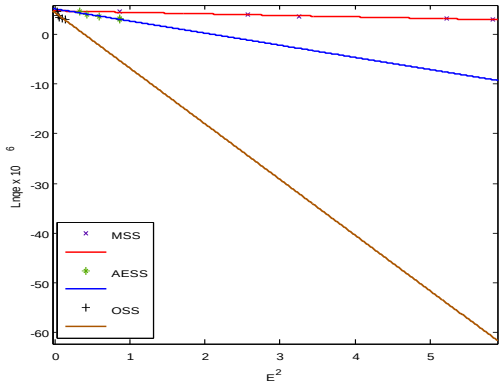

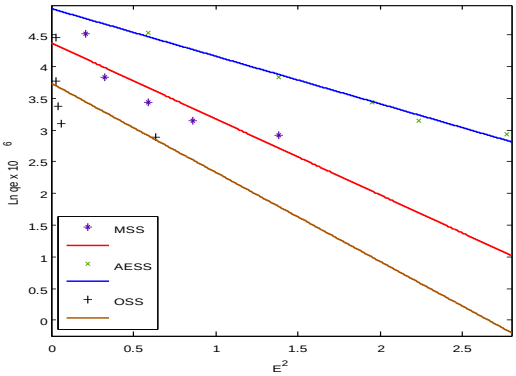

(pH4)

(pH6) (pH8)

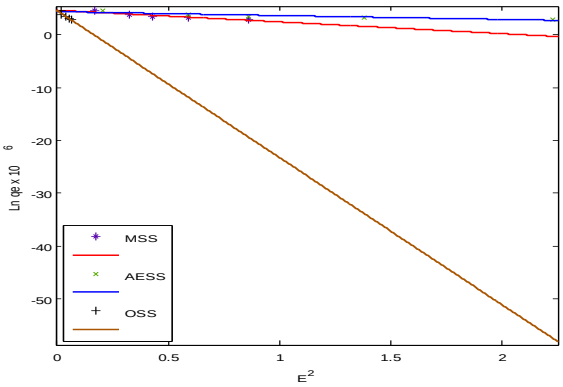

(pH10)

Figure C8A plot of Ln($1/q_e$) vs E^2 at various pH for salt treated adsorbent in brewery effluent (BRE)

APPENDIX D

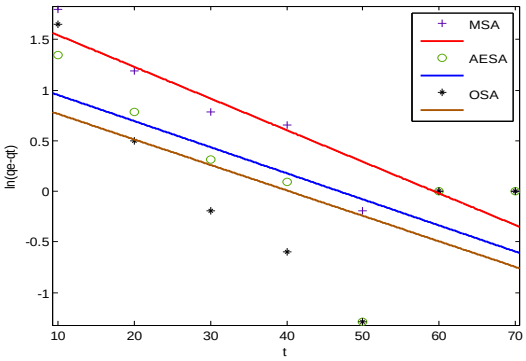

pH2.0

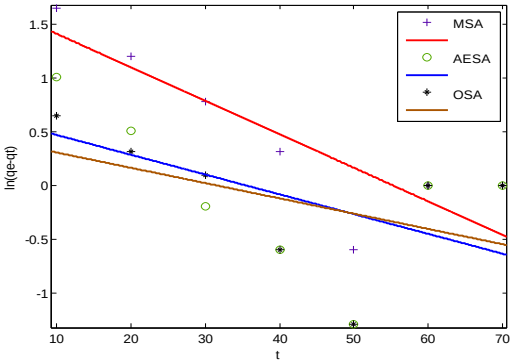

pH4.0

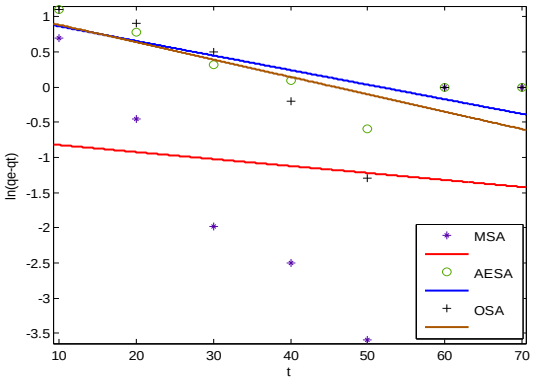

pH6.0

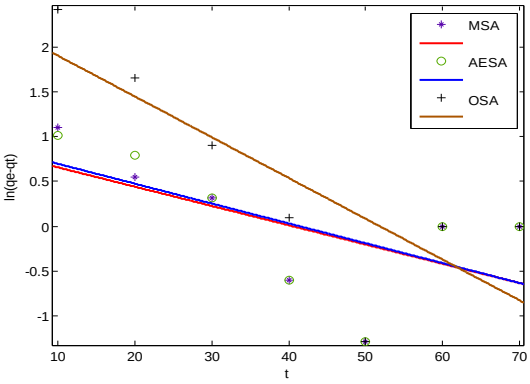

pH8.0

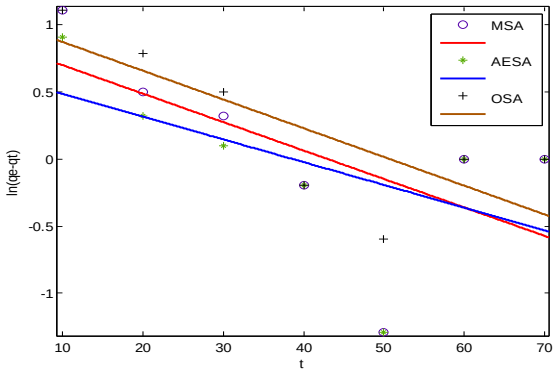

pH10.0

Figure D1 Linearized plot for Pseudo first order kinetic adsorption of TSS and TDS at different pH with 20mg acid treated adsorbents in BRE

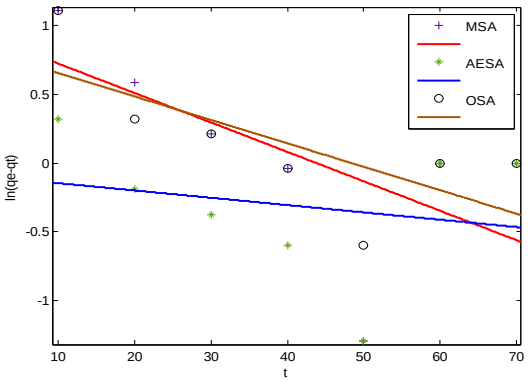

pH2.0

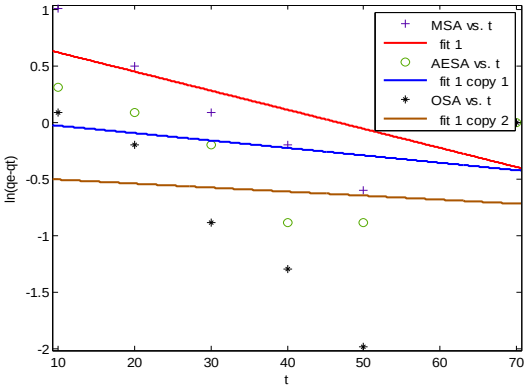

pH4.0

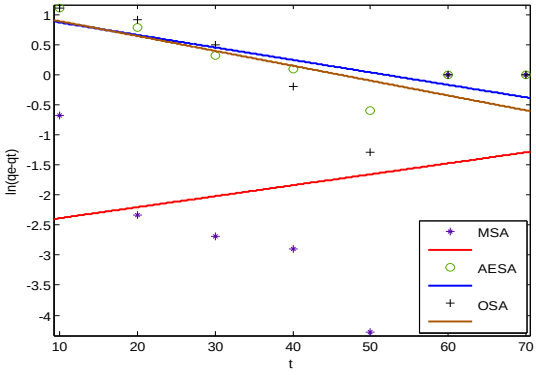

pH6.0

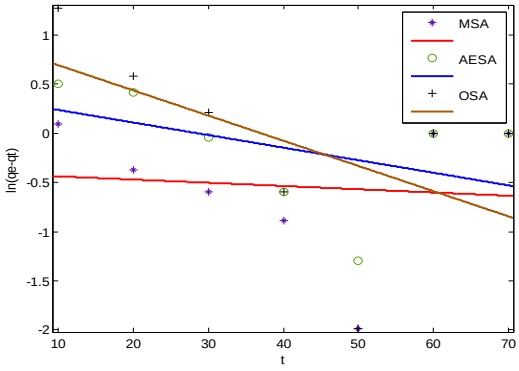

pH8.0

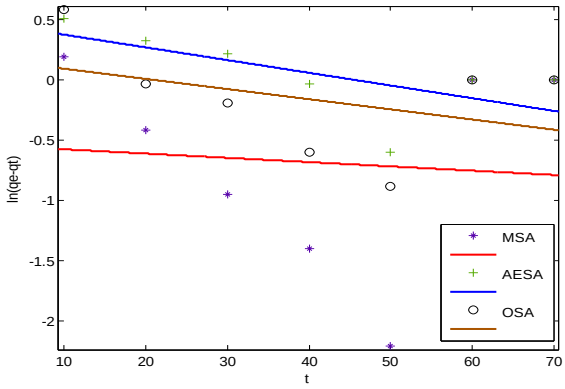

pH10.0

Figure D2 Linearized plot for Pseudo first order kinetic adsorption of turbidity at different pH with 40mg acid treated adsorbents in BRE

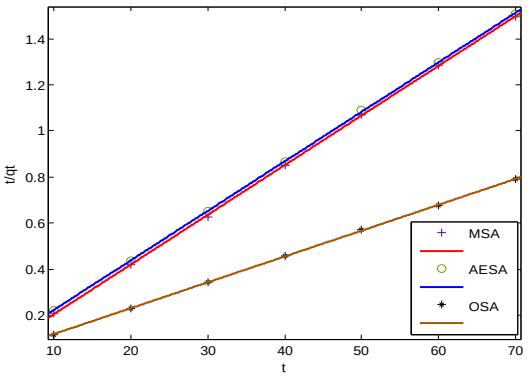

pH2.0

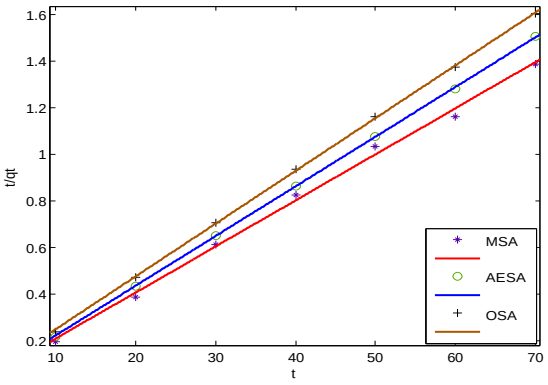

pH4.0

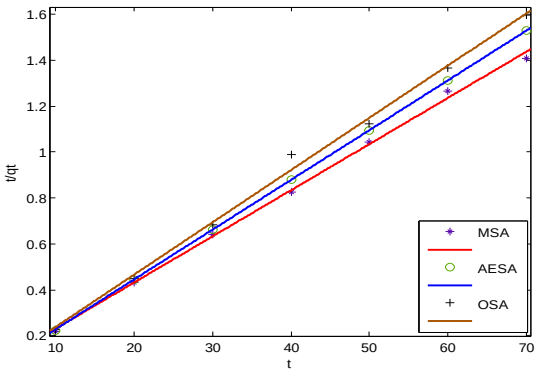

pH6.0

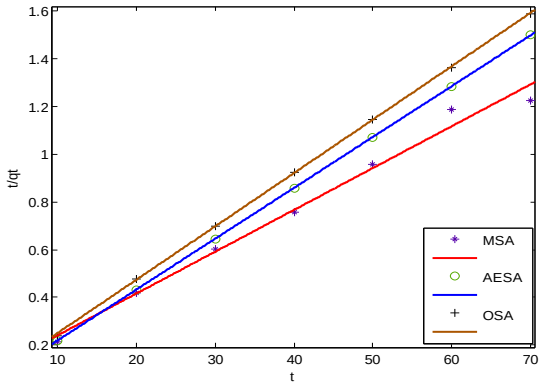

pH8.0

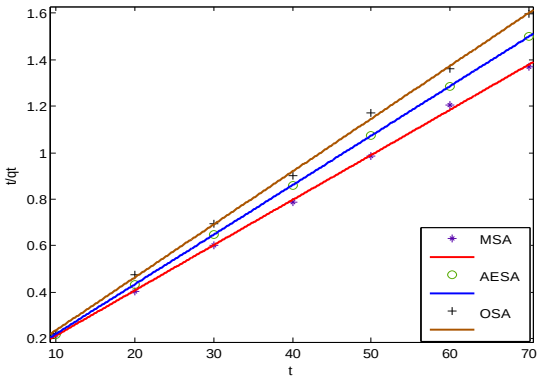

pH10.0

Figure D3 Linearized plot for Pseudo second order kinetic studies for adsorption at different pHs for 40mg acid treated adsorbent in PW

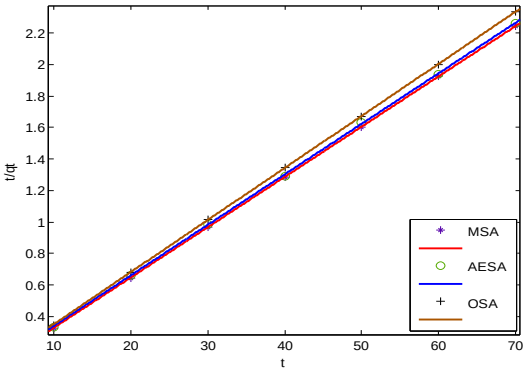

pH2.0

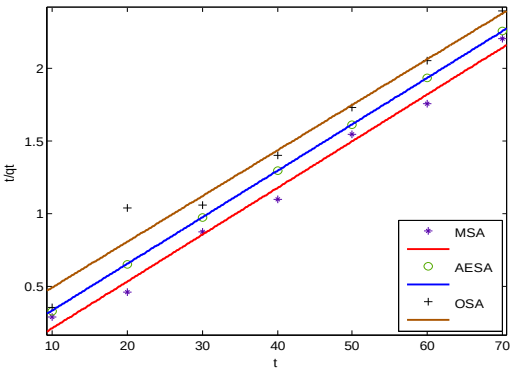

pH4.0

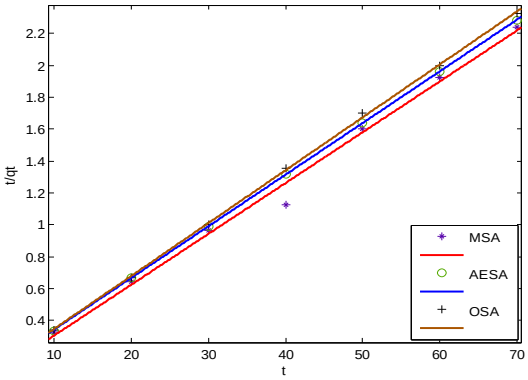

pH6.0

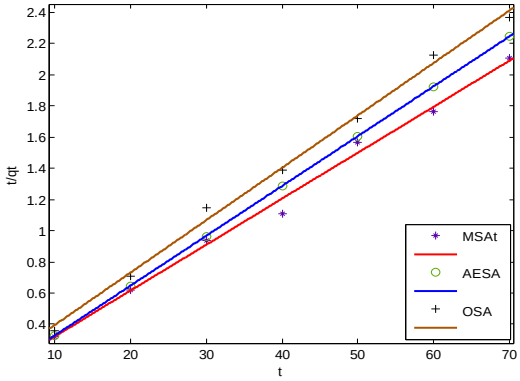

pH8.0

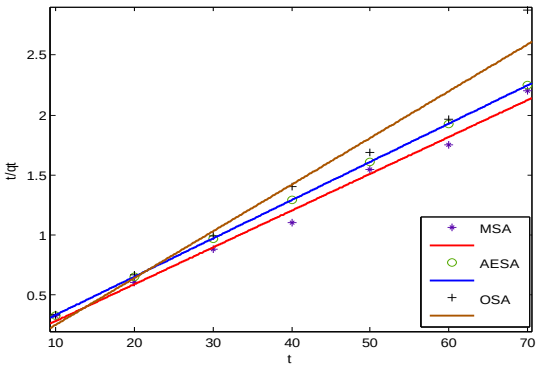

pH10.0

Figure D4 Linearized plot for Pseudo second order kinetic studies for adsorption at different pHs with 60mg acid treated adsorbent in PW

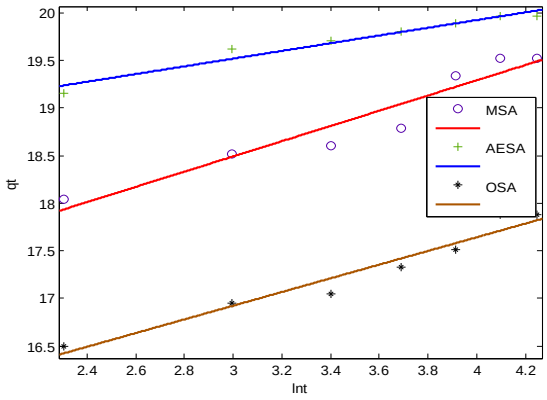

pH2.0

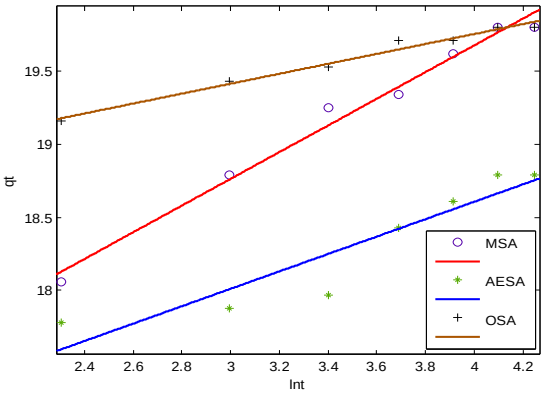

pH4.0

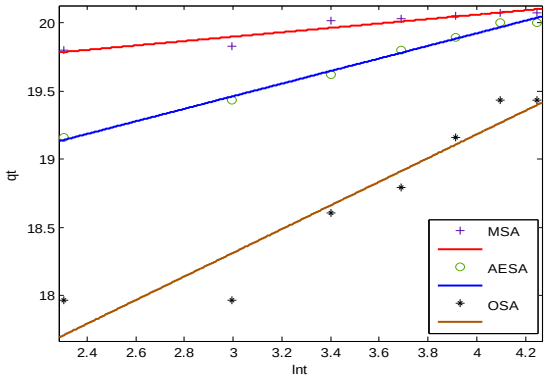

pH6.0

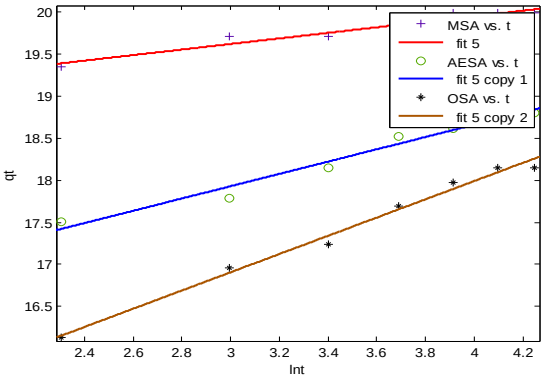

pH8.0

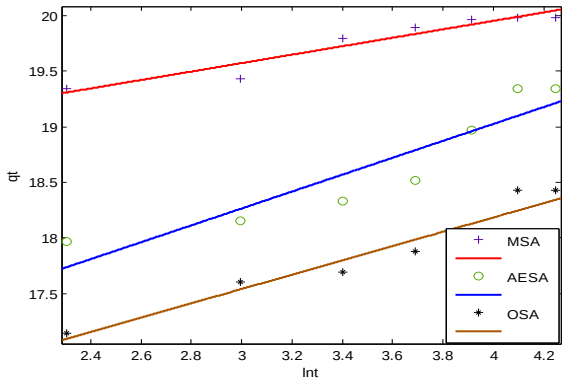

pH10.0

Figure D5 Linearized plot for Elovich equation for adsorption of turbidity different pHs with 60mg acid treated adsorbent in BRE

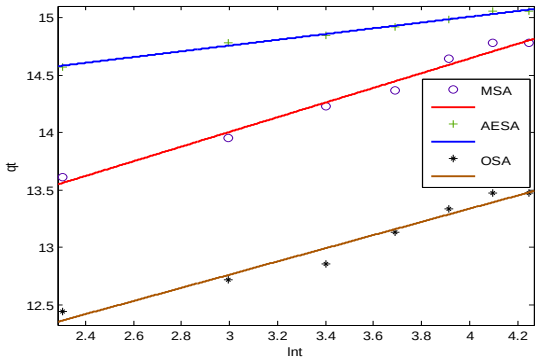

pH2.0

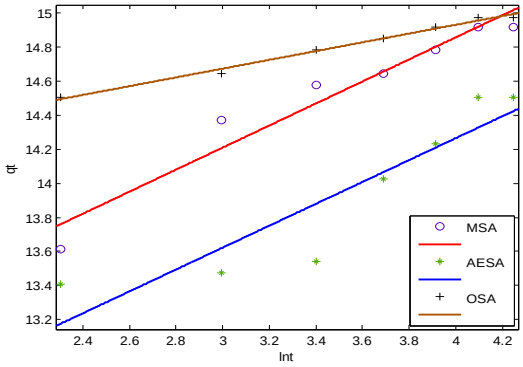

pH4.0

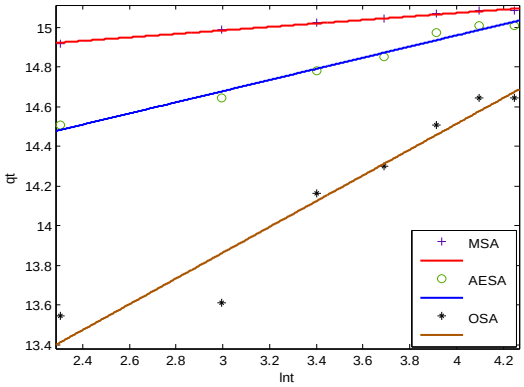

pH6.0

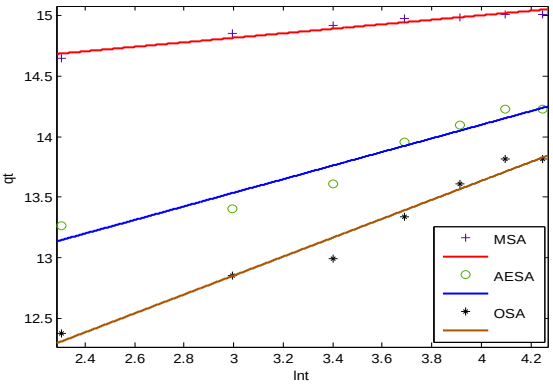

pH8.0

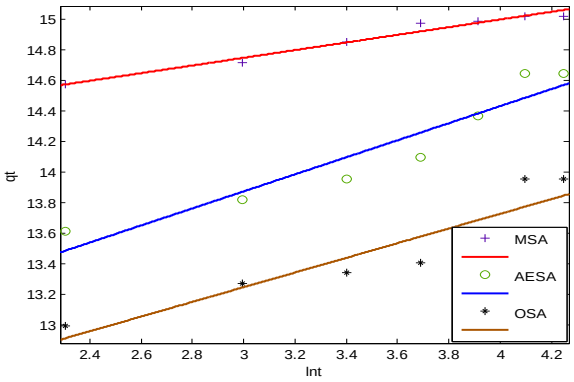

pH10.0

Figure D6 Linearized plot for Elovich equation for adsorption of TSS and TDS at different pHs and 80mg acid treated in BRE

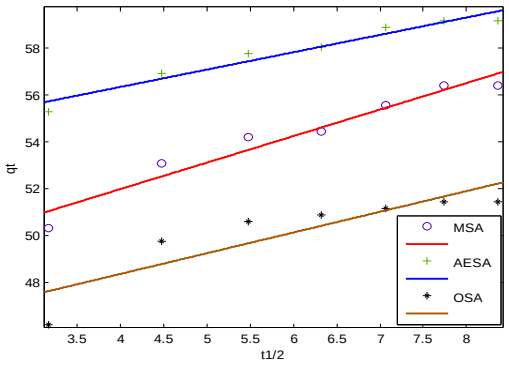

pH2.0

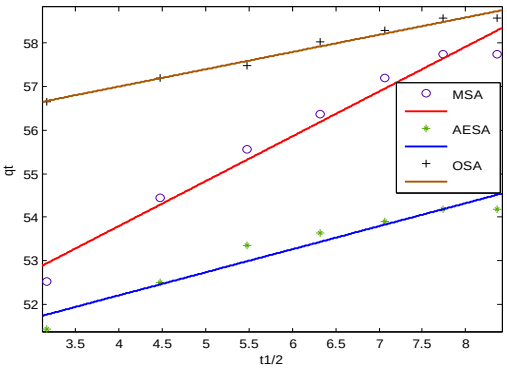

pH4.0

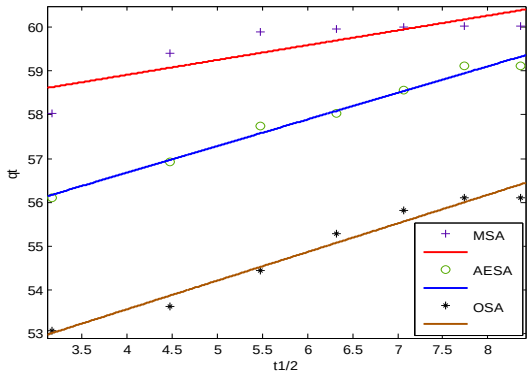

pH6.0

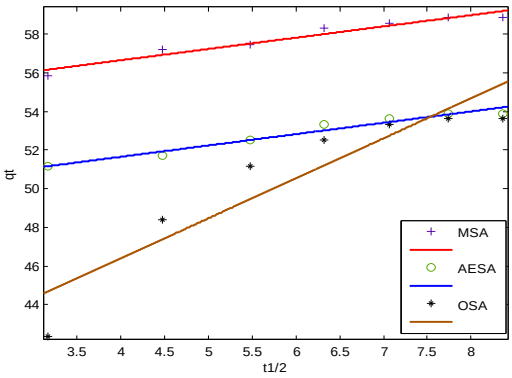

pH8.0

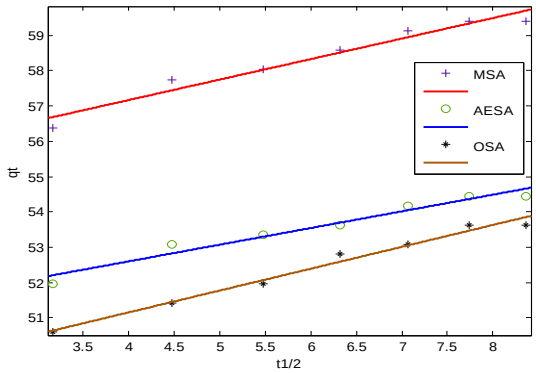

pH10.0

Figure D7 Linearized plot of intra particle diffusion studies for adsorption of TSS and TDS at different pH with 20mg acid treated adsorbents on BRE

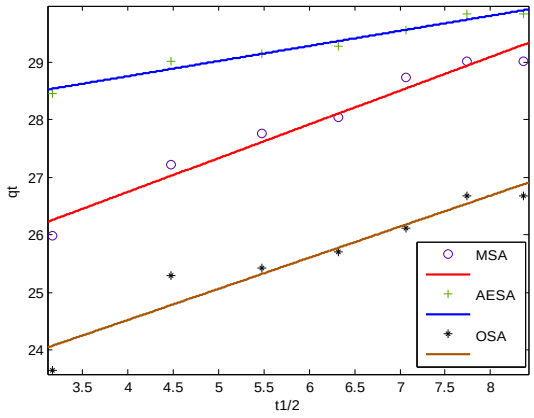

pH2.0

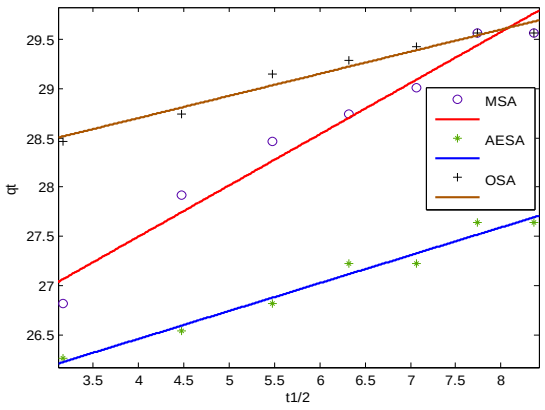

pH4.0

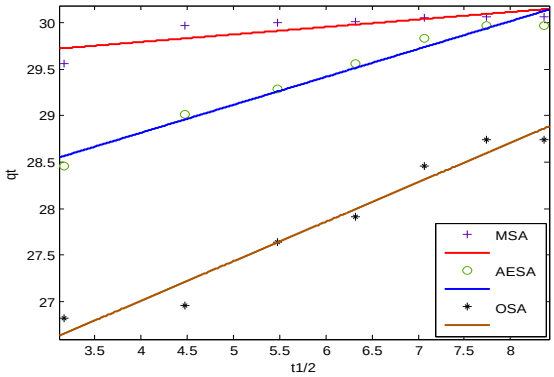

pH6.0

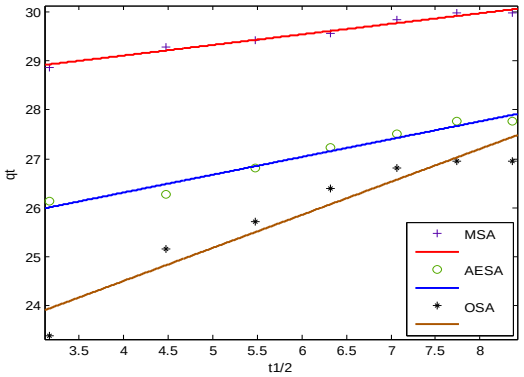

pH8.0

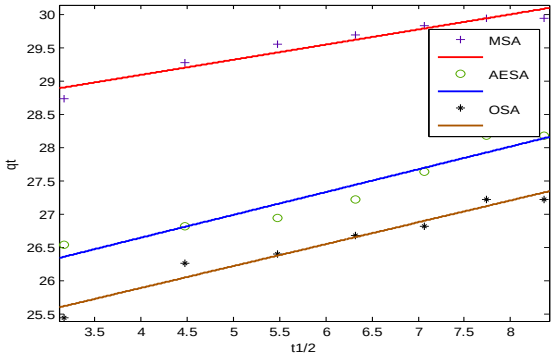

pH10.0

Figure D8 Linearized plot of intra particle diffusion studies for adsorption of TSS and TDS at different pH with 40mg acid treated adsorbents on BRE

APPENDIX E

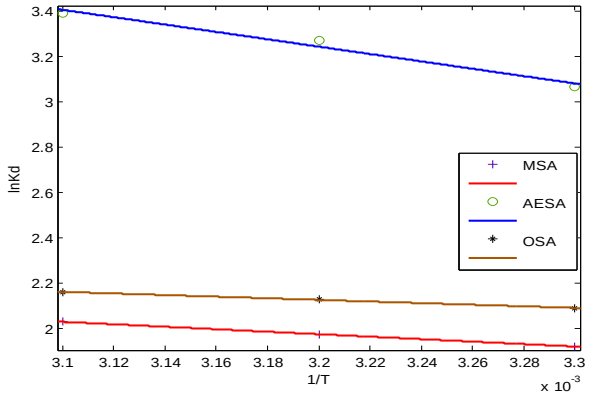

Figure E1 Von't Hoff plot of effect of temperature on adsorptionof TSS and TDS on acid treated adsorbent in BRE.

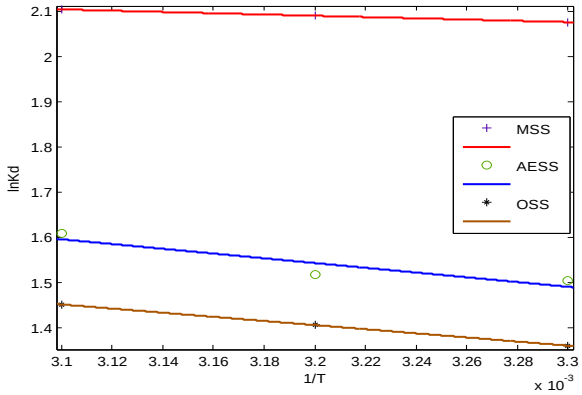

Figure E2 Von't Hoff plot of temperature effect on adsorption of TSS and TDS on salt treated adsorbent in BRE.

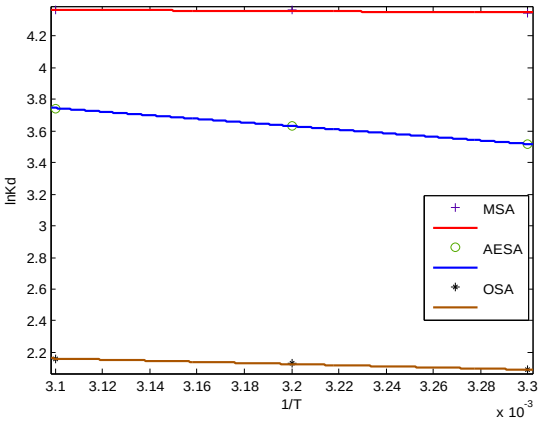

Figure E3 Von't Hoff plot of temperature effect on adsorption of TSS and TDS on acid treated adsorbent in PW

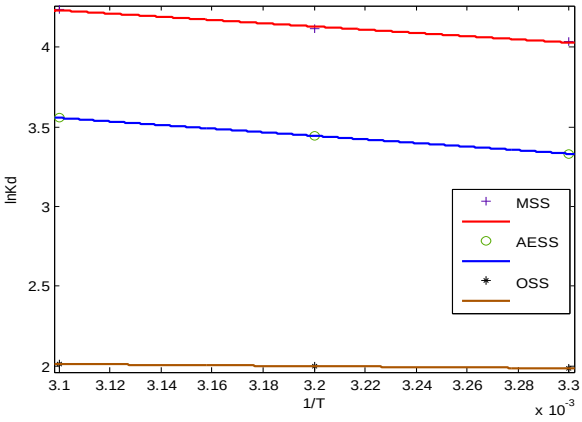

Figure E4 Von't Hoff plot of temperature effect on adsorption of TSS and TDS on salt treated adsorbent in PW.